OPG's DEEP GEOLOGIC

REPOSITORY

FOR LOW & INTERMEDIATE LEVEL WASTE

Postclosure Safety Assessment: Gas Modelling

March 2011

Prepared by: Geofirma Engineering Ltd. and
Quintessa Ltd.

NWMO DGR-TR-2011-31

Geofirma Engineering Ltd

Quintessa

OPG's DEEP GEOLOGIC

REPOSITORY

FOR LOW & INTERMEDIATE LEVEL WASTE

Postclosure Safety Assessment: Gas Modelling

March 2011

Prepared by: Geofirma Engineering Ltd. and
Quintessa Ltd.

NWMO DGR-TR-2011-31

THIS PAGE HAS BEEN LEFT BLANK INTENTIONALLY

DOCUMENT HISTORY

Title:	Postclosure Safety Assessment: Gas Modelling		
Report Number:	NWMO DGR-TR-2011-31		
Revision:	R000	**Date:**	March 2011
Geofirma Engineering Ltd. [1] and Quintessa Ltd.			
Prepared by:	J. Avis, N. Calder, P. Humphreys, F. King, P. Suckling, R. Walsh		
Reviewed by:	J. Pickens, R. Little		
Approved by:	R. Little		
Nuclear Waste Management Organization			
Reviewed by:	H. Leung, F. Garisto		
Accepted by:	P. Gierszewski		

[1] Previously known as Intera Engineering Ltd.

THIS PAGE HAS BEEN LEFT BLANK INTENTIONALLY

EXECUTIVE SUMMARY

Ontario Power Generation (OPG) is proposing to build a Deep Geologic Repository (DGR) for Low and Intermediate Level Waste (L&ILW) near the existing Western Waste Management Facility at the Bruce nuclear site in the Municipality of Kincardine, Ontario. The Nuclear Waste Management Organization, on behalf of OPG, is preparing the Environmental Impact Statement (EIS) and Preliminary Safety Report (PSR) for the proposed repository.

The project involves investigation of the site's geological and surface environmental characteristics, conceptual design of the DGR, and safety assessment. The postclosure safety assessment (SA) evaluates the long-term safety of the proposed facility and provides supporting information for the EIS and PSR.

This report describes numeric modelling work undertaken to calculate the generation and build-up of gas in the repository, the exchange of gas and groundwater between the repository and the surrounding rock, and between the rock and the surface environment. The results are used to inform the postclosure safety assessment modelling of potential dose impacts of the repository gases.

Models and Calculation Cases

The conceptual models for gas generation and groundwater flow and transport in the geosphere were based on the repository design and the expected system evolution. The gas modelling included the following key features:

- A repository model with gas generation by various corrosion and degradation reactions, coupled to gas and water inflow and outflow;
- Detailed models for the geosphere and the shaft, which considered transient groundwater flow, two-phase gas transport and dissolved gas transport; and
- The effects of the initial under- and over- pressures, and the presence of initial gas saturation in the deep rock.

The gas modelling approach consists of four separate numerical models.

1. A detailed three-dimensional (3D) representation of the repository, the shafts and the surrounding low-permeability geosphere (the 3DD model). The model includes some simplifications of the actual design such as combined shafts and galleries, but is nonetheless computationally demanding. For this reason, its use was limited.
2. A simplified quarter section 3D model of the repository, the combined shafts, and the surrounding low-permeability geosphere (the 3DSRS model). This model is the primary model used in the analyses and results are available for most calculation cases.
3. A simplified quarter section 3D model of the repository, and the surrounding low-permeability geosphere (the 3DSR model). This model focuses on gas transfer across the repository-geosphere interface and was used primarily for evaluation of calculation cases focussed on geosphere performance. It was also used as a comparison to 3DSRS model results with the differences used to determine the impact of the shaft seal system on results.
4. A two-dimensional radial and vertical axisymmetric representation of the shaft system connecting the repository to the Shallow Bedrock Groundwater Zone (the 2DRS model). Specified repository gas pressure histories from 3DD or 3DSRS model results were applied

to the bottom of the shaft. The model was used to calculate flows of gas up the shaft in the system above the domain of the 3D models.

The rationale for using these models is as follows.

- To provide a detailed representation of the gas behaviour (pressure, saturation) within the repository and its interaction with the surrounding host rock, including two-phase transport and dissolved phase transport. This is accomplished by coupling the gas transport model with a repository gas-generation model (GGM).
- To represent the interaction of the repository and shaft seals with the surrounding host rock. This is accomplished by using a range of model geometries that capture the essential processes of each case.
- To provide gas transport rates up the shaft system and the host rock as input to the assessment modelling of impacts.

The main geometric simplifications were as follows.

- Limiting the vertical extent of the 3D models to reduce computational requirements. The geosphere models focussed on the low-permeability deep groundwater and intermediate groundwater zones around the repository, extending from the top of the Cambrian to the lowest permeable Silurian formation, the Guelph Formation.
- Representation of the repository as homogenized into two panels in the 3DD model and a single panel in the 3DSRS and 3DSR models.
- Representation of the two shafts as a single shaft with the same total cross-sectional area for the shaft and for the associated EDZ.

A series of calculation cases based on the Normal Evolution Scenario (i.e., the expected evolution of the repository and geosphere) have been evaluated. These include a Reference Case, a Simplified Base Case, and a number of variant cases which address various parameter, conceptual model and data uncertainties. Additionally, two variant cases of a single Disruptive Scenario (Severe Shaft Seal Failure Scenario, whereby the shaft seals are assumed to perform greatly below expectations) were considered. Calculations were conducted using TOUGH2, coupled to a custom gas-generation module GGM. The coupled code is referred to as T2GGM.

Gas generation rates calculated by the GGM module are highly dependent upon the availability of water or water vapour to sustain certain degradation reactions. The gas generation module was used in two modes: Water-Limited (WL) and Non-Water-Limited (WL). WL analyses limit reactions to the water inflows available from the geosphere. NWL results allow gas-generation reactions to proceed even if that would require water in excess of that provided by the geosphere. In general, the WL mode results in less gas generation and a delayed repository pressure build up relative to the NWL cases. The WL mode, although a more accurate representation of processes, is very sensitive to assumptions regarding geosphere permeability, which is the most significant control on repository inflow. Therefore, it is conservatively assumed that the NWL cases represent expected behaviour.

In all cases, groundwater was assumed to be of constant density; the gas species generated in the repository were converted to a single bulk gas for transport through the geosphere and shaft seals; no horizontal hydraulic gradients (e.g., in the Guelph and Salina A1 upper carbonate formations) were implemented; and glaciation related impacts were not analyzed. The impacts of these are addressed qualitatively; they do not affect the main conclusions.

Uncertainties

Uncertainties in model results presented in this report arise from a variety of sources, including: the modelling approach, limitations of the model, parameterization (for both the gas generation and gas transport models), and the conceptual model of the geosphere. Uncertainties have been managed through the use of multiple modelling approaches, sensitivity cases and adoption of conservative assumptions.

The primary uncertainties are the parameterization of the shaft seals, shaft excavation damage zone, the highly damaged zone (HDZ) surrounding the concrete monolith, and of lesser significance, more complete characterization of the pressures, saturation state and two-phase flow parameters of the geosphere. Conservative values have been used for these parameters and variability is addressed with sensitivity cases.

Further geosphere uncertainties relate to the hydromechanical response of the repository and geosphere system to glaciation events. These uncertainties are addressed with conservative conceptualization of the models.

Results and Analysis

Gas generation and consumption processes within the repository occur in the following sequence:

1. Oxygen within the repository is consumed and conditions become anaerobic.
2. Metals and organic wastes are subject to anaerobic corrosion and degradation, supported by moisture, resulting in the generation of hydrogen, CO_2 and CH_4 gases. The gas pressure in the repository rises gradually.
3. Over the 1 Ma assessment period, the peak repository gas pressure is in the range of 7 to 9 MPa, converging towards or somewhat higher than the steady-state geosphere hydraulic pressure at the repository horizon.
4. Methane is generally the dominant gas throughout the evolution of the repository.

The following describes the general flow of gas and water within the host-rock and shaft system in qualitative terms:

1. Rock formation porewater and gas (if present) flow into the shaft from the rock after closure.
2. Porewater and formation gas (if present) very slowly flow into the repository from the host rock. The shaft is a minor source of water and gas.
3. If the geosphere contains gas above a residual level of gas saturation, formation gas will continue to seep into the repository until an equilibrium between repository and geosphere pressures is reached. This may take millions of years.
4. As pressures in the repository develop, small amounts of gas are pushed out into the shaft and the rock mass. The properties of the Ordovician rock mass and bentonite/sand seals ensure that leakage of gas out of the repository is very slow.
5. In the most cases repository gas pressure never reaches a pressure sufficient to cause gas to flow up the shaft.
6. In the several sensitivity cases where gas does flow up the shaft, it leaves the shaft at the more permeable formations in the Silurian, particularly the Guelph Formation. This prevents gas from reaching the Shallow Bedrock Groundwater Zone.
7. Some dissolved gas does reach the top of the Intermediate Groundwater Zone, in very small amounts and at long times.

8. The repository remains nearly completely dry over the 1 million years evaluated in the normal evolution scenario. As gas generation is completed, slow gas dissolution and permeation may allow eventual resaturation on very long time scales.

Results from cases presented in this report show that the site geosphere acts as a very effective barrier, with no significant flow of free-phase or dissolved gas within the host rocks. For most cases, there is also no transport through the shaft seal. In cases where transport does occur, the shaft seals are an effective barrier and, in conjunction with the higher permeability Guelph and Salina A1 upper carbonate formations, prevent the transport of any free phase gas to the Shallow Bedrock Groundwater Zone (i.e., the near-surface aquifer). Only under the Severe Shaft Seal Failure Scenario does free-phase gas reach the Shallow Bedrock Groundwater Zone, and then only if extreme assumptions are made about the properties of the degraded shaft materials that characterize the scenario.

TABLE OF CONTENTS

LIST OF TABLES

Page

LIST OF FIGURES

Page

1. INTRODUCTION

Ontario Power Generation (OPG) is proposing to build a Deep Geologic Repository (DGR) for Low and Intermediate Level Waste (L&ILW) near the existing Western Waste Management Facility (WWMF) at the Bruce nuclear site in the Municipality of Kincardine, Ontario (Figure 1.1). The Nuclear Waste Management Organization (NWMO), on behalf of OPG, is preparing the Environmental Impact Statement (EIS) and Preliminary Safety Report (PSR) for the proposed repository.

The project involves investigation of the site's geological and surface environmental characteristics, conceptual design of the DGR, and safety assessment. The postclosure safety assessment (SA) evaluates the long-term safety of the proposed facility and provides supporting information for the EIS (OPG 2011a) and PSR (OPG 2011b).

The work builds upon the previous safety assessment (QUINTESSA et al. 2009) and has been refined to take account of the revised waste inventory and repository design, and the greater understanding of the site that has been developed.

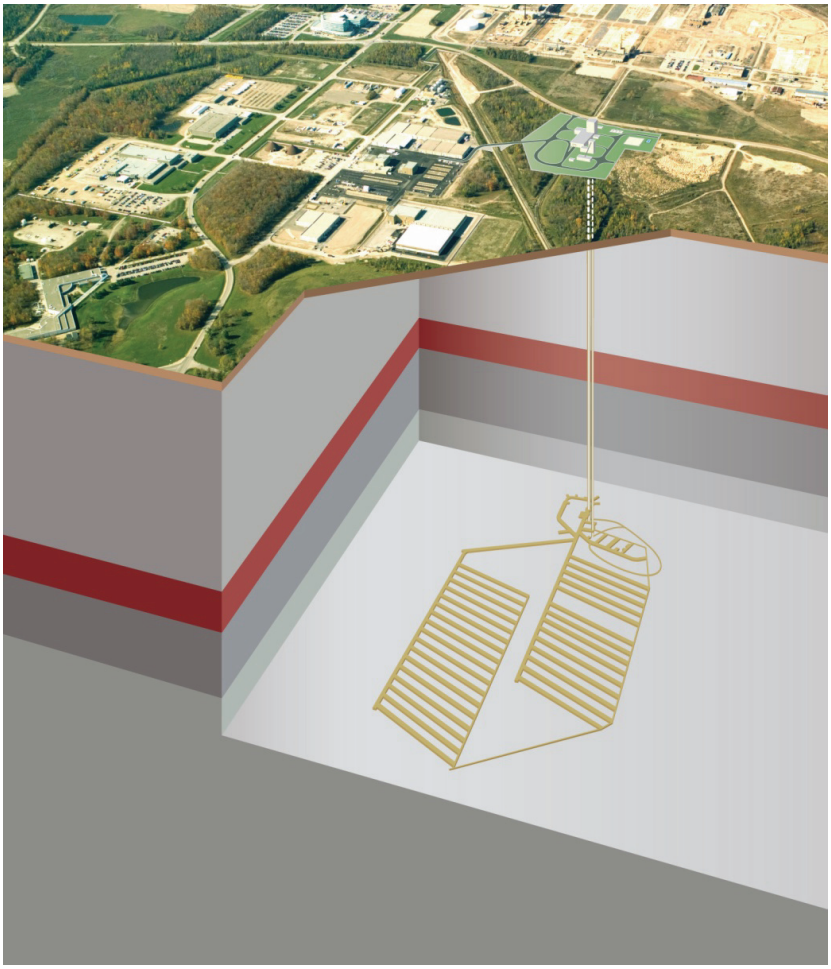

Figure 1.1: The DGR Concept at the Bruce Nuclear Site

This report (Gas Modelling) is one of a suite of documents that present the postclosure safety assessment (Figure 1.2), which also includes the Postclosure SA main report (QUINTESSA et al. 2011a), the Normal Evolution Scenario Analysis report (QUINTESSA 2011a), the Human Intrusion and Other Disruptive Scenarios Analysis report (QUINTESSA and SENES 2011), the System and Its Evolution (QUINTESSA 2011b), the Features, Events and Processes report (QUINTESSA et al. 2011b), the Data report (QUINTESSA and GEOFIRMA 2011a), and the Groundwater Modelling report (GEOFIRMA 2011).

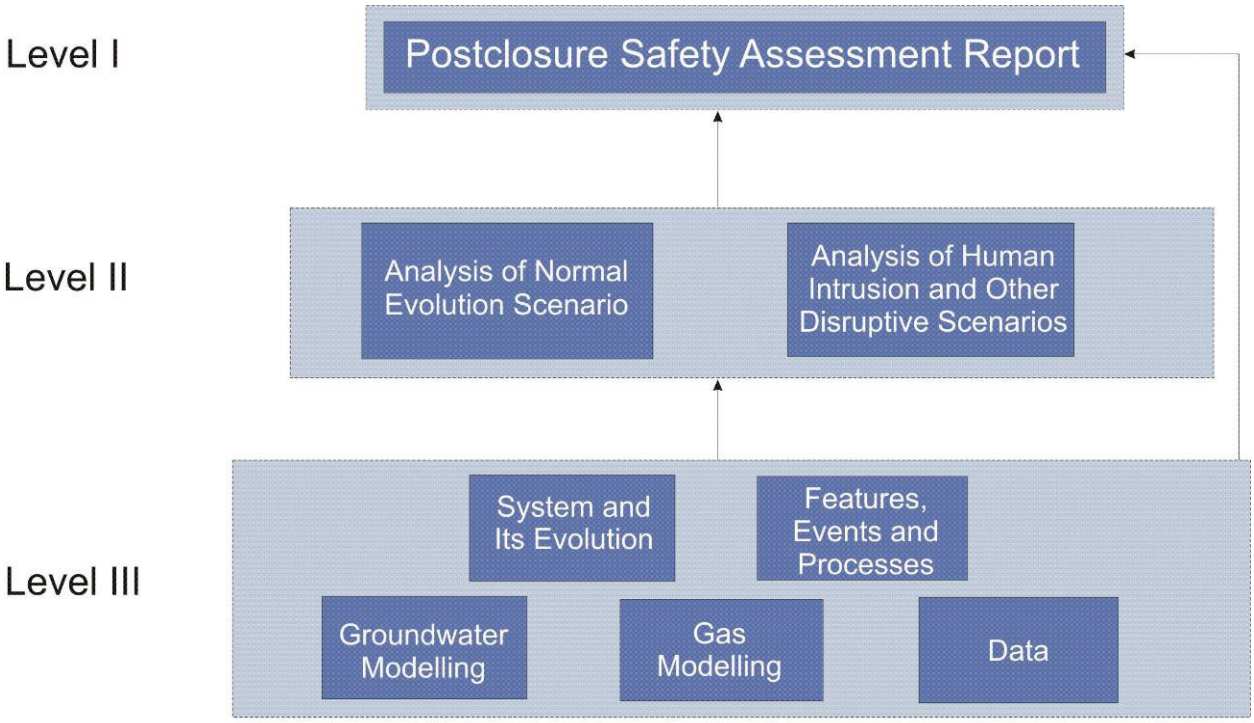

Figure 1.2: Document Structure for the Version 2 Postclosure Safety Assessment

1.1 Purpose and Scope

This report describes numeric modelling work undertaken to calculate the generation and build-up of gas in the repository, and the potential two-phase flow of gas and groundwater from the proposed repository to the surface environment. The modelling was performed using a coupled gas generation and two-phase flow transport code that allows for detailed representation of repository and geosphere.

The detailed models capture most relevant aspects of overall system performance for both Normal Evolution Scenarios (i.e., those that model the expected evolution of the repository and geosphere) and possible Disruptive Scenarios (i.e., unlikely or “what if” cases that test the robustness of the DGR). These are documented in Chapters 7 and 8 of the System and Its Evolution report (QUINTESSA 2011b).

The detailed models were simulated for a Reference Case set of parameters and initial conditions that approximate the Normal Evolution Scenario with the exception that glaciation-cycle related impacts were not assessed. A number of calculation cases addressing sensitivity to Normal Evolution Scenario assumptions were also simulated, such as alternative geosphere initial conditions, engineered barrier system performance, and gas generation parameters. An additional calculation case was defined to simulate a "what if" Disruptive Scenario.

Calculation cases include both conservative Non-Water-Limited (NWL) and more realistic Water-Limited (WL) gas generation modes. NWL cases do not remove water consumed in gas generation reactions from the repository. This allows gas-generation reactions to continue even if they would require water in excess of that provided by the geosphere. WL cases remove consumed water from the repository. Both modes limit reactions if there is insufficient water in the repository to support the reactions. Results of calculation cases are compared to provide a quantitative assessment of significance of this parameter.

Results from the detailed gas modelling provide direct input to the gas transport pathway for the assessment modelling (QUINTESSA 2011a; QUINTESSA and SENES 2011). The assessment modelling describes the performance of the total system (repository through to biosphere) for all radionuclides, and calculates metrics that can be compared to regulatory standards, such as peak dose rate.

1.2 Report Outline

The report is organized as follows.

- Chapter 2 describes the conceptual models of gas generation, flow and transport and the approach used to create numeric models representing the conceptual models.
- Chapter 3 describes the defined calculation cases.
- Chapter 4 provides an overview of the data used in the numeric modelling and the implementation of the detailed numeric models.
- Chapter 5 presents results of modelling for the Normal Evolution Scenario's reference and sensitivity calculation cases for the NWL mode.
- Chapter 6 presents results for Disruptive Scenarios based on Severe Shaft Seal Failure Scenario for the NWL mode.
- Chapter 7 presents summary results for WL mode simulations.
- Chapter 8 presents graphical and tabular summaries and a discussion of all case results.
- Chapter 9 describes uncertainties in the modelling scenarios and results.
- Chapter 10 provides overall conclusions on the detailed gas modelling results.

Appendix A contains an audit of the mathematical model for gas generation and transport against the FEPs (Features, Events and Processes) set out in the FEP report (QUINTESSA et al. 2011b). Appendix B provides a simple repository gas pressure and flow calculation. This calculation estimates peak repository gas pressures from initial waste inventories and assumptions about the key gas generation processes. Estimates of gas flow rates up the shaft are also calculated.

The report has been written for a technical audience that is familiar with the scope and objectives of the DGR project, the Bruce nuclear site, and the process of assessing the long-term safety of radioactive waste deep geological repositories.

2. CONCEPTUAL MODELS

This section of the report describes the general conceptual models of gas and water generation and consumption within the repository and the detailed modelling of the groundwater and gaseous pathways through the geosphere at the Bruce nuclear site. These conceptual models are generally consistent with the system and its evolution described in the Normal Evolution and Disruptive Scenarios. Differences required to best simulate the integrated repository and geosphere system while maintaining computational tractability are described.

A coupled conceptual model of gas generation has been developed and implemented in a code (T2GGM). The code comprises a component (GGM), which models gas generation within the DGR due to corrosion and microbial degradation of the waste packages, and a component (TOUGH2), which models the subsequent two-phase transport of the gas through the repository and into the DGR shafts and geosphere (Figure 2.1). The following sections provide a description of the underlying gas generation and gas and water transport conceptual models.

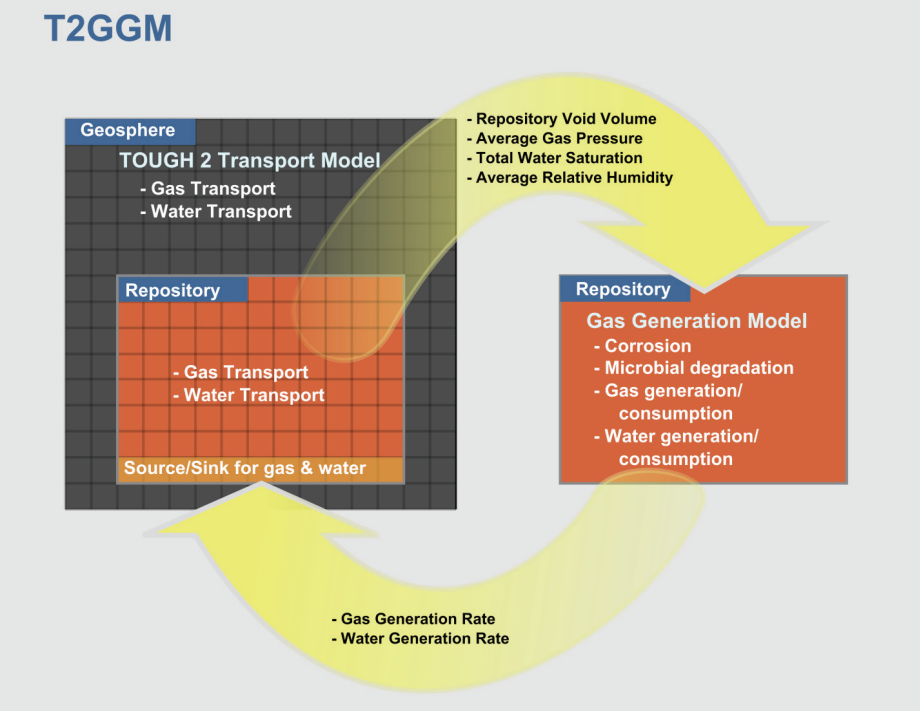

Figure 2.1: Coupling Gas Generation and Transport in T2GGM

2.1 Gas Generation Overview

Gas generation within the repository is one of the key factors in the postclosure safety of the proposed facility. Gas is generated and consumed within the repository by various microbial and corrosion processes. The repository interacts with the geosphere through the fluxes of gas and water into and out of the repository. Following closure, the build-up of gas within the sealed repository affects the water resaturation time and could lead to the release of gaseous radionuclides.

GGM has been developed to simulate various microbial and corrosion processes, the gas evolution of the repository, and its interaction with the geosphere. GGM tracks the production and consumption of the key chemical species (e.g., metals, organic wastes, gases, water) and tracks the fluxes of the water and gases into and out of the repository. It is designed to fully conserve Fe and C, and to ensure that reactions only proceed when there is sufficient water. Other elements are conservatively assumed not to be limiting and are not tracked for mass balance (e.g., N needed to support microbial reactions).

A complete description of all the processes included in GGM is given in the theory section of the T2GGM software documentation (QUINTESSA and GEOFIRMA 2011b). QUINTESSA and GEOFIRMA (2011b) also includes a description of the approach used in coupling GGM to TOUGH2, and describes various other minor enhancements made to TOUGH2 to support the postclosure gas modelling. This T2GGM report also provides documentation of the verification of T2GGM.

The following sections summarize the key waste streams and processes included in the GGM.

2.1.1 Non-Water-Limited and Water-Limited Modes

In applying T2GGM to simulate the defined calculation cases, two modes are used to reflect different assumptions concerning the availability of water in the repository: non-water-limited (NWL) and water-limited (WL).

- The NWL mode does not enforce a full water balance in the repository. Specifically, the repository saturation and humidity levels are a function of geosphere inflow or outflow only, which are controlled by geosphere and shaft permeabilities and pressure gradients. The generation or consumption of water by corrosion and other reactions within the repository is not included in the water balance. In practice, this means that reactions – including gas generation - proceed in all circumstances except when water has been expelled from the repository due to repository pressures exceeding geosphere liquid pressures.
- The WL mode enforces a water balance. Water consumed in repository reactions is withdrawn from the repository. The repository saturation and humidity levels are a function of geosphere inflow or outflow, and of repository water consumption/generation reactions. As the humidity decreases, water vapour dependent reaction rates are also decreased so that they are in balance with calculated water repository inflow from the geosphere. In general, the WL mode results in less gas generation and a delayed repository pressure build up relative to the NWL mode.

The WL cases are sensitive to the uniformly low host rock permeability, which is the most significant control on repository water inflow. It is, therefore, conservatively assumed that the NWL cases represent expected behaviour.

2.1.2 Classification of Organic and Metallic Wastes

The organic and metallic wastes are classified into a number of waste streams. This allows the degradation/corrosion of each waste stream to be modelled independently and assigned different reaction rates.

Organic wastes are classified into three groups: cellulosic wastes, ion-exchange resins, and plastics and rubbers.

Metallic wastes are classified into four groups: carbon and galvanized steels; passivated carbon steels; stainless steels and nickel alloys; and zirconium alloys.

2.1.3 Key Processes

GGM includes four key mechanisms for the generation of gas and consumption of water (see Sections 4.2 and 4.3 of QUINTESSA and GEOFIRMA 2011b for complete supporting references):

1. The microbial degradation of organic wastes;
2. Methanogenesis via the microbial hydrogen mechanism;
3. The corrosion of metallic wastes; and
4. The CO_2 enhanced corrosion of metallic wastes and formation of siderite ($FeCO_3$).

These processes may occur in either the saturated (water submerged) or vapour phases. These four mechanisms above are summarized in Sections 2.1.3.1 to 2.1.3.4 below.

Gases are modelled as partitioning between the saturated and vapour phases according to Henry's law, where dissolved gas and free-phase gas are in equilibrium. The relative humidity of the vapour phase is calculated by TOUGH2 and provided as an input to the GGM model (Figure 2.1). The dependence on relative humidity of vapour phase microbial and corrosion processes is taken into account, with reaction rates decreasing linearly to zero between a relative humidity of 80% and 60%.

Under ideal conditions, microbial systems employ a range of terminal electron acceptors in oxidation-reduction reactions, which are consumed in a well-defined order depending on the amount of energy provided by each reaction: oxygen, nitrate, ferric ion, manganese, sulphate, and carbon dioxide. All of these stages, apart from manganese (IV), are included in GGM. Mn(IV) has been excluded from GGM as a terminal electron acceptor, because it is not expected to be present in significant quantities. Also, scoping calculations have shown that these initial stages take place over a relatively fast time scale (decades) and that they have a minimal impact on the composition and amounts of the gases that play the main role in generating the peak gas pressures in the final stage: methane, hydrogen and carbon dioxide.

GGM also includes the growth and death of biomass from organic materials and models the recycling of dead biomass as a mix of easily recycled and recalcitrant organic matter. The results show the primary effect of biomass is to lock up a small fraction of the carbon in the system. This reduces the amount of carbon available for methane and carbon dioxide formation, reducing peak pressures slightly.

2.1.3.1 Microbial Degradation of Organic Wastes

The microbial degradation of organic wastes will in general involve various intermediate compounds. However, for this model, the emphasis is on the end state, in which organic matter is broken down into simple gaseous forms.

Specifically, cellulosic wastes are modelled as cellulose $(C_6H_{10}O_5)_n$, which degrades in the presence of water through several steps, according to the following effective reaction:

$$C_6H_{10}O_5 + H_2O \rightarrow 3CO_2 + 3CH_4 \qquad (2\text{-}1)$$

The microbial degradation of cellulose is controlled by the first main step in the process, the rate of cellulose hydrolysis. Reaction (2-1) describes the degradation of the cellulose monomers, with the rate of this process controlled by that of the hydrolysis reaction.

Ion-exchange resins are modelled as styrene that has degraded from polystyrene $(C_8H_8)_n$, which degrade according to the following reaction:

$$C_8H_8 + 6H_2O \rightarrow 3CO_2 + 5CH_4 \quad (2\text{-}2)$$

The limiting reaction rate is that for styrene hydrolysis. The functional groups and bound water on the resins are an appreciable fraction of the resin mass, but do not contain carbon, and so do not contribute to the gas generation.

Plastics and rubbers represent a heterogeneous mix of materials such as PVC, polyethylene, neoprene, nitrile and latex. In order to assess the impact of potential plastic and rubber degradation on the overall gas generation these components are modelled in the same manner as ion-exchange resins.

The degradation of polymeric organic substrates is modelled as being first order (proportional) with respect to their amounts.

Conditions in the DGR may not be favourable for microbial activity, due to the high salinity of the water in general, and the low porosity in the host rock or the chemical conditions within the repository. In the reference case, it is assumed that microbes will be active given that energy sources are present; additional cases consider little or no microbial activity.

2.1.3.2 Methanogenesis via the Microbial Hydrogen Mechanism

In radioactive waste disposal sites, significant amounts of hydrogen may be produced via anaerobic corrosion of metals. Hydrogen gas can be consumed by several microbial reactions, and in particular the methanogenic reaction:

$$4H_2 + CO_2 \rightarrow CH_4 + 2H_2O \quad (2\text{-}3)$$

provided that there is sufficient humidity to support microbial processes and conditions are sufficiently reducing. The minimum relative humidity required for microbial activity is approximately 60%. The rate for this reaction is modelled as being first order with respect to CO_2 concentration, but limited by the availability of hydrogen.

2.1.3.3 Corrosion of Metallic Wastes

Corrosion of metallic wastes and container materials occurs within the saturated (water submerged) and vapour phases. Aqueous corrosion processes are possible in humid atmospheres provided the relative humidity is sufficiently high. The relevant vapour-phase rate constants are ramped linearly down to zero between 80% and 60%.

The inventory of carbon and galvanized steels in the repository will comprise various carbon steel wastes, as well as carbon and galvanized steel waste containers. Galvanized and carbon steels are treated as a single metallic source, represented by the corrosion of Fe as carbon steel (C-steel). The initial presence of ferric corrosion products (rust) due to corrosion in air is neglected – all steel is conservatively assumed available for anaerobic corrosion.

The overall reaction for the anaerobic corrosion of C-steel is given below:

$$3Fe + 4H_2O \rightarrow Fe_3O_4 + 4H_2 \quad (2\text{-}4)$$

The reaction proceeds at a rate determined by the C-steel corrosion rate.

Passivated carbon steel comprises waste forms grouted in cementitious materials and structural steel (rebar, rails, etc.) in contact with concrete. These materials are treated separately from the plain carbon and galvanized steel inventories because of the effect of the cementitious material on the corrosion rate. Although the rate of corrosion of passivated carbon steel is lower, the mechanism is treated in exactly the same fashion as for the plain carbon and galvanized steel.

Stainless steels and nickel alloys are present as container materials and waste from steam generators and end fittings from pressure tubes, as well as miscellaneous waste forms. These materials contain Fe, Ni, Cr, Mo, and other minor alloying elements, in amounts dependent on the composition of the particular alloy.

For simplicity, the corrosion of the passive materials is treated in the same manner as carbon steel (i.e., Equation 2-4). The passive materials and stainless steels/nickel alloys are modelled as 100% Fe and as fully reacting, but at a slower rate based on the effective corrosion rate of each type of metal.

Zirconium alloy waste comprises pressure tubes and other components of the decommissioned reactors. Typically these alloys contain small amounts of Nb, which is approximated as corroding similar to Zr. The corrosion of zirconium alloys is represented by the following reaction:

$$Zr + 2H_2O \rightarrow ZrO_2 + 2H_2 \quad (2\text{-}5)$$

2.1.3.4 CO_2 Enhanced Corrosion of Metallic Wastes

Carbon steel undergoes accelerated corrosion in the presence of high CO_2 partial pressures. The enhanced corrosion rate is primarily a consequence of the decrease in pH that accompanies the dissolution of CO_2 in water to form carbonic acid (H_2CO_3). However, because of the high HCO_3^- concentration, the stable corrosion product is siderite ($FeCO_3$) rather than Fe_3O_4. The corrosion rates for metallic wastes undergoing CO_2 enhanced corrosion are taken to be a function of the CO_2 partial pressure, with the overall corrosion reaction given by the following reaction (EU 1999):

$$Fe + H_2CO_3 \rightarrow FeCO_3 + H_2 \quad (2\text{-}6)$$

Although the pH of the environment is not specifically calculated within the model, the use of an enhanced corrosion rate in the presence of CO_2 implicitly takes into account the acidification resulting from the dissolution of CO_2 in the aqueous phase. In terms of the model, the rate of reaction is treated as a multiplier of the anaerobic corrosion rate. Therefore, depending upon the partial pressure of CO_2, the anaerobic corrosion rate is enhanced by an appropriate factor:

$$1 + \left(\frac{P_{CO2}}{P_{CO2}^{ref}} \right)^q \quad (2\text{-}7)$$

where P_{CO_2} is the partial pressure of CO_2, $P_{CO_2}^{ref}$ is a reference partial pressure of CO_2, and q is the reaction order with respect to the partial pressure of CO_2 and has a value of 0.67. If there is no CO_2 present, the factor is 1. The relative amounts of Fe_3O_4 and $FeCO_3$ formed are determined by the values of the respective rate constants which, in the case of $FeCO_3$, are the enhanced additional corrosion rate due to the partial pressure of CO_2.

In addition to the carbon and galvanized steels, the stainless steels and nickel alloys are also modelled as undergoing enhanced CO_2 corrosion and forming carbonate-containing corrosion products based on the experience of using these materials in CO_2-containing environments in the oil and gas industry. No CO_2 enhancement is included for Zr alloys.

2.1.4 Interaction between the Repository and Geosphere

The GGM model of the repository and TOUGH2 model of the geosphere are coupled via the repository pressure, saturation state, relative humidity, and void volume. These couplings determine the flows of water and of gas into and out of the repository. The TOUGH2 model simulates a single bulk gas only. For the purpose of modelling the fluxes of individual gas components into and out of the repository, it is assumed that the composition of gas leaving or entering the repository is the same as that currently in the repository.

2.2 Gas and Water Transport Overview

Two-phase flow processes within the geosphere, repository, and shaft are controlled by pressure gradients: liquid moves according to Darcy's law under the control of liquid pressure gradients while gas moves according to Darcy's law in response to gas pressure gradients. The relationship of gas and liquid pressures is complex and is characterized by the capillary pressure curve, which expresses the difference between gas and liquid pressures as a function of gas saturation (the proportion of the porosity that is occupied by a separate gas phase). Essentially, the capillary pressure curve represents the ability of liquid surface tension to impede the flow of gas into a liquid saturated pore-space. The capillary pressure curve is a function of pore space size, geometry, and other physical properties of the material, and can be determined from petrophysical testing procedures. Results from petrophysical tests conducted on DGR borehole core samples are described in INTERA (2011). These results are used to determine the parameters of functional representations of capillary pressure response that are used in the two-phase flow modelling presented in this report.

Given a specified gradient, gas and liquid flux or mass flow rate is also proportional to the permeability of the material to a specific phase. In general, the permeability to a single phase increases with the saturation level of that phase, while permeability to the other phase is reduced. This process is represented in the model through use of a relative permeability function which scales the absolute, or intrinsic, permeability according to the phase saturation.

Capillary pressure and relative permeability functions are further described in Section 4.2.1.

As described in Section 2.3.6.2 of the System and Its Evolution report (QUINTESSA 2011b), groundwater flow at the Bruce nuclear site can be divided into four basic zones, delineated by stratigraphy. The stratigraphic column at the Bruce nuclear site is based on results from boreholes DGR-1 through DGR-4 described in INTERA (2011), and presented in Figure 2.2.

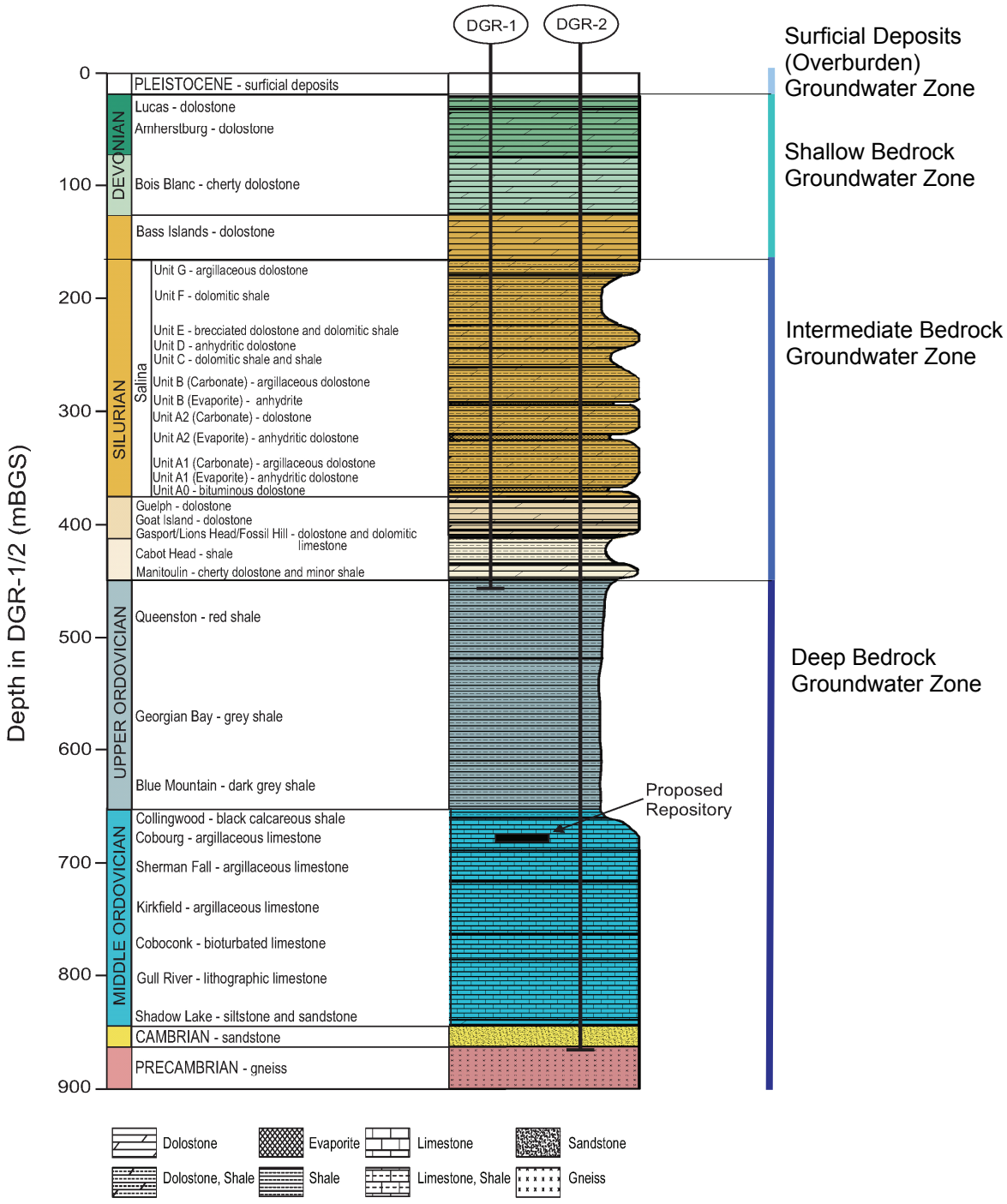

Figure 2.2: Reference Stratigraphic Column Showing Groundwater Zones at the Bruce Nuclear Site

The groundwater zones are as follows.

1. Surficial deposits (overburden) groundwater zone – Local flow of fresh water providing precipitation driven recharge to the underlying shallow groundwater zone. The surficial zone is approximately 20 m thick.

2. Shallow Bedrock Groundwater Zone – The relatively high permeability sequence consisting of Devonian and Upper Silurian (to top of Salina G) sediments to an approximate depth of 170 m below ground surface (mBGS), or an elevation of +15 m above sea level (mASL). Groundwater in this zone is fresh to brackish and flow is primarily horizontal, driven by topographic features with discharge to Lake Huron. Hydraulic gradients in this zone are sufficiently high to create advection dominated flow.

3. Intermediate Bedrock Groundwater Zone – The Silurian sediments from the Salina G down to the Manitoulin. Some zones of medium permeability exist in this sequence (Salina A1 upper carbonate, Guelph Formation), but the formations are primarily low-permeability shales and dolostones, with some extremely low permeability anhydrite beds. Slow horizontal groundwater flow may occur in the medium permeability units, albeit under very low horizontal gradients. Groundwater in the zone is highly saline (20 to 310 g/L). The intermediate zone is approximately 280 m thick (to an approximate depth of 450 mBGS, or an elevation of -265 mASL).

4. Deep Bedrock Groundwater Zone - All stratigraphic units below the Manitoulin. Transport in the low-permeability Ordovician shales and limestones is expected to be diffusion dominated. Site characterization results (Figure 2.3) show elevated environmental heads in the Cambrian sandstones and underpressured conditions throughout the Ordovician sequence, indicating that the system is not in hydrodynamic equilibrium. Groundwater in the zone is highly saline (150 to 350 g/L).

It is clear that the formations in the Deep Bedrock Groundwater Zone above the Cambrian have very low permeability with no known transmissive vertical fractures, that there are significant over- and under- pressures, and that there is a separate gas phase within some of these rock formations (INTERA 2011). Transport of contaminants within the intact rock will be diffusion dominated (NWMO 2011a). Important uncertainties are the full extent of underpressures in the Ordovician sequences, and the actual gas saturations. The underlying causes of the non-equilibrium conditions are not known for certain, but plausible hypotheses are described in the Geosynthesis report (NWMO 2011a). More importantly for the postclosure safety assessment, these features are indicative of a low vertical permeability host rock, and will likely persist for very long times.

The modelling approach presented in this report uses a conservative approach to account for these uncertainties by including cases based on transient responses to the observed underpressures with specified gas saturations (the NE-RC and derived cases, Section 3.1), and cases based on a steady-state fully liquid saturated geosphere that assume instantaneous decay of the underpressures (the NE-SBC and derived cases, Section 3.1).

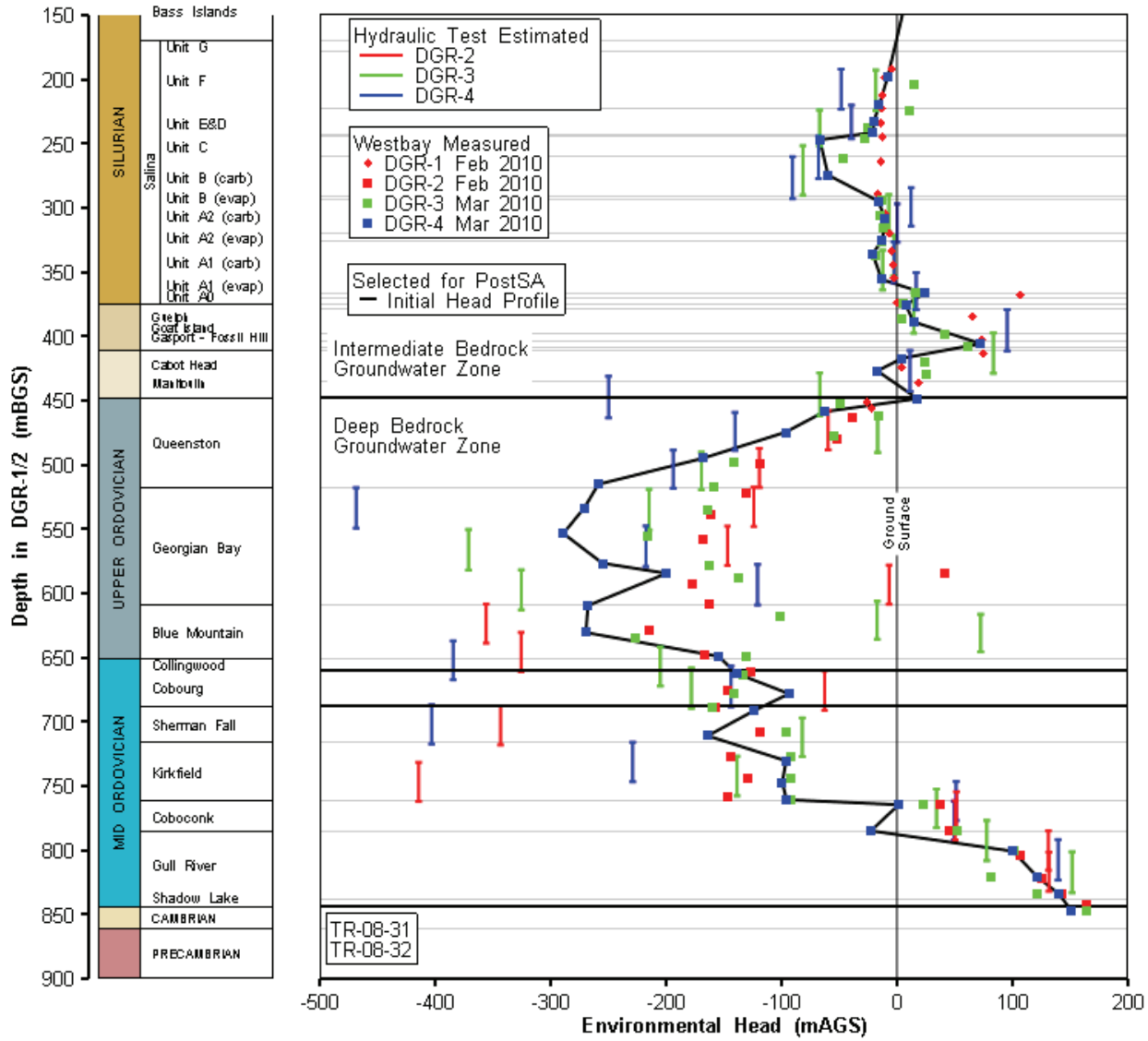

Note: Monitoring data from (INTERA 2011).

Figure 2.3: Environmental Head Profile from DGR Site Investigation Boreholes based on Winter 2010 Monitoring Data

2.3 Repository Location and Characteristics

The final preliminary repository design is described in Chapter 6 of the Preliminary Safety Report (OPG 2011b). The underground layout is shown in Figure 2.4 in relation to the site Universal Transverse Mercator (UTM) coordinate system. The figure also shows the location of current site characterization deep boreholes.

The final preliminary facility design is shown in Figure 2.4a. However, detailed modelling of the repository presented in this report was initiated based on the original preliminary design shown in Figure 2.4b. The change was made after the present detailed analyses were completed. The change from single-ended emplacement rooms with return ventilation ducting, to the final preliminary design with flow-through ventilation was made for operational safety and reliability reasons. However, while the changes are important for operations, and while they may affect the long-term gas transport numerical results in detail, the overall gas transport results are not expected to be substantively changed. This was specifically tested through two cases presented in this report which are based on detailed modelling of the final preliminary design. In this report, most results therefore are from a numerical model based on the original preliminary design (Figure 2.4b). Results based on the final preliminary design (Figure 2.4a) are specifically indicated as such, and designated by PD for Preliminary Design.

Note that the shafts and the shaft seal concept are unchanged.

The repository design includes two waste emplacement panels (Panel 1, to the north, and Panel 2, to the south) and two shafts; access tunnels connecting the shaft services area to the waste emplacement panels, a main access shaft (9.14 m diameter at closure) and a smaller ventilation shaft (7.45 m diameter at closure).

The repository is located at a depth of approximately 680 mBGS in the Cobourg Formation.

An aspect of the design which is relevant to the detailed gas modelling is the void volume of 1) the access tunnels (including shaft service area), and 2) the emplacement rooms, accounting for emplaced materials and for concrete volumes on floors, walls, and ceilings. These volumes are 64,780 m^3 and 353,000 m^3, respectively, for the original preliminary design, and 84,200 m^3 and 365,000 m^3 for the final preliminary design (Table 4.5 of QUINTESSA and GEOFIRMA 2011a).

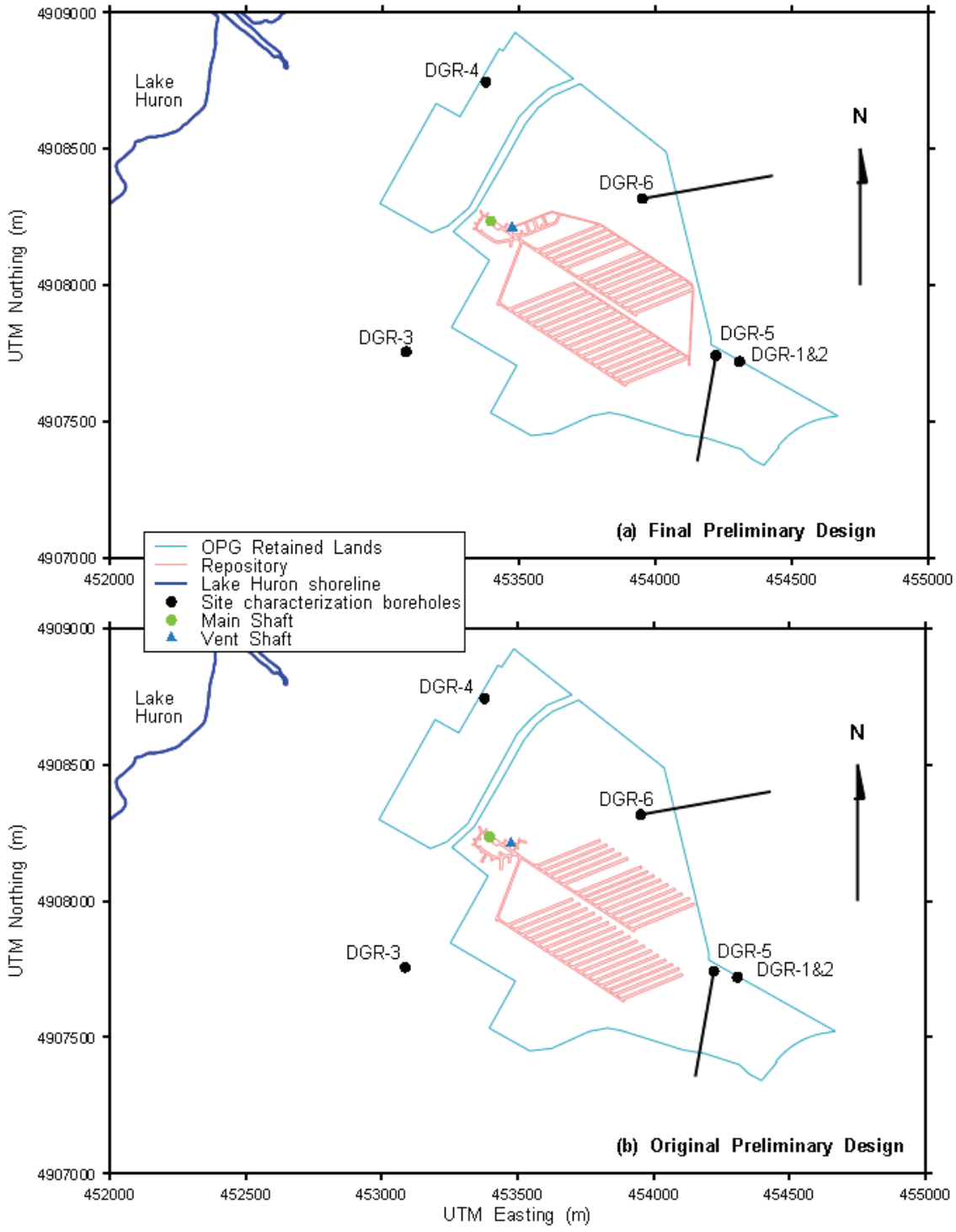

Figure 2.4: Repository Layout in UTM Coordinate System: (a) Final Preliminary Design, (b) Original Preliminary Design

The closure shaft seal design is based on a concrete monolith base and a primary compacted bentonite/sand seal, supported by an asphalt seal layer and concrete bulkheads. The reference seal design is illustrated in Figure 2.5, and parameters are given in Section 4.3.2 of the Data report (QUINTESSA and GEOFIRMA 2011a). The shaft sealing system is designed to limit groundwater and gas flow through the shafts.

The repository itself is not backfilled on closure, which ensures that there is space available for gas generated by corrosion or degradation of wastes and waste packages. However, the area around the base of the shafts is filled with a large concrete monolith. Figure 2.6 illustrates the extent of the monolith.

The envelope of sedimentary rock surrounding underground excavations, including the shafts that connect the DGR with the ground surface, will have enhanced hydraulic conductivity as a consequence of excavation-induced damage due to excavation techniques and stress change resulted from excavation in a stressed rock. This damaged zone can be subdivided into three sub-zones (Lanyon et al. 2001).

- Highly Damaged Zone (HDZ) where macro-scale fracturing or spalling may occur. The effective permeability of this zone is dominated by the interconnected fracture system.
- Excavation Damaged Zone (EDZ) with hydromechanical and geochemical modifications inducing changes in flow and transport properties.
- Excavation disturbed Zone with possible hydromechanical and geochemical modification, without material changes in flow and transport properties. This zone is not explicitly represented in the model since it has no property changes, and changes in flow and transport within this zone due to the nearby shaft are automatically calculated by the numerical model.

In the shafts, the HDZ will be removed during closure from repository level up to the top of the Salina F formation in order to provide a more effective seal (see Section 5.2.1 of the Data report, QUINTESSA and GEOFIRMA 2011a). An EDZ will be present, and is modelled as a region of about one shaft radius, based on geomechanical modelling (Section 6, NWMO 2011a). To reflect the variation in properties across the EDZ in shafts, the EDZ is modeled as two zones, an inner EDZ extending from the shaft wall to an additional radius equal to one half the shaft radius; and an outer EDZ extending an additional one half shaft radius beyond the inner EDZ (Figure 2.5).

At the repository level, the HDZ is not removed during closure. For gas transport modelling, the HDZ along the tunnels filled with concrete monolith is an important pathway, and is explicitly included.

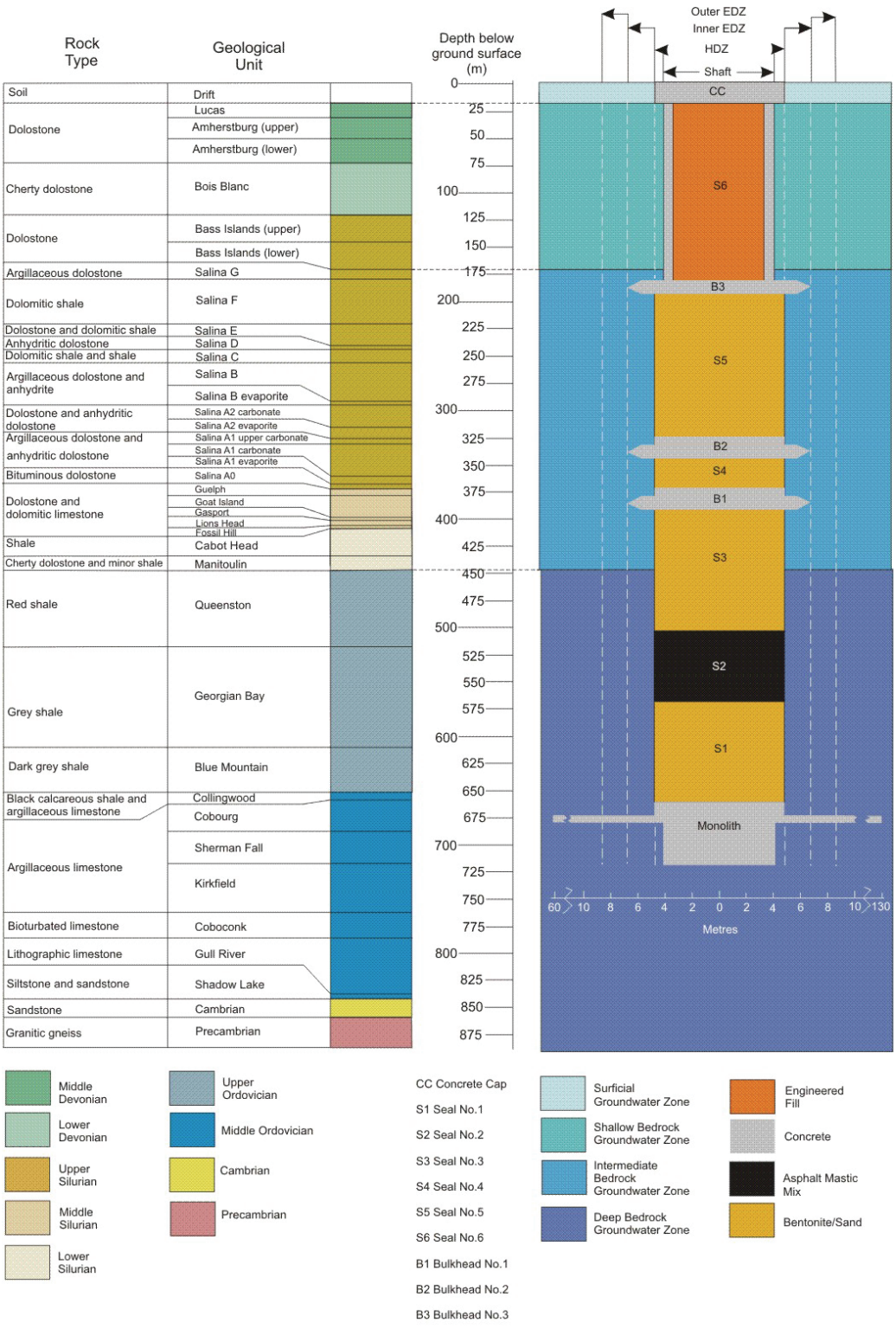

Note: Figure from QUINTESSA and GEOFIRMA (2011a).

Figure 2.5: Lithology and Shaft Sealing System

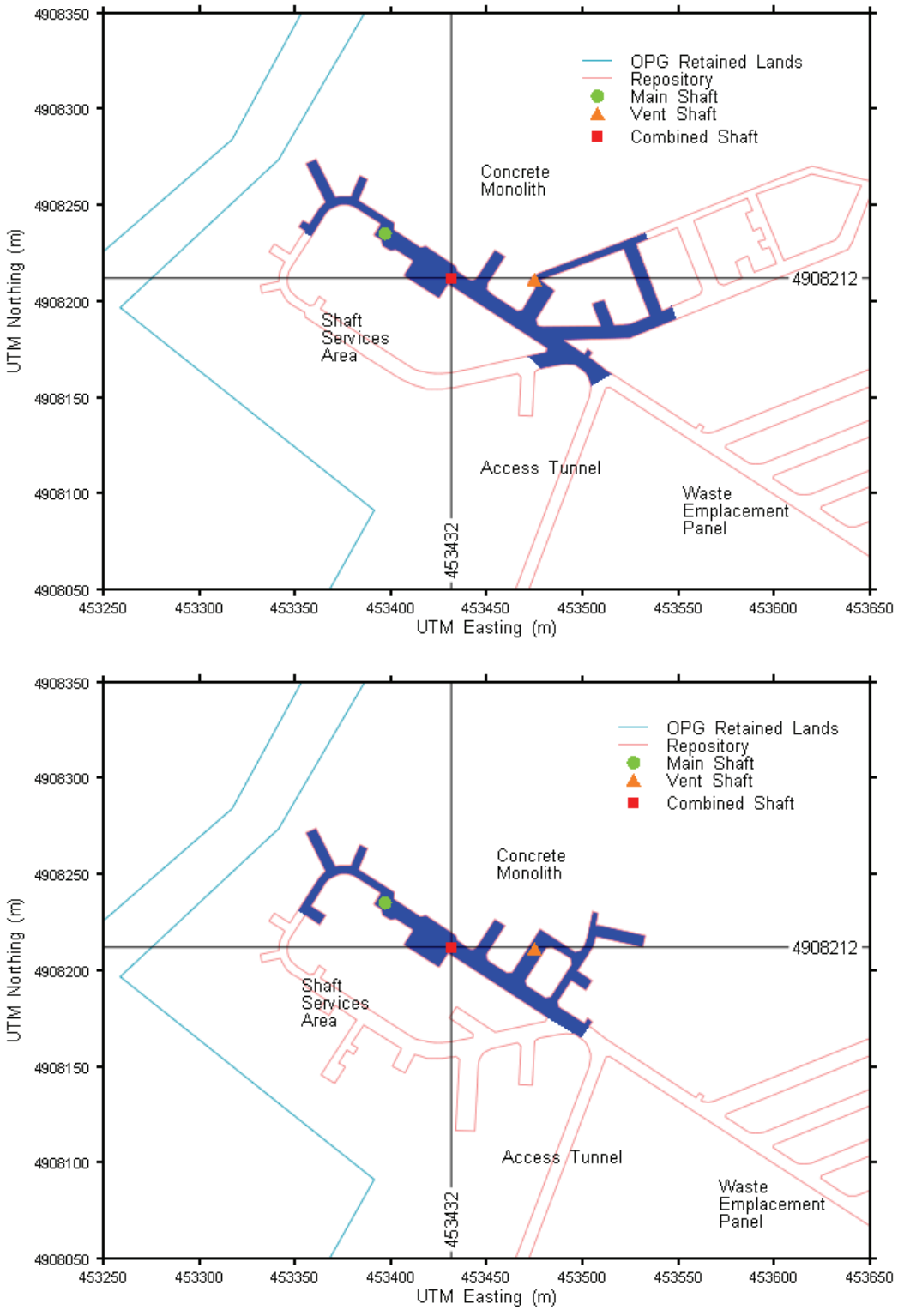

Figure 2.6: Concrete Monolith at the Base of Shaft: (a) Final Preliminary Design, (b) Original Preliminary Design

2.4 Normal Evolution and Disruptive Scenarios

The Normal Evolution Scenario, described in detail in Chapter 7 of the System and Its Evolution report (QUINTESSA 2011b), is the expected evolution of the geosphere and repository system as a function of time. It includes likely changes in the waste forms, repository conditions, geosphere evolution, and climate conditions.

The modelling of gas generation and transport is numerically complicated, given the desire to include geometric details, disparate distance and time scales, very long times, two-phase gas and water transport, and large ranges in permeabilities. The Normal Evolution Scenario implemented in the detailed gas modelling makes the following assumptions and simplifications.

- Impacts due to glaciation are not modelled. From a hydrogeologic perspective, the impact of glaciation events can be extensive. Glacial advance and retreat provide large transient changes in mechanical and hydraulic loading of the geosphere. However, regional data and modelling indicate that this loading has little influence on the deep groundwater system (NWMO 2011a). Furthermore, this modelling did not consider gas phase processes, in which gas may offer additional capacity to reduce pressure changes associated with mechanical loading. The mechanical loading would reach the repository level, and the aggregate geomechanical impacts of multiple glacial cycles on the repository are included by making conservative assumptions about rockfall within the facility. Specifically, possible rockfall associated with glaciation is assumed to occur immediately at repository closure. Finally, glaciation over the DGR site would occur after the peak period of gas generation within the repository, and after the key gaseous radionuclides (C-14 and H-3) had decayed, so its influence on contaminant transfer in the gas phase would be limited.

- For the majority of the modelling cases presented in this report, the flow system is conservatively assumed to be at steady-state, with vertical gradients driven by a constant head boundary condition at the Cambrian. That is, the Cambrian overpressure is assumed to persist indefinitely, while the Ordovician underpressures are conservatively assumed to dissipate instantly. The steady-state flow system assumptions results in a prevailing upwards vertical gradient driven by the constant Cambrian head boundary condition. This simplification is tested through the inclusion of underpressures derived from Figure 2.3 in some modelling cases.

- Groundwater is constant density. Site characterization results indicate that highly saline waters are found in the deep and intermediate systems. Ignoring varying salinity simplifies the modelling, which significantly improves the numerical tractability and helps allow more complete treatment of geometry. The main impact of salinity on vertical gradients is incorporated by using environmental heads to calculate boundary conditions. Environmental heads in Figure 2.3 were calculated from formation pressures following the methods of Lusczynski (1961) and Jorgensen et al. (1982). These heads are suitable for assessing vertical groundwater flow potentials in variable-density groundwater flow systems. Modelling of salinity is important in systems with topographic driving forces for horizontal groundwater flow, as increases in density with depth tend to moderate the horizontal gradients in deeper saline waters, thus reducing transport. However, in the current local site system, where transport is primarily by diffusion, topographic driving forces are small, and any flow is vertical due to the Cambrian overpressure and Ordovician underpressures, the environmental head gradients incorporate the salinity profile in these vertical gradients. GEOFIRMA (2011) presents results from variable density groundwater flow modelling that

show very good consistency with flow fields from constant-density environmental head models.

- The geosphere is assumed to be fully liquid saturated in most modelling cases. Results from the site characterization program show partial gas saturations are prevalent in the geosphere at the Bruce nuclear site (INTERA 2011). However, there is considerable uncertainty in the gas saturation measurements, and the presence of background levels of formation gas makes it difficult to distinguish the flow of contaminated gas generated within the repository. In general, the geosphere gas content is not important for gas releases from the repository (which occur primarily through the shaft). Several sensitivity cases in this report examine the impact of varying initial gas content of the geosphere.

- While the T2GGM gas generation model considers multiple gas species in the repository, only a single bulk gas (methane in most calculation cases) is considered for gas transport through the geosphere, repository and shaft seals. This is justified on the grounds that methane is expected to be the predominant gas present within the repository. This simplification allows use of the single gas TOUGH2/EOS3 module for the gas transport portion of T2GGM rather than a more computationally demanding TOUGH/TMVOC module. The generation rate of the multiple gas species calculated internally by GGM is converted to a molar equivalent single gas generation rate for use by TOUGH2. This assumption is partially tested by considering gases other than methane.

Four Disruptive Scenarios were also identified in which the major geosphere barriers were breached (Chapter 8 of the System and Its Evolution report, QUINTESSA 2011b). Briefly stated, the scenarios and their treatment in the detailed groundwater modelling are as follows.

1. Human Intrusion – An exploration borehole penetrates the repository and is abandoned. The intrusion is assumed to occur once institutional control over the site is no longer effective. Furthermore, the borehole is then poorly sealed, resulting in the loss of contaminants into permeable geosphere horizons above the repository.

2. Severe Shaft Seal Failure – The shaft seals are assumed to perform greatly below expectations. As the main control on flow within the shaft is permeability of shaft materials, this scenario is modelled by greatly increasing shaft sealing material permeability and modifying two-phase flow parameters to remove impediments to gas flow.

3. Poorly Sealed Borehole – A DGR site investigation/monitoring borehole near, but not intersecting, the repository is assumed to be poorly sealed on closure. Standard practice is that boreholes that are no longer to be used are sealed with bentonite or cement to prevent contamination of potable water supplies. If this step is improperly performed or the seal significantly degrades, the closed borehole can provide a path for the flow of contaminants.

4. Vertical Fault – A transmissive fault is assumed to exist within the vicinity of the repository. The permeable vertical fault extends from the Precambrian basement to the Guelph.

Only the Severe Shaft Seal Failure Scenario is considered in the present report on detailed gas transport modelling (see Section 3.2).

The Human Intrusion Scenario was not considered as gases would vent to surface upon intersection of the borehole with the repository, negating the requirement for a detailed gas model. The release rate of gas would be controlled by the operation of a blow-out preventer normally installed on such deep boreholes. The Normal Evolution Scenario's Reference Case

gas model results can be used to estimate the available repository gas pressure and volumes that could be released. The other two Disruptive Scenarios (Poorly-Sealed Borehole and Vertical Fault) are also not considered in this report as the results from the Normal Evolution Scenario's Reference Case indicate that they are unlikely to have any effect on gas transport near the repository as transport of gas through the geosphere to the borehole or fault will not occur. These scenarios are treated in detailed groundwater modelling (GEOFIRMA 2011) and assessment-level modelling (QUINTESSA and SENES 2011). Results from the groundwater modelling indicate that the cases do not significantly alter the pressure distribution in the vicinity of the repository, and thus do not impact inflow from the geosphere which could potentially change gas generation.

2.5 Modelling Approach

The model domain for the detailed two-phase flow and transport modelling presented in this report encompasses the repository and a several kilometre radius around the repository. This allows the modelling to focus on the impact of the repository on gas flow and transport and to effectively represent the relatively small-scale features of the repository design such as shafts and shaft seals.

One effect of this limited domain is to require the regional flow processes be incorporated as boundary conditions. Regional flow modelling has been undertaken to support the Phase II site Geosynthesis (NWMO 2011a). Results of this modelling, and indications from site characterization, show that regional gradients exist only within several moderate permeability units, that flow rates within the low-permeability deep and intermediate bedrock groundwater zones are very low, and that transport within the low-permeability zones is diffusion dominated. Consequently, the domain selected is appropriate for modelling transport in the vicinity of the repository with most vertical boundary conditions specified as zero-flow. This ignores horizontal flow within the moderate permeability units. From the perspective of gas modelling, this is conservative as any flow within these units would reduce the vertical flux to the key receptors above the repository. Discharge points (if any) for the moderate permeability units are likely tens of kilometres from the site (NWMO 2011a), and would involve further dilution, dispersion and decay.

Two-phase flow and transport modelling is non-linear and is a computationally difficult task, frequently requiring many more numeric calculations than similar scale groundwater flow and transport modelling problems. Typically, gas transport modelling uses simplified geometries and will selectively include only those components of a system with significant impact on gas transport. Here, four different, but complimentary, numerical models have been developed:

1. A detailed three-dimensional representation of the simplified geometry of the repository, the shaft, and the surrounding low-permeability geosphere (the 3D Detailed or 3DD model);

2. A simplified three-dimensional quarter section representation of the repository, the shaft, and the surrounding low-permeability geosphere (the 3D Simplified Repository and Shaft, or 3DSRS model);

3. A further simplified three-dimensional representation of the repository and surrounding geosphere (the 3DS Repository or 3DSR model); and

4. A two-dimensional vertical and radial axisymmetric representation of the shaft system connecting the repository to the Shallow Bedrock Groundwater Zone (the 2D radial shaft, or 2DRS model).

In the 3DD, 3DSRS, and 2DRS models the main and ventilation shafts have been combined to form a single shaft with properties representing the aggregate of both shafts. In the 3DD, 3DSRS and 3DSR model the pressure and saturation response within the repository system is self-consistently calculated with the gas generation model. For the 2D radial shaft model (2DRS), the boundary conditions at the bottom of the shaft are extracted from the repository pressure results calculated by the 3D models. The rationale for using four models is described below.

1. The combined geometry of the repository, access shafts and tunnels is sufficiently complex as to warrant a 3D representation. Simplifying the geometry to a 2D representation may eliminate or obscure some of the important details. Interactions of the shaft and repository are important for some cases, particularly those cases where shaft and/or EDZ performance is degraded. Furthermore, the actual tunnel and panel layout may have an effect on flows. The combined groundwater and gas flow in the repository and shaft can only be simulated if both components are present, as is the case in the 3DD model. The 3DD model maintains fidelity with the repository design by including separate repository panels connected to the shaft by access tunnels. Comparison of the available 3DD model results to corresponding 3DSRS model results helps to build confidence in the appropriateness of the simpler 3DSRS model, which is used for the majority of the calculation cases.

2. Two-phase flow and transport is computationally demanding. Reducing the complexity of the system while still including the most important features can increase the computational tractability and allow more cases to be evaluated. The 3DSRS model includes a simplified repository connected to a single shaft similar to that in the 3DD model.

3. In cases where the shaft sealing system performs as expected, gas and groundwater flow in the shaft is negligible and the pressure/resaturation response of the system is controlled entirely by processes occurring in or around the repository. These cases do not require the significant numeric complications of a shaft and are satisfactorily represented by the significantly simpler 3DSR model. Comparison of 3DSRS and 3DSR models results for similar cases builds further confidence in the modelling approaches.

4. The vertical extents of the 3D models needed to be limited to reduce computational requirements. In particular, gas flow from the shaft into permeable formations requires very small time steps to capture accurately. Time step requirements are such that the 3DD or 3DSRS models would not complete the 1 Ma simulation period in a reasonable amount of time, if this process were included. Consequently, an appropriate upper boundary is the lowest permeable Silurian formation, the Guelph Formation. However, in order to assess the impacts of gas releases from the repository, the assessment model requires gas flows into the Shallow Bedrock Groundwater Zones, so transport through the Silurian is needed. The only significant pathway for gas is through the higher permeability shaft and EDZ system, which can be effectively simplified as a 2D axisymmetric model. This model reduces the size of the model grid and allows the processes of gas flow into the permeable formations to be captured in a reasonable amount of time. The 2DRS model is used only for those calculation cases where 3DD or 3DSRS model results indicate that gas flow up the shaft is occurring.

In all models, the geosphere is described as horizontal layers with properties varying on a formation basis. Horizontal formations are a minor simplification of actual stratigraphy given the model domain and relatively shallow dip of formations at the Bruce nuclear site.

The 3DD conceptualization of the repository and shaft is shown in Figure 2.7.

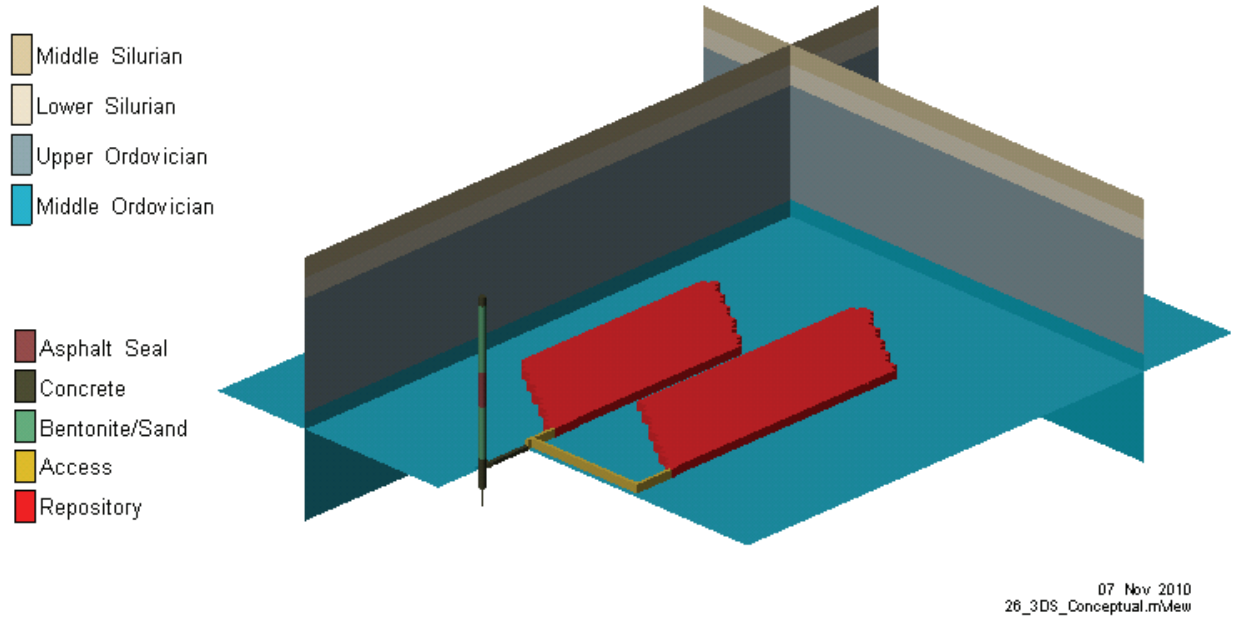

Figure 2.7: Illustration of the Repository, Shaft and Rock in the 3DD Model

The 3DSRS model represents the repository panel as a single square section, with a connected shaft. Only a quarter section is modelled to take advantage of symmetry, as shown in Figure 2.8.

The 3DSR model removes the shaft from the 3DSRS model (Figure 2.9). The 2DRS model of the shaft system is shown in Figure 2.10.

Figure 2-7 to Figure 2.10 illustrate the conceptual models for the original preliminary design. The models for the final preliminary design are similar to those for the original preliminary design. The same numerical gridding was used, but the specified total volumes for the repository and tunnel elements were increased to correspond to the final preliminary design values. This caused a slight increase in the calculated porosity of repository model elements. There is no change to the shaft seal design.

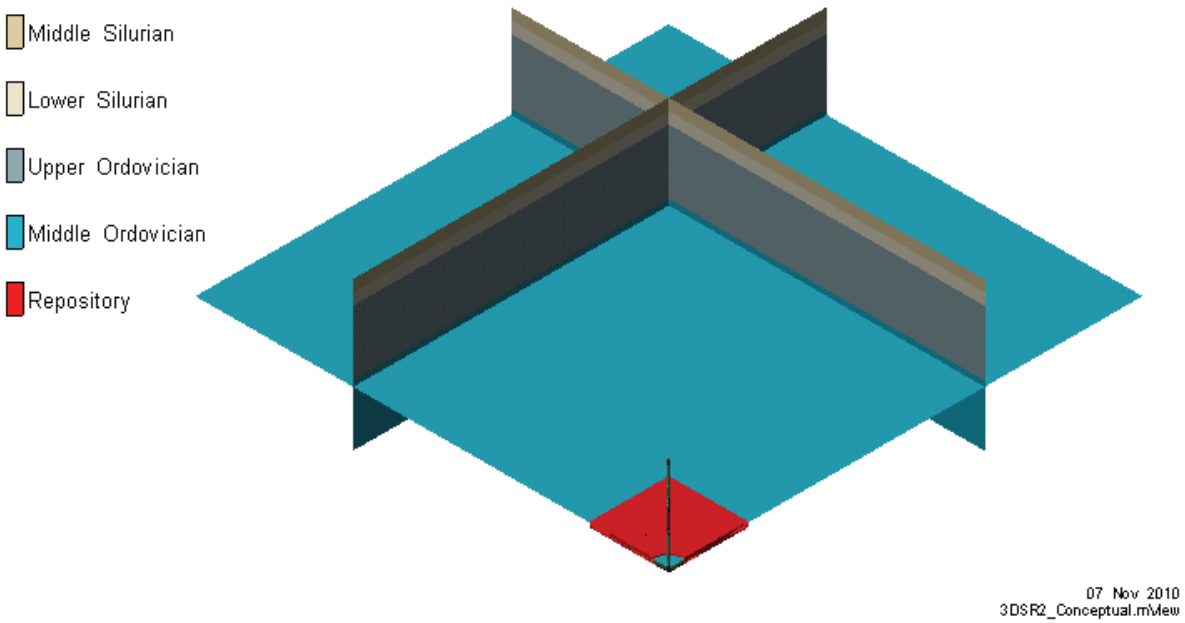

Figure 2.8: Illustration of the Repository and Rock in the 3DSRS Model

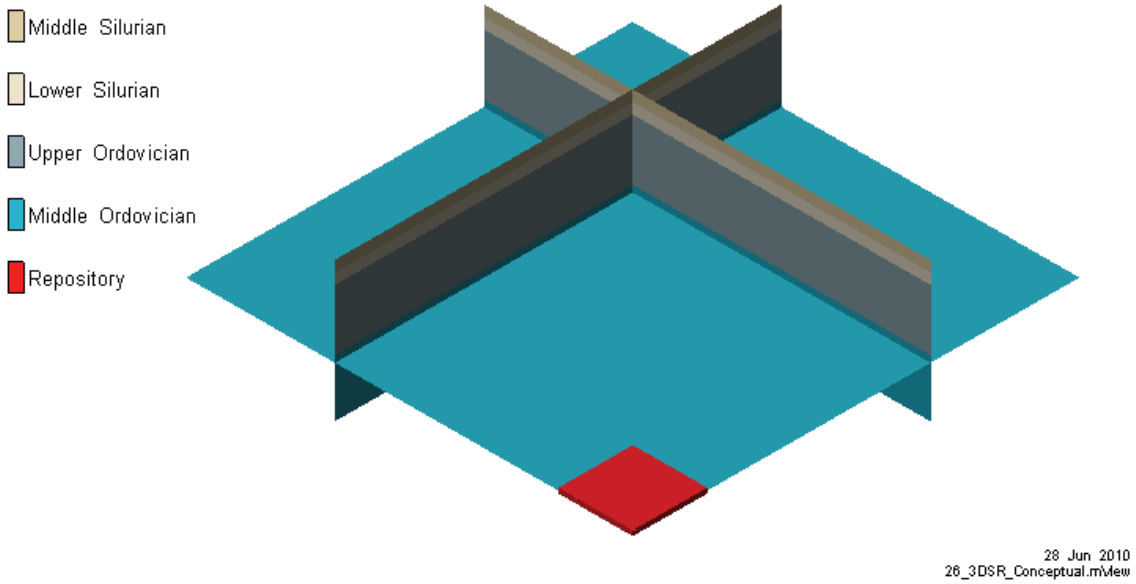

Figure 2.9: Illustration of the Repository and Rock in the 3DSR Model

The 2DRS model extends from the Salina G in the Upper Silurian to the repository elevation in the Cobourg as shown in Figure 2.10. The model includes the shaft, shaft EDZ, and a limited radius (500 m) of intact rock.

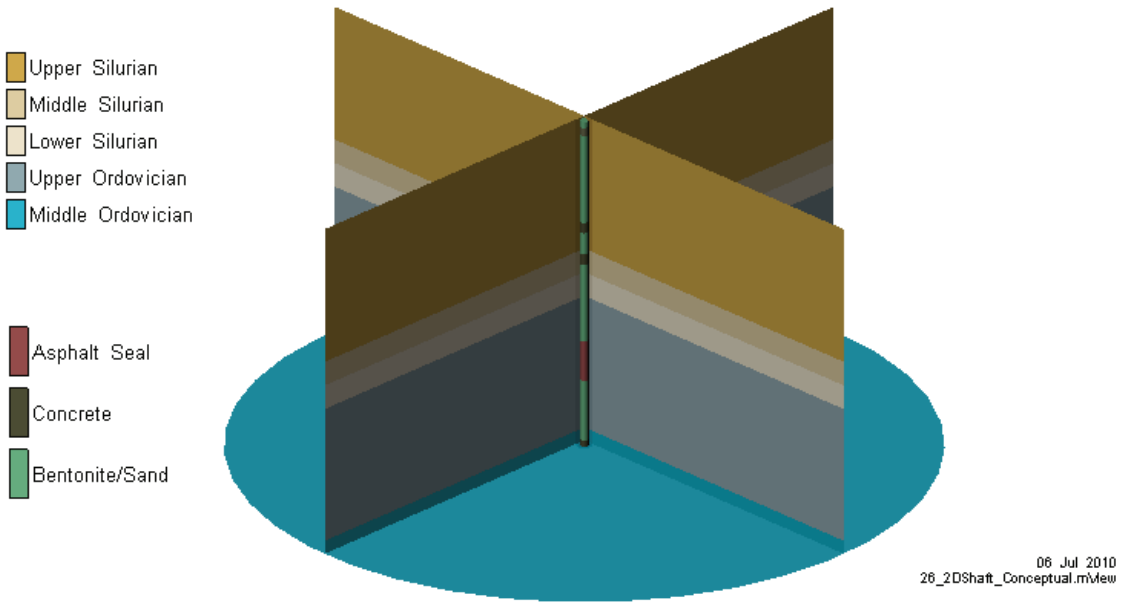

Figure 2.10: Illustration of the Shaft and Rock in 2DRS Model

3. CALCULATION CASES

Detailed gas modelling was performed for a number of parameter and conceptual model sensitivity cases. All cases were derived from a Reference Case characterization of the system as described in the Data report (QUINTESSA and GEOFIRMA 2011a). The Reference Case assumes a constant present-day climate, with no change in boundary conditions during the 1,000,000 a simulation period. Transient flow is assumed. For the Reference Case, all stratigraphic, hydrogeologic, and transport properties are as outlined in Chapter 5 of the Data report (QUINTESSA and GEOFIRMA 2011a).

Some key geometric parameters for the repository are:

- 7 m high access tunnels and repository;
- 10 m (immediate) rockfall above access tunnels and repository, where these are unsupported by concrete, effectively extending the unsupported access tunnels and repository to a height of 17 m from time of closure;
- 8.5 m EDZ above, below and on sides of unsupported access tunnels and repository and associated rockfall;
- 5 m EDZ above, below and on sides of supported access tunnels (i.e., around concrete monolith); and
- Highly Disturbed Zone (HDZ) extending 2 m above and below and 0.5 m laterally from supported access tunnels (i.e., concrete monolith).

The shaft geometry is characterized by:

- Removal of concrete liner and 0.5 m thick HDZ from repository level to the top of the Salina F;
- Main and ventilation shaft combined into one shaft with radius of 5.90 m in the model;
- Below the base of the main shaft the radius reduces to 3.73 m to represent the deeper bottom of the ventilation shaft; and
- Inner EDZ thickness is 0.5 times shaft radius, outer EDZ extends beyond the inner EDZ another 0.5 times the shaft radius.

Boundary conditions for the Reference Case model are:

- 165 m hydraulic head fixed boundary at the bottom of the modelled system (the top of the Cambrian geological unit);
- 0 m fixed head boundary at the top of the upper bedrock unit for the 2DRS models (top of Salina F geologic unit for the detailed gas models). 3D model upper boundary pressures were extracted from initial 2DRS steady-state case results, and corresponded to a hydraulic head of approximately 7 m. This was consistent with steady-state groundwater modelling results presented in GEOFIRMA (2011);
- No flow boundaries on all vertical model boundaries; and
- No horizontal gradient in the more permeable Silurian units.

Initial conditions for the Reference Case model are summarized:

- Initial head distribution includes underpressures in Ordovician shales (see Figure 2.3);
- Initial gas saturation in the repository based on initial water content of waste;
- Gas saturation of 10% in intact rock;

- Initial repository void volume of 4.2×10^5 m^3 (based on emplacement rooms, access tunnels and shaft service area) for the original preliminary design, and 4.5×10^5 m^3 for the final preliminary design, as reported in Table 4.5 of the Data report (QUINTESSA and GEOFIRMA 2011a); and
- Initial waste inventories and reaction rates as provided in Chapter 3 of the Data report (QUINTESSA and GEOFIRMA 2011a).

The Reference Case model also assumes:

- Higher permeability of all concrete in the monolith and shaft-sealing system due to presumed partial degradation over time (but assumed to occur immediately after closure);
- Constant density water; and
- Single bulk gas of methane used for gas transport calculations in geosphere and shaft.

Additional formation specific parameters, e.g., calculated permeabilities, are presented in Section 4.2.

Calculation cases were derived for the Normal Evolution Scenario and for the Severe Shaft Seal Failure Scenario. A common calculation case naming convention has been specified for the detailed groundwater, detailed gas and assessment modelling. The calculation case identifier is made up of the scenario (NE – normal evolution, HI - human intrusion, SF – shaft failure, BH – poorly sealed borehole, and VF – vertical fault), and additional identifiers describing the case (described below).

3.1 Normal Evolution Scenario

A number of parameter and conceptual model sensitivity cases have been developed to assess the impact of alternative likely parameterizations of the EDZ, engineered barrier systems, geosphere, and gas generation processes. Cases with PD designation are for the final preliminary design, e.g., NE-PD-RC; otherwise, the cases are for the original preliminary design-see Figure 2.4.

Figure 3.1 is an overview showing a schematic representation of the cases and their derivation. Table 3.1 describes the modelling cases for the Normal Evolution Scenario.

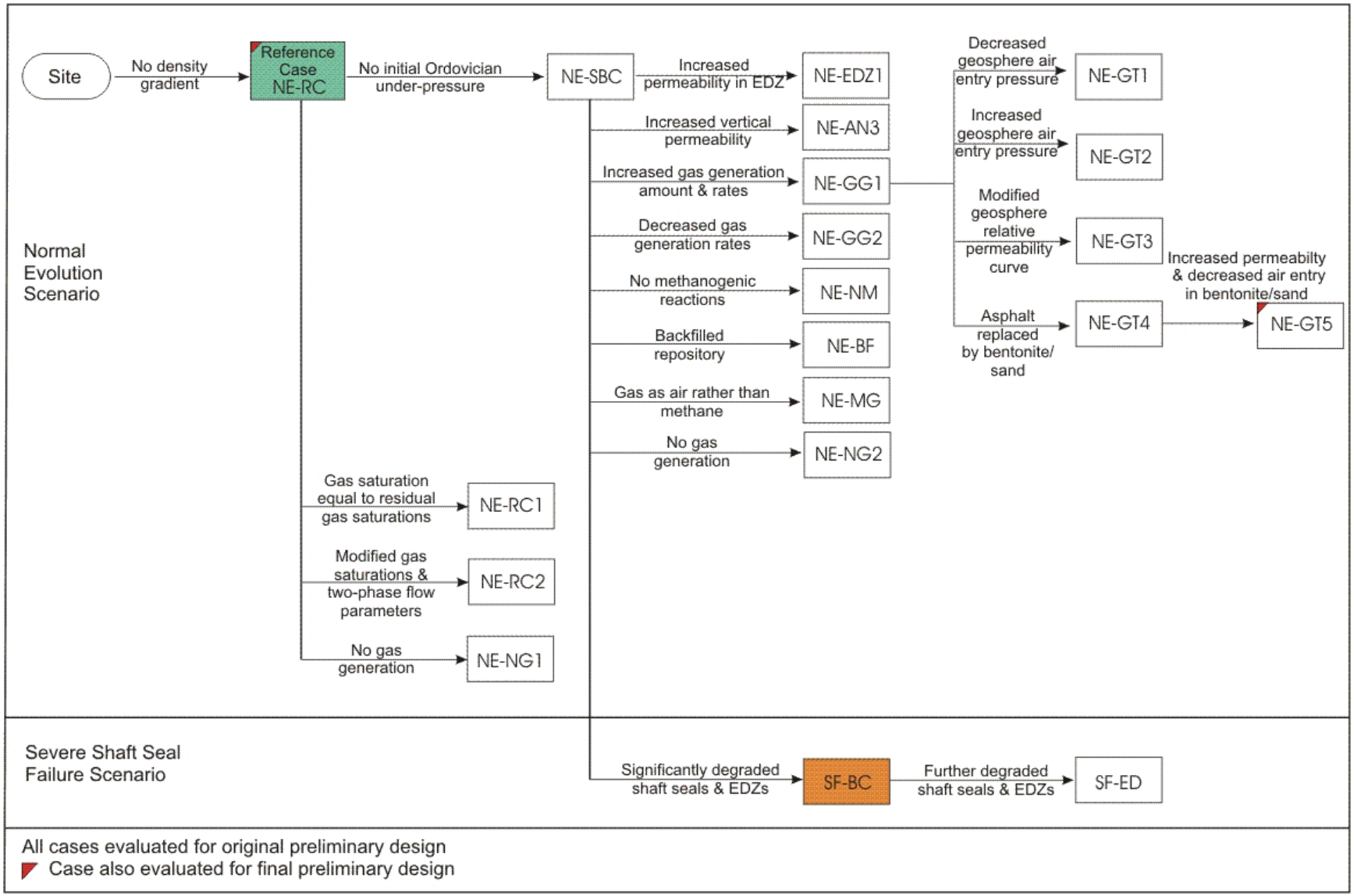

Figure 3.1: Gas Modelling Calculation Cases

Table 3.1: Gas Modelling Cases for the Normal Evolution Scenario

Case ID	Case Description
NE-RC	(Reference Case) Reference case parameters based on original preliminary repository design, reference inventory, and site characterization data, with gradual repository (including shaft) resaturation, and gas generation. Assume initial Cambrian overpressure (+165m), initial underpressures and partial gas saturations of 10% in Ordovician, no salinity gradient, rockfall in emplacement rooms and tunnels, and no horizontal gradients applied to any formations.
NE-PD-RC	(Reference Case - Final Preliminary Design) As NE-RC, but with the final preliminary repository design.
NE-SBC	(Simplified Base Case) As NE-RC, but with steady-state Cambrian overpressure (+165m), and no underpressures or partial gas saturations in Ordovician.
NE-AN3	(Reduced Geosphere Anisotropy) As NE-SBC with increased vertical permeability resulting in no horizontal to vertical anisotropy in most of the Ordovician formations. Anisotropy of the Coboconk and Gull River Formations is reduced from 1000:1 to 10:1.
NE-EDZ1	(Increased Permeability EDZ) As NE-SBC, but with permeability for shaft inner EDZ assumed to be four orders of magnitude greater than intact geosphere, and permeability for shaft outer EDZ assumed to be two orders of magnitude greater than intact geosphere with a corresponding reduction in gas air-entry pressure.
NE-GG1	(Increased Gas Generation) As NE-SBC, but with increased gas generation achieved by increasing the inventory (and hence surface area) of metals disposed in the repository and increased corrosion and degradation rates using the maximum values given in Tables 3.20 and 3.21 of the Data report (QUINTESSA and GEOFIRMA 2011a).
NE-GG2	(Reduced Degradation Rates) As NE-SBC, but with reduced degradation rates, i.e., minimum values from Table 3.21 of the Data report (QUINTESSA and GEOFIRMA 2011a), which, for anaerobic conditions, are a factor of ten less than the best estimate values.
NE-GT1	(Decreased Geosphere Air Entry Pressure) As NE-GG1, but with decreased van Genuchten air-entry pressure and less steep air-entry curve for geosphere. NE-GG1 is used as comparison case because it generates overpressures in the repository which are more suitable for testing gas transport in the intact rock near the repository.
NE-GT2	(Increased Geosphere Air Entry Pressure) As NE-GG1, but with increased geosphere van Genuchten air-entry pressure and steeper air-entry curve.
NE-GT3	(Modified Geosphere Relative Permeability) As NE-GG1, but with geosphere relative permeability curve modified with residual liquid saturation and residual gas saturation set to zero.
NE-GT4	(Asphalt Replacement) As NE-GG1, but with asphalt seal removed from shaft and replaced with bentonite/sand.

Case ID	Case Description
NE-GT5	(Reduced Shaft Seal Performance) As NE-GT4, but with permeability of bentonite/sand seal increased by a factor of 10, and air-entry pressure reduced by a factor of two to 5 x 10^6 Pa.
NE-PD-GT5	(Reduced Shaft Seal Performance - Final Preliminary Design) As NE-GT5, but with final preliminary repository design.
NE-MG	(Gas as Air) As NE-SBC, except that gas used is air rather than methane. Case recognizes the different gases generated in the DGR will have different characteristics than the "bulk" gas (methane) considered in NE-SBC.
NE-NG1	(No Gas Generation for Reference Case) As NE-RC, but with no gas generation.
NE-NG2	(No Gas Generation for Simplified Base Case) As NE-SBC, but with no gas generation.
NE-NM	(No Methanogenic Gas Reactions) As NE-SBC, but with all methanogenic reactions turned off. Conditions are assumed unfavourable for methanogens and so there is no organic degradation by methanogens and H_2 and CO_2 are not converted to CH_4 via the microbial hydrogen methanogenic reaction (Equation 2-3). This simulation uses gas parameters (molecular weight, viscosity) consistent with H_2 rather than CH_4.
NE-RC1	(Geosphere Gas Phase at Residual Saturation) As NE-RC, except partial gas saturations in Ordovician equal to residual gas saturation of 5%.
NE-RC2	(Variable Geosphere Gas Saturation and Transport Properties) As NE-RC except initial gas saturations and two-phase flow parameters on a formation basis as given in INTERA (2011).
NE-BF	(Backfilled Repository) As NE-SBC, except the repository is backfilled with a coarse aggregate material of approximately 30% porosity. This may increase the structural integrity of the repository and decrease rockfall, but would also decrease the void space available for gas pressurization.

3.2 Disruptive Scenarios

As noted in Section 2.4, the Human Intrusion, Poorly Sealed Borehole, and Vertical Fault Scenarios are not analyzed in this report.

However, two calculation cases are considered for the Severe Shaft Seal Failure Scenario (SF). The SF-BC case simulates improper repository closure or other unexpected events that lead to very poor shaft seal performance. In this case, the hydraulic properties of all seals and shaft EDZs are set to significantly degraded values from repository closure (e.g., hydraulic conductivity of 10^{-9} m/s for the seals). The SF-ED case is based on the SF-BC case; however the assumed shaft seal hydraulic conductivity is increased to 10^{-7} m/s in order to understand the sensitivity of the model performance to shaft seal properties.

Note that the specific disruptive scenario cases analyzed here are based on the original preliminary design. The shaft seal is unchanged in the revised final preliminary design, and the

changes at the repository level are not expected to significantly change the conclusions with respect to disruptive scenarios. This is supported by the small difference in results between the original preliminary design and the final preliminary design for key normal evolution scenario cases as discussed later in this report.

3.3 Models Used for Calculation Cases

Table 3.2 describes the models used and the gas generation modes for the defined normal evolution scenario and disruptive event scenario calculation cases. In general, the 3DSRS model was used for all cases where flows in the shaft could influence the simulated repository pressure, while the 3DSR model was used for cases where geosphere performance was the primary focus of the case. The 3DD model was used on a limited number of cases only. With several minor exceptions (3DSR NE-GG1 and NE-GG2), all 3D models were run for both NWL and WL modes. The 2DRS model was used for those 3DSRS cases that showed free-phase gas transport up the shaft, which occurred for NWL mode simulations only.

Table 3.2: Models Used for Calculation Cases

Case ID	3DD	3DSRS	3SDR	2DRS
NE-RC	X	X	X	
NE-PD-RC		X		
NE-SBC	X	X	X	
NE-AN3		X		
NE-EDZ1		X		
NE-GG1	X	X	X	X
NE-GG2		X	X	
NE-GT1			X	
NE-GT2			X	
NE-GT3			X	
NE-GT4		X		
NE-GT5		X		X
NE-PD-GT5		X		
NE-MG			X	
NE-NG1	X	X	X	
NE-NG2	X	X	X	
NE-NM		X	X	X
NE-RC1			X	
NE-RC2			X	
NE-BF		X	X	X
SF-BC		X		
SF-ED		X		

4. MODEL IMPLEMENTATION AND DATA

4.1 Software Codes and Quality Assurance

All detailed gas modelling presented in this report has been performed using T2GGM (Version 2.0), which couples the Gas Generation Model (GGM, Version 2.0) and TOUGH2 (Version 2.0, EOS3 equations of state). Quality assurance information for T2GGM is provided in QUINTESSA and GEOFIRMA (2011b), which also includes a description of the approach used in coupling GGM to TOUGH2 (Section 7.2 of QUINTESSA and GEOFIRMA 2011b), and the various other minor enhancements made to TOUGH2 to support the current gas modelling (see Chapter 8 and Appendix A of QUINTESSA and GEOFIRMA 2011b).

GGM is a project-specific code that models the generation of gas within the DGR. It was written and is maintained by Quintessa Ltd. Based on the current state of the repository as supplied by TOUGH2 and knowledge of the waste inventories, GGM calculates the rate of generation or consumption of water and gases within the repository based on a model for corrosion and microbial degradation of the wastes. These rates are used as sources for water and gas within TOUGH2's 2-phase flow model of the repository.

TOUGH2 is a general-purpose numerical simulation program for multi-phase fluid and heat flow in porous and fractured media developed by Lawrence Berkeley National Laboratory (Pruess et al. 1999). TOUGH2 is provided with several different equation-of-state (EOS) modules that support modelling different combinations of liquids and gases in isothermal or non-isothermal conditions. The EOS3 equation of state module used in the modelling presented in this report simulates the transport of a single separate phase gas in water. EOS3 also models the transport of dissolved gas in water by diffusion and advection. Dispersive processes are not modelled. The EOS3 equation of state module uses steam table equations for the properties of water and assumes that the bulk gas is air, with properties of an ideal gas. Modifications to EOS3 were performed to use alternative gases including: methane (CH_4), carbon dioxide (CO_2), hydrogen (H_2), and air. The modifications entailed changes to Henry's law constants, molecular weights, and viscosity calculations. CH_4 was used for most of the simulations documented in this report, although H_2 and air were used for the NE-NM and NE-MG calculation cases respectively. Integration of GGM with TOUGH2 and development of TOUGH2 modifications have been performed by Geofirma Engineering Ltd.

Two versions of TOUGH2 were used in developing the models presented in this report: a single-processor version, and a multi-processor version (TOUGH2 MP) which distributes the matrix solution across multiple processors. The multi-processor version was used for initial development of the 3DD models, although all final runs presented here were simulated with the single-processor version. All other models were simulated with the single processor version. The MP version offered relatively quick solutions, but was prone to numeric instabilities at longer simulation times, as the system approached steady-state conditions.

Model pre- and post-processing has been performed using mView 4.03, a proprietary modelling support tool developed by Geofirma. Pre-processing procedures consist primarily of discretization and property assignment. Post-processing includes all summary calculations and visualizations. mView 4.00A has been qualified to Yucca Mountain Project (YMP) Software Quality procedures. Additional capabilities added to mView since the YMP qualification have been verified in compliance with Geofirma's internal, ISO 9001 compliant, software development procedure.

The detailed gas calculations have been conducted to standards specified in the project's quality plan (QUINTESSA 2010) and the Geofirma Engineering ISO 9001 Registered Quality Management System. There is a specific Work Instruction (WI), Numeric Modelling, which describes model input file management and archiving using a version control system.

4.2 Data

4.2.1 Formation Properties

This sub-section presents the rock property data from Chapter 5 of the Data report (QUINTESSA and GEOFIRMA 2011a) and describes how the data are used to delineate model units.

Stratigraphy outlined in the Data report (QUINTESSA and GEOFIRMA 2011a), and previously presented in Figure 2.2, serves as the basis for the assignment of properties to the layers of the numerical model. The numerical models used in this report cover the Intermediate and Deep Bedrock Groundwater Zones. This is the region of rock that is expected to dominate gas transport from the repository. Formation properties presented in this report and used in the gas modelling are restricted to these zones and consist of formations from the top of the Salina G down to the top of the Cambrian.

The implications of gas transport over the full domain of rock, from the repository to the surface, are included within the assessment level modelling. In particular, assessment modelling in the Normal Evolution Scenario Analysis report considers the Shallow Bedrock Groundwater Zone pathway for gas release to the surface (QUINTESSA 2011a).

Table 4.1 describes the full stratigraphic sequence at the site, based on the reference stratigraphy at the DGR-1/DGR-2 borehole location. Stratigraphic nomenclature in Table 4.1 is taken from the Data report (QUINTESSA and GEOFIRMA 2011a). The table column "Model ID" designates the material property name used for the geologic units in the gas transport modelling, and indicates the geologic units in the detailed gas transport models. The Model ID is limited to a maximum of five characters for the T2GGM model, and the text "R" indicates intact rock mass rather than the EDZ.

Table 4.2 provides the physical and hydrogeologic properties for each model unit obtained from the Data report (QUINTESSA and GEOFIRMA 2011a). Horizontal and vertical permeability (K_{xy} and K_z) values for the model layers are shown graphically in Figure 4.1. QUINTESSA and GEOFIRMA (2011a) reports hydraulic conductivities in Table 5.5. These were converted to the permeabilities shown in Table 4.2 using a fluid density of 1000 kg/m^3 and viscosity of 1.1×10^{-3} kg/(m s). These fluid density and viscosity values are close approximations of the values that are used internally by the EOS3 module in T2GGM to calculate Darcy flow of gas and liquid.

Porosity values are taken from Table 5.6 of QUINTESSA and GEOFIRMA (2011a). Tortuosity values are calculated to yield effective diffusion coefficients consistent with formation D_e HTO values given in Table 5.14 of QUINTESSA and GEOFIRMA (2011a).

Table 4.1: Geological Units and Model IDs

Stratigraphic Unit	Hydro-stratigraphic Zone	Model ID	Top Elevation	
			mBGS	mASL
Drift	Surficial	N/A	0	186
Lucas	Shallow	N/A	20	166
Amherstburg (top 20 m)		N/A	30	155
Amherstburg (lower 25 m)		N/A	50	136
Bois Blanc		N/A	75	111
Bass Island (upper 20 m)		N/A	124	62
Bass Island (lower 25 m)		N/A	144	42
Salina G	Intermediate	SALGR	169	16
Salina F		SALFR	179	7
Salina E		SALER	223	-37
Salina D		SALDR	243	-57
Salina C		SALCR	245	-59
Salina B		SALBR	260	-75
Salina B Evaporite		SLBER	291	-105
Salina A2 Carbonate		SA2CR	293	-107
Salina A2 Evaporite		SA2ER	320	-134
Salina A1 Upper Carbonate		SA1UR	326	-140
Salina A1 Carbonate		SA1CR	329	-143
Salina A1 Evaporite		SA1ER	367	-181
Salina A0		SLA0R	371	-185
Guelph		GUELR	375	-189
Goat Island		GOATR	379	-193
Gasport		GASPR	397	-212
Lions Head		LIONR	404	-219
Fossil Hill		FOSSR	409	-223
Cabot Head		CABOR	411	-225
Manitoulin		MANIR	435	-249
Queenston	Deep	QUEER	448	-262
Georgian Bay		GBAYR	518	-332
Blue Mountain		BLUMR	609	-423
Collingwood		COLLR	652	-466
Cobourg		COBGR	660	-474
Sherman Fall		SFALR	688	-502
Kirkfield		KIRKR	716	-530
Coboconk		COBOR	762	-576
Gull River		GULLR	785	-599
Shadow Lake		SHADR	839	-653
Cambrian		N/A	844	-658
Precambrian		N/A	861	-675

Table 4.2: Physical and Hydrogeologic Properties for Each Geological Unit for the NE-RC Models

Unit	Porosity (-)	Horizontal Permeability (K_{xy}) (m^2)	Vertical Permeability (K_z) (m^2)	Pore Compressibility* (1/Pa)	Tortuosity (-)
SALGR	0.172	1.16E-18	1.16E-19	2.91E-09	0.0100
SALFR	0.128	5.81E-21	5.81E-22	1.95E-09	0.1281
SALER	0.135	2.33E-20	2.33E-21	1.85E-09	0.1393
SALDR	0.098	2.33E-20	2.33E-21	3.57E-10	0.1918
SALCR	0.205	4.65E-20	4.65E-21	1.80E-09	0.2146
SALBR	0.165	4.65E-20	4.65E-21	1.52E-08	0.2909
SLBER	0.098	3.49E-20	3.49E-21	3.57E-10	0.0031
SA2CR	0.145	3.49E-17	3.49E-18	1.17E-09	0.0331
SA2ER	0.098	3.49E-20	3.49E-21	3.57E-10	0.0031
SA1UR	0.070	2.33E-14	2.33E-14	1.33E-09	0.1400
SA1CR	0.019	1.05E-18	1.05E-19	4.89E-09	0.0379
SA1ER	0.007	3.49E-20	3.49E-21	5.00E-09	0.0171
SLA0R	0.027	3.49E-20	3.49E-21	4.44E-10	0.0044
GUELR	0.057	3.49E-15	3.49E-15	1.49E-09	0.1123
GOATR	0.020	2.33E-19	2.33E-20	1.80E-09	0.0300
GASPR	0.020	2.33E-19	2.33E-20	1.80E-09	0.0300
LIONR	0.031	5.81E-19	5.81E-20	1.16E-09	0.8000
FOSSR	0.031	5.81E-19	5.81E-20	1.16E-09	2.0645
CABOR	0.116	1.05E-20	1.05E-21	2.16E-08	0.1069
MANIR	0.028	1.05E-20	1.05E-21	6.07E-09	0.0214
QUEER	0.073	2.33E-21	2.33E-22	4.79E-09	0.0548
GBAYR	0.071	3.49E-21	3.49E-22	1.23E-08	0.0383
BLUMR	0.078	5.81E-21	5.81E-22	1.67E-08	0.0421
COLLR	0.012	2.33E-21	2.33E-22	8.33E-09	0.1633
COBGR	0.015	2.33E-21	2.33E-22	3.67E-09	0.0987
SFALR	0.016	1.16E-21	1.16E-22	1.69E-08	0.0550
KIRKR	0.021	9.30E-22	9.30E-23	8.57E-09	0.0800
COBOR	0.009	4.65E-19	4.65E-22	2.00E-08	0.1200
GULLR	0.022	8.14E-20	8.14E-23	8.18E-09	0.0473
SHADR	0.097	1.16E-16	1.16E-17	1.03E-09	0.2515
CAMBR	0.071	3.49E-13	3.49E-13	1.41E-09	0.2169

Notes: *Pore compressibilities are calculated from rock compressibility divided by porosity. Rock compressibility data are the high values described in Walsh (2011).

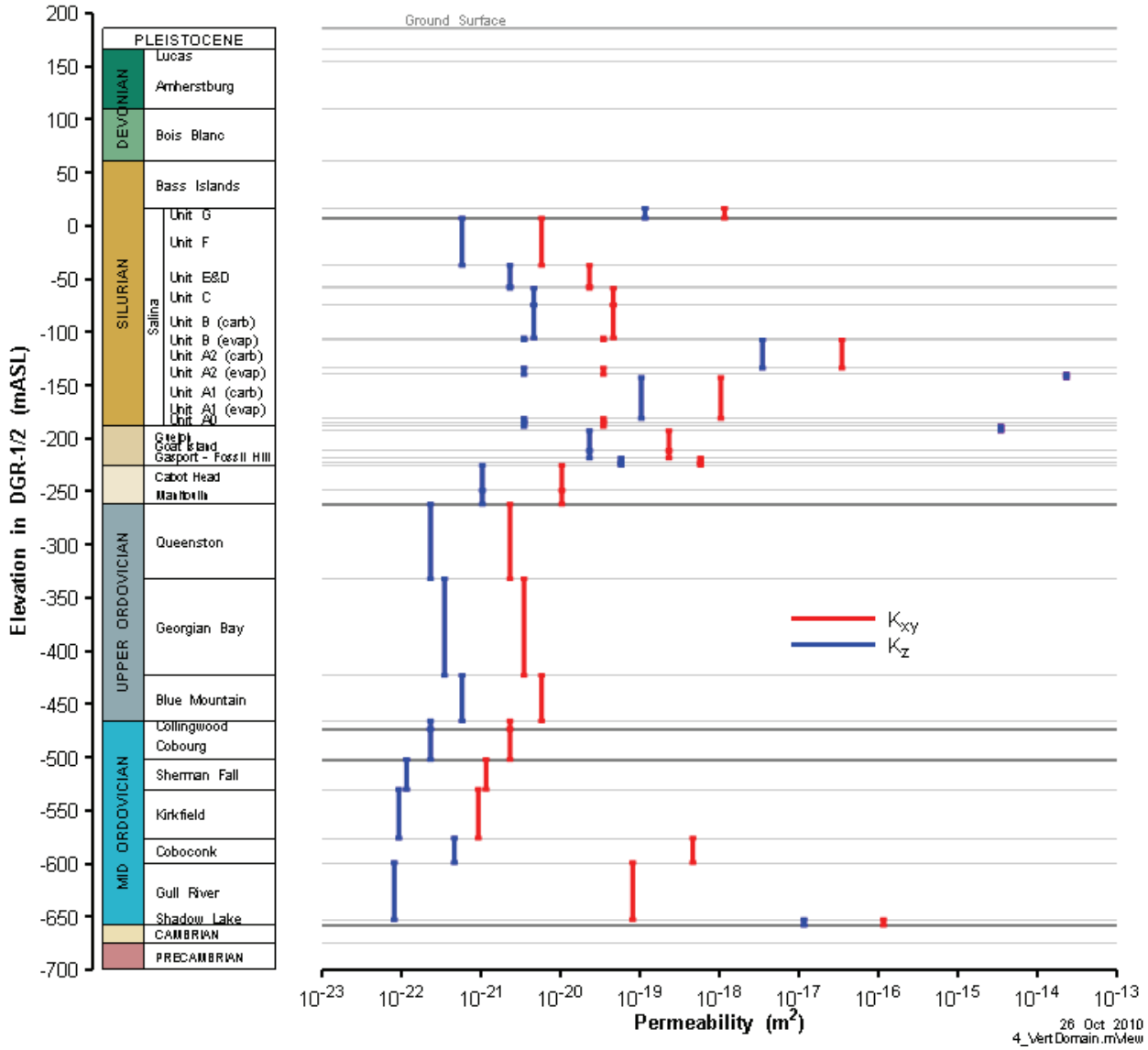

Figure 4.1: Vertical and Horizontal Permeability in the NE-RC Models

Capillary pressure and relative permeability curves are represented using the modified Van Genuchten equations (Luckner et al. 1989) as presented in Finsterle (1999) as a function of the water saturation fraction S_l. The capillary pressure relationship is given by:

$$P_c = -\frac{1}{\alpha}\left[S_{ec}^{-1/m} - 1\right]^{1/n} \tag{4-1}$$

$$S_{ec} = \frac{S_l - S_{lr}}{1 - S_{lr}} \tag{4-2}$$

The van Genuchten-Mualem-Luckner relative permeability curves are given by:

$$k_{rl} = S_{ek}^{1/2}\left[1 - (1 - S_{ek}^{1/m})^m\right]^2 \tag{4-3}$$

$$k_{rg} = (1 - S_{ek})^{1/3}\left[1 - S_{ek}^{1/m}\right]^{2m} \tag{4-4}$$

$$S_{ek} = \frac{S_l - S_{lr}}{1 - S_{lr} - S_{gr}} \tag{4-5}$$

Finally, the gas or liquid permeability is calculated by multiplication with the relative permeability:

$$k_g = k_{rg}\ k \quad and \quad k_l = k_{rl}\ k \tag{4-6}$$

where:

P_c	is the capillary pressure (Pa);
k_{rl}	is the liquid phase relative permeability (ratio);
k_{rg}	is the gas phase relative permeability (ratio);
k	is the intrinsic permeability (m^2);
S_{ec}	is the effective saturation for the capillary pressure relationship (volume ratio);
S_{ek}	is the effective saturation for the relative permeability relationship (volume ratio);
S_l	is the liquid saturation (volume ratio);
S_{lr}	is the residual liquid saturation (volume ratio);
S_{gr}	is the residual gas saturation (volume ratio);
m	is a van Genuchten fitting parameter (unitless);
n	is a van Genuchten fitting parameter (unitless); and
α	is a van Genuchten fitting parameter (1/Pa).

Table 5.15 of the Data report (QUINTESSA and GEOFIRMA 2011a) reports two-phase flow properties for all formations. The values in the report were calculated by fitting equations to laboratory petrophysical data calculated from Ordovician core samples (Calder 2011). These properties define the capillary pressure and relative permeability curves in an air-water system.

Preliminary model calculations were performed using the parameters from QUINTESSA and GEOFIRMA (2011a) for all formations. These initial models were generally stable, but two-phase flow is a non-linear process, and this stability came at the cost of very small time-steps within the model, resulting in unacceptably long runtimes, particularly for the 3DD models. Consequently, the two-phase parameters for most Ordovician formations were replaced with a representative curve that captures most of the capillary pressure behaviour, but has a reduced slope at low water saturations, with a maximum capillary pressure limit of 40 MPa. This

modification reduced the non-linearity in the model and improved the numeric stability, allowing longer timesteps and reduced runtimes. The NE-GT1 and NE-GT2 cases assess sensitivity of model results to this representative curve, while the NE-RC2 case presents results obtained using the formation-specific QUINTESSA and GEOFIRMA (2011a) two-phase flow properties. Results of these cases show that the representative curve is appropriate for use and gives near-identical results.

Formations below the bottom of the shafts did not affect model stability, and the Data report values were retained for the Gull River, Coboconk, and Shadow Lake Formations. Similarly, in the 3D models, where the top of the Guelph Formation is the upper model boundary (see Section 4.3.1), the unmodified van Genuchten parameters from the Data report (QUINTESSA and GEOFIRMA 2011a) were used for the Guelph Formation.

The two-phase flow properties used for modelling are presented in Table 4.3, and are referred to as the NE-RC gas parameters elsewhere in this report. Note that the 2DRS model used the representative parameters for the Guelph Formation and Salina A1 upper carbonate unit with a reduced air-entry pressure ($1/\alpha$). The 3D models used the QUINTESSA and GEOFIRMA (2011a) values for all gas properties for the Guelph. The measured air-entry pressure is substantially lower for the Guelph Formation and Salina A1 upper Carbonate unit than for the other, lower permeability, formations. Since these units have relatively high permeability and low air-entry pressures, they are important gas sinks in those scenarios where gas does travel up the shaft.

Figure 4.2 shows the representative NE-RC capillary pressure curve (solid line) compared with petrophysics data (shown as symbols) for the four different formations. Numbers in the sample legend are sample identifiers. While the modified curve presents a departure from the original analysis of the laboratory petrophysics data (as reported in Section 5.6.1 of the Data report, QUINTESSA and GEOFIRMA 2011a), the modified characteristic curves are similar to and largely within range of the original petrophysical data. As illustrated by the NE-GT1 and NE-GT2 sensitivity cases, the actual capillary pressure curve has very little impact on repository pressures and shaft gas flows.

Table 4.3: Two-Phase Flow Properties (Van Genuchten) for Each Geological Unit

Unit	1/α (MPa)	m (-)	n (-)	S_{lr} (-)	S_{gr} (-)
2D Shaft Model					
SALGR SALFR SALER SALDR SALCR SALBR SLBER SA2CR SA2ER	40	1.00	1.75	0.25	0.05
SA1UR	0.80	1.00	1.75	0.25	0.05
SA1CR SA1ER SLA0R	40	1.00	1.75	0.25	0.05
GUELR	0.80	1.00	1.75	0.25	0.05
GOATR GASPR LIONR FOSSR CABOR MANIR QUEER GBAYR BLUMR COLLR COBGR SFALR KIRKR	40	1.00	1.75	0.25	0.05
COBOR	66.23	1.732	1.82	0.00	0.02
GULLR	40.00	0.775	4.06	0.21	0.11
SHADR	0.23	0.583	1.20	0.04	0.00
3DD, 3DSRS, & 3DSR Models are same as 2DRS, except for the Guelph:					
GUELR	0.037	0.145	4.89	0.25	0.00

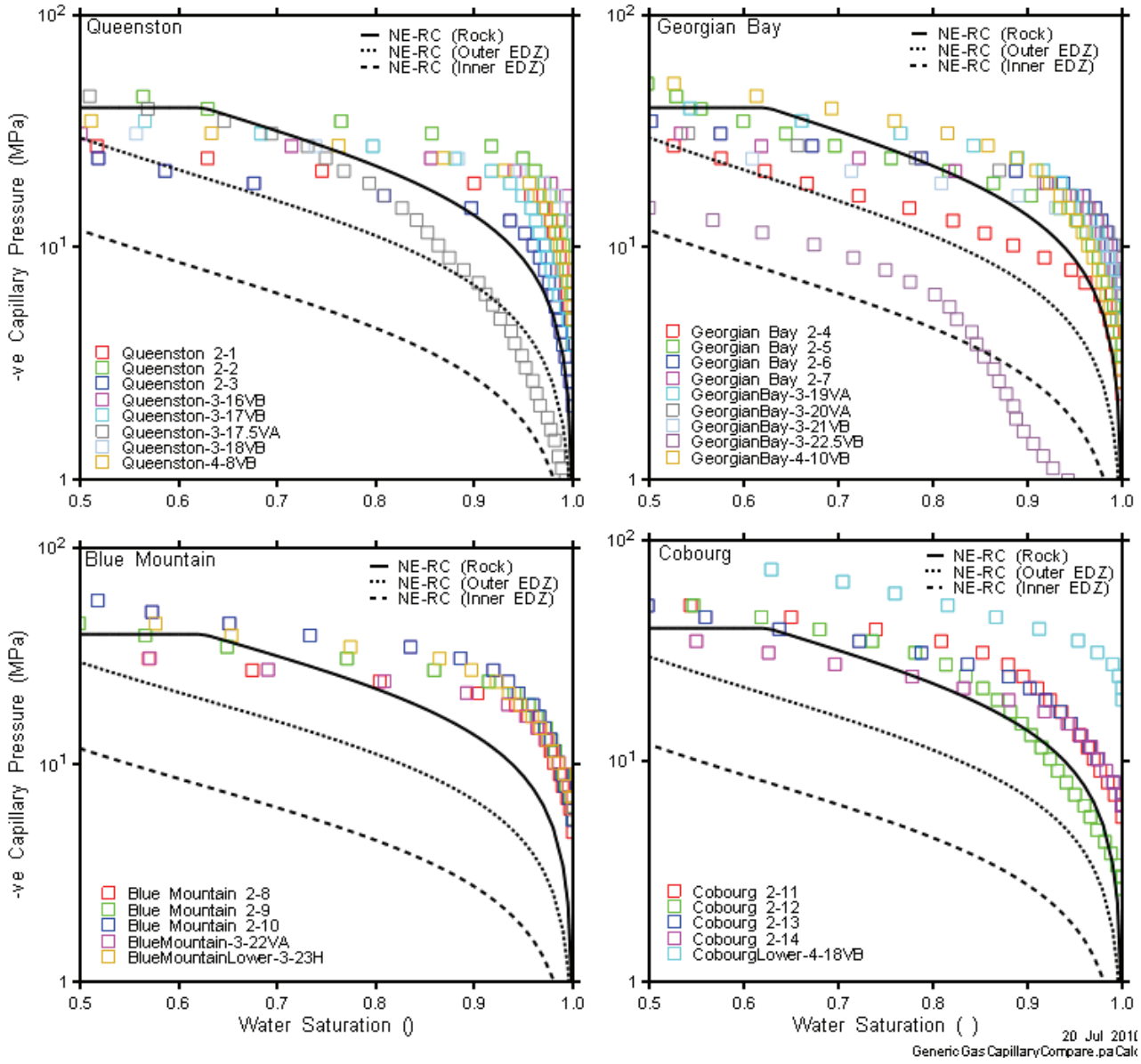

Note: The capillary pressure is a suction pressure.

Figure 4.2: NE-RC Capillary Pressure Curves and Measured Data in Four Ordovician Formations

In the EDZ surrounding the shaft, the development of fractures is expected to alter the capillary pressure and relative permeability relationship. As described in Section 5.6.2 of the Data report (QUINTESSA and GEOFIRMA 2011a), a report from Davies (1991) provides a relationship between permeability and air-entry pressure (1/α). This relationship was used to scale the air-entry pressure within the EDZ, such that the air-entry pressure in the inner EDZ was divided by five, and the outer EDZ air entry pressure was divided by two. The effect of changing this parameter on the representative characteristic curve is shown in Figure 4.2. Further details of the application of the Davies (1991) relationship are provided below in Section 4.2.2.

Capillary pressure curves for the gas parameter sensitivity cases NE-GT1, NE-GT2, and NE-GT3 are shown in Figure 4.3. For cases NE-GT1 and NE-GT2 the air-entry pressure and van Genuchten fitting parameter **n** were modified, with 1/α set to 10 MPa and 200 MPa and **n** set to 1.5 and 2.5, respectively. For case NE-GT3, S_{lr} and S_{gr} are both set to 0.0. The primary purpose of NE-GT3 is to modify the relative permeability curve, as described below, however, changing S_{lr} also slightly impacts the shape of the capillary pressure curve.

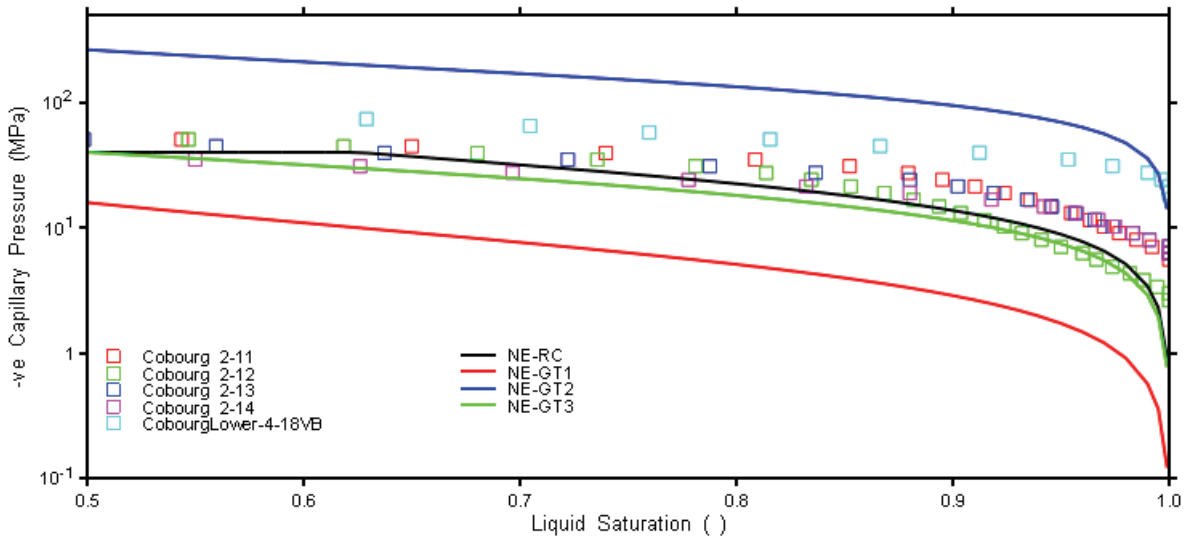

Note: Capillary Pressure is a Suction Pressure

Figure 4.3: Capillary Pressure Curves for NE-GT Sensitivity Cases

Relative permeability curves are a function of the fitted S_{lr}, S_{gr}, and the van Genuchten **m** parameter (see Equations 4-3 through 4-6). In general, there are very high uncertainties to the residual saturations calculated from the analyses of petrophysics testing data. S_{lr} values presented in Table 5.15 in the Data report (QUINTESSA and GEOFIRMA 2011a) range from 0.0 to 0.377 over the formations of interest, while S_{gr} ranges from 0.0 to 0.265. For the NE-RC representative parameters, a residual liquid saturation of 25% and a residual gas saturation of 5% were assumed. The values are a reasonable selection for representative parameters applicable to most formations. In particular, the S_{gr} value is lower than the assumed initial gas saturation in the intact rock for the NE-RC case (10%). Advective transport of gas will only occur when the gas saturation is above the residual gas saturation (otherwise k_{rg} in Equation 4-6 is 0.0), so these parameter selections allow for advective movement of gas in the formations for which the representative parameters are used. As with the capillary pressure curves, the QUINTESSA and GEOFIRMA (2011a) values of S_{lr} and S_{gr} are used for the Coboconk, Gull River and Shadow Lake Formations.

The relative permeability curves for the NE-RC and NE-GT3 gas parameters are shown in Figure 4.4, as well as data points representing relative permeability to gas from the petrophysics analyses used in the determination of van Genuchten parameters in Table 5.15 of the Data report (QUINTESSA and GEOFIRMA 2011a). The NE-GT3 case assumes that both residual saturations are zero.

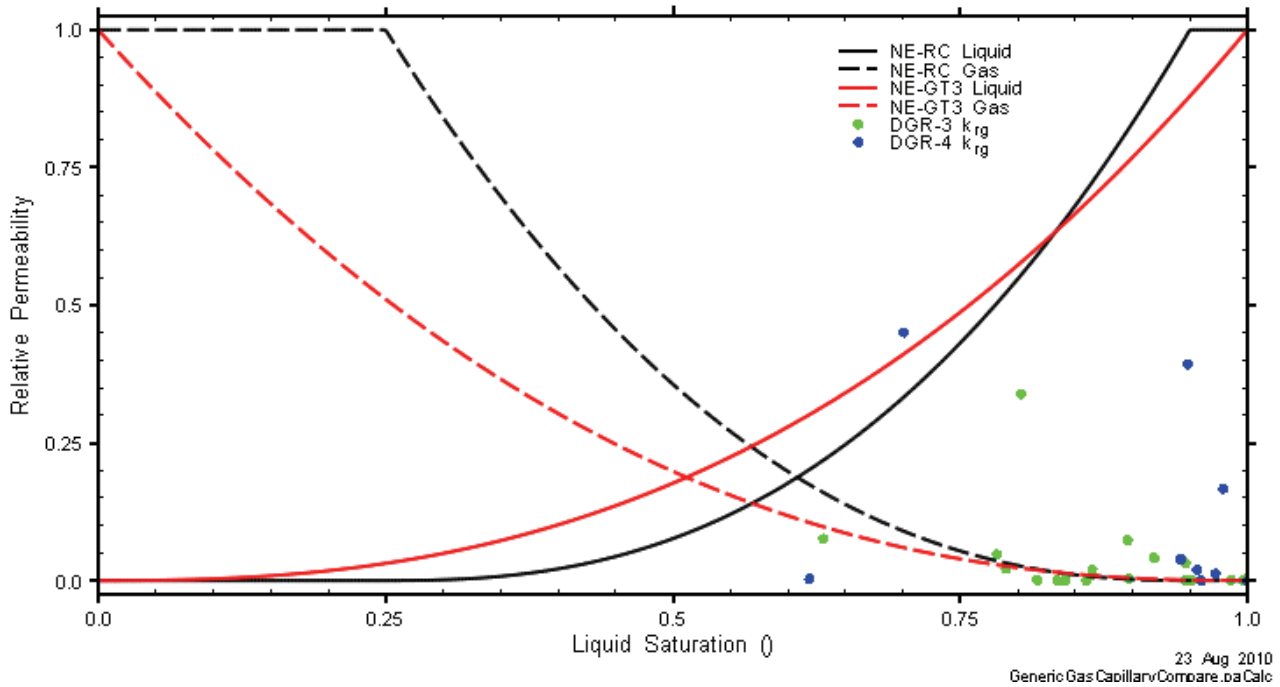

Figure 4.4: NE-RC and NE-GT3 Relative Permeability Curves

There is significant uncertainty in the shape of the relative permeability curve. It is assumed to be represented by the van Genuchten equations; however, laboratory measurements are restricted to a single point on the curve. As noted in Calder (2011), it was not always possible to have the van Genuchten relative gas permeability curve pass through the measured relative gas permeability data. Generally, for these cases, the measured relative gas permeability was greater than provided by the van Genuchten curve with S_{gr} of 0. Given the minimal data available and the uncertainty in the data, no further adjustments were made in the relative permeability curves. The NE-GT3 case provides quantification of some of the uncertainty associated with these assumptions.

4.2.2 Shaft, Repository and Sealing Material Properties

The emplacement rooms, access tunnels, shaft services area, main shaft, the ventilation shaft, and their associated EDZ, HDZ, and sealing systems form the engineered portion of the modelled system. For these components of the model, there is no directionality to the material and the vertical and horizontal permeabilities are equal. Model IDs in this section are shown in bold text to make them easily distinguishable.

As described in Section 4.3.1, the repository is conceptually divided into two components, each with slightly different properties: the waste disposal area, consisting of emplacement rooms and

access tunnels joining the emplacement rooms (referred to as **REPO** for repository); and access tunnels joining the shafts and surrounding tunnels to the waste disposal area (**TUNN**). The porosity for both these components is calculated from the ratio of the total void volume of repository and tunnels in Table 4.5 of the Data report (QUINTESSA and GEOFIRMA 2011a) and the total element volume assigned to the property in the model (**REPO** and **TUNN**). The porosity of the rock pillars and the rock above the repository (rockfall) is low and, therefore, neglected in this calculation. It should be noted that the repository and access tunnels will have a very high permeability, as they are primarily void space. However, numeric issues associated with permeability contrasts required that a nominal permeability be assigned to these elements for successful calculations. After initial testing simulations, a value of 10^{-6} m/s was chosen as an acceptable value that would not materially impact flow or transport results.

The HDZ (**RPHDZ**) and EDZ surrounding the monolith, access tunnels and the repository is assumed to be entirely within the Cobourg unit (**COBGR**), and is assumed to have uniform properties. The repository EDZ was not included in any of the 3D models as the high repository permeability would essentially eliminate any impact from the EDZ as a gas pathway. The permeability of **RPHDZ** is set to 1.16×10^{-15} m^2 in all directions. This is much higher than the host rock, and is based on the possibility that there may be connected fractures in this HDZ as it is aligned with the bedding planes. This is equivalent to a hydraulic conductivity of 10^{-8} m/s, and is lower than the 10^{-6} m/s given in Table 5.8 of the Data report (QUINTESSA and GEOFIRMA 2011a). The lower permeability was required for reasons of numerical stability, but still provides a very high permeability in contrast to the surrounding rock. Repository HDZ porosity is based on the Cobourg rock mass property, with a porosity four times that of the intact rock.

In the reference DGR closure plan, the base of the shafts and all of the tunnels in the vicinity of the main and ventilation shafts will be filled with concrete (called a concrete monolith) (see Figure 2.6). This extends to the junction where the access tunnels from the two panels meet. Above the monolith, the shafts will be backfilled primarily with a compacted bentonite/sand seal (**BENTS**). The shaft seal also contains a section of asphalt (**ASPH**) in the upper Ordovician sequence. The monolith and concrete bulkheads in the deep and intermediate groundwater zones within the shaft are assumed to have identical properties and are designated as lower concrete (**CONCL**). The concrete bulkheads above -10 mASL are in a separate material group than the more deeply buried concrete (called **CONCS**, shallow concrete). **CONCS** is assigned the same values as **CONCL**, as all concrete is assumed to have degraded and therefore have somewhat higher permeabilities than newly placed concrete (Table 4.22 of QUINTESSA and GEOFIRMA 2011a). **CONCS** is only present in the upper portion of the 2DRS model.

The shaft has an inner and outer EDZ, with separate model properties defined for each geologic unit intersected by the shaft. EDZ property IDs are identical to the geologic unit IDs, with the "R" in the model ID replace by an "I" for the inner EDZ and an "O" for the outer EDZ. For example, the Cobourg unit has rock, inner EDZ and outer EDZ model property IDs, labelled respectively of **COBGR**, **COBGI** and **COBGO**. In the Reference Case, the inner EDZ has a vertical hydraulic conductivity 100 times greater than the associated rock mass K_v, and the outer EDZ has a vertical hydraulic conductivity 10 times greater. (In the alternative case NE-EDZ1, the inner EDZ has a vertical hydraulic conductivity 10,000 times greater than that of the host rock.) Inner EDZ has twice the porosity of the associated rock mass, while the outer EDZ porosity is the same as for the intact rock. For example, the Cobourg unit inner EDZ has a vertical permeability of 2.33×10^{-20} m^2 and a porosity of 0.03, and the Cobourg unit outer EDZ has a vertical permeability of 2.33×10^{-21} m^2 and a porosity of 0.015. Within the EDZ it is assumed that vertical and horizontal permeability are equal.

Based on Table 4.28 of the Data report (QUINTESSA and GEOFIRMA 2011a), two-phase flow parameters were also specified for all shaft and sealing materials. In the EDZ, the development of fractures is expected to alter the capillary pressure and relative permeability relationship. As described in Section 5.6.2 of QUINTESSA and GEOFIRMA (2011a), reduction of air-entry pressures (1/α) in the EDZ was accomplished by applying the Davies relationship (Davies 1991) to the formation permeability:

$$P_{ae} = 5.6 \times 10^{-7} k^{-0.346} \quad (4\text{-}7)$$

where:

P_{ae} is the air-entry pressure, MPa; and
k is the rock permeability, m^2.

This relationship was used to scale the air-entry pressure within the EDZ, such that the air-entry pressure in the inner EDZ was divided by five, and the outer EDZ air-entry pressure was divided by two. The effect of changing these parameters on the representative characteristic curve is shown in Figure 4.2 above.

Physical, hydrogeologic and two-phase flow properties for repository, shaft, and sealing system materials, based on Table 4.28 of the Data report (QUINTESSA and GEOFIRMA 2011a), are given in Table 4.4. Due to the large number of geologic units, and consequently the large number of inner and outer EDZ material types, Table 4.4 does not provide the properties for each EDZ material. The preceding two paragraphs sufficiently describe the differences between EDZ properties and those of the surrounding intact rock.

Table 4.4: Physical, Hydrogeologic, and Two Phase Flow Properties for Shaft, Repository, HDZ, and EDZ for the RC

Unit	Porosity (-)	Permeability (m^2)	Pore Compressibility (1/Pa)	1/α (MPa)	m (-)	n (-)	S_{lr} (-)	S_{gr} (-)
ASPH	0.02	1.16E-19	1.49E-08	-	-	-	0.001	0.001
CONCL	0.10	1.16E-17	6.00E-10	1.0	0.5	2.0	0.20	0.10
BENTS	0.29	1.16E-18	1.48E-09	10.0	0.4	1.8	0.01	0.01
TUNN	0.50	1.16E-13	1.10E-10	-	-	-	0.01	0.00
REPO	0.50	1.16E-13	1.10E-10	-	-	-	0.01	0.00
RPHDZ	0.06	1.16E-15	9.17E-10	-	-	-	0.25	0.001

Table 4.4 does not provide two- phase flow properties for the repository, access tunnels, repository HDZ, or asphalt as a different approach was taken to describe the two-phase flow behaviour for these materials. The repository and tunnels are actually a void space without porous media type behaviour. Capillary pressure is assumed to be zero. Relative permeability is modelled using a simple linear model that allows gas and water to move freely within the repository void, except for some restrictions at very low saturations that are required to maintain numeric stability.

Asphalt (**ASPH**) is also treated differently from other materials. As discussed in QUINTESSA and GEOFIRMA (2011a), asphalt is hydrophobic, and should therefore not produce capillary suction. Capillary pressure is therefore assumed to be zero at all liquid saturations. The relative liquid permeability is assumed to vary linearly between 0 and 1 between liquid saturations of 0.001 and 0.999. The relative gas permeability is assumed to vary linearly between a minimum of gas saturation 0.001 and a maximum of 0.999.

Two- phase flow in the repository HDZ (**RPHDZ**) is modelled by assuming that all significant flow occurs in the fraction of the **RPHDZ** porosity comprised of fractures. Because the fracture apertures in the permeable part of the HDZ are likely to be relatively large, capillary pressure is assumed to be negligible, and is set to zero at all saturations. 75% of the HDZ porosity is considered to be fracture porosity (this corresponds to the increase in porosity above that of the host rock). Consequently, the residual liquid saturation is set to 0.25, as any saturation reduction below this level will not significantly affect the relative liquid porosity. Conversely, gas permeability does not increase beyond a gas saturation of 75% (See Figure 4.5).

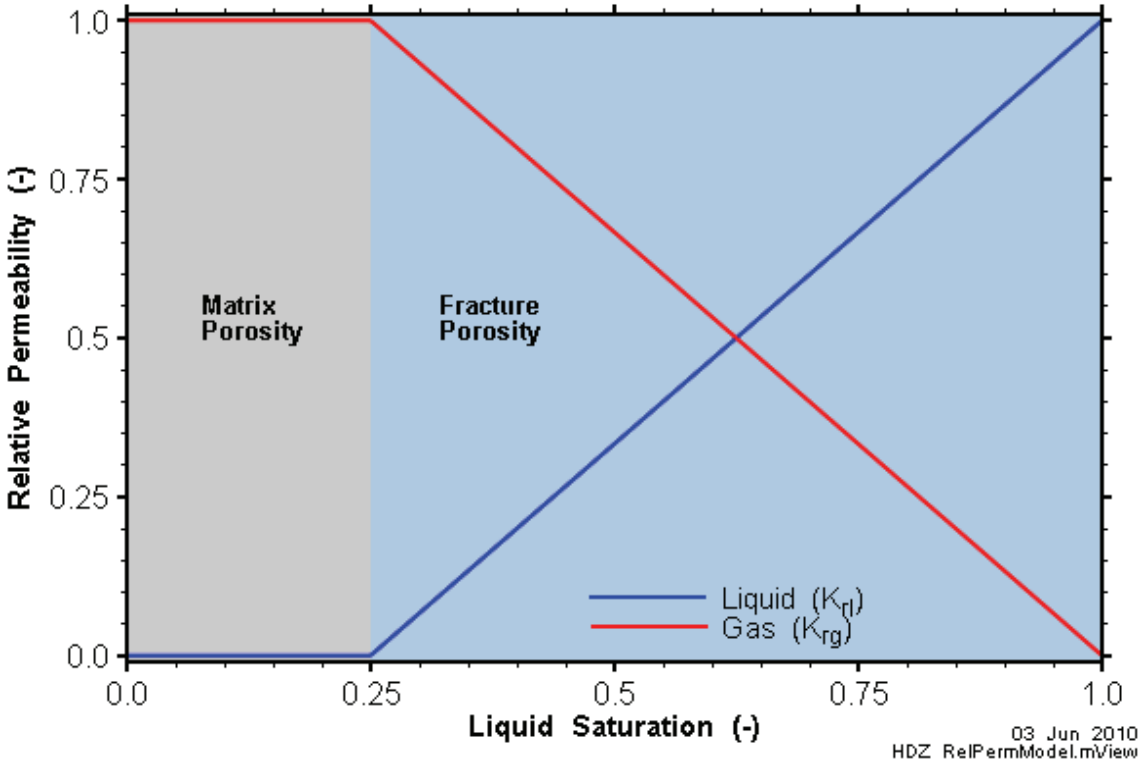

Figure 4.5: Gas and Water Relative Permeability Curves for Repository HDZ

The NE-EDZ1 modelling case examines the impact if the maximum shaft EDZ hydraulic conductivity estimates from Tables 5.7 and 5.8 of the Data report (QUINTESSA and GEOFIRMA 2011a) are applied and the air-entry pressure of the EDZ is reduced (by reducing 1/α values). For the EDZ sensitivity case NE-EDZ1, the inner EDZ and outer EDZ permeability for the shaft are 10,000 and 100 times the rock mass vertical conductivity, respectively. As described earlier in this section, the reduction of air-entry pressures (1/α) for the NE-EDZ1 case

was accomplished by applying the Davies relationship (Davies 1991) to the formation permeability. For a factor of 10,000, the Davies relationship indicates an approximate factor of 25 reduction. The revised air-entry pressure for the NE-EDZ1 representative characteristic curve for the Inner EDZ is 1.6 MPa, as compared to 8 MPa for the NE-RC. For the outer EDZ, air-entry pressure drops from 20 MPa down to 8 MPa. This approach addresses the basic assumption that air-entry pressures in the EDZ for the NE-EDZ1 case should be lower than those of the NE-RC case.

For the shaft failure case SF-BC, the shaft seal material is assumed to have degraded to a conductivity of 10^{-9} m/s (1.16×10^{-16} m^2 permeability) and a porosity of 0.30. The SF-ED case assumes a shaft conductivity of 10^{-7} m/s (1.16×10^{-14} m^2 permeability). In both cases, shaft material capillary pressure is set to zero at all saturations, and a linear relative permeability curve is used. EDZ permeabilities for these shaft seal failure case were also to be degraded as per the NE-EDZ1 case. Initial simulations indicated that these values would cause unacceptably long run-times. The SF-BC and SF-ED case were actually conducted with EDZ conductivities consistent with the NE-RC case. Since the SE-BC degraded shaft seal permeability is two orders of magnitude higher than NE-EDZ1 inner EDZ permeabilities, there will be no perceptible impact on calculated gas and liquid flow rates up the shaft as a result of these modifications.

4.2.3 Gas Generation Input Parameters

GGM requires information about: the initial surface areas of the metallic wastes; the inventories of metals and organic wastes in all waste groups; the reaction rates for the corrosion and degradation reactions under the various conditions (saturated phase, vapour phase); and physical properties such as densities, molar masses and solubility constants. A full listing of those parameters is provided in Table 7.8 of the T2GGM Report (QUINTESSA and GEOFIRMA 2011b), and the values and documentation are in the Data report (QUINTESSA and GEOFIRMA 2011a).

One parameter, PMINSAT (minimum saturation), was set to 0.00011 for numeric reasons. Experience with initial versions of T2GGM had shown that time steps reduced to impractically small values if the repository was allowed to entirely dry out. Accordingly, PMINSAT was set to turn-off water consuming reactions when the overall repository liquid saturation approached 0.0001, a very low but non-zero value.

4.2.4 Gas Properties

The modified TOUGH2 (EOS3 module) component of the T2GGM model simulates transport of a single bulk gas, and is configured to use methane as the bulk gas for most calculation cases. As will be discussed below, the GGM component of the T2GGM model simulates multiple gas components, which are then converted to the single bulk gas for transport in the TOUGH2 component of the model. Methane was selected as the bulk gas in the TOUGH2 component of the T2GGM model since initial GGM results showed that it becomes the dominant gas in the repository.

The GGM component of T2GGM converts the mass flow rate of individual gas components generated at each time step to an equivalent mass rate of a single gas for injection into the TOUGH2 model. The conversion is calculated by multiplying the sum of the molar rates (mol/s) of individual gas components by the molar mass of the specified bulk gas (CH_4 for most cases).

The diffusion coefficient of water vapour and air in gas at 20°C is 2.1 x 10^{-5} m^2/s (Pruess et al. 1999; Incropera and DeWitt 1996). This value is assumed representative for all gases. At the isothermal conditions simulated, diffusion of water vapour in air will not impact simulation results. For diffusion of dissolved gas in water, a free-water diffusion coefficient of 10^{-9} m^2/s is specified. This results in calculated D_e for dissolved gas in water that are consistent with formation D_e HTO presented in Table 5-14 of QUINTESSA and GEOFIRMA (2011a). T2GGM scales calculated D_e by the relative permeability function to determine reductions in diffusion due to partial gas saturations. The diffusion of all gases was assumed to be similar to HTO. As water is the main component of the liquid phase (i.e., dissolved gas is a dilute solution), the diffusion coefficient of water in the liquid phase is zero. Mass flux of dissolved gas is, in general, of far less significance than mass flux of free-phase gas in those instances where either or both are transmitted up the shaft. Uncertainties in diffusion coefficients will, therefore, have minimal impact on results.

The solubilities of selected gases are specified within the T2GGM model and are given in Table 3.19 of QUINTESSA and GEOFIRMA (2011a). The solubility constant for methane in brine is given as 4.0 x 10^{-3} mol/(L MPa).

4.3 Model Implementation

4.3.1 Model Structure

The site geology is represented as a flat "layer cake" system in the all models. The vertical domains of each model are shown in Figure 4.6. Two sets of extents are required for the 2DRS model. The intact rock model is used to specify initial pressures in the pre- and post- closure models, and must therefore extend to the lower hydrogeologic boundary of the system. The 2DRS pre- and postclosure models calculate the response of the shaft to repository induced pressures, and thus its domain is limited to the formations above the repository.

4.3.1.1 3D Detailed (3DD) Model

For the 3DD model, the model domain extends from the top of the Guelph Formation (at -188.8 mASL or approximately 374.5 mBGS) down to the top of the Cambrian sandstone at an elevation of -658 mASL (or 844 mBGS). The choice of the Cambrian sandstone as the lower boundary was dictated by the need to include the high pressure boundary condition within this unit. The omission of Silurian units above the Guelph in these models improves model tractability. In trial simulations with model domains extending above the Guelph, and where free-phase gas flow occurred in the shaft, the ingress of free-phase gas into the Guelph formation was a limiting factor on time-step size. Eliminating this effect allowed the 3DD and 3DSRS models to execute in an acceptable time period. The Guelph Formation forms a natural upper boundary for the 3D models, as it is the first higher permeability layer above the Ordovician and lower Silurian formations. Transport above the Guelph is addressed using the 2DRS model.

Set within the layer cake hydrostratigraphic system is the deep geological repository, represented with reasonable fidelity to the design, although with certain simplifications. First, the main shaft and the ventilation shaft design are combined and represented by a single shaft in the model. This simplification serves to reduce the complexity of the discretization. This combined shaft has been located mid-way between the ventilation shaft and main shaft locations. The radius of the modelled "combined shaft" was calculated to match the summed cross-sectional areas of the main and ventilation shafts, as shown in Table 4.5.

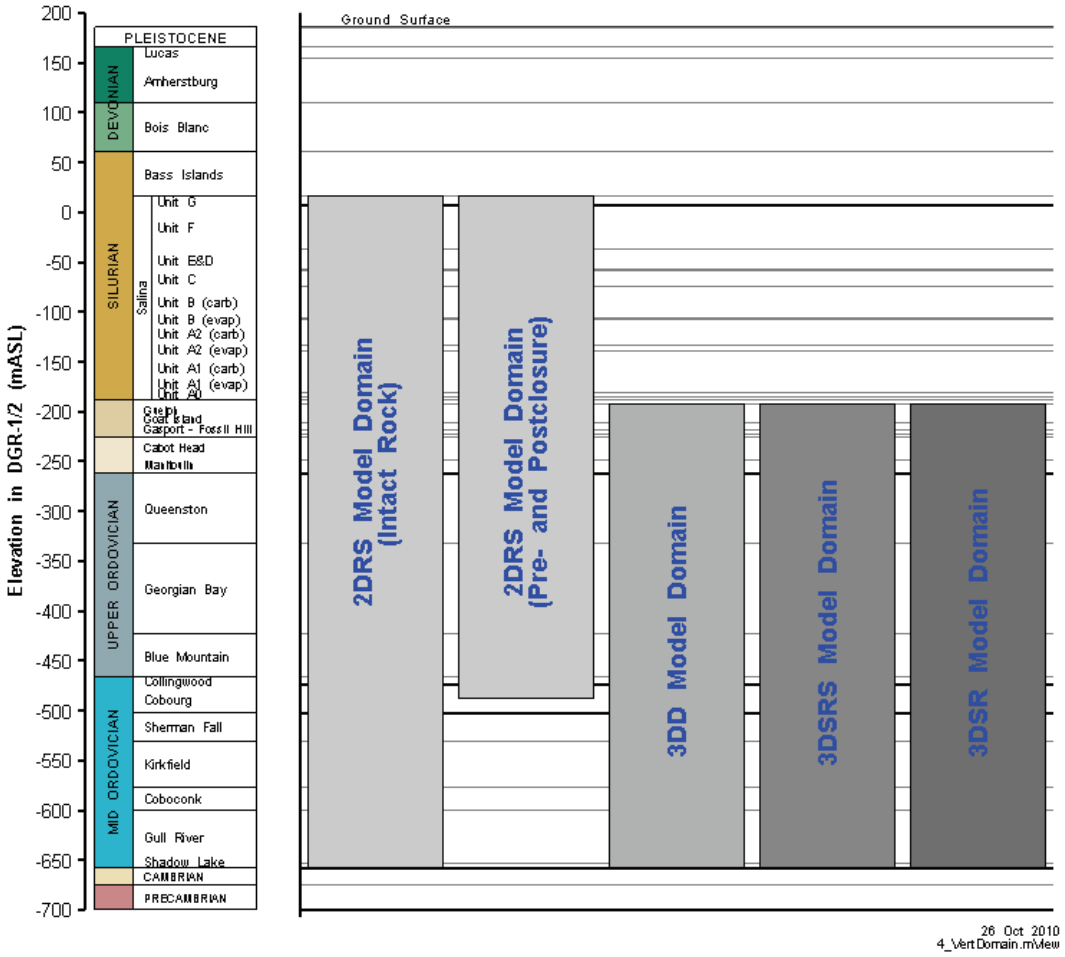

Figure 4.6: Geologic Domains of Gas Transport Models

For the combined shaft, the radii of the inner EDZ, and the outer EDZ above -535.2 mASL were chosen so as to best match the cross sectional areas of these features with the sum of the main shaft and ventilation shaft EDZ, as shown in Table 4.5. The 2D geometry of the 2DRS model by necessity implements a circular EDZ. The 3D models also implement a circular EDZ to simplify gridding. EDZ radii are defined in terms of the shaft radius following removal of the 0.5 m thick HDZ (R_{shaft}), with the inner EDZ extending from the shaft wall to a radius of 1.5 R_{shaft}, and the outer EDZ extending from 1.5 R_{shaft} to 2.0 R_{shaft}. (See Section 5.4.2 of QUINTESSA and GEOFIRMA 2011a). Any shaft HDZ is removed during shaft sealing so is not part of this model.

Although the actual geometry of the EDZ may be elliptical, to reflect major and minor axes of principal stress (NWMO 2011a), there are few data available to justify the orientation and magnitude of permeability changes. The EDZ geometry and properties used in the modelling is based on a review of experimental data and site-specific geomechanical modelling (Section 5.4.2 of QUINTESSA and GEOFIRMA 2011a). The resulting conceptualization is a conservative approach as the radius of the circular EDZ zones includes the major axes of the elliptical zones predicted from the geomechanical modelling.

Table 4.5: Radii and Cross-Sectional Areas of Combined Shaft

Shaft	Shaft radius (after HDZ removal) m	Inner EDZ Radius m	Outer EDZ Radius m	Shaft Area m^2	Inner EDZ Area m^2	Outer EDZ Area m^2
Main shaft	4.575	6.86	9.15	65.75	82.09	115.18
Ventilation shaft	3.725	5.59	7.45	43.59	54.58	76.20
Combined shaft	5.900	8.85	11.80	109.35	136.70	191.38

Note: From QUINTESSA and GEOFIRMA (2011a).

Since the ventilation shaft extends approximately 32 m below the bottom elevation of the main shaft (-535.2 mASL), the radius of the combined shaft was equal to that of the ventilation shaft below that depth. To simplify gridding, and since initial scoping simulations indicated that these were not important for gas transport, the model does not include the ramp to the shaft bottoms, nor the HDZ in the shaft bottoms. However, the shaft EDZ is modelled in a similar manner as described above.

As a further simplification, the tunnels and tunnel stubs of the shaft services area (shown in Figure 2.6 and Figure 4.7) are not represented in the model. Only the shortest route linking the shaft to the repository is present. The shaft tunnel is connected to the repository panels by orthogonal access tunnels, sized according to the design.

Note that Figure 4.7 uses a modelling coordinate system with its origin at the location of the combined shaft (i.e., mid-way between the main shaft and ventilation shaft) and a positive X axis extending along the main access tunnel for the north panel. This modelling coordinate system will be used in all further 3DD figures for this report.

The closure plan calls for the tunnels to be used for disposal of concrete debris from the shaft liner removal and for disposal of all used equipment. At closure, however, there will still be void space, and for these simulations it is assumed that there is an immediate 10 m of roof collapse above all access tunnels not filled with concrete (see Section 4.4.1 of the System and Its Evolution report, QUINTESSA 2011b). These tunnels have been modelled as a high permeability and porosity zone with properties as described in Table 4.4.

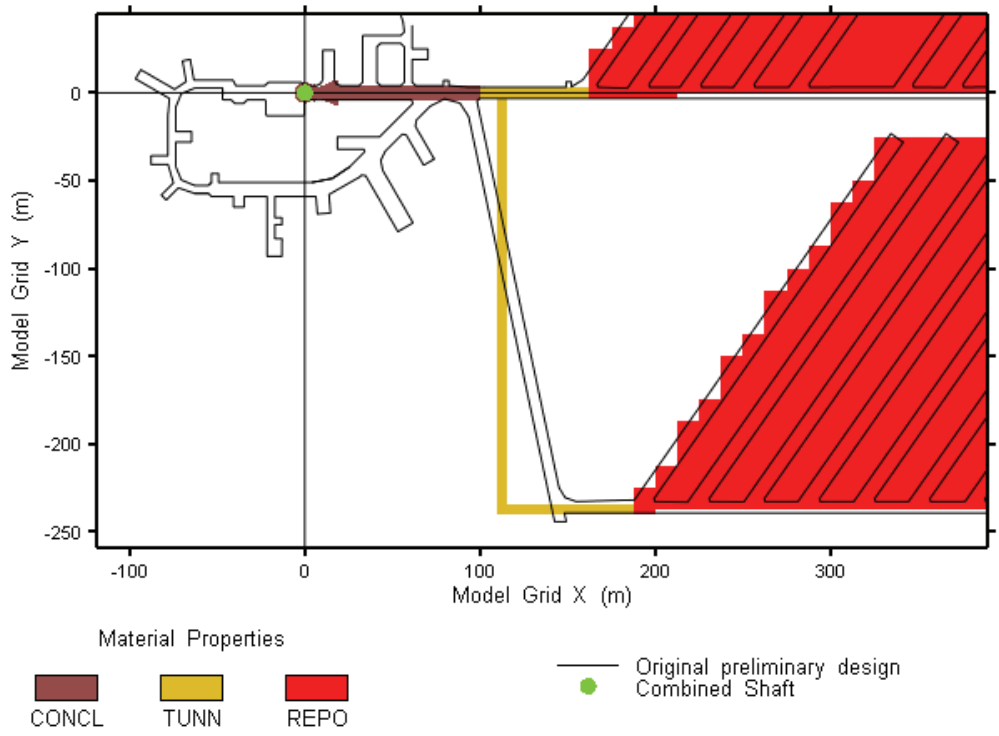

Note: Final preliminary design is discussed in Section 2.3.

Figure 4.7: Repository Plan Outline and 3DD Model Representation (Near the Shafts)

Where the concrete monolith is in place (100 m from the shaft along the tunnel, Figure 2.6), there will be no roof collapse, but an HDZ is modelled, extending 2 m above the concrete monolith (Table 5.8 of QUINTESSA and GEOFIRMA 2011a). The HDZ (described in QUINTESSA and GEOFIRMA et al. 2011a) below and to the sides of the monolith was not included. The HDZ above the concrete monolith provides the most significant flow pathway linking the repository to the base of the shaft and shaft EDZ.

The individual emplacement rooms are not explicitly represented, but are rather combined with the repository pillars in a repository panel unit with the same total porosity. Thus, the repository panels are modelled as two volumes, which roughly approximate the plan outline of the repository as shown in Figure 4.8. This approach simplifies the modelling process by reducing the required level of discretization, while being consistent with the expected relatively easy mobility of water and gases within the panels. It may also reflect the long term conditions for stabilized rockfall within a panel. Similar to the access tunnels, an immediate 10 m roof collapse is assumed for the repository.

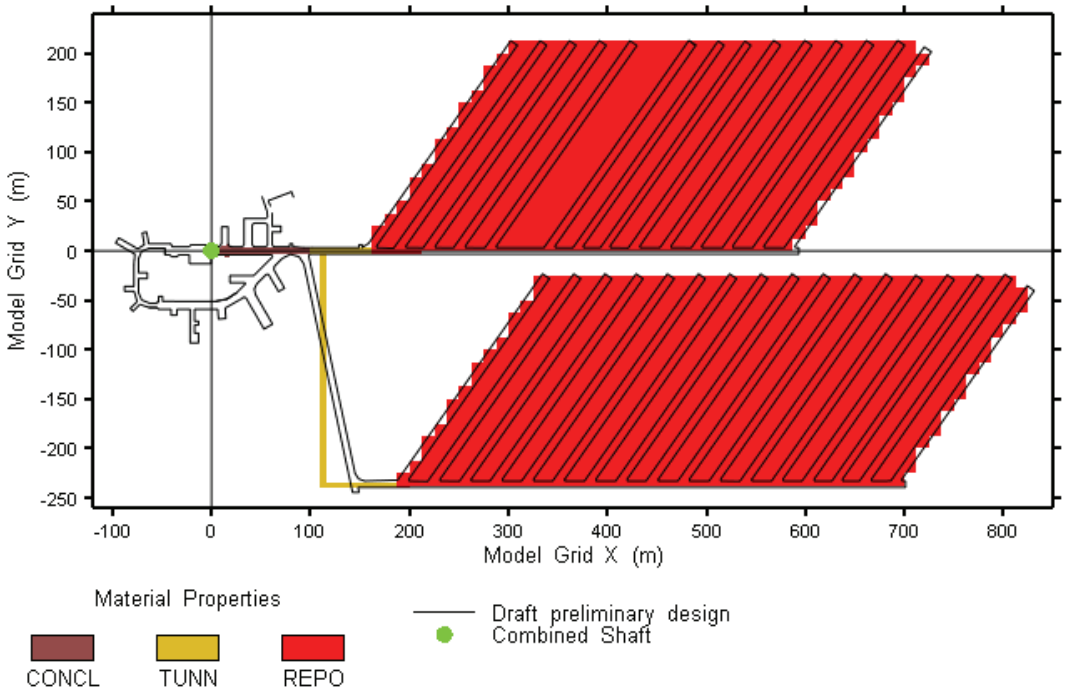

Figure 4.8: Repository Plan Outline and 3DD Model Representation

Repository panels, access tunnels and monolith will be surrounded by an EDZ. However, the presence of EDZ around the tunnels and repositories in the model caused numerical difficulties, without contributing to the transport of gas given the much higher permeability of the repository and access tunnel zones. Thus, the repository and access tunnel EDZ was not included in the model.

4.3.1.2 3D Simplified - Repository & Shaft (3DSRS) Model

The 3DD model, while providing a comprehensive representation of repository features, is very large. Initial simulations with the model were time consuming, and prone to numeric difficulties. These factors led to development of the 3DSRS model. This is a reduced scale model that captures the main aspects of the system by including repository and shaft seals, repository HDZ and shaft EDZ in a simplified system.

The 3DSRS model represents the repository as a square with approximately the same plan surface area and thickness as the original repository. The repository plan surface area is approximately 200,000 m^2, which is equivalent to a square with 447 m long sides. The 3DSR model has sides that are 500 m. The 500 m length allows for integer sized grid blocks when subgridded and results in a slightly larger total seepage face than a 200,000 m^2 model. The vertical seepage face (i.e., at the sides of the square) is smaller than the combined seepage face of the two panels in the 3DD model.

A round shaft is located in the middle of the square, surrounded by a concrete monolith of 50 m radius. The shaft extends upwards from the monolith and has the same dimensions as the combined shaft in the 3DD model above the monolith. Finally, to take advantage of the two planes of symmetry in a square, only a quarter of the total square is actually modelled (i.e., a

square with 250 m long repository sides, two of which are no-flow boundaries. The 3DSRS representation of the repository footprint is shown in Figure 4.9.

The HDZ was implemented as a single channel of grid blocks connecting the bottom of the shaft EDZ to the repository. This leads to an overstatement of HDZ permeability as the single channel is in effect wider than the HDZ around the tunnel after a multiplier factor of four is incorporated to account for the quarter section model. In practice, the extra permeability has little impact, as the permeability of the shaft materials is the main control on gas and liquid flow.

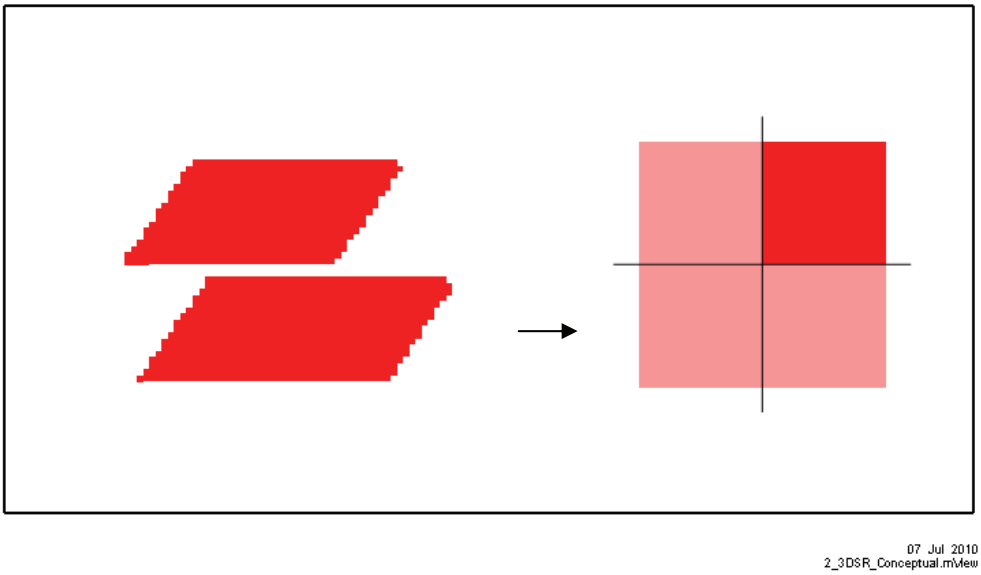

Figure 4.9: 3DSRS Representation of Repository

4.3.1.3 3D Simplified - Repository (3DSR) Model

In several of the calculation cases, performance of the geosphere alone is the main focus of the case. For these cases, the 3DSR model, which does not include a shaft, provides a further simplified representation of the repository system. The 3DSR model is identical to the 3DSRS with the shaft, shaft EDZ, monolith and HDZ removed. 3DSR simulations were conducted for most cases. Comparison of 3DSR and 3DSRS results provides a direct indication of the impact of the shaft on the model results.

4.3.1.4 2D Radial Shaft (2DRS) Model

The 2DRS model is separated into two model domains: intact rock and pre-/postclosure. The intact rock model extends from the top of the Cambrian at a depth of 844 m (elevation -658 mASL) to the top of Salina G at a depth of 169.3 m (elevation 16.41 mASL). This model represents a column of intact rock, and is used to generate initial and boundary conditions for 2DRS preclosure models. Both the pre- and postclosure model domains extend from the top of the supported access tunnel highly damaged zone (-487.3 mASL, within the Cobourg unit) to the top of the Salina G.

The 2DRS model represents only the transport up the shaft and the interaction of the shaft with the surrounding rock. The model represents the combined shaft and the surrounding rock as a two-dimensional radial section with an arc length of 2 degrees. Subsequently, the fluxes crossing this slice are multiplied by 180 to get the total flow and the mass flow from within the shaft and shaft EDZ. The shaft radii are the same as shown in Table 4.5 with the combined shaft used in the simulations. The model extends beyond the shaft to a radius of 500 m.

4.3.2 Model Discretization and Property Assignment

Model grid and property assignments for the 3DD, 3DSRS, 3DSR and 2DRS models are presented in this section.

4.3.2.1 3DD Model

The 3DD has 126,352 nodes with 389,248 connections. Plan view discretization of the 3DD model from overall scale, to repository scale, to access tunnel and shaft services area scale, to shaft scale, is shown in Figure 4.10 through Figure 4.14, respectively. The plan view discretization in Figure 4.10 contains 2401 nodes. The model is greatly refined in the vicinity of the repository and the shaft. Away from the shaft and repository, the grid size increases gradually. This progressive coarsening of the grid occurs both horizontally and vertically. Figure 4.12 shows a plan view of the grid at a higher elevation where compared to Figure 4.11 the mesh refinement has been reduced above the repository footprint.

The vertical parameter distribution of the 3DD model from repository scale, to monolith scale to shaft scale, is shown in Figure 4.15 to Figure 4.17. Note that individual formations are not shown in the figure and that the grid blocks have been colour coded according to their lithography. In the model, layers were assigned their unique property according to formation in Table 4.2 and Table 4.3 and according to their distance from the shaft (e.g., FOSSI, FOSSO, and FOSSR for inner EDZ, outer EDZ, and intact rock of the Fossil Hill formation). Figure 4.15 to Figure 4.17 all present a vertical cross section through the centre of the shaft (i.e., through model coordinate y=0). Element boundaries are shown on Figure 4.16 only.

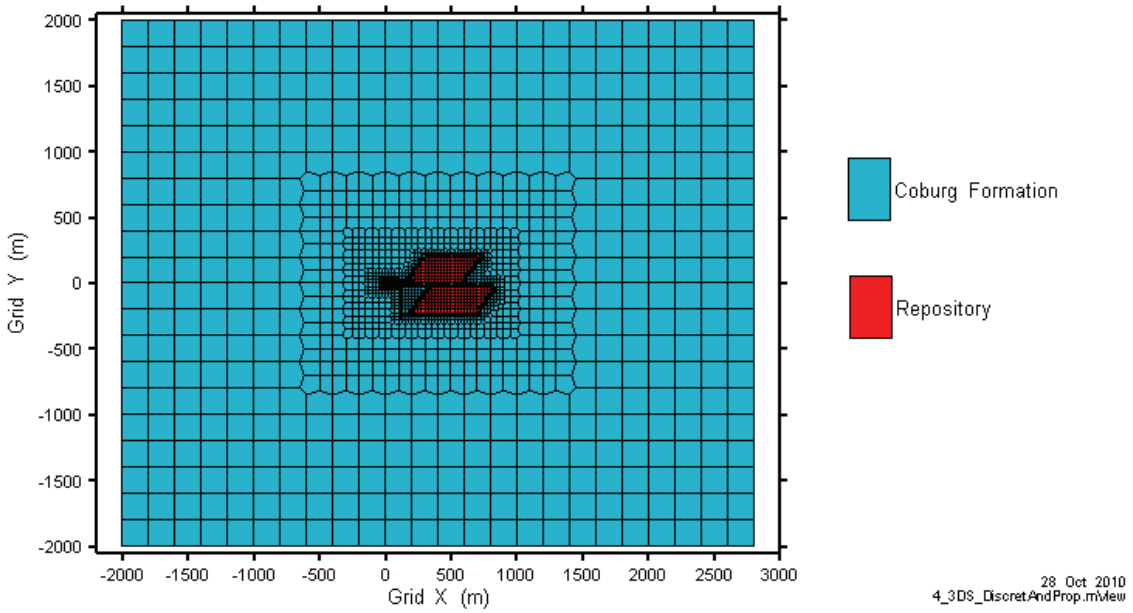

Figure 4.10: 3DD Model Plan Section View of Entire Model Domain (at Repository Depth)

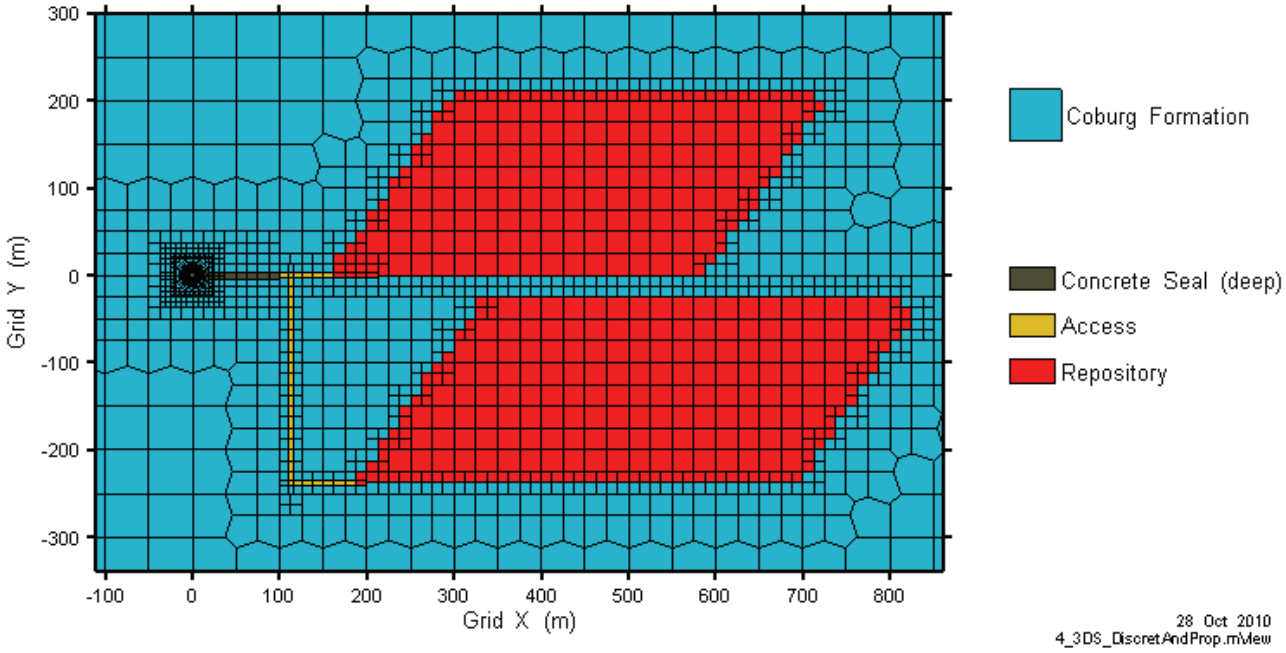

Figure 4.11: 3DD Model Plan Section View - Repository Horizon

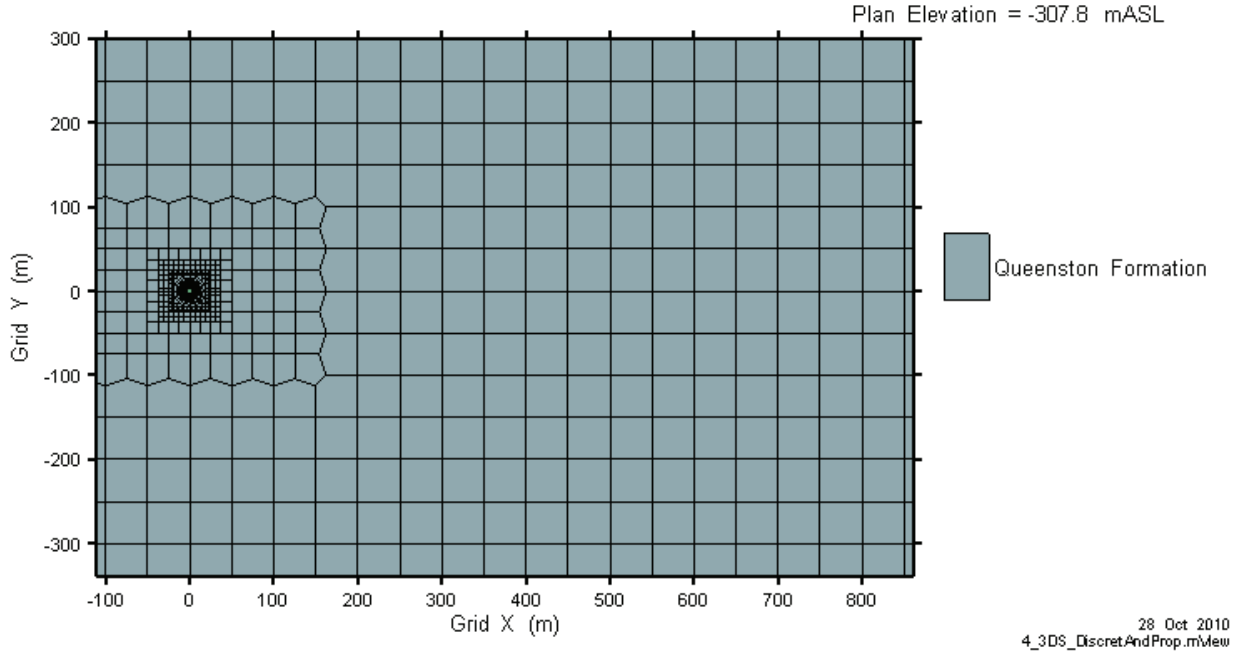

Figure 4.12: 3DD Model Plan Section View – Queenston Formation

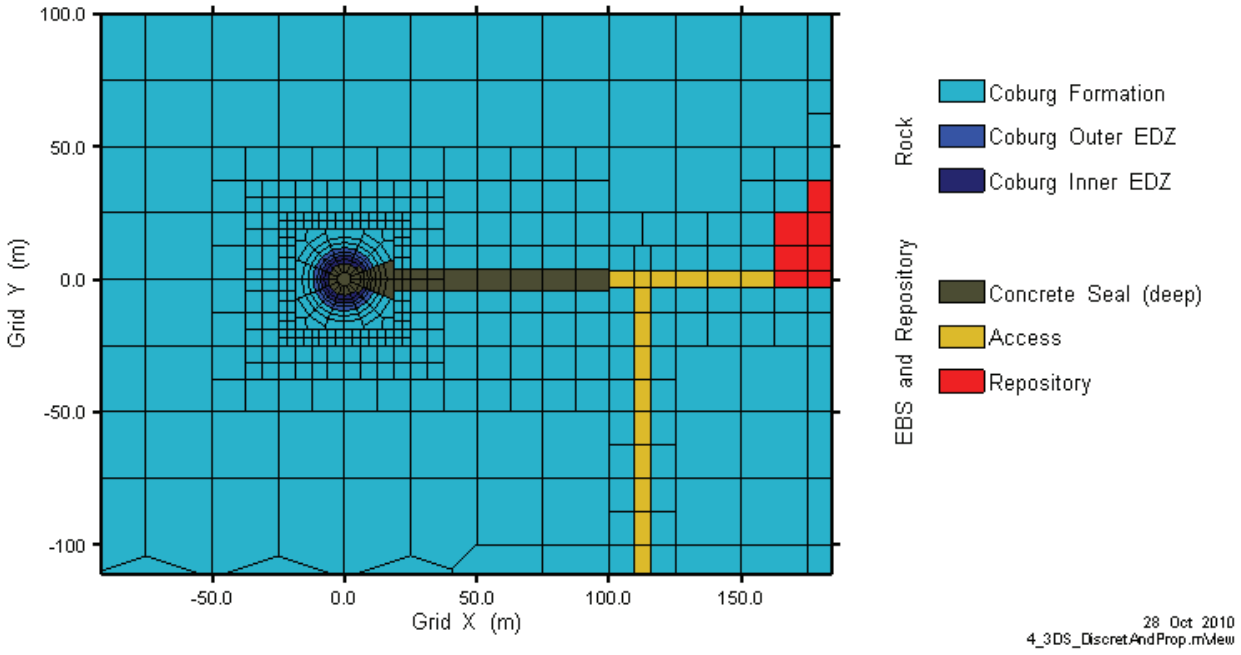

Figure 4.13: 3DD Model Plan Section View – Shaft Area and Tunnel Detail

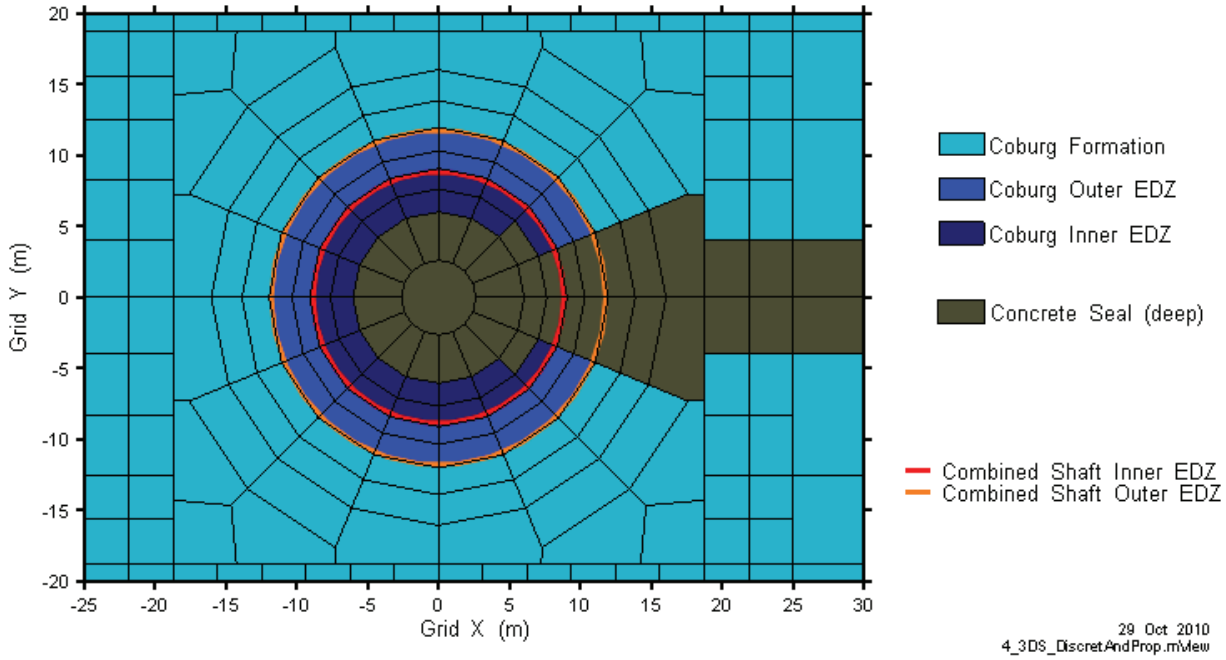

Figure 4.14: 3DD Model Plan Section View – Shaft, EDZ, and Tunnel Detail

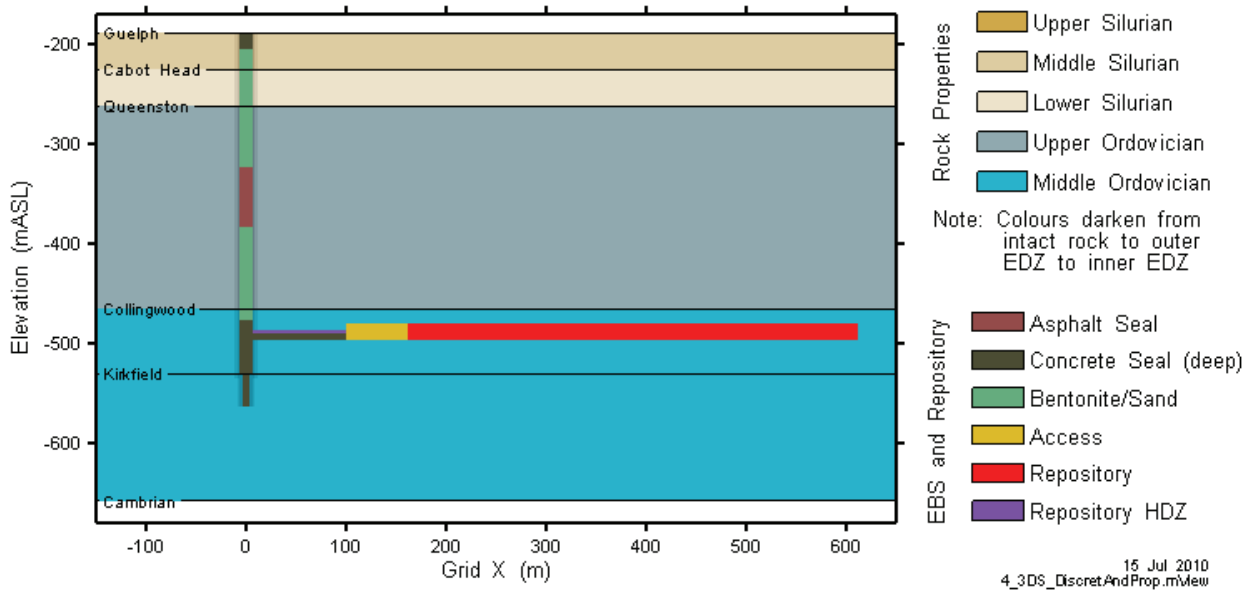

Figure 4.15: 3DD Model Cross-Section View – Property Assignment

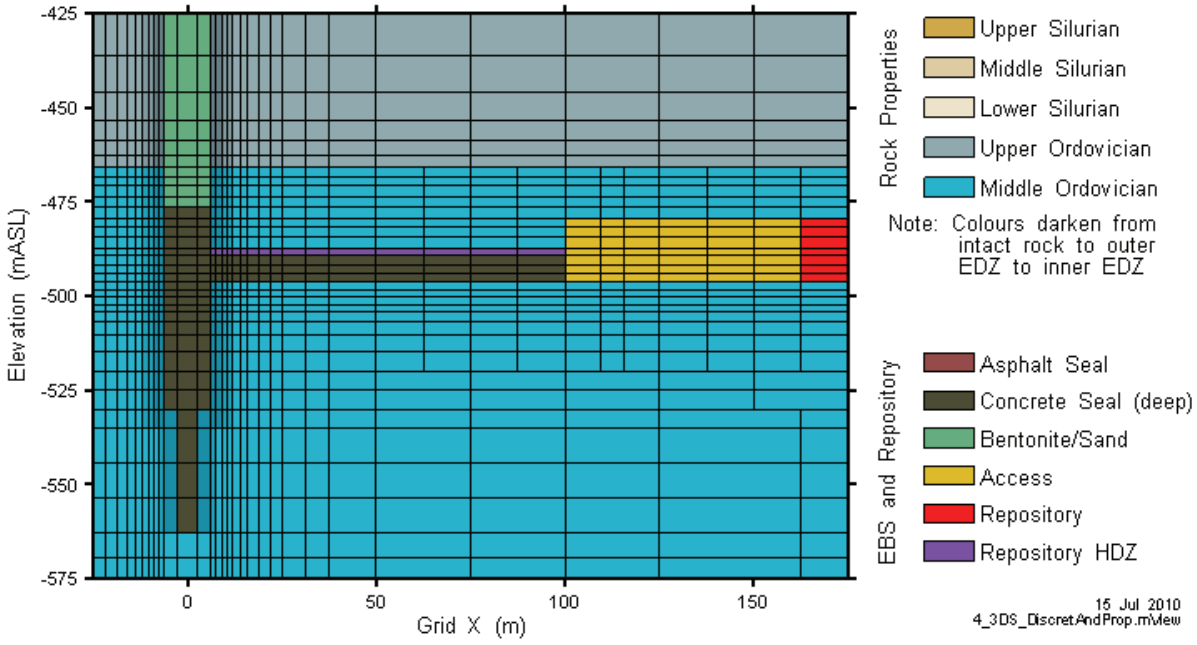

Figure 4.16: 3DD Model Cross-Section View – Property Assignment near Monolith

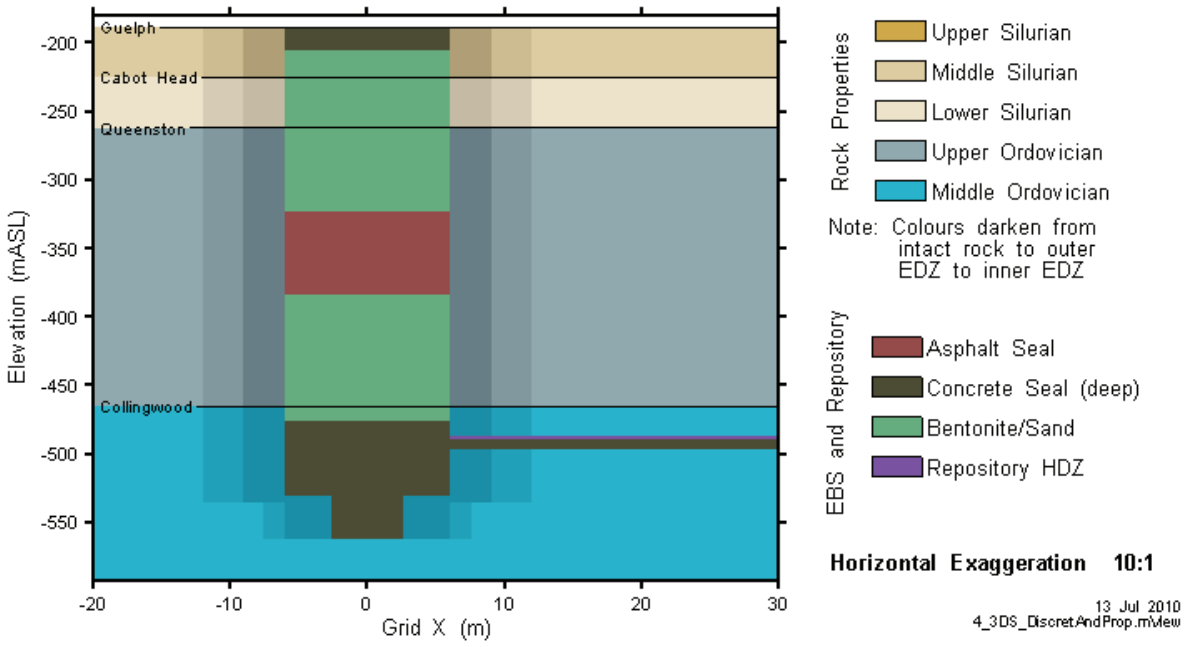

Figure 4.17: 3DD Model Cross-Section View – Property Assignment in Shaft

Figure 4.18 shows the vertical permeability of the system. Individual formations can be differentiated. The very high permeability contrast between the shaft and tunnels and surrounding intact rock is also evident.

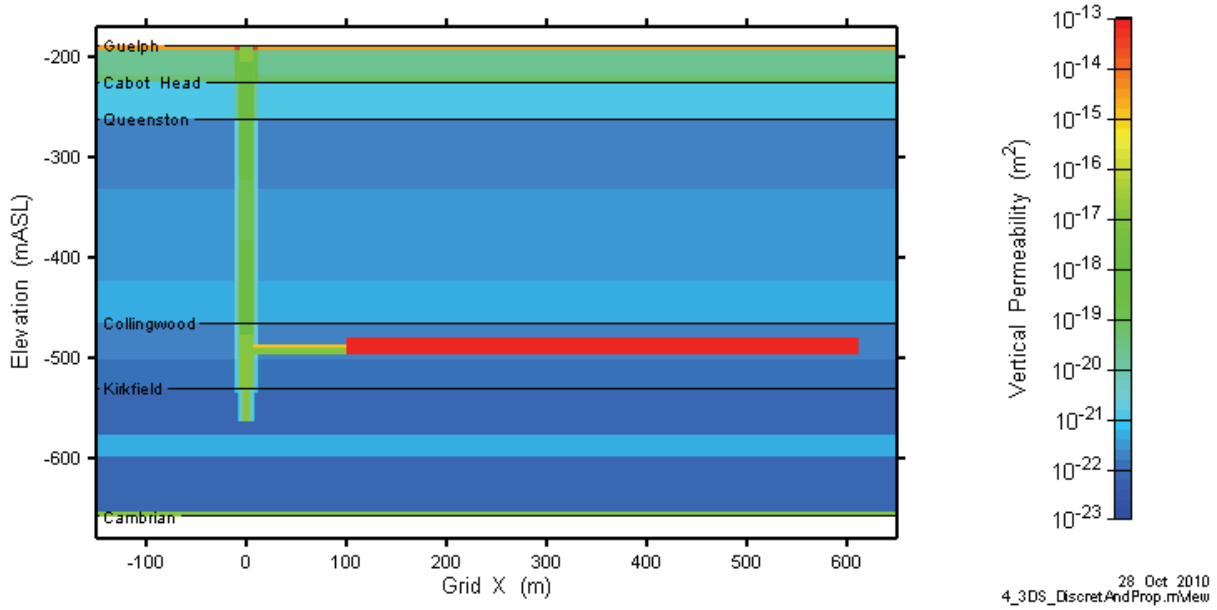

Figure 4.18: 3DD Model Cross-Section View – Vertical Permeability

Figure 4.19 is a three-dimensional illustration of the 3DD repository. As described previously, there is no EDZ surrounding the repository and the monolith. However, the layer of HDZ above the monolith provides a permeable connection which effectively transmits gas or liquid between the repository and the shaft.

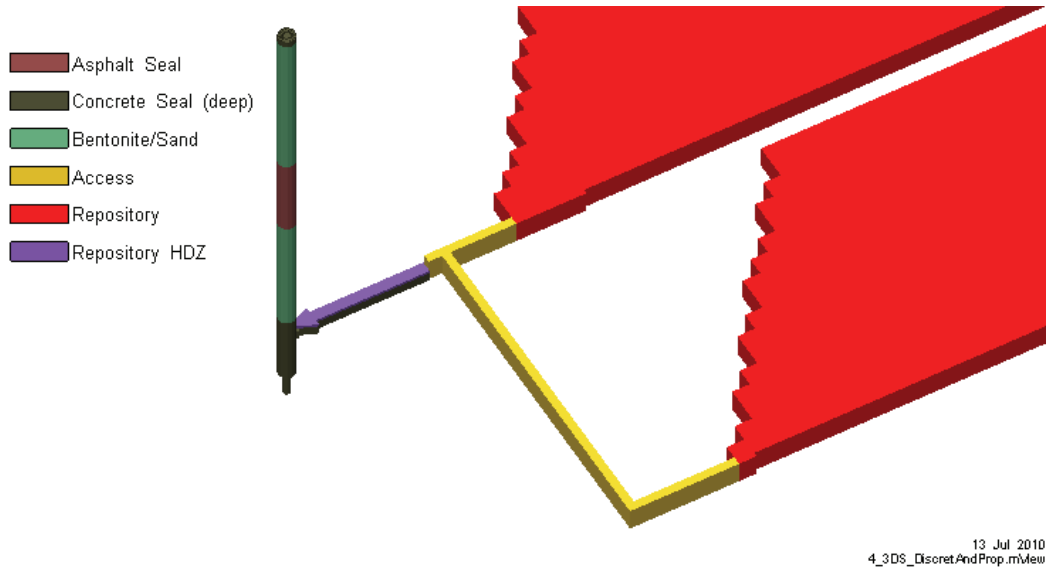

Figure 4.19: 3DD: Repository, Access Tunnels, Monolith, HDZ, and Shaft Sealing System

4.3.2.2 3DSRS Model

Compared to the 3DD model, the 3DSRS model is greatly simplified, having 10,089 nodes with 28,739 connections. The mesh is much coarser than the 3DD model (see Figure 4.20 through Figure 4.22).

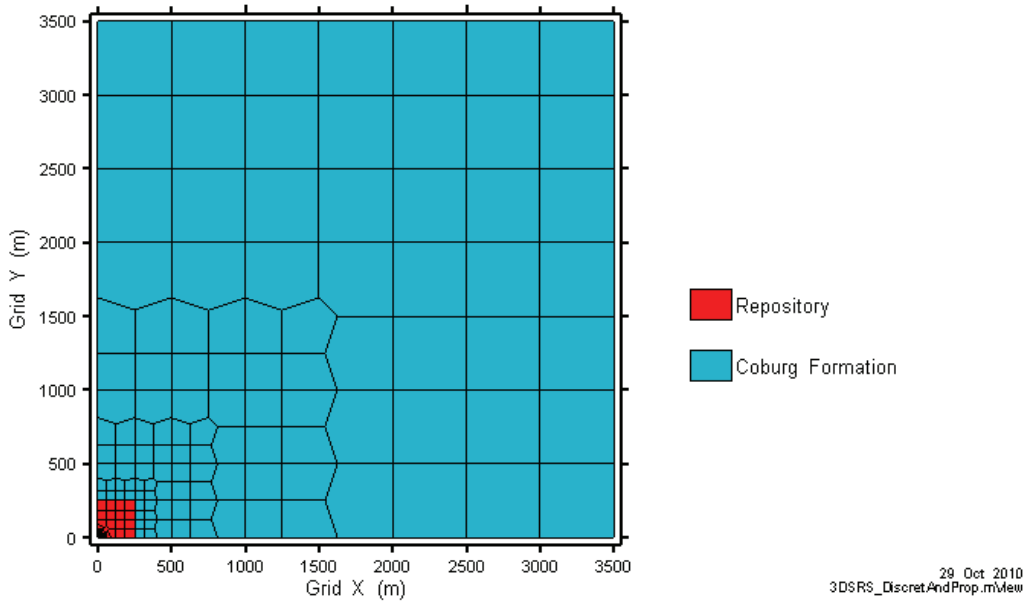

Figure 4.20: 3DSRS Model Plan Section View of Entire Model Domain (at Repository Depth)

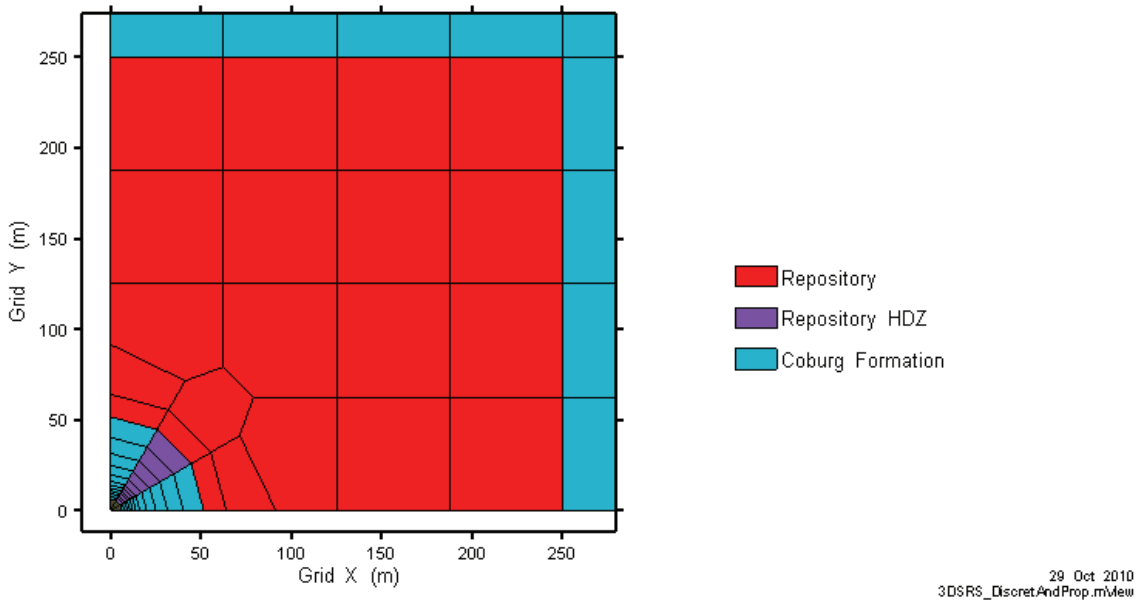

Figure 4.21: 3DSRS Model Plan Section View of Repository and HDZ (at Repository Depth)

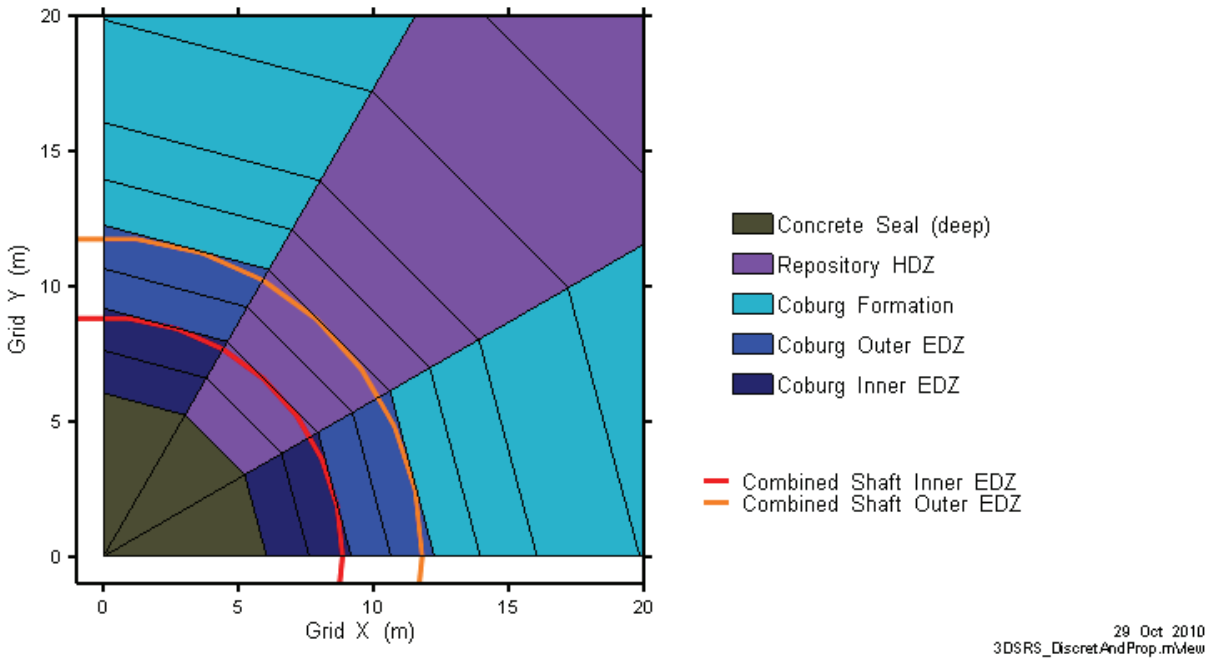

Figure 4.22: 3DSRS Model Plan Section View – Shaft, EDZ, and HDZ Detail

As shown in Figure 4.23 and Figure 4.24, the vertical discretization of the shaft system is similar to the 3DD model except there is no shaft extending below the repository. The figures portray a vertical slice at 45 degrees to show the HDZ, which is placed on a single line of elements to more closely approximate the actual geometry. Access tunnels are not represented in the 3DSRS model. Figure 4.25 is a three-dimensional illustration of the 3DSRS repository.

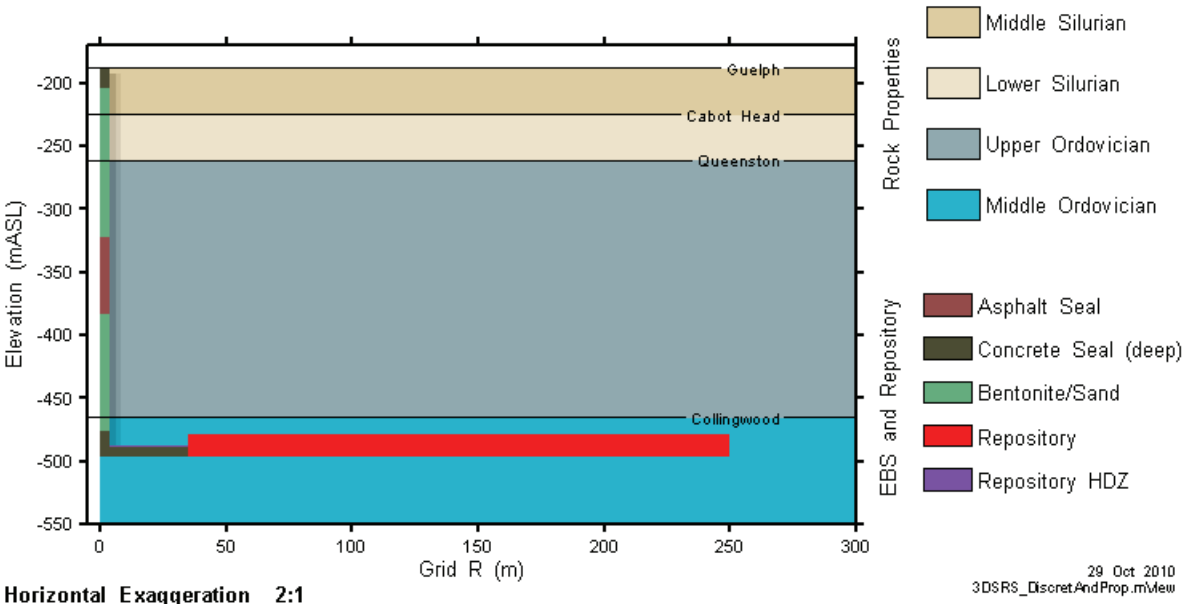

Figure 4.23: 3DSRS Model Cross-Section View – Property Assignment

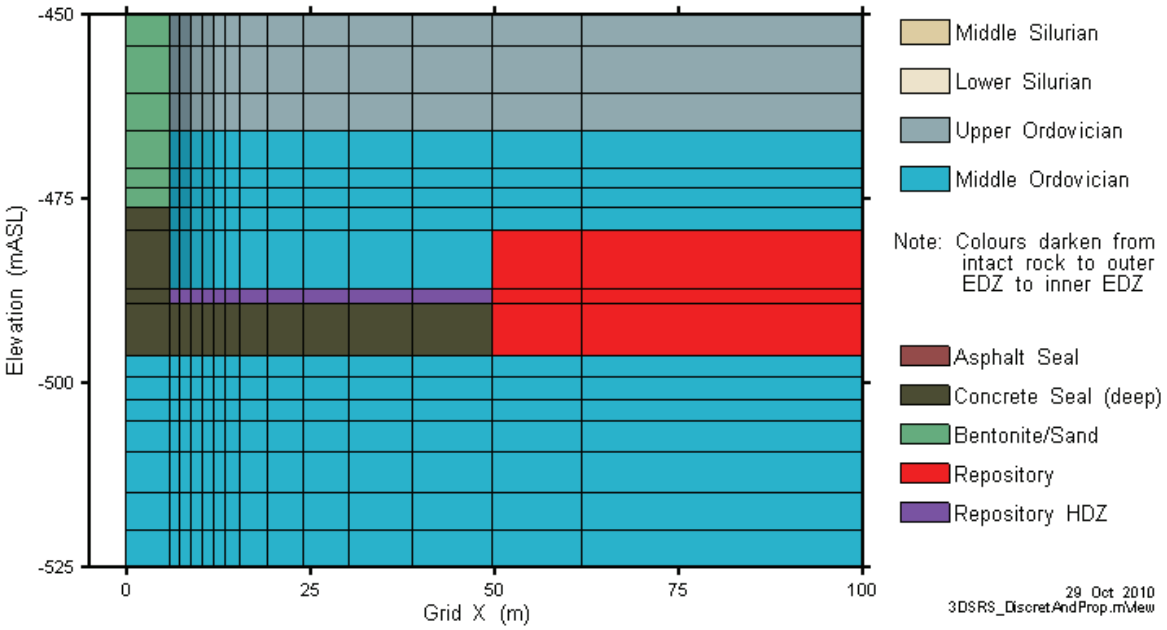

Figure 4.24: 3DSRS Detailed Discretization of Monolith and HDZ

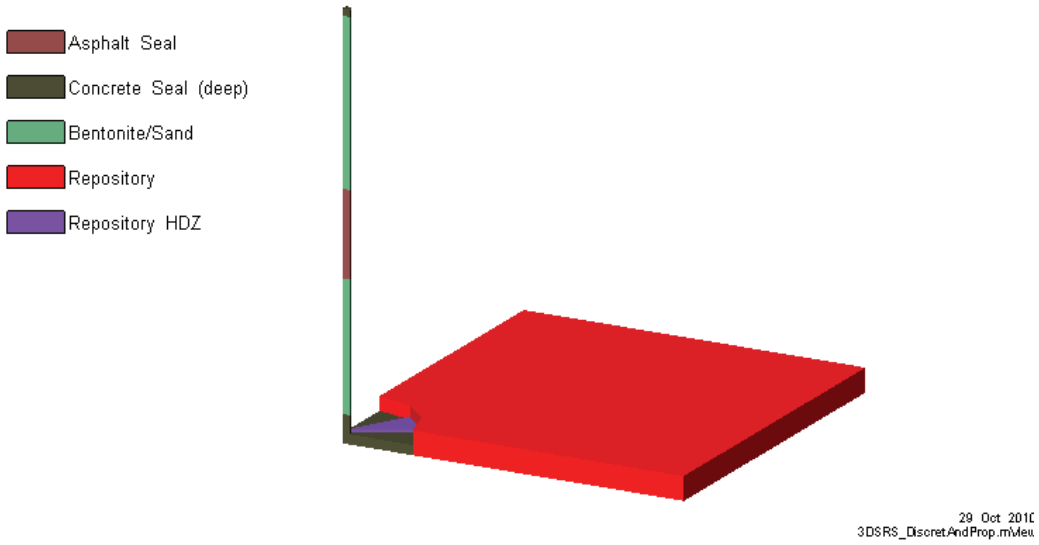

Figure 4.25: 3DSRS Model 3D Layout of Repository, Access Tunnels, Monolith, HDZ, and Shaft Sealing System

4.3.2.3 3DSR Model

The 3DSR model is a further simplified version of the 3DSRS, with the monolith, shaft seals, shaft EDZ and repository HDZ eliminated. It is essentially a repository located in the middle of the geosphere. The 3DSR model consists of 8710 nodes and 25 263 connections. Plan and vertical cross-sections are shown below in Figure 4.26 and Figure 4.27.

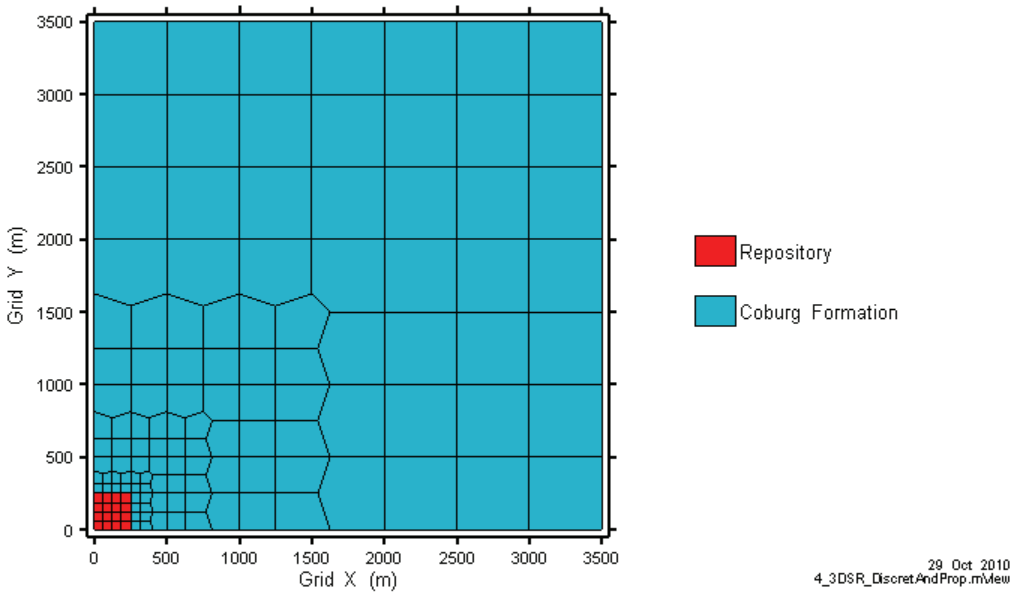

Figure 4.26: 3DSR Model Plan Section View of Entire Model Domain (at Repository Depth)

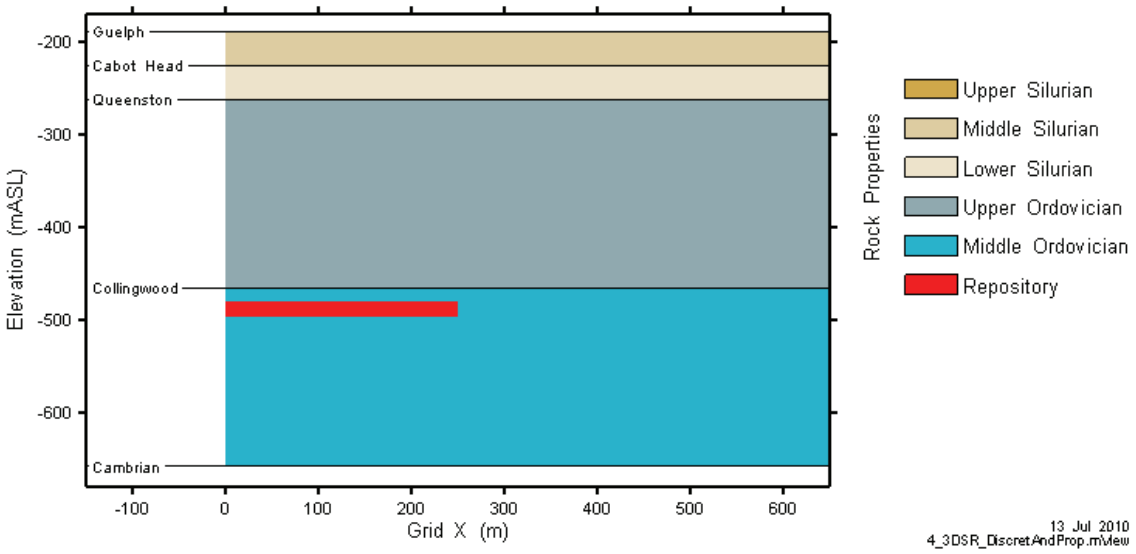

Figure 4.27: 3DSR Model Cross-Section View – Property Assignment

4.3.2.4 2DRS Model

The 2DRS model is a simple radial model designed to assess gas transport up the shaft, which is the primary pathway for gas leaving the repository. This model is a two-dimensional radial slice centered on the shaft and extending 500 m into the surrounding rock (see Figure 4.28). The model has 3040 nodes and 5953 connections, and covers a 2 degree arc.

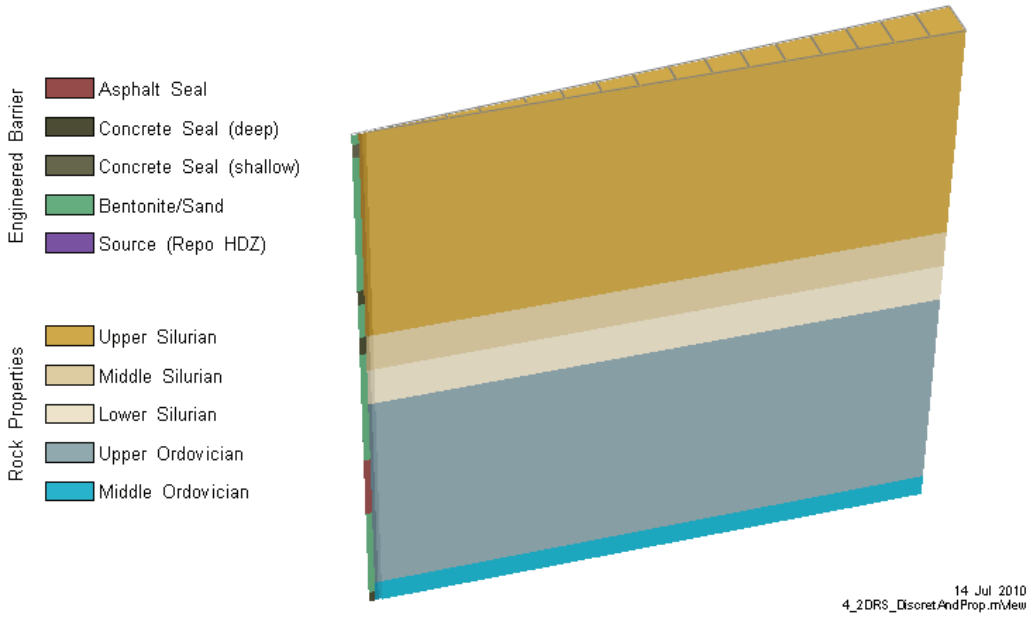

Figure 4.28: 2DRS Model Domain with Geology and Shaft Sealing System

The 2DRS postclosure model extends from the top of the supported access tunnel HDZ (the primary pathway connecting the repository and the shaft in the 3DD and 3DSRS models) to the top of the Salina G formation (the bottom of the Shallow Bedrock Groundwater Zone) (see Figure 4.29). As described in Section 4.3.1 and Figure 4.6, a 2DRS intact rock model was used to generate initial conditions for the 2DRS preclosure model. This model has a very similar structure to that in Figure 4.28, but extends down to the top of the Cambrian, and does not include the shaft and engineered barrier system.

Figure 4.30 shows a detail of the grid and property assignment in the lower left corner of the model domain. Of particular interest in this figure is the source location and property assignment at the base of the shaft EDZ. In the model, these source nodes are defined as very large volume nodes that are always gas saturated. Gas is injected into these nodes at a rate that will reproduce the repository pressure evolution calculated by the 3D models.

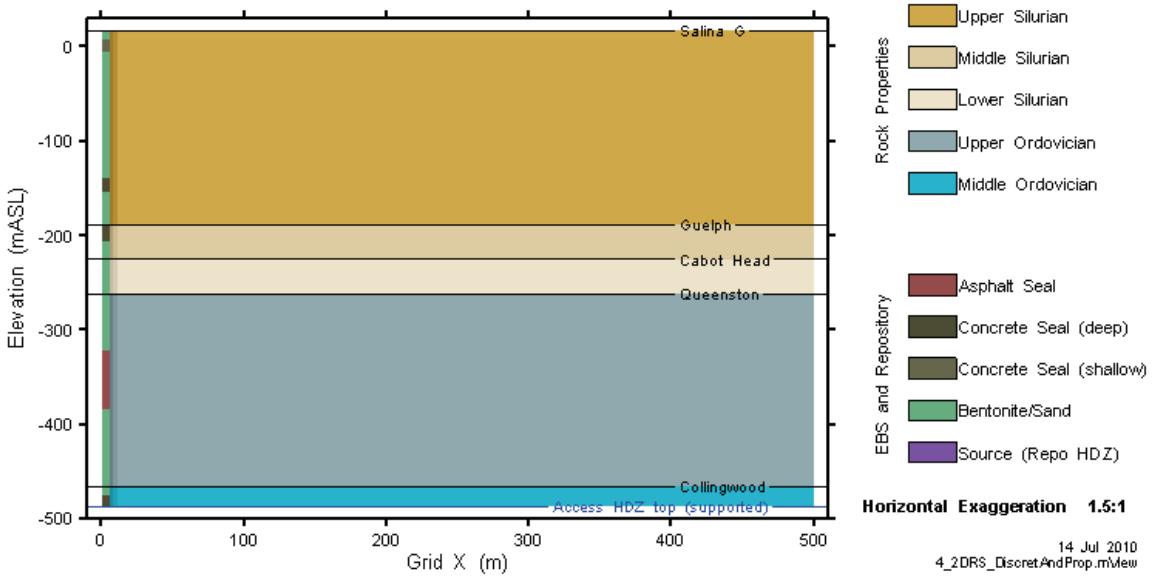

Figure 4.29: Cross–Section of 2DRS Model Domain with Geology and Shaft Sealing System

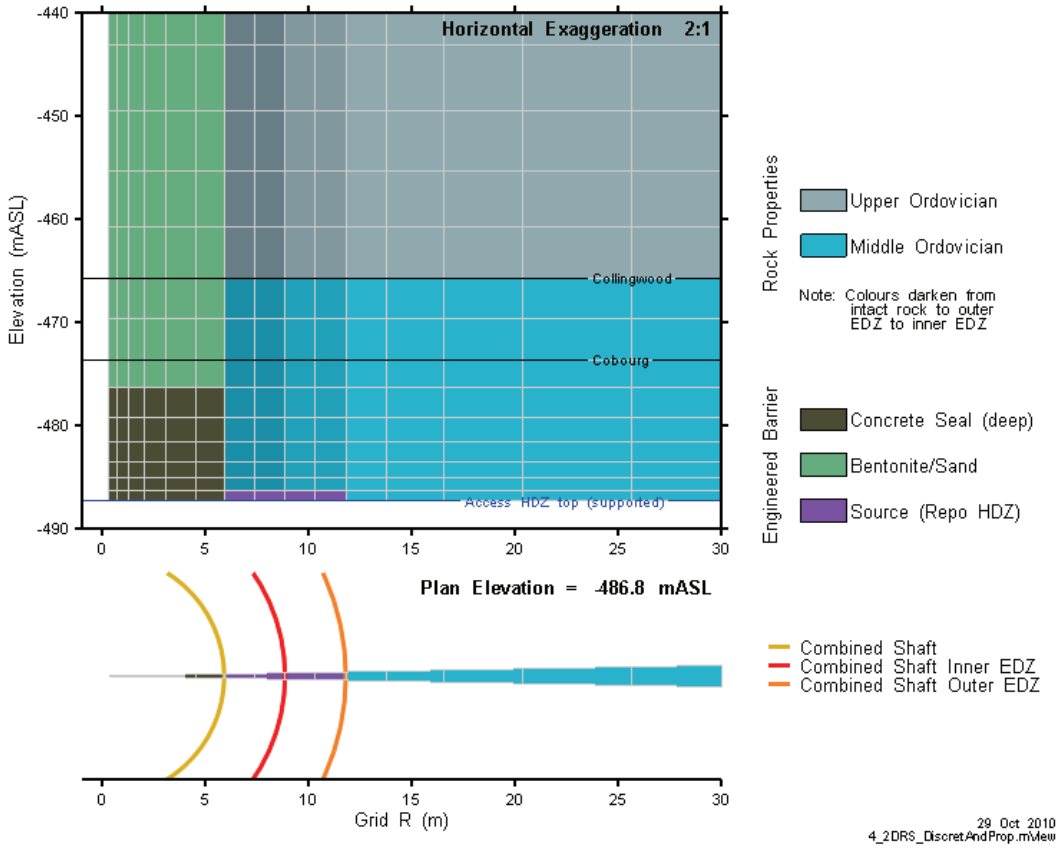

Figure 4.30: 2DRS Grid and Property Assignment near Base of Shaft

4.3.3 Boundary and Initial Conditions

4.3.3.1 Flow Boundaries and Initial Pressure Conditions

All models have fixed head boundary conditions on the top and bottom layers of the model, defining a vertical upward hydraulic gradient in the system. The 3D models assumes a 158 m total gradient, with the top model surface (at -190 mASL) defined with a head of 7 m, and the bottom surface (at -658 mASL) defined with a head of 165 m. The 7 m head was based on the steady-state simulated pressure for the NE-SBC 2DRS intact rock model and was corroborated by head for the NE-SBC case groundwater model (Section 5.3.1 of GEOFIRMA 2011).

For the 2DRS model, the head at the top of the system was set to 0 m. Applying this head at the top of the Salina F Formation assumes no substantial vertical gradients in the Devonian system, which is slightly conservative for these transport calculations below Salina F. These heads are converted to the absolute pressures required by T2GGM based on the depth below ground surface plus imposed head converted to pressures, assuming a density of 1000 kg/m^3. Atmospheric pressure is taken to be 101.3 kPa.

The 2DRS model cannot account for lateral advective flow in the model domain. All flow is radial, vertical, or a combination of the two. The external boundary at R = Rmax (where Rmax = 500 m) is zero-flow, for both gas and groundwater. The boundary is sufficiently distant so as not to significantly affect simulation results.

The 3DD, 3DSRS, and 3DSR models are also assigned zero lateral flow boundaries, but these boundaries are located at a much larger distance from the repository. All 3D models neglect regional horizontal flow within the more permeable Guelph Formation. This is a reasonable assumption as the site characterization information indicates that any flow in these units is slow, and neglecting the flow is conservative as this maximizes any contaminant upward flux through the shaft above the repository.

For all cases except the NE-RC, NE-RC1, and NE-RC2, the models are first simulated without the repository and shaft/EDZ (i.e., just the intact rock system) to obtain a steady-state pressure profile for the initial conditions in the rock mass. For the NE-RC, NE-RC1 and NE-RC2 cases, the initial rock mass pressure profile is developed directly from the DGR-4 environmental head profile (see Figure 2.3).

The initial rock mass pressures are then combined with atmospheric pressures in the repository, tunnels and shaft to provide the initial pressure conditions for a preclosure, or operational, period of 60 a.

Pressure and saturation results from the end of the operational period are then combined with specified initial saturations in the shaft seal materials (see Section 4.3.3.2 below) to produce initial conditions for the postclosure simulations.

4.3.3.2 Gas Saturation Initial Conditions

The NE-RC and NE-RC1 cases include initial gas saturations in the intact geosphere of 10% and 5% respectively. These represent saturations above (NE-RC) and at (NE-RC1) the assumed residual gas saturation of 5%. For the NE-RC2 case gas saturations are initialized on a formation basis at the measured values given in INTERA (2011).

For all other cases, the rock mass was assumed fully saturated with water. This simplifying assumption was made due to the uncertainty in two-phase flow parameters and in the magnitude of initial gas saturations. This assumption is conservative with respect to gas generation in the repository as it maximizes the inflow of liquid available to sustain reactions. It is non-conservative with respect to flux of gas through the intact rock; however, results show that this pathway is insignificant in all cases.

The repository and tunnels are initially full of gas, except for the bottom layer of the repository, where an initial water saturation is assigned representative of the initial mass of available or unbound water in the waste of 5.0×10^5 kg (Section 3.4.1 of QUINTESSA and GEOFIRMA 2011a).

The bentonite/sand shaft seal materials were assumed initially saturated with gas at 20%. Concrete initial gas saturation was 50%, and the asphalt seal was 100% gas saturated in the porosity. This represents the partial saturation of the shaft materials when emplaced. These values are discussed in Section 4.7.5 of the Data report (QUINTESSA and GEOFIRMA 2011a).

4.3.4 Gas and Water Source Terms

The GGM component of the T2GGM model calculates the gas generation and water consumption rates within the repository. These source terms are then applied to the TOUGH2 component of the T2GGM model. TOUGH2 is responsible for simulating the flow of water and bulk gas into and out of the repository (see Figure 2.1).

Unlike TOUGH2, GGM does not model any spatial dependence within the repository. Instead it treats the repository as a specified volume within which the time dependence of the gas generation processes is modelled in detail. The following are explicitly modelled within the repository: the evolution of the individual gas components (partial pressures, concentrations in the saturated phase and total amounts within the repository and leaked from the repository); the generation/consumption of water due to the reactions; metallic wastes and their corrosion; organic wastes and their degradation; terminal electron acceptor stages; biomass recycling; and corrosion and degradation products (see Chapter 4 of QUINTESSA and GEOFIRMA 2011b).

As input, GGM takes information about the current (repository averaged) total gas pressure, saturation, water inflow from the geosphere, relative humidity (RH), repository void volume and molar mass of bulk gas from TOUGH2. For the water-limited (WL) simulations, RH is calculated to a reduced value as the repository approaches a fully unsaturated state. This reduces gas generation reaction rates to balance with water inflow from the geosphere. The gas pressure and saturation are used to determine the flux of gas out of the repository.

As output, GGM calculates the rates of gas and water production and/or consumption within the repository as a whole. For gas, GGM calculates gas generation rates for individual gas components, and then calculates a molar equivalent rate of bulk gas for the TOUGH2 source term. These rates for the whole repository are distributed spatially by TOUGH2, with gas injected into or withdrawn from specified repository elements. GGM calculated water production and consumption is similarly distributed through repository nodes for WL simulations. NWL simulations ignore GGM calculated liquid consumption or production.

For the Non-Water-Limited cases, the generation or consumption of water by reactions within the repository is not included in the repository water balance. For the Water-Limited cases, it is included.

4.4 Audit of Features, Events and Processes

The Features, Events and Processes (FEPs) report (QUINTESSA et al. 2011b) presents a comprehensive review and screening of FEPs that are relevant to the conceptual models developed for the Normal Evolution and Disruptive Scenarios. Appendix A presents an audit of the FEPs to indicate which FEPs are addressed in the detailed gas modelling presented in this report and which are excluded. Reasons for exclusion are given and include: not applicable to DGR; not applicable to the current gas transport model; simplifications in modelling approach in the T2GGM models; and considered in safety assessment modelling using AMBER rather than detailed gas modelling using T2GGM.

5. RESULTS FOR THE NORMAL EVOLUTION SCENARIO

This section presents the detailed modelling results for the Normal Evolution Scenario. For each case, results are presented and discussed for:

- Gas generation within repository; and
- Transport of gas, both in gaseous form and dissolved form, out of the repository and into the shaft and rock mass, and water flow from the rock mass into the repository.

The Reference Case and Simplified Base Case are presented in detail, and all other cases are then compared (See Section 3.1 for description of all Normal Evolution Scenario cases).

The results presented here are based on the more conservative Non-Water-Limited assumption for repository reactions. Water-Limited results are presented in Section 7.

Most results are presented based on analyses of the original preliminary design. Specific analyses for the final preliminary design are presented in Section 5.15, Section 5.16 and Section 7.5.

It is useful to briefly describe some terminology and visualization conventions here before actual results are presented.

For gas generation figures, the evolution of all quantities is given as a function of time in years on a logarithmic scale. All concentrations are given per volume of water unless otherwise stated. Stack plots are used to demonstrate mass balance. Each band on the stack plot represents a different form that the given quantity can be in. The thickness of a band on a stack plot shows the number of moles of the quantity that is currently in the given form. Some quantities can take negative values (such as the amount of water that has entered the repository if more has left than has entered), in which case the band is shifted by a constant value to ensure a positive band thickness. Mass balance is demonstrated by the sum of all contributions – that is the height of the stack – being constant. The y-axes of some plots have been given a logarithmic scale, in which case this is indicated in the figure caption.

For most advective velocity gas transport figures presented in this report, velocity vectors are shown only for those regions where velocities exceed 10^{-4} m/a (i.e., at least 100 m of advective transport in 1,000,000 a). In general, the vector length is scaled by log velocity, however the scaling factor varies depending upon figure scale, and vector lengths should be regarded as a qualitative indication only.

The term “repository” refers to the repository and unsealed access tunnels, unless specified otherwise, as the gas and water flow processes in the two model zones are generally the same.

Use of the term “gas” refers to the free-phase gas, and includes water vapour, although this is usually only a trace component. “Dissolved gas” refers to the gas dissolved in the water. "Bulk gas" refers to free-phase and dissolved gas. “Water” refers to the liquid groundwater present in the geosphere or repository. While water includes dissolved gas, the dissolved gas is a dilute component of the water. T2GGM simulations presented in this report assume fresh water as the liquid phase within the gas transport model.

Gas saturation is the volumetric proportion of the porosity occupied by free-phase gas. Liquid saturation is the volumetric proportion of the porosity occupied by water, and is equal to one minus the gas saturation. Gas saturations are presented to show the extent of gas transport

within the shaft and geosphere, and only gas saturations greater than 10^{-4} are shown unless otherwise noted. Areas with liquid saturation greater than 0.9999 are shown as blank on gas saturation figures. Dissolved gas is only present if liquid is present, and is only shown on figures in areas where: a) the dissolved gas concentration exceeds 10^{-4} kg/m^3, and b) where liquid saturation is greater than 10%.

Summary figures presenting repository pressures and liquid saturations are shown for most cases. On the pressure figures there are horizontal lines indicating "Model steady-state pressure at repository" and "Freshwater hydrostatic pressure at repository". The former is the steady-state liquid pressure that the model would attain in the absence of a repository. The latter is the pressure of a column of fresh water at the repository horizon. The difference between these pressures represents the contribution of the overpressured Cambrian boundary condition to the system. For the NE-RC case and derived cases (NE-RC1, NE-RC2), the initial liquid pressures in the Ordovician system are much lower than the steady-state pressure. For all other cases, the steady-state pressures are the initial conditions for the preclosure models.

The simulations reported here use a single bulk gas in the geosphere and shafts. Consequently, there is no way to discriminate between gas generated in the repository due to degradation reactions, formation gas (in the NE-RC, NE-RC1, and NE-RC2 cases), and gas initially present in shaft sealing materials or repository (all cases). In nearly all cases, early time gas flows in the shaft, and dissolved gas in the vicinity of the shaft, are due entirely to gas present initially in the seal materials when they are emplaced.

In describing gas and water flows, the time in years is provided. Note that these times are restricted to the time resolution available for specification of model output. GGM results have a greater time resolution than spatial TOUGH2 results, and consequently TOUGH2 results are typically rounded to the closest 1000 a when discussed in the text.

Results are presented from 3DD, 3DSRS, 3DSR and 2DRS models. In general, 3DSRS results are used most extensively, with 3DSR results for comparison. Where 3DD results are available, they are used by preference, with 3DSRS results are presented for comparison. 3DSR results are used for cases where geosphere performance is the main issue (NE-GT1, NE-GT2, NE-GT3, NE-RC1, and NE-RC2). 2DRS results are used to show transport processes above the vertical limits of the 3D models in cases where free-phase gas transport up the shaft is indicated by the 3DSRS or 3DD model results.

5.1 Reference Case (NE-RC)

This section provides a detailed description of gas generation and transport for the Reference Case (Table 3.1). The case assumes an initial Cambrian overpressure (+165m), initial underpressures, and initial gas saturations of 10% in the Ordovician formations. The Reference Case model was simulated with all three 3D models.

5.1.1 Gas Generation

Gas generation results discussed below are based on 3DSRS model results.

5.1.1.1 Terminal Electron Acceptor Stages

Figure 5.1 shows the terminal electron acceptor stages. These are:

1. Aerobic degradation;
2. Nitrate reduction;
3. Ferric iron reduction;
4. Sulphate reduction; and
5. Methanogenesis.

The first four stages complete within a decade. The third and fourth stages are short due to the small initial inventories of ferric iron and sulphates.

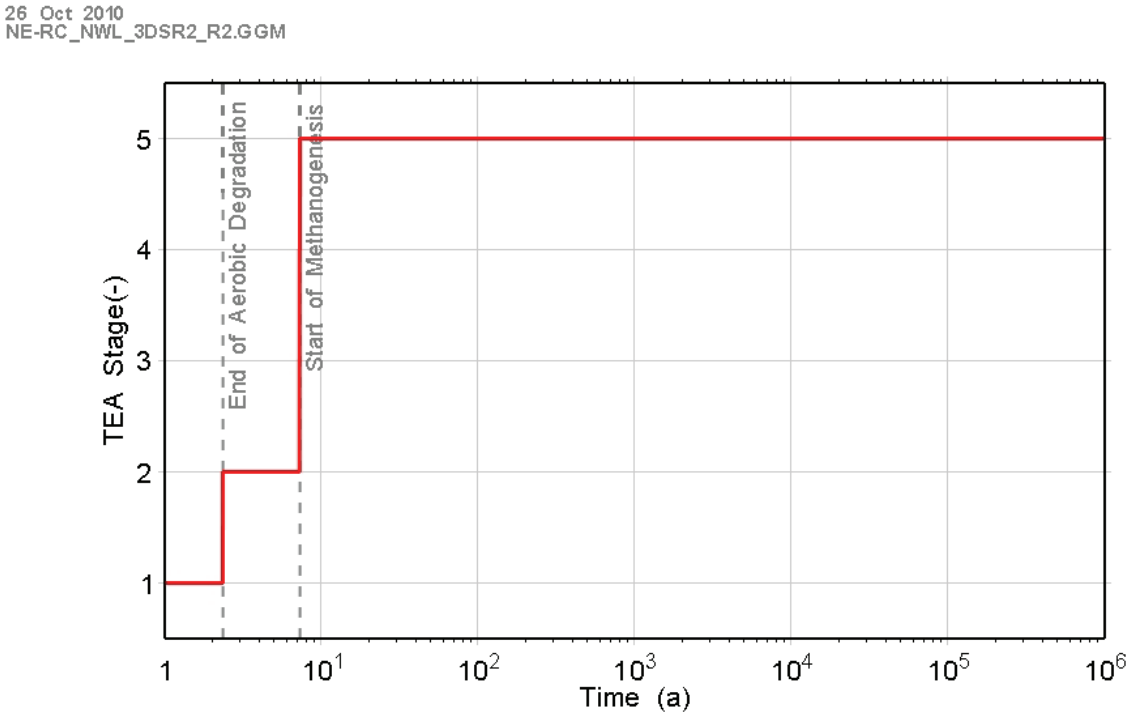

Figure 5.1: NE-RC: Terminal Electron Acceptor Stages

5.1.1.2 Water Balance and Saturation

Figure 5.2 describes the generation and flow of water for the repository. The water profile (solid dark-blue line) evolves in response to geosphere gas and water flow, build-up of gas pressure and flux of gas between the repository and geosphere, but is not affected by the consumption of water due to gas generation as this is a non-water-limited case. The amount of water that entered from the geosphere is shown as a dotted line. This can be seen to follow the profile for the amount of water in the repository. Water vapour entering or leaving the repository is negligible (less than 10^5 mol).

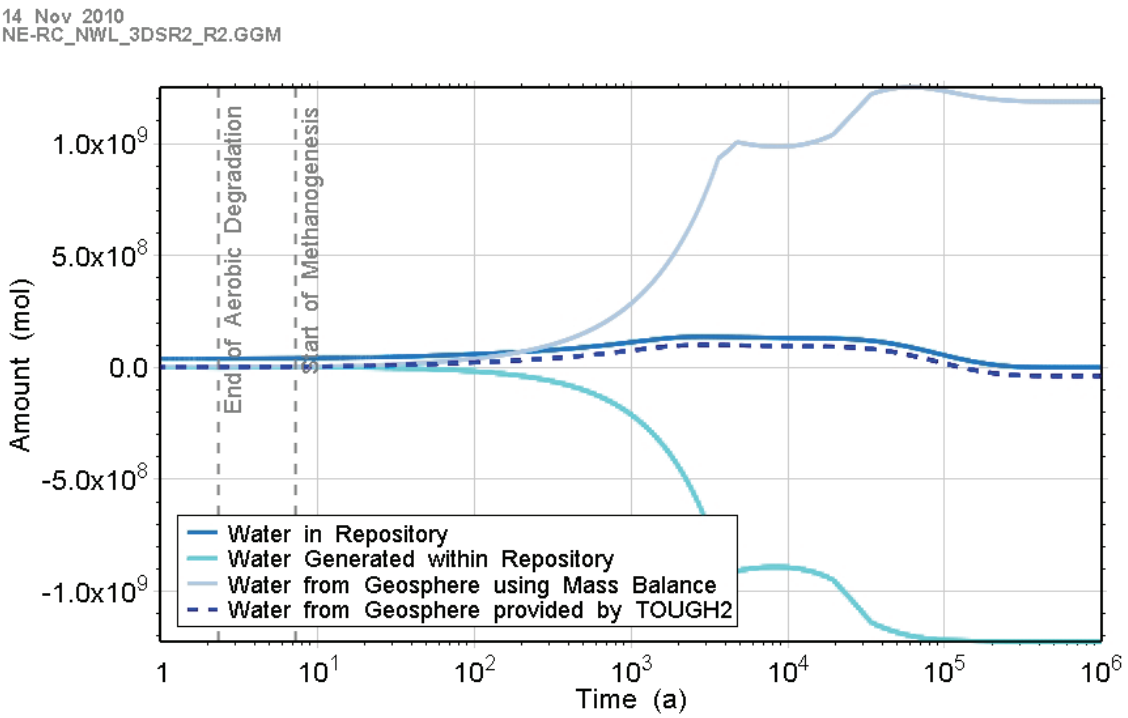

Figure 5.2: NE-RC: Water Sources

The cyan line shows the amount of water that the gas generation reactions would consume and the dark blue line shows the amount of water that would have had to enter from the geosphere to maintain the observed water level. This additional amount of water is approximately 2 m^3/a. If the water consumed by gas generation reactions is taken into account, then the water saturation drops to zero much sooner, resulting in water-limited conditions that inhibit gas generation. See Section 7.1 for a full account of this water-limited case.

The evolution of the repository water saturation is shown in Figure 5.3. This is the fraction of the void volume in the repository occupied by water, as calculated by T2GGM from detailed modelling of the distribution of water within the repository. Water seeps slowly from the surrounding host rock and shafts into the repository. Repository water saturation peaks at approximately 0.7% at 3000 a. Thereafter, a build-up of gas pressure, due to corrosion and microbial degradation of the waste, results in a reduction in the amount of water in the repository, reaching effectively zero saturation at approximately 300,000 a.

The implication of the expulsion of the small amount of potentially contaminated water is studied in the assessment modelling (QUINTESSA 2011a).

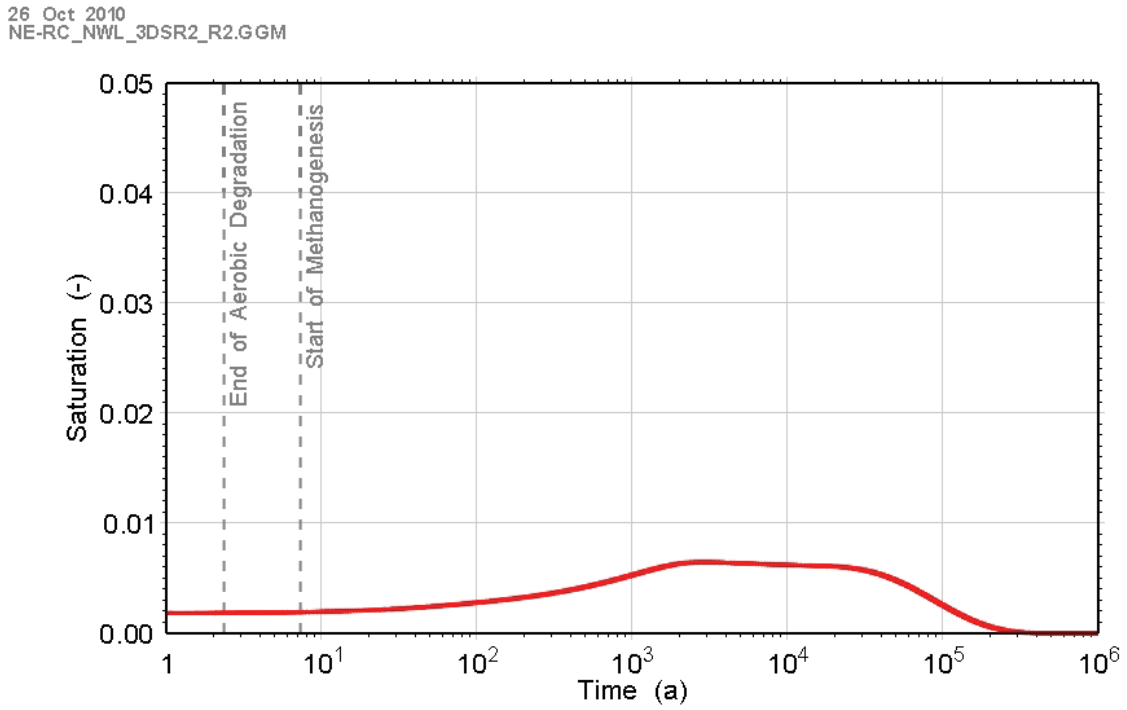

Figure 5.3: NE-RC: Water Saturation within the Repository

5.1.1.3 Gases

Figure 5.4 shows the evolution of the amounts of the gases in the vapour phase in the repository and Figure 5.5 shows the cumulative total amount of gas that has left the repository. The negative profile in this figure indicates a net influx of formation gas from the geosphere into the repository. T2GGM assumes this incoming gas makes no change to the existing composition of gas within the repository; since the geosphere bulk gas is methane and the repository is primarily methane, this is a reasonable estimate. There is no outflow of gas from the repository.

At approximately 8 a after the completion of the aerobic degradation and nitrate reduction stages, nitrogen is the dominant gas in the repository. There is then a short period of rapid gas consumption due to hydrogen oxidization via iron and sulphate reduction. This is associated with a small gas influx, partly a numerical artefact of the model mass balance for such a short pulse.

The general influx of gas from the rock is due to the initial gas content within the intact rock (10% gas saturation in the NE-RC reference case). Capillary pressure within the rock causes this formation gas to bleed into the repository, increasing the pressure above the hydrostatic level. After the water saturation reaches effective zero at approximately 300,000 a, the gas pressure evolution is dominated by this effect. This is a slow influx of about a few kg per year.

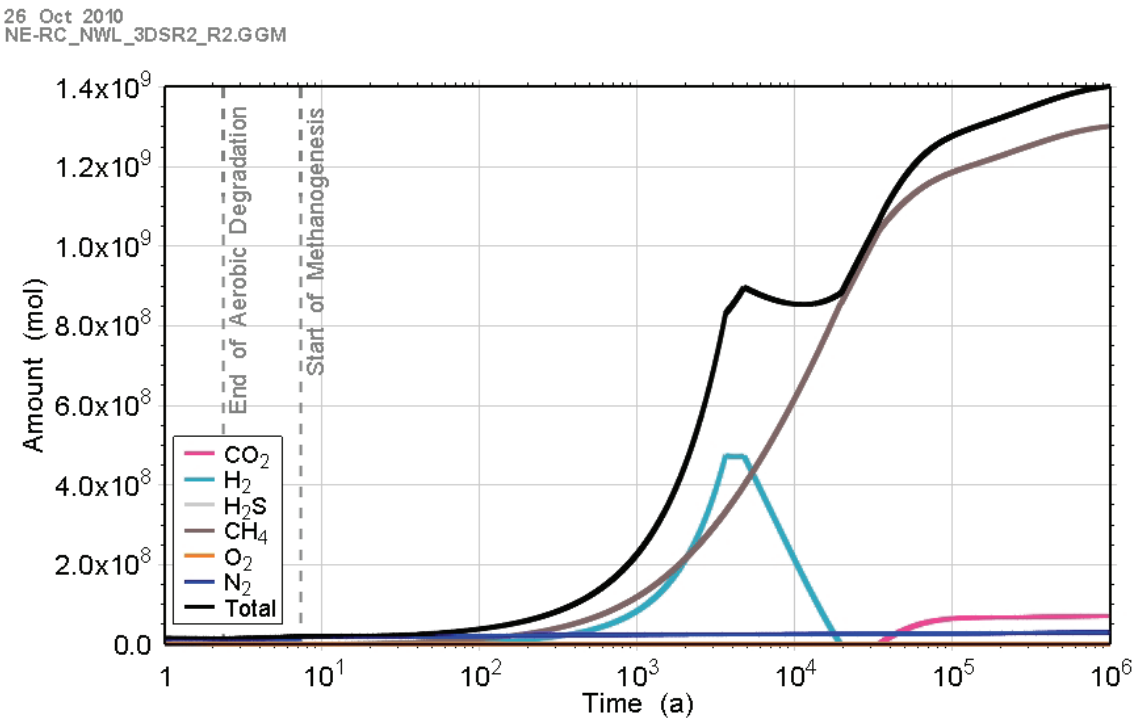

Figure 5.4: NE-RC: Amounts of Gases in the Vapour Phase within the Repository

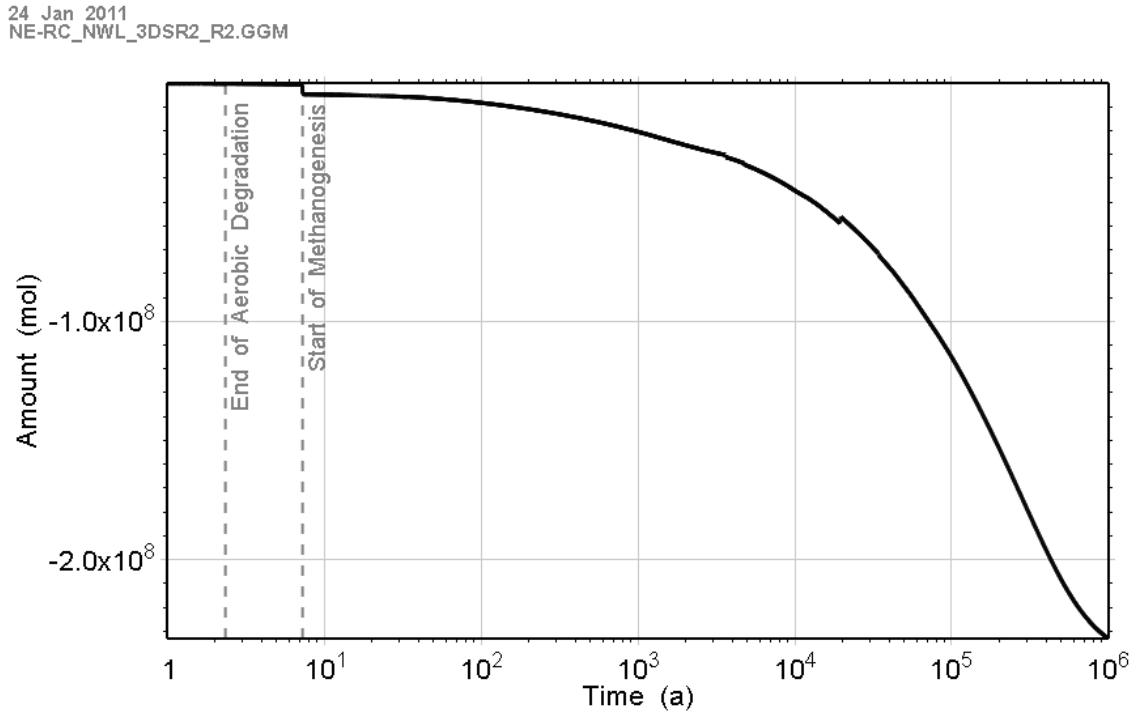

Note: The negative values indicate that (uncontaminated) gas has flowed from the geosphere into the repository.

Figure 5.5: NE-RC: Total Amount of Gas that has Left the Repository

Figure 5.6 gives the concentrations of the gases dissolved in the water saturated part of the repository. The calculated water vapour content (relative humidity) is provided in Figure 5.14.

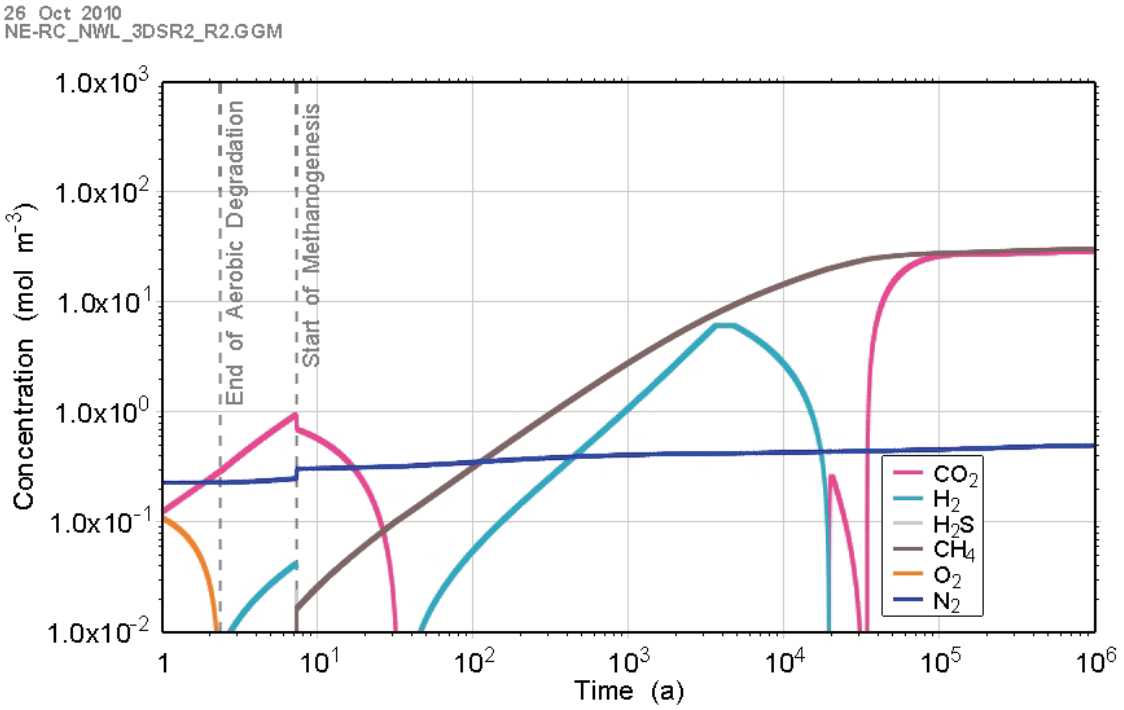

Figure 5.6: NE-RC: Concentrations of Dissolved Gas within the Repository (Log scale)

The gas partial pressures and total gas pressure within the repository are given in Figure 5.7. The total gas pressure undergoes its biggest rise during a phase of methane and hydrogen generation. A local peak of approximately 5 MPa is reached at approximately 5000 a. This local peak pressure can be checked using the ideal gas law (PV=nRT); the void volume of the repository ($V = 4.2 \times 10^5$ m^3); the total number of moles of gas in the repository at the time of peak pressure, determined from Figure 5.4 ($n = 9 \times 10^8$ mol); and a temperature of 22°C. This calculation yields a pressure of 5.2 MPa. After this time the pressure continues to increase above hydrostatic due to an inflow of gas (methane) from the geosphere, reaching 8.2 MPa at 1,000,000 a. This is discussed in Section 5.1.2.

The evolution of the individual gas components will now be described in turn.

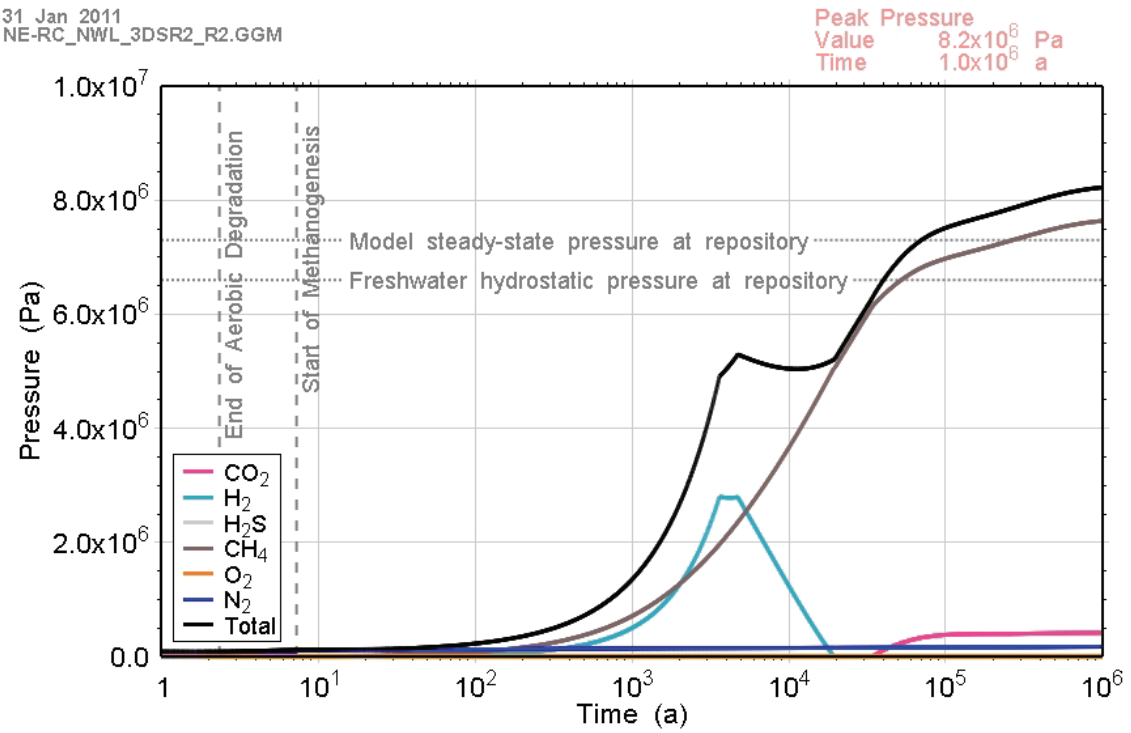

Figure 5.7: NE-RC: Total and Partial Gas Pressures within the Repository

Nitrogen

Apart from the nitrate reduction stage during which degradation of organic matter gives rise to the generation of a small amount of nitrogen, this gas is not involved in the corrosion, degradation or microbial reactions within the repository. The concentration and partial pressure of nitrogen within the repository remain fairly constant.

Methane

Methane is the dominant gas within the repository, produced by both the microbial degradation of organic wastes and the metabolism of carbon dioxide and hydrogen (Figure 5.4).

Most of the carbon initially in the organic waste streams is finally converted to methane gas. See the carbon atom stack plot, Figure 5.12. No mechanisms for the consumption of methane are modelled.

Methane generation through the degradation of organic wastes decreases as the organic wastes become degraded, ceasing at approximately 100,000 a. Thereafter, the increase in the amount of CH_4 is due to the inflow of methane from the host rock.

Methane generation via the microbial metabolism of carbon dioxide and hydrogen given in Equation (2-3) can proceed very rapidly. After 20,000 a, this reaction becomes limited by the availability of hydrogen and the rate at which it is produced through the anaerobic corrosion of the remaining stainless steel and nickel based alloys and zirconium alloy waste. See Figure 5.8.

Carbon Dioxide

Carbon dioxide is produced via the microbial degradation of organic wastes. Carbon dioxide production decreases as the organic waste streams are degraded and will cease once all the organic waste has been degraded – which occurs at approximately 200,000 a for the Reference Case. See Figure 5.11.

Carbon dioxide is consumed via the microbial generation of methane, the growth of biomass and via the enhanced corrosion of metallic wastes. It will also be controlled by chemical equilibrium with the cement within the repository, and the limestone rock around the repository.

Enhanced corrosion of the carbon and galvanized steels and the stainless steels and nickel alloys leads to a more rapid consumption of carbon dioxide when pressures are significantly higher than the reference partial pressure for enhanced CO_2 corrosion: 0.025 MPa (QUINTESSA and GEOFIRMA 2011a). Partial pressures of carbon dioxide rise sufficiently high for this to occur at approximately 30,000 a (see Figure 5.7). However, by the time this peak in CO_2 partial pressure has arrived, those metallic waste streams susceptible to enhanced corrosion have already been almost completely corroded (see Figure 5.8). Thus there is only a small increase in the corrosion product $FeCO_3$ at that time (see Figure 5.9) and enhanced corrosion due to high partial pressures of CO_2 does not play a significant role.

It is methane generation via the microbial metabolism of carbon dioxide and hydrogen which has the greatest impact on the evolution of CO_2 in this reference case. Sufficient hydrogen is generated from the metallic wastes to sustain this reaction, keeping the amount of CO_2 in the repository at a low level until those metallic waste streams are consumed at 300,000 a. Approaching this time the amount of hydrogen in the repository decreases as the metallic waste streams are corroded and hydrogen is finally completely consumed. The methane generation reaction then becomes limited by the rate at which hydrogen can be produced through the anaerobic corrosion of zirconium alloy wastes. Since the microbial methane generation reaction becomes hydrogen limited, CO_2 consumption is reduced and CO_2 accumulates in the repository until the organic wastes have been consumed.

Hydrogen

Hydrogen is produced by corrosion of metallic wastes. Hydrogen production decreases as each of the metallic waste streams are corroded and undergoes sharp decreases as each metallic waste stream is completely exhausted[2]. For example, it can be seen from Figure 5.8 that at 4 000 a, the carbon and galvanized steel wastes are exhausted. In this case, the rate of generation of hydrogen drops sufficiently to change the balance to net consumption of hydrogen (see Figure 5.4).

Hydrogen is rapidly consumed via the microbial generation of methane from carbon dioxide and hydrogen and is also consumed due to methanogen biomass growth. Once all hydrogen has been consumed, these reactions become limited by the rate at which hydrogen is produced through corrosion. Provided sufficient carbon dioxide is available these reactions will continue

[2] Note that these appear as step decreases on the timescale of interest, with the apparent sharpness enhanced by the logarithmic timescale. In practice, variability within the waste and the rates at which they corrode will smooth these transitions.

to consume all hydrogen made available through corrosion. It can be seen from Figure 5.4 that this occurs after 20,000 a.

Oxygen

During the initial aerobic degradation stage the oxygen initially present in the repository is rapidly consumed through the oxidation of organic wastes and aerobic corrosion of carbon and galvanized steels. Figure 5.1 and 5.7 show that this process is complete after just a few years.

Hydrogen Sulphide

The initial concentration of sulphates in the repository is sufficiently small that only a trace amount of H_2S is produced during the sulphate reduction stage. Incoming sulphate in groundwater is not explicitly included, but expected to be small due to the low water inflow rate. Insufficient H_2S is produced to show on the plots. Any H_2S produced precipitates rapidly to iron sulphide.

5.1.1.4 Metallic Wastes

The different types of metallic wastes can be seen to be consumed over time scales varying from 4000 a to more than 300,000 a in Figure 5.8. The various corrosion products are given in Figure 5.9. Figure 5.10 shows the complete balance of Fe atoms on a stack plot. It can be seen that only approximately 1% of the iron in the metallic waste ends up as $FeCO_3$ produced through enhanced carbon dioxide corrosion, with most ending up as Fe_3O_4.

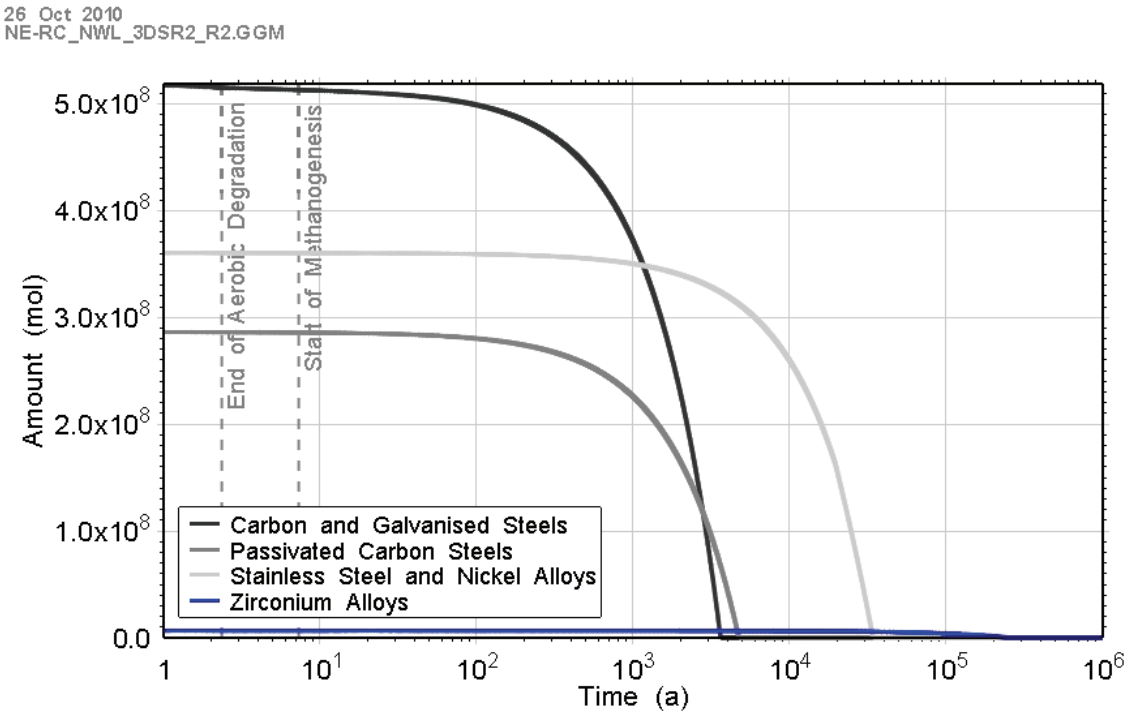

Figure 5.8: NE-RC: Amounts of Metallic Waste

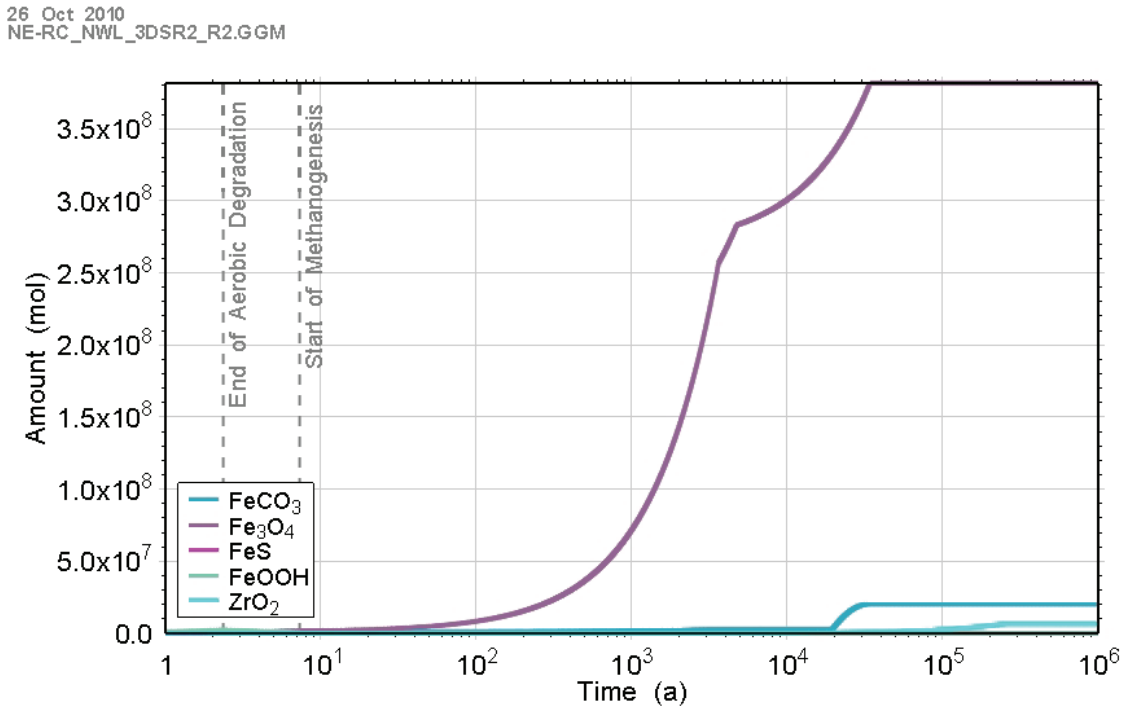

Figure 5.9: NE-RC: Amounts of Corrosion Products

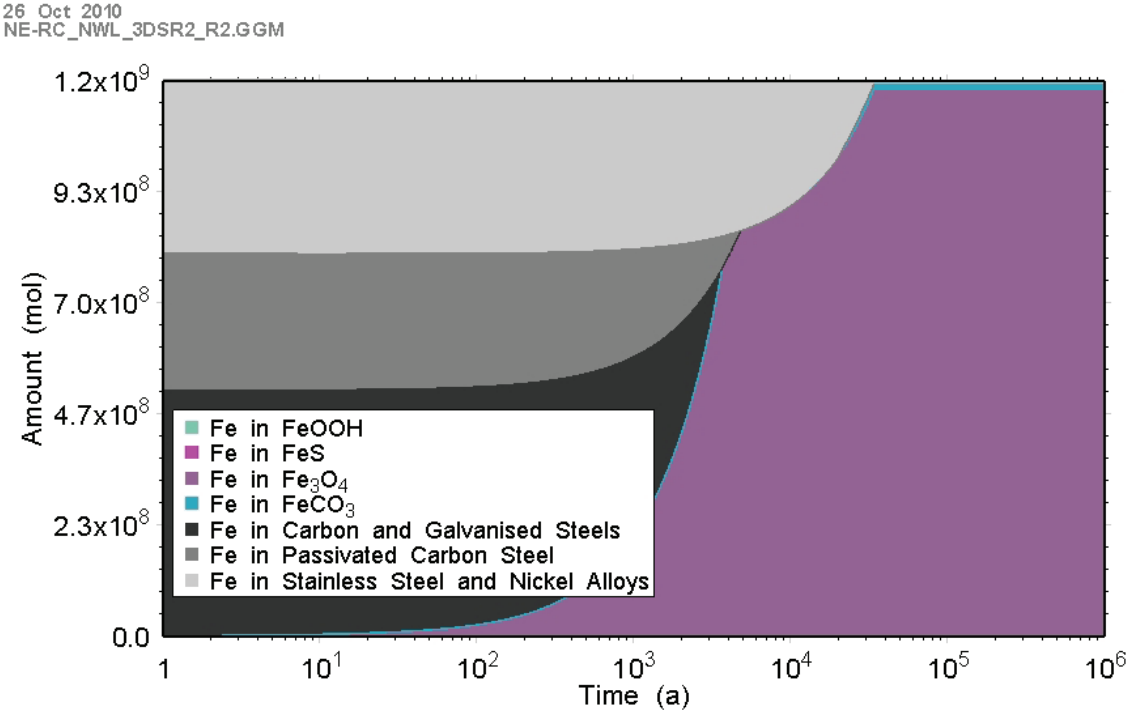

Figure 5.10: NE-RC: Iron Atom Stack Plot

About 2 x 10^6 mol of FeOOH are produced through corrosion by the end of the aerobic degradation stage, but this amount is too small to appear on the plots. The FeOOH is rapidly consumed under anaerobic conditions such that it is completely exhausted by the end of the nitrate reduction stage. It then plays no further part in gas evolution.

The generation of corrosion products slows each time a metallic waste stream is completely corroded. The complete consumption of the carbon and galvanized steels at 4000 a causes a drop in the rate of production of the Fe_3O_4 corrosion product for example (Figure 5.9). Production of corrosion products ceases once all the metallic waste streams are completely corroded at 400,000 a.

5.1.1.5 Organic Wastes

The degradation of the organic wastes is shown in Figure 5.11. Degradation of the waste streams is almost complete by about 100,000 a. Figure 5.12 shows the complete balance of carbon atoms. It can be seen that most carbon in the organic wastes ends up as CH_4 in the repository, while only a very small fraction becomes locked up in $FeCO_3$ or recalcitrant organic material.

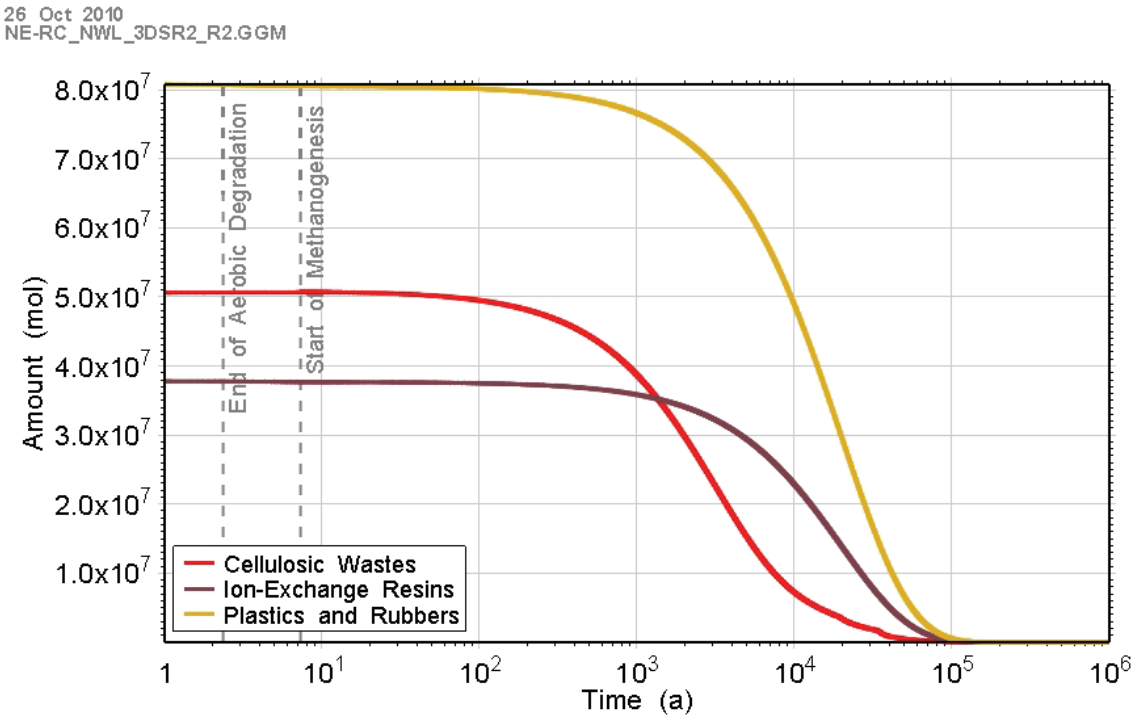

Figure 5.11: NE-RC: Amounts of Organic Waste

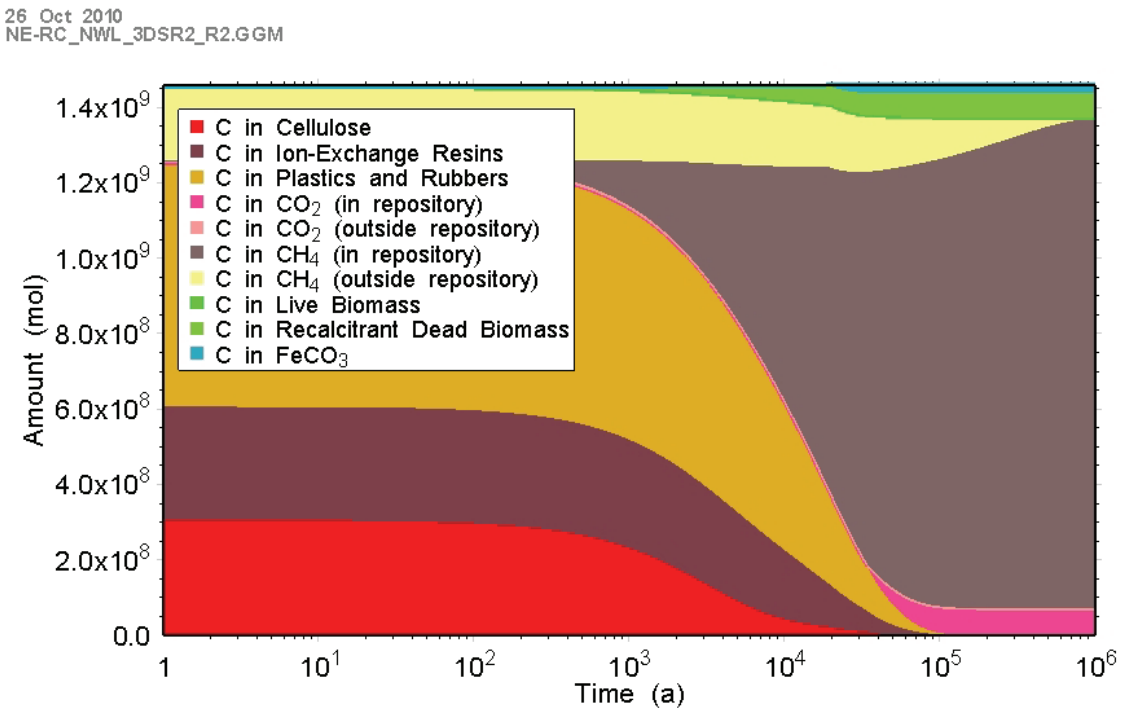

Figure 5.12: NE-RC: Carbon Atom Stack Plot

5.1.1.6 Biomass

The amounts of microbial biomass are given in Figure 5.13. During the long methane generation stage, biomass growth is limited by the availability of carbon dioxide and hydrogen. At approximately 20,000 a, hydrogen gas within the repository is completely consumed and from that point on methanogen biomass production is limited by the rate at which hydrogen is produced through corrosion, resulting in a decrease in the amount of live biomass.

Biomass growth consumes water and carbon. The water and carbon are subsequently released as the microbes die, and most of the organic carbon is decomposed and available for gas generation. A fraction of the microbial biomass (10%) is assumed to be recalcitrant and not decomposed on relevant timescale. The carbon atom stack plot shows that only a small fraction of the carbon atoms in the system originally in the form of organic waste end up as recalcitrant biomass. See Figure 5.12.

5.1.1.7 Relative Humidity

The relative humidity is calculated by T2GGM as the partial pressure of vapour divided by the saturated vapour pressure (at 20°C, this is 2340 Pa). In this (non-water-limited) case, the relative humidity remains at 100% for the entire simulation (see Figure 5.14), and vapour phase microbial and corrosion processes are fully active for the whole simulation.

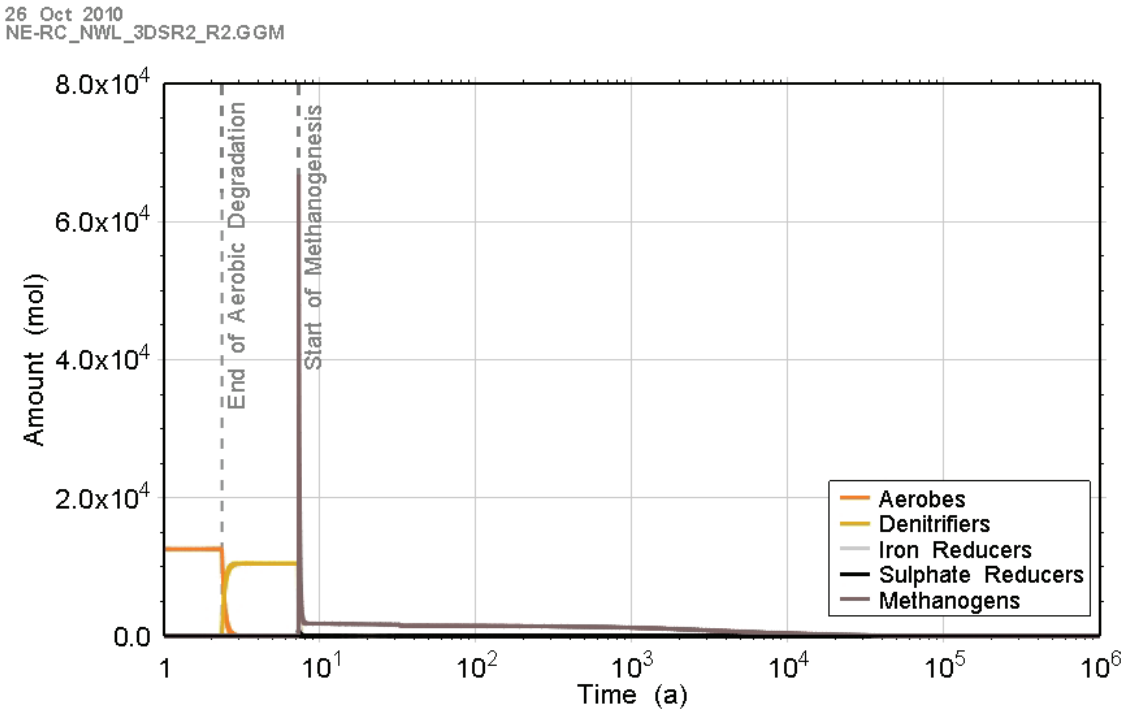

Figure 5.13: NE-RC: Amounts of Live Biomass

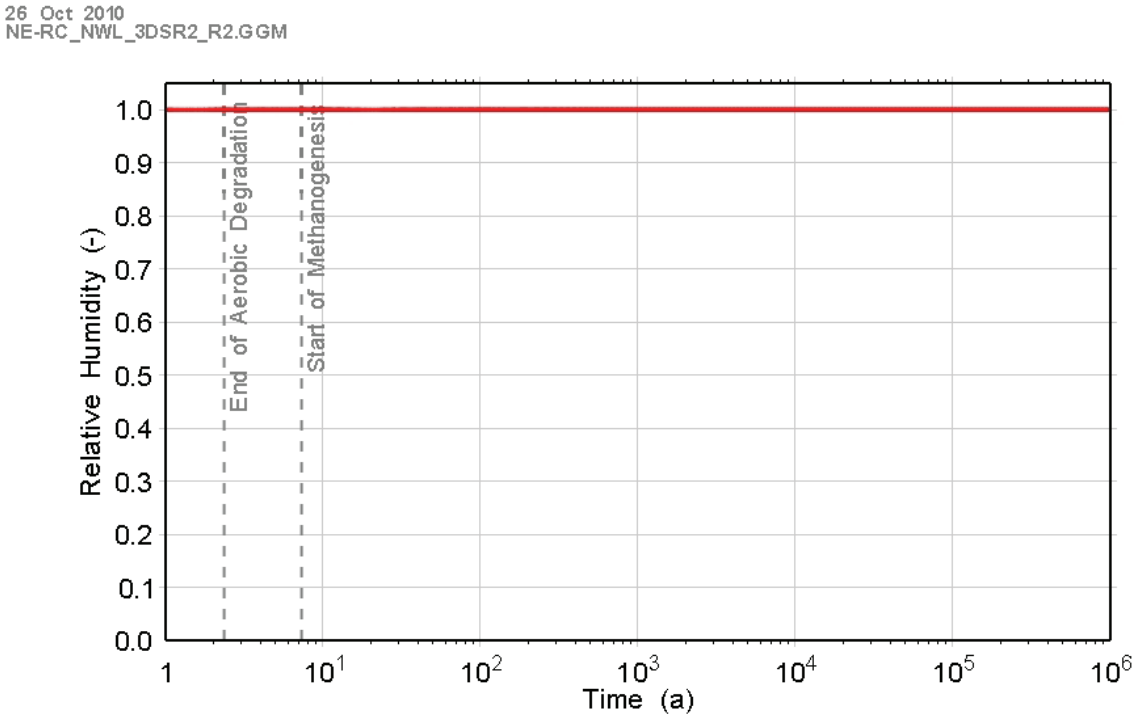

Figure 5.14: NE-RC: Relative Humidity

5.1.1.8 Gas and Water Generation

The rates of gas and water generation (or consumption) due to the various corrosion and microbial processes occurring within the repository are given in Figure 5.15.

The first few years involve sustained gas and water consumption due to aerobic degradation. There is a sharp peak in the rate of gas consumption (primarily hydrogen) and water production during the ferric iron and sulphate reduction stages due to hydrogen oxidation.

The longest sustained period of gas generation occurs during the organic degradation stage up to 4000 a. The gas generation here is primarily due to the production of hydrogen through the corrosion of the carbon and galvanized steels.

Gas and water generation rates then both continue to decline towards 1 million years as the waste packages become fully degraded.

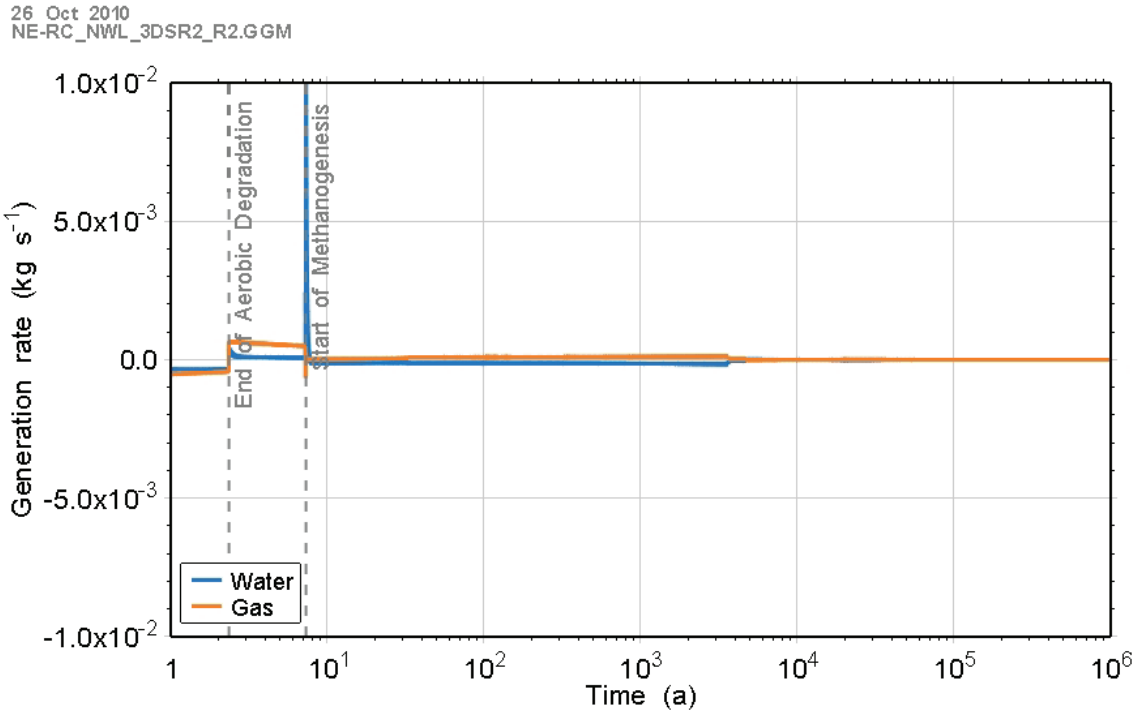

Figure 5.15: NE-RC: Gas and Water Generation Rates

5.1.1.9 Gas Generation Summary

- The oxygen, nitrates and sulphates initially present have virtually no impact on the long-term repository conditions stage during which the peak gas pressure occurs.
- Microbial activity is an important factor in causing gas generation. But biomass itself plays only a minor role in locking up carbon and limiting the amount of gas formed.
- The repository pressure approaches steady-state pressures at about 10^5 a, after the gas generation from the wastes has completed.

- The peak gas pressure is 8.2 MPa at 1,000,000 a. The continued rise of the peak pressure after 10^5 a is due to the slow inflow of gas from the geosphere.

5.1.2 Gas and Water Flows

Results presented in this section are primarily from the 3DD and 3DSRS model. Selected results from the 3DSR models are also presented for comparison. The description of shaft resaturation and repository behaviour is based on the 3DD model results, while the discussion of long-term geosphere behaviour is based on the 3DSRS model results.

The initial pressures for the models are calculated from the head profile presented in Figure 2.3. Initial geosphere gas saturations were set to 10%. The capillary pressure calculated using Equation (4-1) is approximately -13.7 MPa. Total pressure, or gas pressure, is used as initial conditions and is calculated as liquid pressure minus capillary pressure. In the van Genuchten formulation used by T2GGM, capillary pressure is a negative value or suction pressure, so the gas pressure is higher than the liquid pressure for all formations. The intact geosphere model (no repository) was simulated for a short period (100 a) to smooth some of the more abrupt head transitions. The slightly smoothed pressure profile was used as input initial conditions (pressure and saturation) for the geosphere in the preclosure model. The initial conditions in the repository and shaft system for the preclosure model are set to atmospheric pressure and 100% gas saturation. The preclosure model was simulated for 60 a. Results from the preclosure period are not presented here.

In turn, the calculated pressures and saturations from the preclosure model were used as initial conditions for the intact and disturbed geosphere in the postclosure model. Initial saturations in the shaft seal materials are as described in Section 4.2.2.

The presentation of these NE-RC Reference Case results is different than that for the subsequent Simplified Base Case and other calculation cases where a fully water saturated geosphere is assumed. The differences are as follows.

1. Pressure is presented in terms of liquid pressure which is total pressure plus capillary pressure (capillary pressure is always a negative value). This allows determination of liquid flow by gradient, although it leads to initial large negative pressures for bentonite and concrete (i.e., suction). Note that capillary pressures are zero in the repository, tunnels and asphalt seal.
2. Gas saturation is presented on a linear scale. The gas initially present in the geosphere or repository cannot be distinguished from gas resulting from gas generation reactions. The initial geosphere gas saturation of 10% also eliminates the ability to see small changes of saturation in the geosphere.
3. Dissolved gas concentrations are not presented. The model does not distinguish repository sourced gas from formation gas, and dissolved gas is prevalent in the geosphere since there is an initial gas phase present.

5.1.2.1 Shaft

The evolution of pressures and saturations in the shaft is due to both gas and water flowing into the shaft from the adjacent geosphere and vertical upward flows within the shaft seal materials driven by pressures transmitted from the repository. Figure 5.16 shows the general condition in the shaft immediately after closure. Note that the gas saturations in the rock mass are due to the initial saturation of 10% in the intact rock pore (about 1.5%). Liquid pressures in the rock

reflect the environmental head profile presented in Figure 2.3. Gas and liquid flow into the shaft from the formation in the Manitoulin and Gasport is driven by the overpressure at that depth. Flow from the EDZ into the shaft is driven by the low gas pressures in the seal (atmospheric) and the strong negative liquid pressures (suction) caused by high capillary pressures within the bentonite and concrete). The gas pressure in the EDZ system is slightly reduced relative to the formation due to the effect of the preclosure 60 a simulation period. Figure 5.16 indicates that liquid flows are outwards from the EDZ into the rock. This is a result of the imposition of the initial gas pressures from the rock model on the reduced capillary pressures of the EDZ, resulting in a higher liquid pressure and consequent outward gradient. This is an unavoidable artefact of the modelling approach that is dissipated within a few hundred years and has no impact on the longer term results.

Note that advective flows are indicated as arrows only in those cases where the flow rate exceeds 10^{-4} m/a.

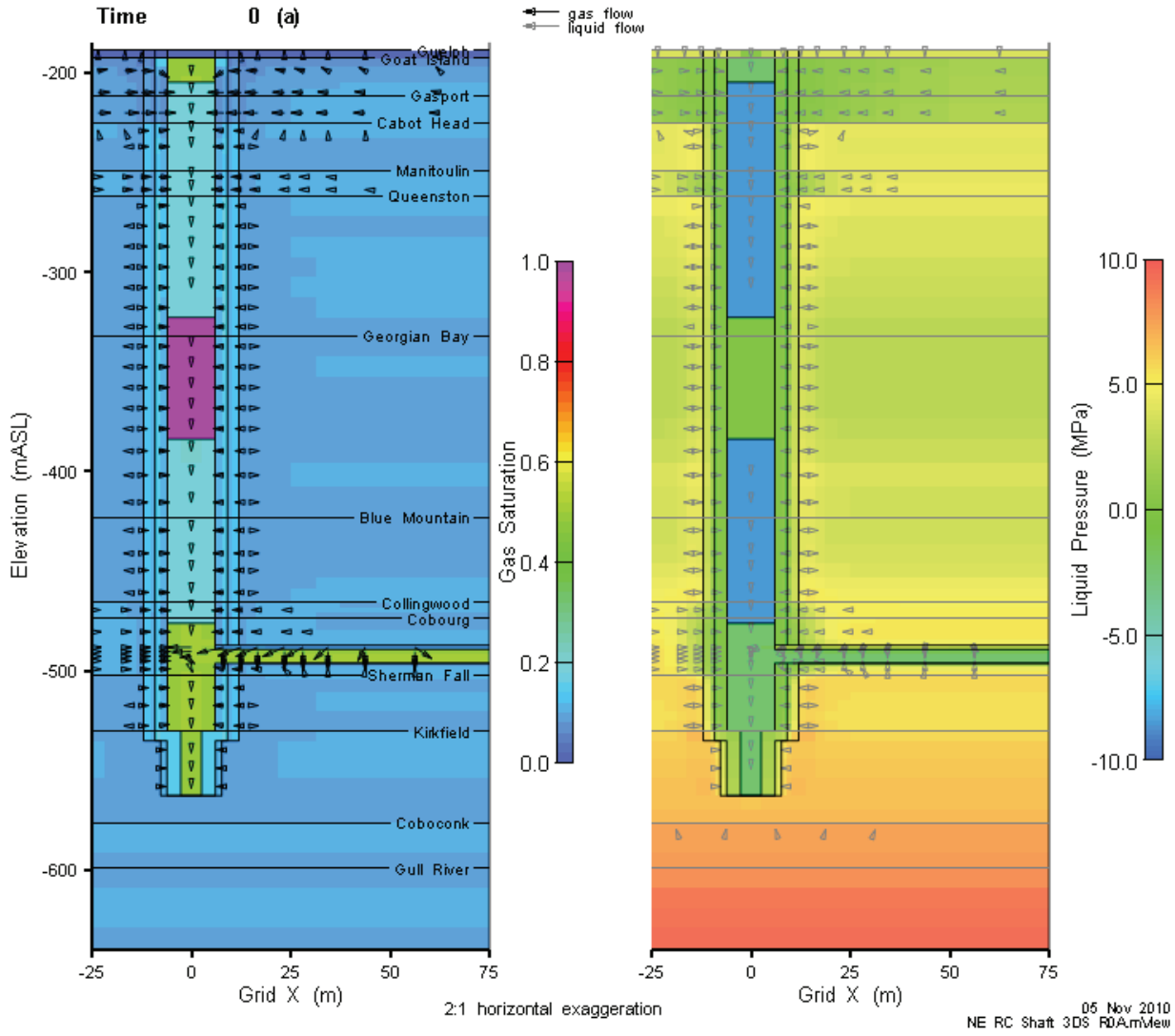

Figure 5.16: NE-RC: 3DD Shaft Saturations, Flows and Pressures (0 a after Closure)

By 500 a (Figure 5.17), the flows have stabilized, with gas and liquid moving from the rock into shaft materials, as the shaft materials continue to equilibrate. Flow within the shaft materials is downwards below the Cabot Head formation and upwards above it. Liquid pressure in the asphalt seal is elevated in comparison to the bentonite/sand due to the asphalt capillary pressure function (zero at all saturations). Gas pressure in the asphalt (not shown in the figure) is similar to that in the adjacent bentonite/sand seal material.

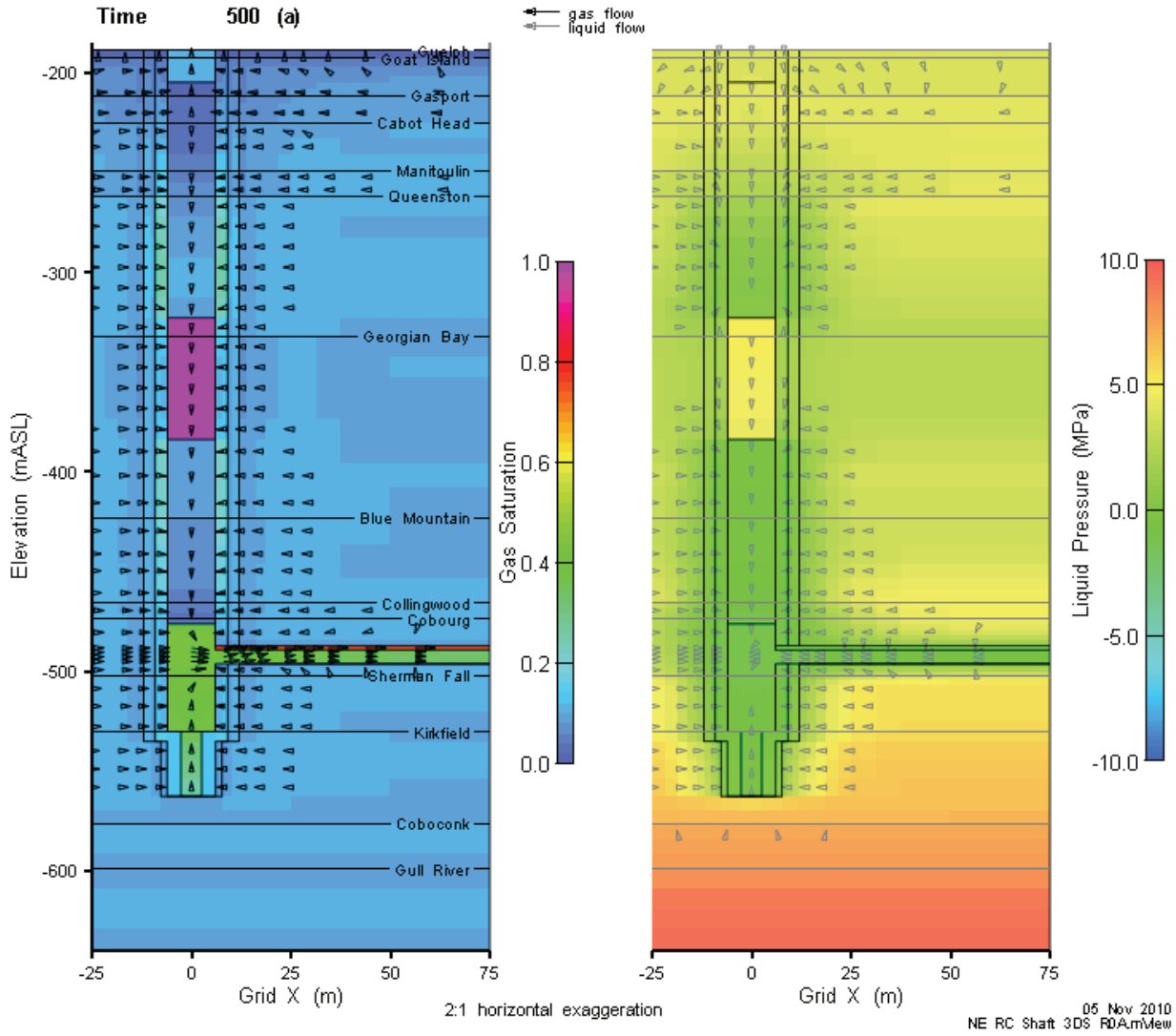

Figure 5.17: NE-RC: 3DD Shaft Saturations, Flows and Pressures (500 a)

At 5000 a (Figure 5.18), the increased pressure in the repository is driving liquid flows upwards in the shaft seals and inner EDZ above the repository and below the asphalt seal. However, gas is still flowing into the shaft from the rock and downwards towards the repository.

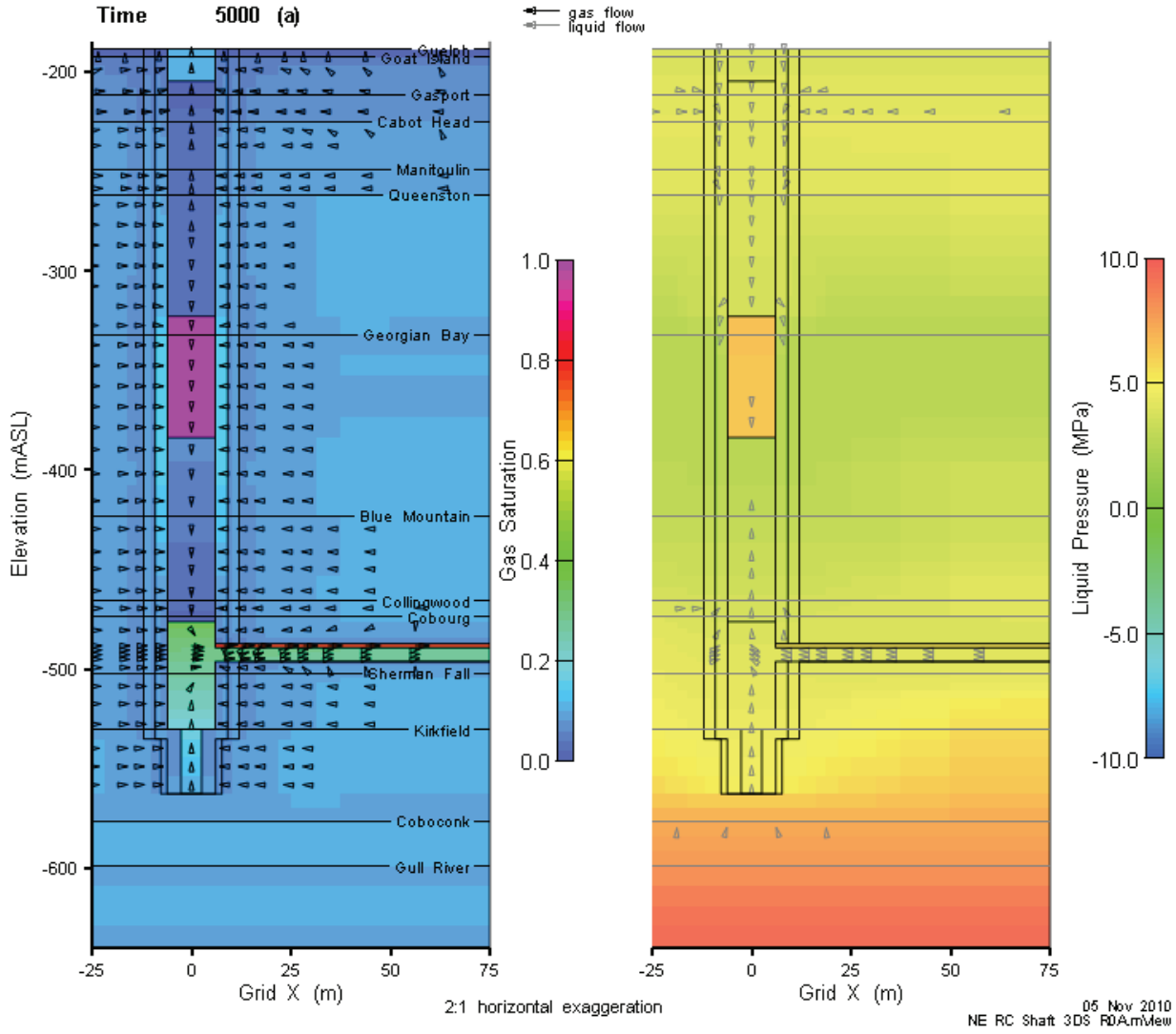

Figure 5.18: NE-RC: 3DD Shaft Saturations, Flows and Pressures (5000 a)

The increasing pressures in the repository dominate shaft flow below the asphalt at 50,000 a as shown in Figure 5.19. Liquid flow entering the shaft from the repository and below is exiting the shaft above the repository. Gas is continuing to flow in from the rock as gas pressure in the rock exceeds that in the shaft due to the differences in capillary pressures and the ongoing equilibration of shaft and repository pressures. Within the shaft, gas flow directions divide in the middle of the Blue Mountain formation, reflecting the competing influences of repository and upper shaft pressures. Above the Blue Mountain all gas flow is upwards, responding to the low pressure boundary at the top of the model. Below the Blue Mountain, the gradient is towards the repository.

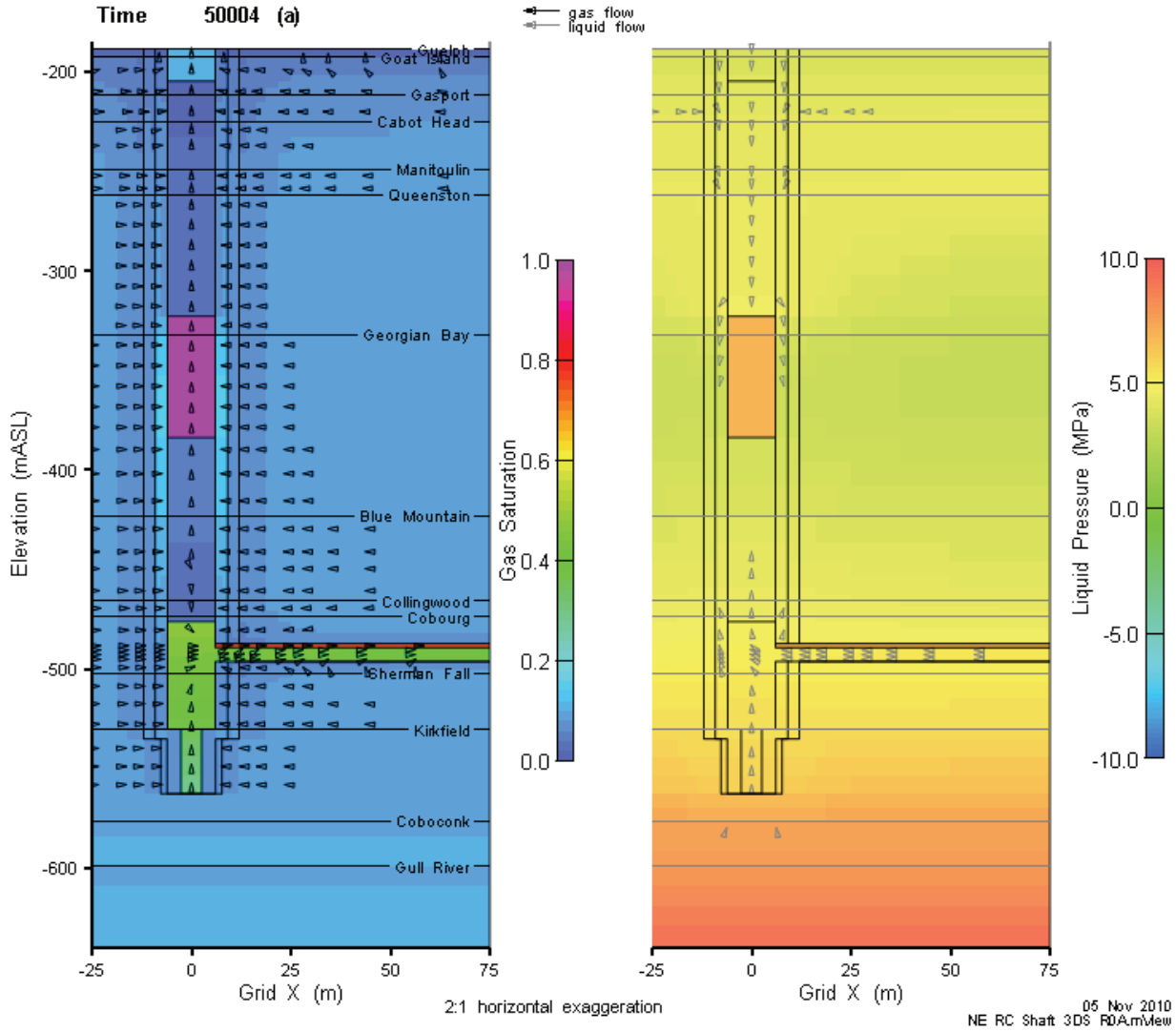

Figure 5.19: NE-RC: 3DD Shaft Saturations, Flows and Pressures (50,000 a)

At 60,000 a (Figure 5.20), gas is flowing out of the repository as gas pressures in the repository exceed those in the shaft. Rock formation gas continues to flow into the shaft from the adjacent rock and then upwards. Groundwater flows from the rock into the shaft EDZ below the repository and above the Queenston formation. Within the Ordovician shales, groundwater flows from the EDZ out into the underpressured formation. Groundwater flow in the shaft seal and EDZ is downward above the Georgian Bay formation.

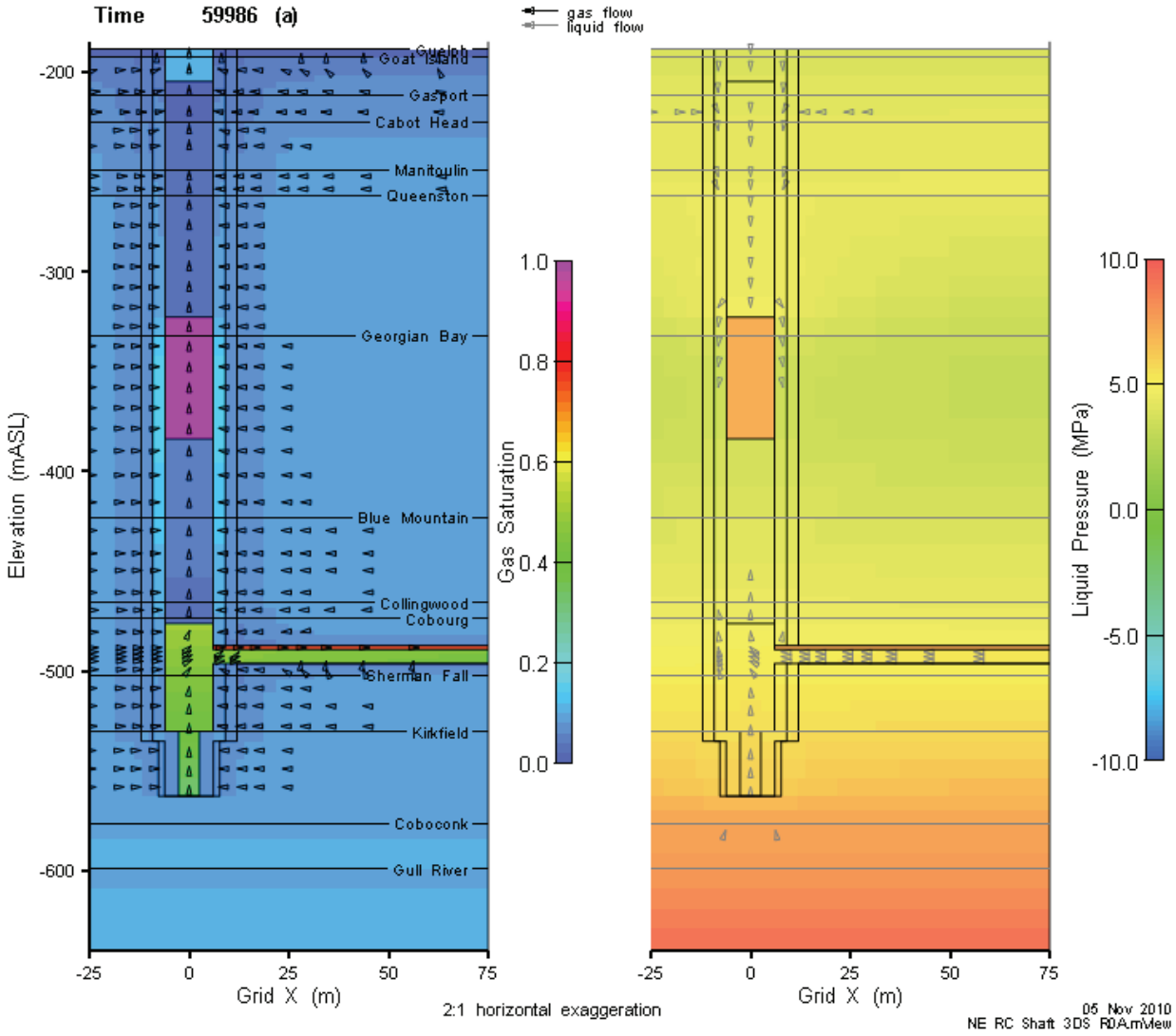

Figure 5.20: NE-RC: 3DD Shaft Saturations, Flows and Pressures (60,000 a)

These conditions remain for the remainder of the 1 Ma period. The rate of gas flow from the formation into the shaft will drop slightly as the gas saturations in the rock adjacent to the shaft are reduced and as pressures within the formation equilibrate. Figure 5.21 shows results at 1,000,000 a.

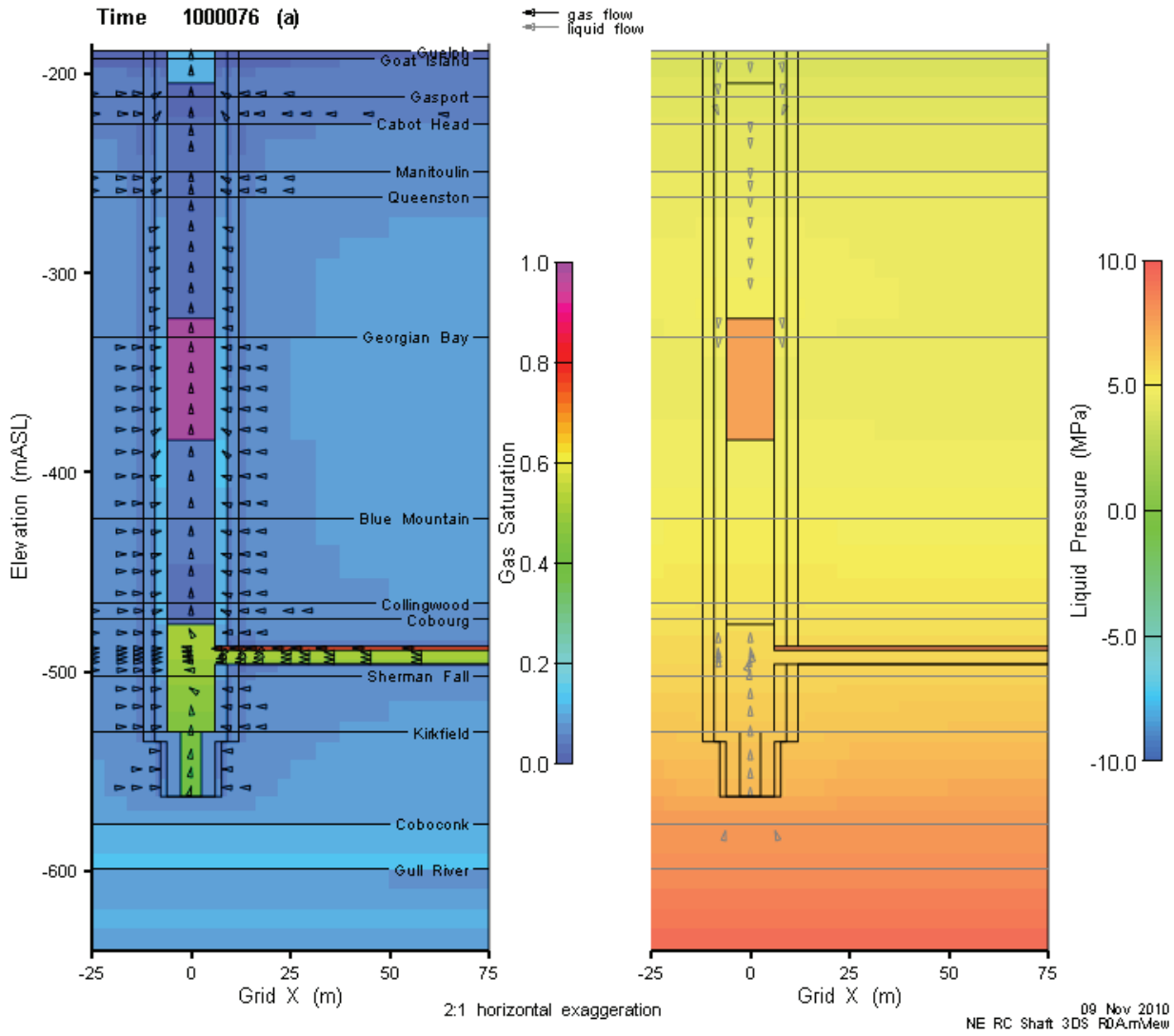

Figure 5.21: NE-RC: 3DD Shaft Saturations, Flows and Pressures (1,000,000 a)

Throughout the simulation, the asphalt seal is an effective barrier to liquid flow, as it remains nearly completely gas saturated and pressurized relative to the other shaft materials. (Water flows instead through the EDZ around it.) However, capillary processes for the asphalt plug are highly uncertain. Sensitivity case NE-GT4 examines the results for a shaft with the asphalt seal replaced by bentonite/sand.

The 3DSRS model results are consistent with the 3DD model. Flows at 1,000,000 a from the 3DSRS model are shown in Figure 5.22. The cross-section shown for the 3DSRS models is extracted from a slice taken at a plan orientation of 45 degrees, so as to include the HDZ within the slice. Consequently, the X axis refers to radius from the shaft centre.

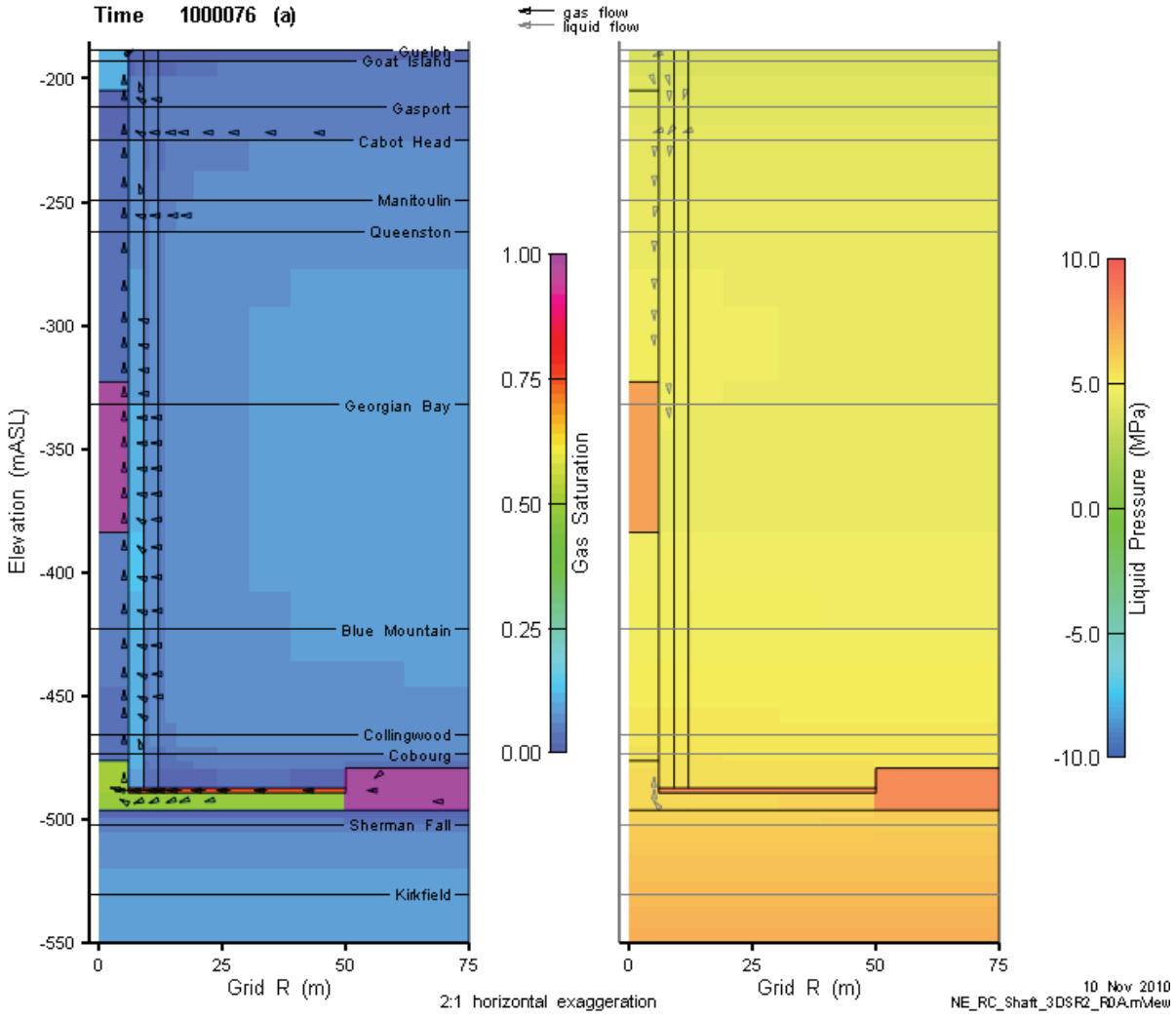

Figure 5.22: NE-RC: 3DSRS Shaft Saturations, Flows and Pressures (1,000,000 a)

Figure 5.23 and Figure 5.24 present time histories of shaft saturations and pressures respectively from the 3DD model. Bentonite/sand behaviour is roughly similar at all monitoring points, while the concrete seal in the Goat Island shows different characteristics than other concrete seals due to its proximity to the liquid saturated Guelph at the top of the modelled domain. Otherwise, the concrete seals resaturate with liquid until the 10% formation gas saturation is reached. Subsequently, as the pressure increases above hydrostatic pressure in the repository (around 75,000 a) and gas is expelled from the repository into the shafts, the concrete seals retain more gas. The monolith has exceeded its initial gas saturation at this time.

Gas mass flux up the shaft through three monitoring planes is presented in Figure 5.25. Below the Manitoulin, gas flows down the shaft until the flow directions reverse at approximately 60,000 a. The gas being measured in this case is formation gas. Upward gas flows occur at all times beyond 100 a above the Manitoulin and, beyond 60,000 a, elsewhere above the repository. At all planes, the majority of gas flux moves through the shaft seal material, with a minor amount through the inner EDZ. 3DSRS model gas mass fluxes are shown for

comparison in Figure 5.26. Results are very similar, with 3DSRS results showing slightly higher mass flux.

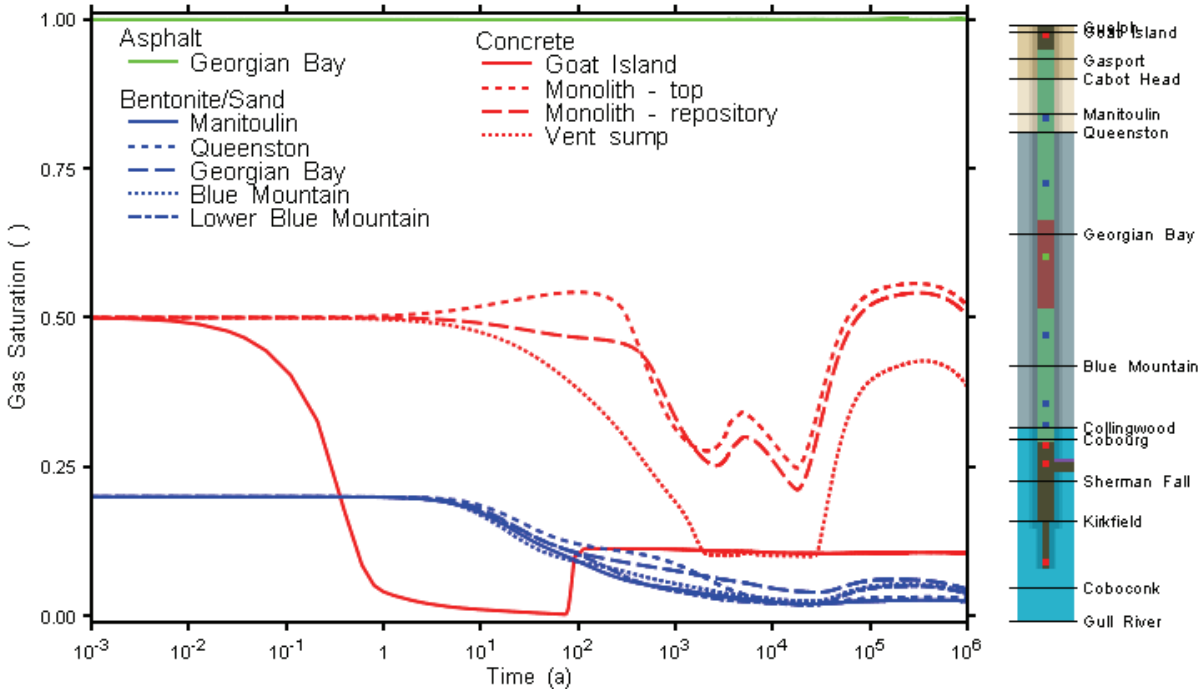

Figure 5.23: NE-RC: 3DD Shaft Saturation at Selected Monitoring Points

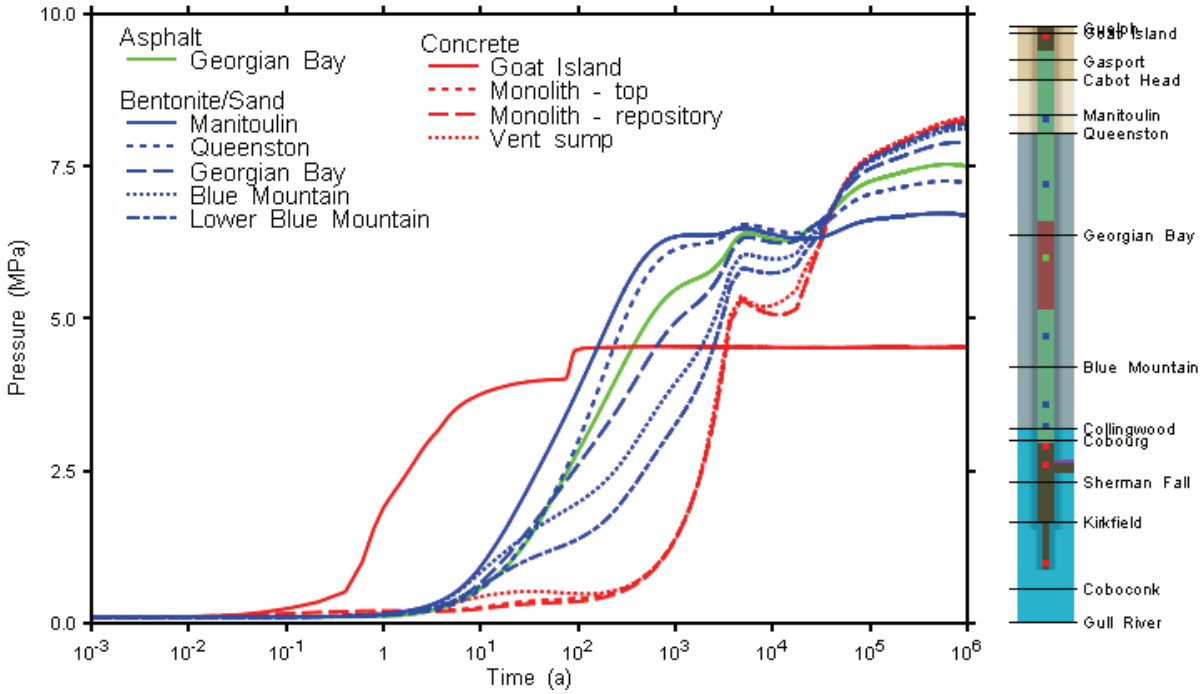

Figure 5.24: NE-RC: 3DD Shaft Gas Pressure at Selected Monitoring Points

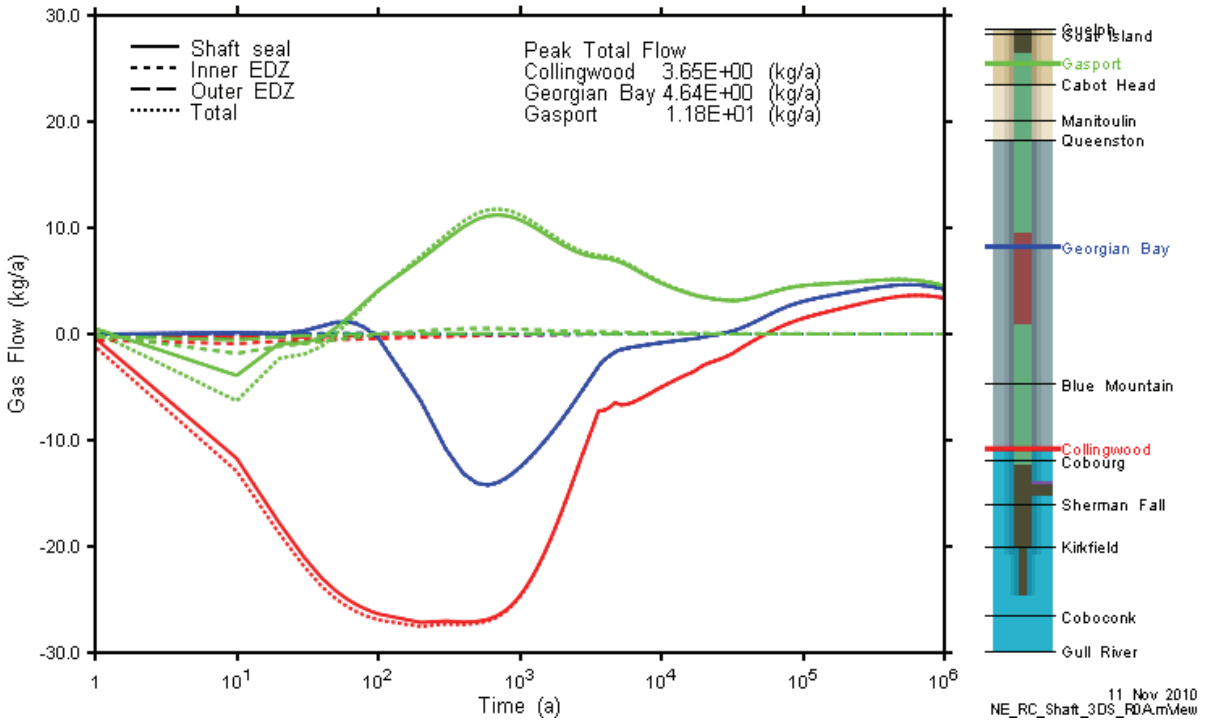

Figure 5.25: NE-RC: 3DD Model Shaft Gas Flows at Selected Monitoring Planes

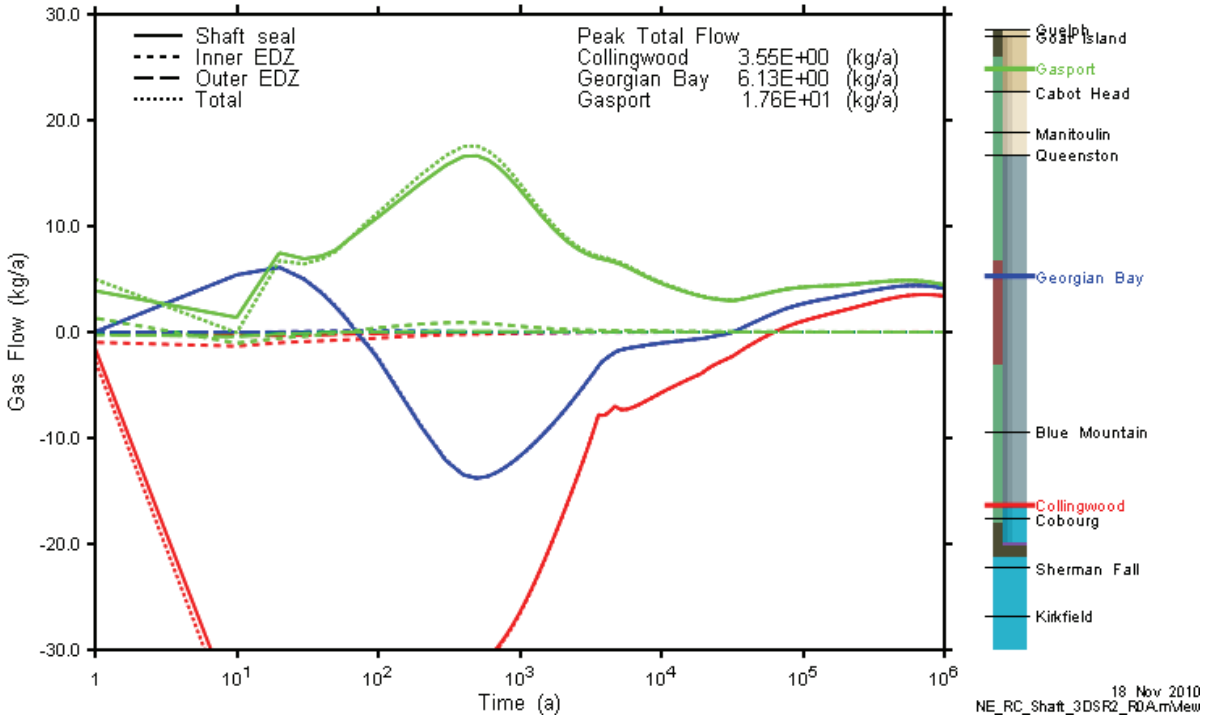

Figure 5.26: NE-RC: 3DSRS Model Shaft Gas Flows at Selected Monitoring Planes

5.1.2.2 Repository System

Figure 5.27 presents a comparison of repository pressures and liquid saturations for the 3DD, 3DSRS and 3DSR models. Pressure results are virtually identical up to approximately 200,000 a. Thereafter, the 3DD and 3DSRS pressures are lower than 3DSR (without shaft) pressures. This is as a result of gas flow up the shaft in the 3DD and 3DSRS models, which mitigates the rate of pressure increase in the repository due to gas flow in from the formation. In contrast, the 3DSR repository pressure continues to increase, as formation gas flows into the repository. As there is no pathway for gas to exit, the 3DSR repository pressures will increase until gas pressure equilibrium is reached with the formation. This in turn is dictated by the capillary pressure relationships of the intact rock. In reality, as partially shown by the 3DD and 3DSRS results, the pressure would stabilize due to a balance between the availability of gas in the near-field rock, the gas pressure in repository, and a slow outflux of gas through the shaft. The net inflow is only a few kg/a at 1,000,000 a.

The slight difference in initial saturation is due to residual liquid saturations required in nominally gas filled (99.9% gas saturation) nodes in the upper layers of the 3DD and 3DSRS repository. This does not impact the 3DSR repository, which is a modelled as a single grid layer. The differences in saturation profiles beyond 20,000 a are also likely due to discretization of the repository. In all cases the repository remains virtually dry for the entire simulation period.

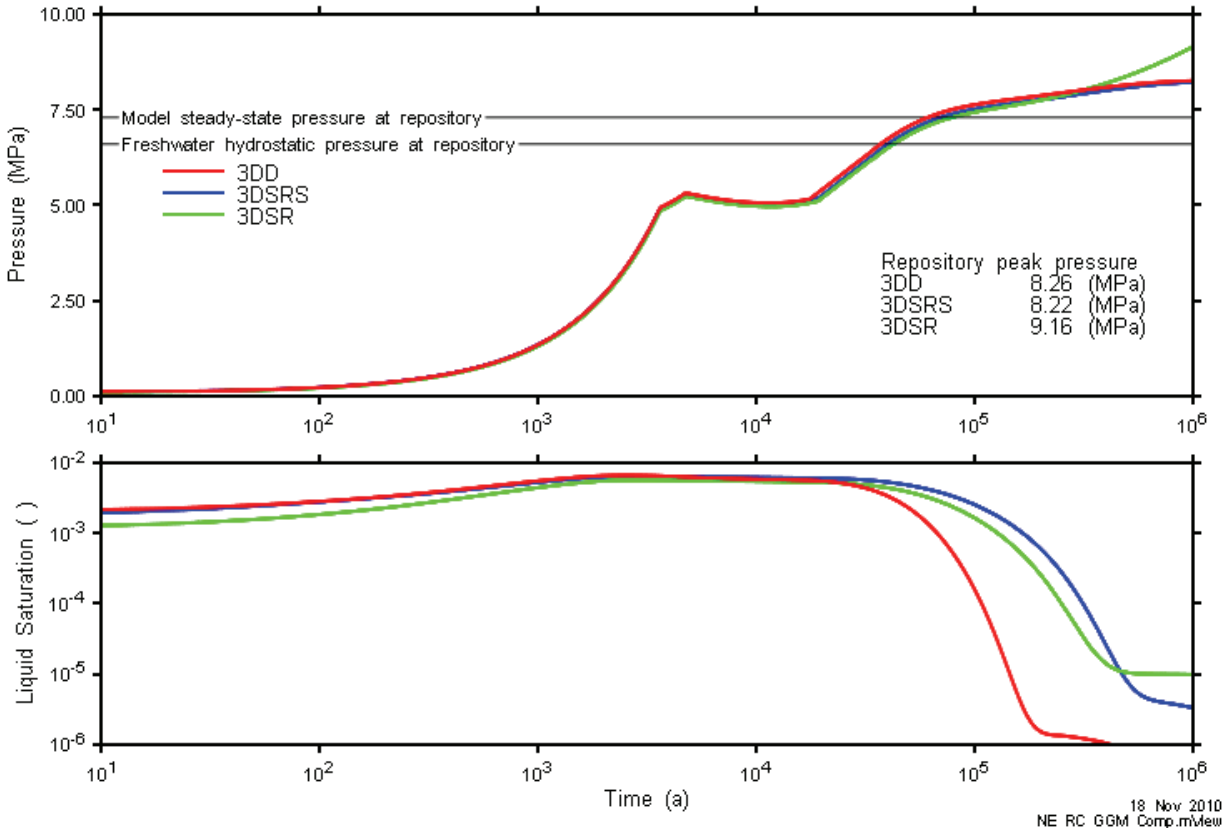

Figure 5.27: NE-RC: Comparison of 3DD, 3DSRS, and 3DSR Model Results

3DD model initial conditions in the repository are shown in Figure 5.28. The repository is almost entirely gas saturated. Liquid pressures are at atmospheric within the repository and HDZ, slightly below zero in the concrete, and significantly negative within the bentonite/sand. Gas and liquid are flowing towards the repository in its immediate vicinity.

Figure 5.29 through Figure 5.31 show the development of the flow system around the repository at 500, 5000, and 50,000 a respectively. By 50,000 a, the repository pressures exceed the liquid pressure of the surrounding bedrock, forcing liquid flow away from the facility in all directions. Liquid saturation in the repository is minimal at this time.

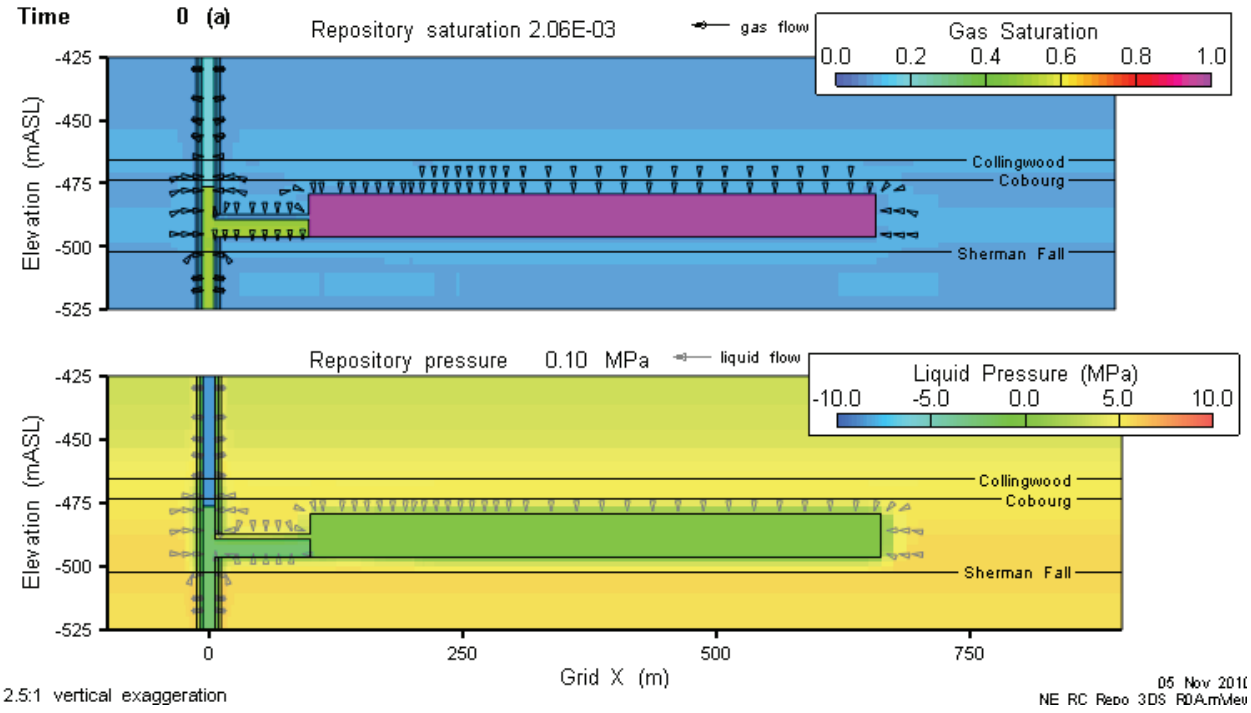

Figure 5.28: NE-RC: 3DD Repository Saturations, Flows and Pressures (0 a after closure)

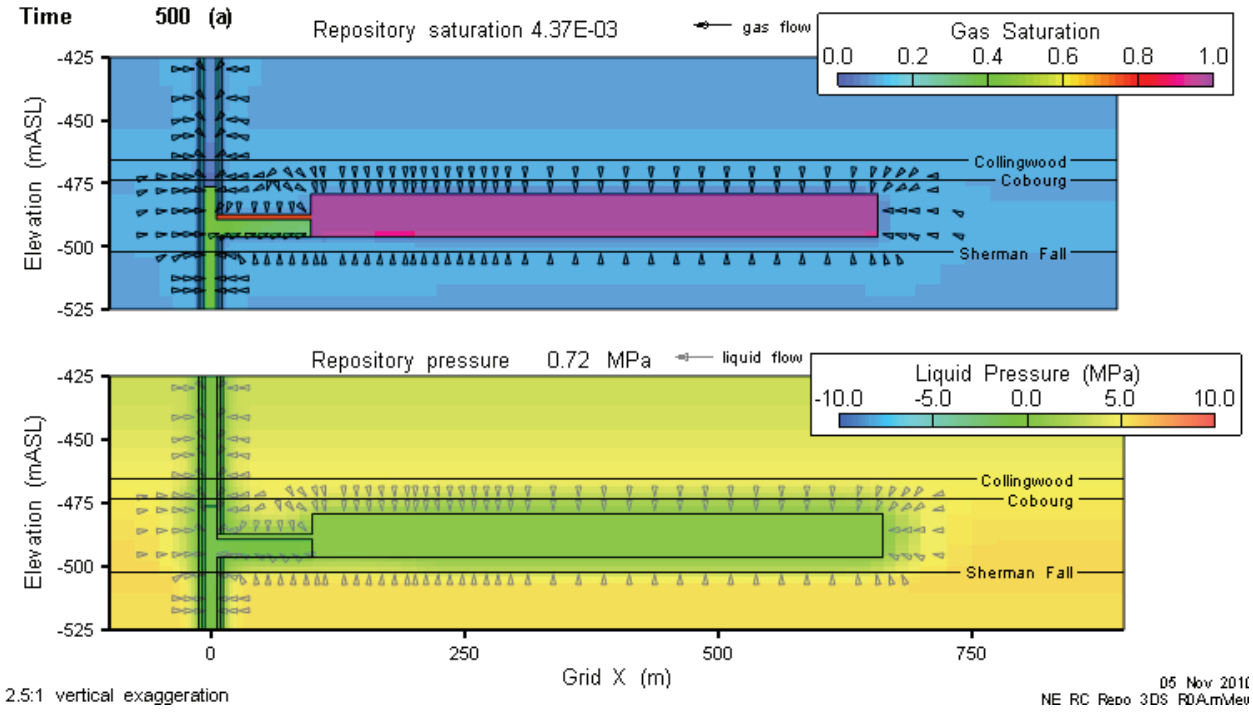

Figure 5.29: NE-RC: 3DD Repository Saturations, Flows and Pressures (500 a)

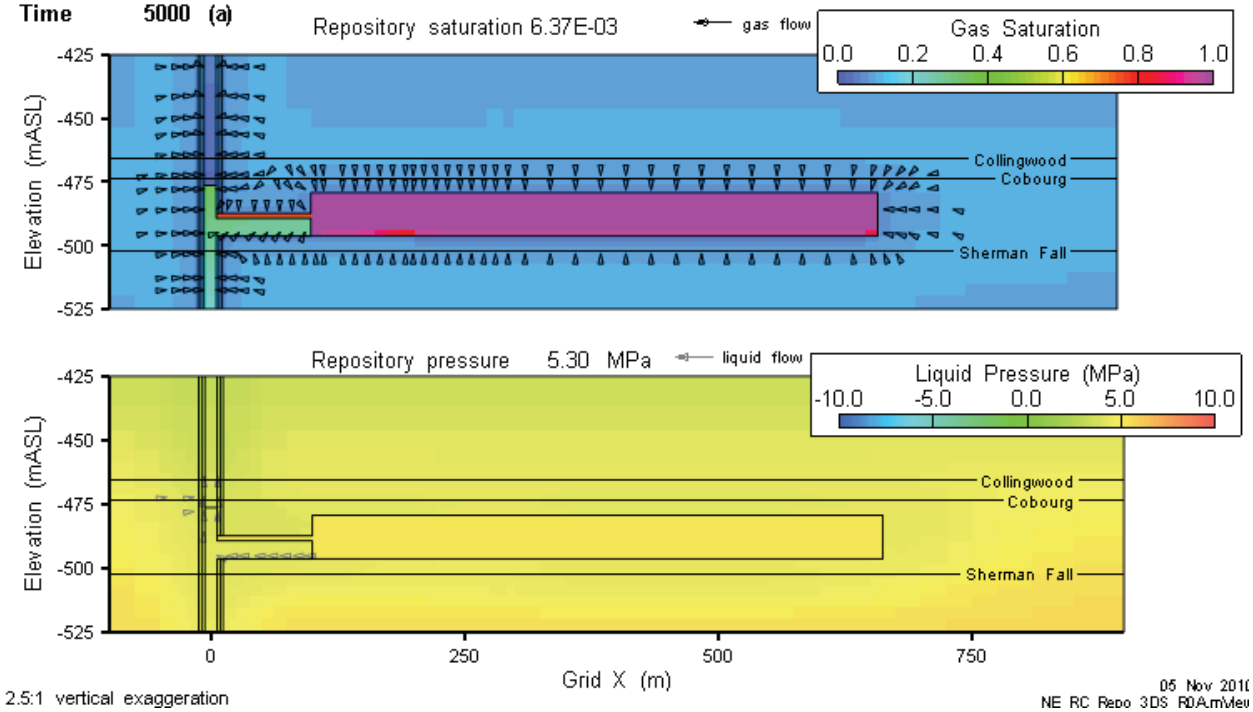

Figure 5.30: NE-RC: 3DD Repository Saturations, Flows and Pressures (5000 a)

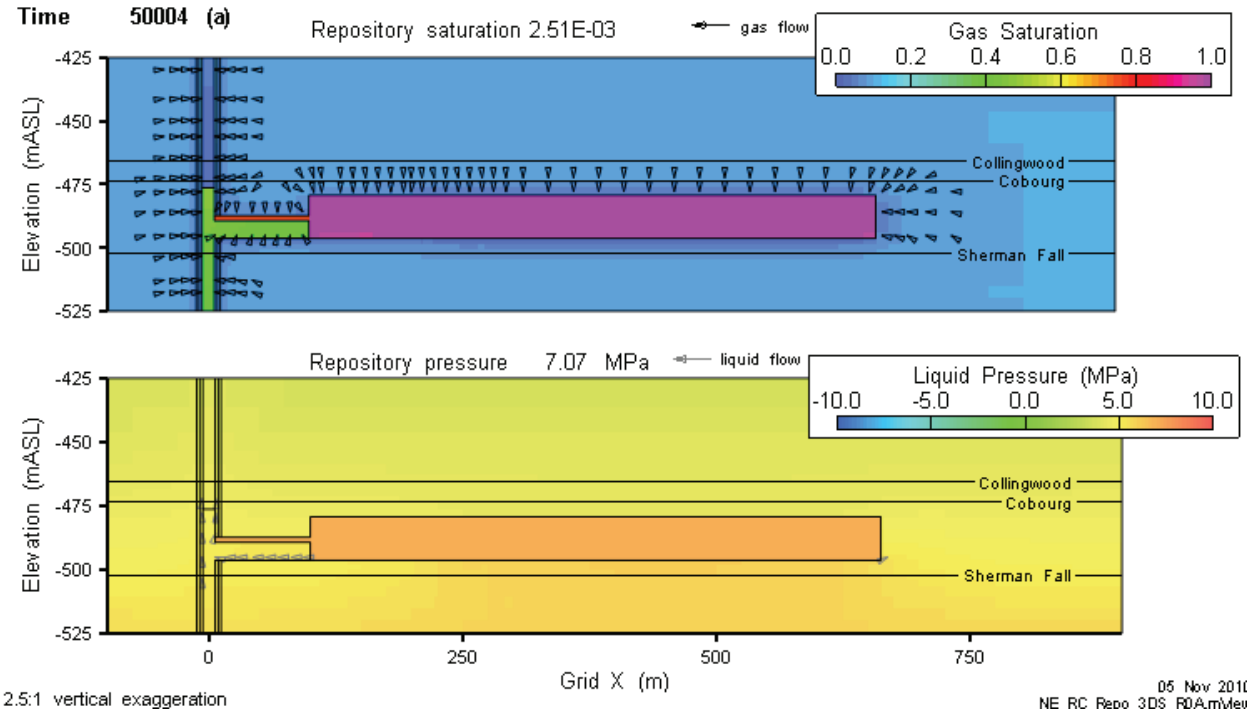

Figure 5.31: NE-RC: 3DD Repository Saturations, Flows and Pressures (50,000 a)

As the repository pressurizes, the pressure gradients reduce, particularly for liquid pressure. This leads to a corresponding reduction in flow rates, which is shown by the progressive elimination of flow vectors in the figures above.

At 100,000 a (Figure 5.32), gas continues to flow from the intact rock into the repository, and subsequently through the tunnels and HDZ and into the shaft seal system. Gas generation within the repository becomes negligible after 100,000 a. Figure 5.33 is a plan section through the HDZ elevation showing gas flow and saturations at 100,000 a.

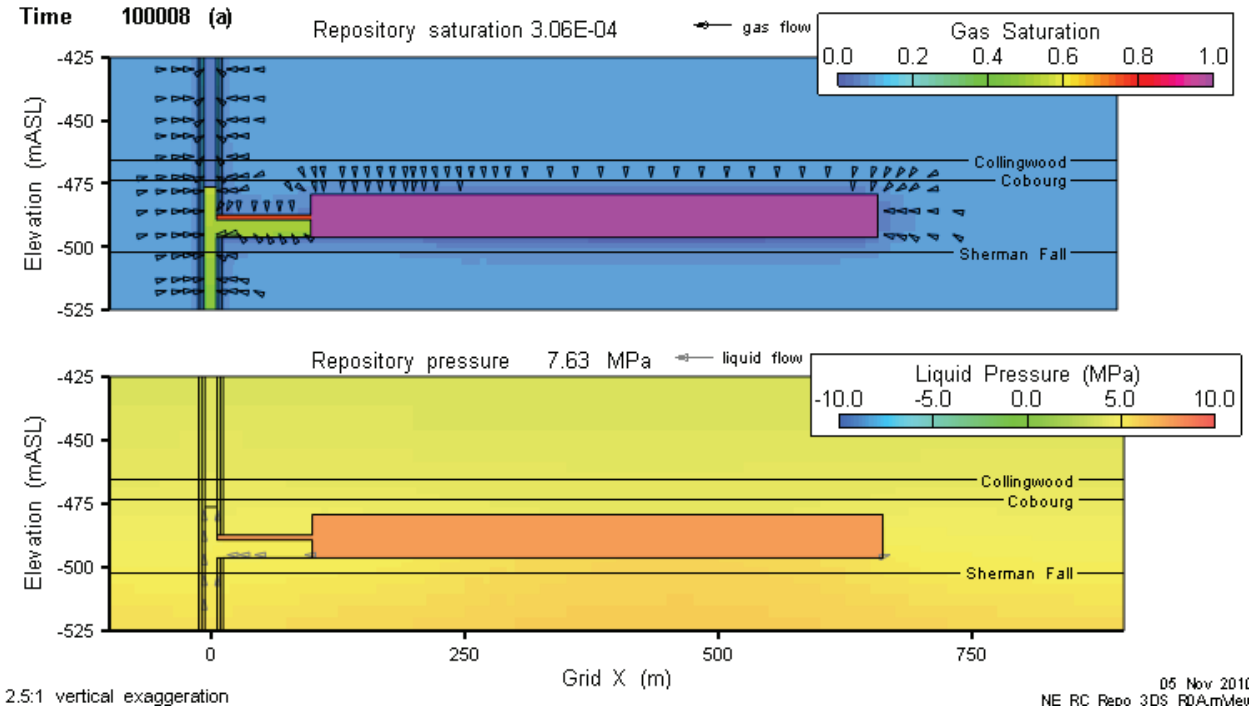

Figure 5.32: NE-RC: 3DD Repository Saturations, Flows and Pressures (100,000 a)

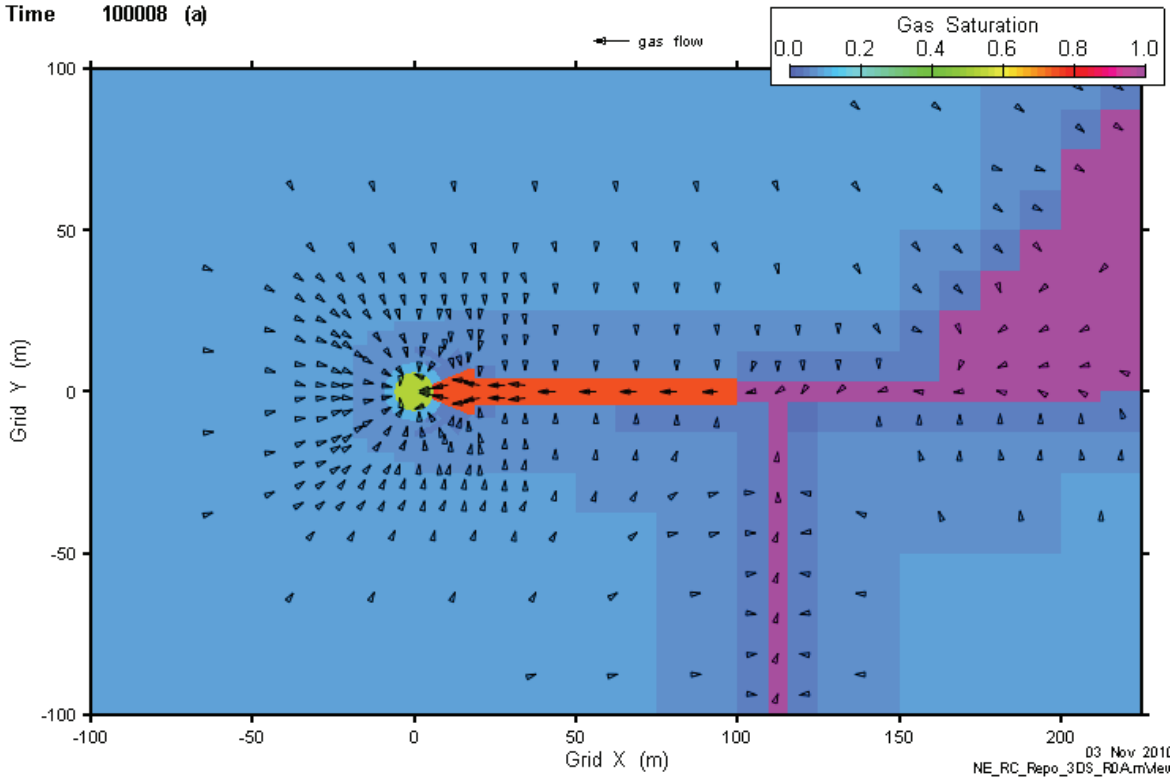

Figure 5.33: NE-RC: 3DD Repository Saturations and Flows - Plan Section (100,000 a)

The general flow domain shown at 100,000 a persists for the duration of the simulation, although velocities slowly decline. Results from the 3DD and the 3DSRS models at 1,000,000 a are shown in Figure 5.34 and Figure 5.35 respectively.

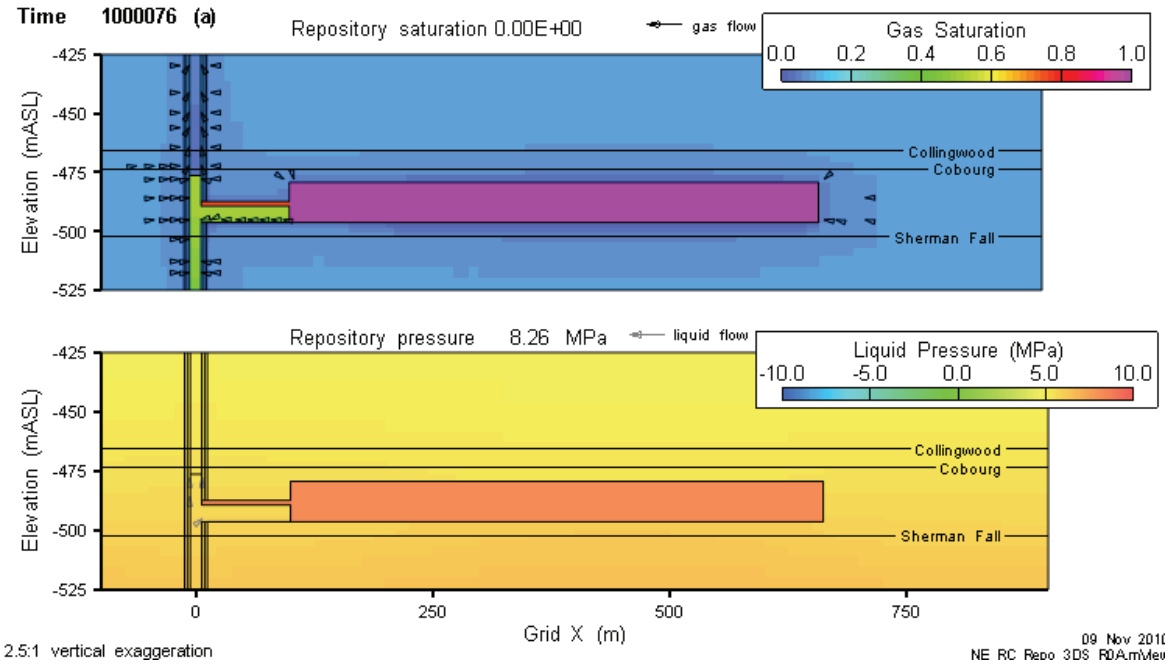

Figure 5.34: NE-RC: 3DD Repository Saturations, Flows and Pressures (1,000,000 a)

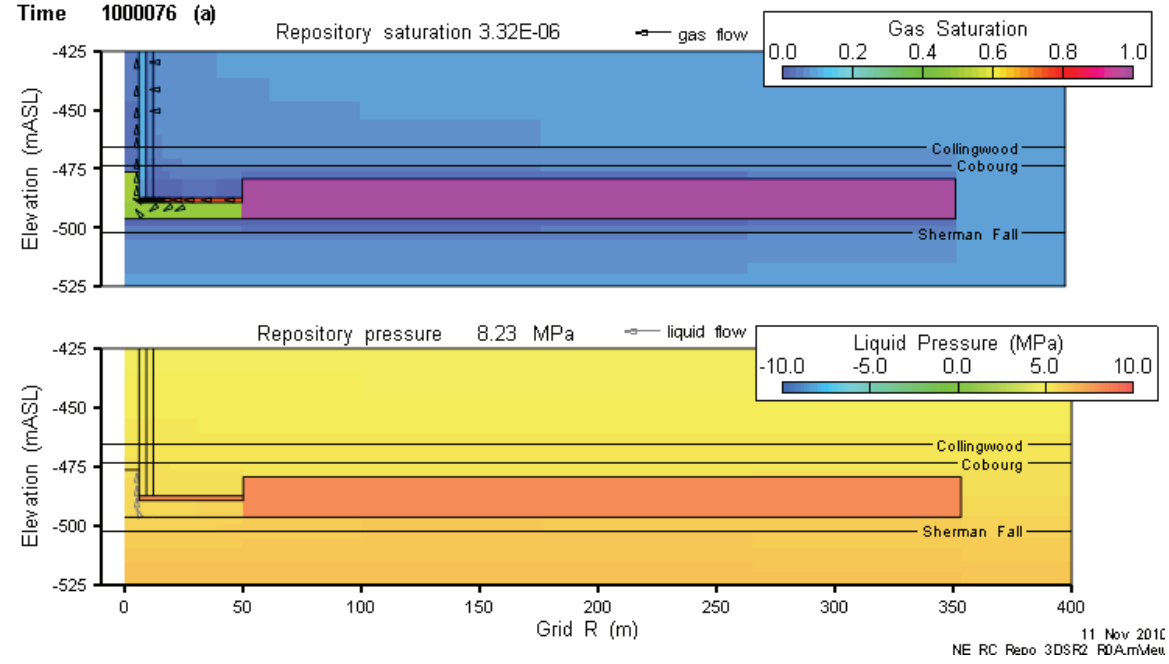

Figure 5.35: NE-RC: 3DSRS Repository Saturations, Flows and Pressures (1,000,000 a)

Figure 5.36 shows cumulative liquid inflow into the repository and gas outflow from the repository, categorized by source. Note that 3DD liquid flow results for rock and total are visually coincident on the plot. It can be seen that HDZ/monolith flow, which is representative of shaft flow, is an insignificant proportion of total flow.

The figure also shows that formation gas is flowing into the repository from the geosphere for the entire simulation period. Late time flow out of the repository and up the shaft is clearly seen.

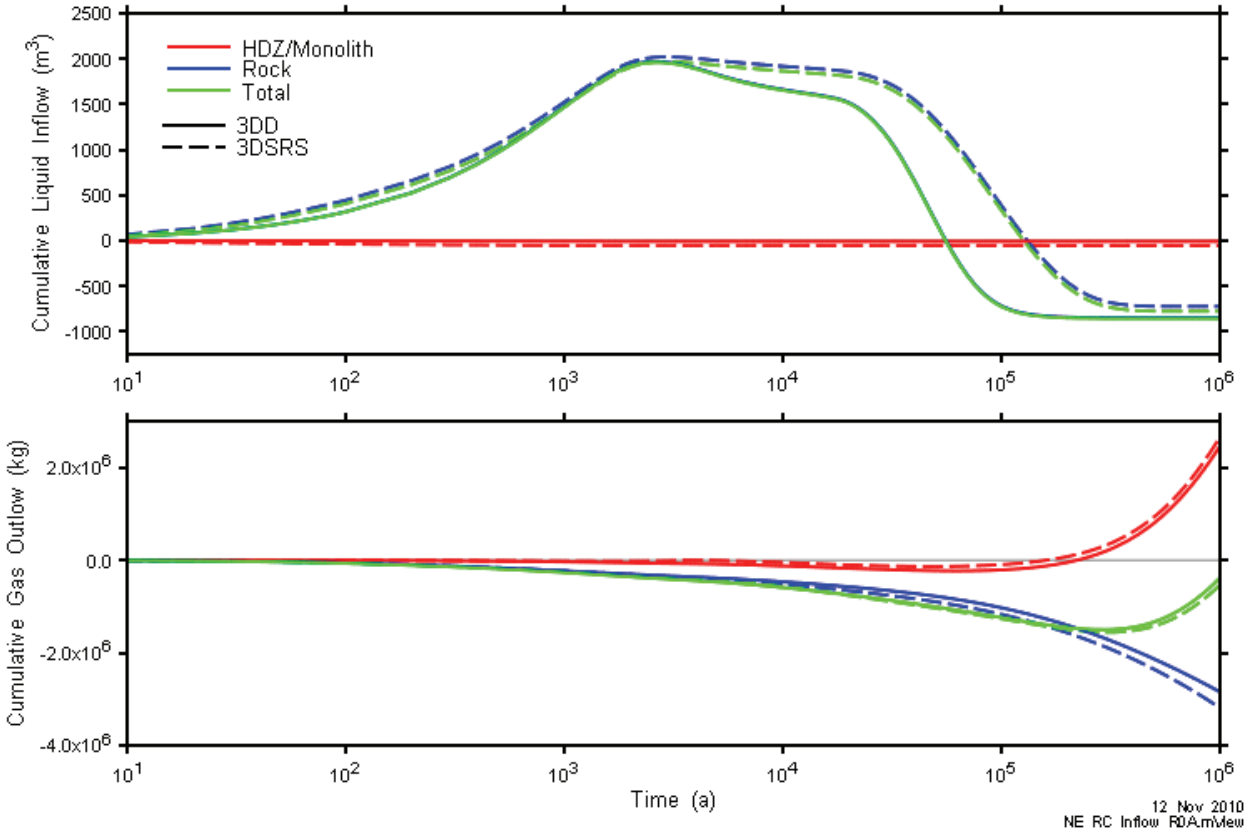

Figure 5.36: NE-RC: Repository Liquid Inflow and Gas Outflow for 3DD and 3DSRS Models

5.1.2.3 Geosphere

The development of the gas and liquid flow system in the geosphere is due to two factors: 1) the influence of the repository, and 2) the ongoing transient behaviour of the two-phase flow system within the Ordovician bedrock. As discussed in NWMO (2011a) and INTERA (2011), the extent and magnitude of gas saturations in the intact bedrock remains uncertain. However, there is compelling evidence that free phase gas exists at some, if not all, locations in all formations. The NE-RC geosphere model is intended to approximate this system. There are significant simplifications: the liquid DGR-4 Westbay pressure measurements are assumed to be representative of current liquid pressures; a constant initial gas saturation is assumed; and the simplified two-phase flow parameters described in Section 4.2.4 are assumed representative of

the bedrock sequence above the Coboconk Formation. The NE-RC1 and NE-RC2 cases explore sensitivity to some of these assumptions.

Figure 5.37, Figure 5.38, and Figure 5.39 present the evolution of the NE-RC Geosphere system, without a repository present. Figure 5.38 and Figure 5.39 show a subset (smaller head range) of the hydraulic head results presented in Figure 5.37. Pressure is presented as hydraulic head, which is useful in determining the direction of liquid flow. Hydraulic head does not capture the effect of gas density variations, and is thus less useful as an indicator of gas flow. However, it does show the difference in pressure between the gas and liquid systems.

In general, there is redistribution of gas pressures and saturations at the upper and lower ends of the system, as the gas drains along the gas pressure and concentration gradient into the permeable (and much reduced capillary pressure) Guelph Formation and Cambrian. In the lower end of the system, within the Gull River, gas flow is by diffusion only as the measured residual gas saturation within that unit is 11%, which is greater than the specified initial gas saturation of 10%. When the residual gas saturation is greater than the actual gas saturation, the relative permeability to gas flow is zero, which precludes advective transport of gas.

Within the centre of the system the gas saturation is reduced very slightly over the 1 Ma period as gas moves upwards very slowly as bulk gas or dissolved gas. As shown most clearly in Figure 5.38, the liquid underpressures in the centre of the system recover somewhat over the 1 Ma period, with the maximum underpressure reducing from -288 mASL to -146 mASL. Liquid gradients are downward from the top of the system and upwards from the bottom, towards a stagnation point in the Georgian Bay and Blue Mountain Formations.

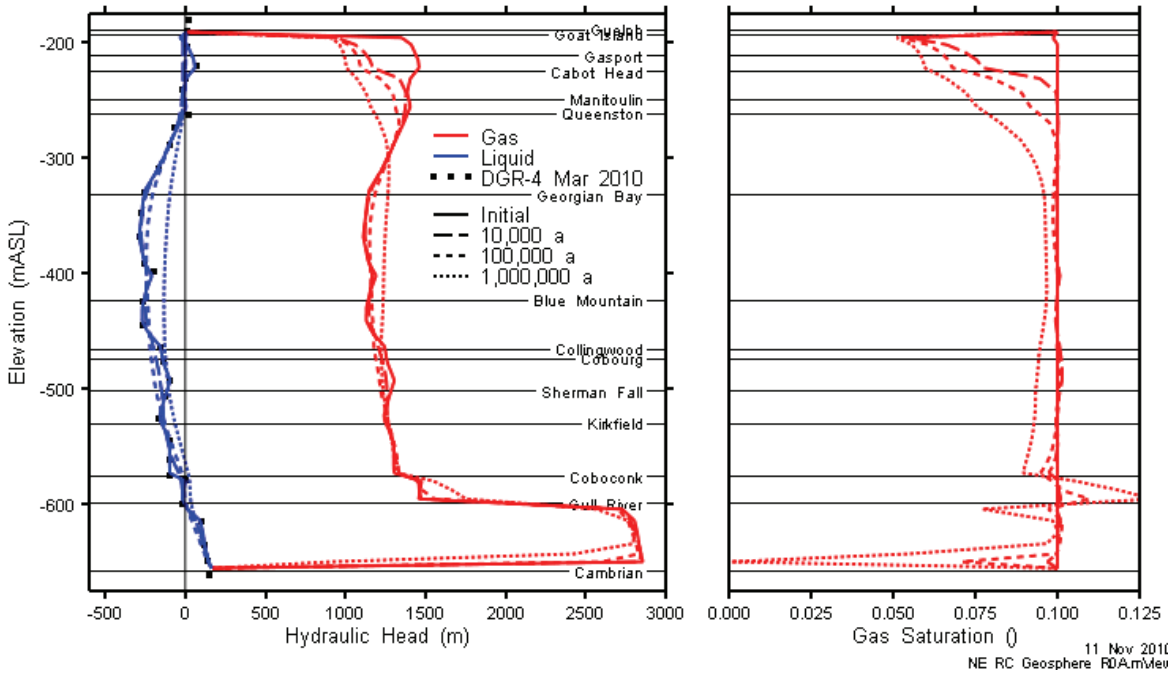

Figure 5.37: NE-RC: 3DSRS Geosphere (No Repository) Gas and Liquid Head and Gas Saturation Profile

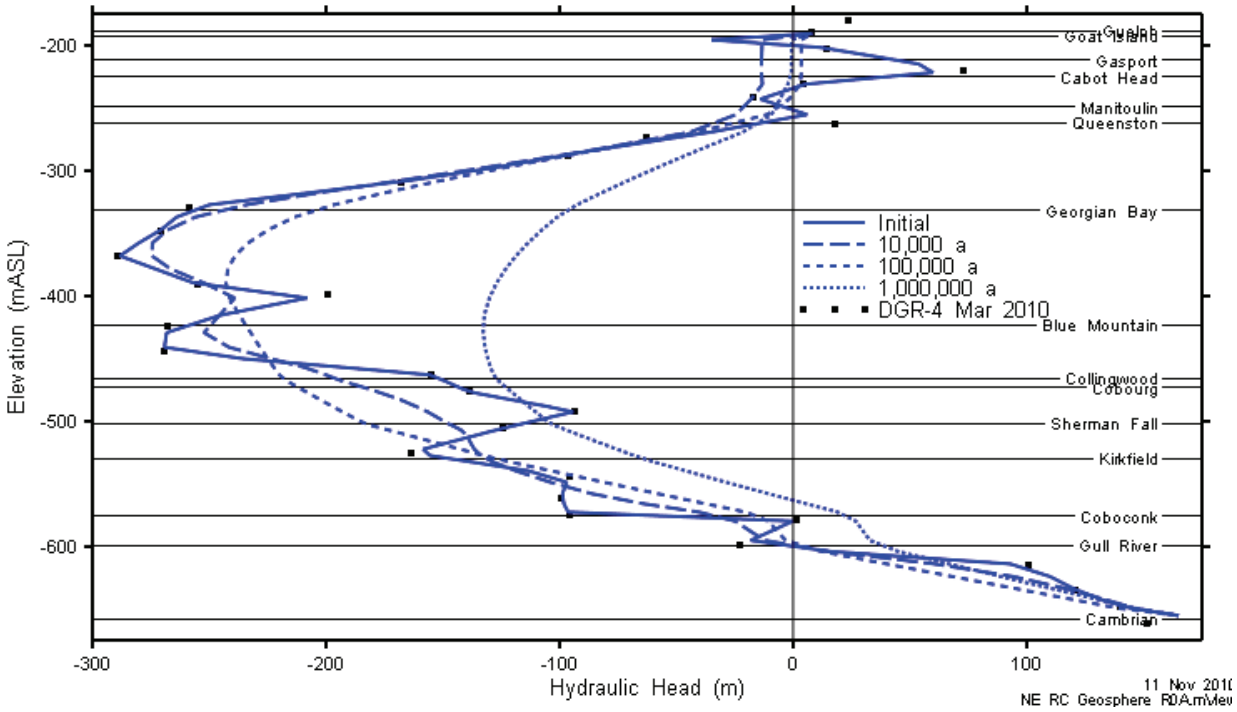

Figure 5.38: NE-RC: 3DSRS Geosphere (No Repository) Liquid Pressure (Expressed as Hydraulic Head) Profile

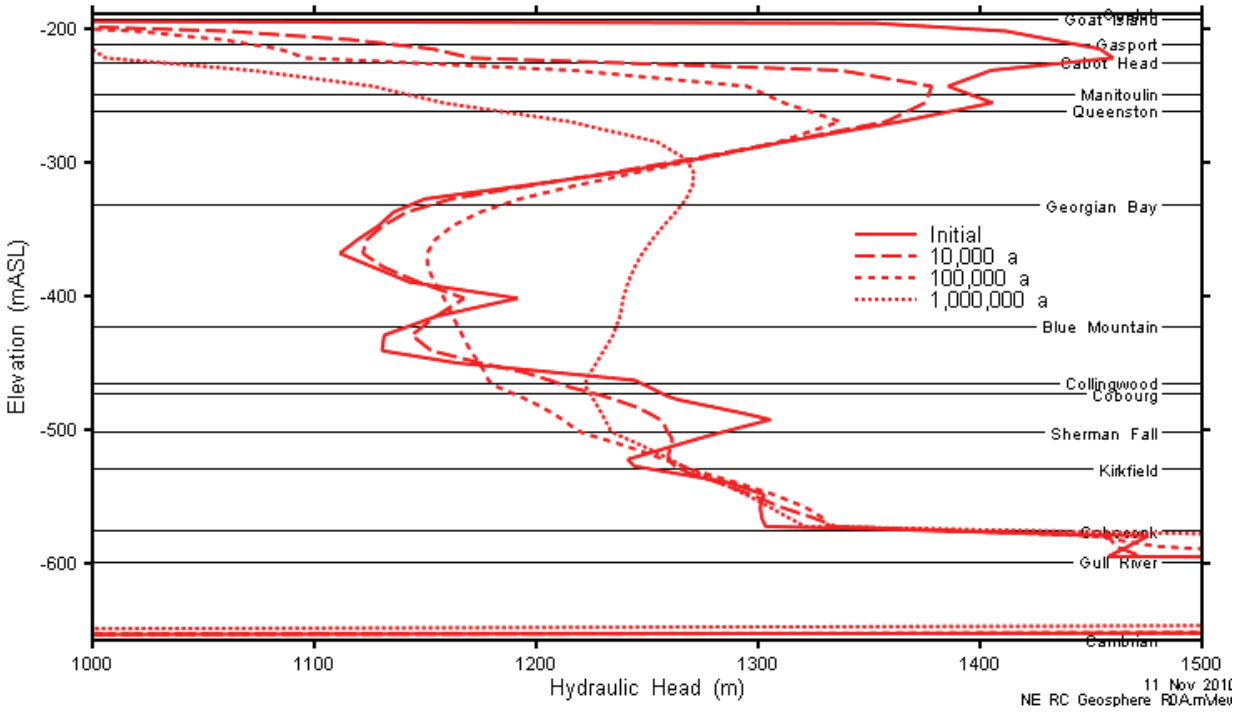

Figure 5.39: NE-RC: 3DSRS Geosphere (No Repository) Gas Pressure (Expressed as Hydraulic Head) Profile

The impact of the repository on the evolution of the geosphere system is shown in Figure 5.40, Figure 5.41 and Figure 5.42. The plots show pressure and saturation on a vertical profile through X = 200, Y= 200m, at a sufficient distance from the shaft (at X =0, Y =0) to minimize impact of the shaft on the profile. The gas saturation within the repository is near 100% and is beyond the X axis limit of the saturation plot in Figure 5.40. The initial liquid hydraulic head is at the repository elevation (approximately 670 mBGS). The repository is a void space and has a capillary pressure of zero, so within the repository the gas and liquid pressures are identical.

At the top and bottom of the system there is little change from the geosphere only model. However, within the immediate vicinity of repository itself, pressure and saturation evolution is considerably different. Initially, both gas and liquid flow towards the repository due to its very low pressure (initialized at atmospheric). By 10,000 a, gas generation processes have raised the pressure in the repository so that it exceeds the liquid pressure of the surrounding rocks, forcing liquid to flow away from the system. The very minor amount of liquid in the repository itself is expelled and the repository is essentially dry from approximately 70,000 a onwards. Gas pressure in the repository remains substantially below the gas pressure in the rock mass, so gas flows from the rock into the repository. Gas flow will continue until the gas saturation in the rocks surrounding the repository is reduced below the specified residual saturation of 5%. At the end of the 1 Ma performance period the repository gas pressure has increased to 8.2 MPa.

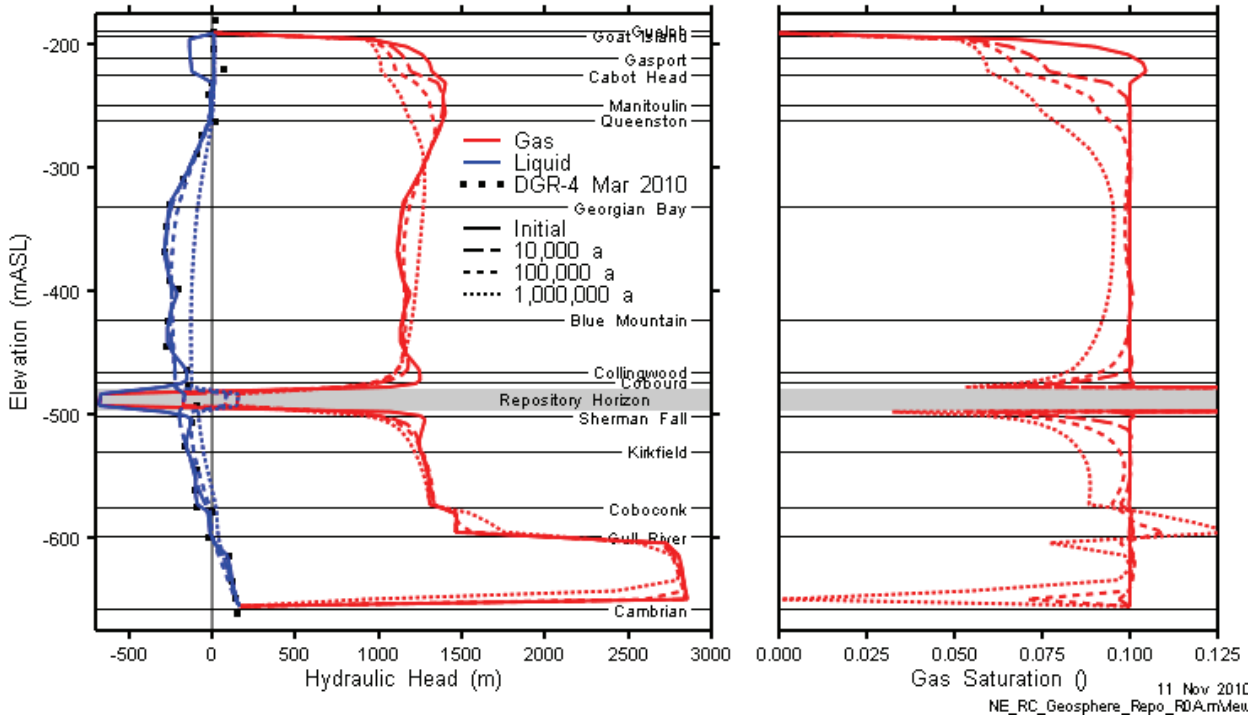

Figure 5.40: NE-RC: 3DSRS Geosphere with Repository Gas and Liquid Head and Gas Saturation Profile

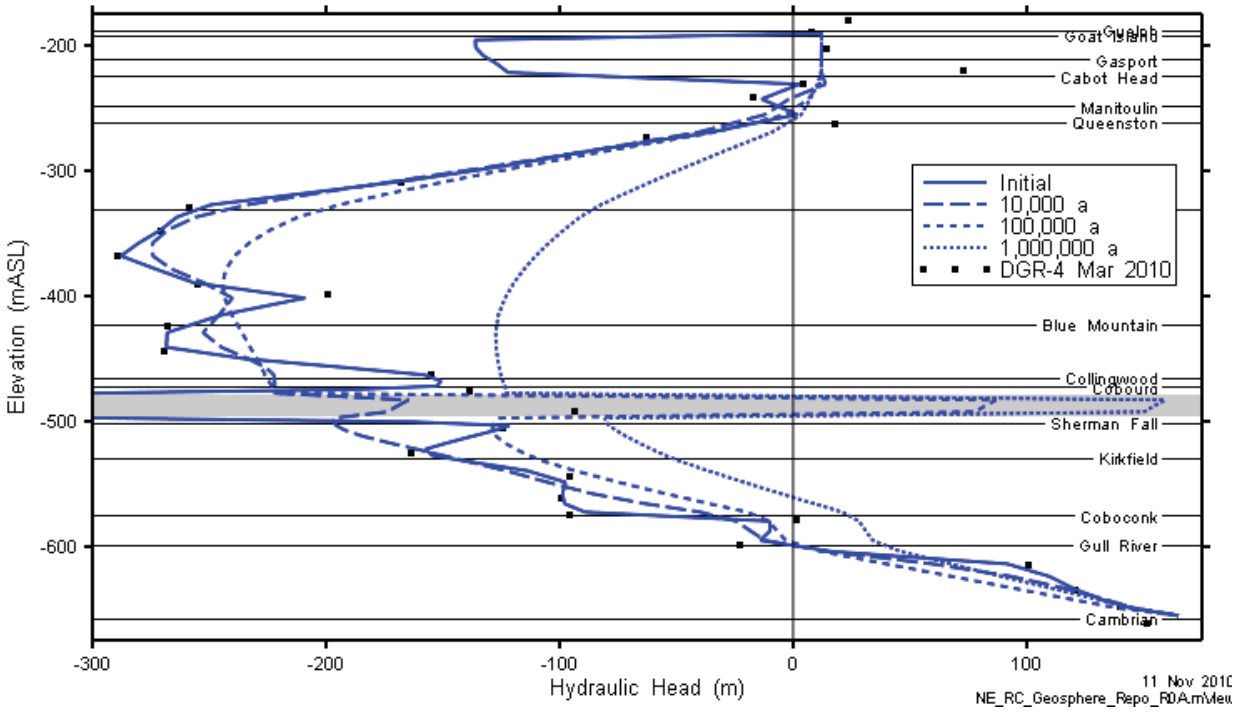

Figure 5.41: NE-RC: 3DSRS Geosphere and Repository Liquid Pressure (Expressed as Hydraulic Head) Profile

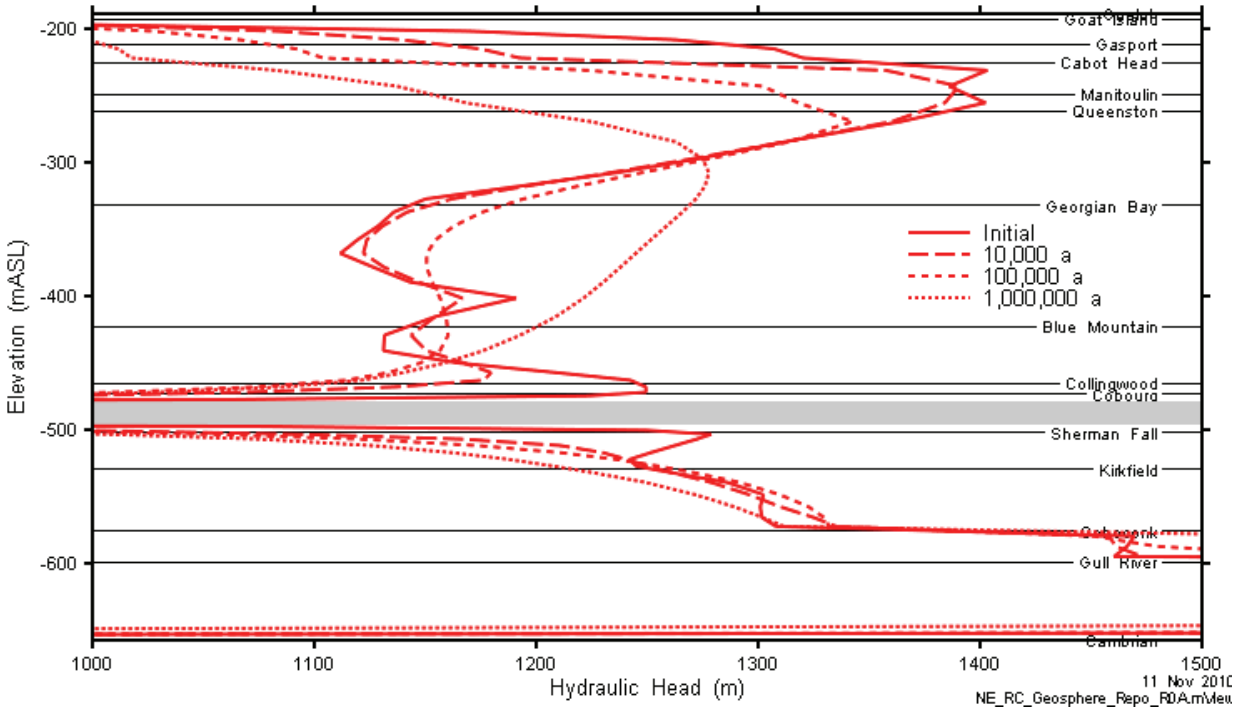

Figure 5.42: NE-RC: 3DSR Geosphere and Repository Gas Pressure (Expressed as Hydraulic Head) Profile

5.2 Case NE-SBC – Simplified Base Case

The results of the NE-RC case represent a simplified parameterization of the Reference Case conceptual model. Alternative estimates of initial gas saturations and gas transport properties, particularly residual gas saturation and capillary pressure, are possible. The NE-RC1 and NE-RC2 cases described in Sections 5.12 and 5.13 explores two such sensitivity cases, while the NE-SBC case assumes no initial gas phase in the intact rock.

The Simplified Base Case model considers flow and transport of gas within a full-saturated geosphere system that is initially (i.e., before construction of the repository) at steady-state conditions (with no underpressures) and with no partial gas saturation in the Ordovician (Table 3.1). Otherwise, all parameters are as described for the NE-RC case. The NE-SBC case was simulated using the 3DD, 3DSRS, and 3DSR models.

5.2.1 Gas Generation

The results presented in this section are from results calculated with the 3DSRS model. The 3DD and 3DSR model produced almost identical results. The key difference between the Simplified Base Case and the Reference Case is that the continued influx of gas into the repository from the geosphere observed for the Reference Case is not observed here. Overall there is a small net outflux of gas over 1,000,000 a (compare Figure 5.43 with Figure 5.5). As a result the pressure does not continue to rise once the wastes have degraded (at about 10^5 a) and a peak constant pressure of 7.2 MPa is attained (see Figure 5.45). A simplified estimate of peak gas pressure for a scenario with the same processes but no leakage of gas from the repository predicts 7.4 MPa for this case (see Case 3 from Appendix B.)

Another consequence is that the water saturation continues to increase during the simulation as liquid flows in slowly from the geosphere, reaching approximately 0.06 at 1,000,000 a (see Figure 5.46). Apart from this, the results are practically identical to the Reference Case.

The small influx of gas at approximately 8 a is in response to rapid gas consumption during the nitrate and sulphate reduction stages as discussed in Section 5.1.1.3. The sharp changes in the amount of gas that has entered or left the repository between 1000 a and 100,000 a are primarily a result of the response to switching between gas and water production and consumption (see Figure 5.44) as waste streams are exhausted and as the system switches to being CO_2 and H_2 limited.

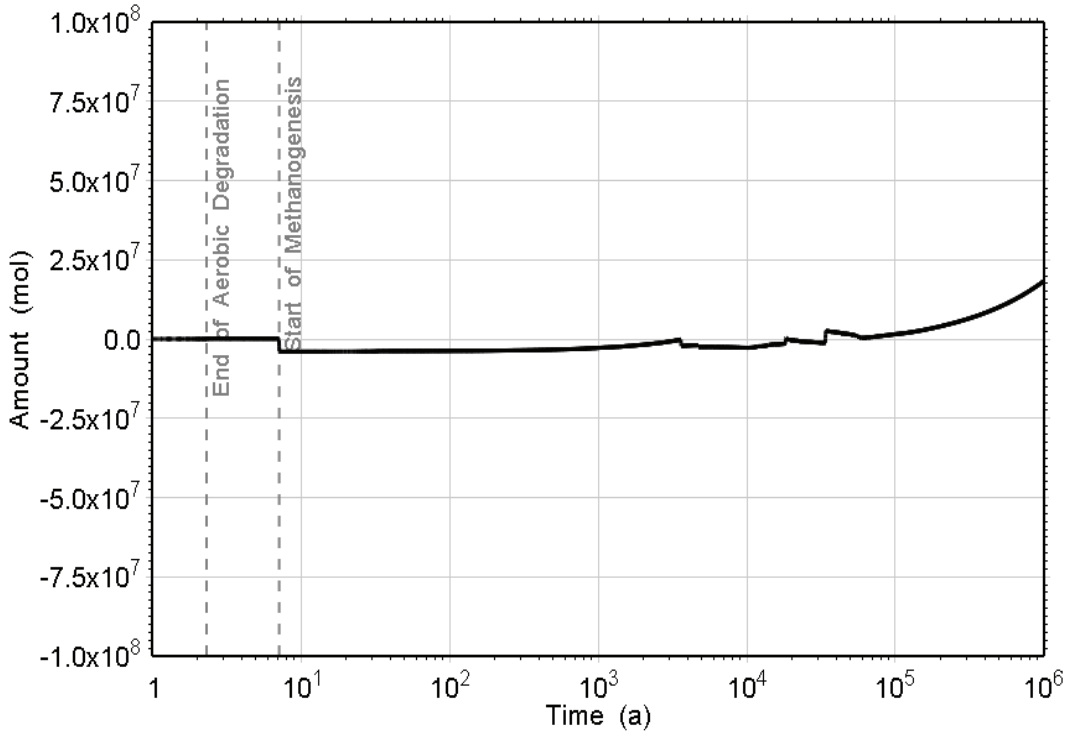

Figure 5.43: NE-SBC: Total Amount of Gas that has Left the Repository

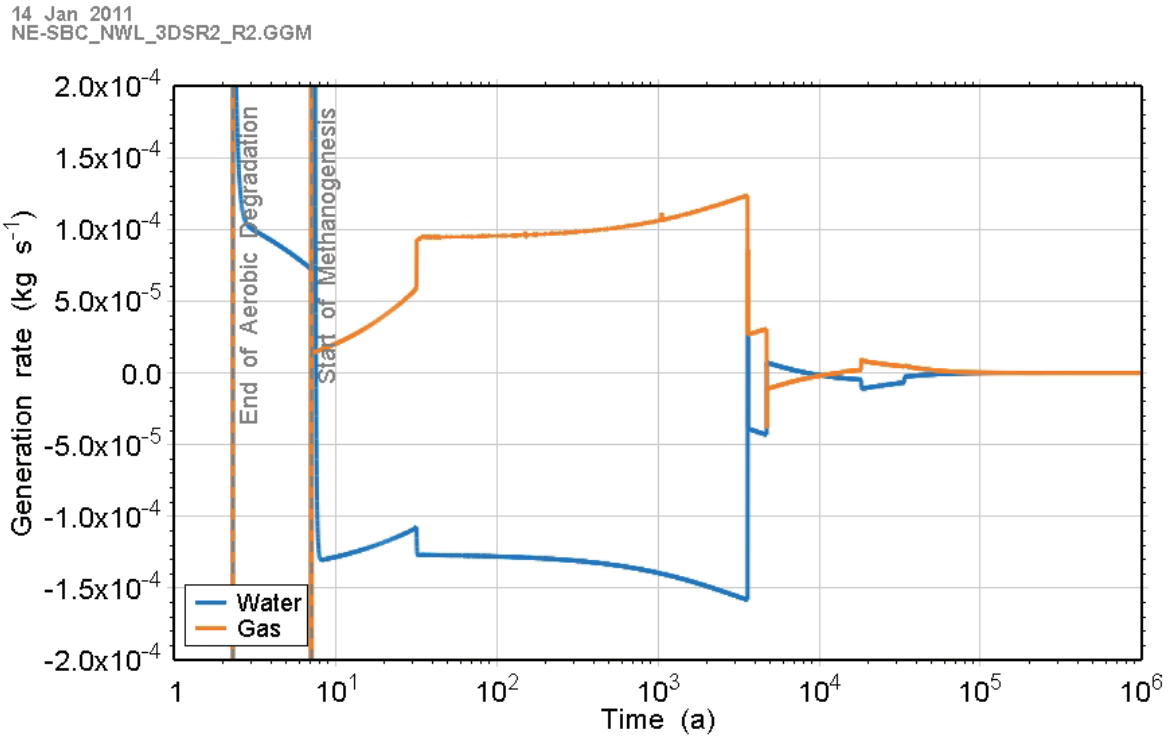

Figure 5.44: NE-SBC: Gas and Water Generation Rates

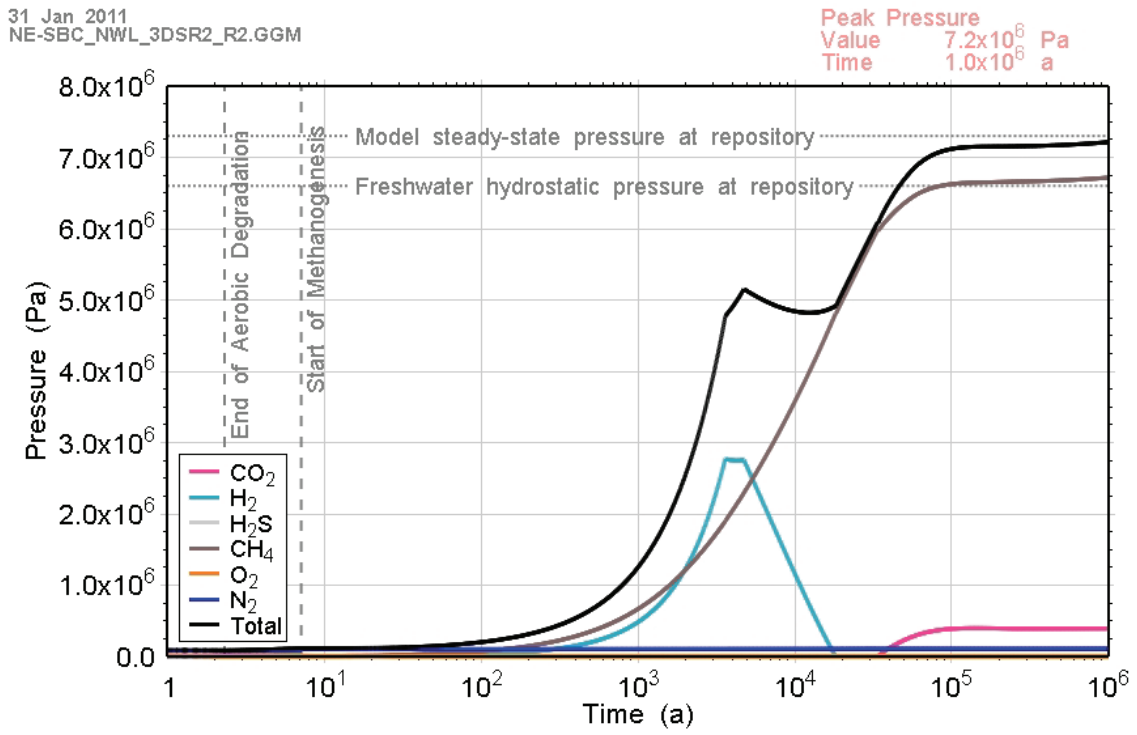

Figure 5.45: NE-SBC: Total and Partial Gas Pressures within the Repository

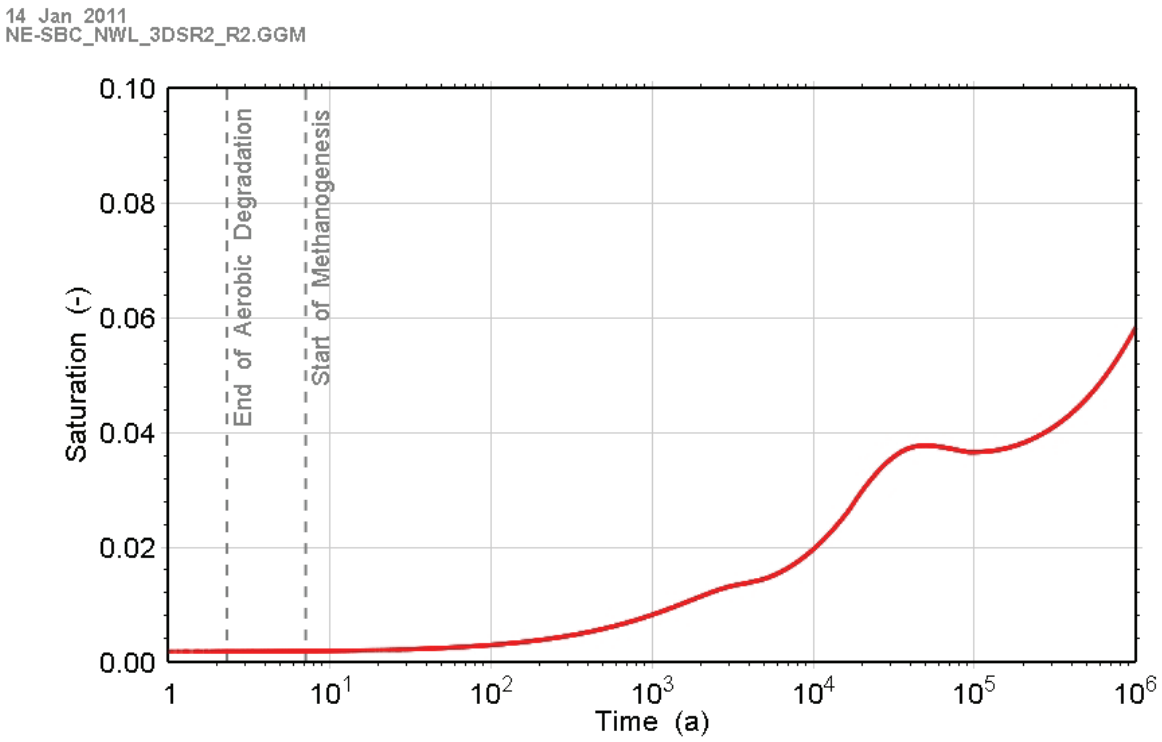

Figure 5.46: NE-SBC: Water Saturation within the Repository

5.2.2 Gas and Water Flows

The description below of shaft resaturation and repository flow is based on 3DD results, with some 3DSRS results presented for comparison. The discussion of long-term repository and geosphere behaviour is based on the 3DSRS model results.

5.2.2.1 Shaft

Shaft results to 1,000,000 a from the 3DD model are presented in Figure 5.47 through Figure 5.53 The figures show a relatively rapid resaturation of the shaft and establishment of groundwater flows down the shaft due to the hydraulic pressure difference between the host rock and initial shaft condition, as the repository repressurizes. Bentonite/sand shaft materials are resaturated by 1000 a, and the asphalt seal by 2000 a. Some portions of the monolith remain partially saturated at low levels (less than 1%) until approximately 20,000 a. Note that gas saturations are shown on a logarithmic scale and only presented where gas saturations exceed 10^{-4}. The uncoloured areas in gas saturation figures represent liquid saturated volumes. Similarly dissolved gas concentrations are shown only where full or partial (greater than 10%) liquid saturation exists and where dissolved gas levels exceed 10^{-4} kg/m^3. The pressure shown in the second panel of each figure is gas pressure.

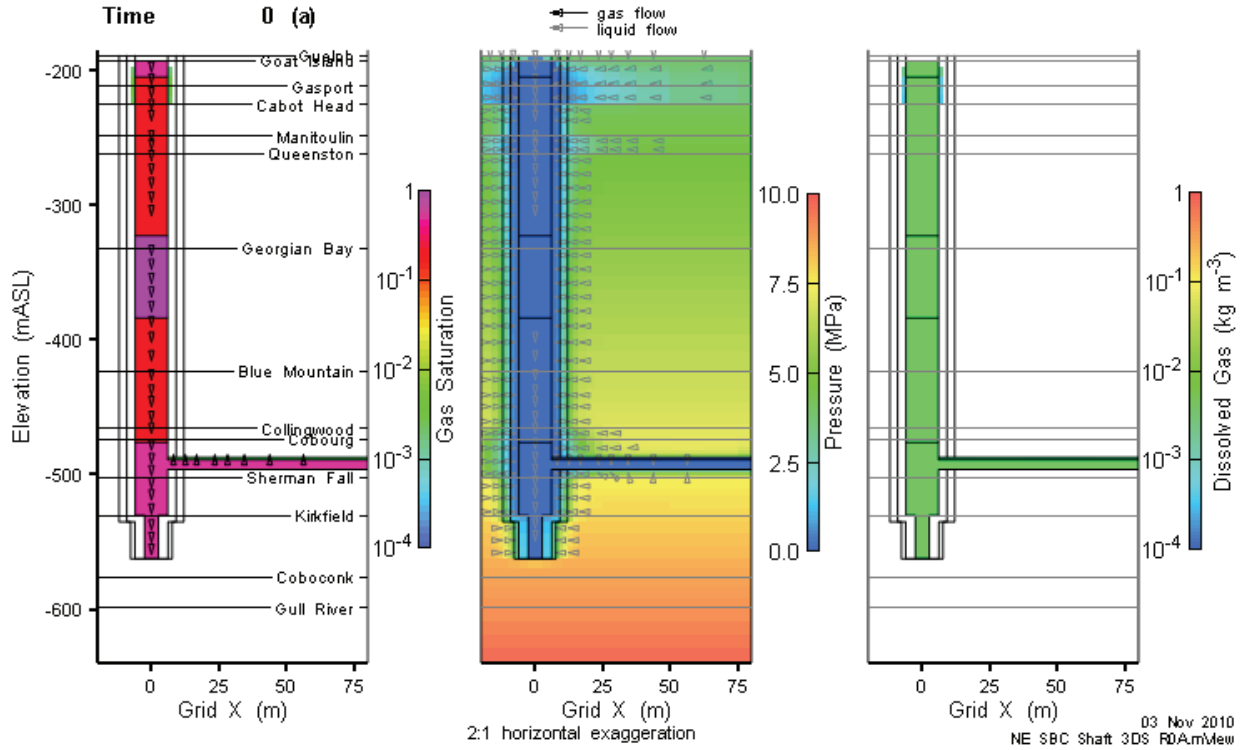

Figure 5.47: NE-SBC: 3DD Model Shaft Saturations, Flows and Gas Pressures (0 a)

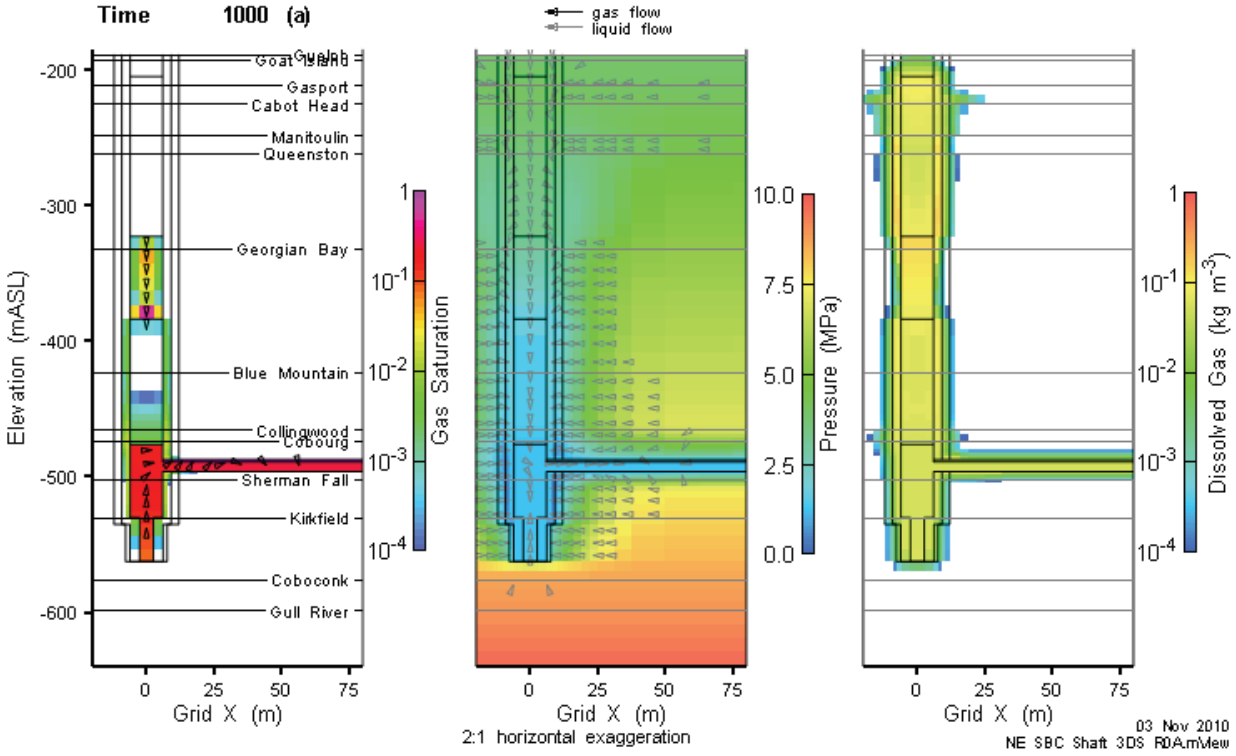

Figure 5.48: NE-SBC: 3DD Model Shaft Saturations, Flows and Pressures (1000 a)

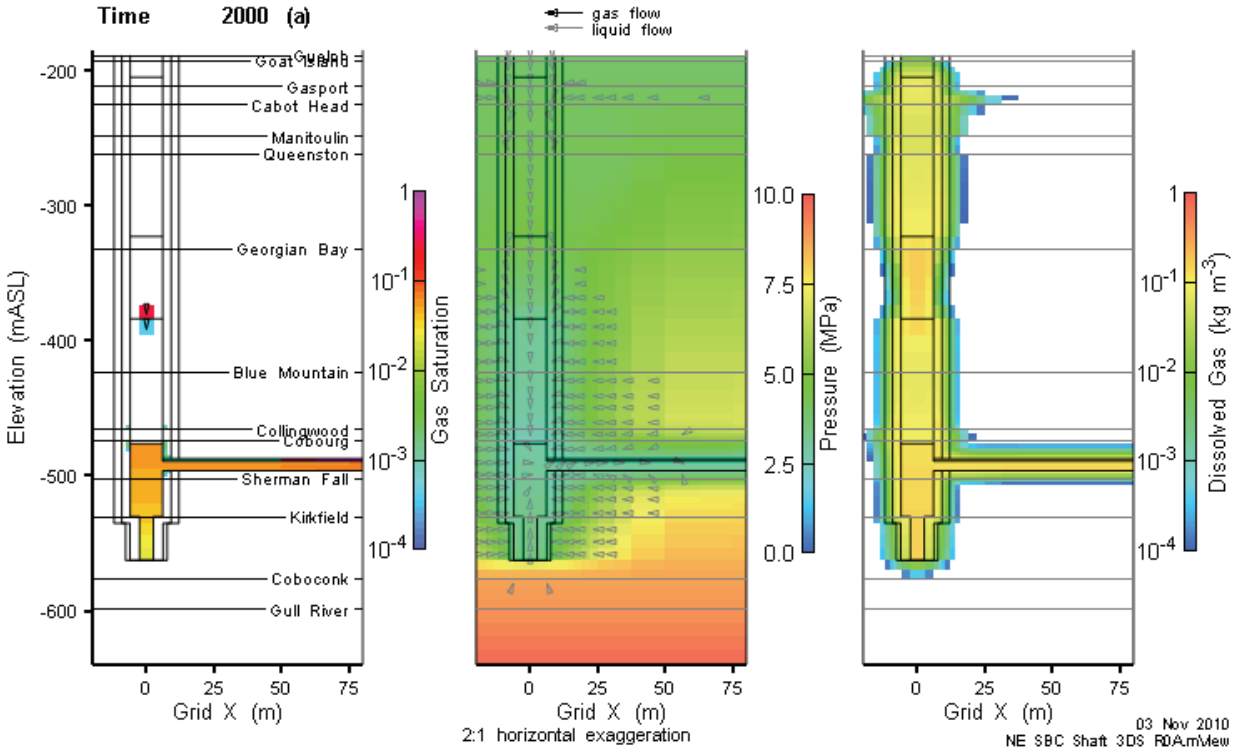

Figure 5.49: NE-SBC: 3DD Model Shaft Saturations, Flows and Pressures (2000 a)

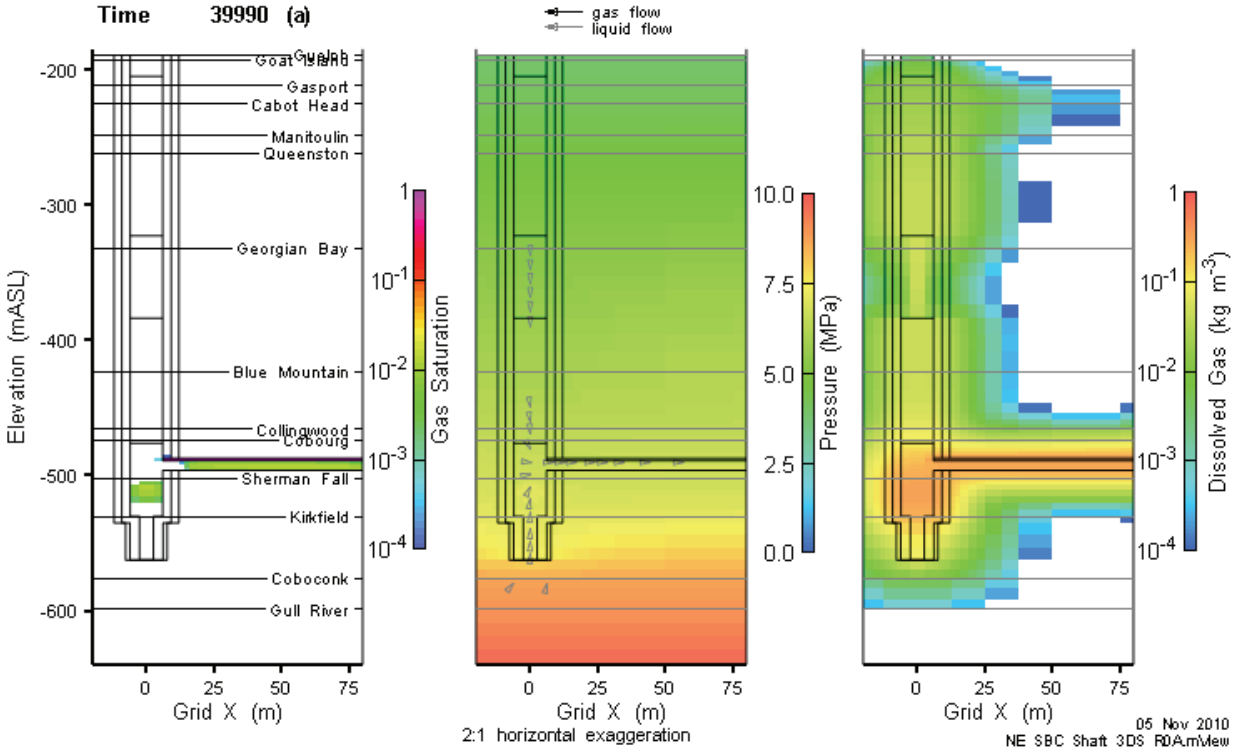

Figure 5.50: NE-SBC: 3DD Model Shaft Saturations, Flows and Pressures (40,000 a)

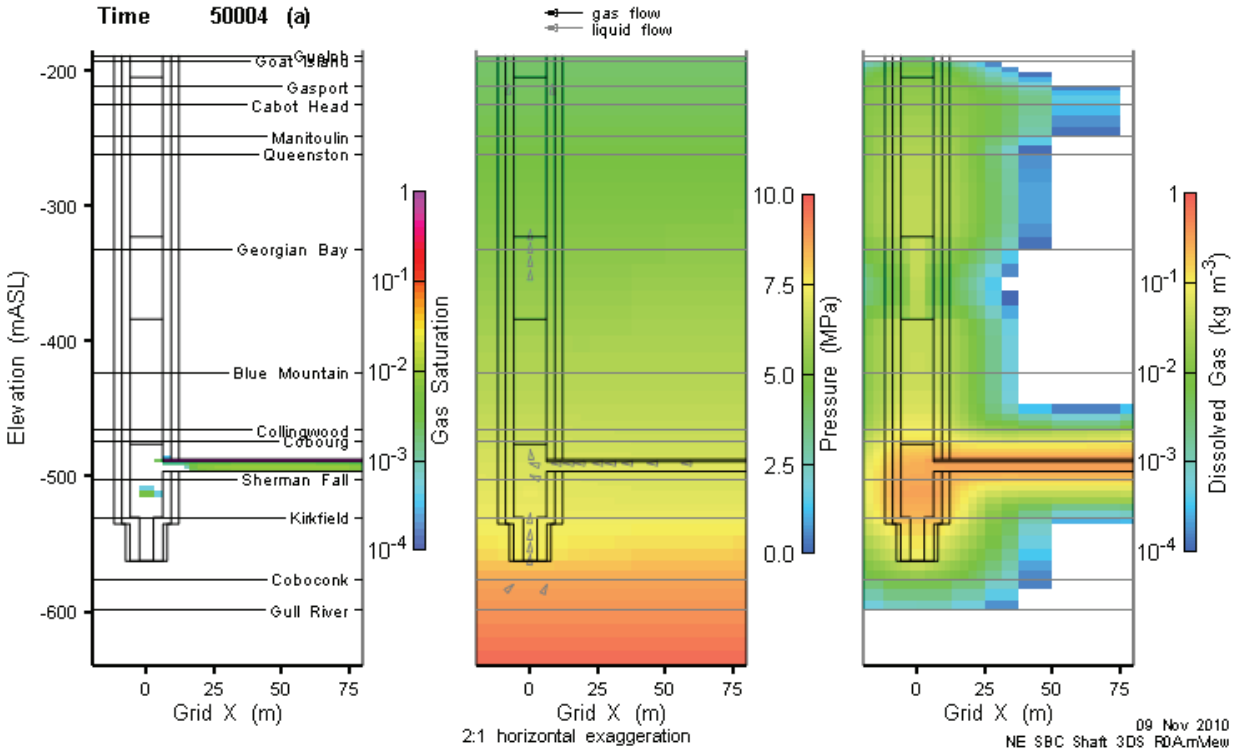

Figure 5.51: NE-SBC: 3DD Model Shaft Saturations, Flows and Pressures (50,000 a)

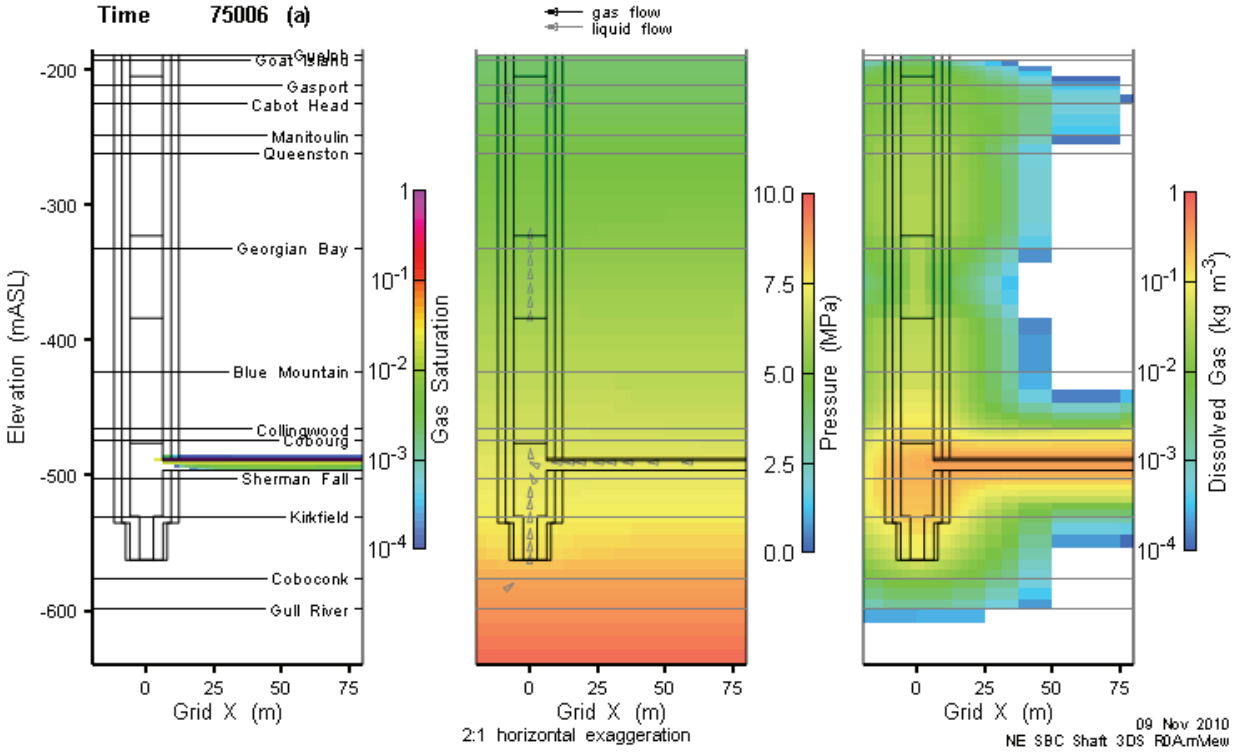

Figure 5.52: NE-SBC: 3DD Model Shaft Saturations, Flows and Pressures (75,000 a)

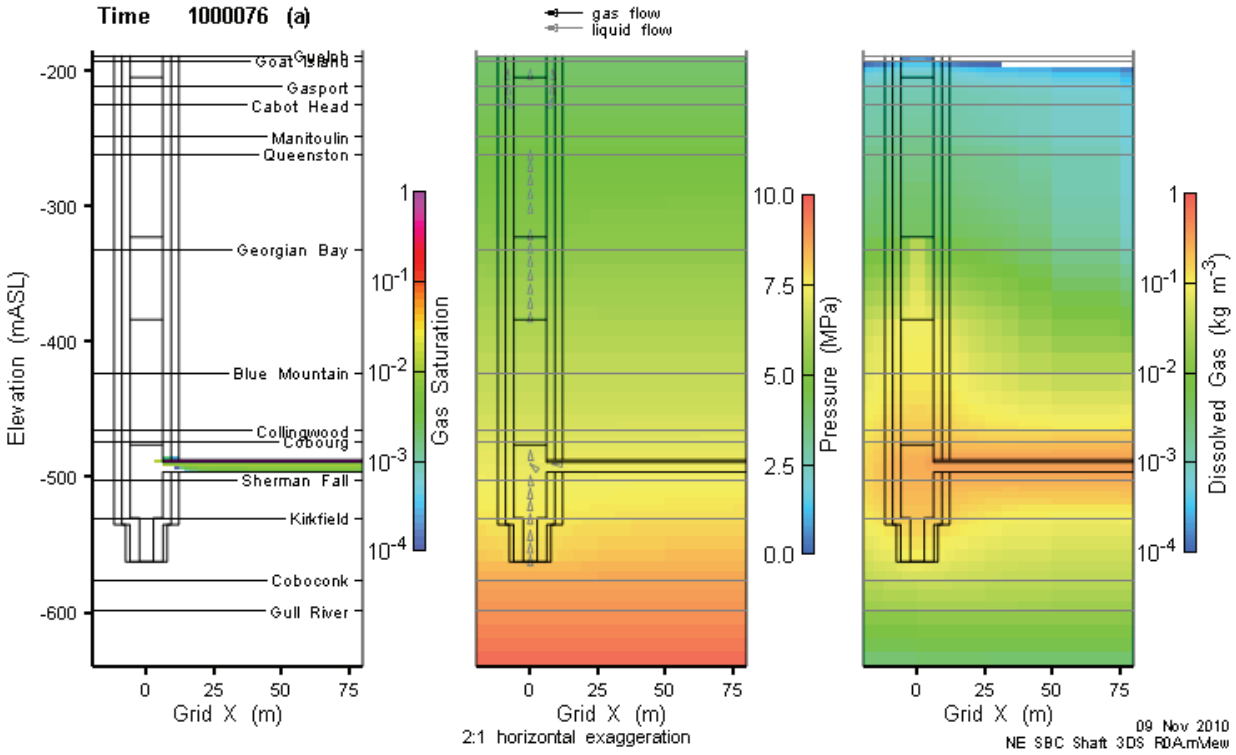

Figure 5.53: NE-SBC: 3DD Model Shaft Saturations, Flows and Pressures (1,000,000 a)

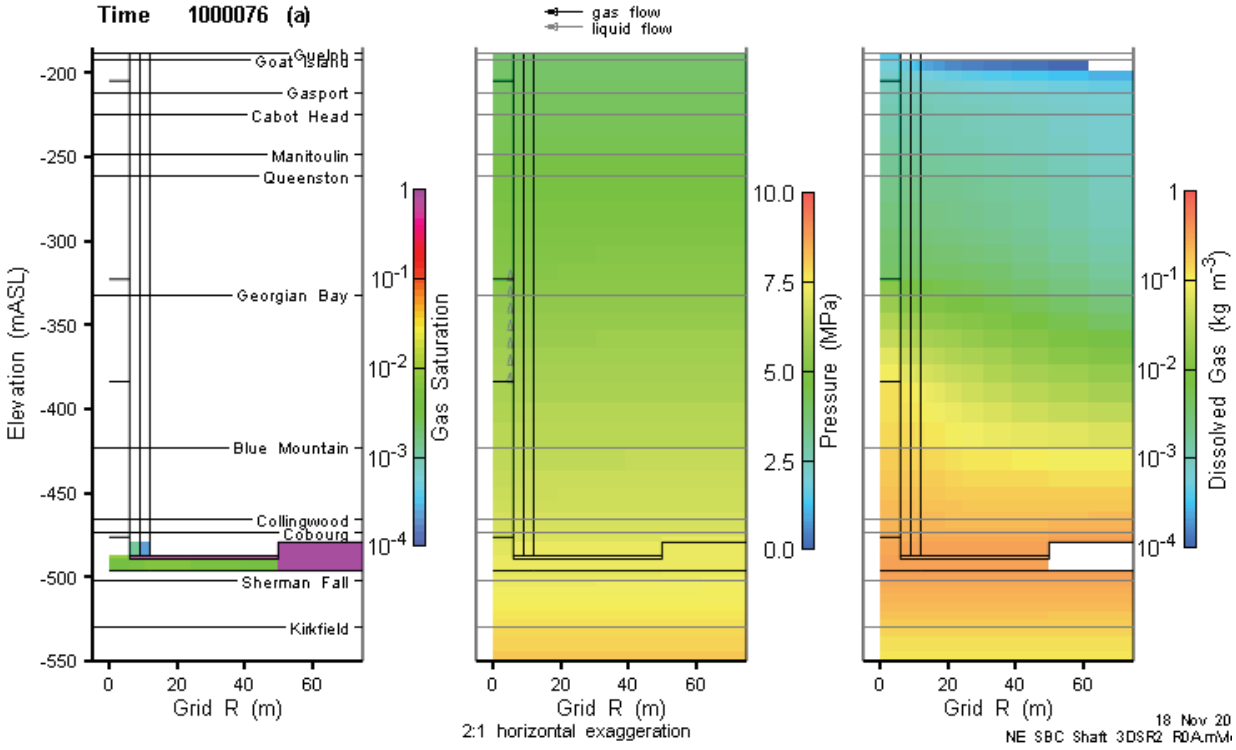

Figure 5.54: NE-SBC: 3DSRS Model Shaft Saturations, Flows and Pressures (1,000,000 a)

Similar results are also seen in the 3DSRS model, as shown in Figure 5.54 at 1,000,000 a.

By 50,000 a, gas pressures in the repository have risen to the point that gas is flowing out of the repository, through the HDZ. Liquid flow directions have also reversed as the rise in repository pressures reverses the liquid pressure gradient. Inflow of liquid into the lower shafts below the repository also contributes to shaft flow as the shaft forms a preferential flow path with a much higher permeability than the rock mass. However, gas flow up the shaft and EDZ is still at very low levels, as indicated by the lack of displayed velocity vectors in Figure 5.50. The presence of gas is apparent in the HDZ and immediately above the monolith in the shaft inner EDZ in Figure 5.51. By 75,000 a liquid flow in the shaft is more strongly upwards as repository pressures have risen further, while gas flow remains negligible (Figure 5.52).

Beyond 75,000 a, pressures remain at near equilibrium, with liquid flow directed upwards from the repository. This flow system (upward liquid flow) remains in place for the remainder of the simulation, as shown in Figure 5.53. Figure 5.54 shows 3DSRS model results at 1,000,000 a for comparison.

Time series profiles of shaft saturation state, pressures and gas flows are given in Figure 5.55 through Figure 5.58.

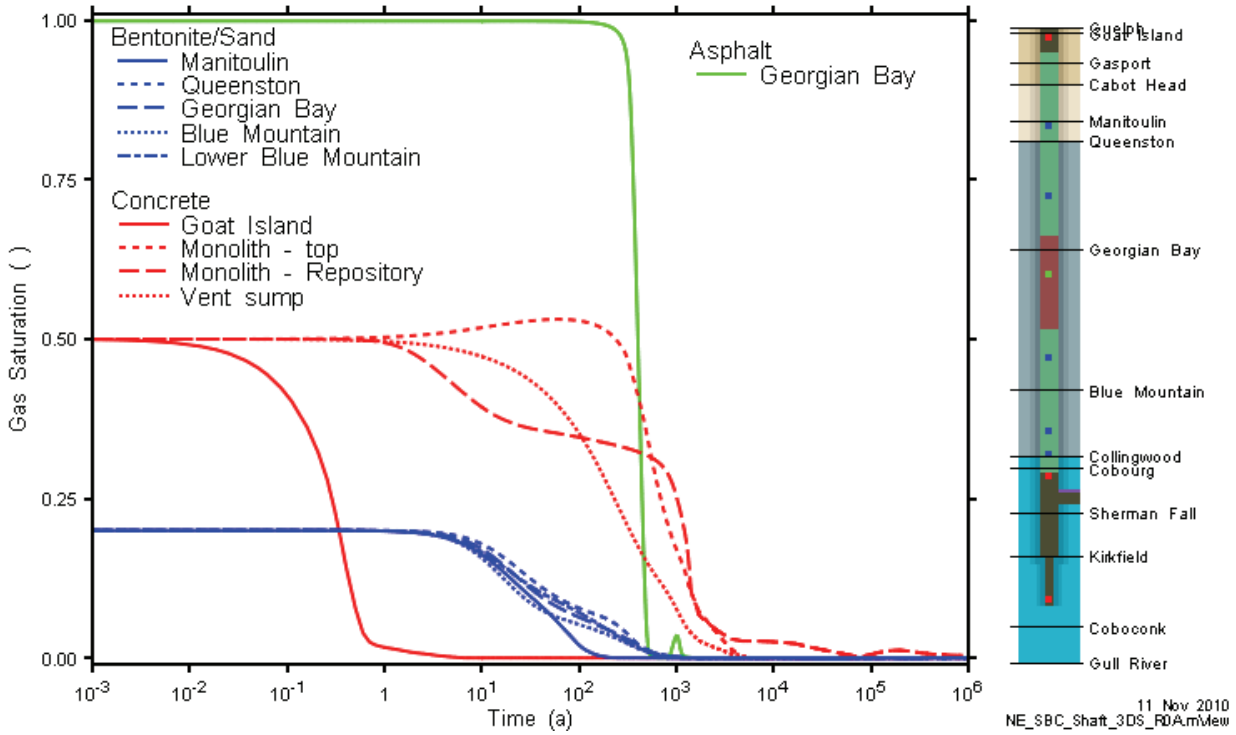

Figure 5.55: NE-SBC: 3DD Shaft Gas Saturation at Selected Monitoring Points

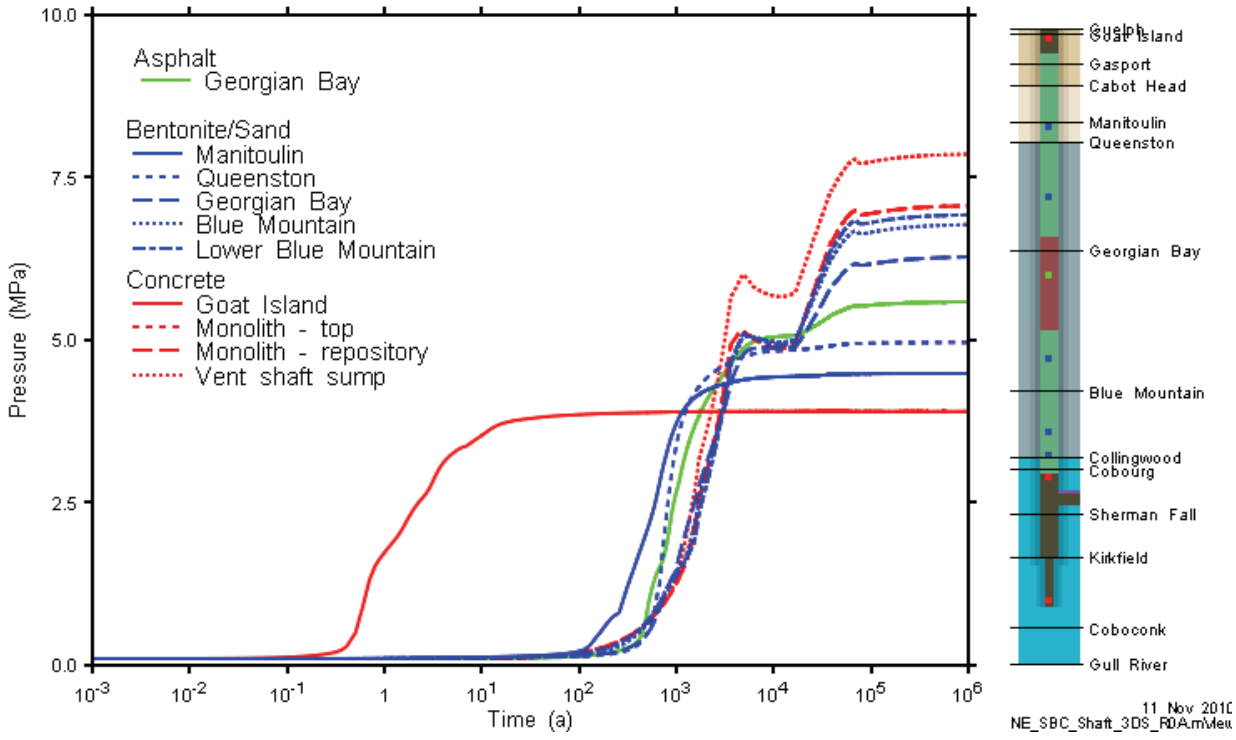

Figure 5.56: NE-SBC: 3DD Shaft Gas Pressure at Selected Monitoring Points

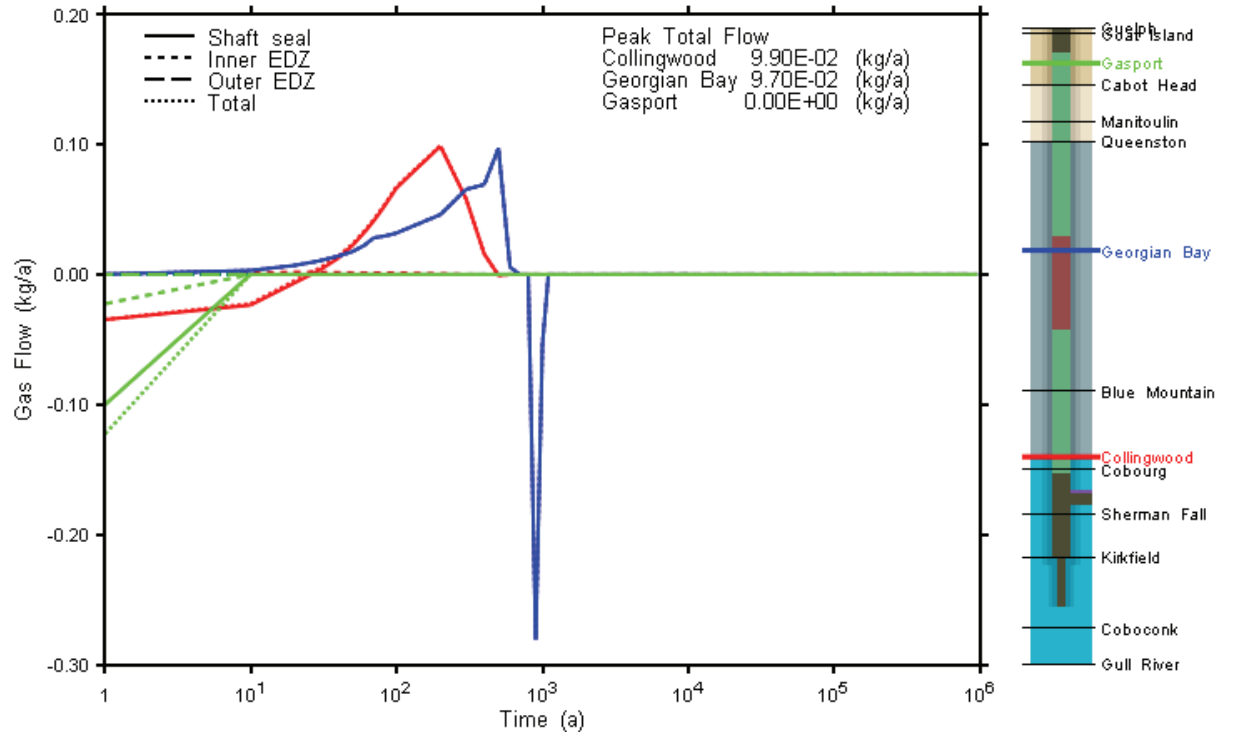

Figure 5.57: NE-SBC: 3DD Shaft Gas Flow at Selected Monitoring Planes

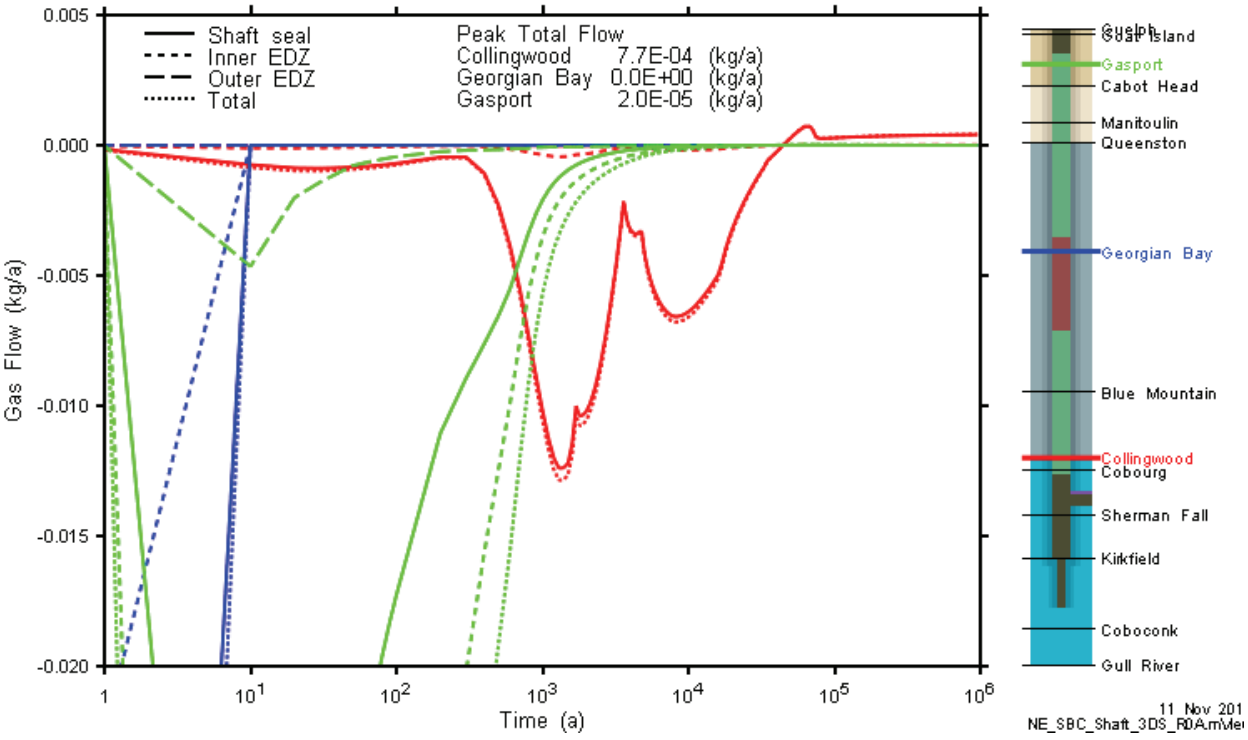

Figure 5.58: NE-SBC: 3DD Shaft Dissolved Gas Flow at Selected Monitoring Planes

Gas flows in the shaft are insignificant, as shown in Figure 5.57 and Figure 5.58. All flows within the shaft system represent the transport of gas that was initially present within the shaft and the flows are largely induced by saturation processes within the shaft. The negative spike in Georgian Bay flows shown at approximately 1000 a in Figure 5.57 is due to resaturation processes within the asphalt seal.

5.2.2.2 Repository System

Figure 5.59 presents a comparison of repository pressures and liquid saturations for the three models. The NE-RC results for the 3DD model are also shown for comparison. Agreement between all NE-SBC models is very good, indicating that the shaft system (not present in the 3DSR model) has little impact on overall performance.

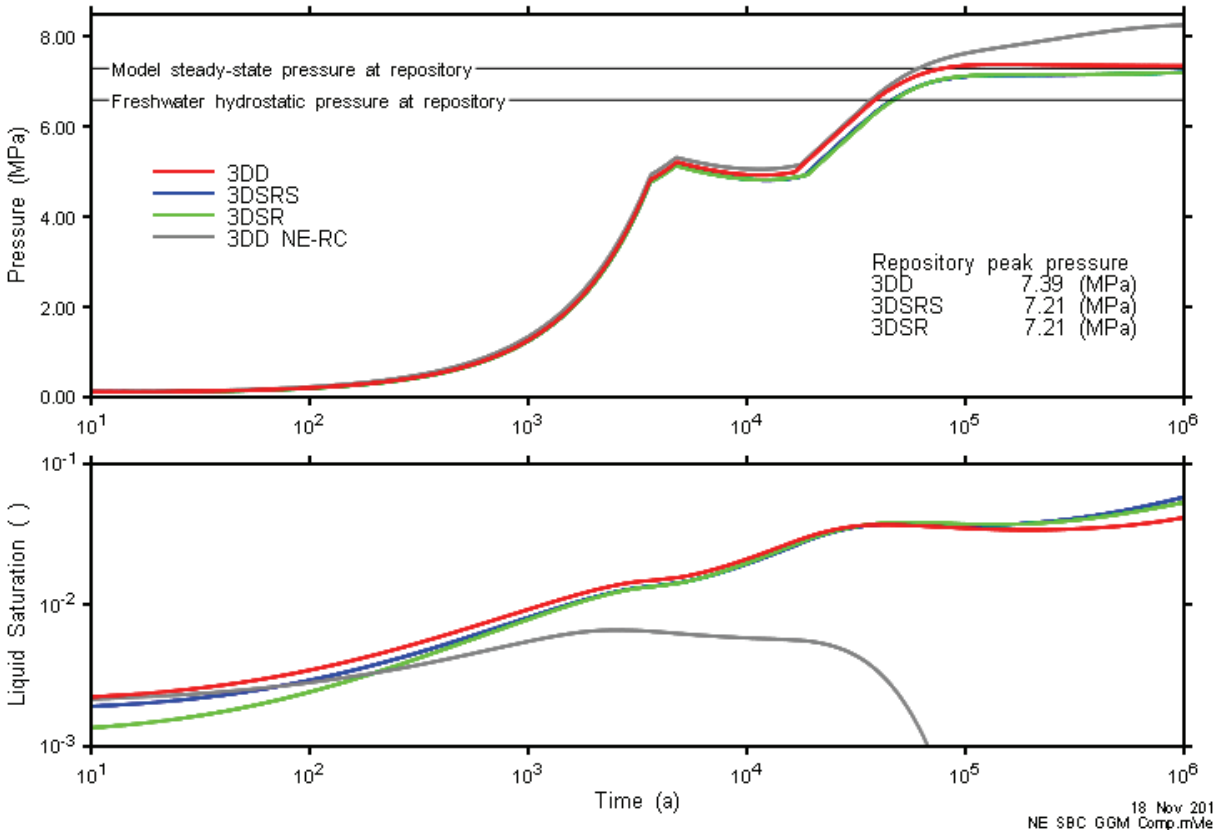

Figure 5.59: NE-SBC: Comparison of 3DD, 3DSRS and 3DSR Model Results

3DD model initial conditions in the repository are shown in Figure 5.60. The repository is almost entirely gas saturated. Pressures are at atmospheric within the shaft seal materials, repository and HDZ. Liquid is flowing towards the repository, while some small amounts of gas are flowing from the shaft seals towards the intact rock.

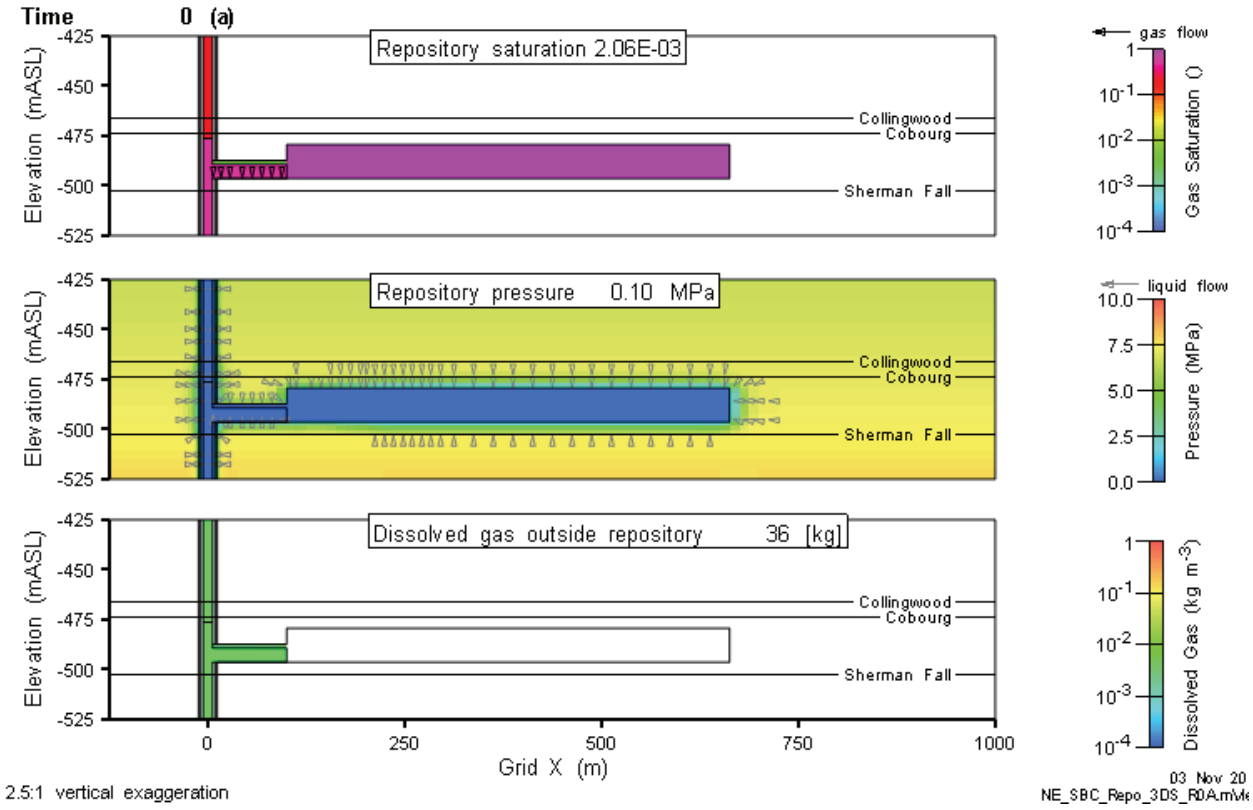

Figure 5.60: NE-SBC: 3DD Repository Saturations, Flows and Pressures (0 a)

Figure 5.61 through Figure 5.64 show the development of the flow system around the repository at 500, 5000, 25,000, and 50,000 a. At 25,000 a, a small amount of liquid resaturation can be seen in the bottom of the repository. Advective gas flow is essentially zero over this period, except for some minor flows associated with resaturation of the concrete monolith. All liquid flow remains directed at the repository and shaft system.

Results at 100,000 a and 1,000,000 a are shown in Figure 5.65 and Figure 5.66. There is very little change in repository saturation, pressure or flows over this period. Gas continues to dissolve in the porewater at the edge of the gas saturation front and thereafter diffuse through the intact rock. Repository pressures have stabilized near the initial steady-state pressure and are very slowly climbing as the geosphere equilibrates.

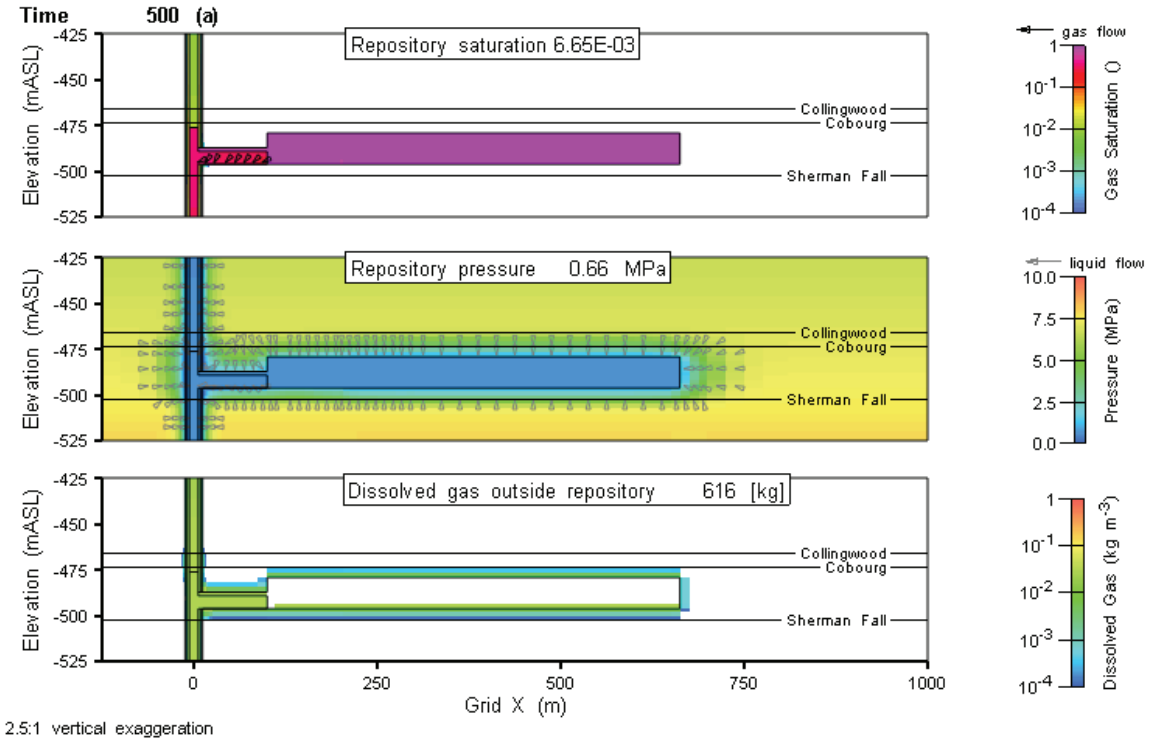

Figure 5.61: NE-SBC: 3DD Repository Saturations, Flows and Pressures (500 a)

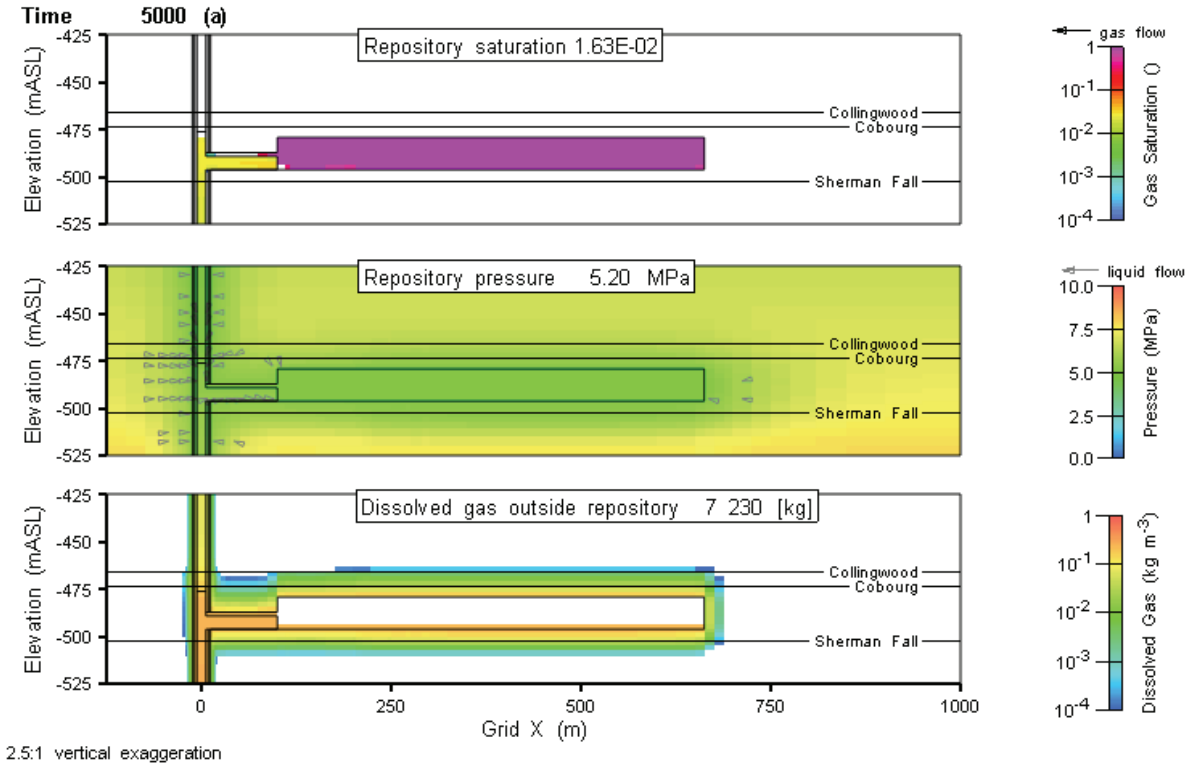

Figure 5.62: NE-SBC: 3DD Repository Saturations, Flows and Pressures (5000 a)

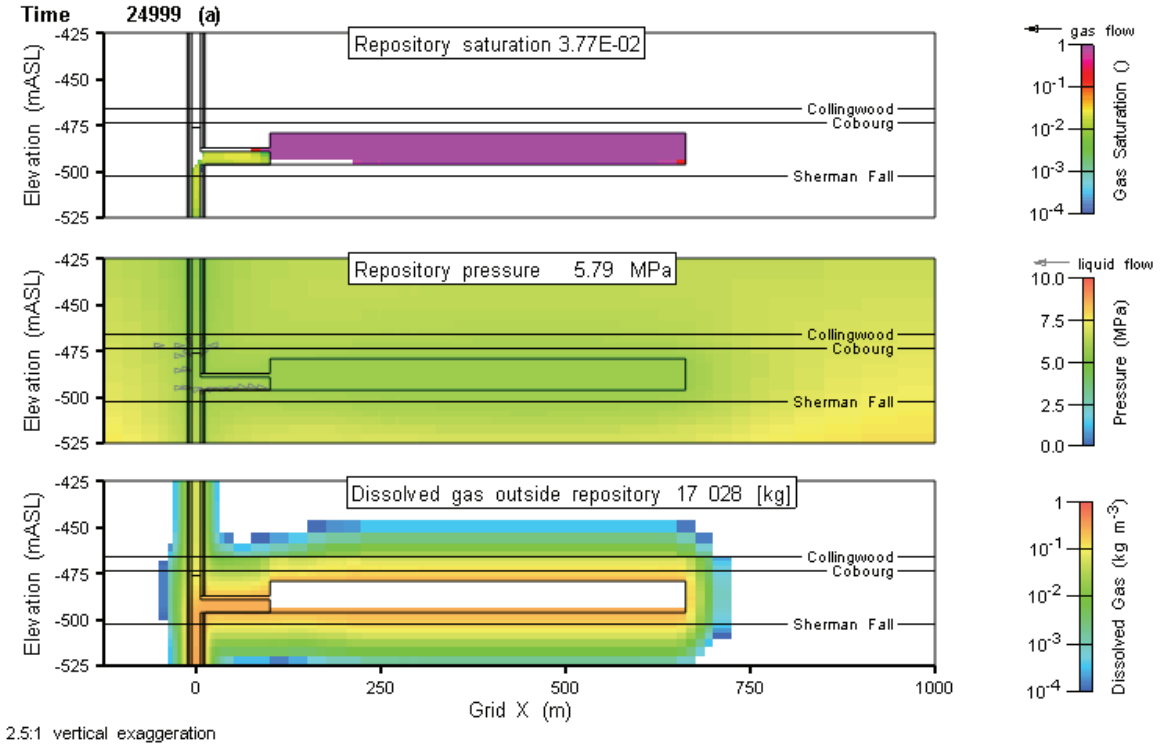

Figure 5.63: NE-SBC: 3DD Repository Saturations, Flows and Pressures (25,000 a)

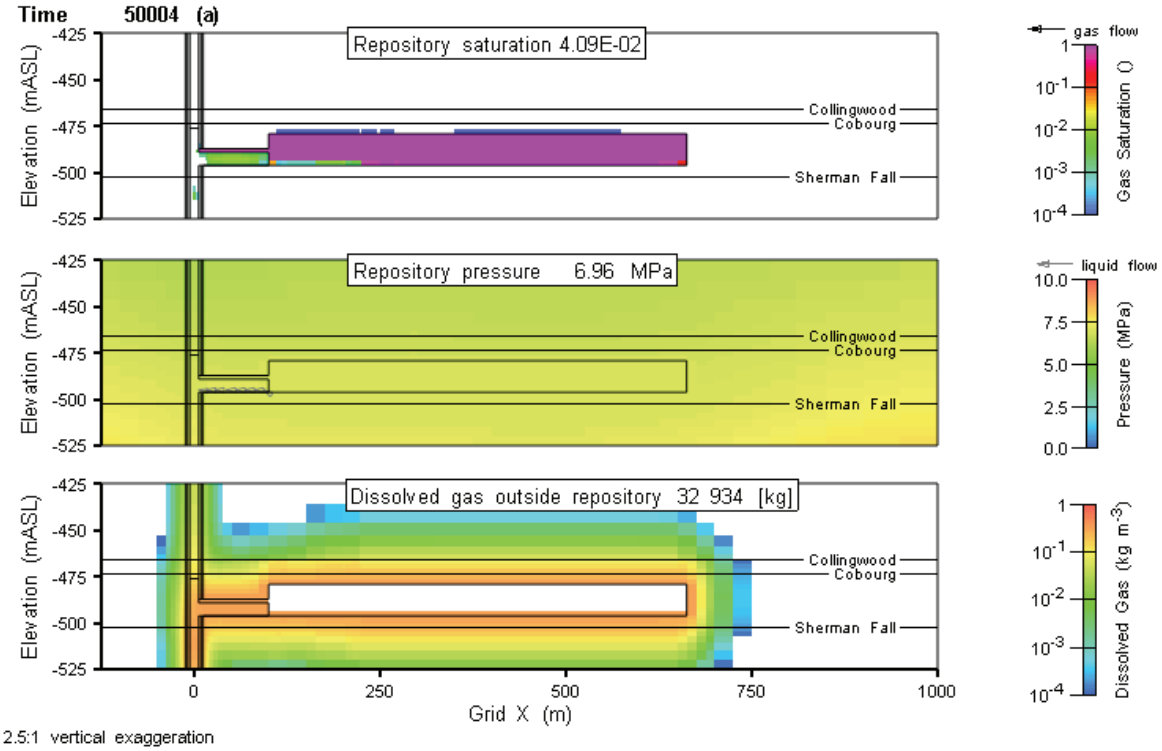

Figure 5.64: NE-SBC: 3DD Repository Saturations, Flows and Pressures (50,000 a)

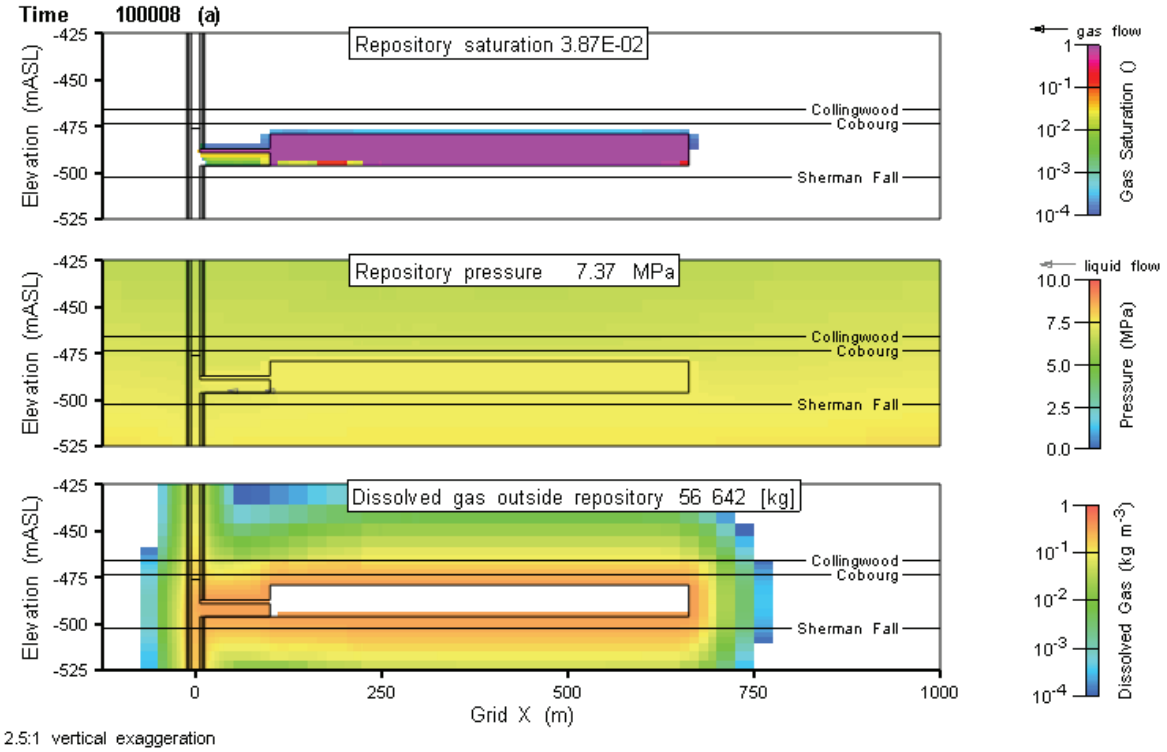

Figure 5.65: NE-SBC: 3DD Repository Saturations, Flows and Pressures (100,000 a)

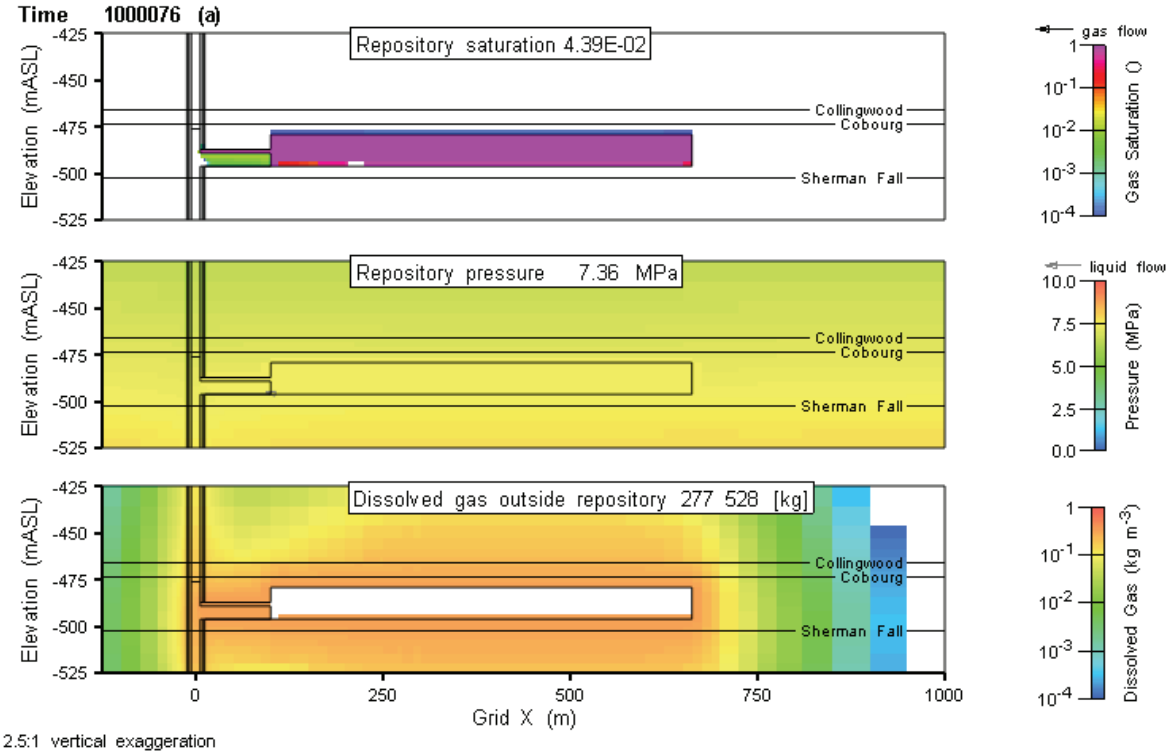

Figure 5.66: NE-SBC: 3DD Repository Saturations, Flows and Pressures (1,000,000 a)

Figure 5.67 shows cumulative inflow of water into the repository, and gas out of the repository, differentiated by source. The small contribution of water via the shaft (and HDZ/Monolith) up to 40,000 a is apparent on the figure.

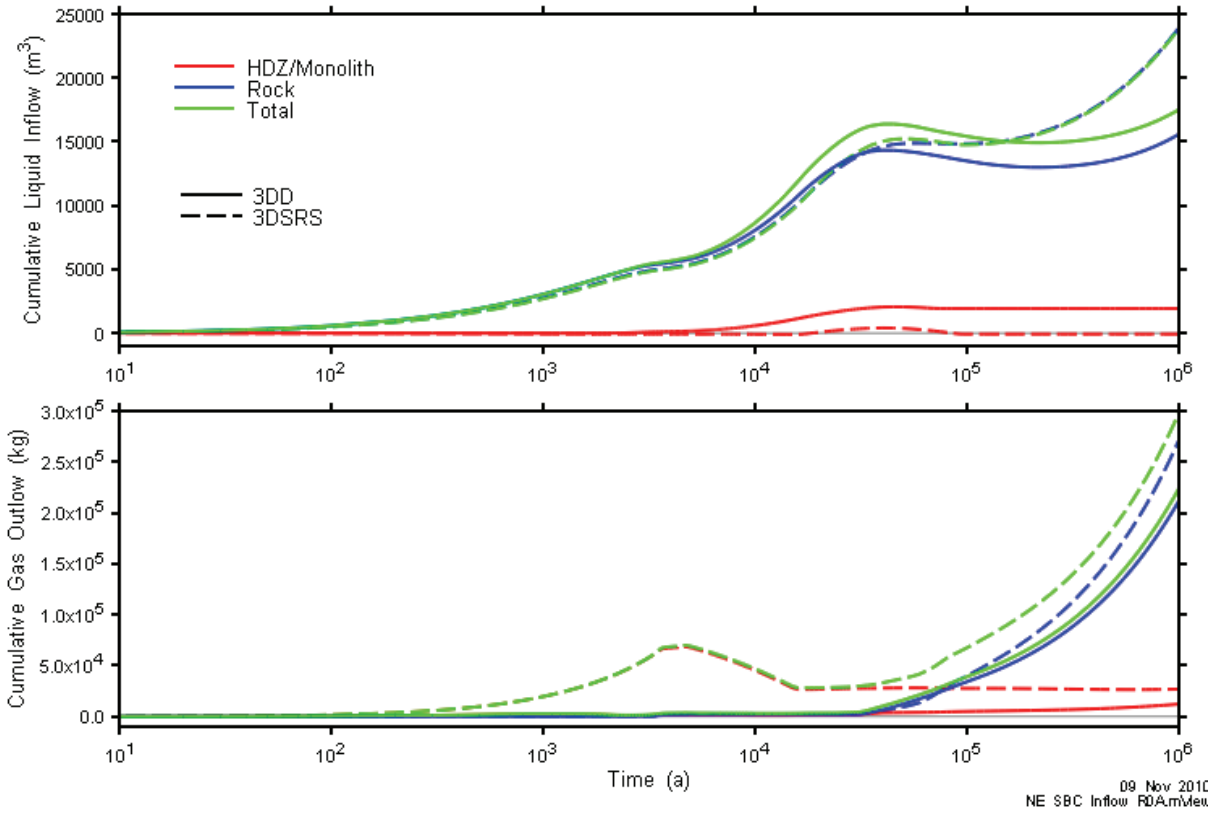

Figure 5.67: NE-SBC: Repository Liquid Inflow and Gas Outflow for 3DD and 3DSRS Models

In general, the flows into the HDZ/monolith can be expected to be representative of shaft flows, although resaturation/desaturation processes within the concrete and HDZ may affect the timing. The volume of monolith concrete is proportionately much greater in the 3DSRS model due to the geometry of the implementation. This is the cause of the larger gas outflows for the 3DSRS model seen in the figure.

Figure 5.68 through Figure 5.73 are three-dimensional visualizations of gas saturation for the 3DD model at 0, 100, 1000, 10,000, 100,000, and 1,000,000 years, respectively. They show the very limited spatial extents of the zones beyond the repository with gas saturation exceeding 10^{-4}.

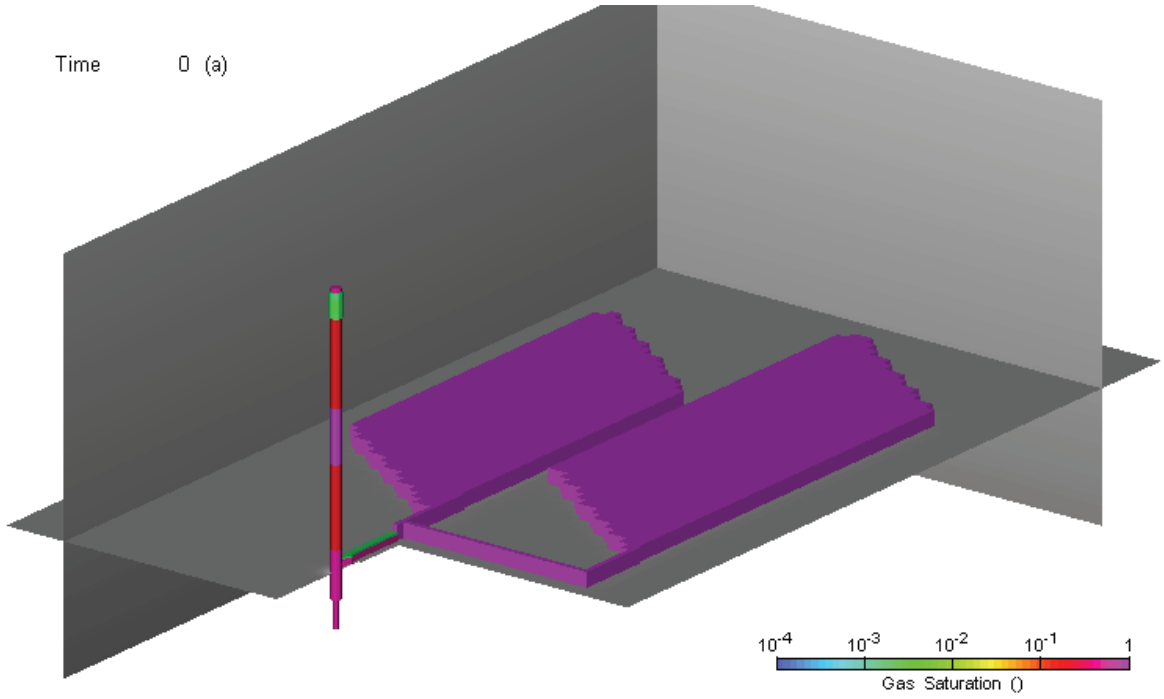

Figure 5.68: NE-SBC: Three-Dimensional Visualization of 3DD Model Gas Saturations at 0 a

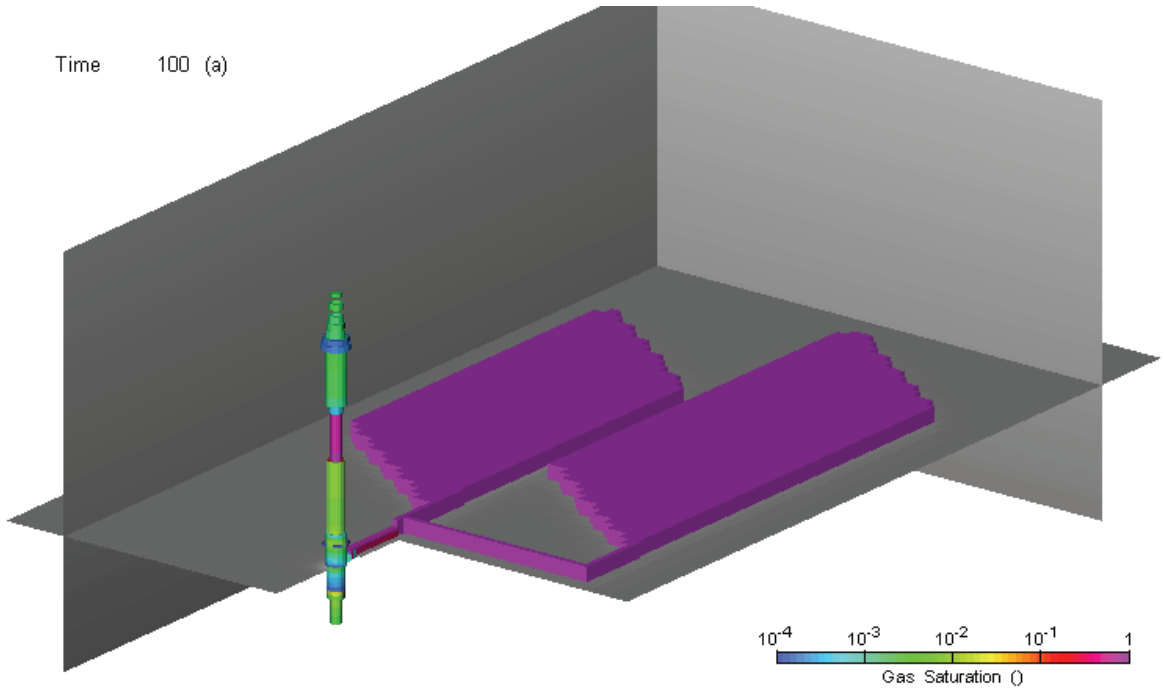

Figure 5.69: NE-SBC: Three-Dimensional Visualization of 3DD Model Gas Saturations at 100 a

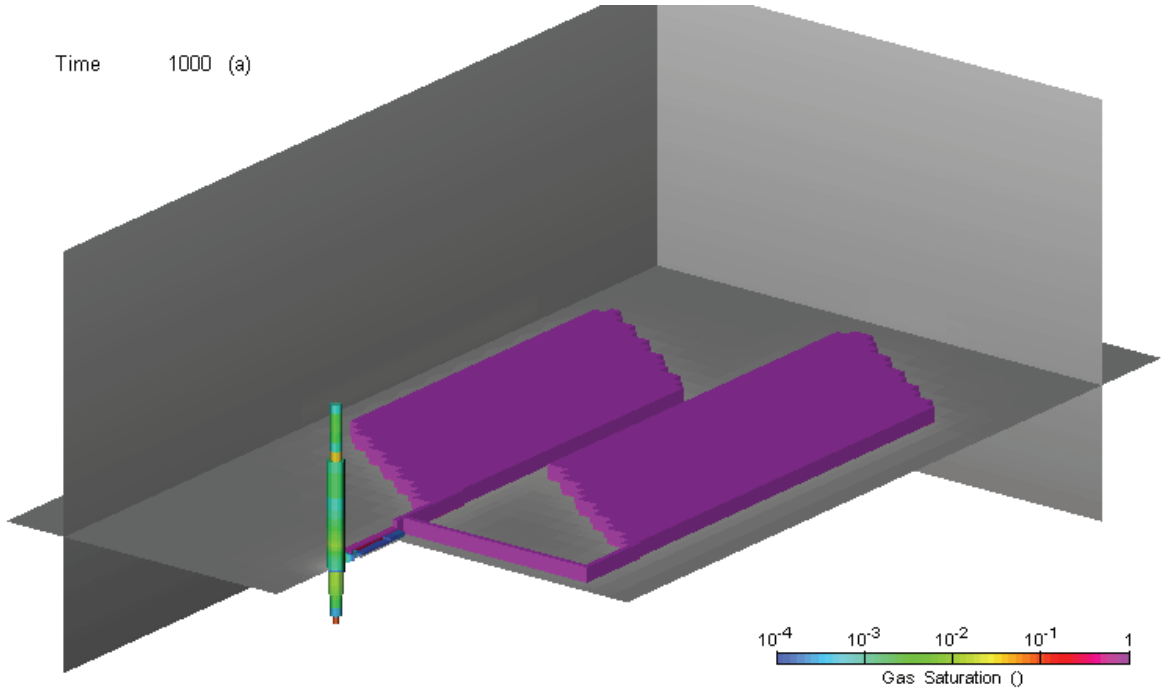

Figure 5.70: NE-SBC: Three-Dimensional Visualization of 3DD Model Gas Saturations at 1000 a

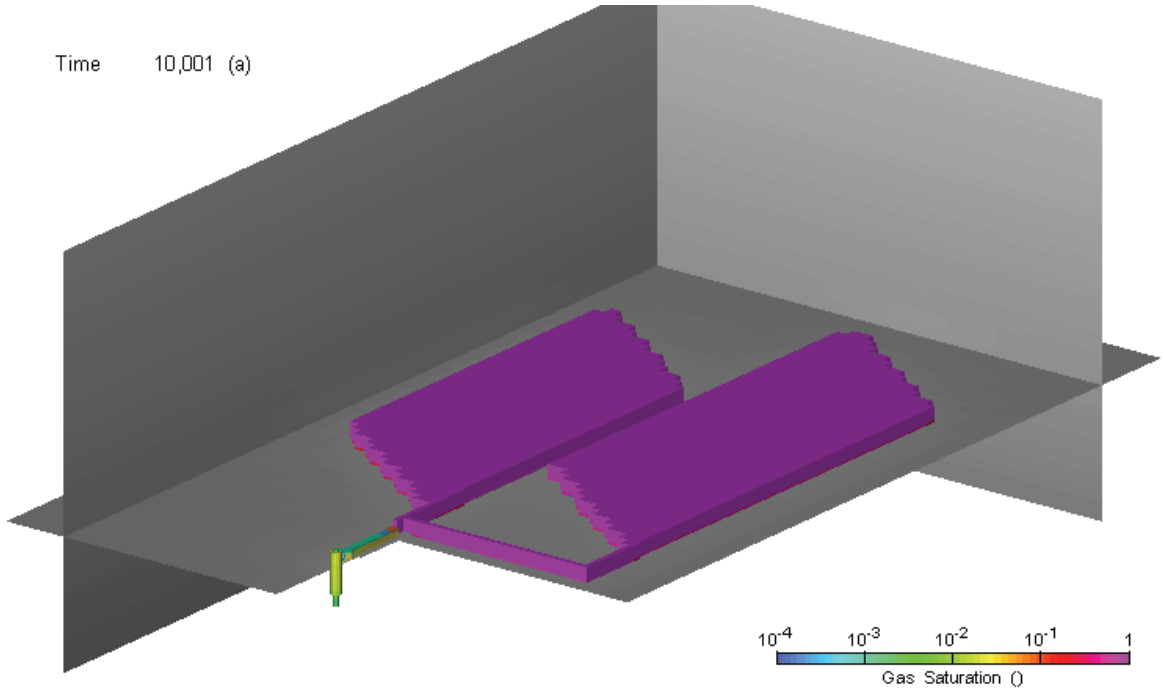

Figure 5.71: NE-SBC: Three-Dimensional Visualization of 3DD Model Gas Saturations at 10,000 a

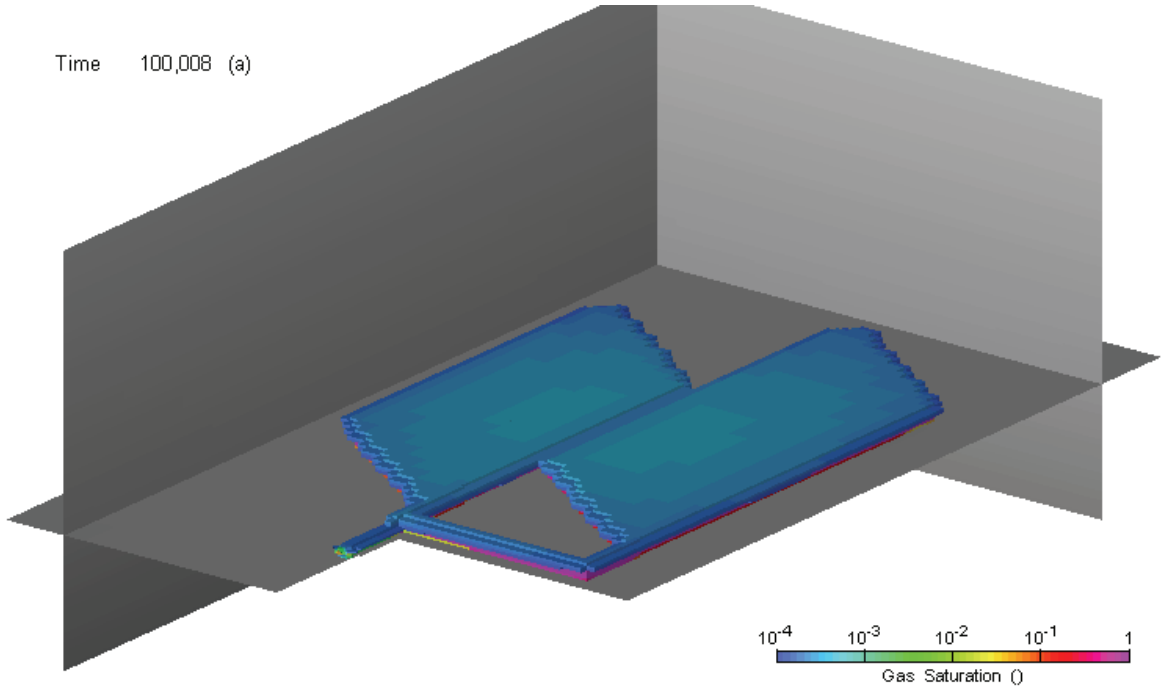

Figure 5.72: NE-SBC: Three-Dimensional Visualization of 3DD Model Gas Saturations at 100,000 a

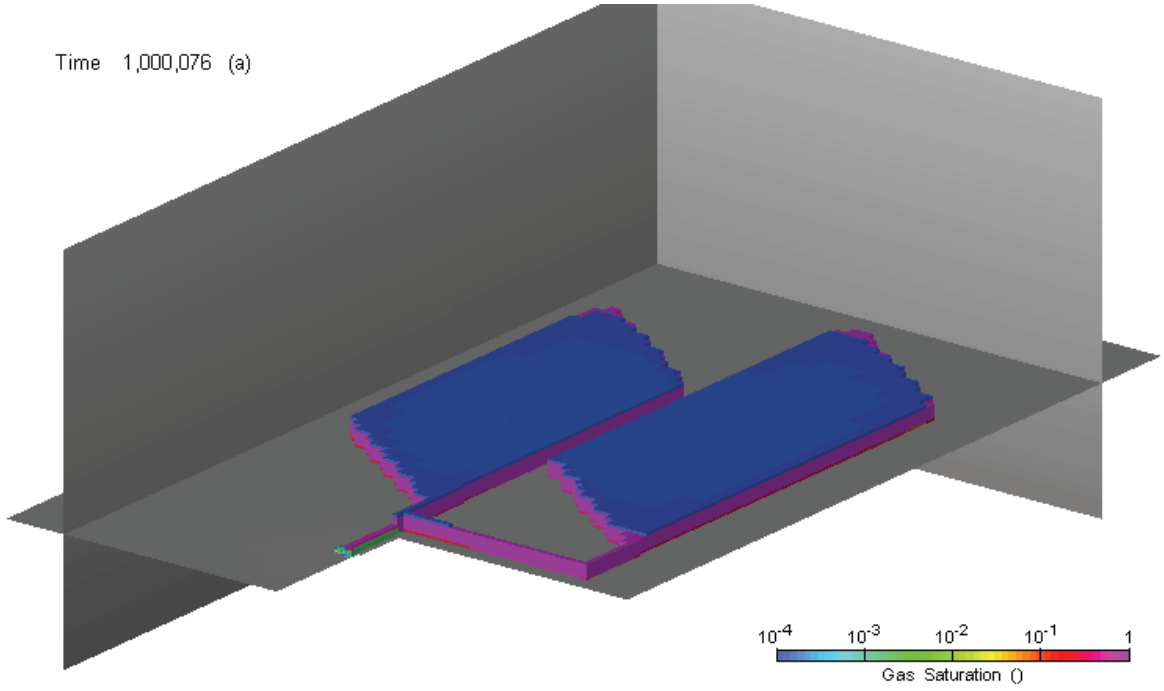

Figure 5.73: NE-SBC: Three-Dimensional Visualization of 3DD Model Gas Saturations at 1,000,000 a

5.2.2.3 Geosphere

The pressure profile (expressed as environmental head) for the NE-SBC case is shown in Figure 5.74. The initial head in the repository is to the left of the Y axis at a value of -670 m (equivalent to depth below ground surface). After 1,000,000 a, the presence of the repository has only slightly perturbed the steady-state pressure distribution. Above the Georgian Bay formation, and below the Kirkfield, pressures are very close to steady-state. The current measured Westbay pressures at DGR-4 are also shown as a point of comparison.

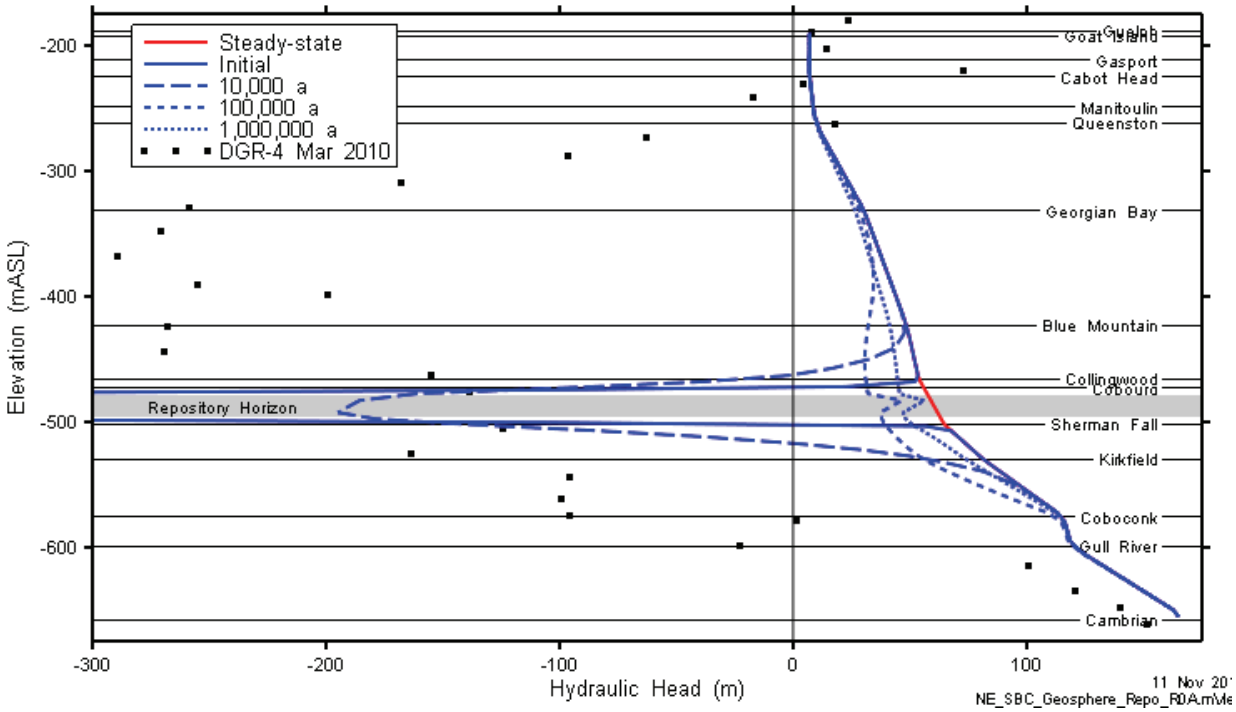

Figure 5.74: NE-SBC: 3DSRS Geosphere Head Profile

5.3 Case NE-AN3 – Reduced Geosphere Anisotropy

This case modifies the NE-SBC case by reducing the vertical permeability anisotropy of most Ordovician formations from 10:1 to 1:1, and that of the Coboconk and Gull River Formations from 1000:1 to 10:1. This increases vertical permeability of the Ordovician system, with the result that inflow of water into the repository is substantially increased relative to the NE-SBC case.

5.3.1 Gas Generation

Gas generation processes and timings are similar to the NE-SBC case and are not discussed further here.

5.3.2 Gas and Water Flows

5.3.2.1 Shaft

The flow system in the shaft develops similarly to that of the NE-SBC model. Long-term liquid flows up the shaft are at a slightly higher rate than NE-SBC due to the slightly overpressured repository system, described in the next section. Figure 5.75 shows the long-term flow system prevalent from approximately 100,000 a to 1,000,000 a.

Shaft resaturation and gas flow are very similar to the NE-SBC case. Figure 5.76 shows shaft resaturation while Figure 5.77 and Figure 5.78 summarize gas and dissolved gas flow through the shaft.

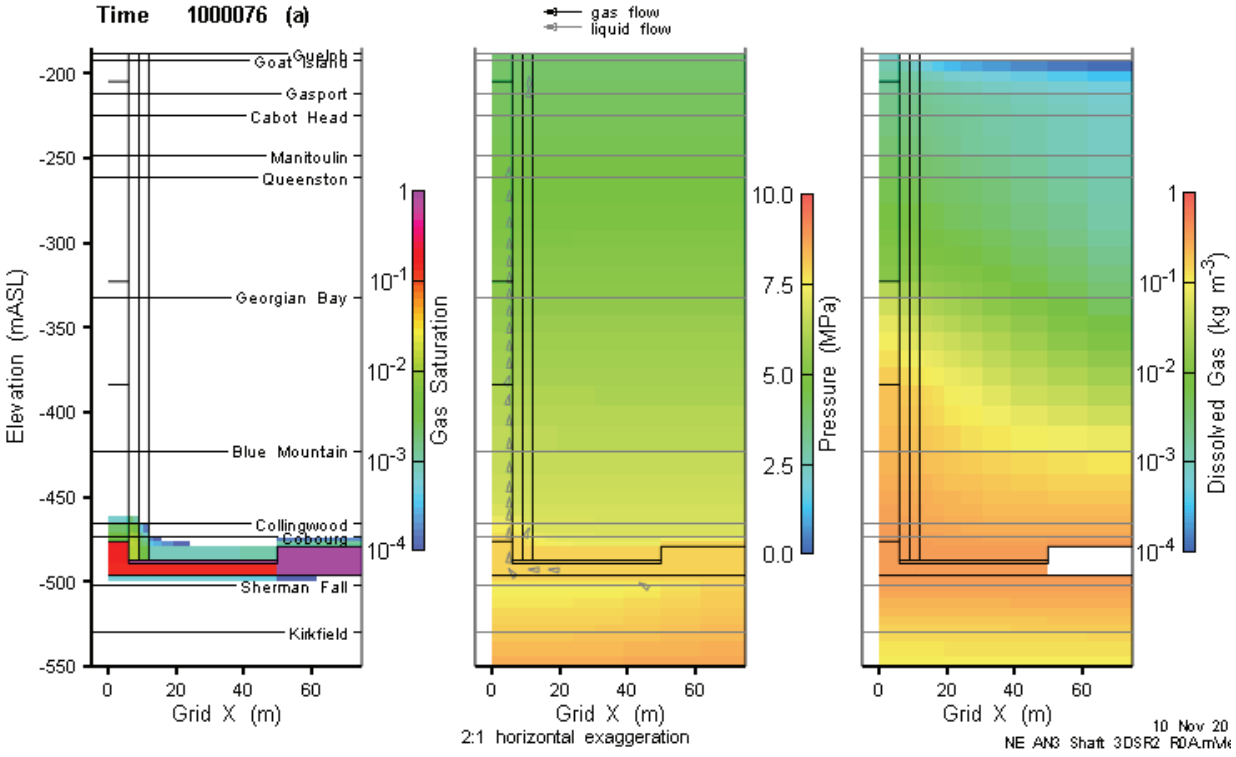

Figure 5.75: NE-AN3: 3DSRS Model Shaft Saturations, Flows and Pressures (1,000,000 a)

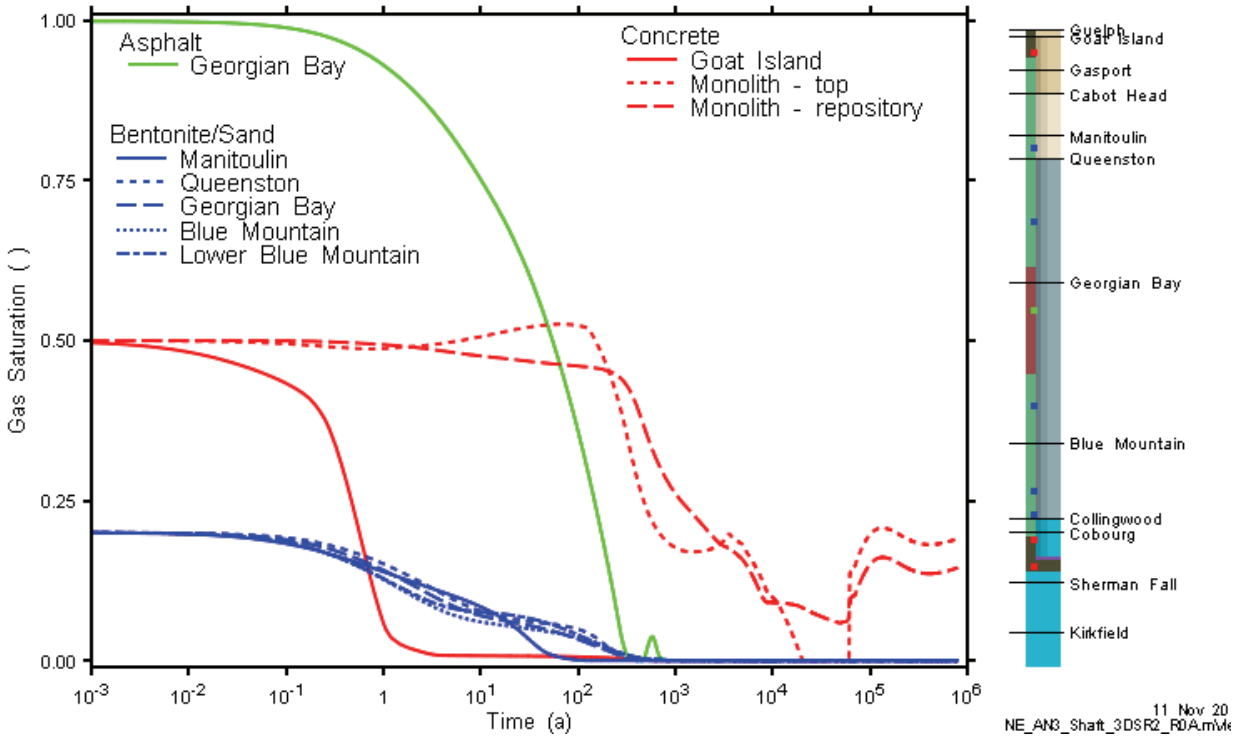

Figure 5.76: NE-AN3: 3DSRS Shaft Gas Saturation at Selected Monitoring Points

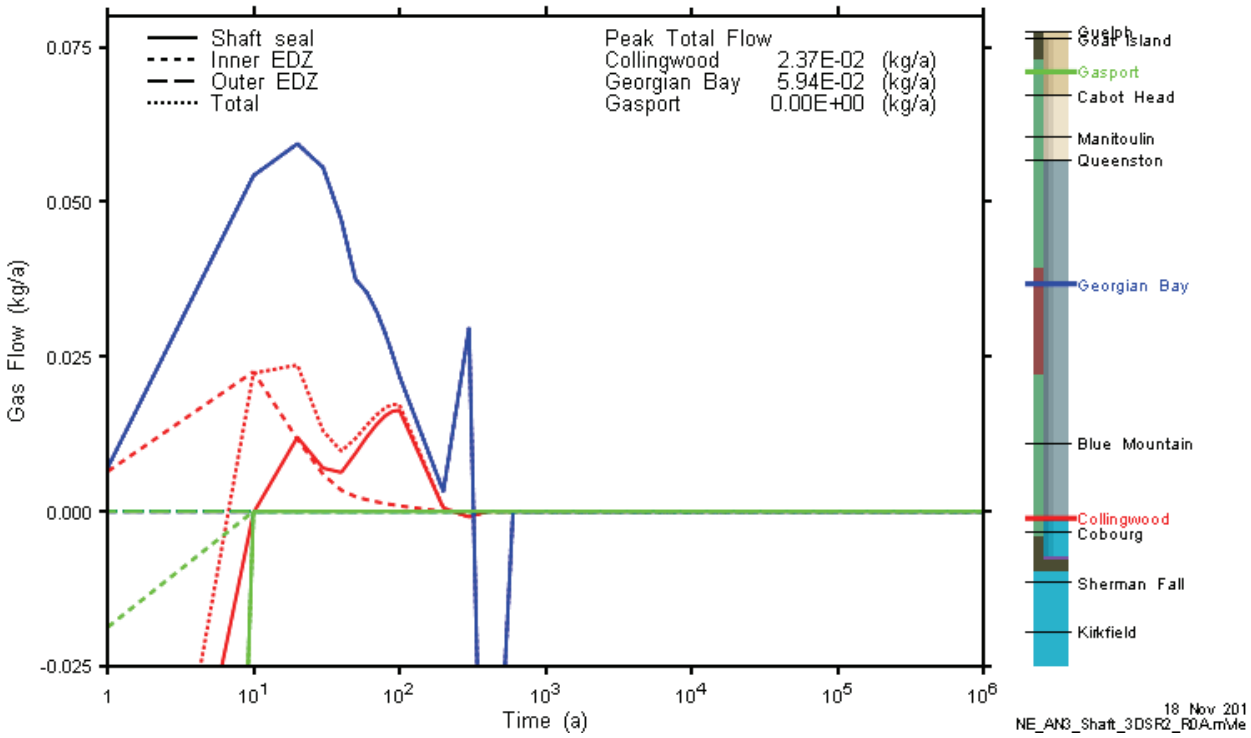

Figure 5.77: NE-AN3: 3DSRS Shaft Gas Flow at Selected Monitoring Planes

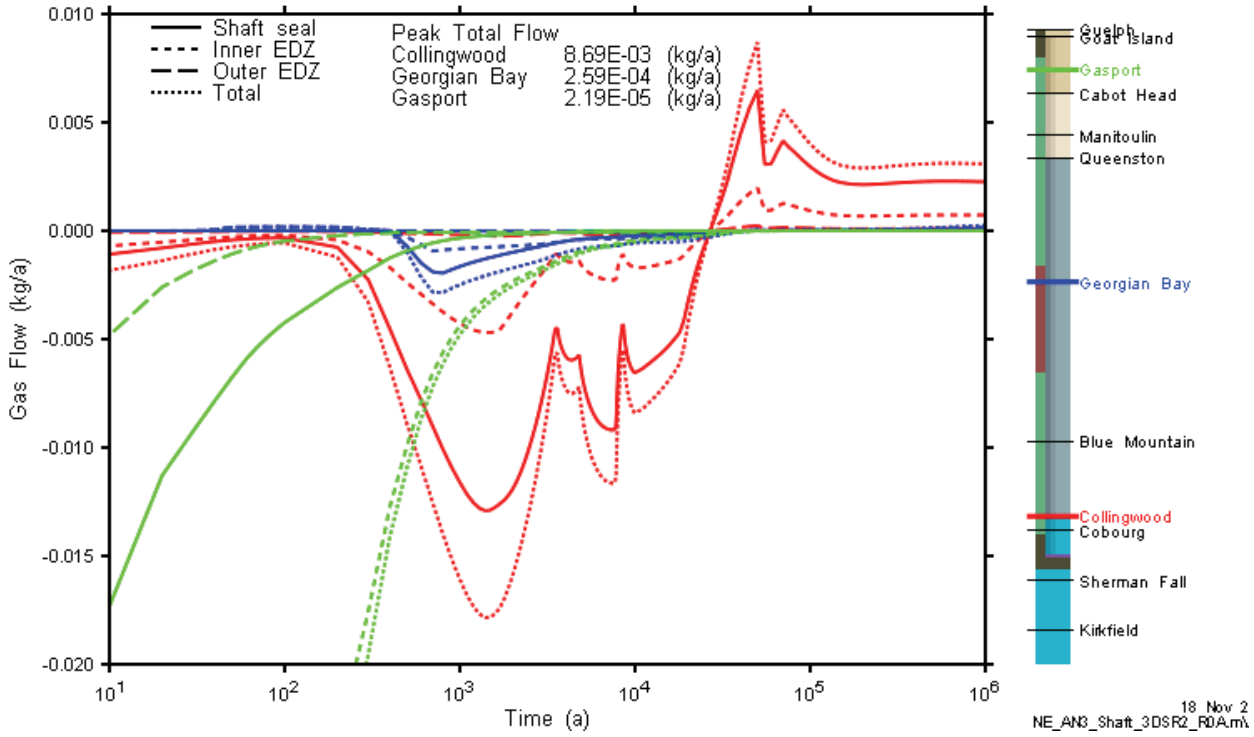

Figure 5.78: NE-AN3: 3DSRS Shaft Dissolved Gas Flow at Selected Monitoring Planes

5.3.2.2 Repository System

Figure 5.79 presents a comparison of repository pressures and liquid saturations for the NE-AN3 and NE-SBC 3DSRS models. Two differences are immediately apparent: 1) repository liquid saturation is much higher for NE-AN3, and 2) the long-term repository pressure is higher than both the NE-SBC case and the initial-steady state pressure at the repository horizon.

The increased liquid inflow is due entirely to the increased vertical conductivity. This in turn leads to a reduction in available repository void volume, which accounts for the increased repository pressure. As shown in Figure 5.80, the shaft is an insignificant contributor to liquid inflow.

The NE-AN3 steady state pressure is higher because of a different geosphere pressure profile. This is discussed in the following section.

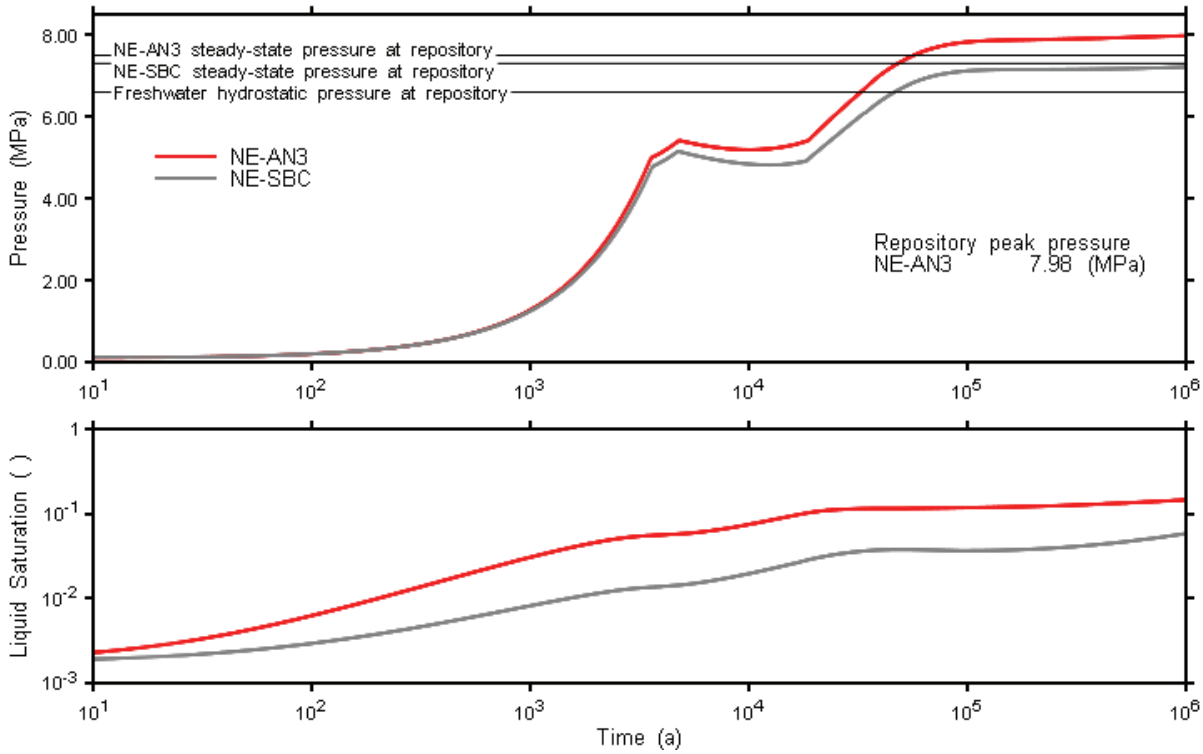

Figure 5.79: NE-AN3: Comparison of NE-AN3 and NE-SBC 3DSRS Model Results

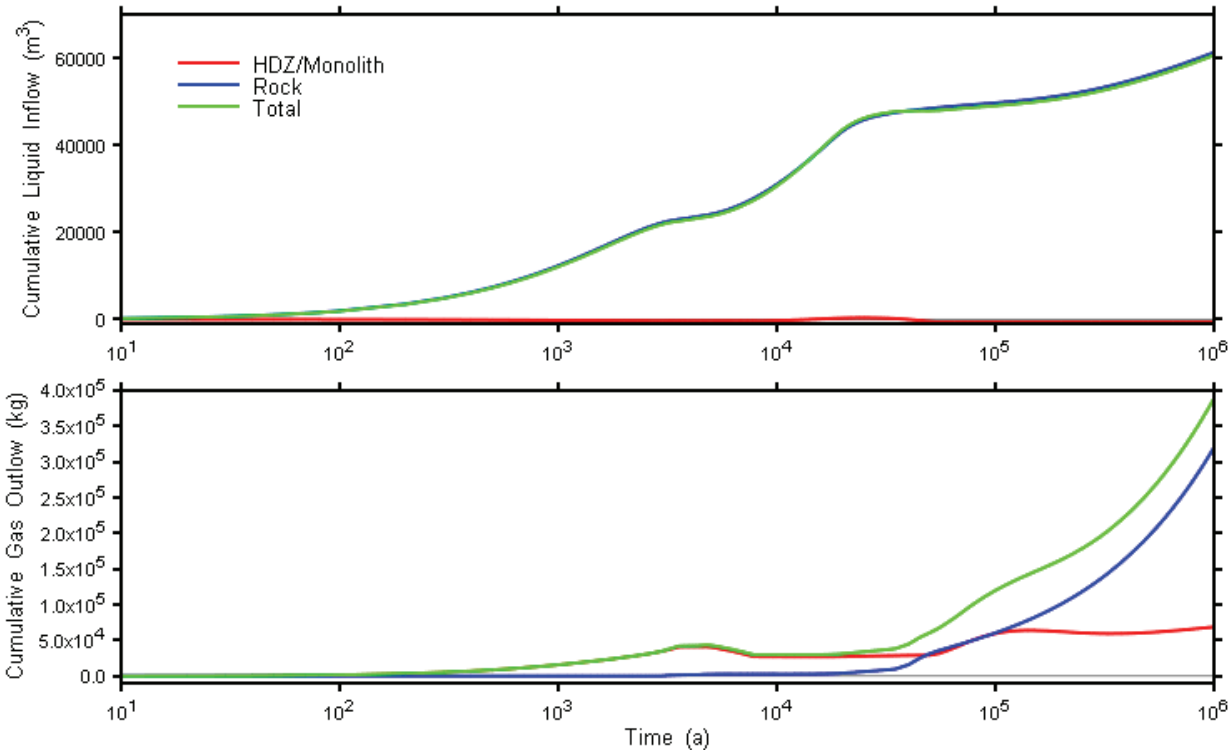

Figure 5.80: NE-AN3: Repository Liquid Inflow and Gas Outflow for 3DSRS Model

5.3.2.3 Geosphere

The pressure profile (expressed as environmental head) for the NE-AN3 case is shown in Figure 5.81. Steady state head profiles for both the NE-AN3 and NE-SBC cases are also shown on the figure.

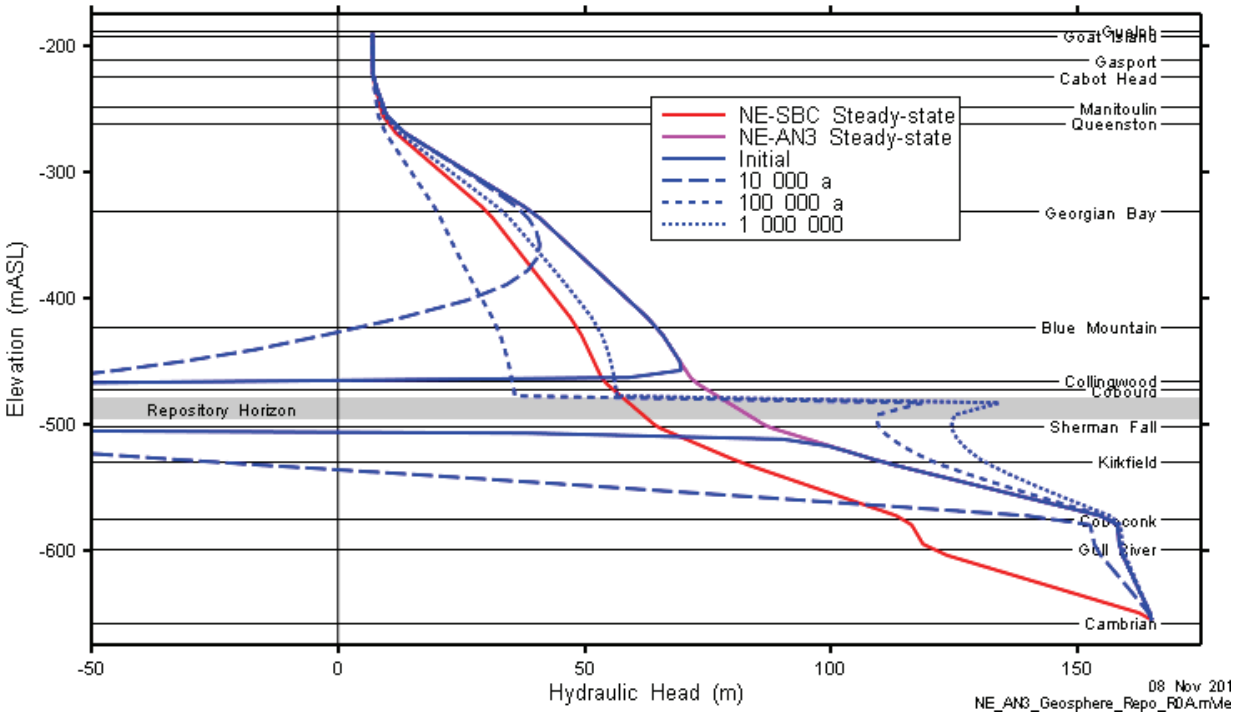

Figure 5.81: NE-AN3: 3DSRS Geosphere Head Profile

The increased permeability of the geosphere results in the repository pressure perturbation extending further vertically above and below the facility. Additionally, the modified permeabilities have a large impact on the steady-state head profile, causing an increase in steady-state pressure at the repository horizon relative to the NE-SBC case.

5.4 Case NE-EDZ1 – Increased Permeability EDZ

In this case, the permeability of the shaft EDZ is increased relative to the NE-SBC parameterization (Table 3.1). The inner EDZ permeability is increased by a factor of 100 and the outer EDZ by a factor of 10. The gas air entry pressures for the inner and outer EDZ are also reduced as described in Section 4.2.2. The NE-EDZ1 case was simulated using the 3DSRS model.

5.4.1 Gas Generation

The NE-EDZ1 case considers Simplified Base Case gas generation but high permeability in the shaft EDZ. As a result, more rapid water ingress and expulsion within the repository is expected. There was a small change in the saturation profile, but for this non-water-limited case it had negligible impact on gas generation and results are practically identical to the Simplified Base Case.

Figure 5.82 and Figure 5.83, and show the water balance and saturation for this case. The peak gas pressure reaches 7.2 MPa as for the Simplified Base Case (see Figure 5.84).

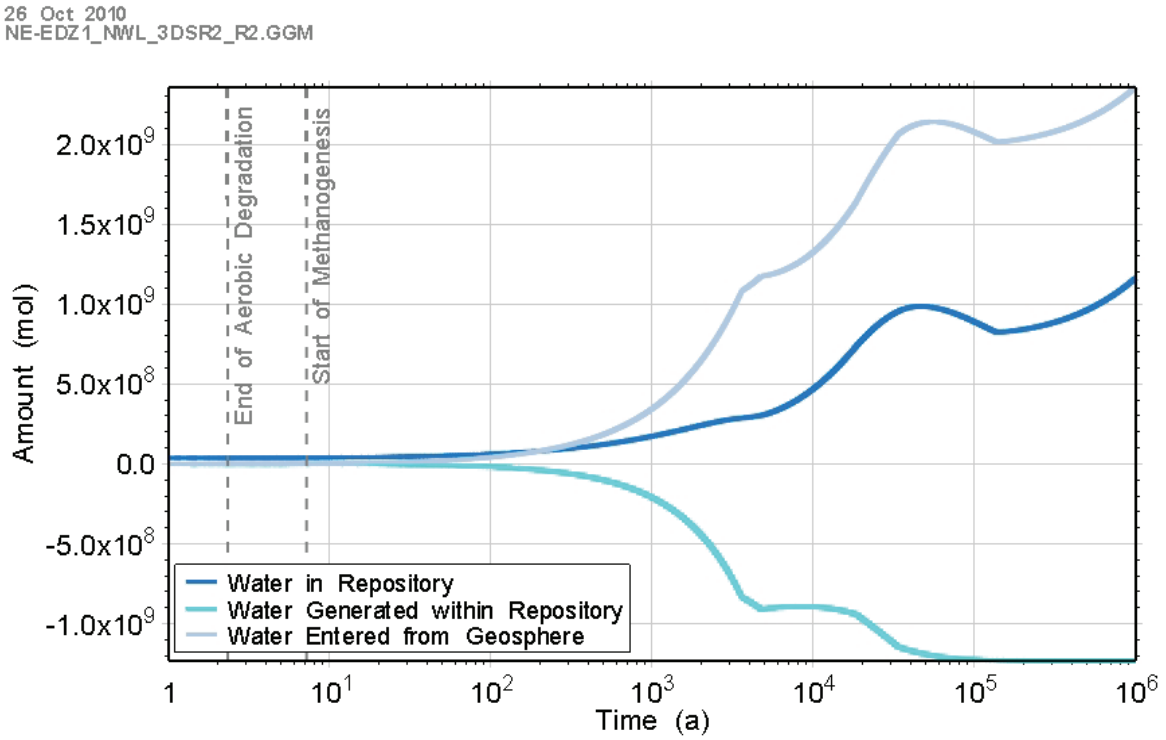

Figure 5.82: NE-EDZ1: Water Balance

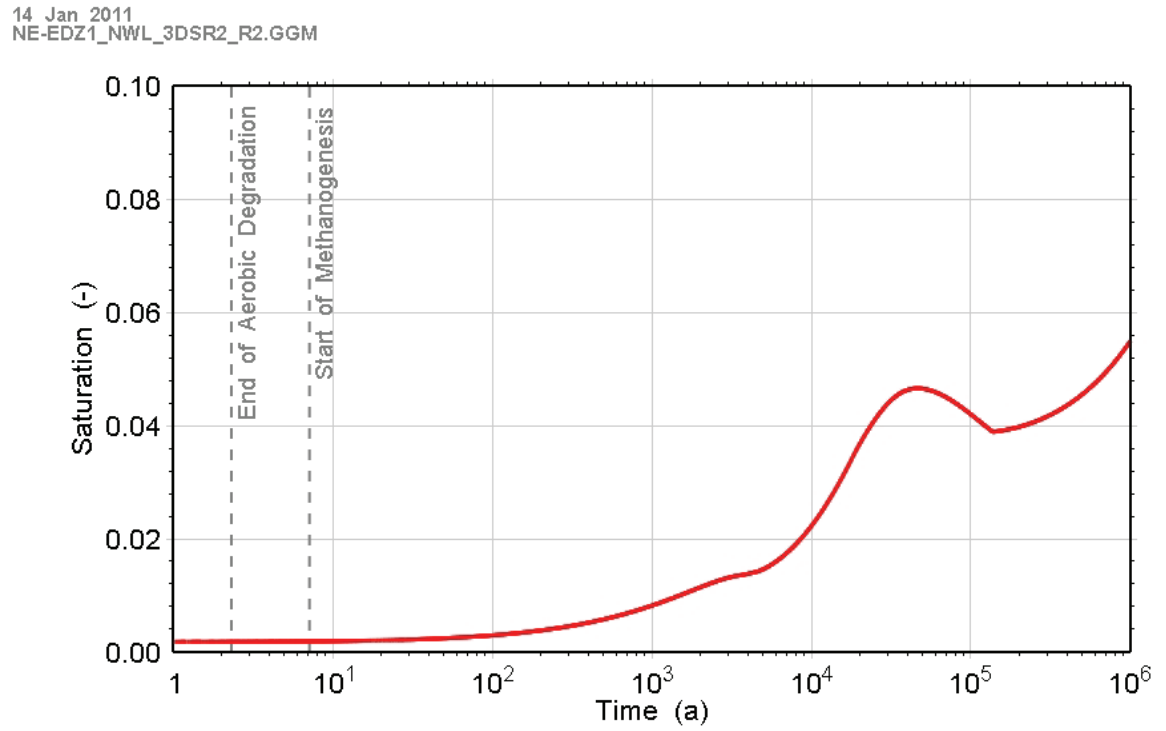

Figure 5.83: NE-EDZ1: Water Saturation within the Repository

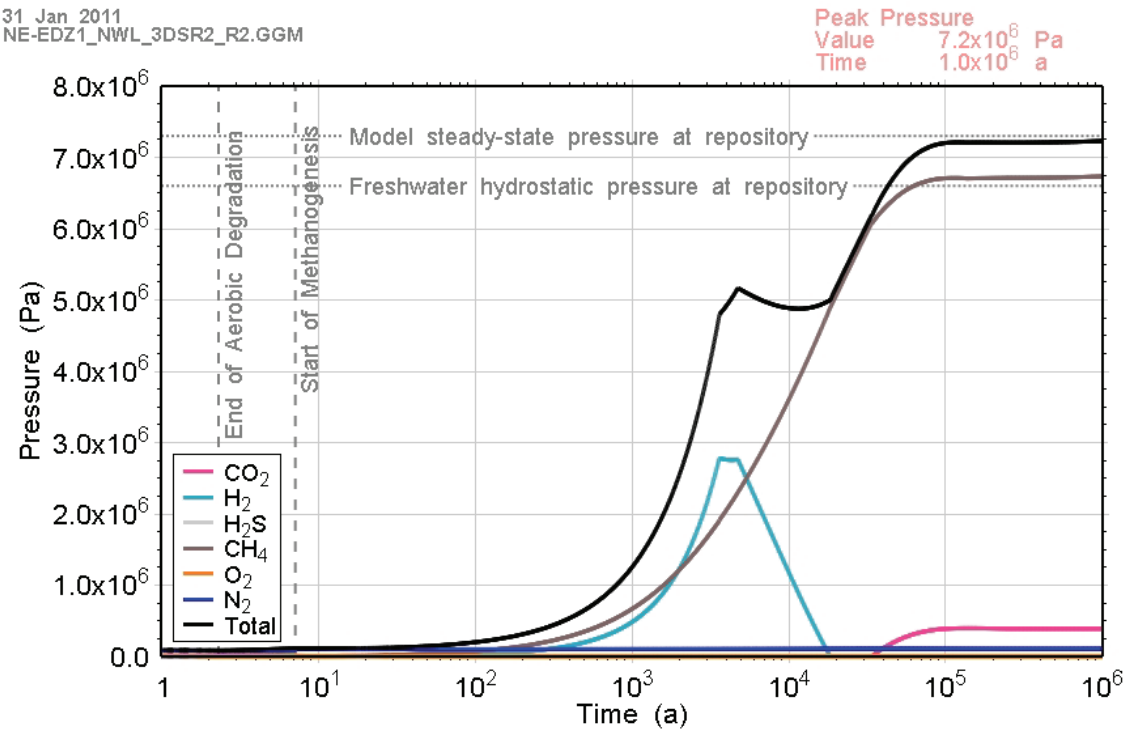

Figure 5.84: NE-EDZ1: Total and Partial Gas Pressures within the Repository

5.4.2 Gas and Water Flows

Gas flows, water flows and repository pressurization responses are virtually identical to the NE-SBC case. This is not surprising as, despite the increase in shaft EDZ permeability and a consequent increase in shaft related flows, the shaft continues to play a relatively minor role in repository pressurization and resaturation.

5.4.2.1 Shaft

Early-time shaft water flows and resaturation are very similar to the NE-SBC case, although occurring somewhat more quickly and at a higher flow rate during the period of shaft inflow and outflow. The higher permeability EDZ provides slightly more water to feed the resaturation process. A comparison of Figure 5.85 below with Figure 5.55 shows that resaturation of the bentonite/sand and Goat Island concrete seal occurs about 3 to 10 times faster in the NE-EDZ1 case.

Up to 40,000 a, shaft water flows are from the intact rock into the EDZ, down the shaft/EDZ, and through the HDZ into the repository (Figure 5.86). Between 40,000 a and 50,000 a, the repository pressure increases to the point that gas flows into the HDZ (Figure 5.87) and liquid flows from the repository towards the shaft, albeit at a very slow rate.

This flow system then persists for the duration of the simulation (Figure 5.88).

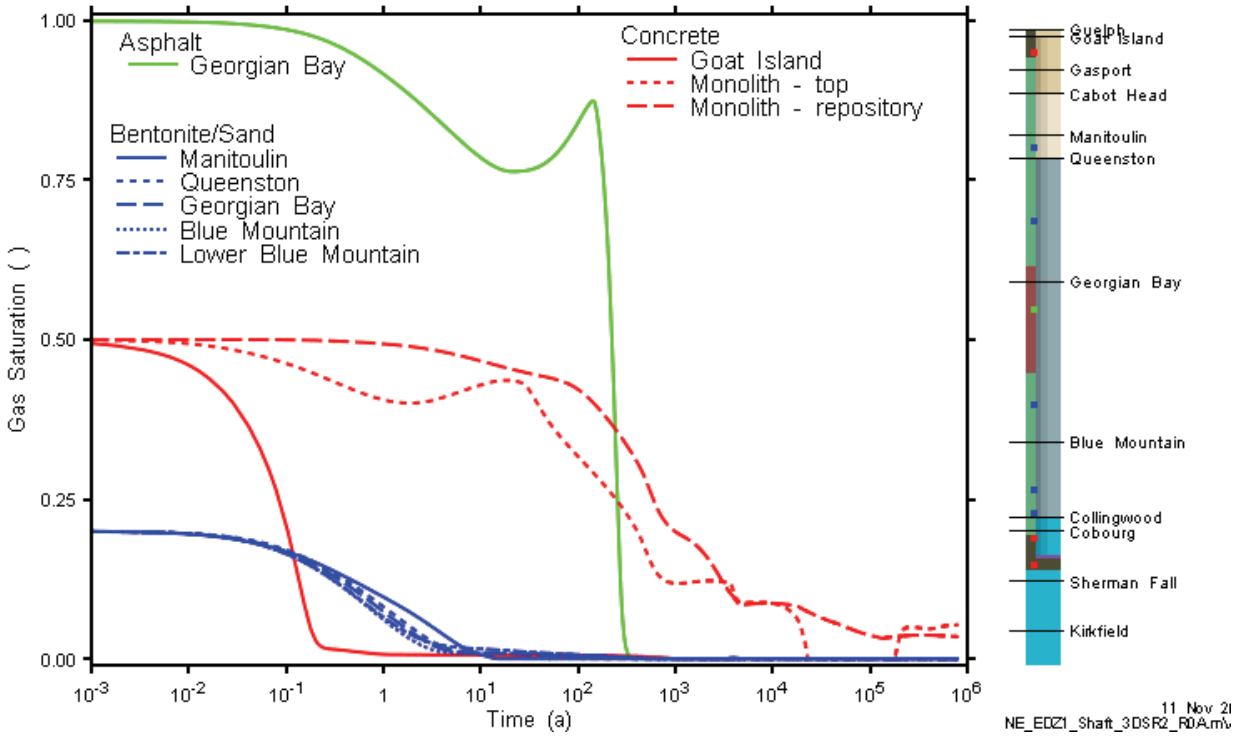

Figure 5.85: NE-EDZ1: 3DSRS Shaft Gas Saturation at Selected Monitoring Planes

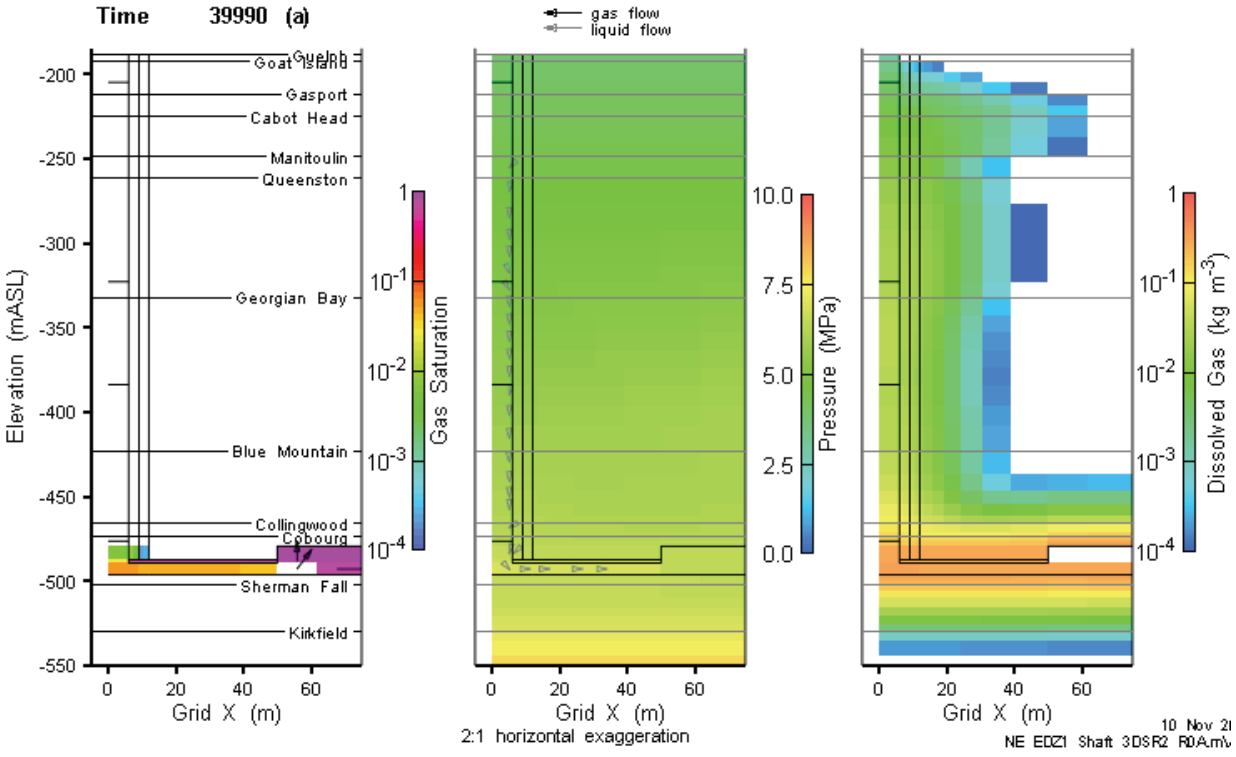

Figure 5.86: NE-EDZ1: 3DSRS Model Shaft Saturations, Flows and Pressures (40,000 a)

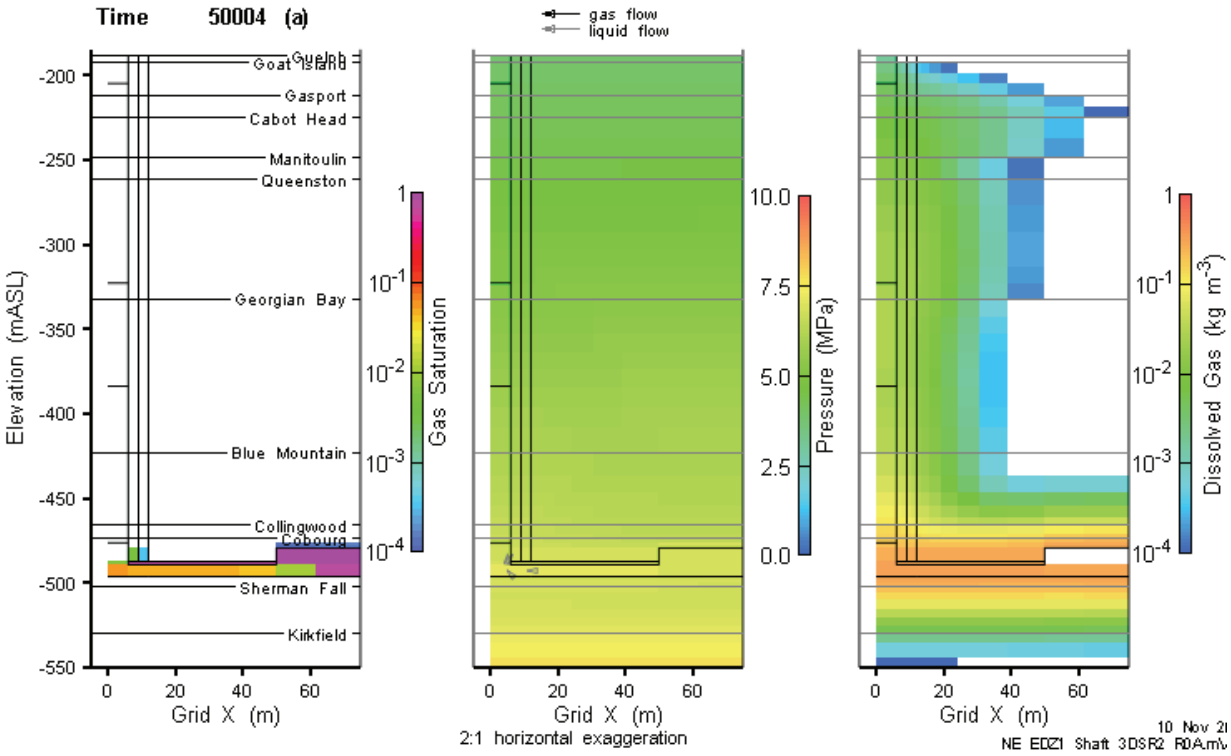

Figure 5.87: NE-EDZ1: 3DSRS Model Shaft Saturations, Flows and Pressures (50,000 a)

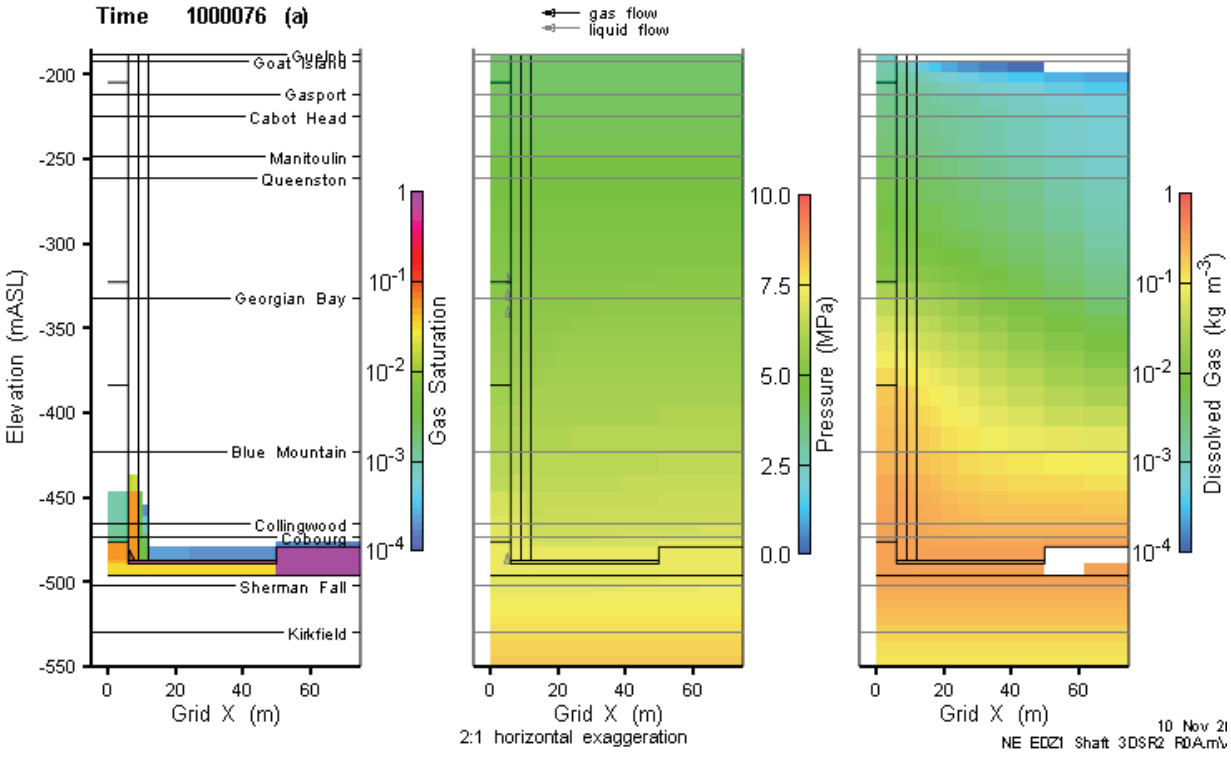

Figure 5.88: NE-EDZ1: 3DSRS Model Shaft Saturations, Flows and Pressures (1,000,000 a)

Gas mass flows up the shaft/EDZ are negligible and are not presented here. Very small amounts of dissolved gas flow up the shaft after the transition in liquid flow directions at 50,000 a. As shown in Figure 5.89, most dissolved gas flow is downwards into the repository through the inner EDZ during the initial resaturation period.

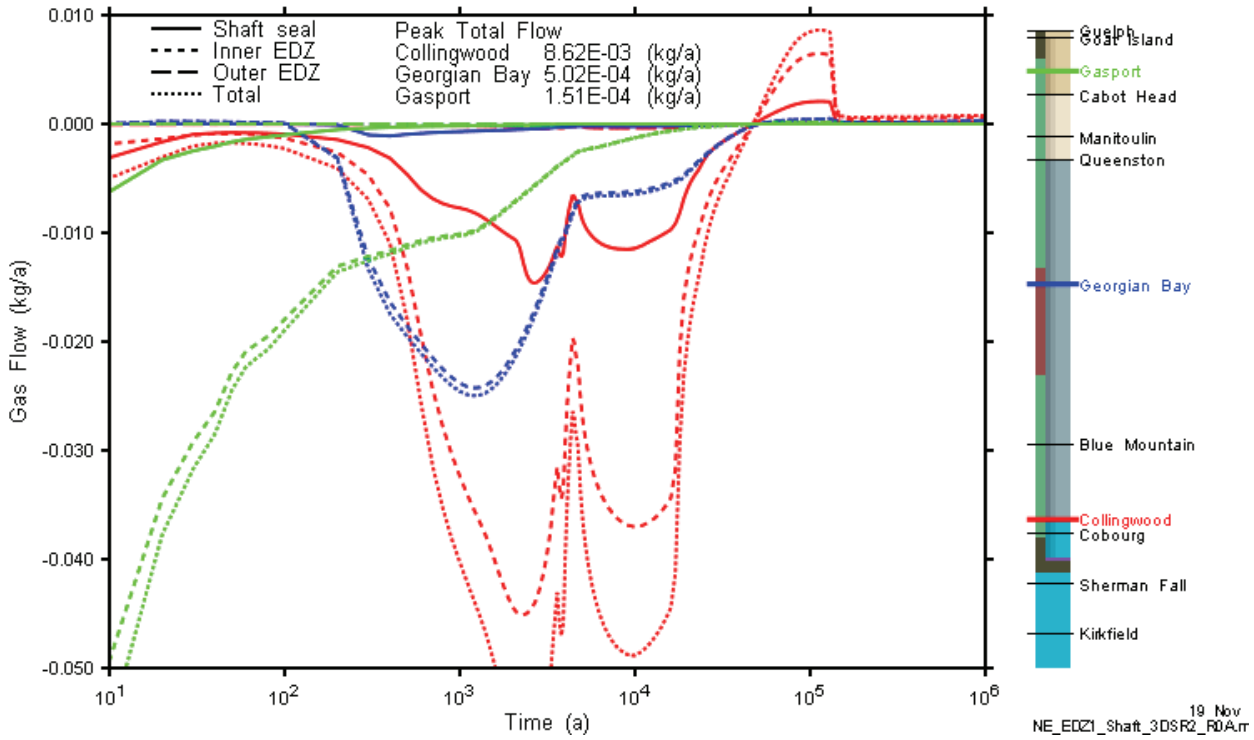

Figure 5.89: NE-EDZ1: 3DSRS Model Shaft Dissolved Gas Flow vs. Time at Selected Monitoring Planes

5.4.2.2 Repository System

Figure 5.90 presents repository pressures and liquid saturations and compares them to NE-SBC 3DSRS model results. Pressures are virtually identical over the range of available results. Repository saturation is slightly higher for the NE-EDZ1 case, which reflects increased water flow down the shaft and into the repository at early time (less than 50,000 a).

The cumulative liquid inflow rates to the repository from the shaft and intact rock are shown in Figure 5.91. The increased inflow flow from the shaft relative to the NE-SBC case (Figure 5.67) is readily apparent. Results are otherwise very similar to the NE-SBC case and will not be discussed further.

5.4.2.3 Geosphere

Results are very similar to the NE-SBC case and will not be discussed or presented further here.

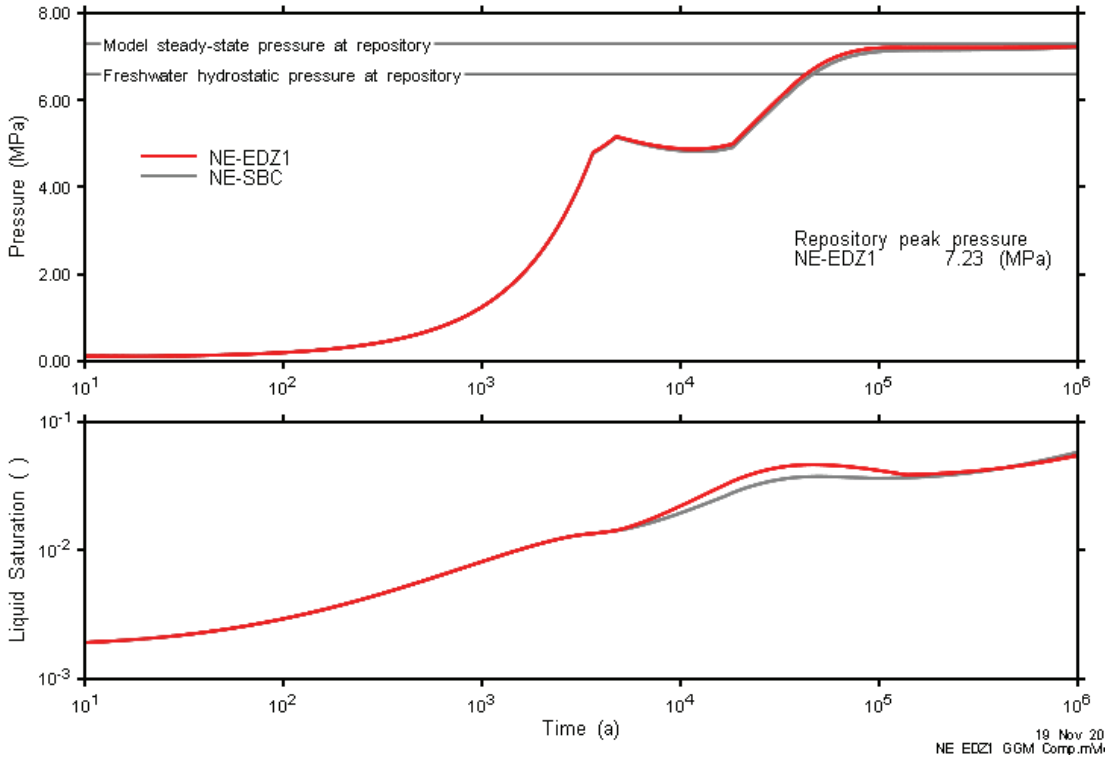

Figure 5.90: NE-EDZ1: 3DSRS Model Repository Pressure and Saturation

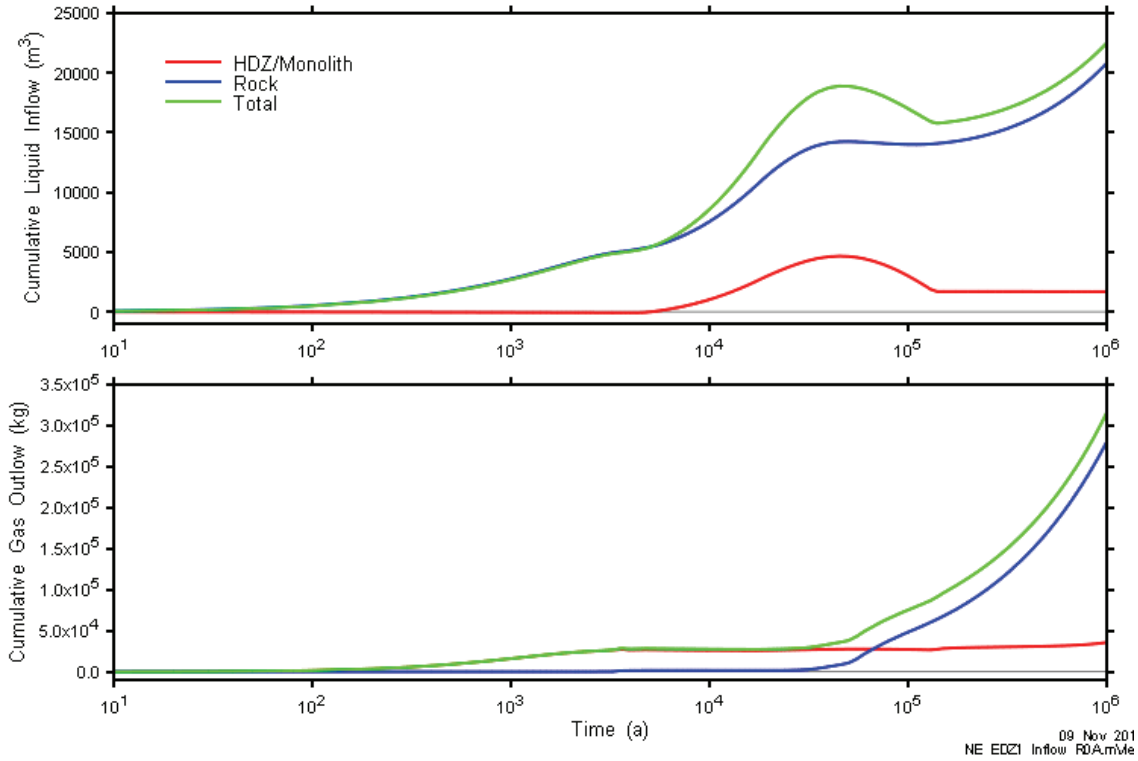

Figure 5.91: NE-EDZ1: Repository Liquid Inflow and Gas Outflow For 3DSRS Model

5.5 Case NE-GG1 – Increased Gas Generation

The NE-GG1 modelling case examines the effect of increased metal inventories (due, for example, to additional overpacking of wastes) plus increased corrosion and degradation rates (Table 3.1). This results in larger and faster gas generation potential. All other parameters were the same as for the NE-SBC case.

The NE-GG1 case was simulated with the 3DD, 3DSRS, 3DSR, and 2DRS models. The 2DRS model was used for the NE-GG1 case as results from the 3DD and 3DSRS model showed some transport of free-phase gas through the shaft to the top of the model. Input pressures to the base of the shaft in the 2DRS model were repository pressures extracted from the 3DSRS model results.

5.5.1 Gas Generation

The gas generation discussion is based on 3DSRS model results.

Case NE-GG1 differs from the Simplified Base Case in that higher metallic inventories and corresponding surface areas are used, as are higher organic degradation and corrosion rates. The metal mass is increased by approximately 23% compared to the Reference Case to 8.1×10^7 kg, and most corrosion and microbial degradation rates are increased by an order of magnitude. As a result of the increased rates, the initial terminal electron acceptor stages complete in approximately one year.

The results show that more gas is produced more rapidly. The gas generation (and water consumption) rates are both approximately an order of magnitude higher than in the Reference Case in the initial 1000 a (see Figure 5.92).

The gas pressure reaches a slightly higher peak than in the Simplified Base Case (7.8 MPa) and is above steady-state pressure at the repository horizon (see Figure 5.93). The increase in gas pressure due to more rapid production of gas was partially mitigated by an increased flux of gas into the geosphere – particularly after the peak pressure was reached (see Figure 5.94). The rapid rise in pressure also reduced infiltration into the repository as the pressure gradient was quickly reversed, with the repository overpressured relative to the intact rock. This eliminated water inflow which resulted in a decreased repository saturation, leaving more volume available for gas.

There is a qualitative difference between this case and the Reference Case caused primarily by the larger inventory of metallic wastes, which leads to hydrogen being the dominant gas within the repository at times less than 3000 a. The degradation of organic wastes causes them to be consumed within approximately 20,000 a (see Figure 5.95). At this time, production of CO_2 ceases. The remaining CO_2 is rapidly consumed by the microbial hydrogen mechanism until it is exhausted.

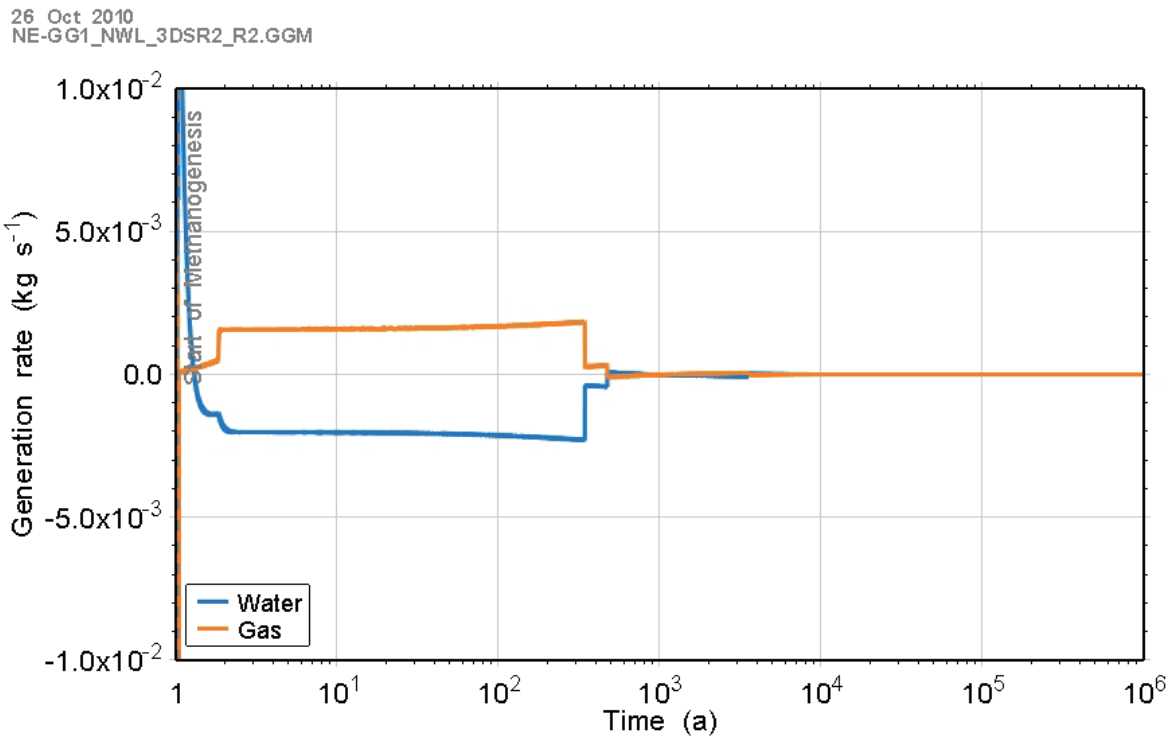

Figure 5.92: NE-GG1: Gas and Water Generation Rates

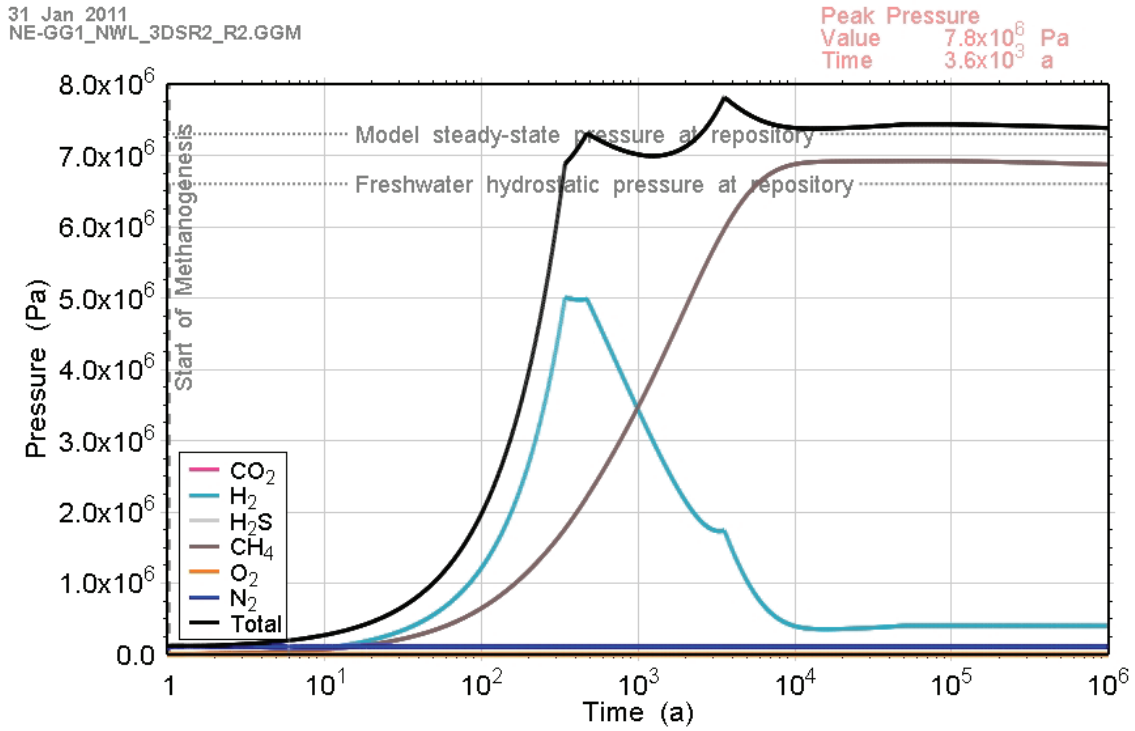

Figure 5.93: NE-GG1: Total and Partial Gas Pressures within the Repository

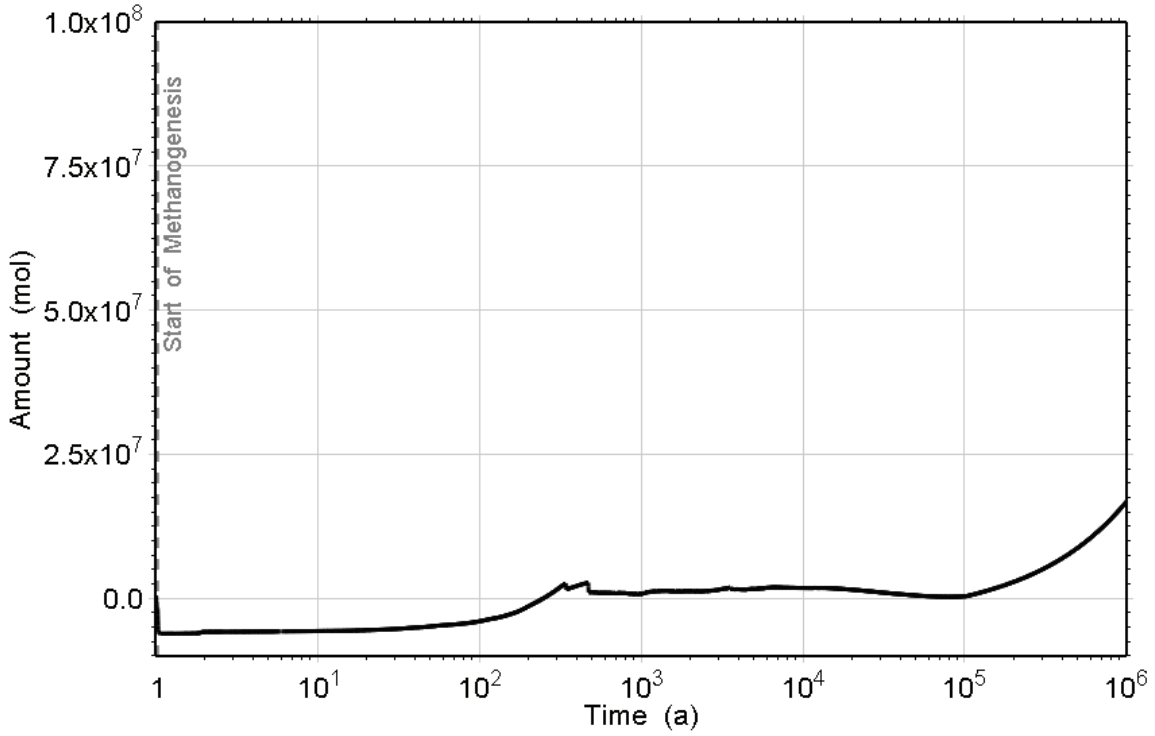

Figure 5.94: NE-GG1: Total Amount of Gas that has left the Repository

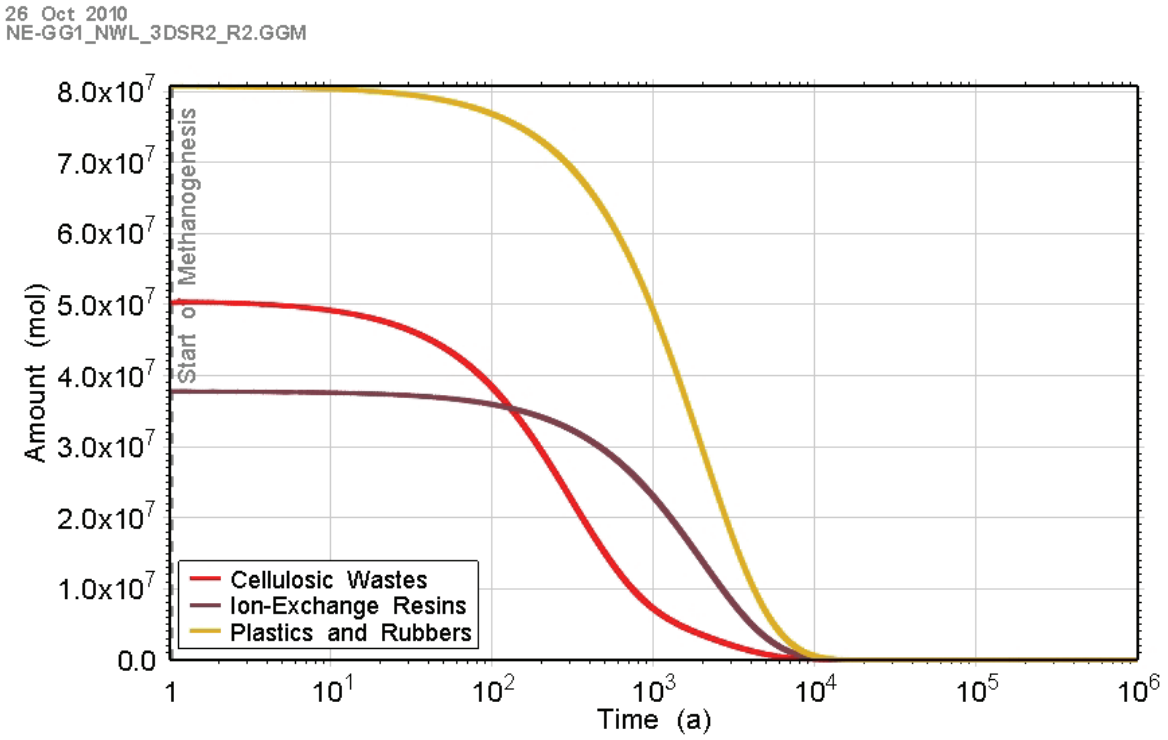

Figure 5.95: NE-GG1: Amounts of Organic Waste

5.5.2 Gas and Water Flows

5.5.2.1 Shaft

Evolution of water flows within the shaft and surrounding intact rock are similar to the NE-SBC case, until the repository pressure exceeds the surrounding geosphere pressure at approximately 500 a (Figure 5.96). Gas flow rates up the shaft are much higher than for the NE-SBC case due to much earlier pressurization, with an initial peak gas flow occurring at approximately 500 a, coincident with the first peak in repository pressure. Subsequently, liquid flow reverses as the repository pressures increase more slowly to a peak pressure at approximately 3500 a (Figure 5.97). Resaturation processes within the shaft slow down as gas is transmitted from the repository, through the HDZ and into the shaft seals and shaft EDZ.

After 3500 a, repository pressure decreases, and consequently liquid flow reverses as water starts to flow very slowly back into the repository access tunnels. Gas flow continues up the shaft, and by 7000 a has reached the top boundary of the model. The system established at this time (Figure 5.98) remains substantially in place until 30,000 a (Figure 5.99), with only minor changes as shaft resaturation slowly occurs, with a commensurate reduction in upwards transport of gas.

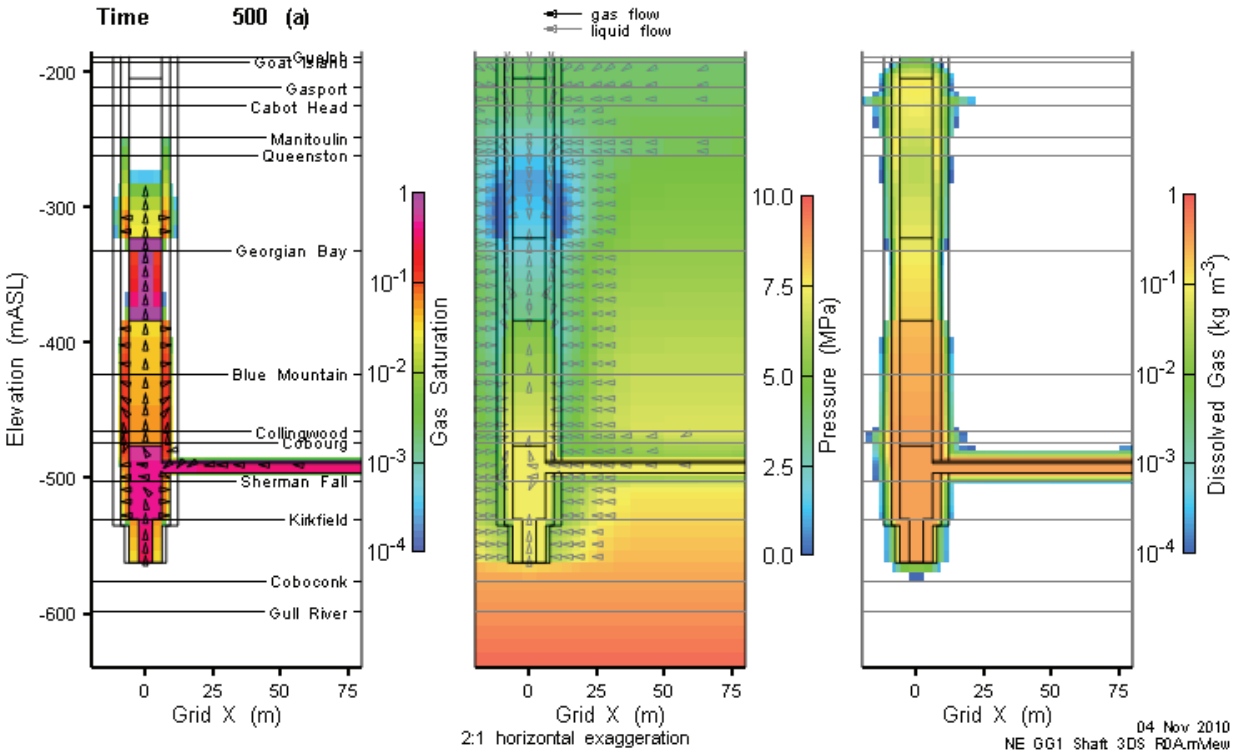

Figure 5.96: NE-GG1: 3DD Model Shaft Saturations, Flows and Pressures (500 a)

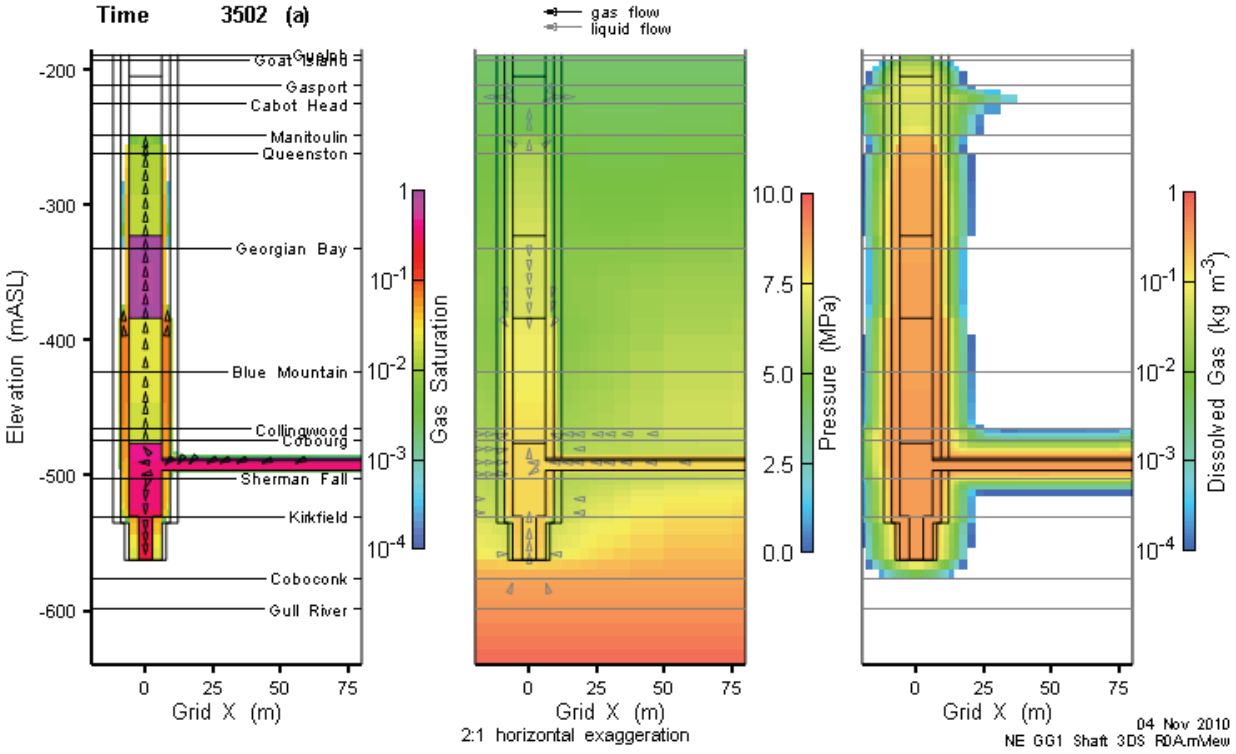

Figure 5.97: NE-GG1: 3DD model shaft saturations, flows and pressures (3500 a)

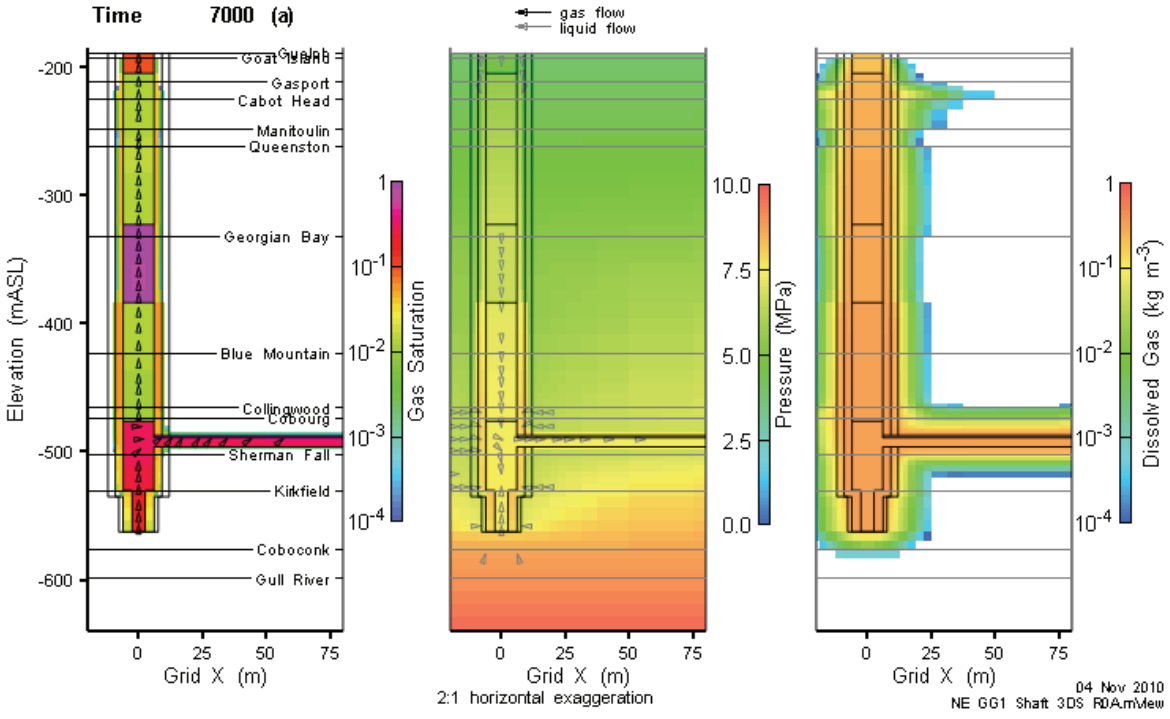

Figure 5.98: NE-GG1: 3DD Model Shaft Saturations, Flows and Pressures (7000 a)

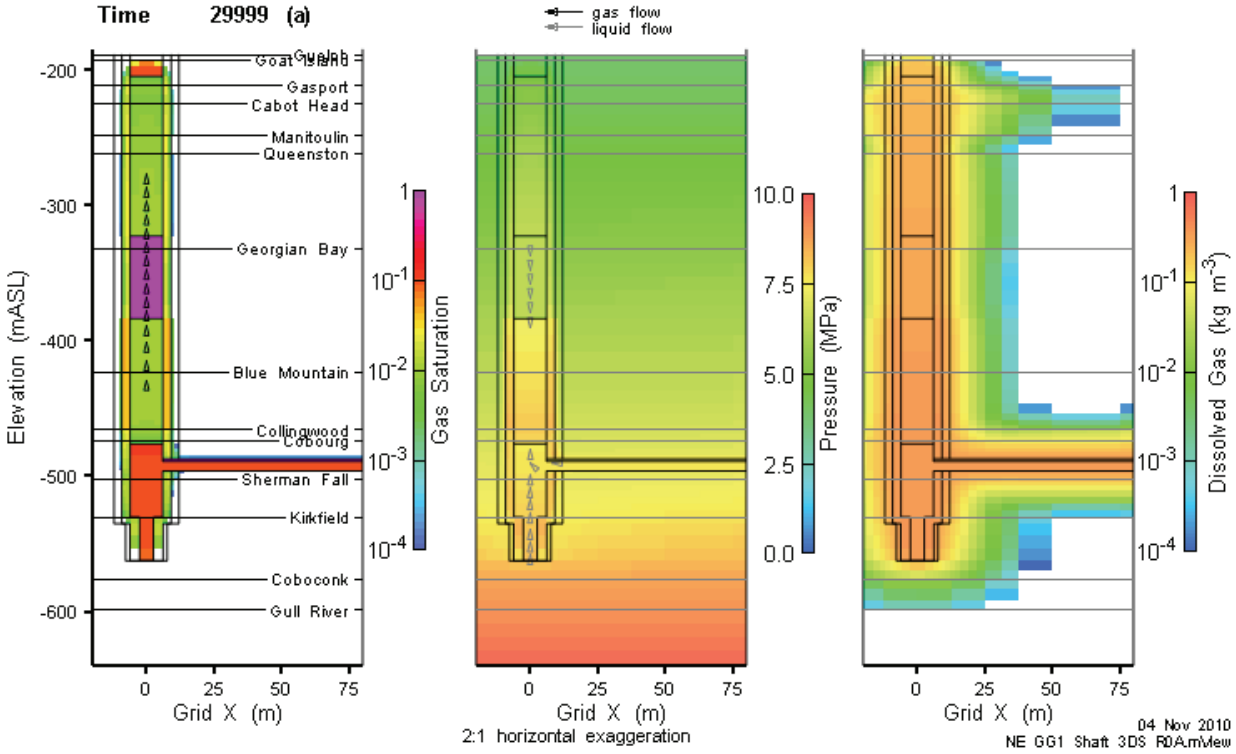

Figure 5.99: NE-GG1: 3DD Model Shaft Saturations, Flows and Pressures (30,000 a)

Beyond 30,000 a, gas flow is nearly eliminated, as evidenced by the disappearance of gas vectors in Figure 5.100 and Figure 5.101.

Beyond 100,000 a, shaft resaturation continues with the asphalt seal retaining vestigial gas until near the end of the simulation period (Figure 5.102).

The residual gas saturation in the shaft is eliminated by 1,000,000 a.

The fate of the early-time gas above the 3D simulation domain was investigated with the 2DRS model. As shown in Figure 5.103, gas reaches the Guelph Formation at about 4600 a (slightly faster than the 3DD model).

Beyond this time, gas exits the shaft into the more permeable Guelph Formation. This transport is driven by the gas pressure gradient, which in turn is dependent upon the capillary pressures of the materials. The Guelph Formation has a much lower air-entry pressure than the concrete seal and the bentonite/sand above the concrete. There is virtually no further upwards transport of the gas phase (see Figure 5.104).

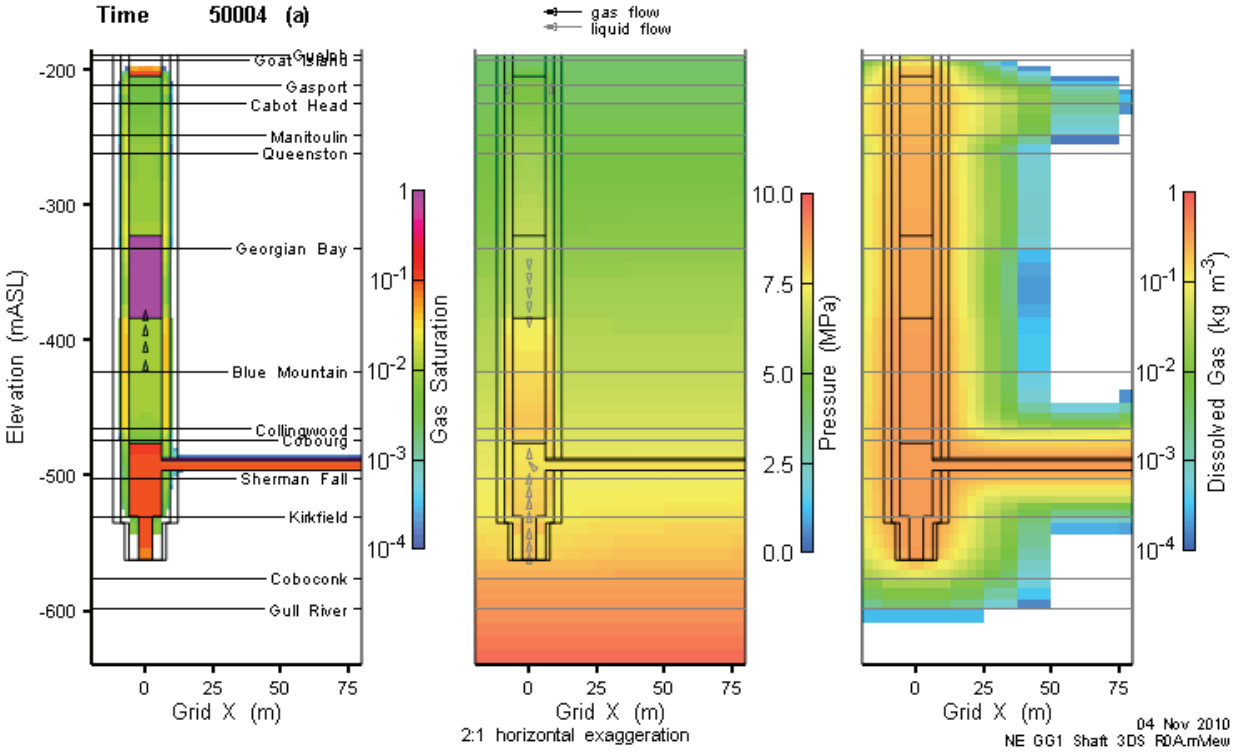

Figure 5.100: NE-GG1: 3DD Model Shaft Saturations, Flows and Pressures (50,000 a)

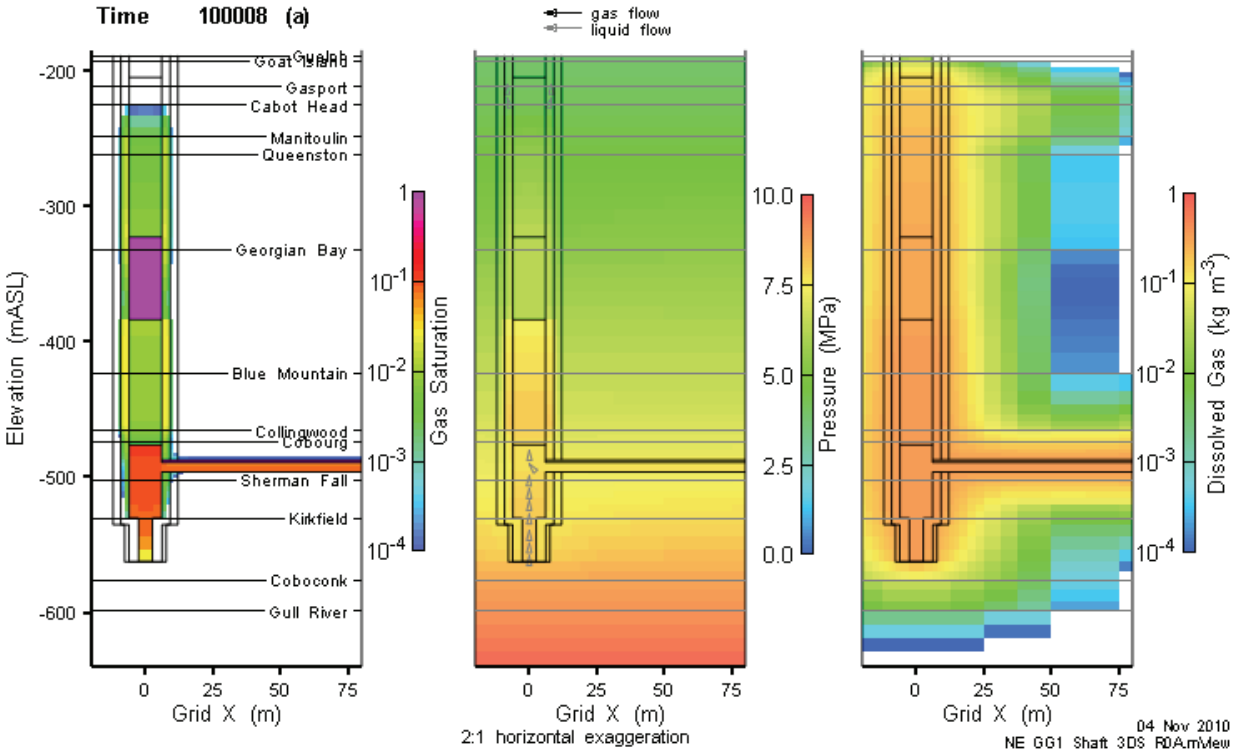

Figure 5.101: NE-GG1: 3DD Model Shaft Saturations, Flows and Pressures (100,000 a)

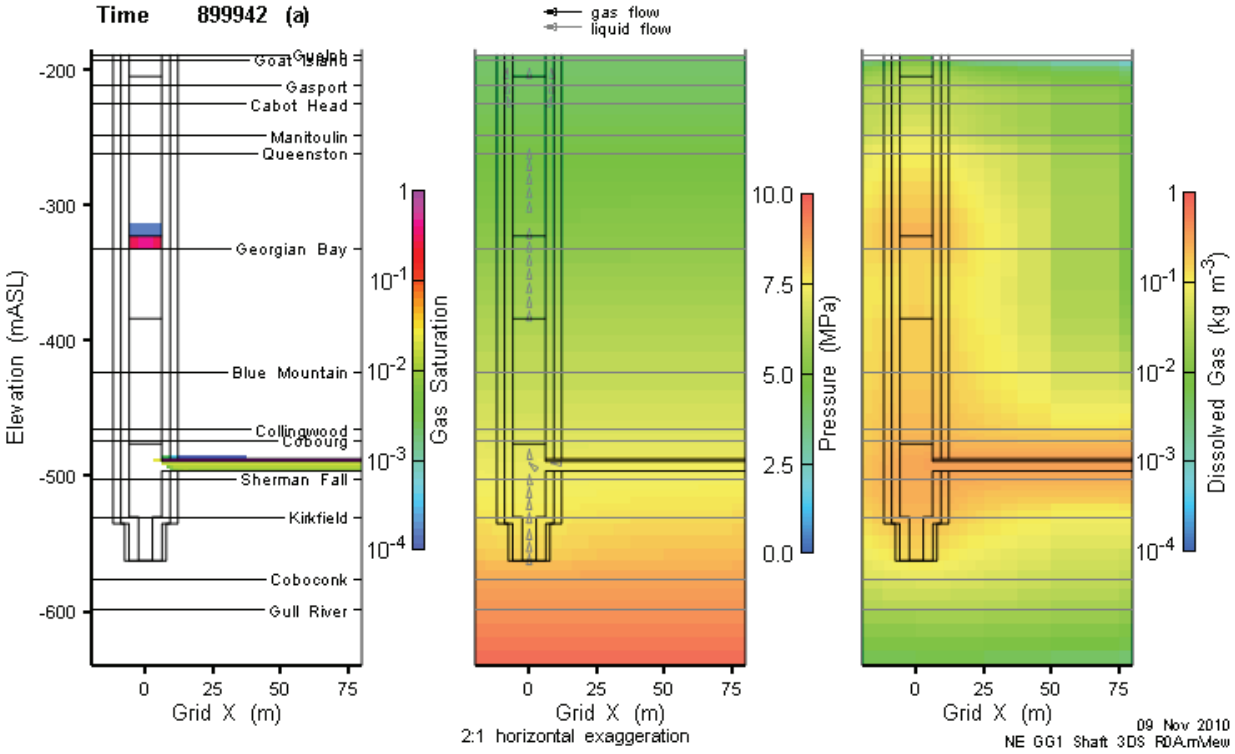

Figure 5.102: NE-GG1: 3DD Model Shaft Saturations, Flows and Pressures (900,000 a)

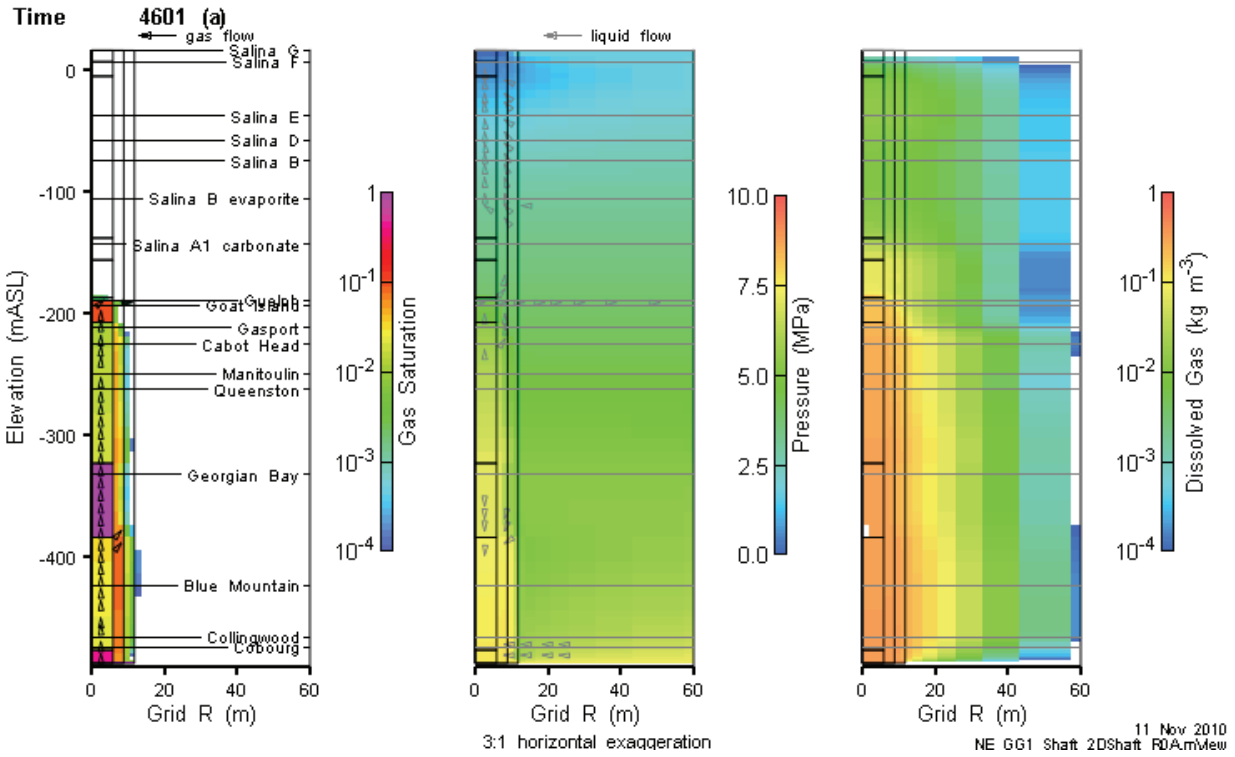

Figure 5.103: NE-GG1: 2DRS Model Shaft Saturations, Flows and Pressures (4600 a)

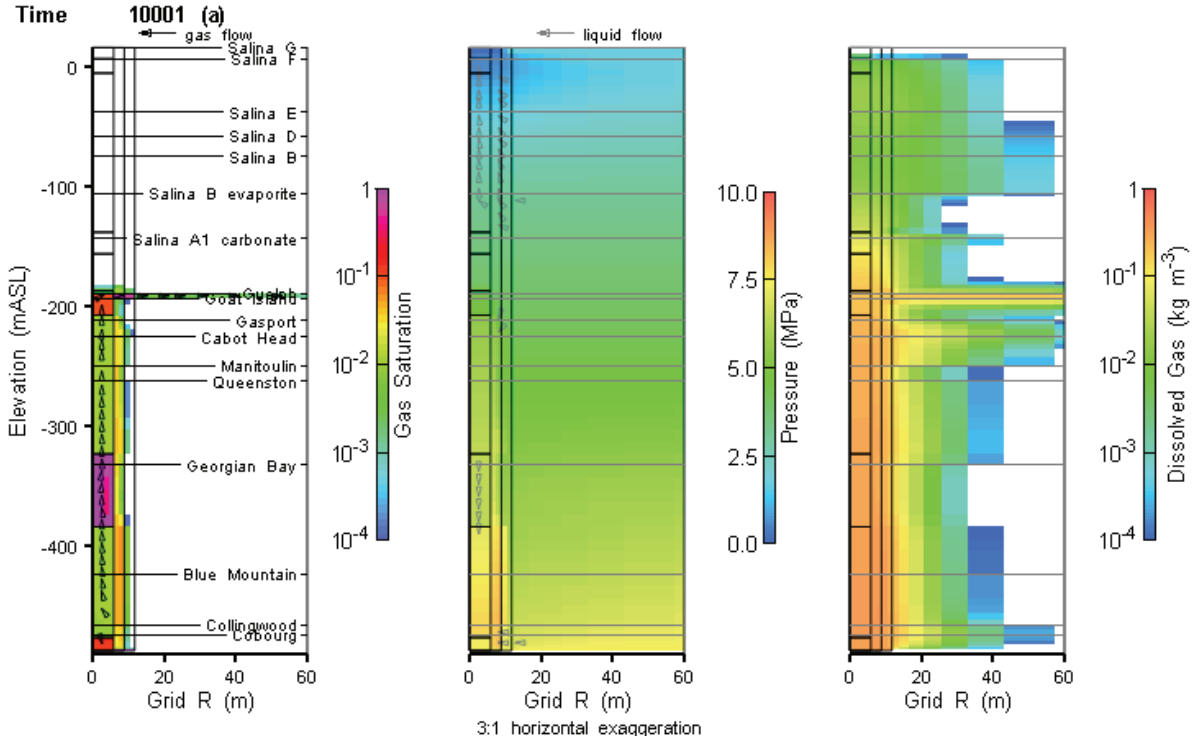

Figure 5.104: NE-GG1: 2DRS Model Shaft Saturations, Flows and Pressures (10,000 a)

The following sets of figures provide a comparison of 3DD and 2DRS time series results and are useful to increase confidence in the two modelling approaches. Shaft gas saturation time profiles are given in Figure 5.105 (2DRS) and Figure 5.106 (3DD). Apart from a minor excursion in the asphalt seal saturation for the 3DD model, results are very similar.

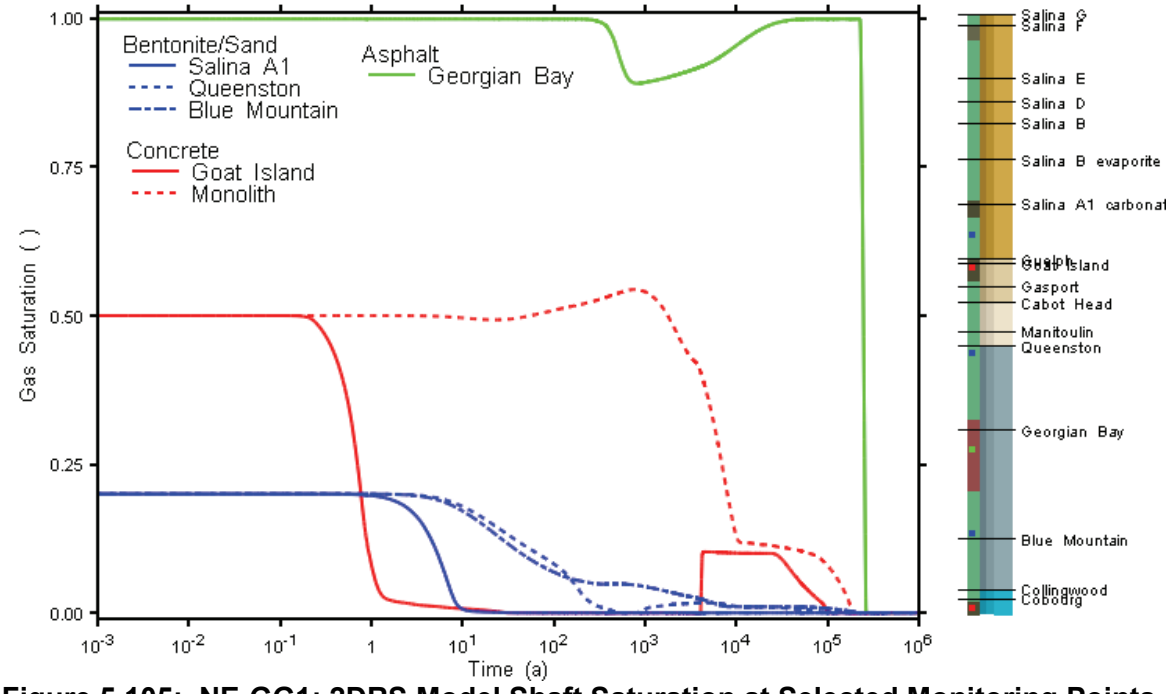

Figure 5.105: NE-GG1: 2DRS Model Shaft Saturation at Selected Monitoring Points

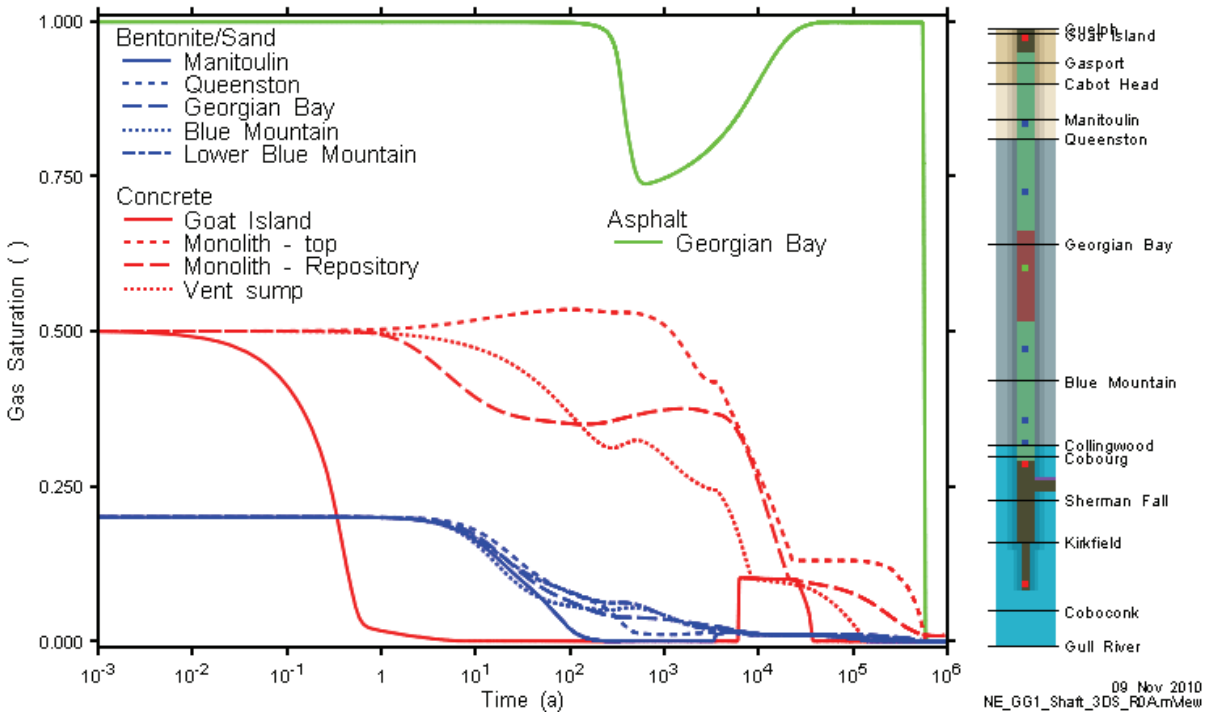

Figure 5.106: NE-GG1: 3DD Model Shaft Saturation at Selected Monitoring Points

Gas flow rates up the shaft are presented in Figure 5.107 (2DRS) and Figure 5.108 (3DD). Results are very similar, with the 2DRS model indicating slightly higher flow rates. The results show that, although a small amount of gas reaches the Gasport, it does not continue past the permeable Guelph to the Salina A2 formation.

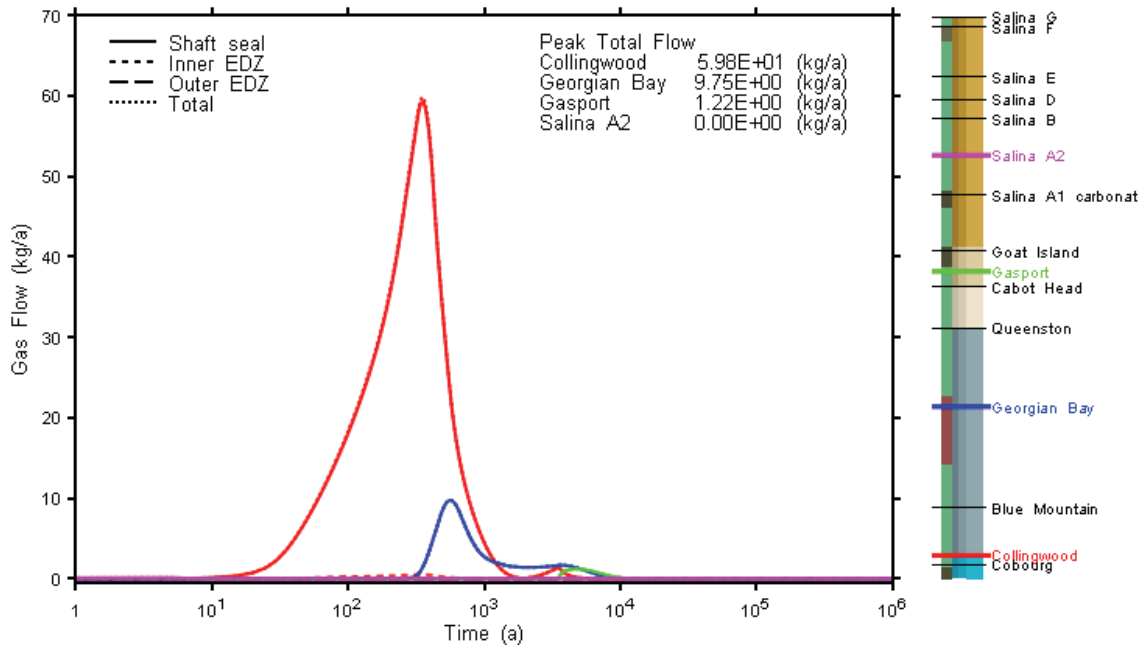

Figure 5.107: NE-GG1: 2DRS Model Shaft Gas Flow at Selected Monitoring Planes

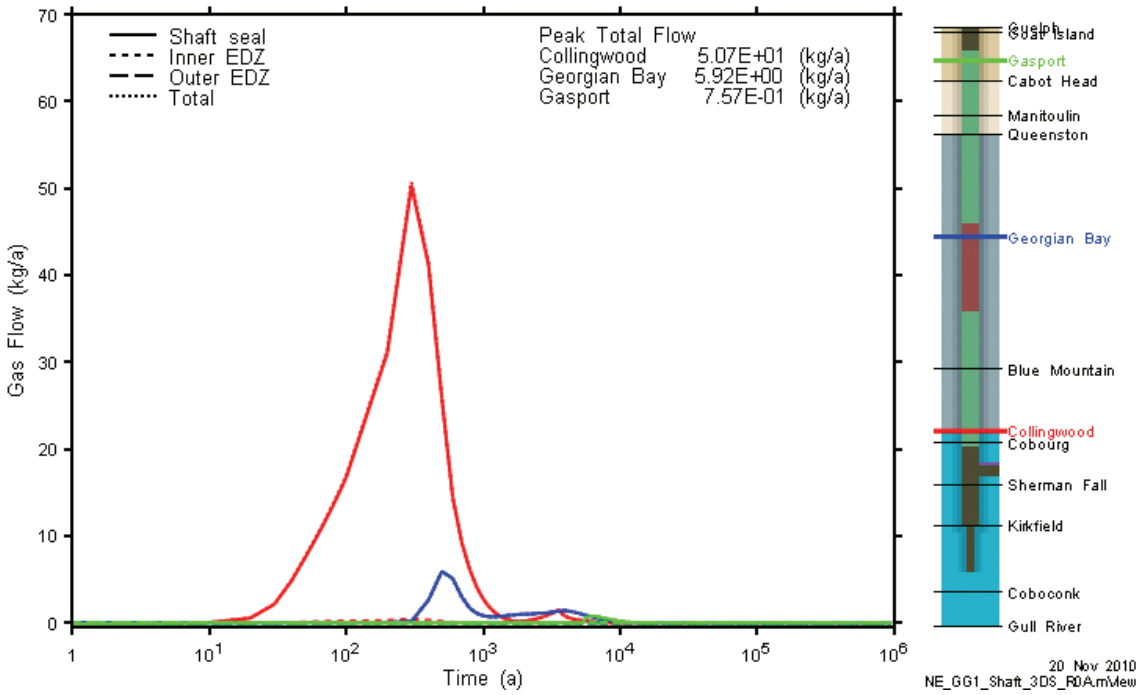

Figure 5.108: NE-GG1: 3DD Model Shaft Gas Flow at Selected Monitoring Planes

Dissolved gas concentration vs. time profiles are relevant only for the 3DD model results as the 2DRS model lower boundary condition assumes full gas saturation. Figure 5.109 shows dissolved gas flow rates in the shaft. Dissolved gas flow which reflects contaminated gas content (as opposed to initial gas present in the shaft seal materials at emplacement) will occur in the event of an outward flux of water from the repository into the shaft, and consequent vertical upwards flow within the shaft, or due to the dissolution of free-gas in the shaft transported from the repository. This upward flux is seen near the bottom of the shaft (Collingwood plane in figure), but significant mass does not travel far up the shaft, likely due to diffusion out from the shaft.

Figure 5.110 and Figure 5.111 present shaft gas and dissolved gas flows. Results are consistent with those for the 3DD and 2DRS models. They are presented here to serve as a basis for comparison to NE-GT4 and NE-GT5 results described in Section 5.8.

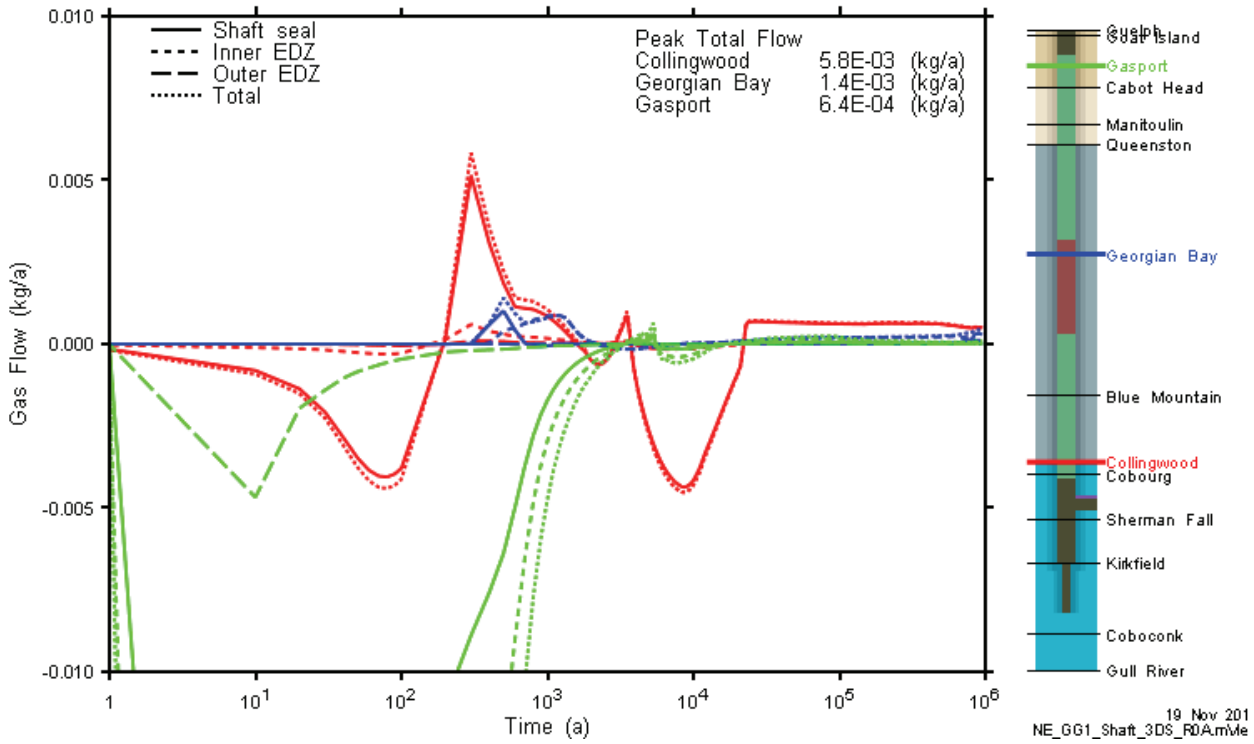

Figure 5.109: NE-GG1: 3DD Model Shaft Dissolved Gas Flow at Selected Monitoring Planes

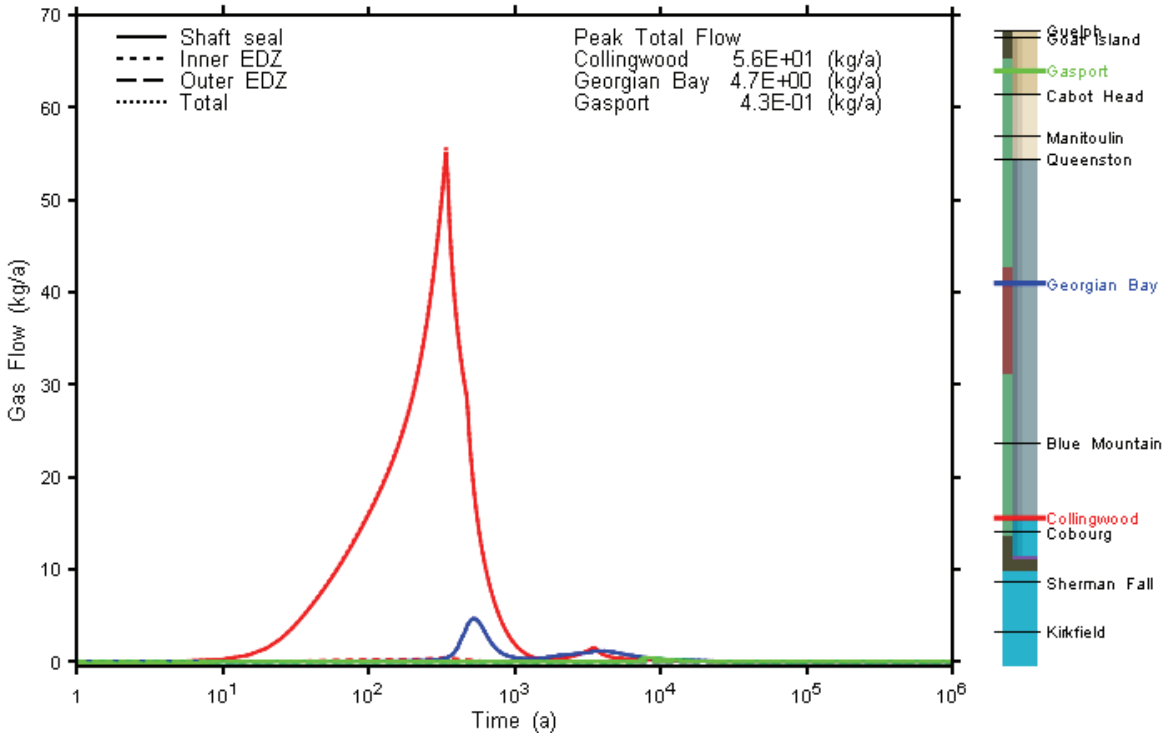

Figure 5.110: NE-GG1: 3DSRS Model Shaft Gas Flow at Selected Monitoring Planes

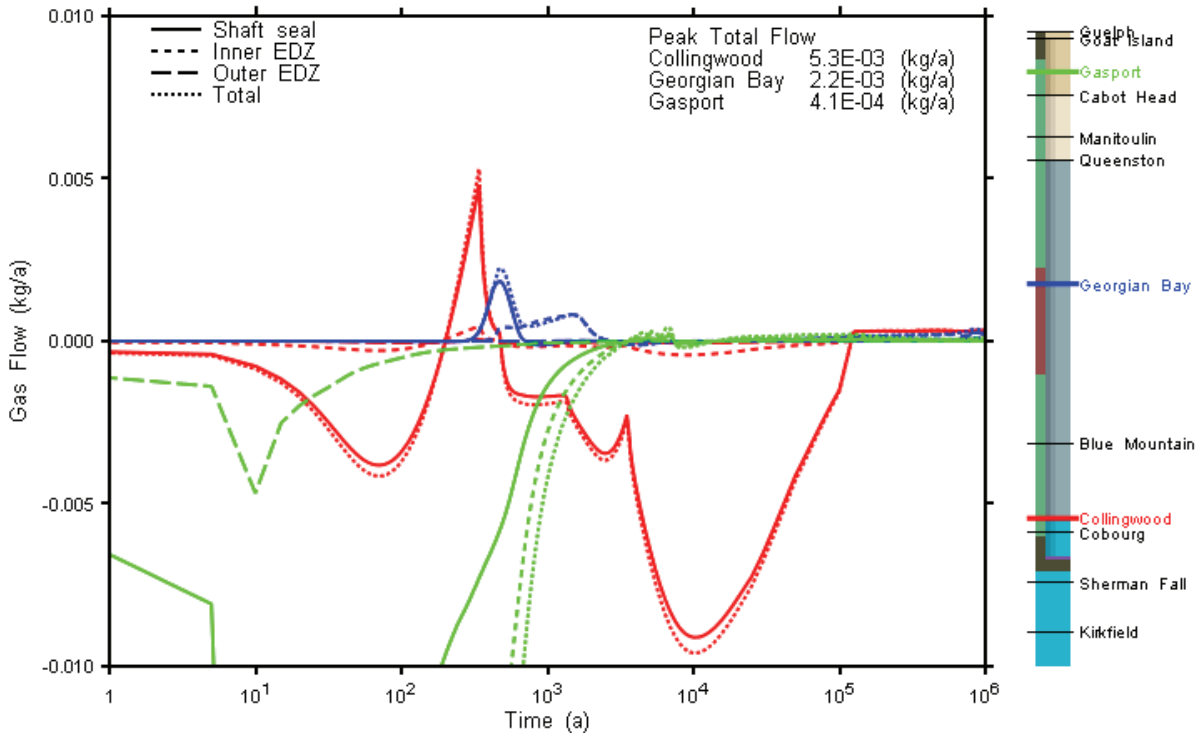

Figure 5.111: NE-GG1: 3DSRS Model Shaft Dissolved Gas Flow at Selected Monitoring Planes

5.5.2.2 Repository System

Figure 5.112 presents repository pressures and liquid saturations for the NE-GG1 3D models. 3DSRS NE-SBC results are also shown for comparison purposes. Pressures are virtually identical for all NE-GG1 models. Initial repository saturation is slightly higher for the 3DD and 3DSRS models, which reflects initial liquid saturations in repository elements which are nominally dry. Maximum saturations are very low, with virtually no water present in the repository. Figure 5.113 shows cumulative gas and liquid flows for the 3DD and 3DSRS models. As described previously, the discrepancy in gas outflow at early times (less than 500 a) is due to gas saturation of excess monolith material present in the 3DSRS model.

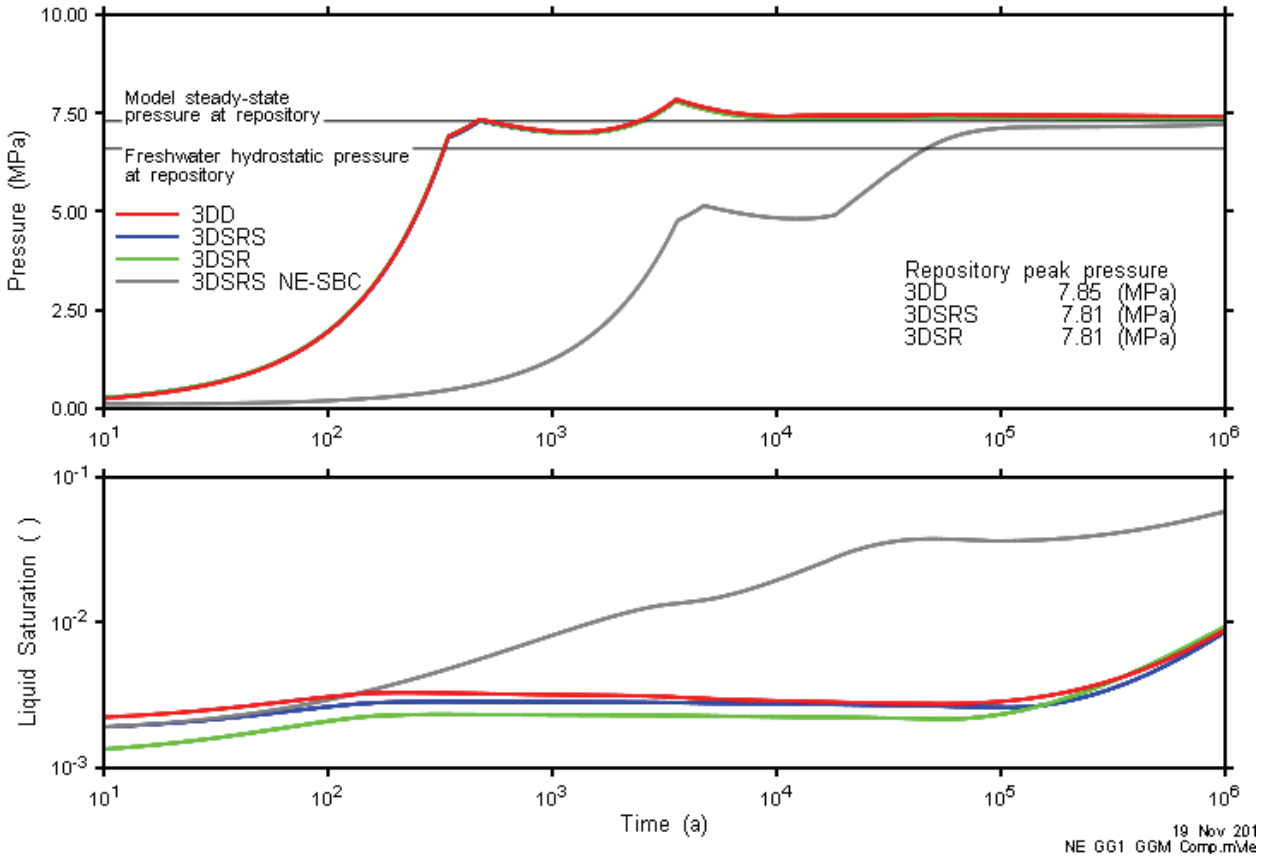

Figure 5.112: NE-GG1: 3DD, 3DSRS and 3DSR Model Repository Pressure and Saturation

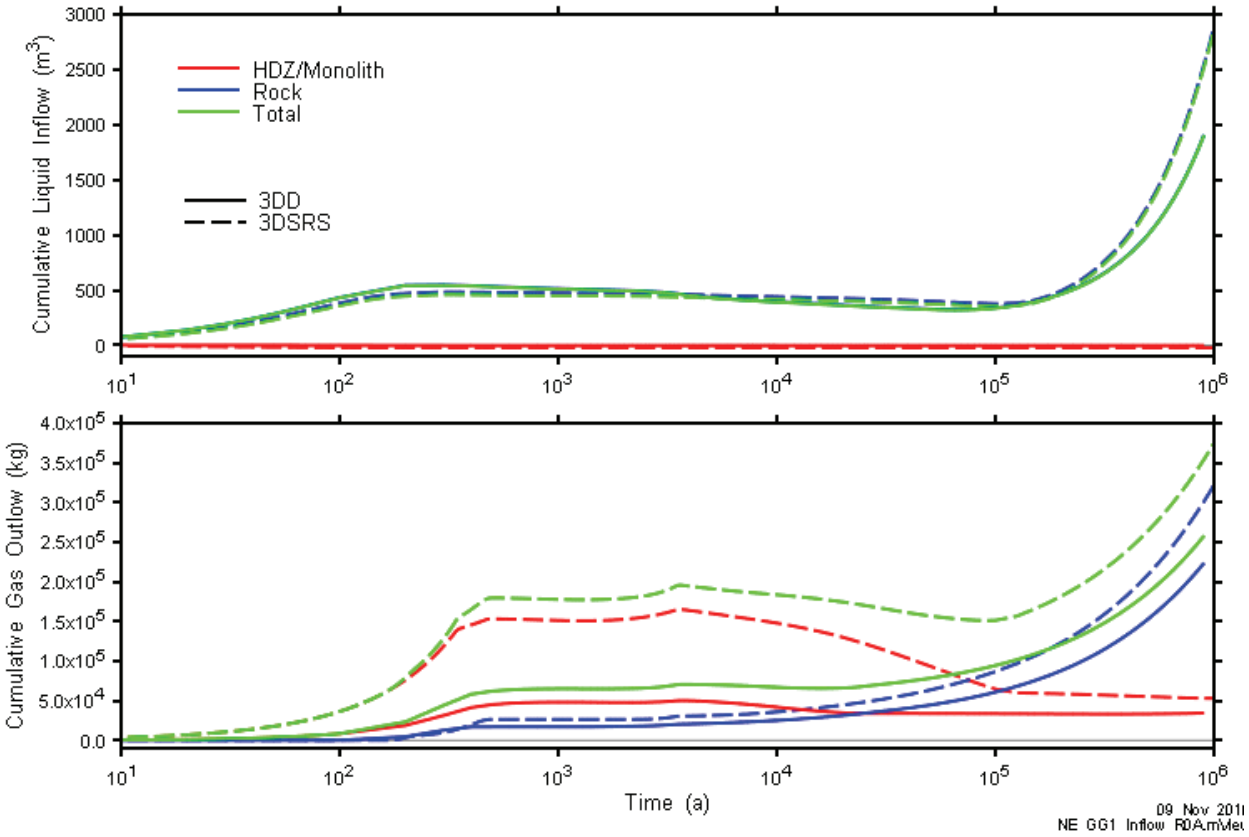

Figure 5.113: NE-GG1: Repository Liquid Inflow and Gas Outflow for 3DD and 3DSRS Models

Detailed flows into the repository at 1000, 10,000, 100,000, and 1,000,000 a are given in Figure 5.114 through Figure 5.117. They show that the higher gas generation rates, and consequent higher repository pressures, result in a near steady-state flow system surrounding the repository and lower shaft.

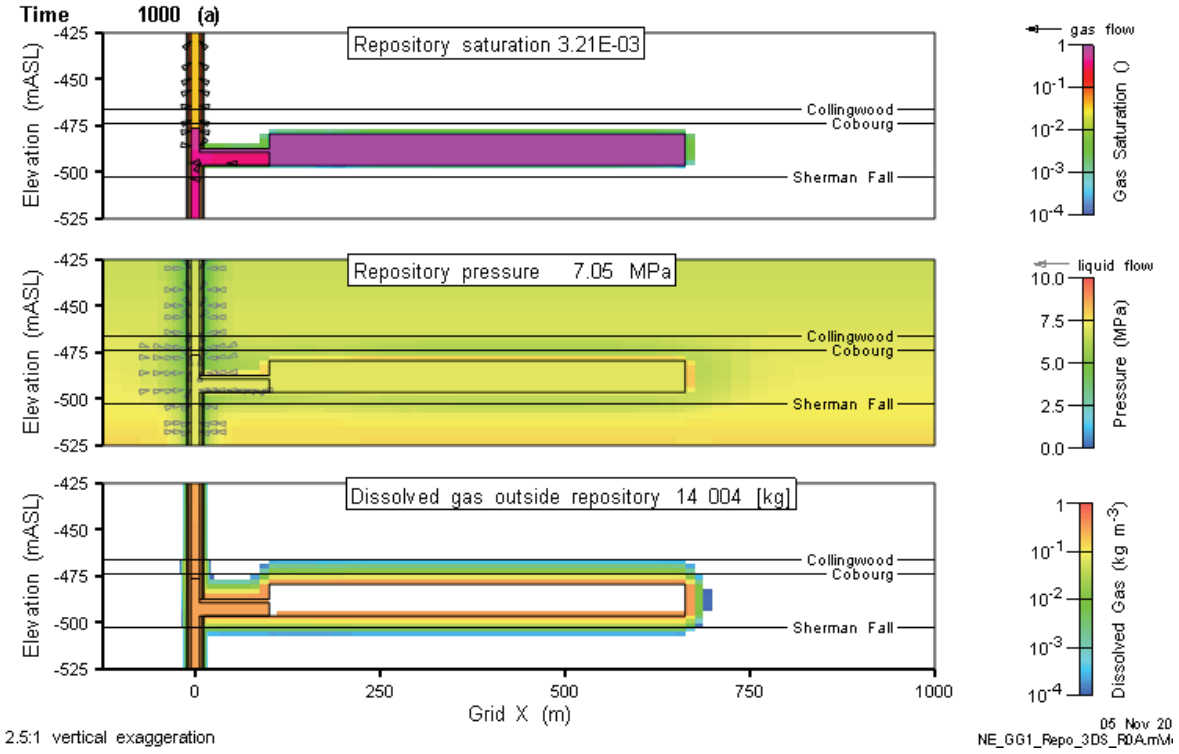

Figure 5.114: NE-GG1: 3DD Repository Saturations, Flows and Pressures (1000 a)

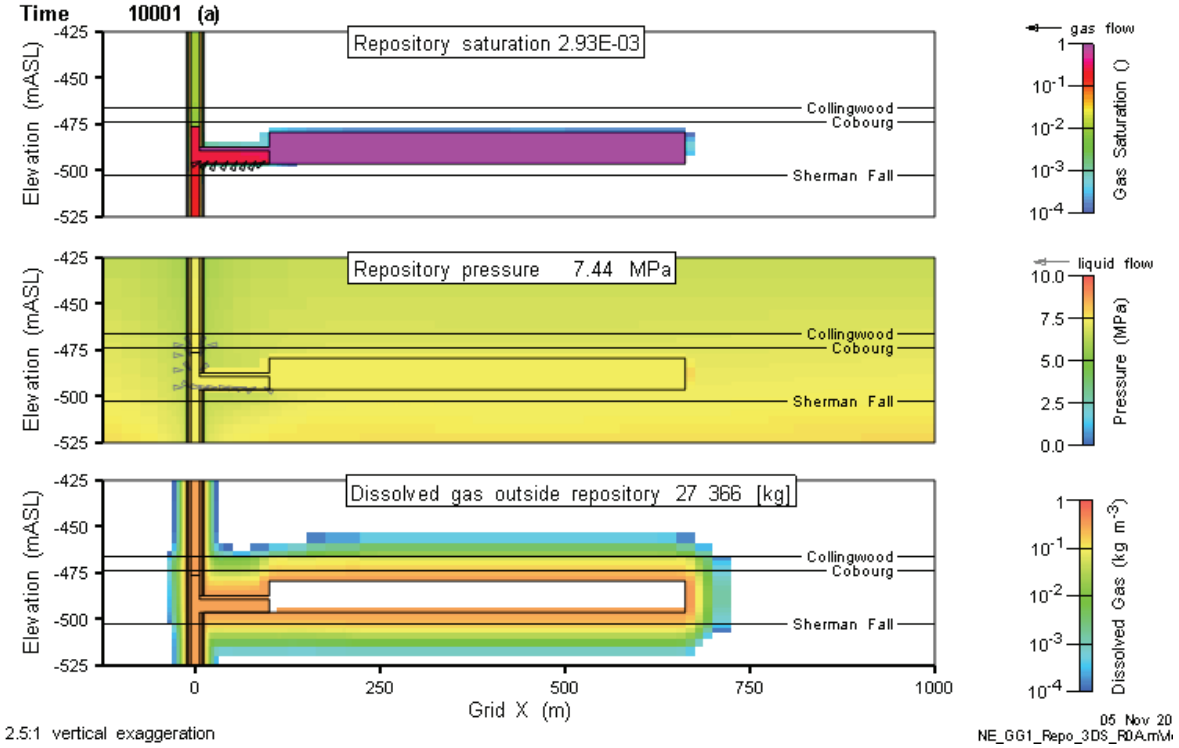

Figure 5.115: NE-GG1: 3DD Repository Saturations, Flows and Pressures (10,000 a)

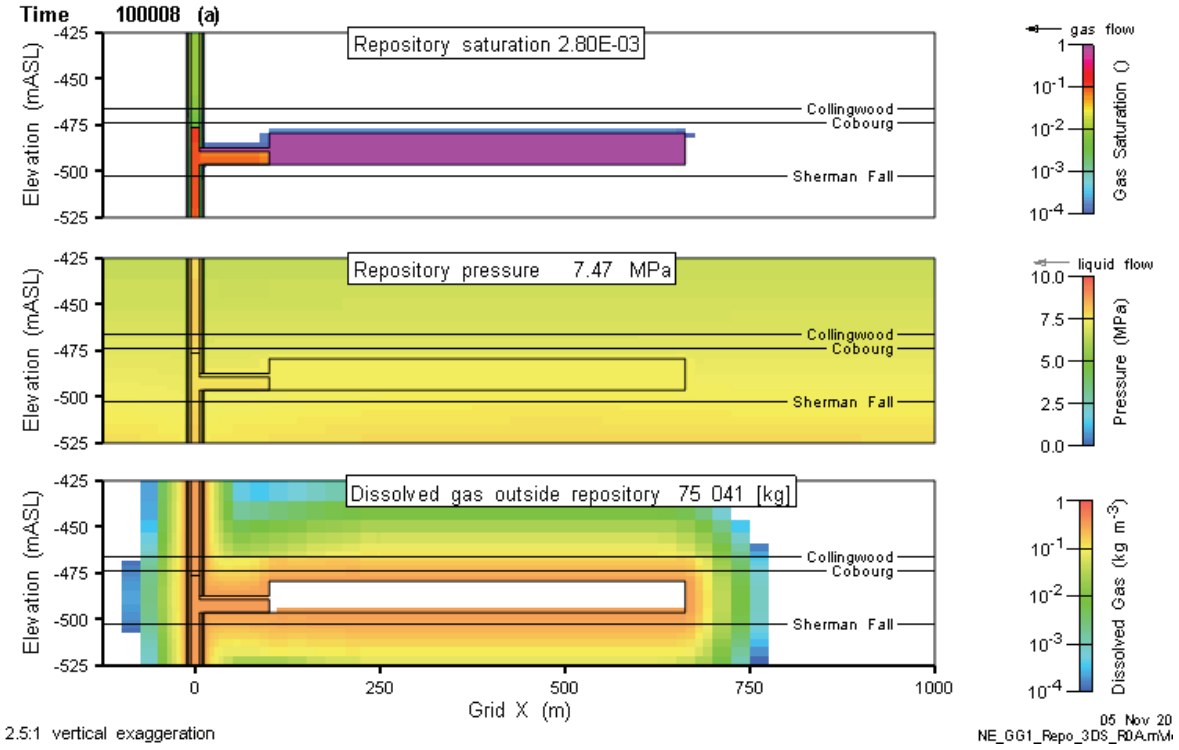

Figure 5.116: NE-GG1: 3DD Repository Saturations, Flows and Pressures (100,000 a)

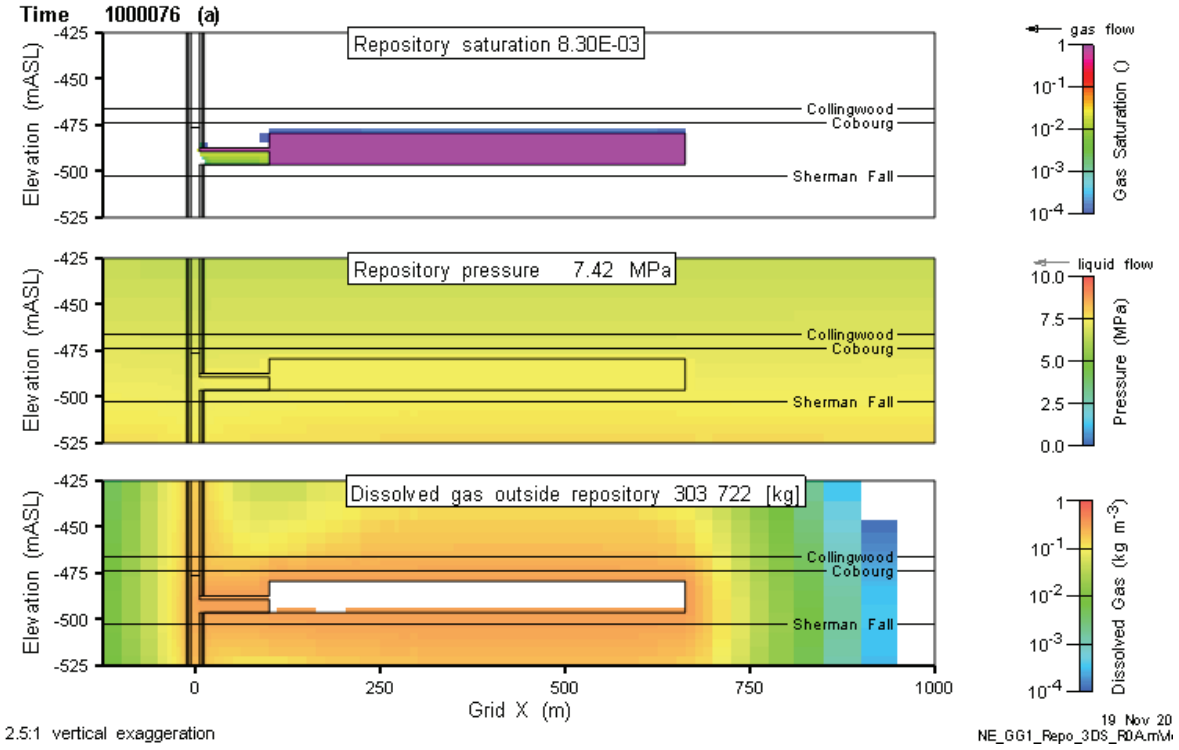

Figure 5.117: NE-GG1: 3DSR Repository Saturations, Flows and Pressures (1,000,000 a)

Figure 5.118 through Figure 5.123 are three-dimensional visualizations of gas saturation for the 3DD model at 0, 100, 1000, 10,000, 100,000, and 1,000,000 a, respectively. They show the limited spatial extent of the zones beyond the repository with gas saturation exceeding 10^{-4}.

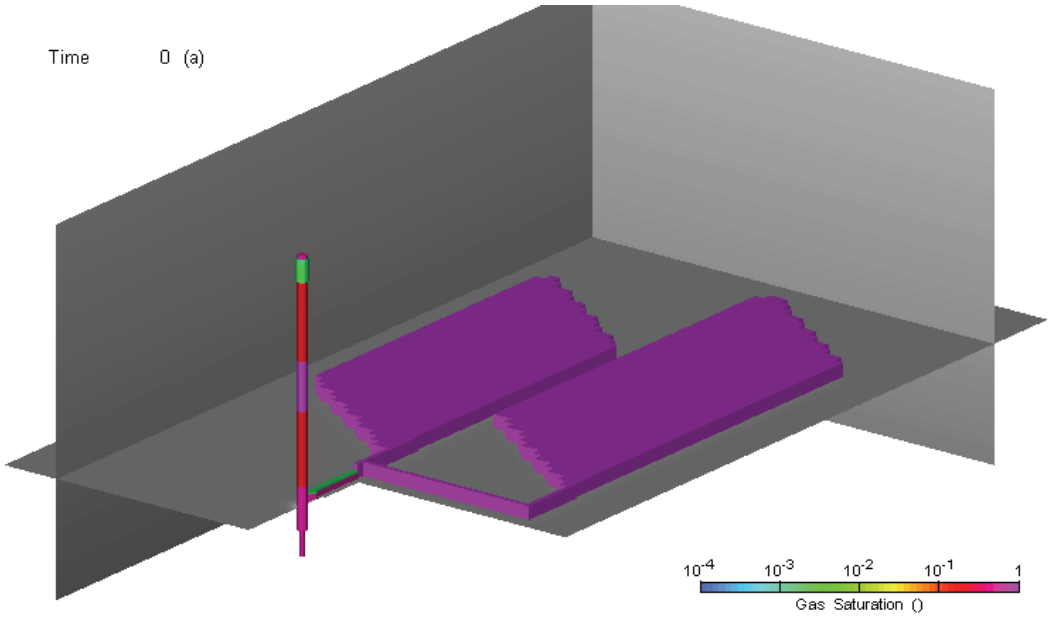

Figure 5.118: NE-GG1: Three-Dimensional Visualization of 3DD Model Gas Saturations at 0 a

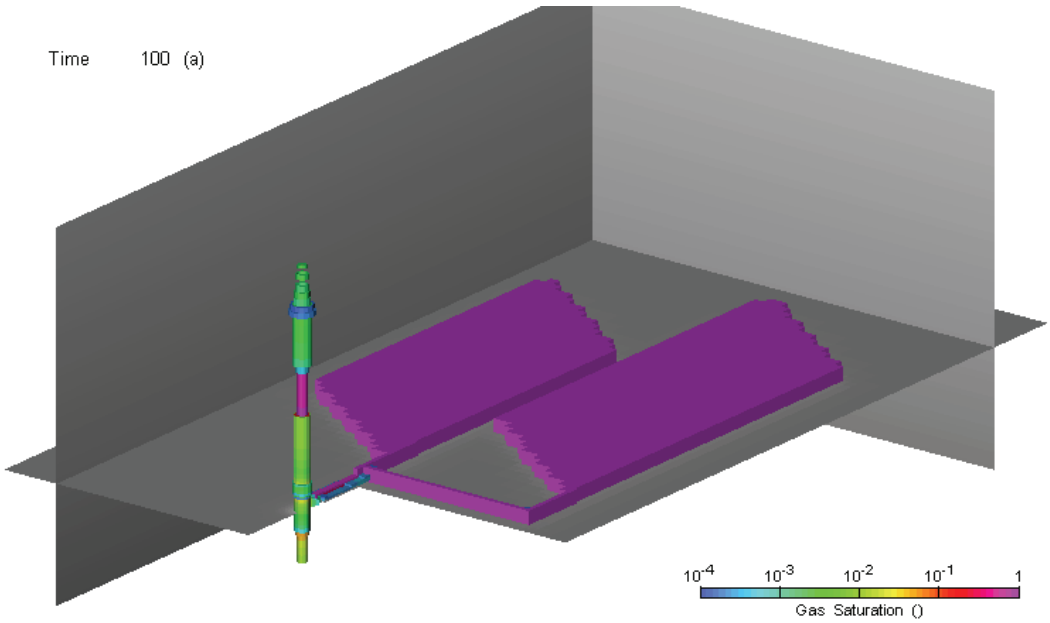

Figure 5.119: NE-GG1: Three-Dimensional Visualization of 3DD Model Gas Saturations at 100 a

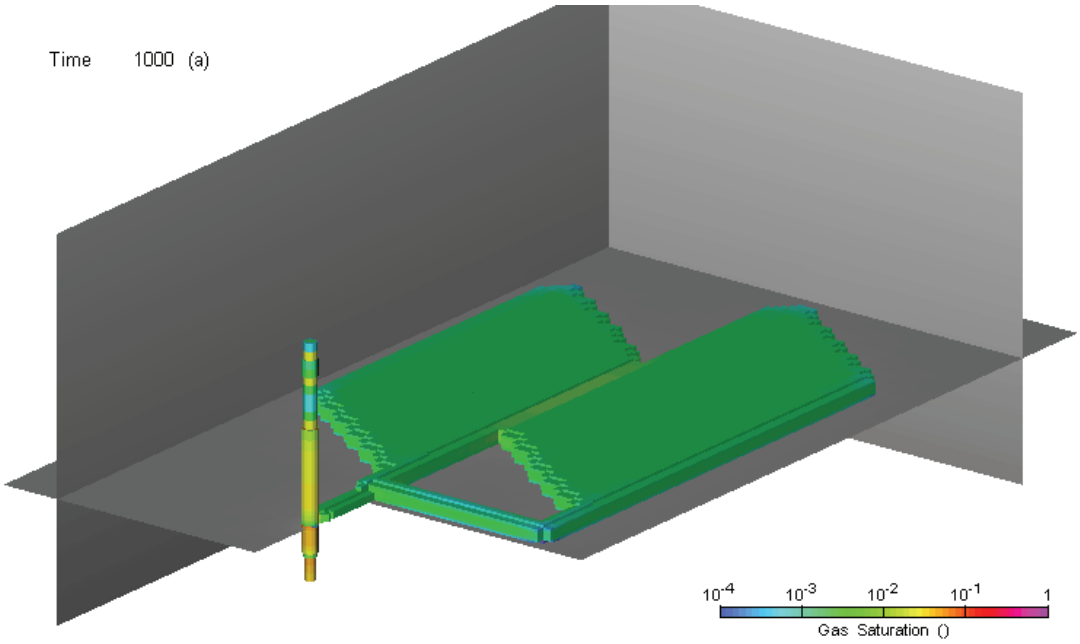

Figure 5.120: NE-GG1: Three-Dimensional Visualization of 3DD Model Gas Saturations at 1000 a

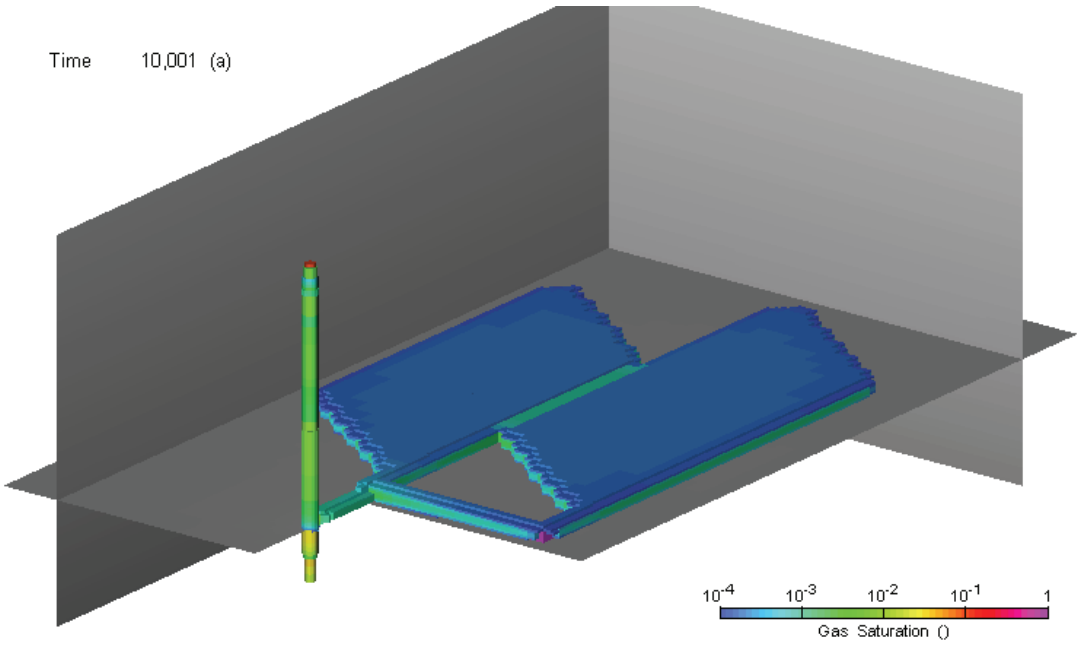

Figure 5.121: NE-GG1: Three-Dimensional Visualization of 3DD Model Gas Saturations at 10,000 a

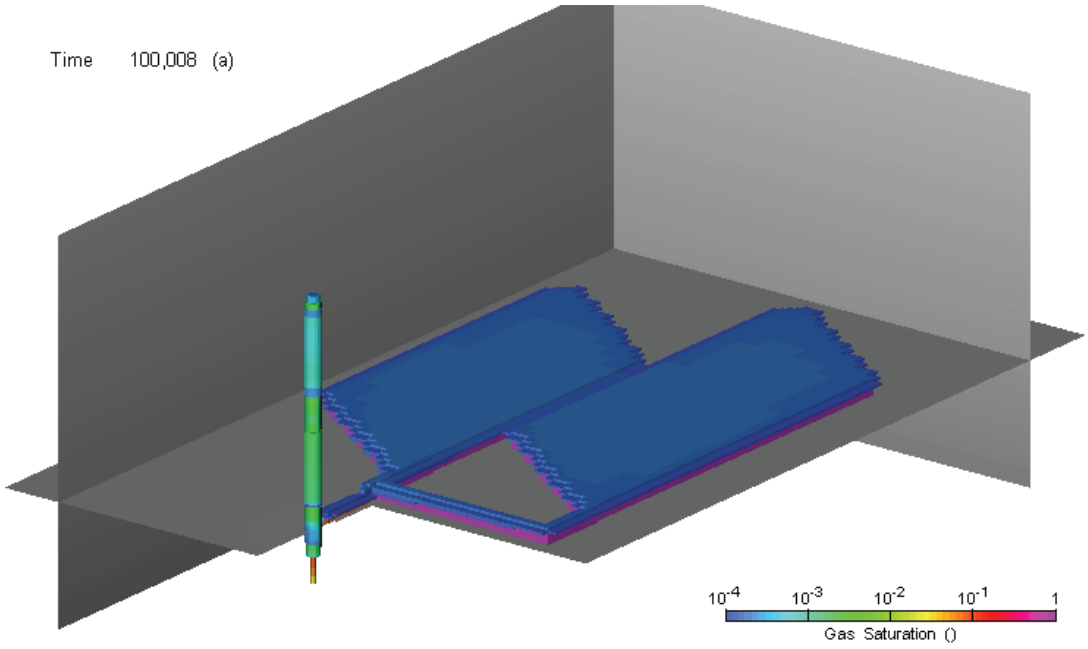

Figure 5.122: NE-GG1: Three-Dimensional Visualization of 3DD Model Gas Saturations at 100,000 a

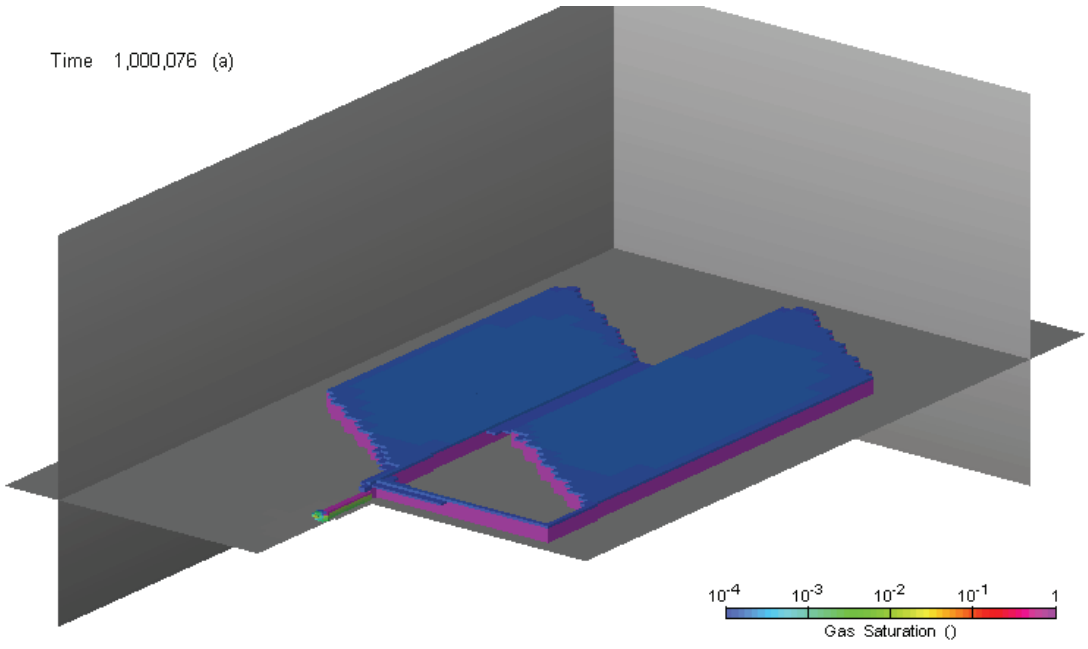

Figure 5.123: NE-GG1: Three-Dimensional Visualization of 3DD Model Gas Saturations at 1,000,000 a

5.5.2.3 Geosphere

The geosphere hydraulic head profile for the NE-GG1 case is presented in Figure 5.124. At the end of the 1 Ma simulation period, repository pressures are slightly in excess of the surrounding rock.

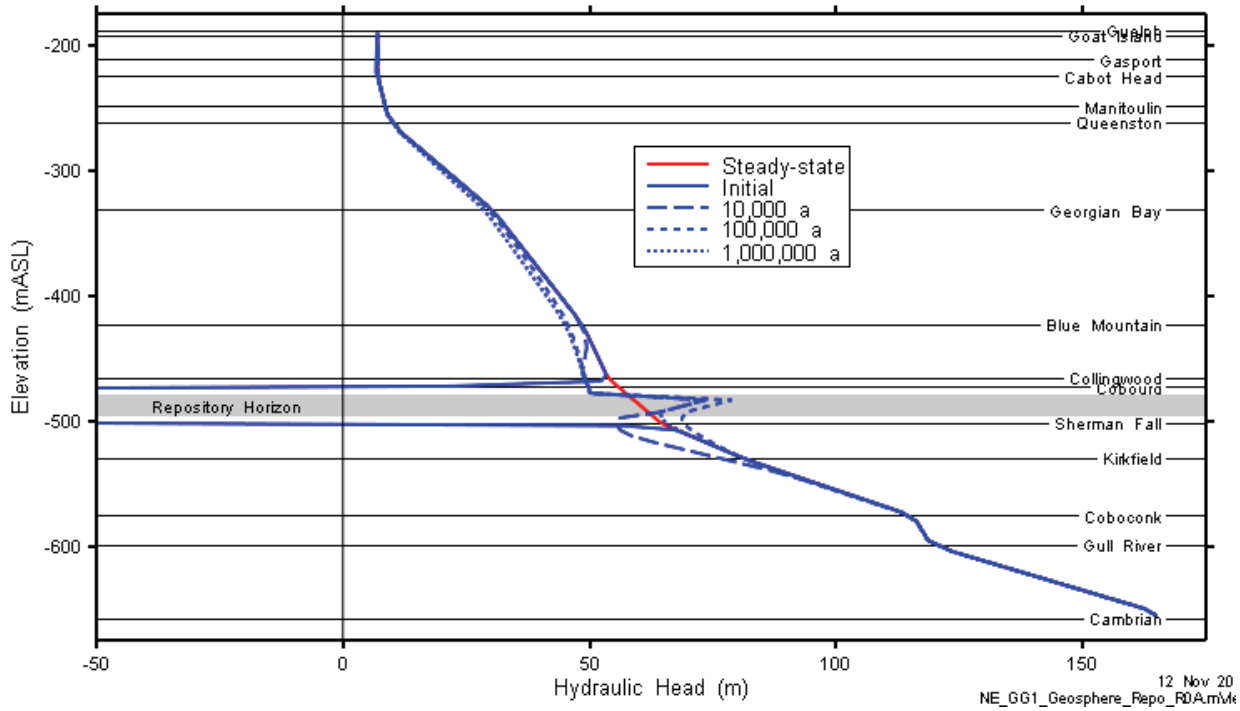

Figure 5.124: NE-GG1: 3DSRS Geosphere Head Profile

5.6 Case NE-GG2 – Reduced Degradation Rates

Case NE-GG2 differs from the NE-SBC case in that reduced organic degradation rates are used (Table 3.1). This corresponds to a scenario in which microbes are present but not as active within the repository as in the Simplified Base Case – for example, due to the high salinity of the groundwaters. The NE-GG2 case was simulated with the 3DSRS and 3DSR models.

5.6.1 Gas Generation

The results presented here are for the 3DSRS model. The 3DSR model produces almost the same results, but with slightly different fluxes of gas between the repository and the geosphere resulting in a marginally higher (0.6 MPa) peak pressure than that for the NE-SBC case.

Case NE-GG2 differs from the Simplified Base Case in that lower organic degradation rates are used. (The rate constant for the microbial hydrogen methanogenic reaction given by Equation (2-3) is unchanged, however.) The results are qualitatively quite different to the Reference Case. There is a higher peak gas pressure and the dominant gas is hydrogen up until 100,000 a as described below.

The complete degradation of the organic wastes can be seen to take a factor of 10 longer than for the Simplified Base Case (see Figure 5.125). The slower degradation results in slower

production of CO_2. Thus, the methanogenic reaction proceeds at a slower rate than that for the Simplified Base Case. This results in hydrogen, rather than methane being the dominant gas in the repository, until eventually there is enough production of carbon dioxide to completely consume the hydrogen at approximately 300,000 a (see Figure 5.126).

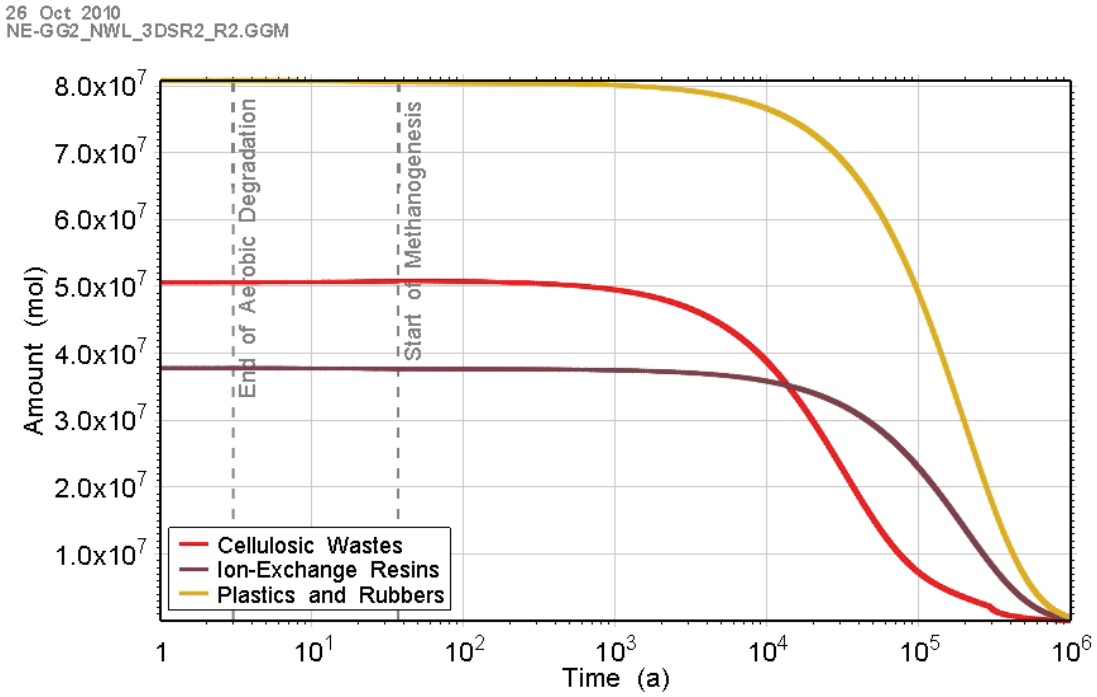

Figure 5.125: NE-GG2: Amounts of Organic Waste

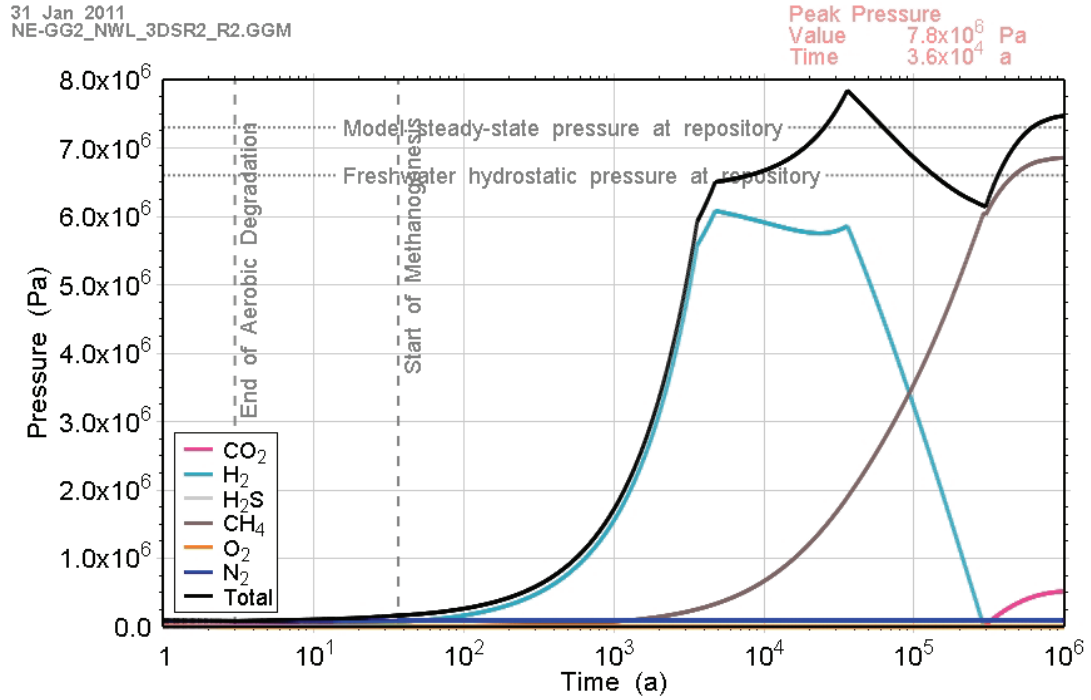

Figure 5.126: NE-GG2: Total and Partial Gas Pressures within the Repository

The slower CO_2 production also limits the rate at which the microbial hydrogen consuming reaction can proceed resulting in a larger total number of moles of gas in the system, until such time that this reaction has converted all available hydrogen and carbon dioxide to methane. This explains the slightly larger peak pressure of 7.8 MPa at 36,000 a (Figure 5.126) compared to the NE-SBC case (Figure 5.45).

Another effect of the slower degradation rates and slower production of CO_2 is that the partial pressure of CO_2 is lower during the first 100,000 a when both the carbon and galvanized steels and stainless steels and nickel based alloys are present. As a result, enhanced carbon dioxide corrosion has a weaker effect and less iron ultimately ends up in the form of $FeCO_3$ (see Figure 5.127), although the amount of $FeCO_3$ formed was small even for the NE-SBC.

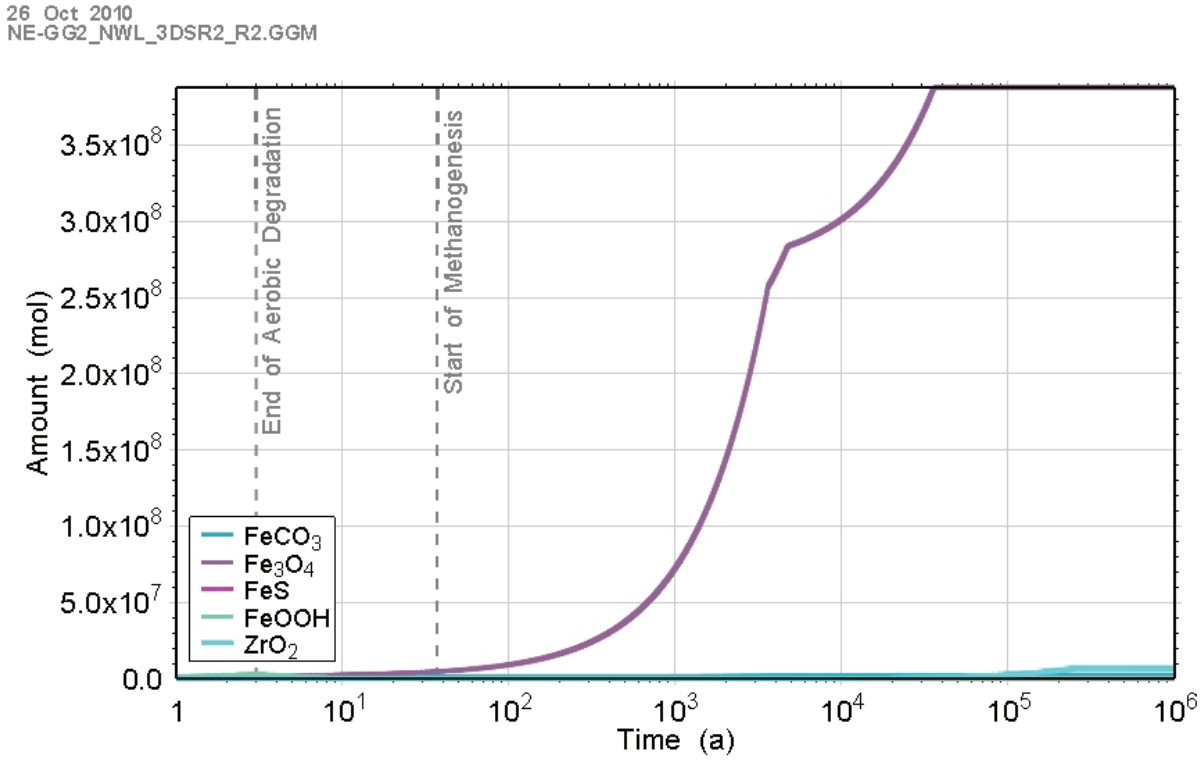

Figure 5.127: NE-GG2: Amounts of Corrosion Products

5.6.2 Gas and Water Flows

5.6.2.1 Shaft

Evolution of gas and liquid flows and saturations within the shaft and surrounding intact rock are very similar to the NE-SBC case. Although the pressure peak exceeds the repository initial pressure briefly at approximately 35,000 a, there is insufficient pressure differential to initiate the flow of gas up the shaft. Figure 5.128 shows gas flow at selected monitoring points. The early time peaks for the Collingwood and Georgian Bay, although small, are artefacts of the shaft resaturation process and do not represent flow of contaminated gas from the repository.

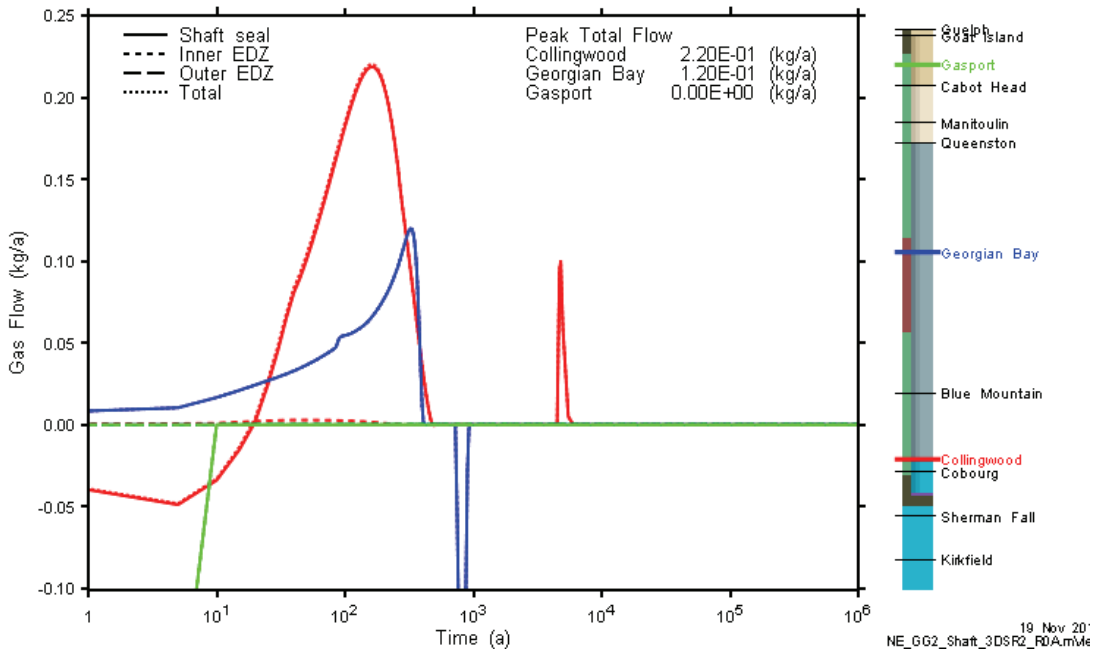

Figure 5.128: NE-GG2: 3DSRS Model Shaft Gas Flow at Selected Monitoring Planes

The dissolved gas concentration vs. time profiles are shown in Figure 5.129. There are two periods of upward flow at the Collingwood monitoring plane, corresponding to the small repository overpressure at 35,000 a, and the longer term overpressure beyond 500,000 a. These flows do not propagate up the shaft.

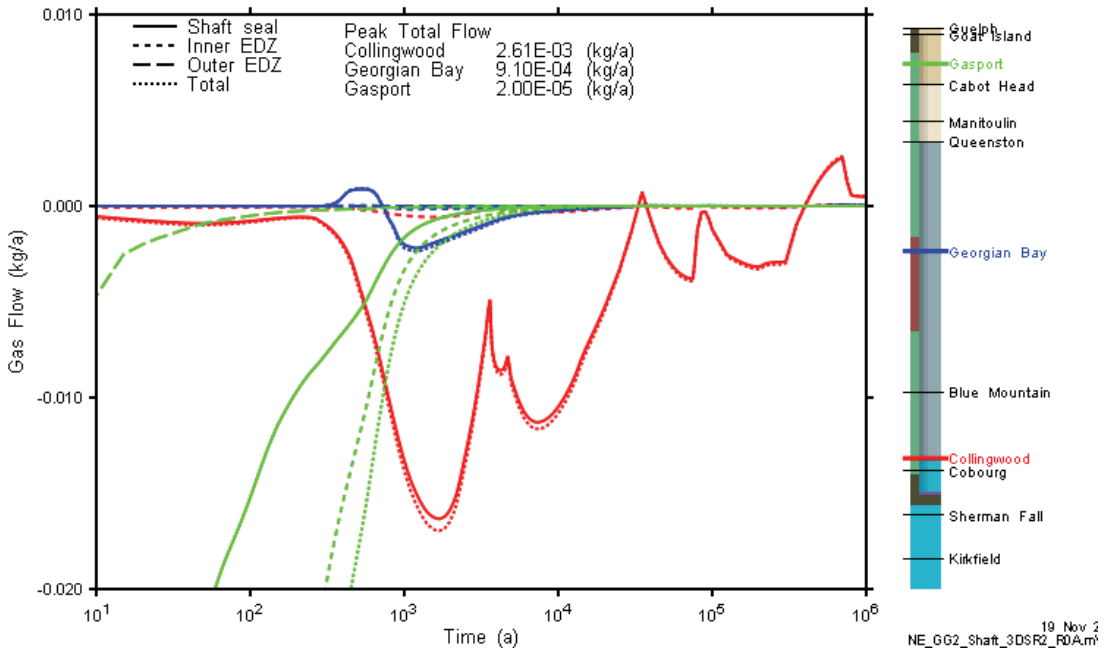

Figure 5.129: NE-GG2: 3DSRS Model Shaft Dissolved Gas Flow at Selected Monitoring Planes

5.6.2.2 Repository System

Figure 5.130 compares repository pressures and liquid saturations for the NE-GG2 3DSRS and 3DSR models to the NE-SBC 3DSRS model. 3DSRS and 3DSR pressures are visually coincident. Peak repository liquid saturations are slightly higher for the NE-GG2 case compared to the NE-SBC due to the period of underpressure, as methanogenic reactions dominate from 100,000 a onward. During this period, liquid flow into the repository is enhanced. Subsequently, saturations fall as the higher pressures return liquid to the geosphere.

Figure 5.131 shows cumulative gas and liquid flows for 3DSRS and 3DSR models. Liquid inflows are very similar, with a small contribution from the shaft in the 3DSRS model during the period repository pressure is below the steady-state geosphere pressure beyond 100,000 a. Calculated gas outflows to the intact rock are nearly identical for both models.

Detailed flows into the repository are shown at 1,000,000 a in Figure 5.132. The extent of gas saturations in the geosphere is minimal.

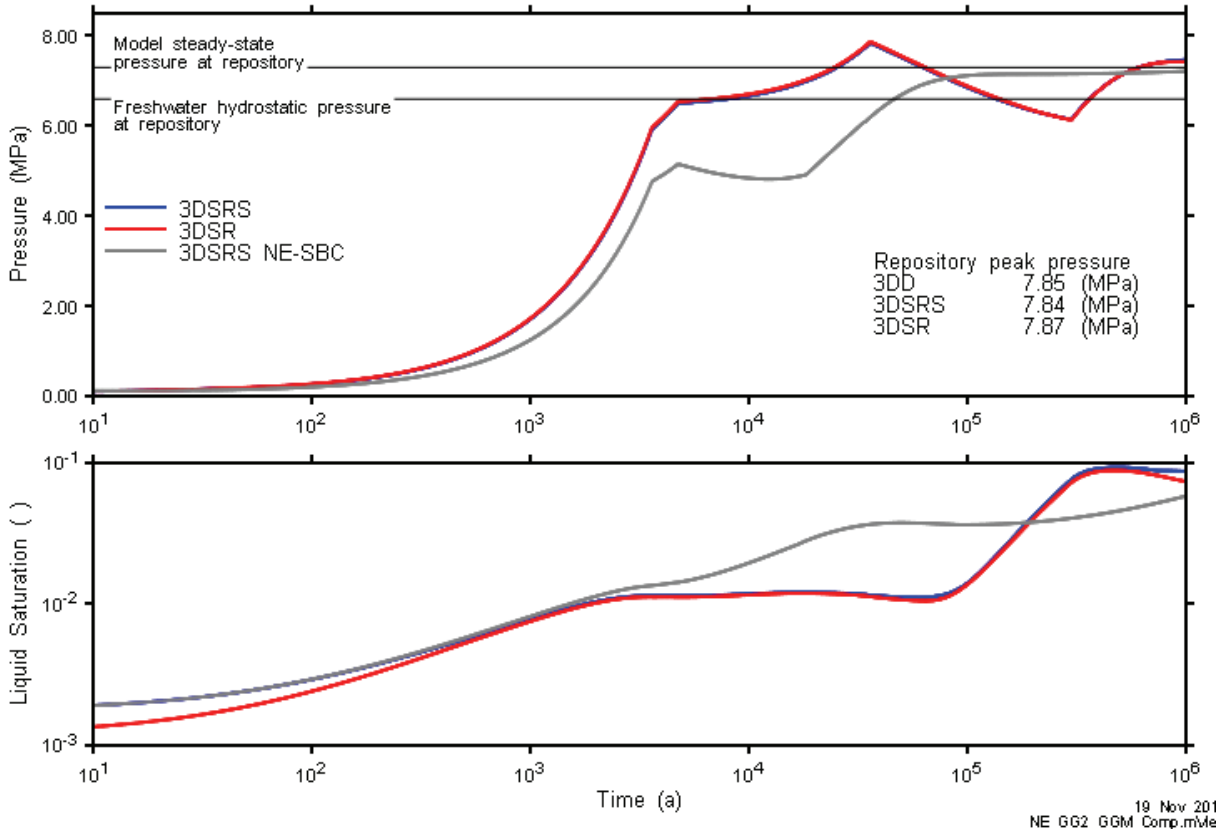

Figure 5.130: NE-GG2: 3DSRS and 3DSR Model Repository Pressure and Saturation Compared to NE-SBC 3DSRS Results.

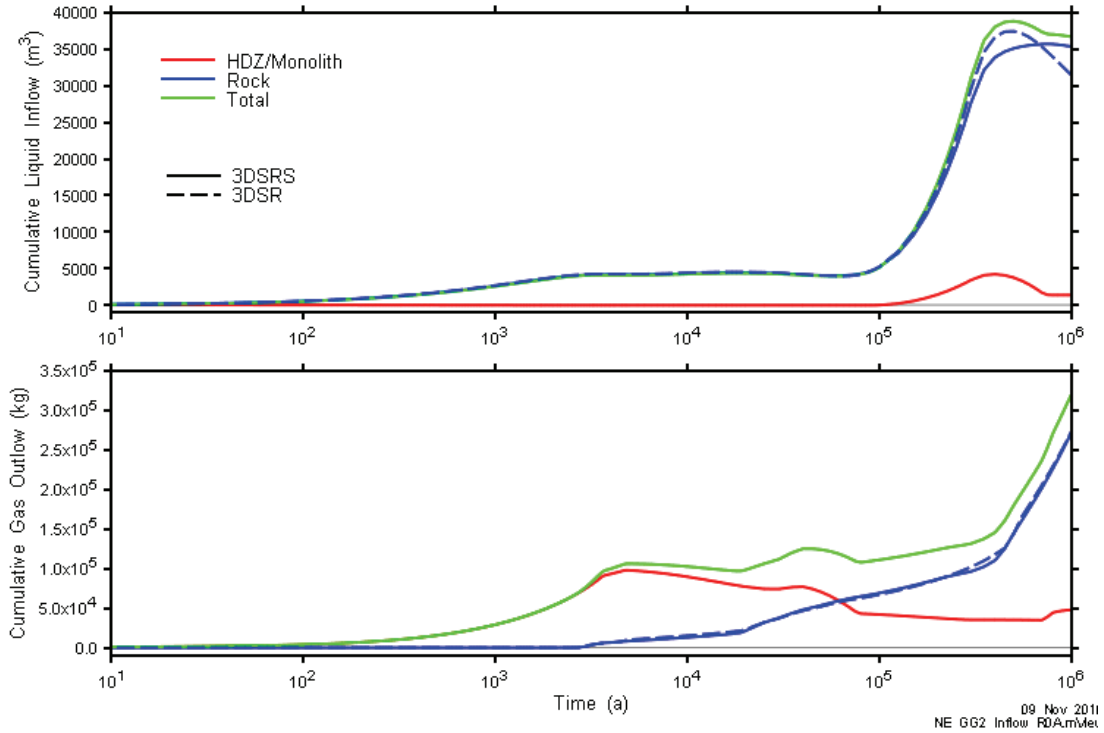

Figure 5.131: NE-GG2: Repository Liquid Inflow and Gas Outflow for 3DSRS and 3DSR Models

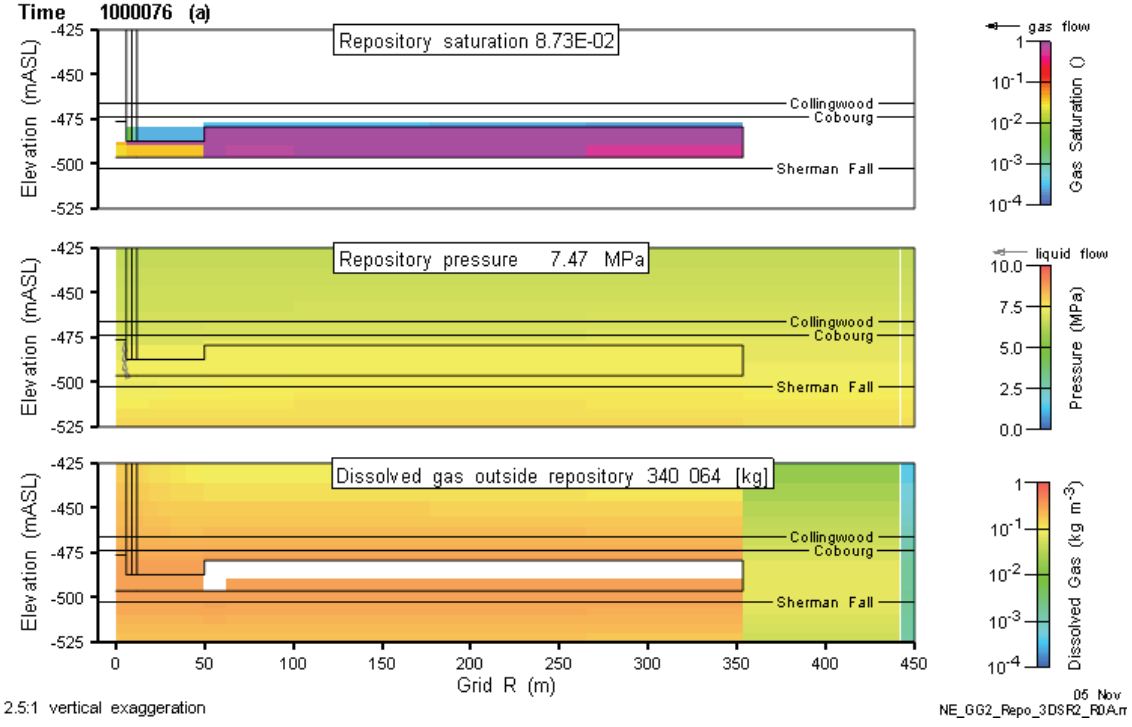

Figure 5.132: NE-GG2: 3DSRS Repository Saturations, Flows and Pressures (1,000,000 a)

5.6.2.3 Geosphere

The geosphere hydraulic head profile for the NE-GG2 case is presented in Figure 5.133. At the end of the 1 Ma simulation period, repository pressures are very slightly in excess of the surrounding intact rock. The extent of the perturbation on the system is minimal as pressures have returned to near steady-state directly above and below the repository.

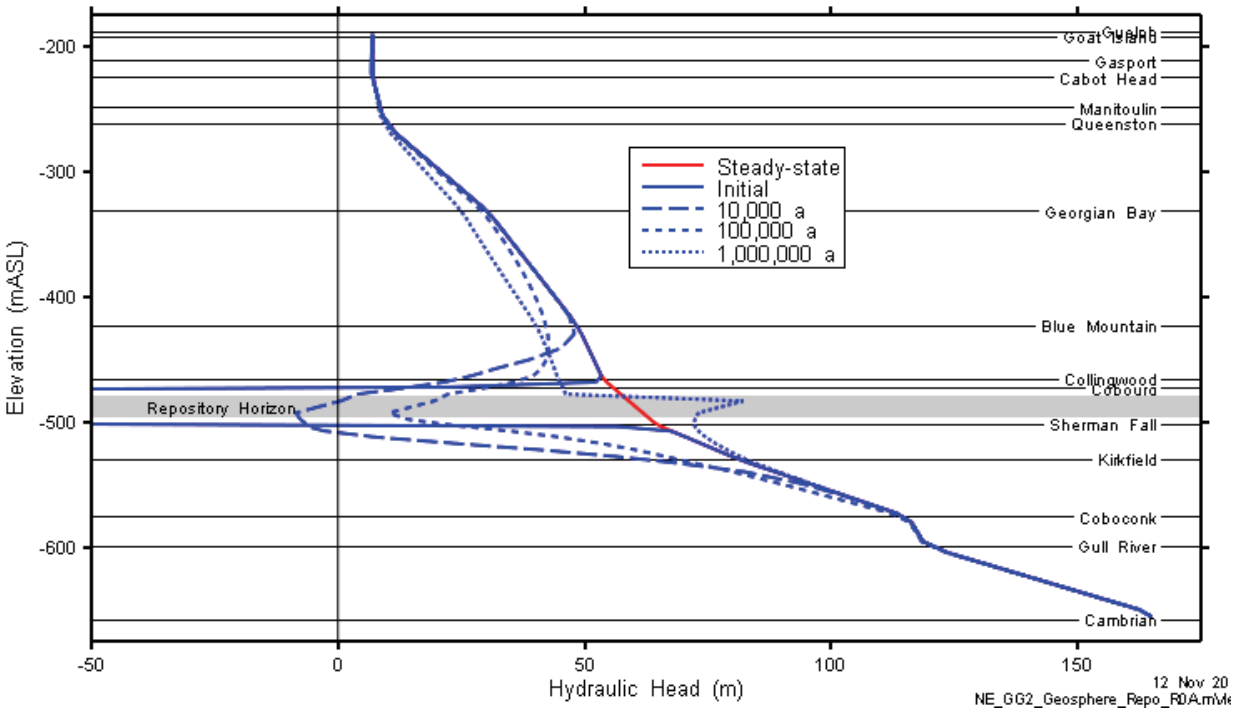

Figure 5.133: NE-GG2: 3DSRS Geosphere Head Profile

5.7 Cases NE-GT1, NE-GT2, and NE-GT3 – Alternative Geosphere Gas Parameters

The three NE-GT cases that test the sensitivity of the results to the gas parameters characterizing the rock formations are described in this section. Case NE-GT1 decreases capillary pressures for the intact rock, NE-GT2 increases capillary pressures, and NE-GT3 modifies the relative permeability curve to reflect zero residual gas and liquid saturations.

Unlike other sensitivity cases, the NE-GT cases are based on the NE-GG1 model rather than the NE-RC or NE-SBC case. This allows the simulations to include a period of repository overpressure where gas flow from the repository into the intact rock may occur, and where the geosphere related parameter changes will be tested.

5.7.1 Gas Generation

The alternative geosphere gas parameters had a negligible impact on gas generation. Results are practically identical to those for NE-GG1.

5.7.2 Gas and Water Flows

All case results are compared to the NE-GG1 model in Figure 5.134. There are virtually no differences in repository pressure between the cases, while repository saturations are very similar, with very minor differences apparent at late times. This indicates that gas and water flows are virtually identical for all four cases.

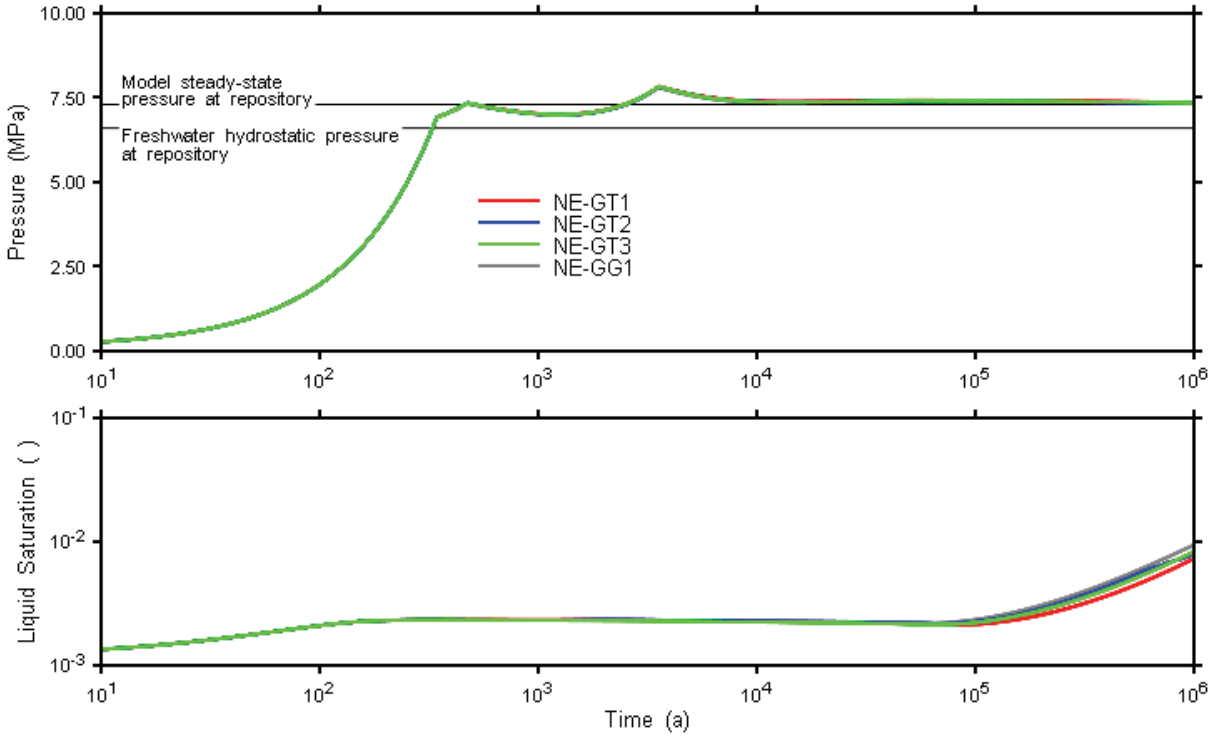

Figure 5.134: NE-GT: 3DSR Model Repository Pressure and Saturation for NE-GT1, NE-GT2, and NE-GT3 Compared to NE-GG1 3DSR Results

The capillary pressure curves used in the intact rock have virtually no impact on repository performance. The capillary pressure curves defined for NE-GT1 and NE-GT2 (see Figure 4.3) bracket the measured range for most formations. The NE-GT3 relative permeability function also has no significant impact on results. As a note of interest, the NE-GG1, NE-GT1, and NE-GT3 cases required similar computing time to complete, while the NE-GT2 case required a factor of 50 more time.

5.8 Cases NE-GT4 and NE-GT5 – Alternative Shaft Parameters

These two NE-GT cases test the sensitivity of the results to the properties of the shaft seal. Case NE-GT4 removes the asphalt seal from the shaft, replacing it with the bentonite/sand material. Case NE-GT5 removes the asphalt seal, and also increases the permeability of the bentonite/sand seal by an order of magnitude, while decreasing the air-entry pressure of the material by a factor of two.

Like the other NE-GT sensitivity cases, the NE-GT4 and NE-GT5 cases are based on the NE-GG1 model rather than the NE-RC or NE-SBC case. The overpressures in the NE-GG1 repository create gas flow up the shaft, which maximizes the effect of the sensitivity case parameter changes.

5.8.1 Gas Generation

For case NE-GT4 the alternative geosphere gas parameters had a negligible impact on gas generation. The results are practically identical to those for NE-GG1.

There were observable differences for the NE-GT5 case, but they had little impact on gas generation. After 10,000 a, the amount of gas leaving the repository increases more rapidly than for case NE-GG1 (see Figure 5.135) as does the water saturation which climbs to approximately 3% at 1,000,000 a (see Figure 5.136). These modified fluxes have very little impact on the gas composition within the repository or overall gas pressure however. The peak gas pressure is calculated as 7.75 MPa compared to 7.81 MPa for NE-GG1.

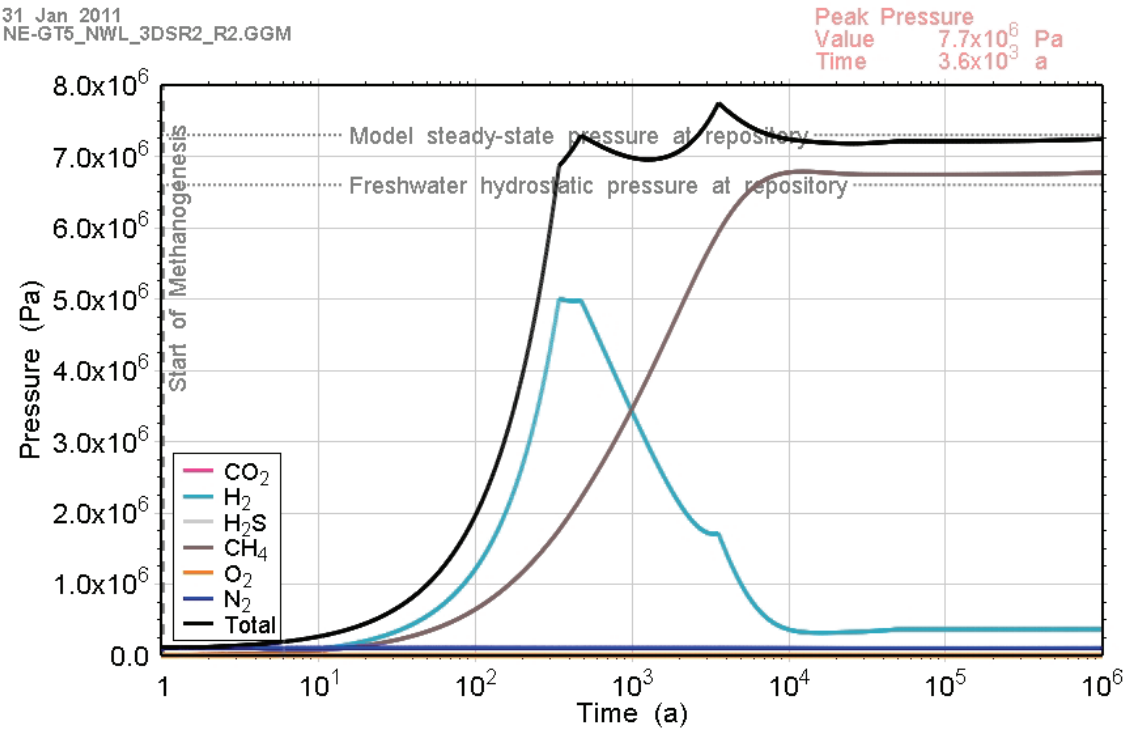

Figure 5.135: NE-GT5: Total and Partial Gas Pressures within the Repository

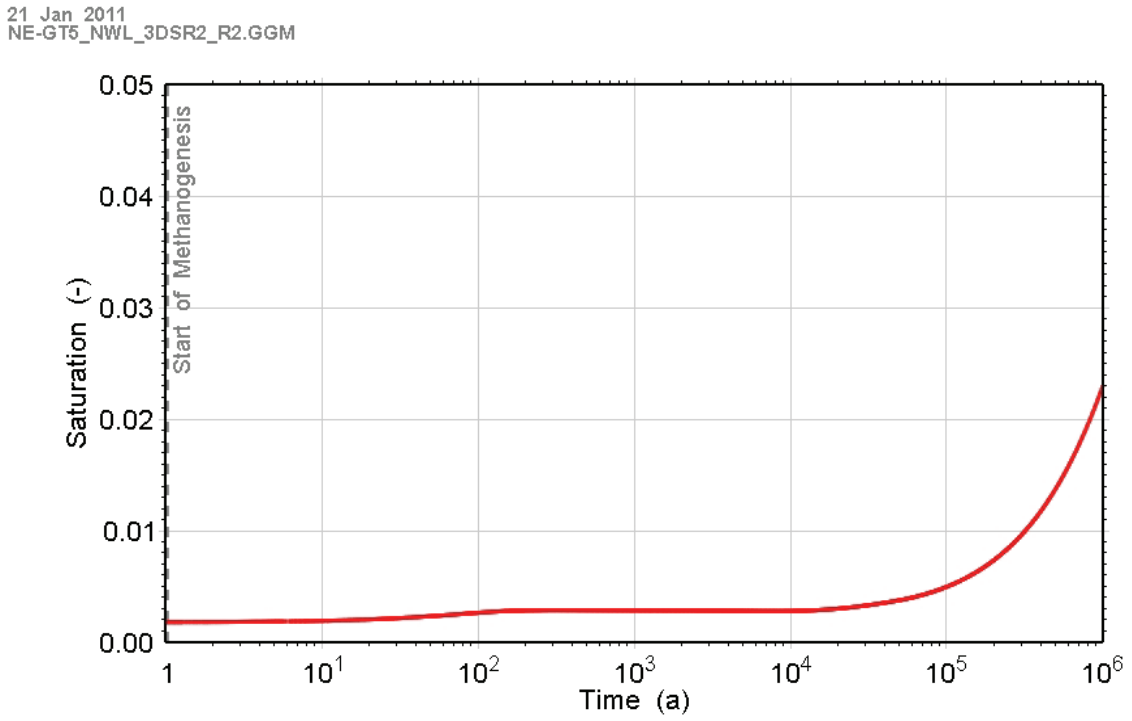

Figure 5.136: NE-GT5: Water Saturation within the Repository

5.8.2 Gas and Water Flows

5.8.2.1 Shaft

Gas and dissolved gas flows in the shaft are affected by the changes in the shaft description (no asphalt seal) and parameterization (increased permeability for NE-GT5 only). For NE-GT4, the elimination of the asphalt seal causes minor increases in predicted gas and dissolved gas flows at the Gasport measuring plane. Although Collingwood peak flows are essentially unchanged, comparing Figure 5.137 and Figure 5.110 shows a factor of 2.8 increase in maximum gas flow rates in the Gasport (0.43 kg/a NE-GG1, 1.2 kg/a NE-GT4), while Figure 5.138 and Figure 5.111 differ by a factor of 1.4 increase in maximum dissolved gas flow at the Gasport. Dissolved gas flow through the Georgian Bay plane is significantly increased. In the NE-GG1 case the asphalt seal has a very high gas saturation and provides the lowest relative permeability to liquid flow, which limits dissolved gas flow.

Shaft gas and dissolved gas flow results for NE-GT5 are presented in Figure 5.139 and Figure 5.140 respectively. In this case the increased permeability of the shaft causes a significant increase in both gas and dissolved gas rates, with Gasport flow increasing by a factor of 55 (gas) and 60 (dissolved gas) relative to NE-GT4. Relatively high flow rates are found up through the entire shaft prior to approximately 30,000 a.

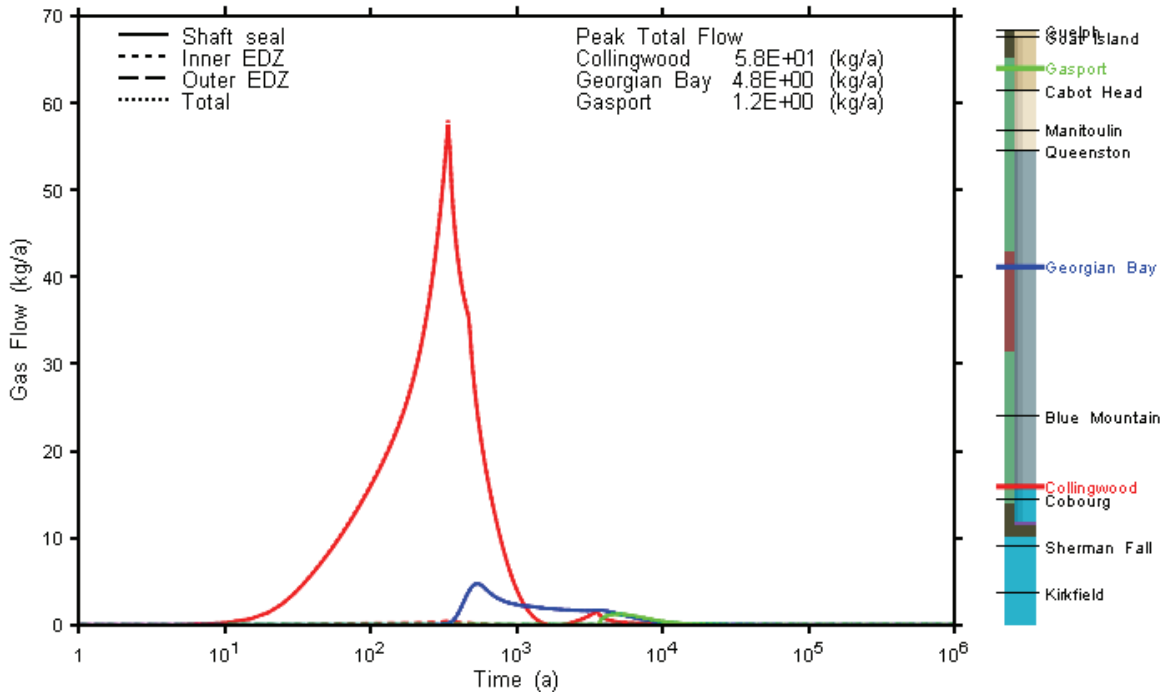

Figure 5.137: NE-GT4: 3DSRS Model Shaft Gas Flow at Selected Monitoring Planes

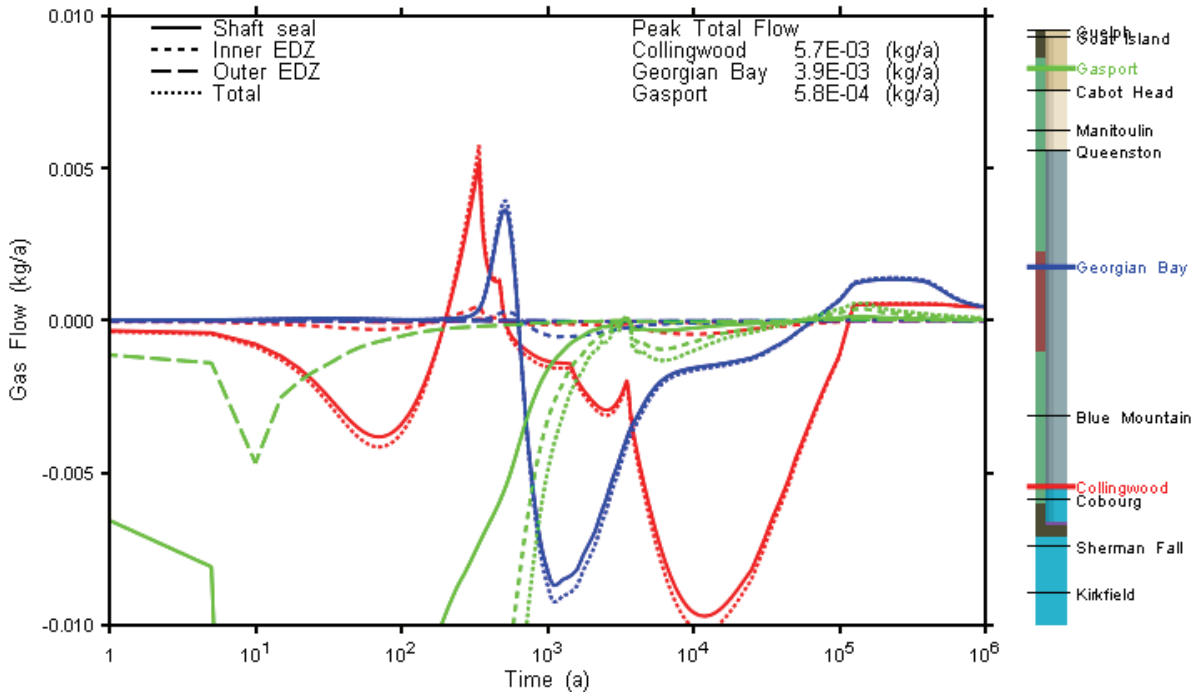

Figure 5.138: NE-GT4: 3DSRS Model Shaft Dissolved Gas Flow at Selected Monitoring Planes

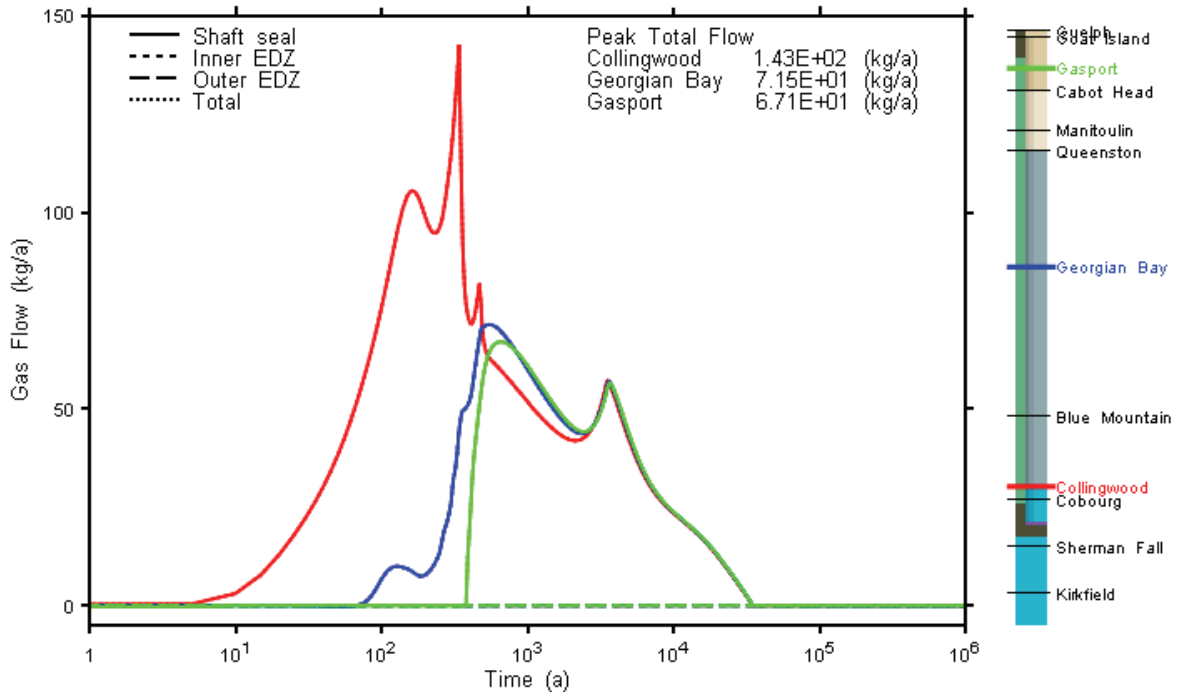

Figure 5.139: NE-GT5: 3DSRS Model Shaft Gas Flow at Selected Monitoring Planes

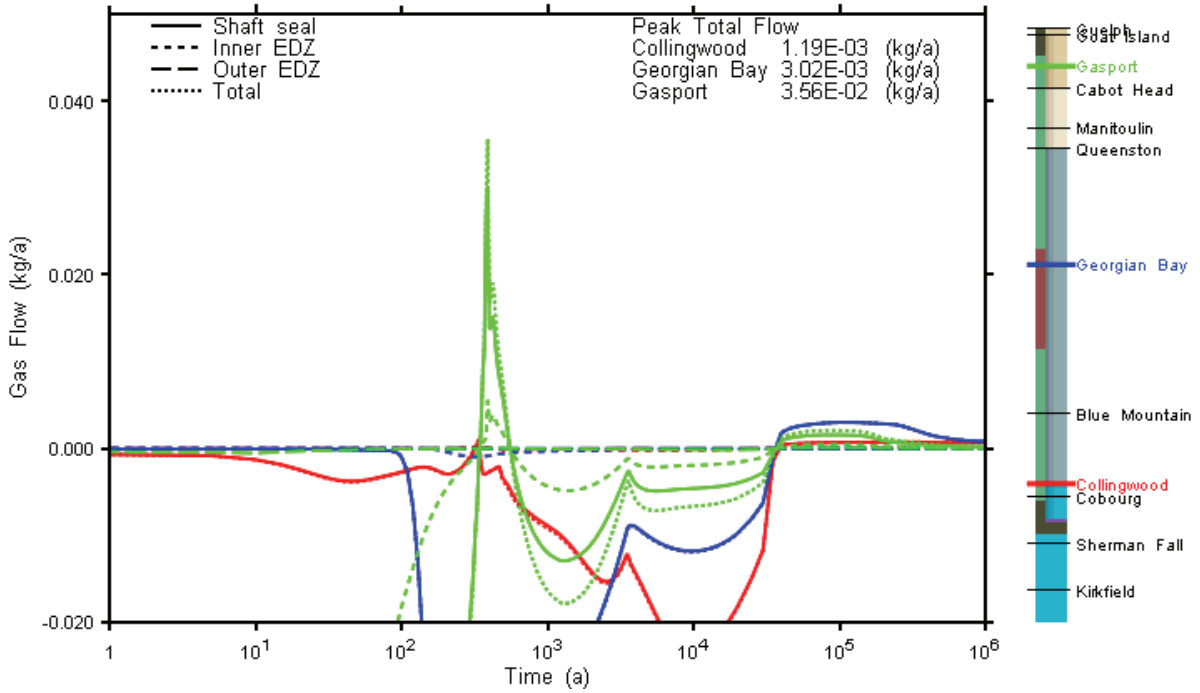

Figure 5.140: NE-GT5: 3DSRS Model Shaft Dissolved Gas Flow at Selected Monitoring Planes

Figure 5.141 describes NE-GT5 gas and liquid flows at 1000 a, during the period of highest gas flows up the shaft. The figure shows high levels of gas saturation throughout the shaft to the top of the model. The 2DRS model was used to investigate the fate of gas in the shaft above the top of the 3D model domain. As shown in Figure 5.142, results are similar to those seen for the NE-GG1 2DRS model; the Guelph Formation is an effective sink for gas and gas is not transported vertically in the shaft beyond that formation.

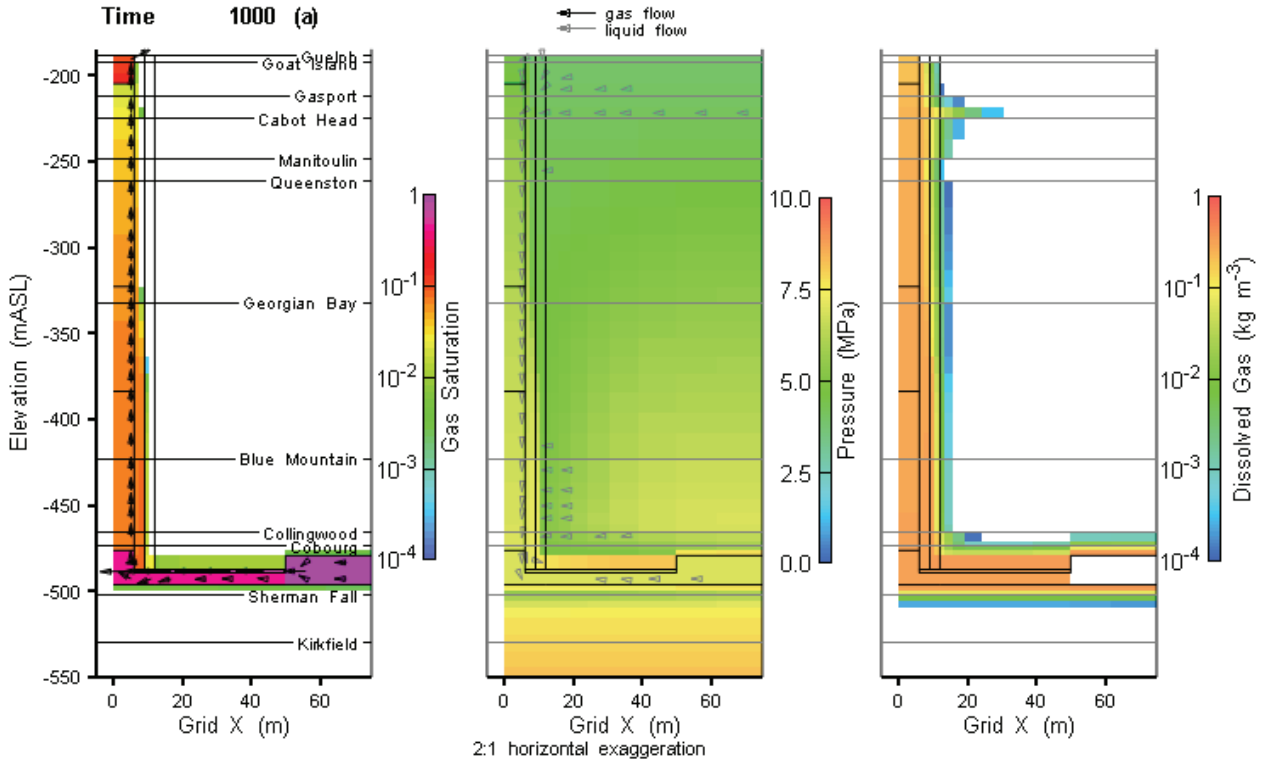

Figure 5.141: NE-GT5: 3DSRS Model Shaft Saturations, Flows and Pressures (1000 a)

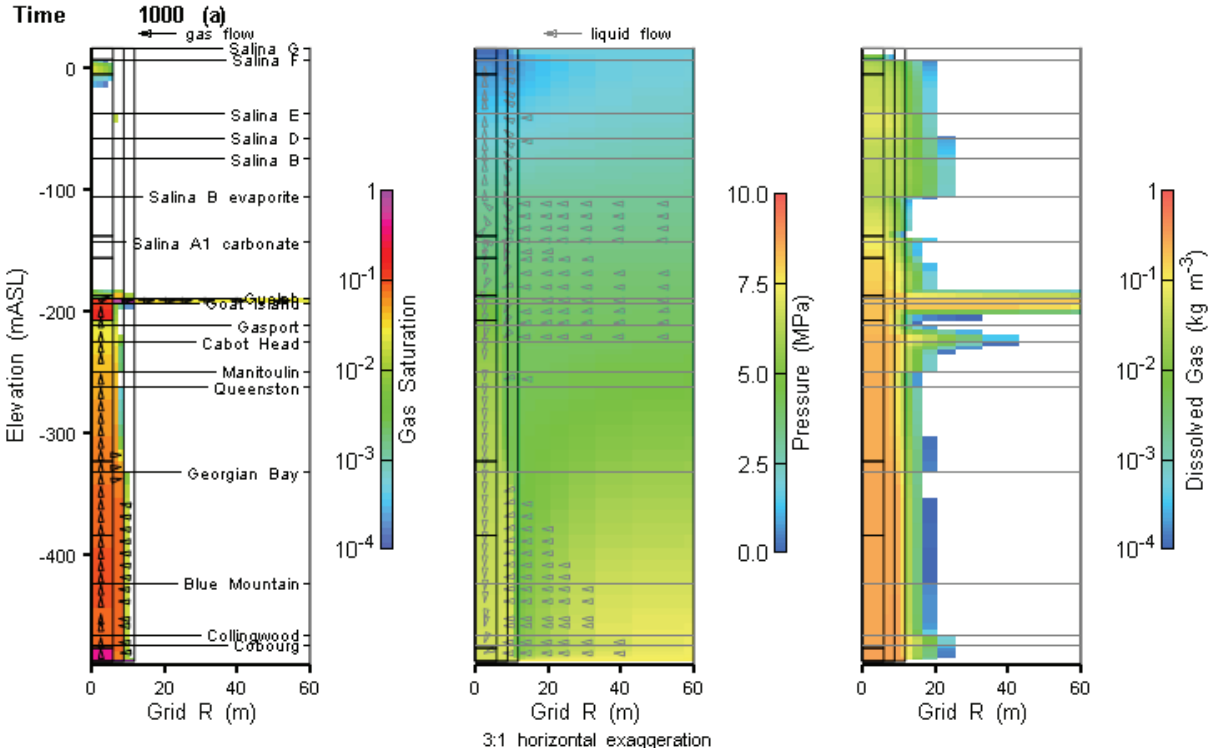

Figure 5.142: NE-GT5: 2DRS Model Shaft Saturations, Flows and Pressures (1000 a)

Gas flow rates up the shaft are presented in Figure 5.143 for the 2DRS model. They are very similar in magnitude and character to the 3DSRS results.

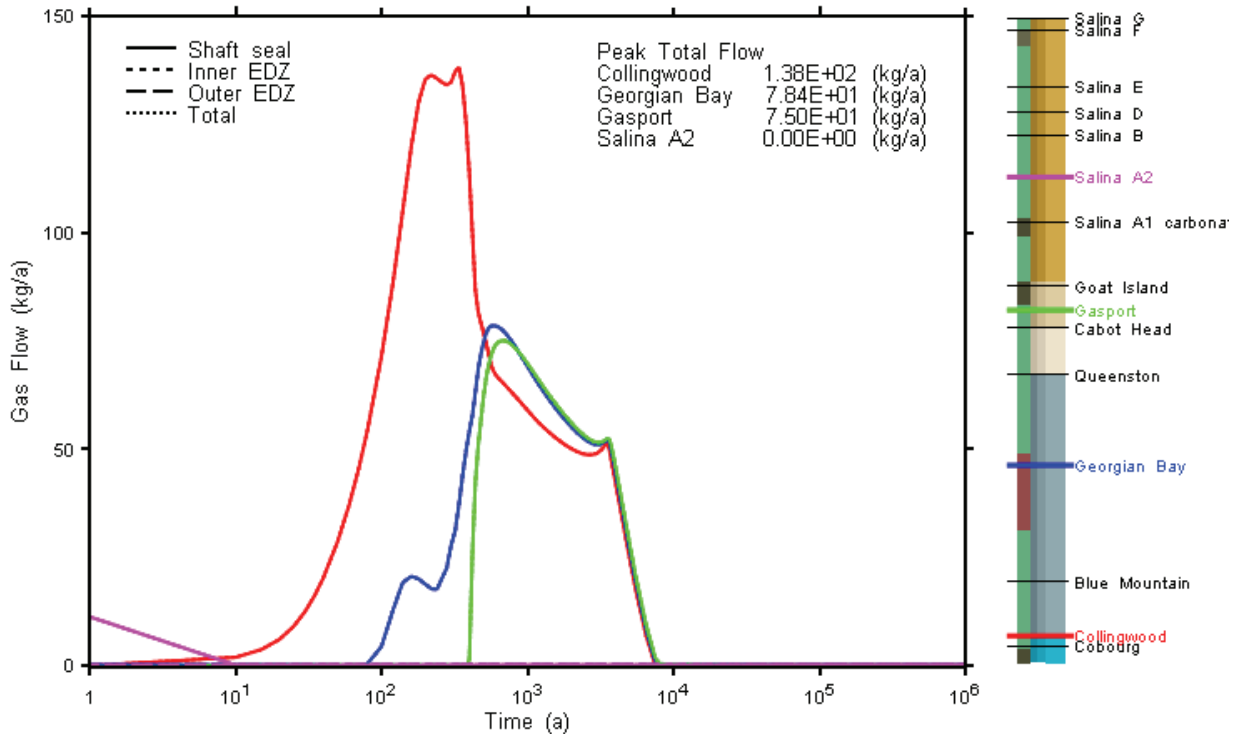

Figure 5.143: NE-GT5: 2DRS Model Shaft Gas Flow at Selected Monitoring Planes

5.8.2.2 Repository System

NE-GT4 and NE-GT5 case results are compared to those of the NE-GG1 model in Figure 5.144. The NE-GT4 case is visually indistinguishable from the NE-GG1 case, while the NE-GT5 case results in lower long-term pressures and noticeably increased repository liquid saturations beyond 10,000 a. The increased saturations are due to higher rates of water inflow from the rock mass caused by the lower repository pressures.

Figure 5.145 compares cumulative gas and liquid flows for the three cases. Liquid flows are consistent with the repository saturations, and show increased flows for the NE-GT5 model. These liquid flows are primarily through the intact rock and are caused by the reduced repository pressure relative to steady-state formation pressure. Liquid inflow from the shaft is negligible in comparison. Gas outflows are significantly higher for the NE-GT5 model, and most of the outflow is up through the shaft, due to the increased shaft permeability. This is consistent with results presented in the previous sub-section.

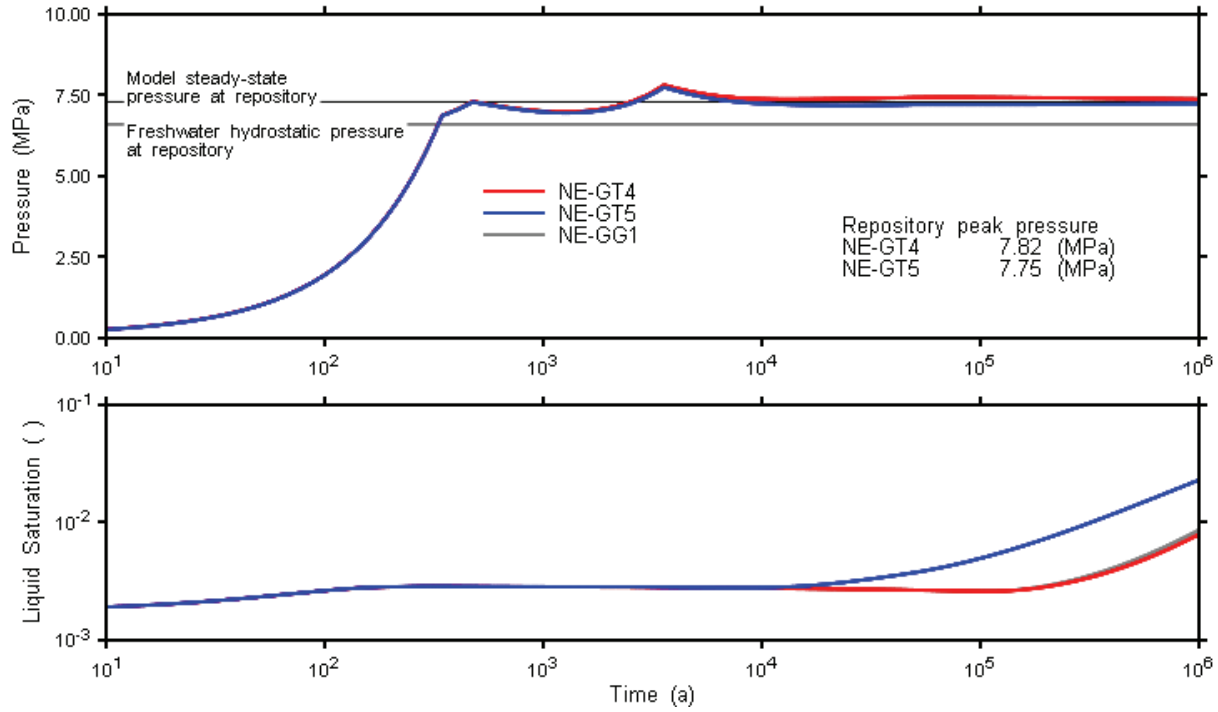

Figure 5.144: NE-GT4/5: 3DSRS Model Repository Pressure and Saturation for NE-GT4, and NE-GT5 Compared to NE-GG1 Results

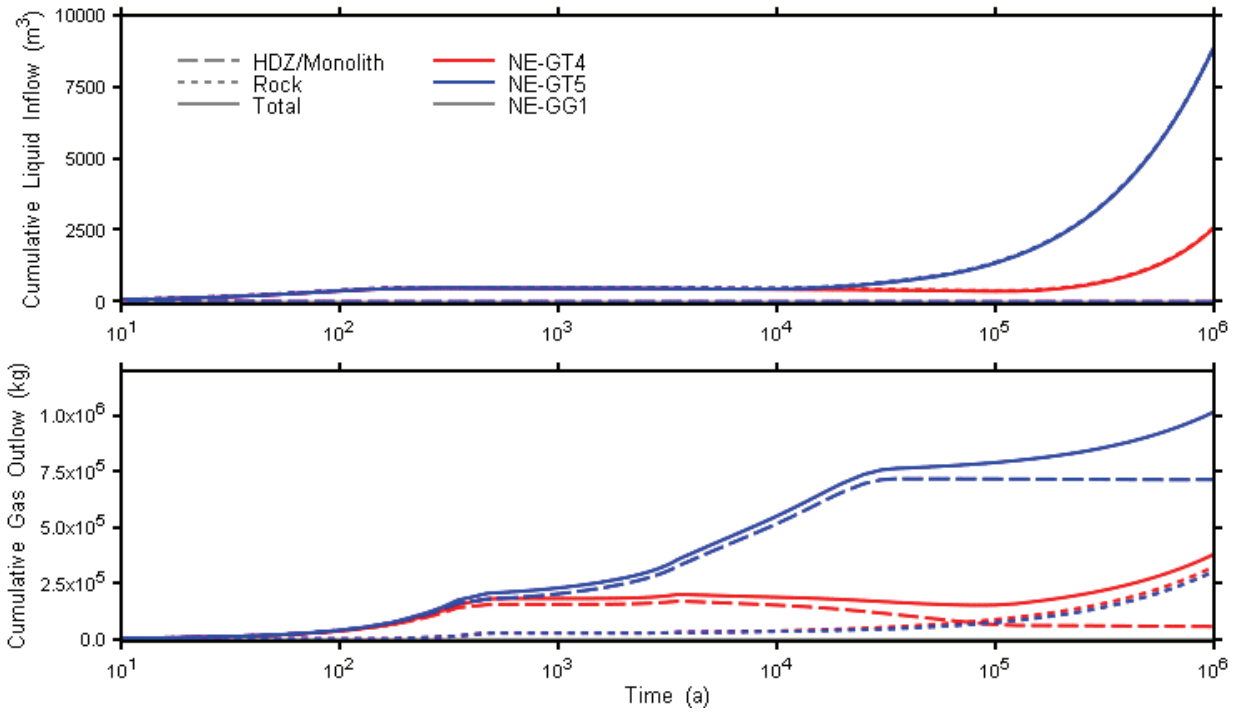

Figure 5.145: NE-GT4/5: Repository Liquid Inflow and Gas Outflow

5.9 Case NE-MG – Alternative Gas

In this case the NE-SBC gas transport simulations are executed using air as the single gas for the TOUGH2 component of the T2GGM model rather than methane. The normal mix of gases was used within the GGM component model. Changing the gas involves changes to molecular weight, Henry's law constant, and viscosity calculation parameters. As described in Section 4.2.4, gas diffusion rates are assumed identical for all gases.

The NE-MG case was simulated using the 3DSR model only. Results are virtually identical to the NE-SBC case, as shown in Figure 5.146. The slight increase in repository liquid saturations at the end of the simulation is due to the very slightly lower peak repository pressure.

There are no significant differences between the gas generation results for this case and for the Simplified Base Case in terms of gas generation or gas and water flows. The key characteristics, such as the peak pressure and saturation profile are all unchanged.

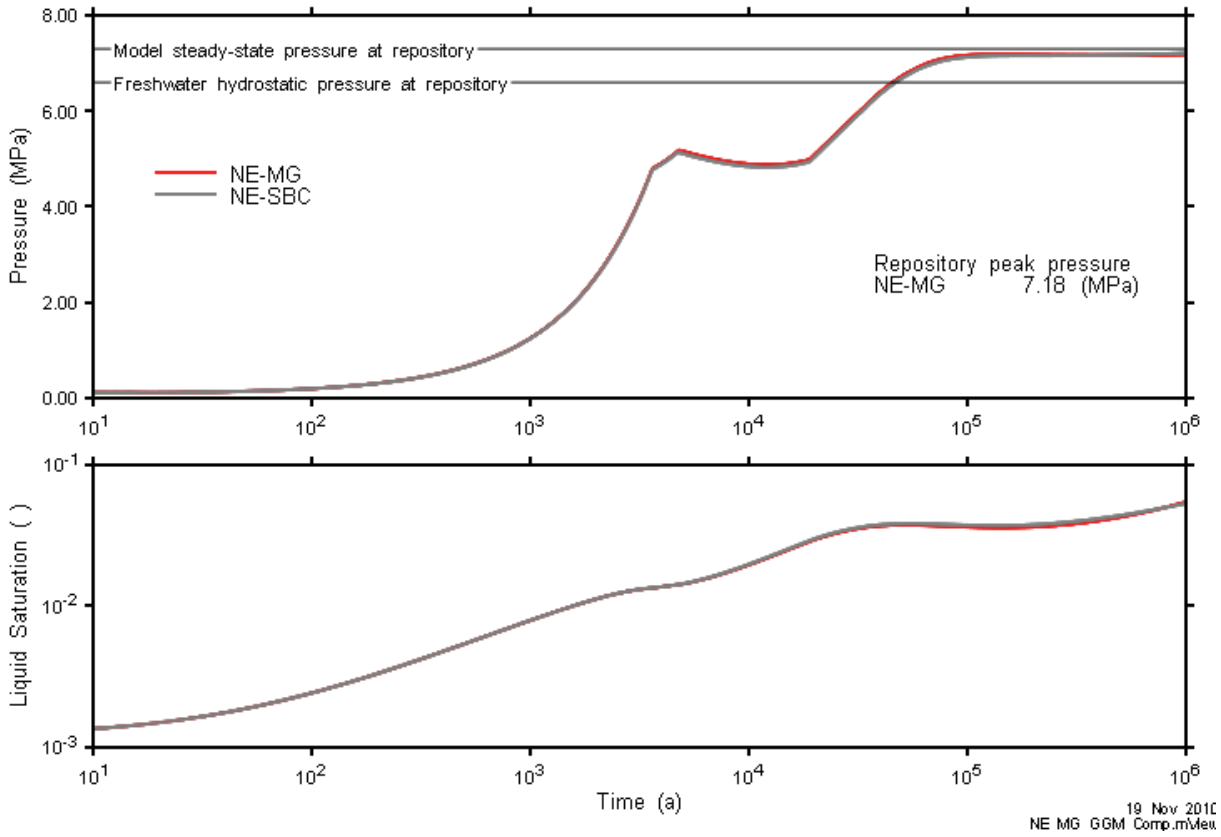

Figure 5.146: NE-MG: 3DSR Model Repository Pressure and Saturation Compared to NE-SBC 3DSR Results

5.10 Case NE-NG – No Gas Generation

The NE-NG1 and NE-NG2 cases are identical to the NE-RC and NE-SBC cases, respectively except that all gas generation reactions are turned off. The case was simulated using 3DD, 3DSRS and 3DSR models. Two cases failed to complete: the 3DD NE-NG1 case stopped at 250,000 a, while the 3DSRS NE-NG2 case stopped at 500,000 a. However, the results were similar between the models up to these times. Figure 5.147 presents pressure and saturation profiles for all models for both cases.

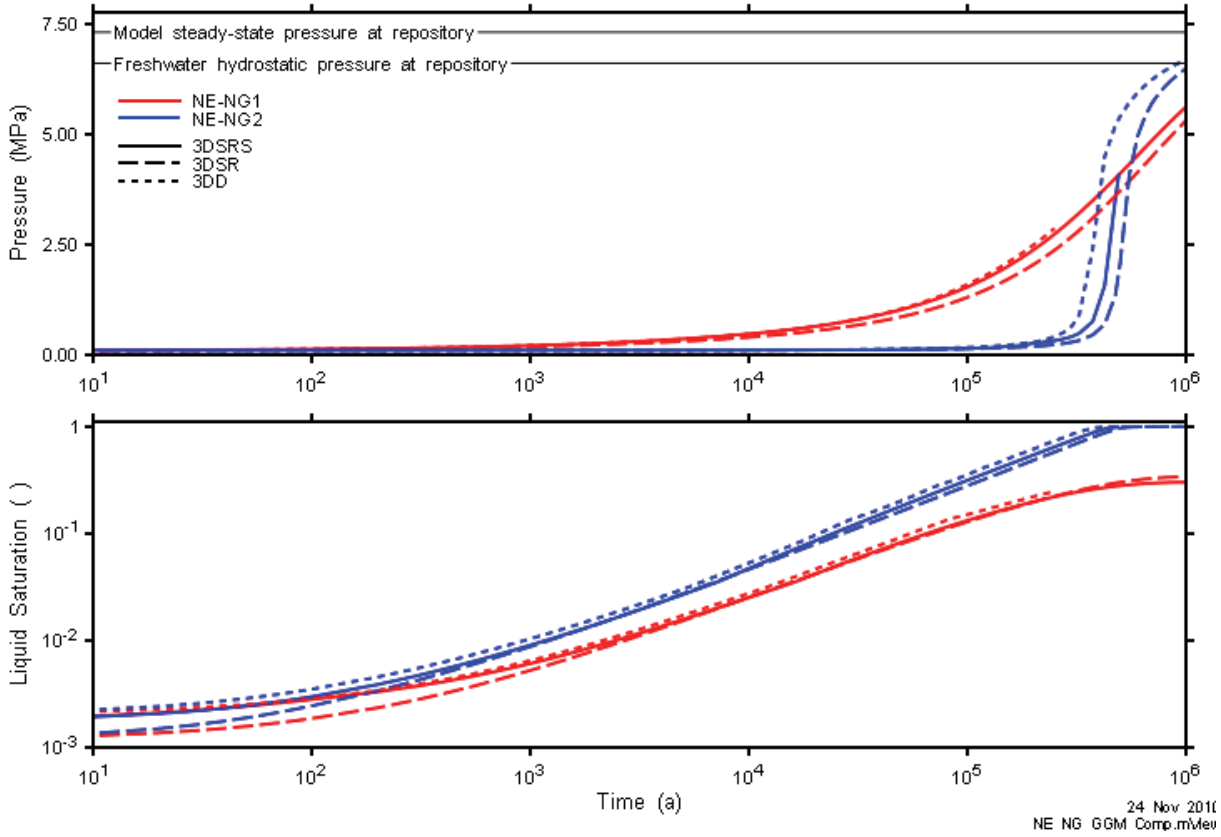

Figure 5.147: NE-NG1 and NE-NG2: 3DD, 3DSRS and 3DSR Model Repository Pressure and Saturation

NE-NG1 pressures are higher than NE-NG2 for nearly 500,000 a, in spite of the lower levels of liquid saturation and inflow. This is due to the distinguishing characteristic of the NE-RC case, which is that higher pressure gas from the formation is flowing into the repository. The difference in the pressure rise between NE-NG1 and NE-NG2 is due to this inflow. Beyond 500,000 a, the compression of the initial gas in the NE-NG2 case exceeds the impact of gas inflow in the NE-NG1 case. At 1,000,000 a, the NE-NG2 case has nearly fully resaturated (but not repressurized), while the rate of liquid saturation change in the NE-NG1 case is decreasing.

Inflows into the repository are compared in Figure 5.148 and Figure 5.149. The 3DD and 3DSRS inflows are categorized by source: rock or HDZ/monolith (i.e., shaft). Inflows for the

NE-NG1 model are decreasing at 1,000,000 a, as increased pressure in the repository due to gas inflows has reversed the liquid flow direction and is driving liquid out of the repository.

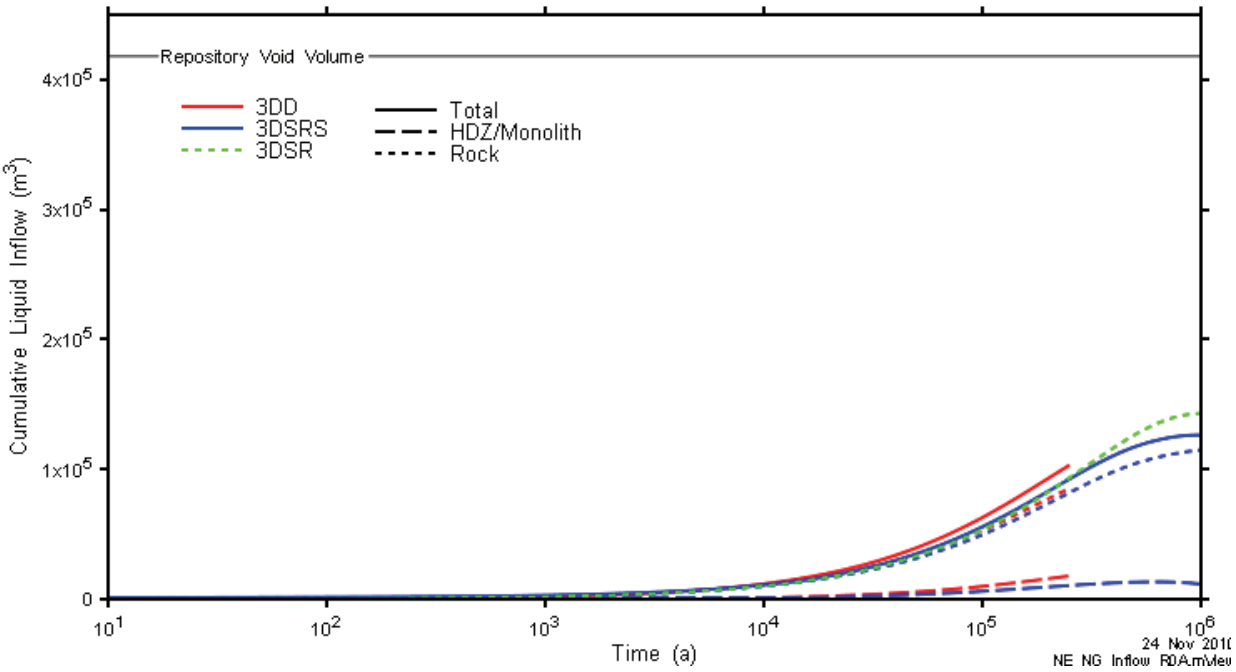

Figure 5.148: NE-NG1: 3DD, 3DSRS and 3DSR Model Liquid Inflows

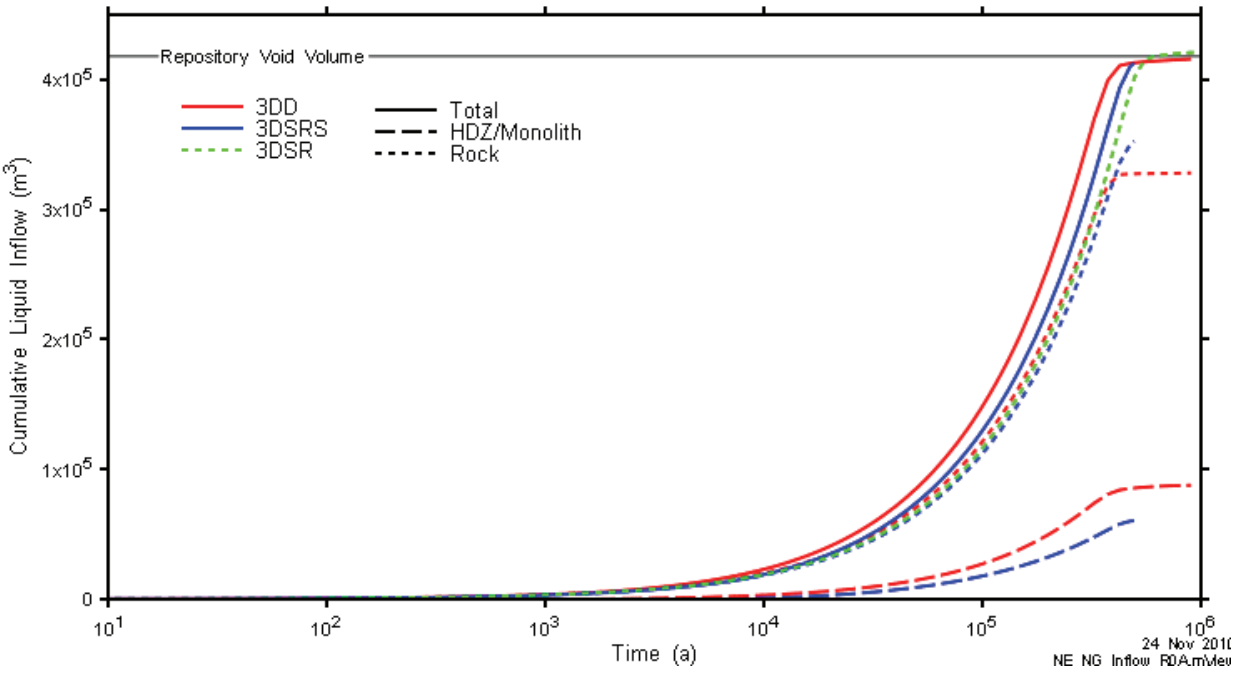

Figure 5.149: NE-NG2: 3DD, 3DSRS and 3DSR Model Liquid Inflows

The 3DD models indicate a slightly higher rate of inflow, with a larger contribution from HDZ/monolith flow than the 3DSR models.

Generally, results from all models are very similar, giving confidence in the simplified geosphere implementation used in the 3DSRS model.

Shaft inflows represent a significant portion of the 3DD and 3DSRS NE-NG2 resaturation and are responsible for their slightly faster resaturation compared to the 3DSR model. The increased shaft flow is largely due to the much longer period of low shaft pressure, driven in turn by the low repository pressure. The gradient towards the shaft in the formations above and below the repository extends for a significant radius (over 500 m at 100,000 a). Combined with the preferential horizontal anisotropy, this causes the shaft to collect a significant quantity of liquid which then is channelled through the HDZ and into the repository.

The case results show, that in the absence of gas generation processes, the repository will never resaturate (NE-NG1), or will resaturate in approximately 500,000 a (NE-NG2), depending upon assumptions of initial gas saturations in the geosphere.

5.11 Case NE-NM – No Methanogenic Gas Generation

This considers the implications of conditions in the repository unfavourable for methanogens. In this case, the NE-SBC model was executed with all methanogenic gas generation reactions turned off, including both organic degradation and CO_2 conversion. As methane concentrations were expected to be minimal, H_2 was specified as the primary gas for transport within the TOUGH2 component of the T2GGM code. The case was simulated using 3DSRS, 3DSR and 2DRS models. 3DSRS model results are available to 780,000 a.

5.11.1 Gas Generation

3DSRS model results are presented here. 3DSR results are almost identical with very slight changes in the gas and water fluxes between the repository and the geosphere but with no significant impact on gas generation. Methane within the repository can be generated via two principal routes:

1. The microbial degradation of organic wastes by methanogens; and
2. The oxidation of hydrogen by which hydrogen and carbon dioxide are consumed to form methane and water.

The first of these two routes typically involves the generation of carbon dioxide and methane and the consumption of water. Thus, the reaction generally acts to increase gas pressures, while the consumption of water can lead to a drop in saturation and hence lowering of gas pressures.

The second of these two routes involves the consumption of hydrogen and carbon dioxide and the production of methane and water. Five moles of hydrogen and carbon dioxide are consumed to produce of one mole of methane via this route, so this reaction acts to decrease the overall gas pressure.

For this case, both microbial methanogenic processes described above are switched off. This simulates the inhibition of methanogens which may happen if the pH is too low or if there are other inhibitory factors, e.g., toxins removes the methane pathways. No other microbial based hydrogen reaction is credited.

A negligible amount of organic degradation takes place during the initial terminal electron acceptor stages, and since methanogens are inactive, no degradation of organic wastes to methane occurs for this case. As a result the composition of gas in the repository was also changed, with hydrogen due to metallic corrosion becoming the dominant gas. See Figure 5.150 and Figure 5.151.

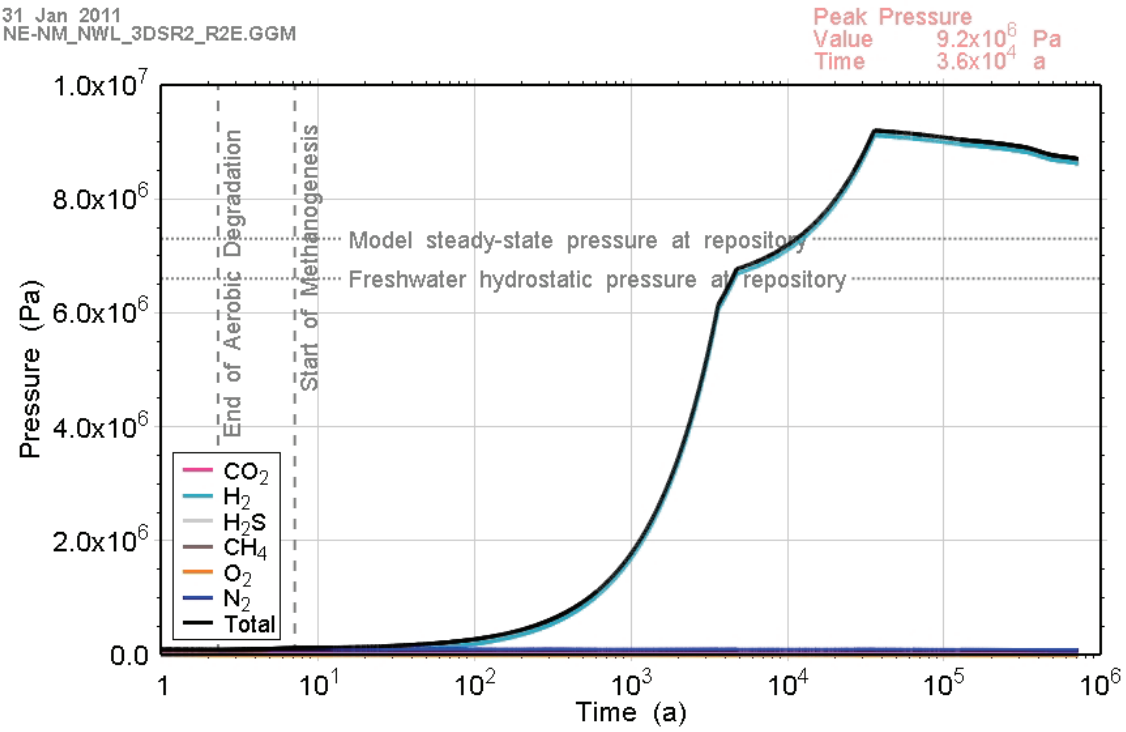

Figure 5.150: NE-NM: Total and Partial Gas Pressures within the Repository

The combined lack of carbon dioxide due to methanogenic organic degradation and the absence of the pressure reducing methane generation reaction (see Equation 2-3) lead to a greater peak pressure: 9.2 MPa as compared to 7.2 MPa for the Simplified Base Case. See Figure 5.150. (H_2-consuming microbial reactions may reduce the peak pressure in this case, but are conservatively not included in the model.)

The increase in gas pressure above the steady-state pressure forces the water saturation to decrease after the peak pressure rather than increase, reaching zero at approximately 1,000,000 a (Figure 5.152).

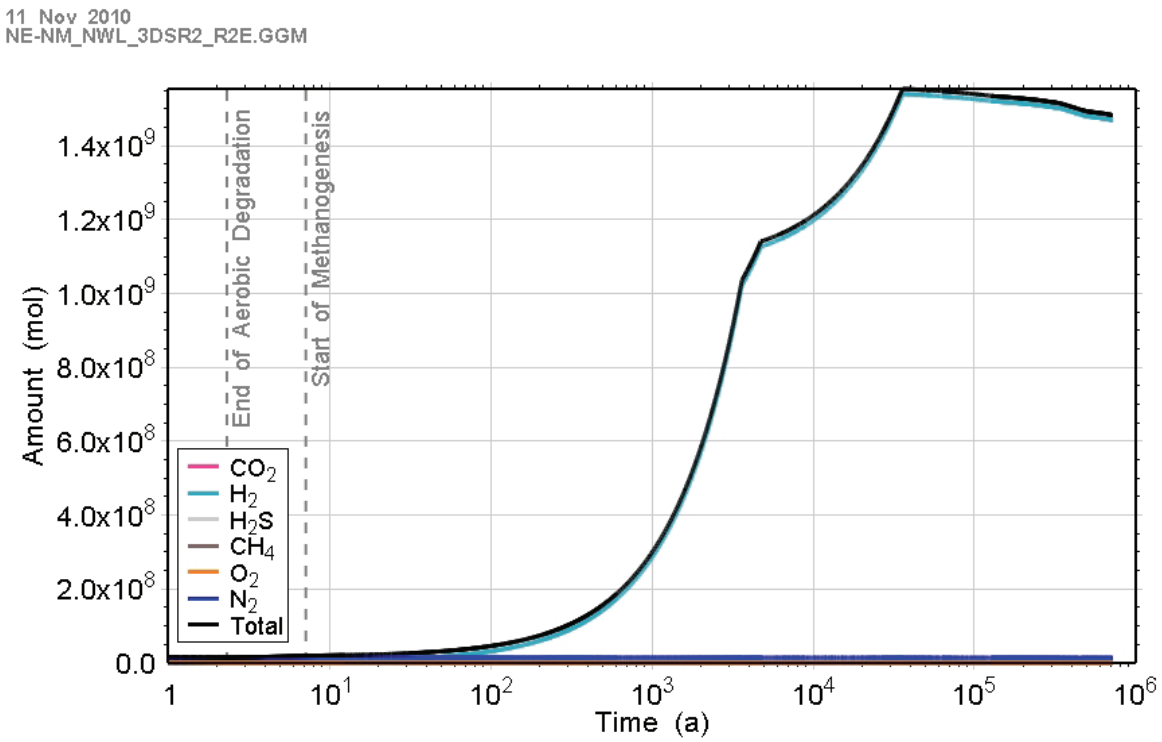

Figure 5.151: NE-NM: Amounts of Gases in the Vapour Phase within the Repository

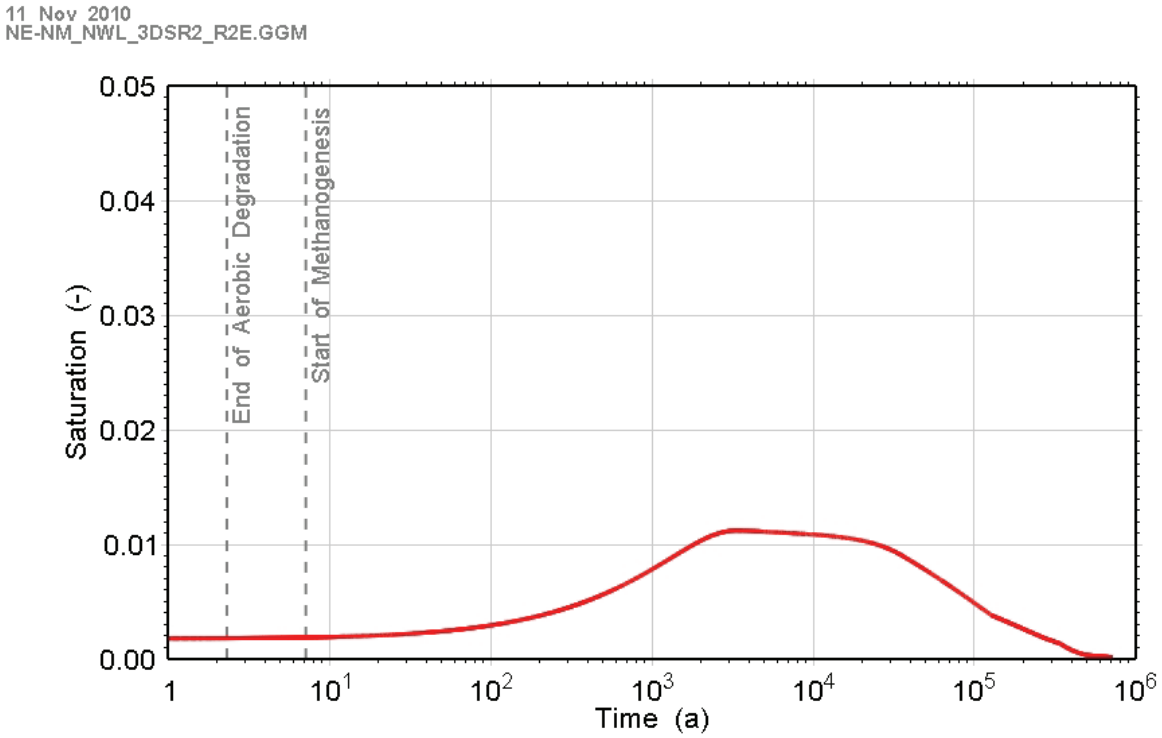

Figure 5.152: NE-NM: Water Saturation

5.11.2 Gas and Water Flows

Gas and water flows in the NE-NM case are characterized by gas flow up the shaft, and very low liquid inflows into the repository.

5.11.2.1 Shaft

Early-time evolution of gas and water flows within the shaft and surrounding intact rock are similar to the NE-SBC case. However, at approximately 5000 a, pressures in the repository exceed the shaft gas pressure and gas flow up the shaft commences (Figure 5.153). Gas flow continues to propagate up the shaft as repository pressure increases. By 40,000 a there is a continuous pathway of non-zero gas saturation through to the top of the modeled shaft (Figure 5.154).

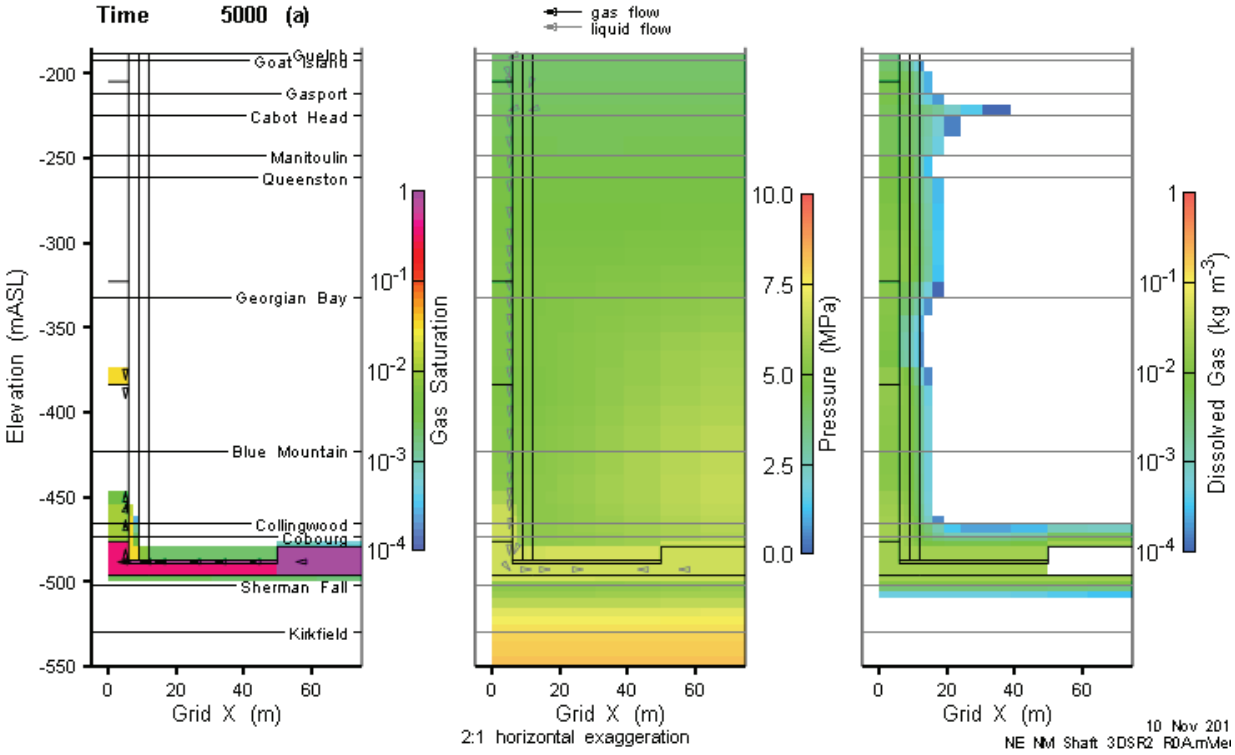

Figure 5.153: NE-NM: 3DSRS Model Shaft Saturations, Flows and Pressures (5000 a)

Peak gas flows occur at approximately 70,000 a (Figure 5.155) with gas flowing up through the shaft seal and, to a limited extent, through the inner EDZ.

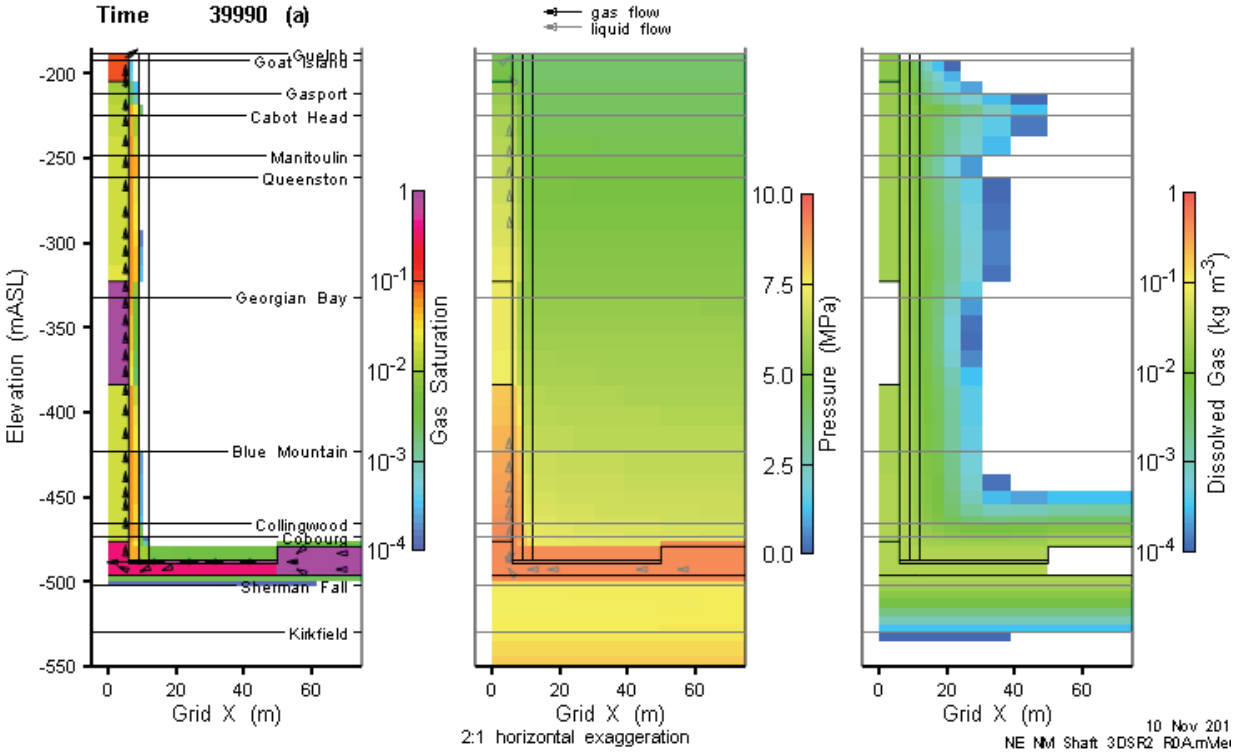

Figure 5.154: NE-NM: 3DSRS Model Shaft Saturations, Flows and Pressures (40,000 a)

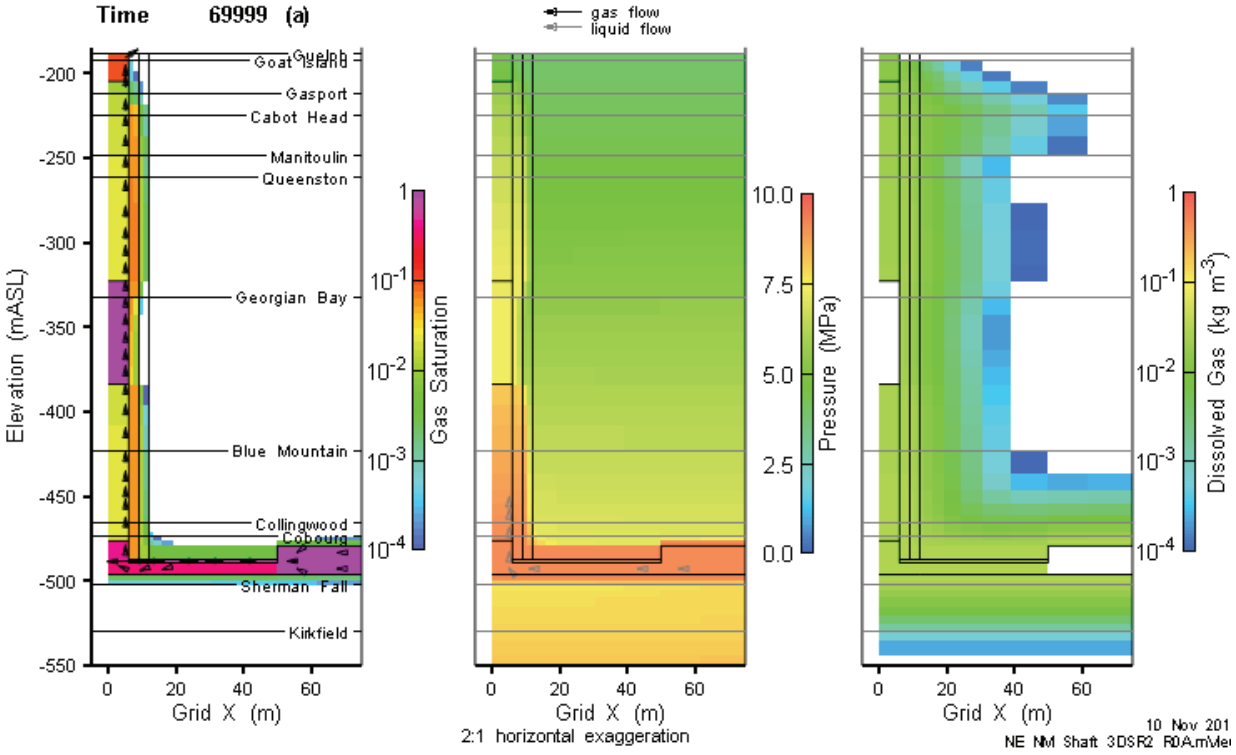

Figure 5.155: NE-NM: 3DSRS Model Shaft Saturations, Flows and Pressures (70,000 a)

Repository pressures are maintained at a relatively high level for the duration of the simulation and gas flow rates decline slowly. Results at 500,000 a are presented in Figure 5.156.

2DRS model results for the NE-NM case are similar qualitatively to those already described for the NE-GG1 and NE-GT5 cases. As shown in Figure 5.157, the role of the Guelph Formation in capturing gas flows is evident.

Gas mass flows vs. time profiles (Figure 5.158) from the 2DRS model further confirm these results. Peak flows are nearly identical for all units below the Guelph, while there is no flow above the Salina A2. The flow profiles also indicate that nearly all gas transport is through the shaft seal materials, with a very small component transported through the shaft inner EDZ. Note that gas flow rates shown for the NE-NM case are for H_2, which has a lower molecular weight than CH_4 used for other cases.

Gas flow time profile results from the 3DSRS model (Figure 5.159) show slightly higher magnitude flows than the 2DRS model. As expected, dissolved gas fluxes peak during the early pressurization period when liquid was flowing up the shaft (Figure 5.160).

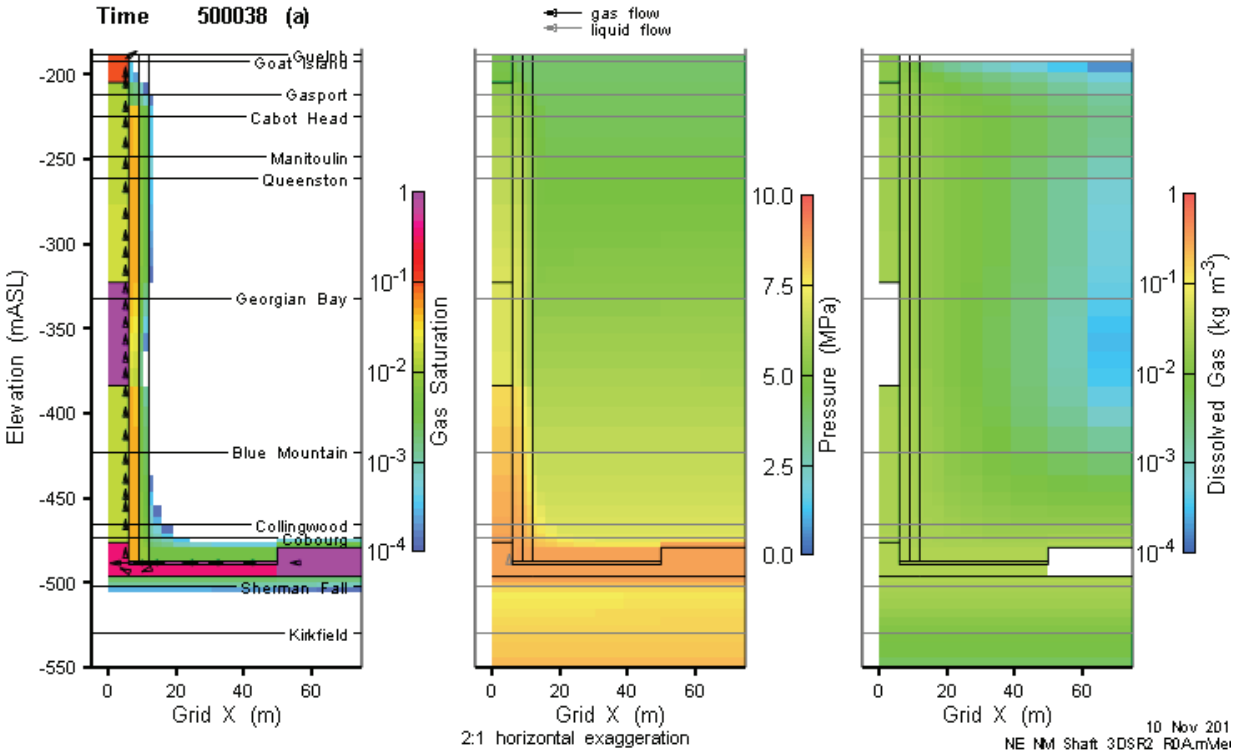

Figure 5.156: NE-NM: 3DSR Model Shaft Saturations, Flows and Pressures (500,000 a)

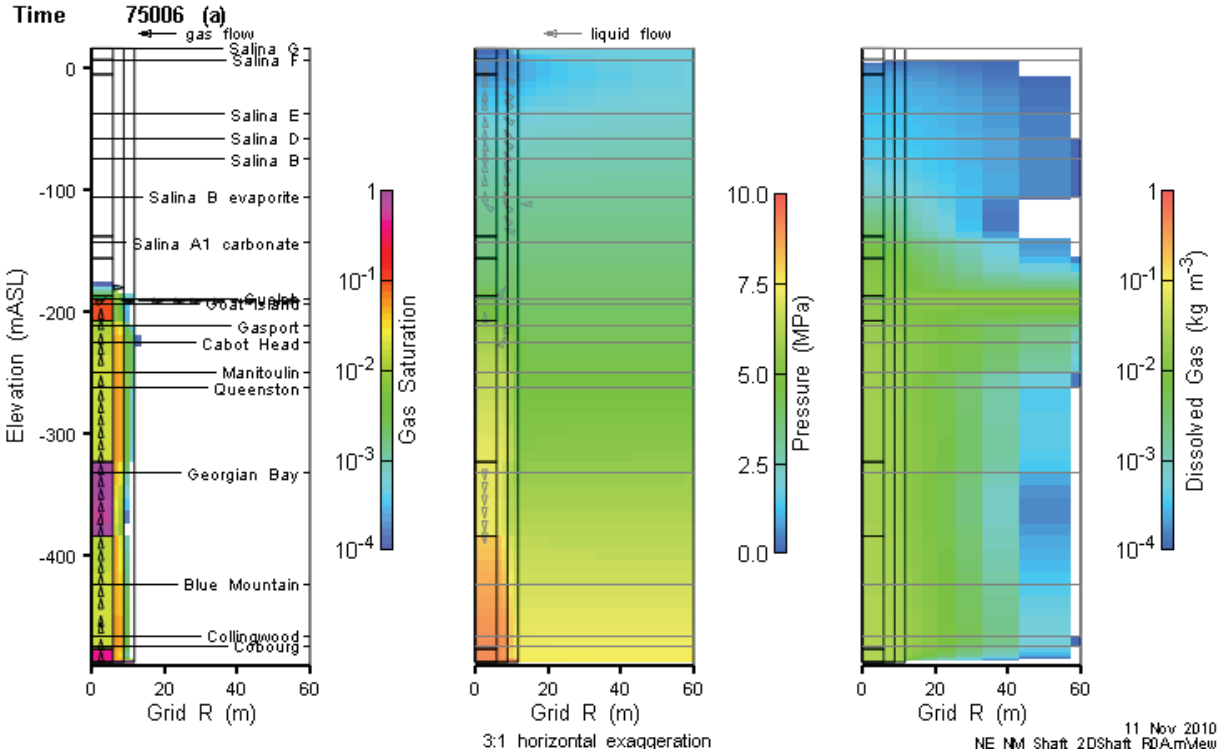

Figure 5.157: NE-NM: 2DRS Model Shaft Saturations, Flows and Pressures (75,000 a)

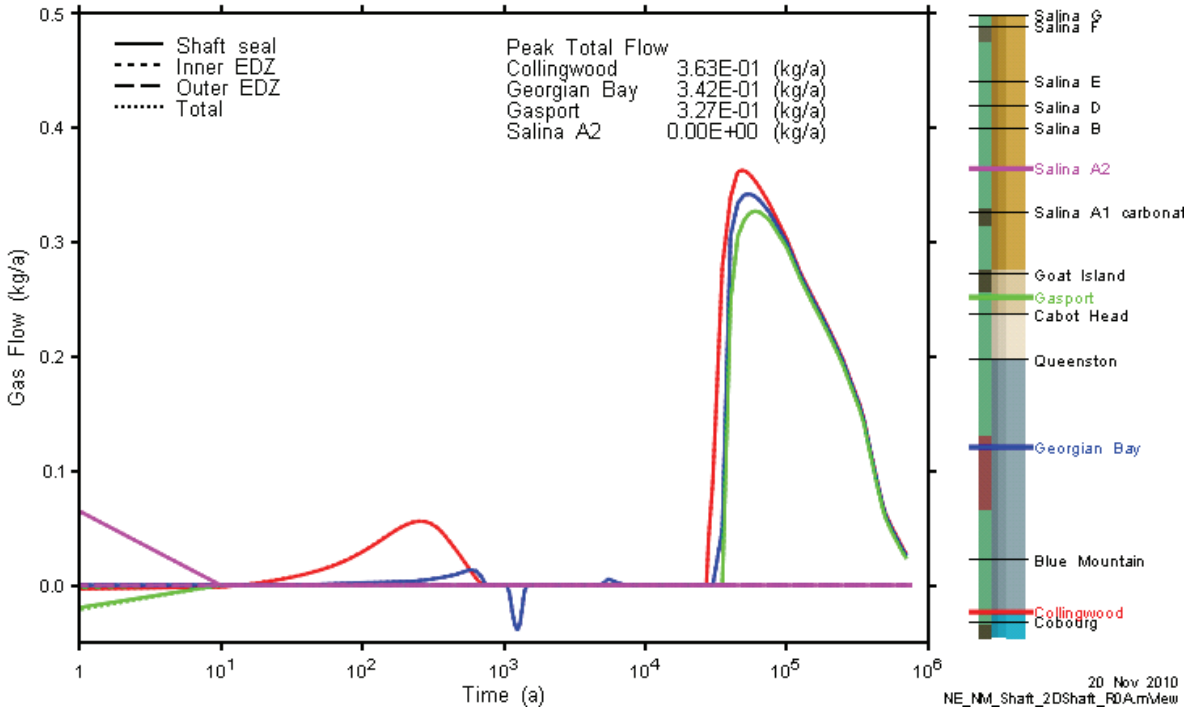

Figure 5.158: NE-NM: 2DRS Model Shaft Gas (H_2) Flow vs. Time at Selected Monitoring Planes

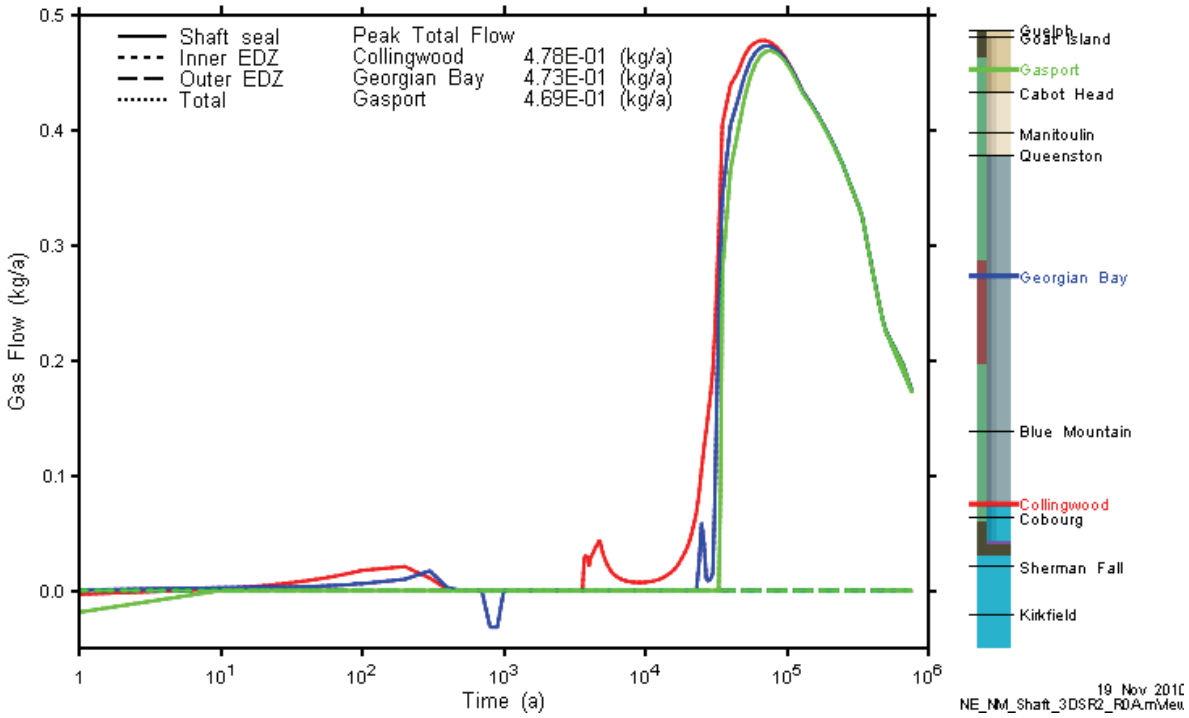

Figure 5.159: NE-NM: 3DSRS Model Shaft Gas (H_2) Flow at Selected Monitoring Planes

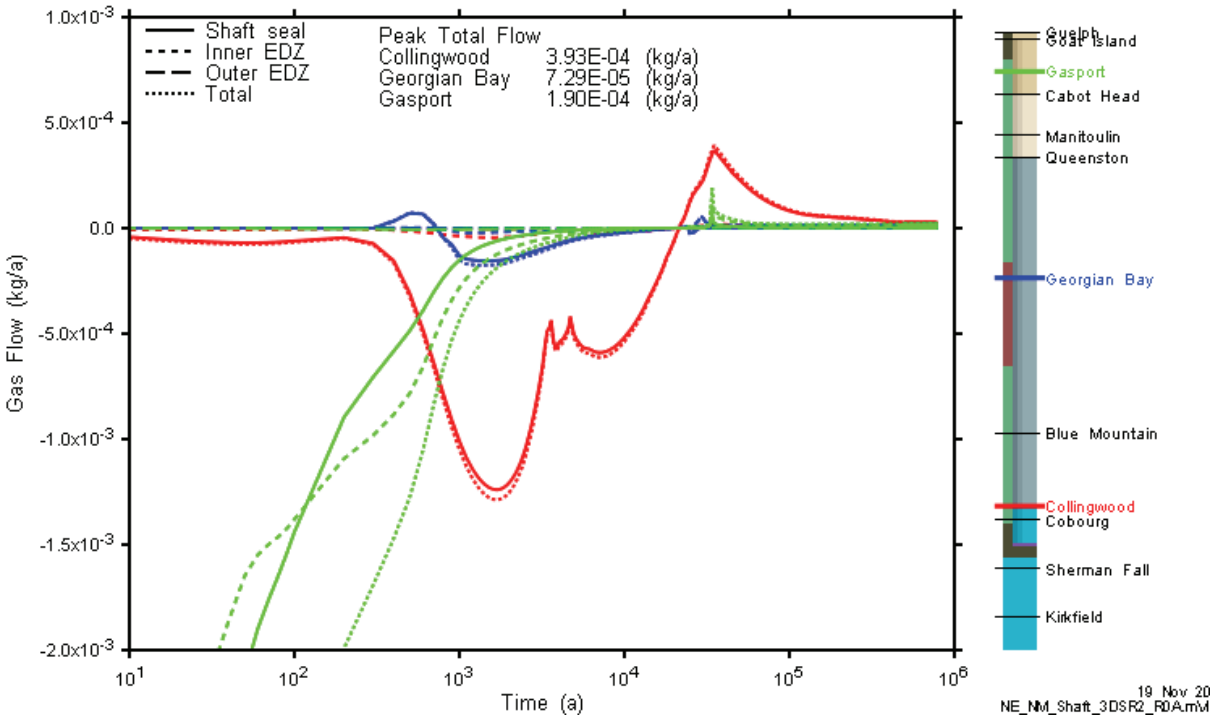

Figure 5.160: NE-NM: 3DSRS Model Shaft Dissolved Gas (H_2) Flow vs. Time at Selected Monitoring Planes

5.11.2.2 Repository System

Repository pressure and liquid saturation profiles for the NE-NM case are shown in Figure 5.161. Pressure results are virtually identical up to the peak pressure time of 35,000 a, after which the 3DSRS results start to decline faster than the 3DSR, due to gas exiting the repository through the shaft in the former model.

Figure 5.162 shows cumulative gas and liquid flows for 3DSRS and 3DSR models. Liquid inflows are very similar, with negligible contribution from the shaft in the 3DSRS model. Calculated gas outflows to the intact rock are nearly identical for both models; however, gas outflow up the shaft is the major component of total gas outflow flow for the 3DSRS model.

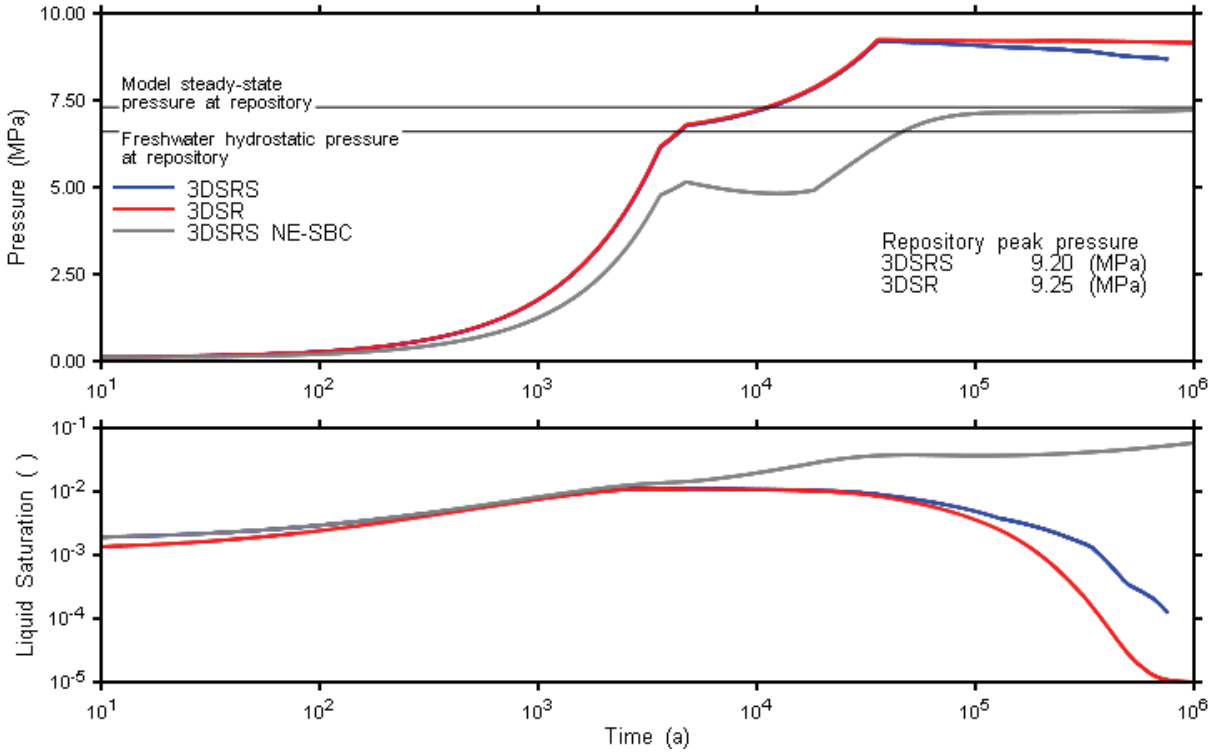

Figure 5.161: NE-NM: 3DSRS and 3DSR Model Repository Pressure and Saturation

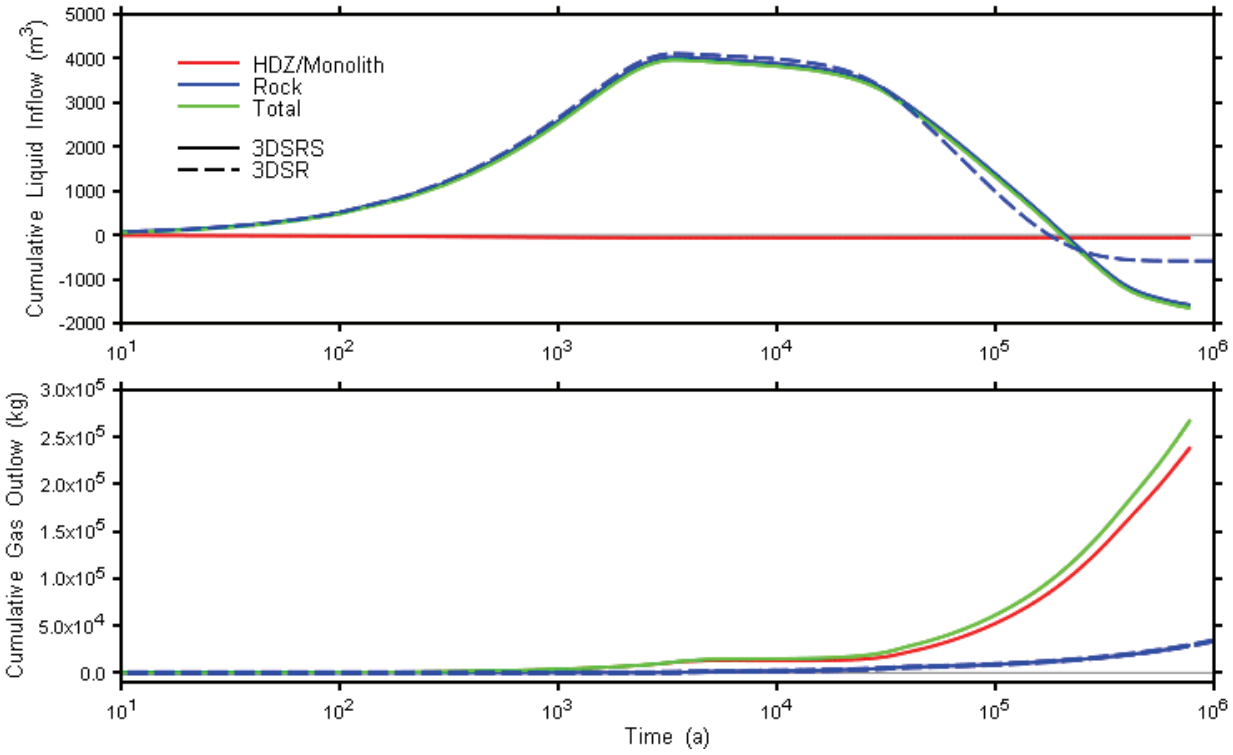

Figure 5.162: NE-NM: Repository Liquid Inflow and Gas Outflow for 3DSRS and 3DSR Models

5.11.2.3 Geosphere

The geosphere hydraulic head profile for the 3DSR NE-NM case is presented in Figure 5.163. At the end of the 750,000 a simulation period, repository pressures have perturbed the natural system within 100 m of the repository.

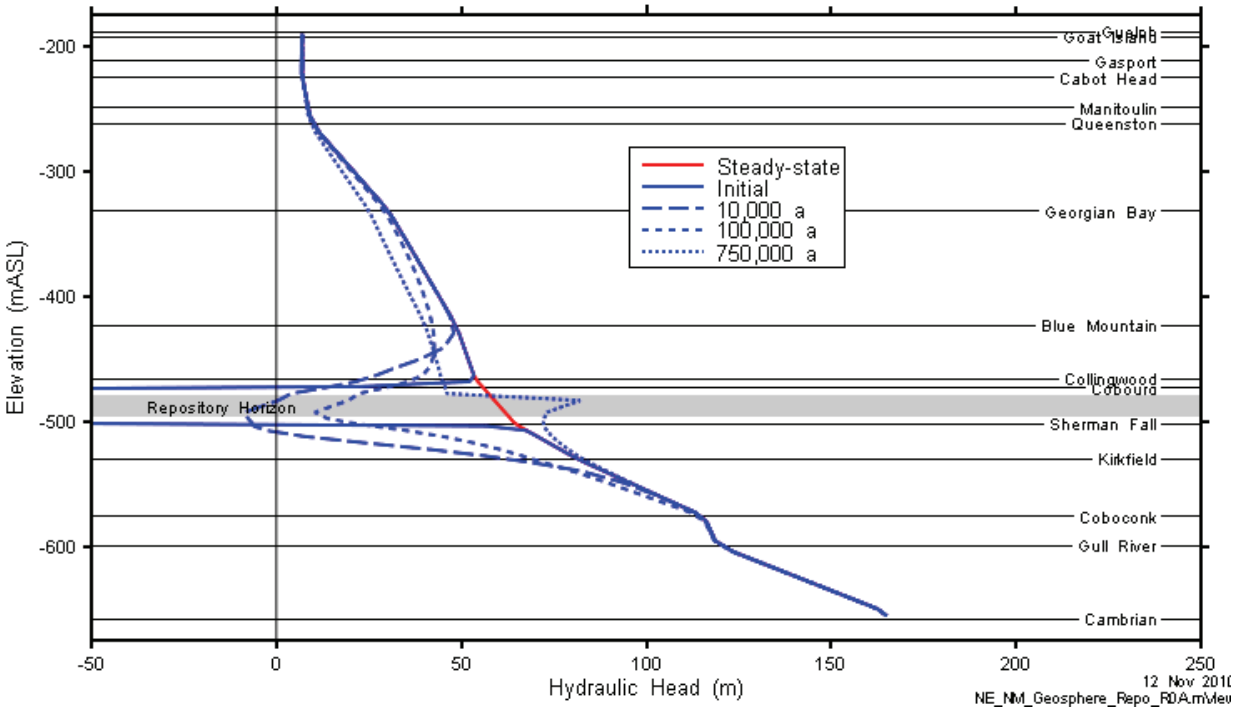

Figure 5.163: NE-NM: 3DSRS Geosphere Head Profile

5.12 Case NE-RC1 – Geosphere Gas Phase at Residual Saturation

This case is identical to the NE-RC except that initial gas saturations in the geosphere are 5%, the residual gas saturation value for the host rock rather than 10% as in NE-RC. This is the residual gas saturation specified in the NE-RC Ordovician rock relative permeability function (see Section 4.2.4). The effect of this is to eliminate long-term transfer of gas from the formation to the repository since the rock is already at its (lowest) residual gas saturation value. The case was simulated using the 3DSR model, and results are compared to the NE-RC 3DSR model results.

5.12.1 Gas Generation

Gas generation is almost the same as for the NE-RC case, except for the fact that the flux of gas from geosphere into the repository is lower in this case, as is to be expected. Figure 5.164 shows that the amount of gas entering the repository is almost an order of magnitude less than for the NE-RC case. As a result of this, the peak gas pressure within the repository is lower in this case, reaching steady-state pressure at the repository horizon at about 1,000,000 a (Figure 5.165).

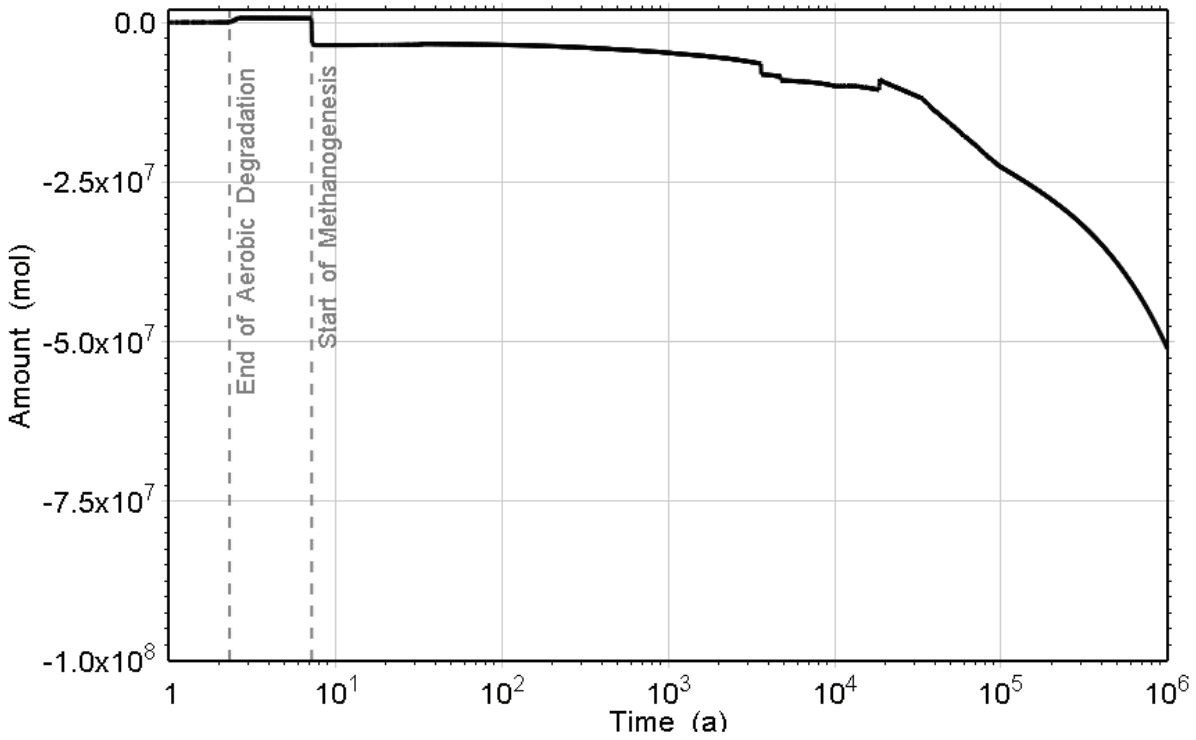

Figure 5.164: NE-RC1: Total Amount of Gas that has Left the Repository. The Negative Values indicate that (Uncontaminated) Gas is entering the Repository

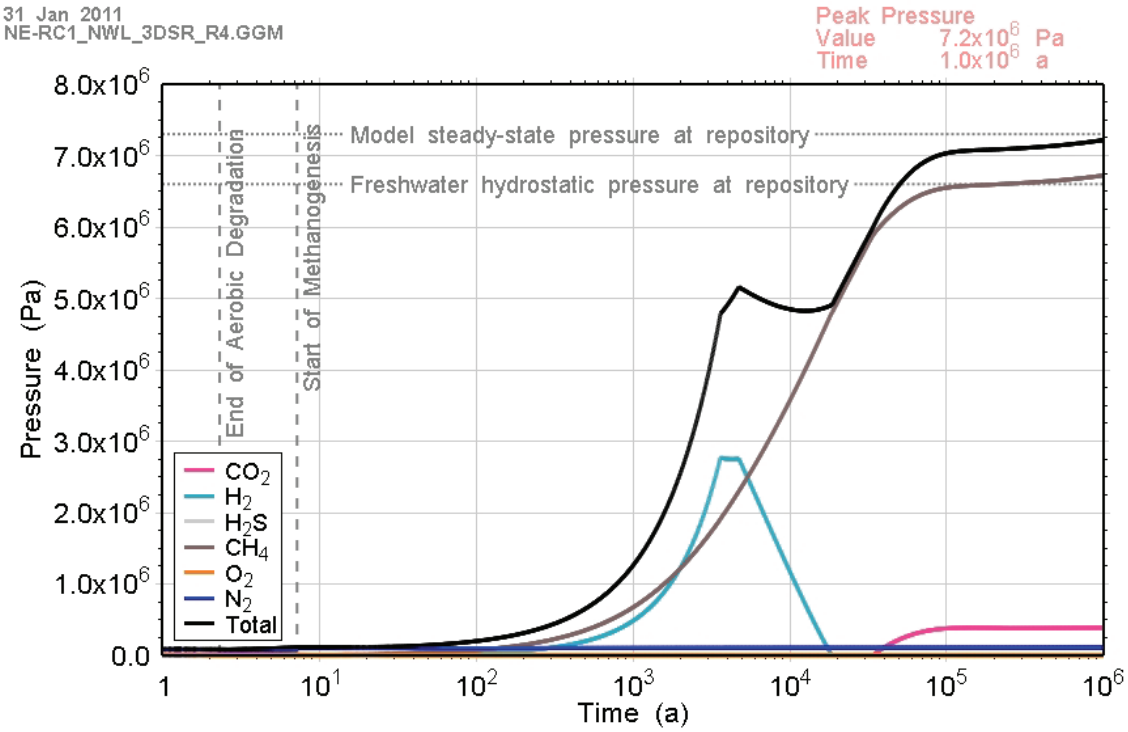

Figure 5.165: NE-RC1: Total and Partial Gas Pressures within the Repository

5.12.2 Gas and Water Flows

Repository pressure and liquid saturation profiles for the NE-RC1 case are shown in Figure 5.166. Results are very similar to the NE-RC case until approximately 100,000 a, where gas flow from the formation into the repository starts to dominate the NE-RC results. Because the NE-RC1 case initial saturations are at specified residual saturations, flow of gas is eliminated. The minor continual pressure rise noted is due to gas diffusing into the repository. These 3DSR results do not include the shaft. As noted in the NE-RC discussion, inclusion of the shaft (3DSRS) provides pressure equilibration on a 1,000,000 a timescale.

Figure 5.167 presents the evolution of the NE-RC1 geosphere system. Gas pressures equilibrate slightly due to diffusion into the geosphere system, but it is apparent that the gas system is largely stagnant, as there is very little change in gas saturation or pressures over the 1 Ma simulation period.

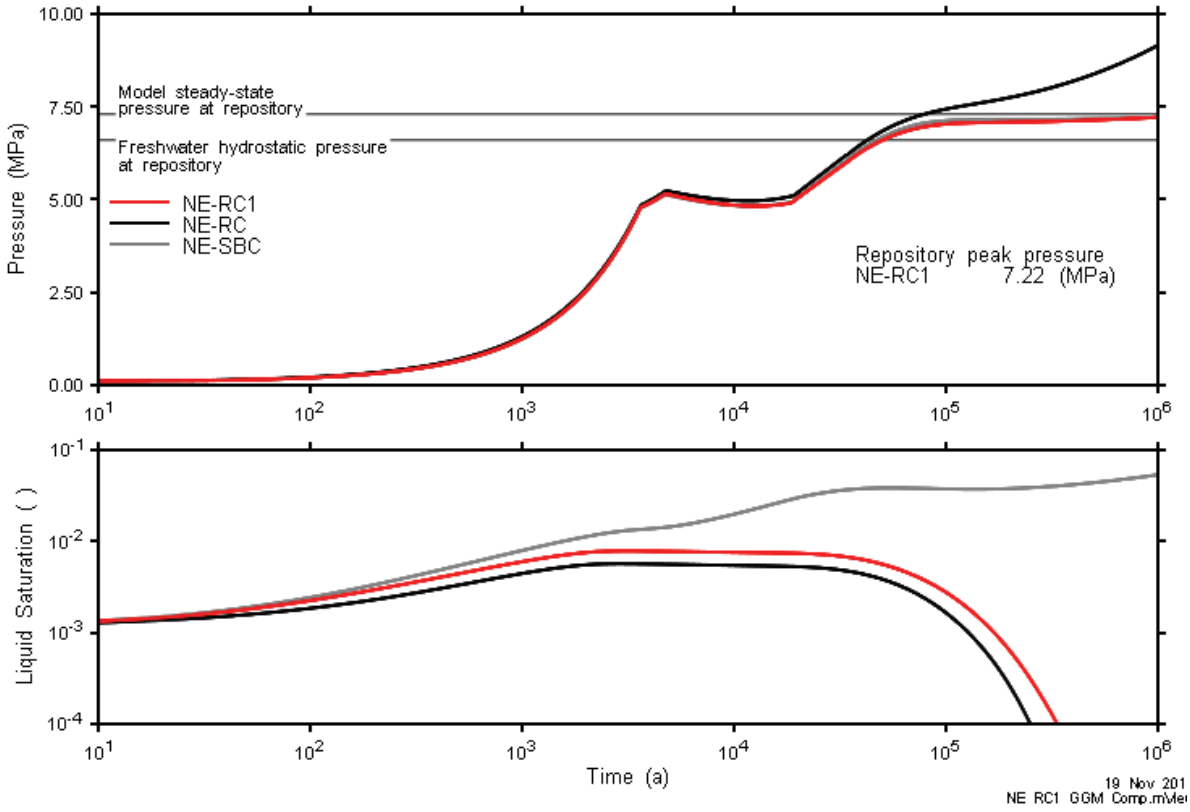

Figure 5.166: NE-RC1: Comparison of NE-RC1, NE-RC and NE-SBC 3DSR Model Repository Pressure and Saturation

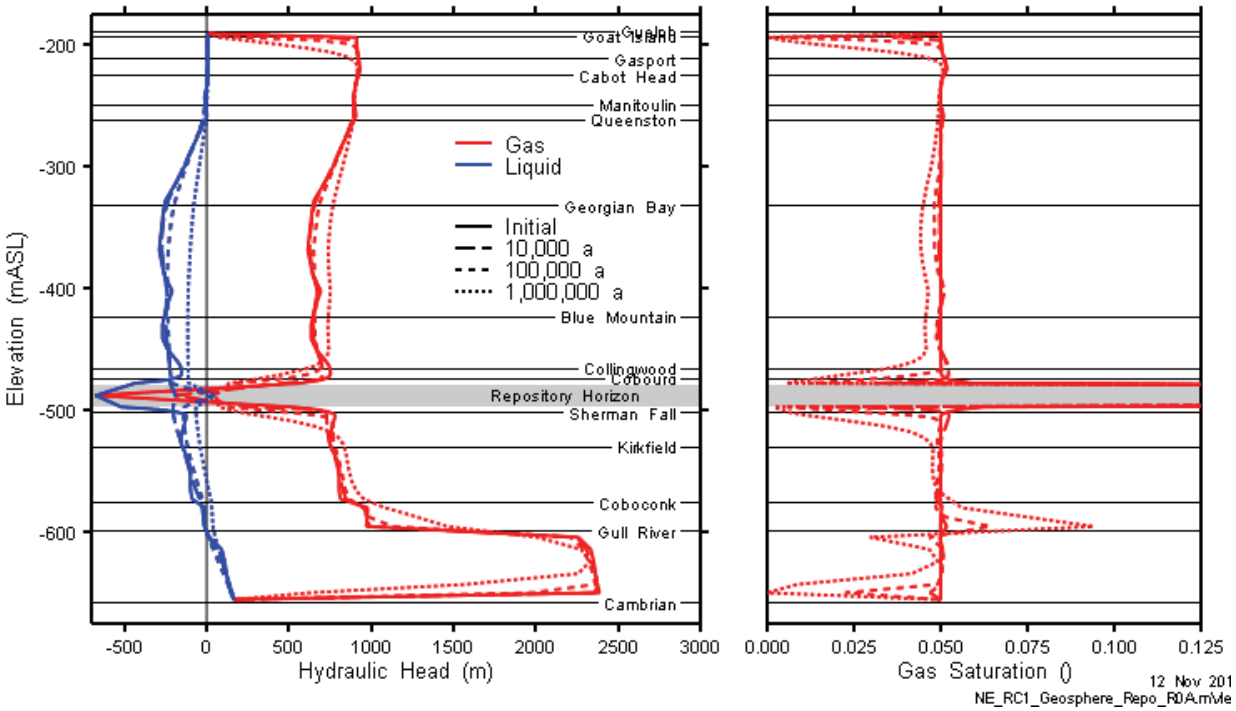

Figure 5.167: NE-RC1: Geosphere Gas and Liquid Head and Gas Saturation Profile

5.13 Case NE-RC2 – Variable Geosphere Gas Saturation and Transport Properties

This case is identical to the NE-RC except that initial gas saturations in the geosphere are set at formation average values from INTERA (2011). There were two variations from the INTERA (2011) data: 1) for the Manitoulin and above where there were no data, so formations saturations were set to 5%, and 2) Coboconk gas saturation is specified as 3.7% in INTERA (2011), which is inconsistent with units above and below, given formation permeability and air-entry pressures and so the Coboconk Formation initial gas saturation was set to 20%.

Two-phase flow parameters for all formations are set at formation specific values as given in the Data report (QUINTESSA and GEOFIRMA 2011a). The case was simulated using the 3DSR model, and results are compared to the NE-RC and NE-RC1 3DSR model results.

5.13.1 Gas Generation

Gas generation results are substantially similar to the NE-RC case and are not discussed further here.

5.13.2 Gas and Water Flows

Repository pressure and liquid saturation profiles for the NE-RC2 case are shown in Figure 5.168. Results are very similar to the NE-RC and NE-SBC case before 100,000 a, after which gas flow from the formation into the repository starts to dominate the NE-RC results. The

difference between the NE-RC and NE-RC2 pressures at 1,000,000 a is primarily due to differences in the capillary pressure curves used for the Cobourg formation in each case.

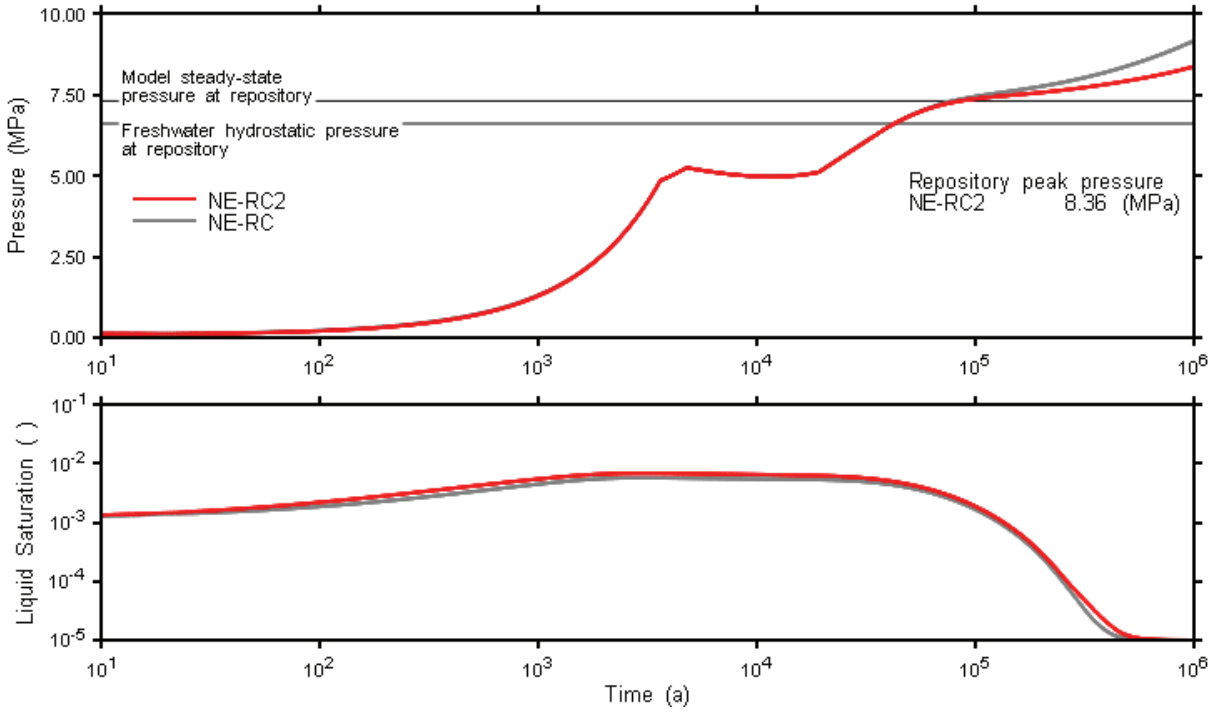

Figure 5.168: NE-RC2: Comparison of NE-RC, NE-RC2, and NE-SBC 3DSR Model Repository Pressure and Saturation

Figure 5.169 presents the evolution of pressures and saturations in the NE-RC2 geosphere. Gas pressures equilibrate at different rates throughout the system. In the lower Ordovician system (Gull River and Coboconk Formations), there are significant changes in the first 10,000 a. This response is either due to a disequilibrium in the system within these formations, or, more likely, due to measurement related uncertainty in initial liquid pressures, gas saturations and/or gas parameters between the different formations. Initial simulations conducted with the Coboconk set at the INTERA (2011) specified initial gas saturation of 3.7% for the Coboconk Formation, showed even greater changes.

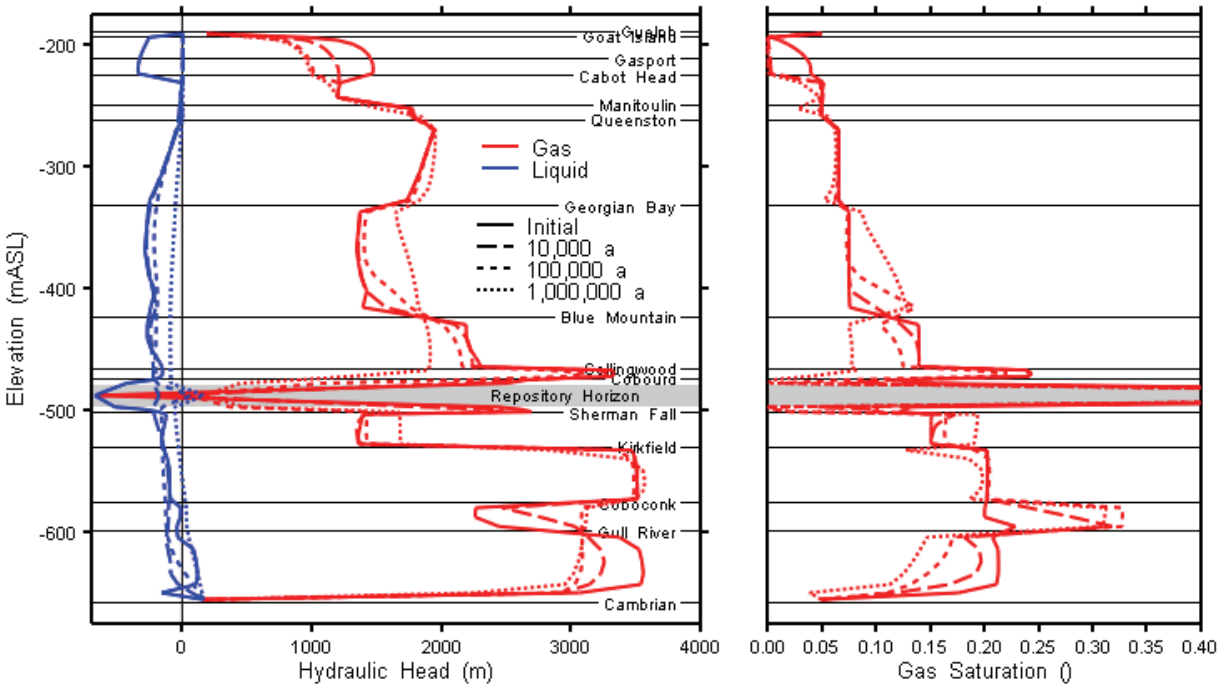

Figure 5.169: NE-RC2: Geosphere System Evolution

Figure 5.170 to 5.173 present vertical liquid pressure profiles (expressed as head) at various times for selected gas and groundwater model results run on geosphere only models (i.e., no repository influence). The purpose of the figures is to compare the evolution of the geosphere system under different assumptions about gas saturations and two-phase flow parameters and to evaluate the impact of these parameters on future system evolution. Results are presented for NE-RC (gas and groundwater), NE-RC2 (gas), and NE-SBC (gas and groundwater). Groundwater model results presented in the figures are described further in GEOFIRMA (2011). Note that the NE-SBC case results are steady-state and are, therefore, the same on all figures.

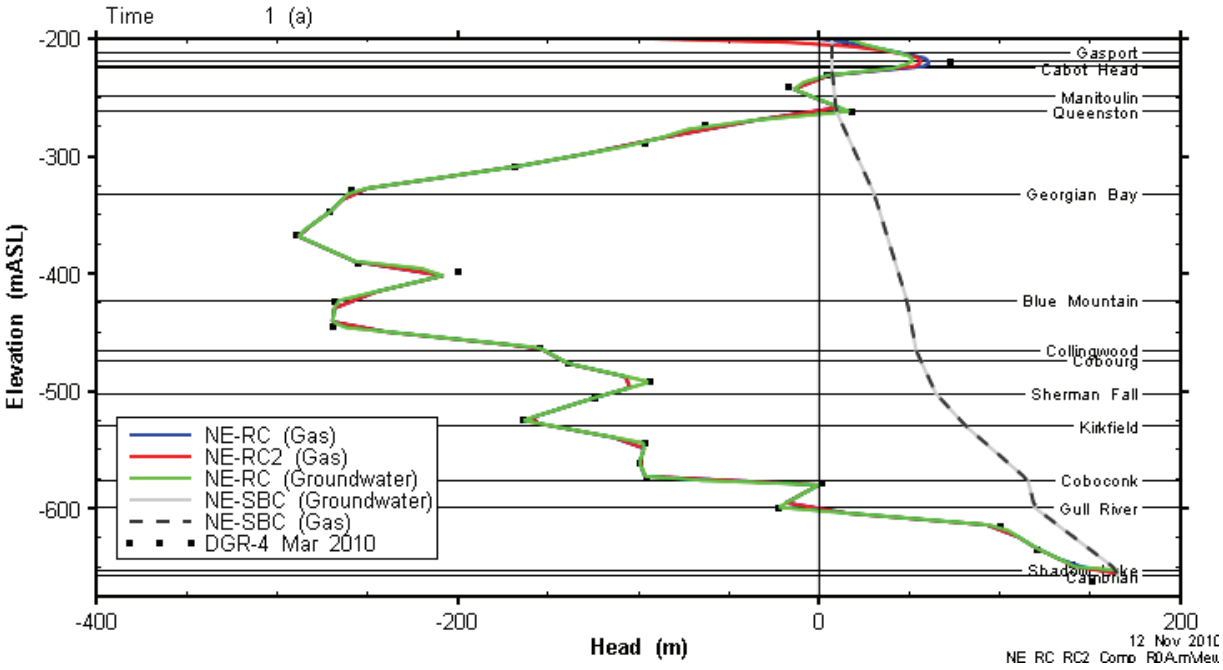

Figure 5.170: NE-RC2: Model Head Comparison at 1 a

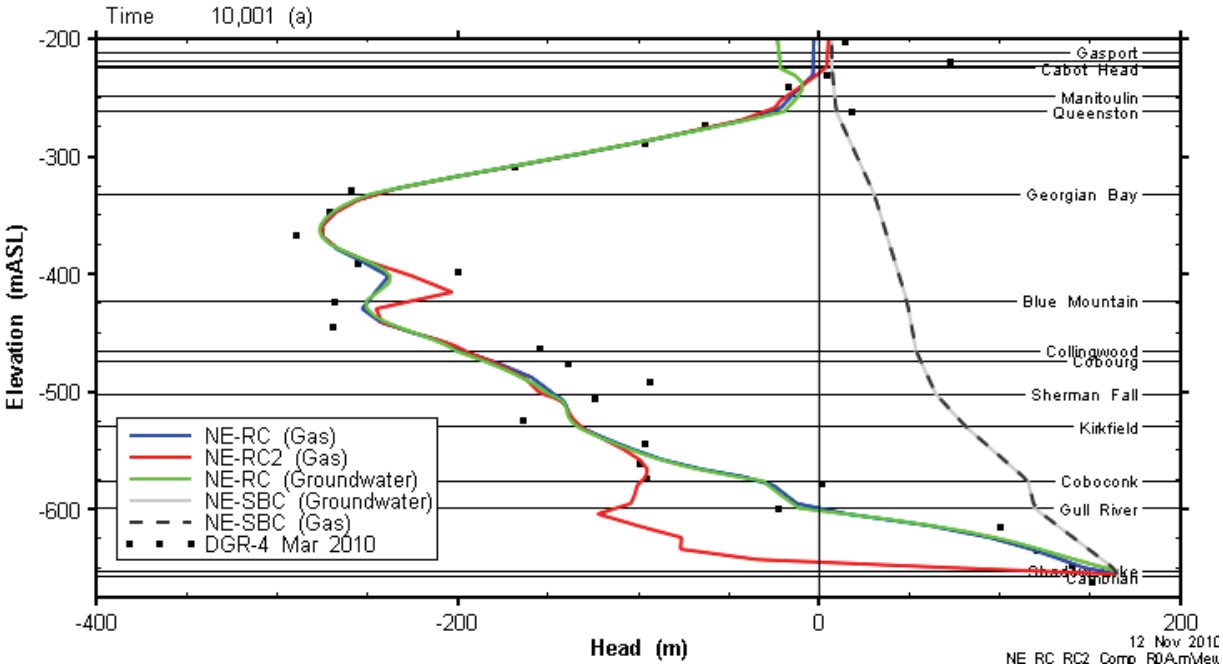

Figure 5.171: NE-RC2: Model Head Comparison at 10,000 a

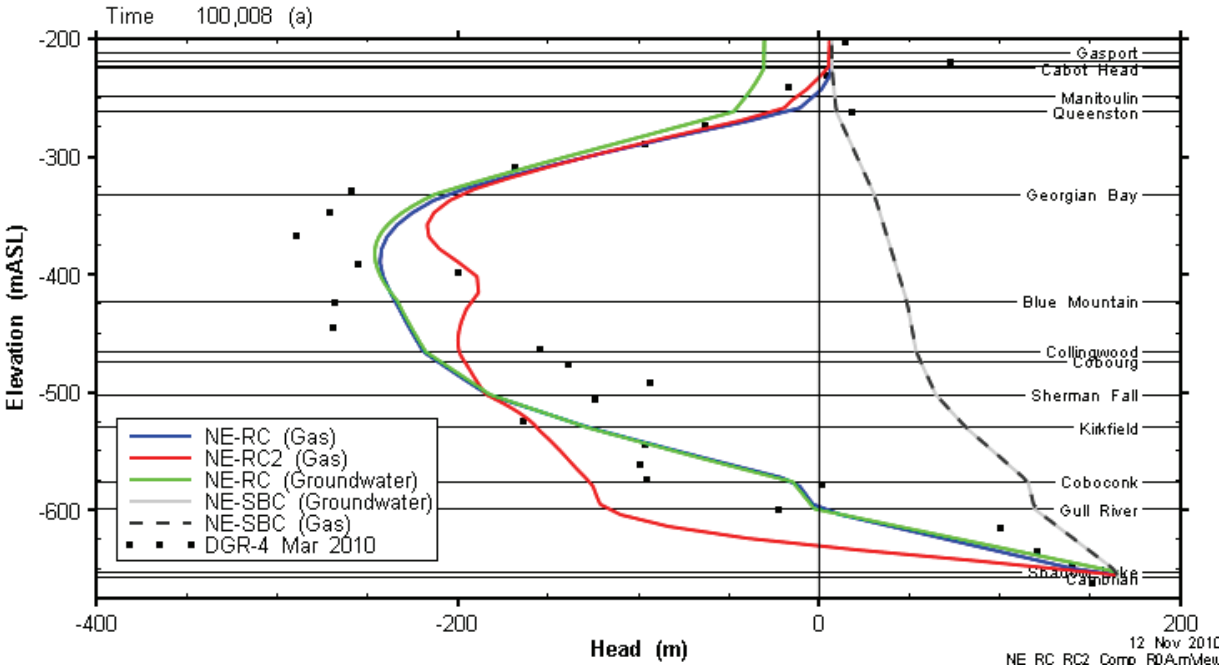

Figure 5.172: NE-RC2: Model Head Comparison at 100,000 a

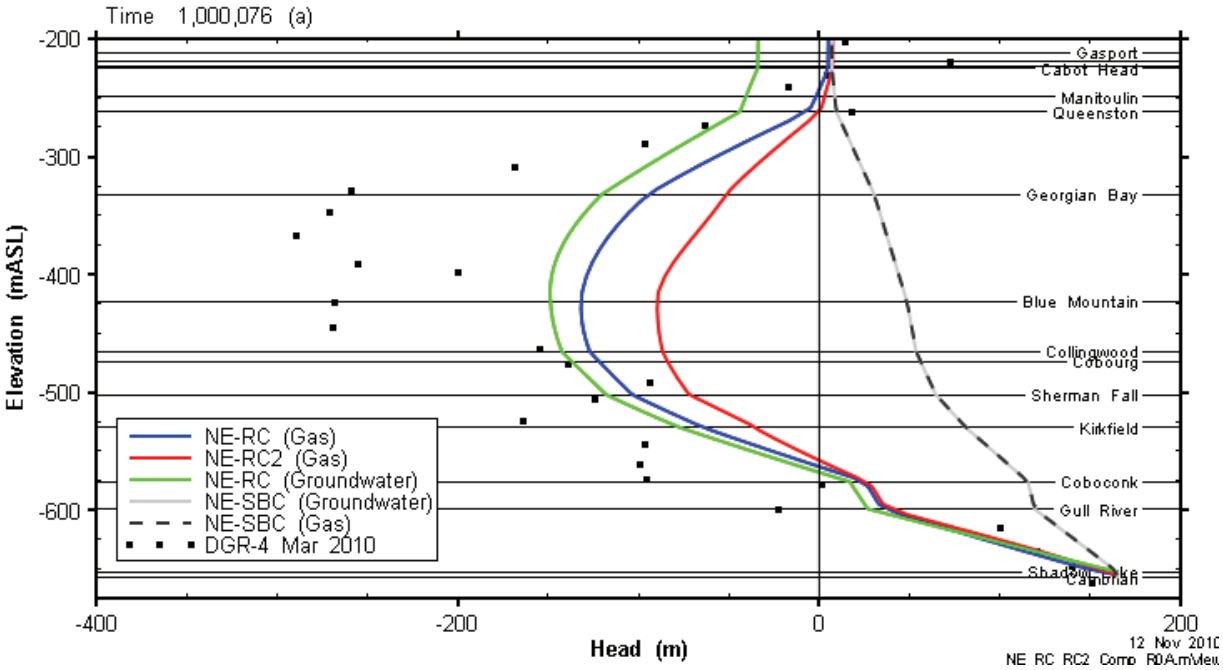

Figure 5.173: NE-RC2: Model Head Comparison at 1,000,000 a

The NE-RC results are virtually identical for both gas and groundwater, indicating that the NE-RC gas system has only a limited impact on the liquid flow domain. Essentially, in the gas

simulations, liquid saturations are always large enough (generally greater than 90%, see Figure 5.37) so that the relative permeability to liquid is not significantly reduced, and the development of the head profile mimics the fully saturated groundwater system. Furthermore, because of the constant saturations and identical capillary pressure curves, there are no substantial pressure gradients initially present in the intact rock. This minimizes gas flow, with a consequent minimal impact on the liquid pressure regime. The divergence near the top of the Ordovician system is due to the different vertical extents of the gas and groundwater models and the development of the transient flow system within the Silurian intervals for the groundwater model.

Liquid pressures for the NE-RC2 gas results are broadly similar to those of the NE-RC case, although the NE-RC2 system shows more strongly transient behaviour. This is due to a much greater degree of gas flow within the system, as it seeks to equilibrate the gas pressure gradients induced by the differing initial gas pressures in each formation. These differences are most apparent in the Gull River and Coboconk Formations, which show significant excursions from the initial conditions by 10,000 a.

One interesting feature of the gas system response is the similarity to the liquid pressure response. This indicates that gas saturations do not increase the effective storage or total compressibility of the system. In fact, the system with the highest level of gas, NE-RC2, equilibrates at the fastest rate (analogous to the lowest total compressibility), although this may be in part due to advective gas movement brought on by the gas pressure gradients.

5.14 Case NE-BF – Backfilled Repository

This case explores a design alternative; it is not the reference design. In this case, the repository is backfilled with a coarse aggregate material that substantially reduces the void space in which gas is generated to a porosity equivalent to a coarse aggregate material (30%). The case is, otherwise, identical to the NE-SBC case. The NE-BF case was simulated using the 3DSRS, 3DSR and 2DRS models.

5.14.1 Gas Generation

The gas generation discussion is based on 3DSRS model results.

The first consequence of the reduced volume for gas is that the aerobic degradation stage completes quicker than for the Simplified Base Case. All oxygen is consumed in under a year, since the initial inventory of O_2 is only 30% of that for NE-SBC.

Another consequence of the reduced void volume is that the gas pressure builds up more quickly. The build-up leads to a peak pressure of 16 MPa at 4800 a, much higher than for NE-SBC. See Figure 5.174. The pressure returns towards the natural steady-state pressure at long-times as in the NE-SBC case. This suggests that the gas pressure build-up in this case is too fast for natural equilibration to occur and the peak pressure overshoots the equilibrium point.

As a result, more gas leaves the repository particularly after the peak gas pressure is reached, totalling approximately 7×10^8 moles of gas by 1,000,000 a as compared with approximately 2×10^7 moles for the Simplified Base Case. In addition, the water saturation drops to zero at approximately the same time as the peak pressure and remains zero for the remainder of the simulation. See Figure 5.175 and Figure 5.176.

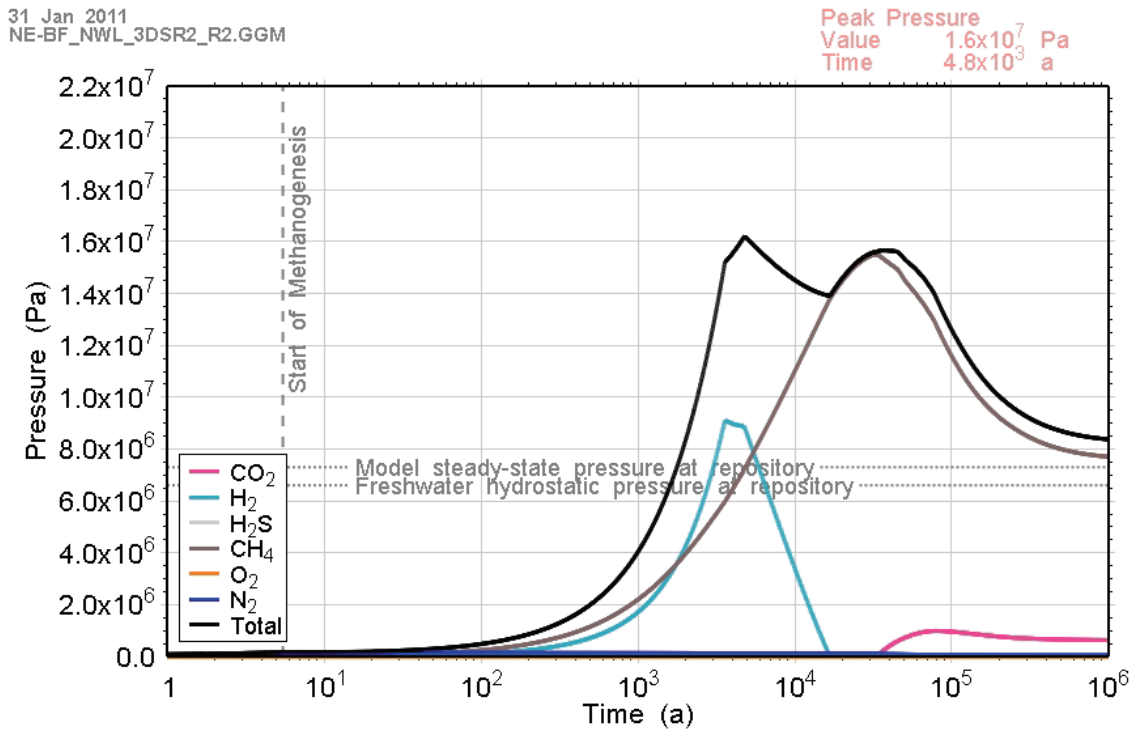

Figure 5.174: NE-BF: (3DSRS) Total and Partial Gas Pressures within the Repository

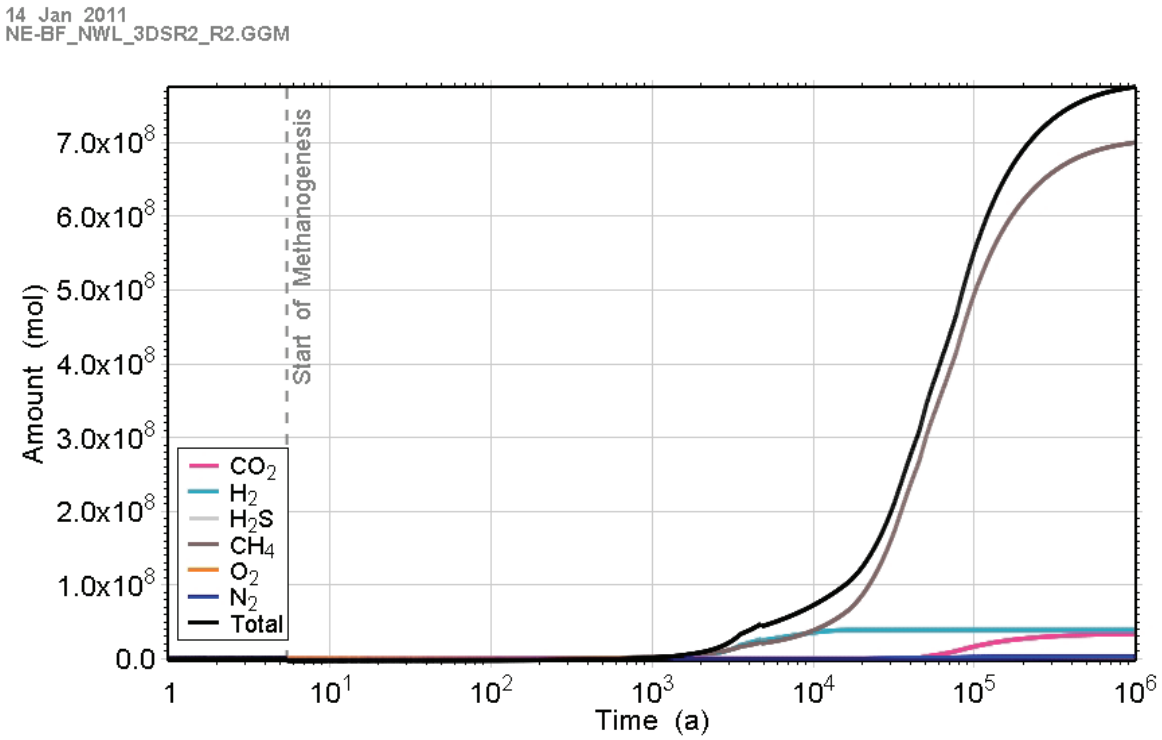

Figure 5.175: NE-BF: (3DSRS) Amounts of Gases which have Left the Repository

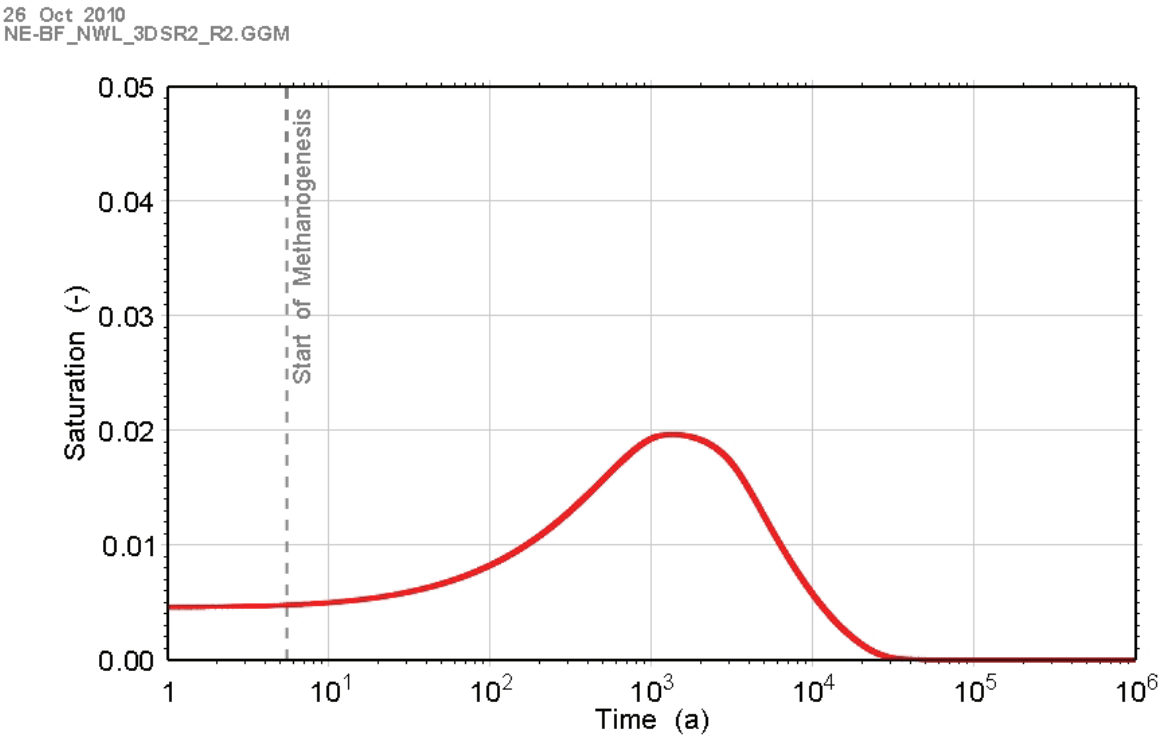

Figure 5.176: NE-BF: (3DSRS) Water Saturation within the Repository

In other respects, such as the dominant repository gas, the times at which wastes are degraded and the amounts of corrosion products, the results are the same as for the Simplified Base Case.

5.14.2 Gas and Water Flows

Unlike most other cases, there is significant variation between the 3DSRS and 3DSR models, as the 3DSR model reaches a much higher peak pressure. Outflow of gas up the shaft in the 3DSRS is the reason for the pressure differences.

5.14.2.1 Shaft

The very-early time (less than 1000 a) response of the shaft is similar to the NE-SBC case and will not be discussed in detail here. In the absence of significant pressures in the repository, the shaft resaturates normally. At 1000 a, pressures are rising rapidly in the repository, and by 2000 a gas is starting to flow up the shaft. As shown in Figure 5.177, by 4000 a gas has reached the top of the 3D model domain.

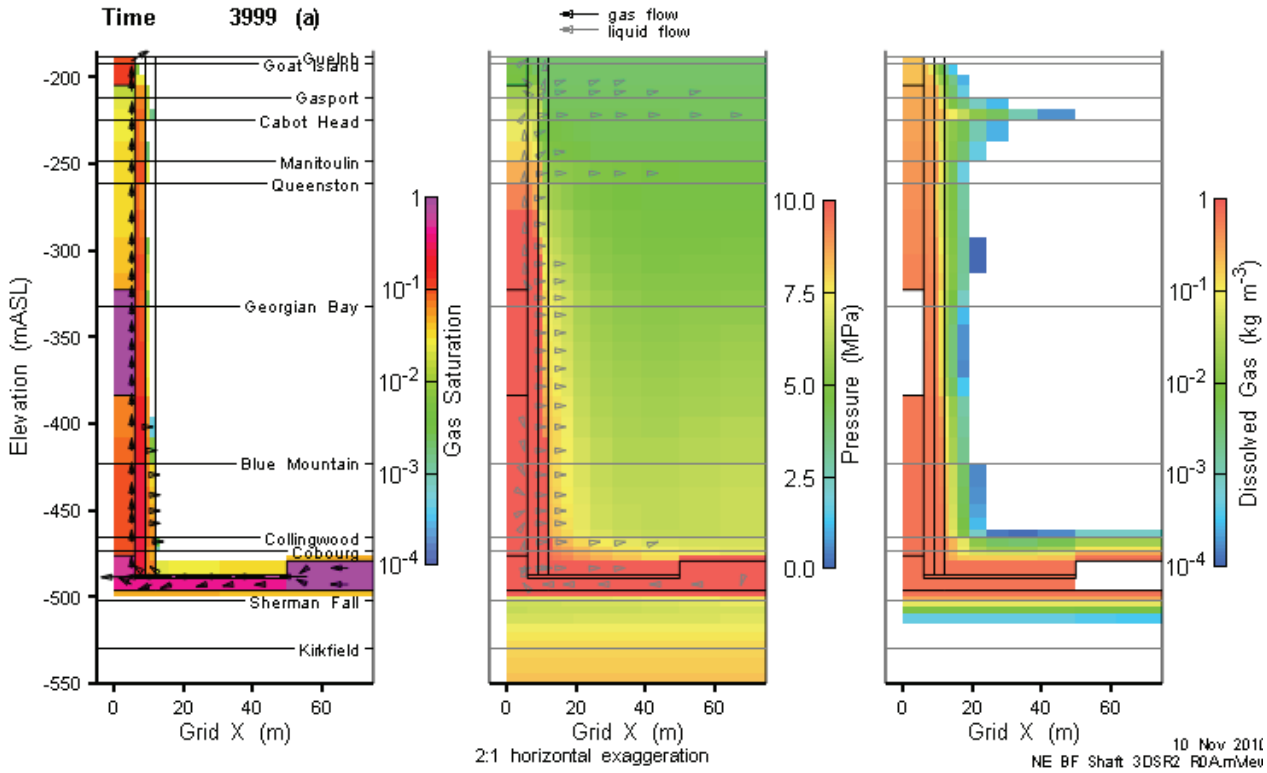

Figure 5.177: NE-BF: 3DSRS Model Shaft Saturations, Flows and Pressures (4000 a)

This system remains established for the duration of the 1 Ma simulation period. Results at 100,000 a and 1,000,000 a are shown in Figure 5.178 and Figure 5.179, respectively.

Typical 2DRS model results are shown in Figure 5.180 and Figure 5.181. As for other cases where repository pressures drive gas flow up the shaft, the higher permeability Guelph Formation acts as an effective sink for any free-phase gas being transported through the shaft.

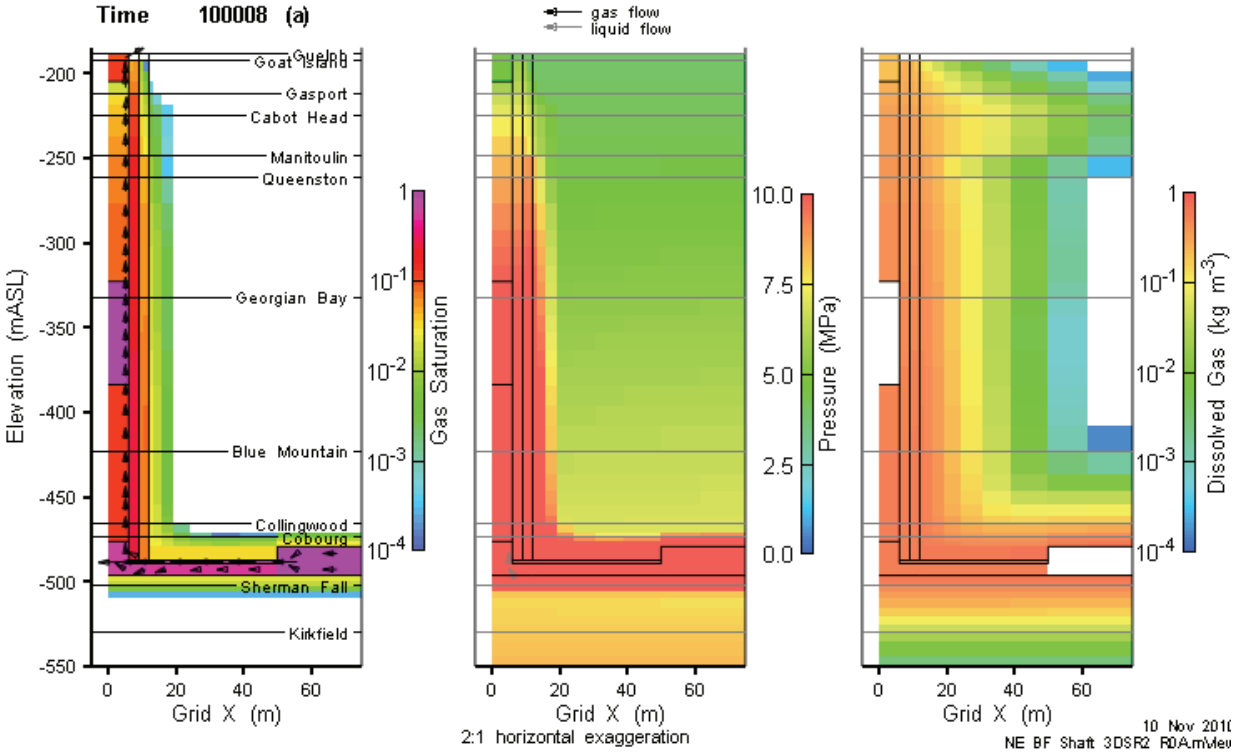

Figure 5.178: NE-BF: 3DSRS Model Shaft Saturations, Flows and Pressures (100,000 a)

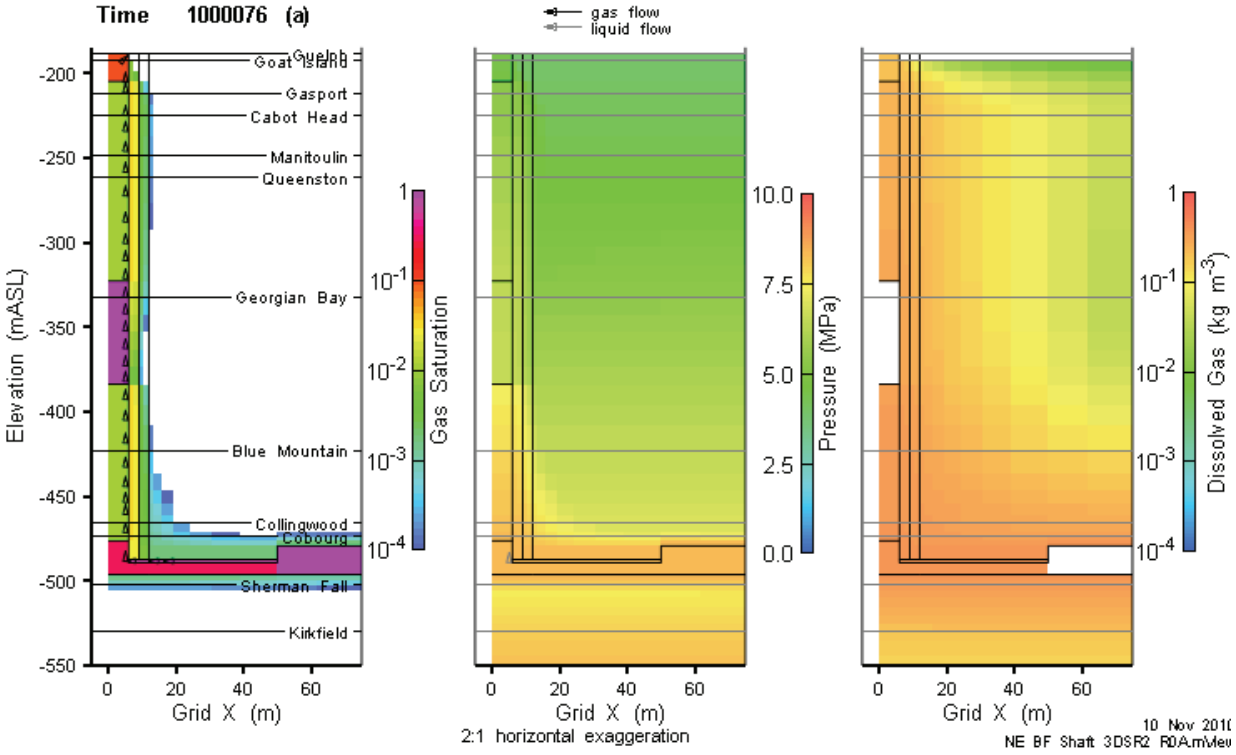

Figure 5.179: NE-BF: 3DSRS Model Shaft Saturations, Flows and Pressures (1,000,000 a)

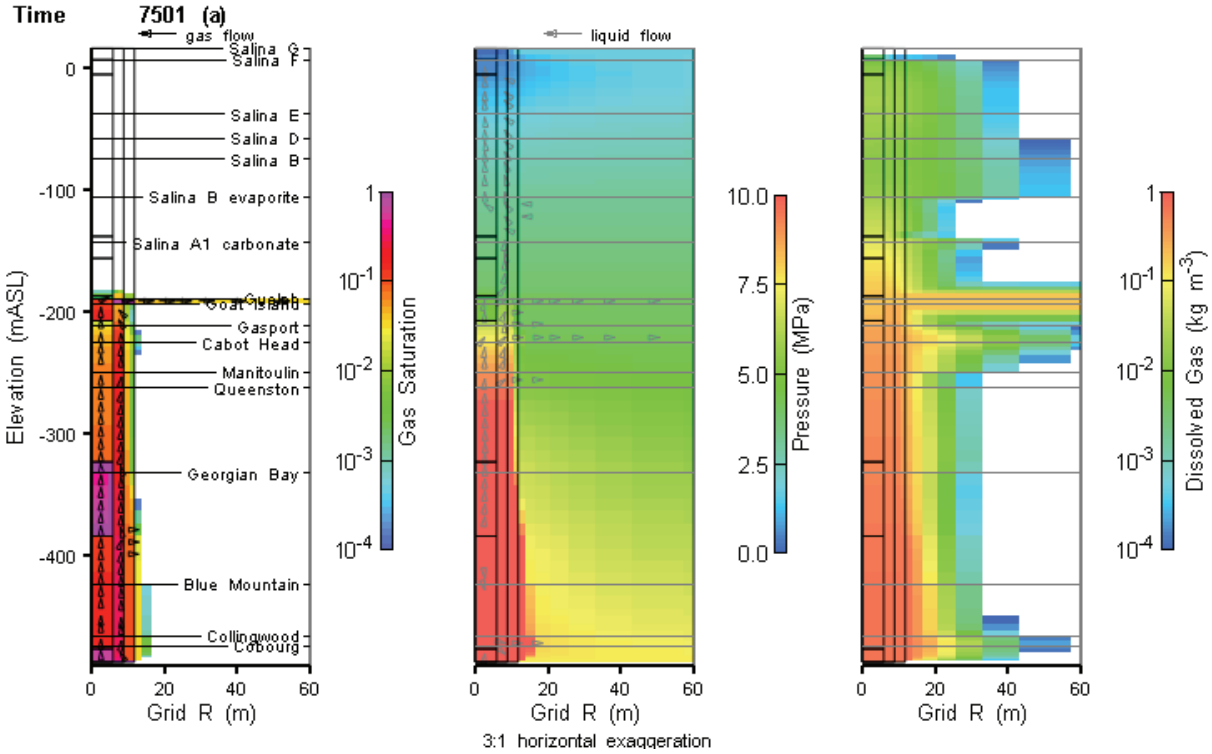

Figure 5.180: NE-BF: 2DRS Model Shaft Saturations, Flows and Pressures (7500 a)

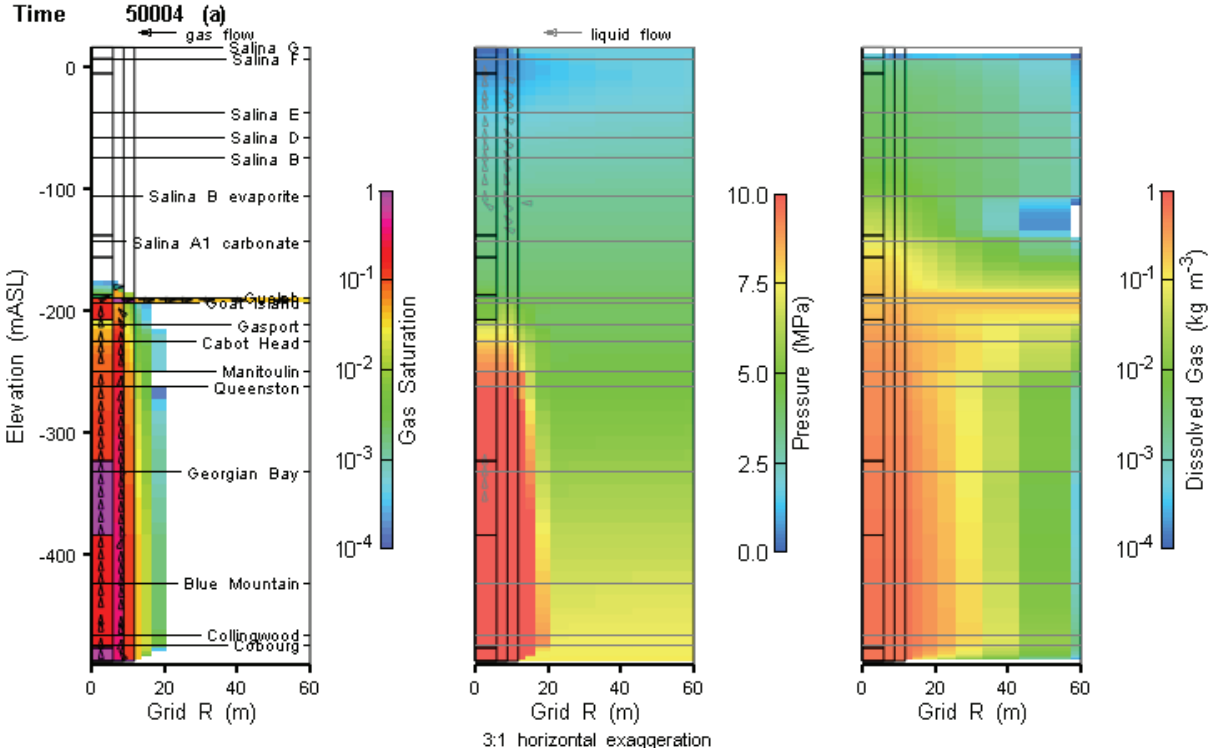

Figure 5.181: NE-BF: 2DRS Model Shaft Saturations, Flows and Pressures (50,000 a)

Early-time resaturation and subsequent desaturation of the shaft seal materials is shown in Figure 5.182. Figure 5.183 shows the calculated gas fluxes up the shaft from the 3DSRS model.

Equivalent 2DRS model results are given in Figure 5.184. They are similar in magnitude to the 3DSRS results. As for other overpressured cases, there is no gas flow above the Guelph Formation.

Dissolved gas flow peaks at an early time, coincident with the initial pressure peak in the repository at approximately 3800 a, as shown in Figure 5.185. The characteristics of the flow are unusual with a higher peak in the Gasport and the majority of flow through the inner EDZ. Dissolved gas flow through the Georgian Bay is low, because the asphalt seal is fully gas saturated when upward flow begins, forcing liquid flow (containing dissolved gas) through the EDZ at lower rates. Above the asphalt seal, gas saturations are lower, and seal material permeability is higher, allowing liquid flow with higher concentrations of dissolved gas. The source of the dissolved gas is also unclear. It may be entrained gas from seal placement; however, the peak dissolved gas rate corresponds with the onset of free gas flow at the Gasport.

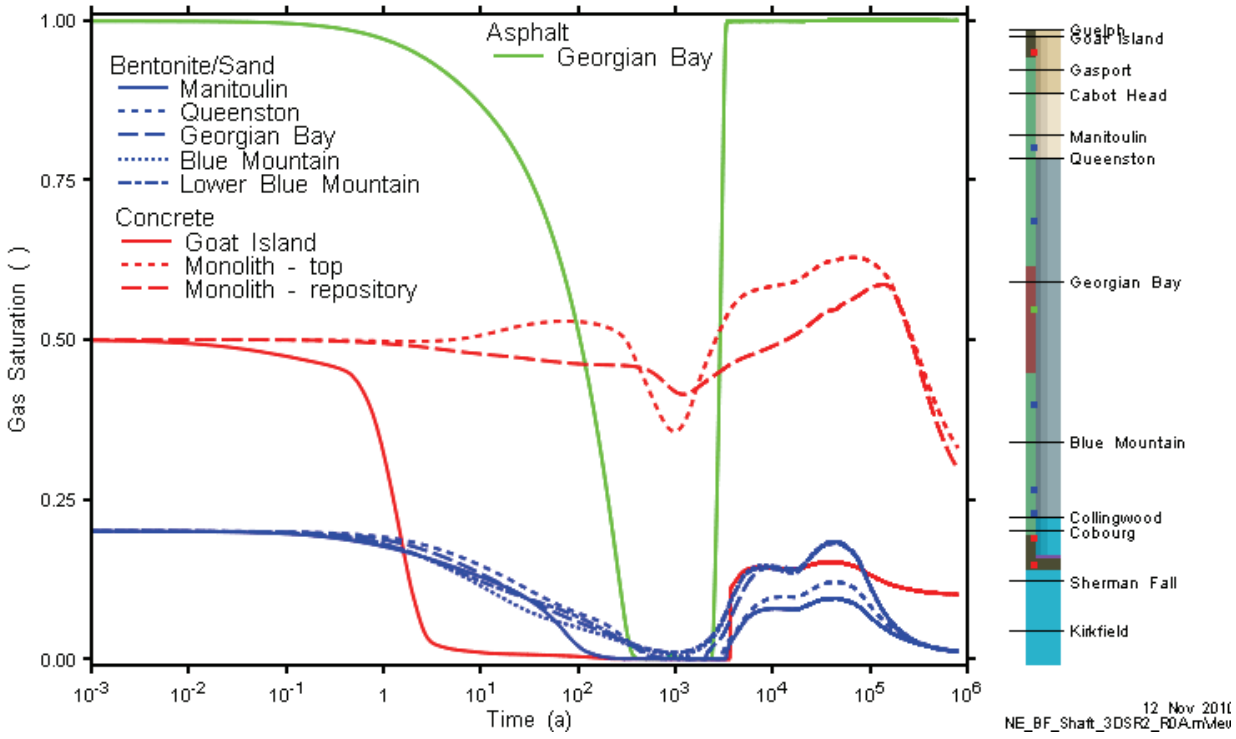

Figure 5.182: NE-BF: 3DSRS Model Shaft Saturation at Selected Monitoring Planes

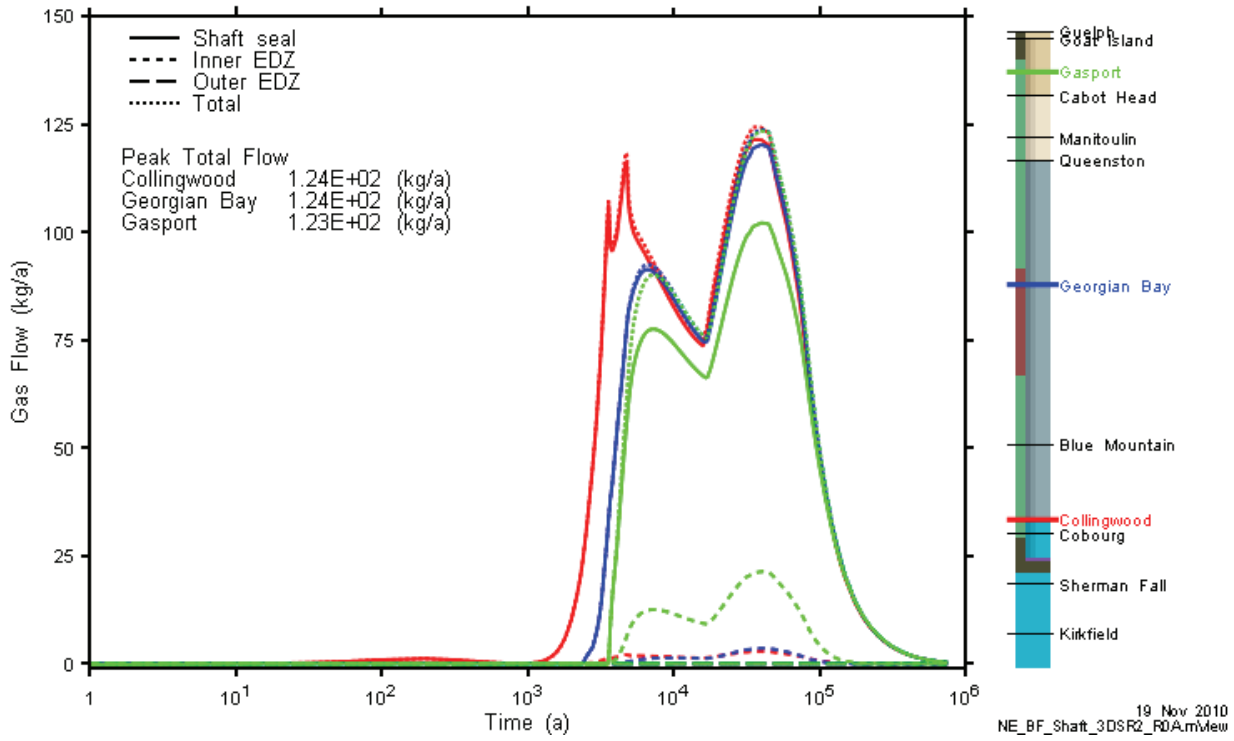

Figure 5.183: NE-BF: 3DSRS Model Shaft Gas Flow at Selected Monitoring Planes

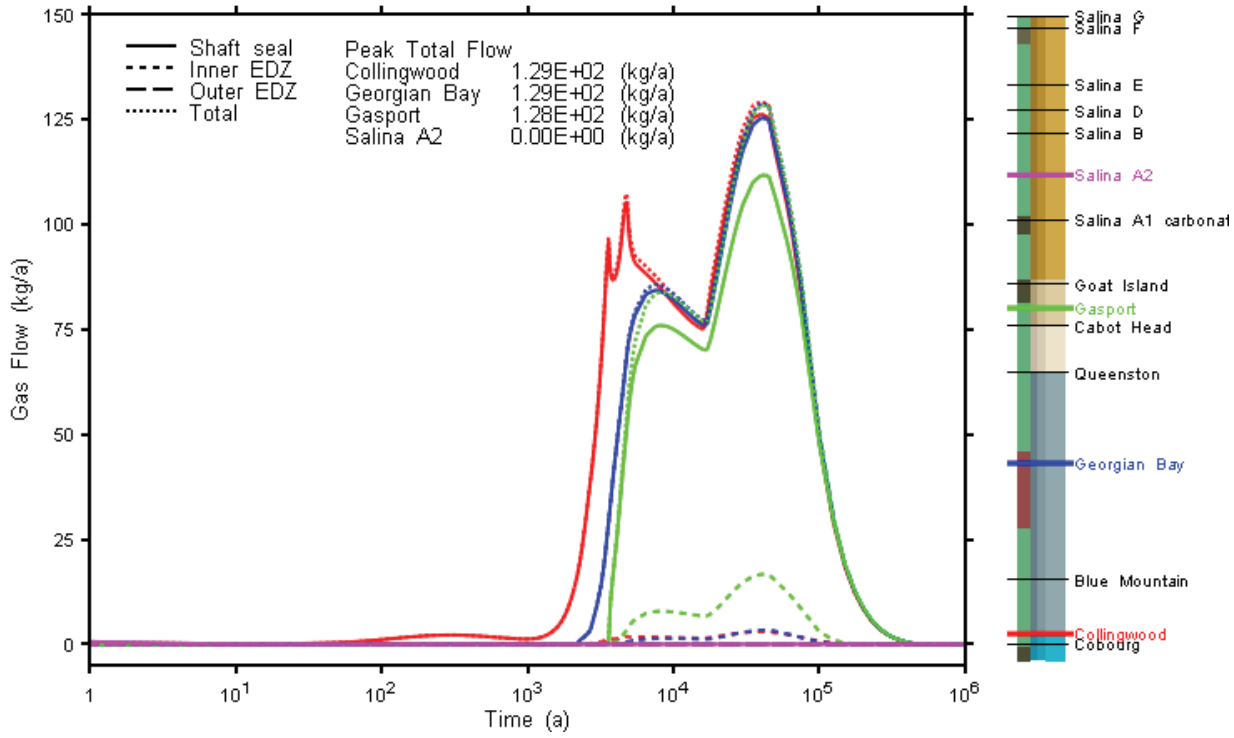

Figure 5.184: NE-BF: 2DRS Model Shaft Gas Flow at Selected Monitoring Planes

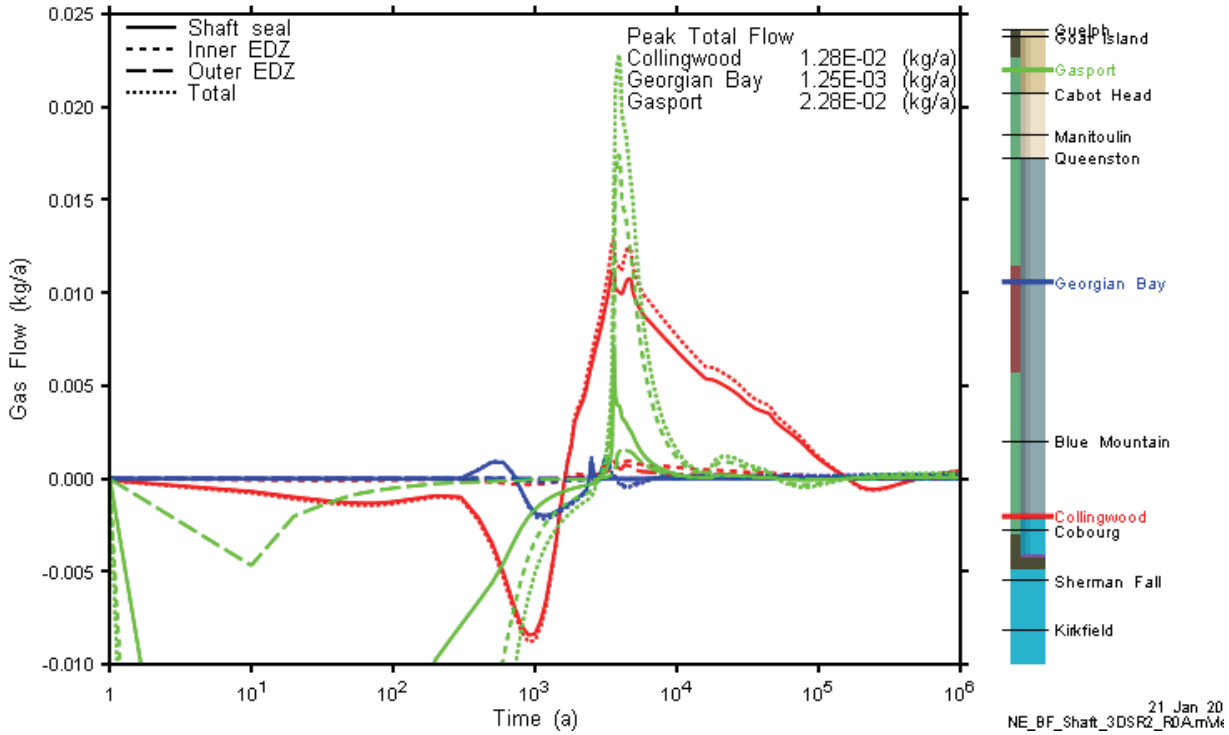

Figure 5.185: NE-BF: 3DSRS Model Shaft Dissolved Gas Flow at Selected Monitoring Planes

5.14.2.2 Repository System

Figure 5.186 presents repository pressures and liquid saturations over the 1 Ma simulation period. It is apparent that the flow up the shaft in the 3DSRS model is sufficient to reduce the peak pressure, and to subsequently speed the pressure decline towards steady-state conditions.

Figure 5.187 shows cumulative gas and liquid flows for 3DSRS and 3DSR models. Liquid inflows are very similar, with negligible contribution from the shaft in the 3DSRS model. Calculated gas outflows are much higher for the 3DSRS model, with the bulk of the gas moving up the shaft.

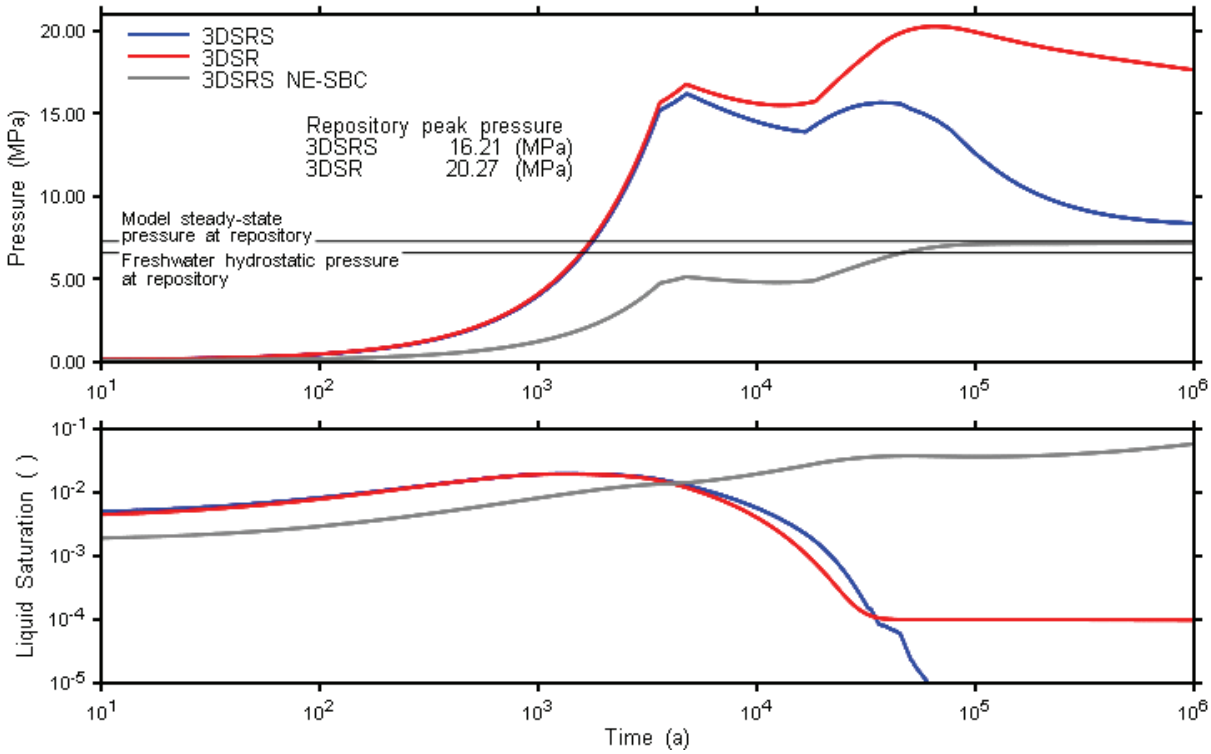

Figure 5.186: NE-BF: 3DSRS and 3DSR Model Repository Pressure and Saturation

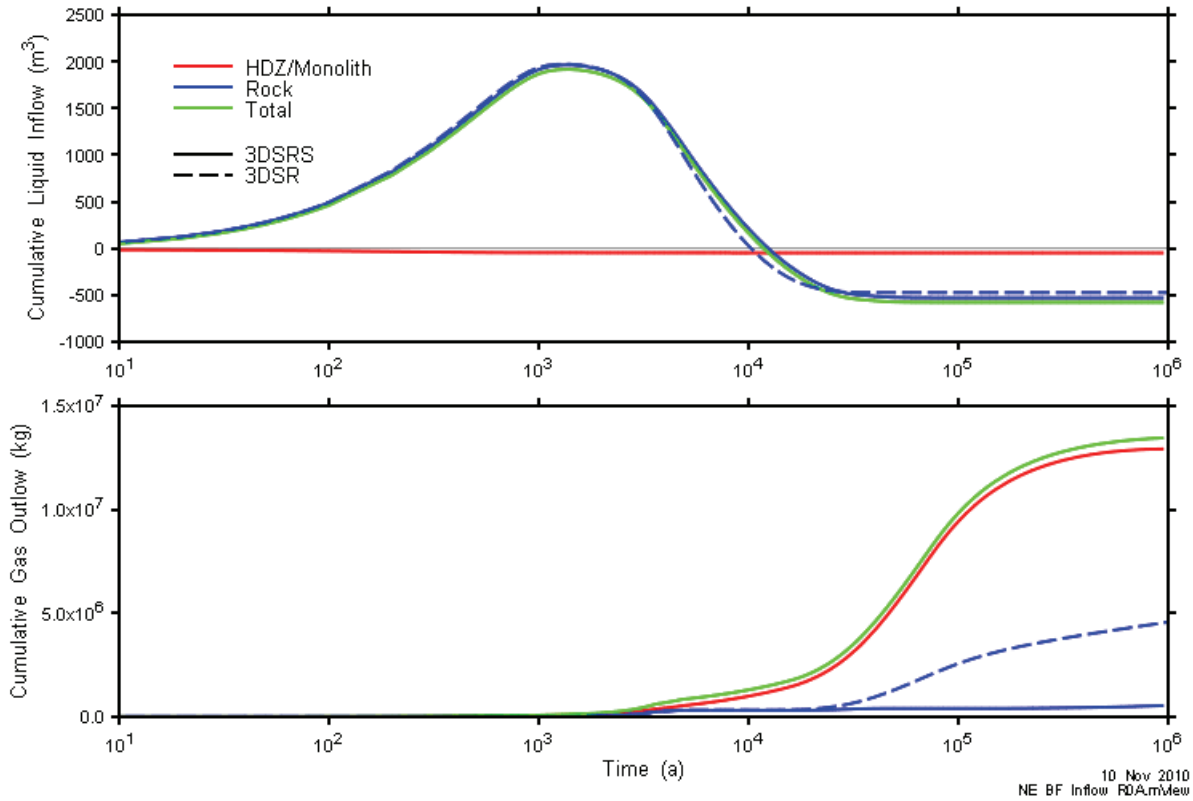

Figure 5.187: NE-BF: Repository Liquid Inflow and Gas Outflow for 3DSRS and 3DSR Models

5.14.2.3 Geosphere

The geosphere hydraulic head profile for the NE-BF case is presented in Figure 5.188. At the end of the 1 Ma simulation period, repository pressures are significantly in excess of the surrounding intact rock. However, the resulting pressure perturbation is of limited vertical extent due to the minimal amount of liquid flow into or out of the repository.

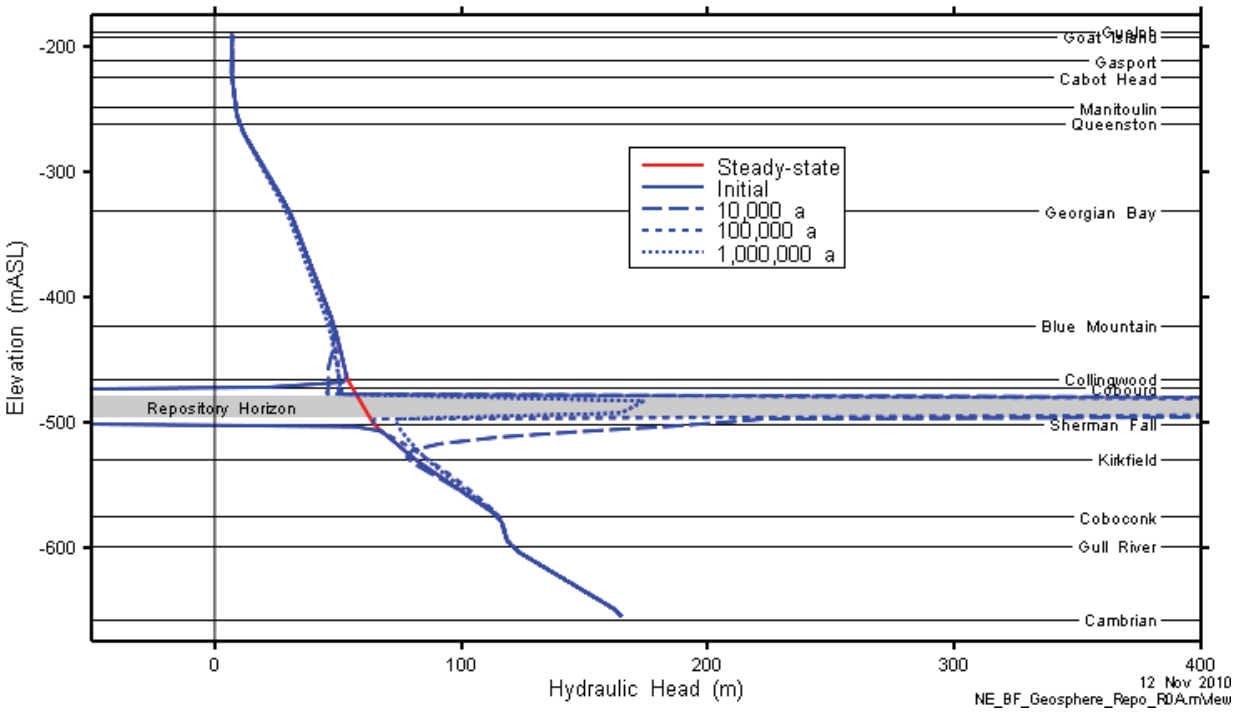

Figure 5.188: NE-BF: 3DSRS Geosphere Head Profile

5.15 NE-PD-RC - Reference Case, Final Preliminary Design

The reference case was updated to the final preliminary design by increasing the repository and tunnel void volume. The change was effected using the 3DSRS model by increasing the calculated porosity of REPO elements to yield the final void volume (total void volume of 449,200 m^3, approximately 8% larger than that of the original preliminary design).

Figure 5.189 compares the repository pressure and saturation response of the NE-PD-RC case to the NE-RC case. The most significant difference is a slight reduction in repository pressure due to the increased void space available to accommodate generated gas. Gas generation processes, shaft flows, and geosphere impact are very similar to the NE-RC case and are not described further here. The final preliminary design has very similar response to the original preliminary design assessed in the NE-RC case.

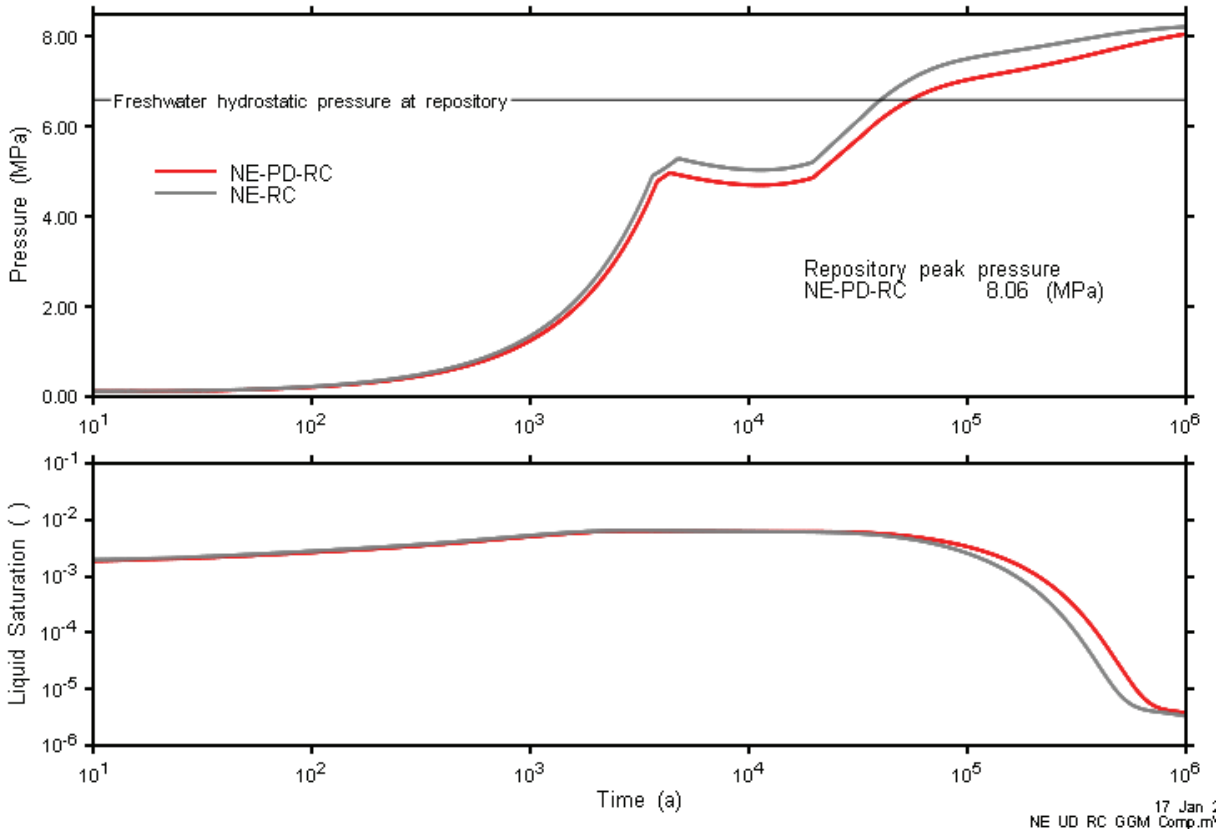

Figure 5.189: NE-PD-RC: 3DSRS Model Repository Pressure and Saturation

5.16 NE-PD-GT5 - Alternative Shaft Parameters, Final Preliminary Design

The NE-GT5 case was updated to the final preliminary design by increasing the repository and tunnel void volume as described above for the NE-PD-RC case.

Figure 5.190 compares the repository pressure and saturation response of the NE-PD-GT5 case to the NE-GT5 case. As for the NE-PD-RC case comparison, the repository pressure is reduced. However, for the NE-PD-GT5 case, this also leads to an increase of liquid inflow into the repository and a decrease in gas flow up the shaft as shown in Figure 5.191 and Figure 5.192 respectively. Dissolved gas flows (not shown) are also slightly reduced relative to the NE-GT5 case. Otherwise, the final preliminary design has very similar characteristics to the original preliminary design assessed in the NE-GT5 case.

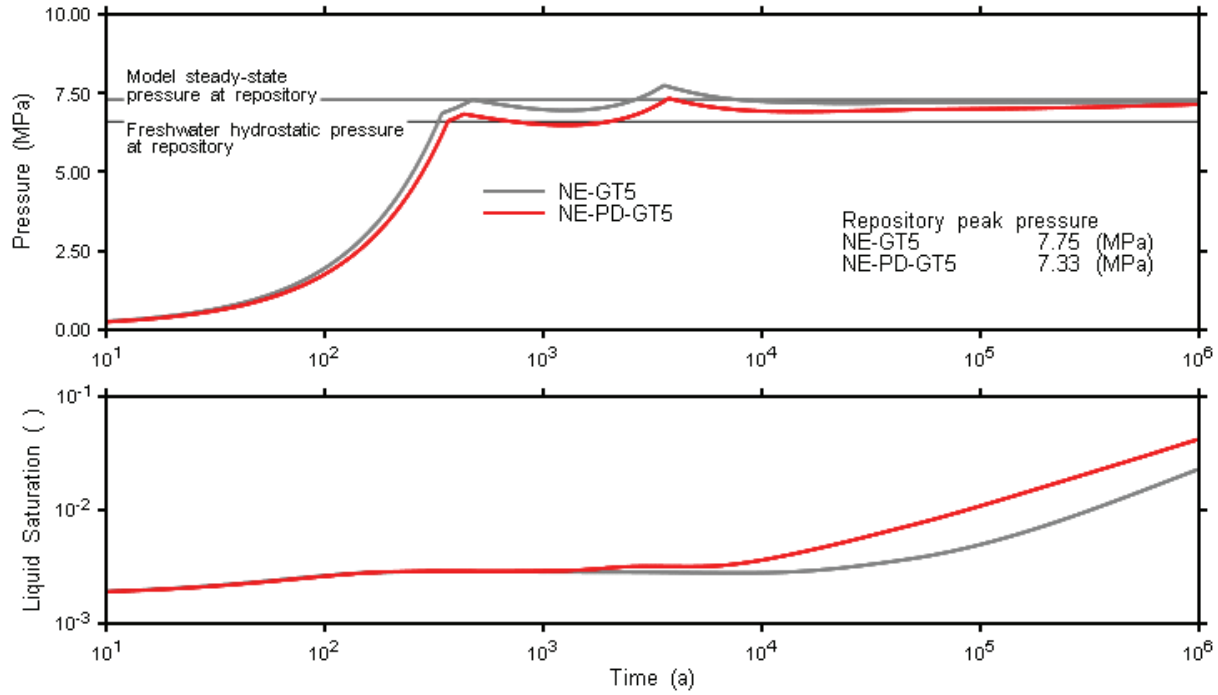

Figure 5.190: NE-PD-GT5: 3DSRS Model Repository Pressure and Saturation

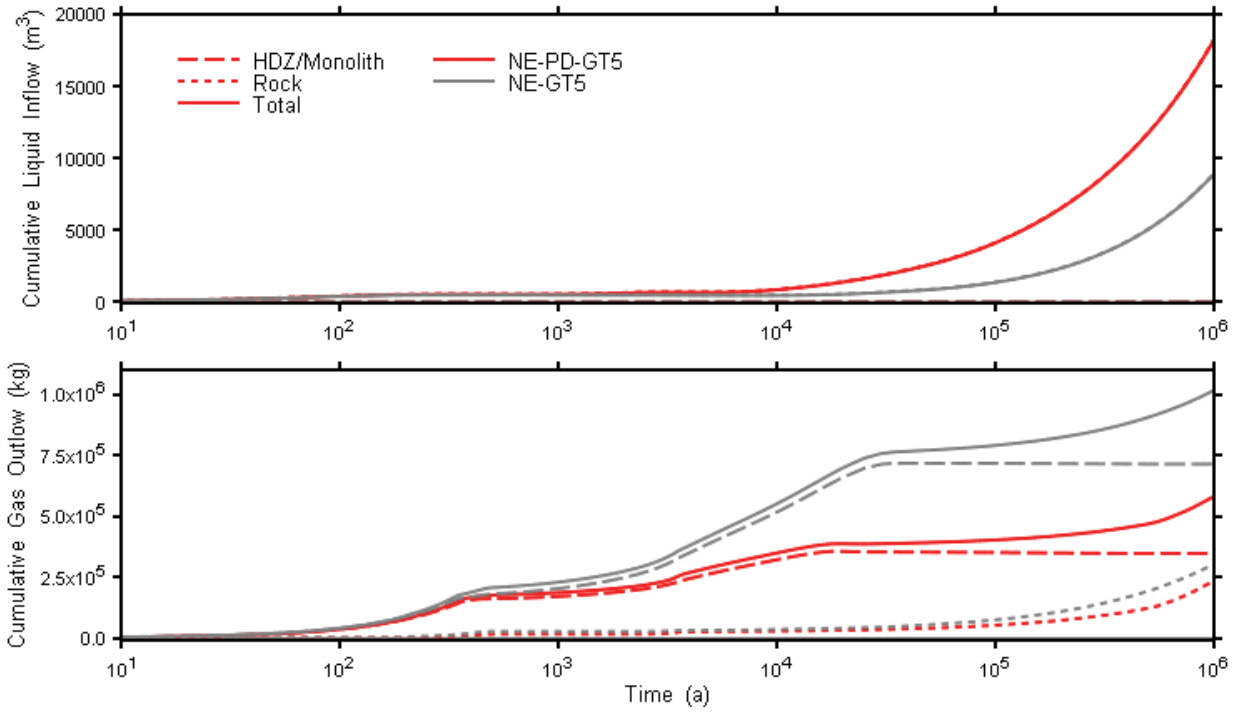

Figure 5.191: NE-PD-GT5: Repository Liquid Inflow and Gas Outflow

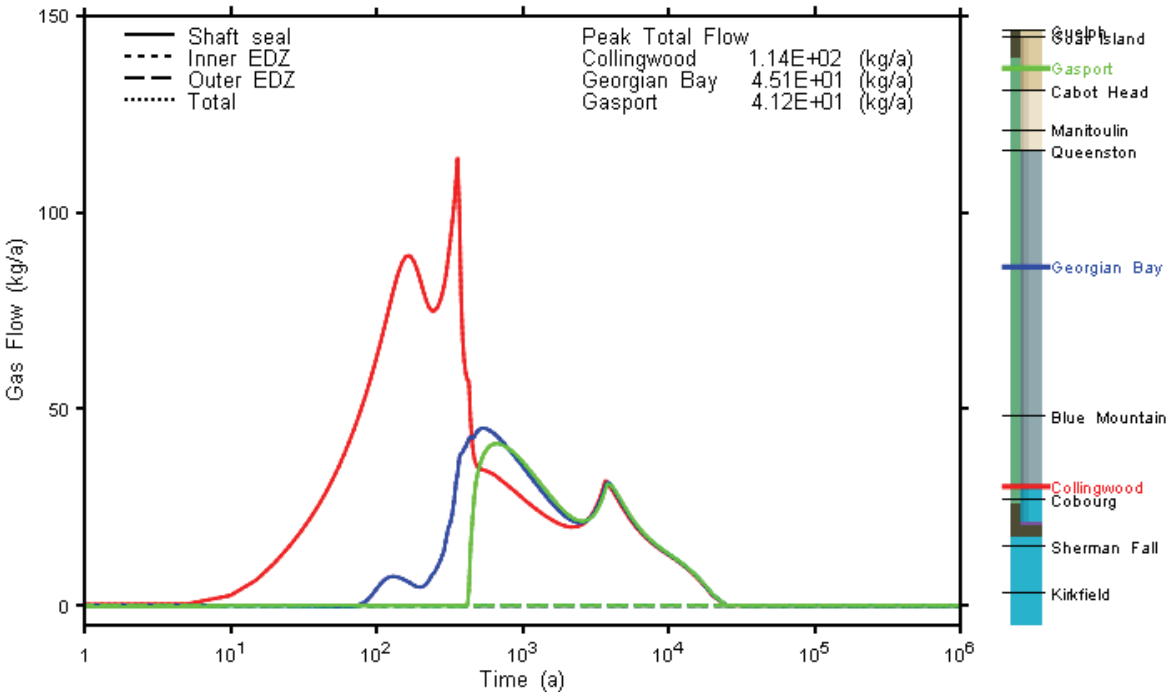

Figure 5.192: NE-PD-GT5: 3DSRS Model Shaft Gas Flow at Selected Monitoring Planes

6. RESULTS FOR THE DISRUPTIVE SCENARIOS

As discussed in Section 3.2, two Disruptive Event calculation cases were specified. Both variants are based on the Severe Shaft Seal Failure Scenario, with different parameterization of the shaft materials. Although the case specification called for inner and outer EDZ parameters for both cases to be as described for the NE-EDZ1 case, numeric difficulties required use of less permeable EDZ parameters. The cases were simulated with the 3DSRS model, with NE-RC inner and outer EDZ permeabilities and two phase flow parameters.

6.1 SF-BC Shaft Seal Failure – Base Case (10^{-9} m/s)

The Severe Shaft Seal Failure Base Case (SF-BC) case assumes NE-SBC case properties, with the exception that that hydraulic properties of all seals are significantly degraded from repository closure (i.e., hydraulic conductivity of 10^{-9} m/s for all shaft seal materials); much higher than that of the as-placed materials. The capillary pressure for the shaft seal material was assumed to be zero at all gas saturations, due to the high permeability. Model results are available to approximately 475,000 a, at which time the simulation terminated as the repository neared saturation. The pressure reaches an intermediate peak of approximately 5.5 MPa at 20,000 a, at which point there is a large evacuation of gas from the repository. The pressure then continues to recover towards the hydrostatic pressure at the repository horizon.

6.1.1 Gas Generation

The results presented in this section are for the 3DSRS geometry. There are two main differences between the results for this case and the NE-SBC case up to the time for which results are available. The first is an enhanced ingress of water into the repository due to the higher permeability seals from 1000 a onwards. For the NE-SBC case the water saturation does not increase above 5%, whereas for this case the saturation has reached 68% by 500,000 a. See Figure 6.1. The second is that very little gas leaves the repository until a large evacuation of gas at approximately 20,000 a (see Figure 6.2) and a corresponding sharp drop in pressure (see Figure 6.3.)

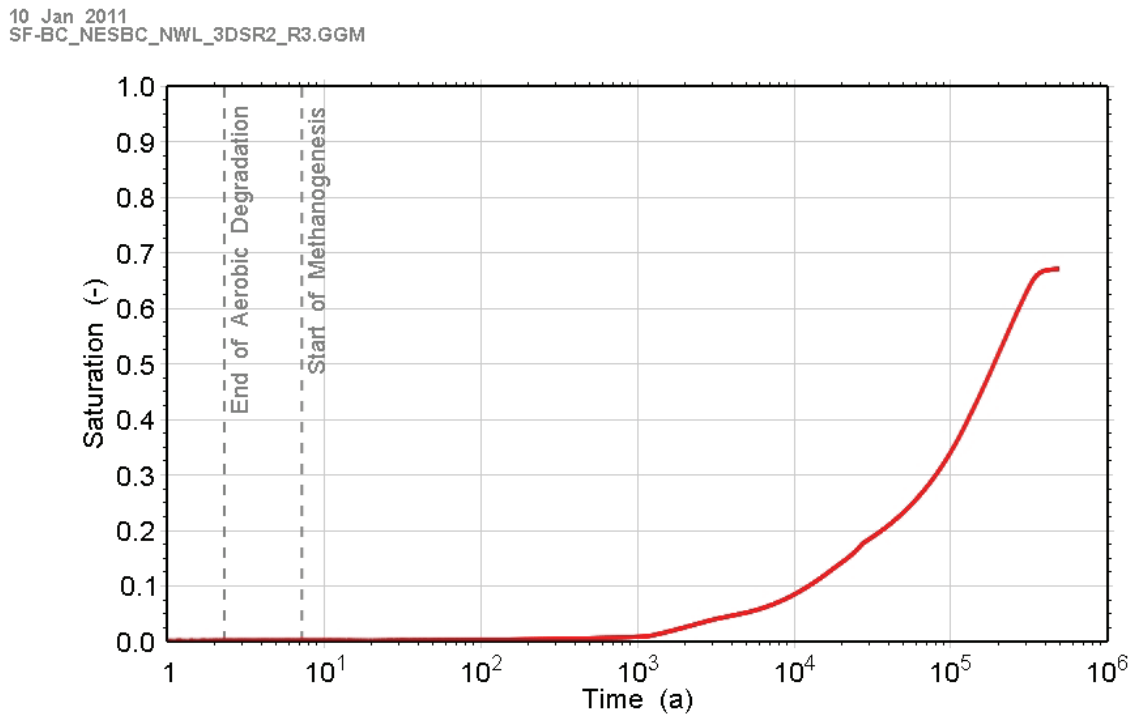

Figure 6.1: SF-BC: Water Saturation

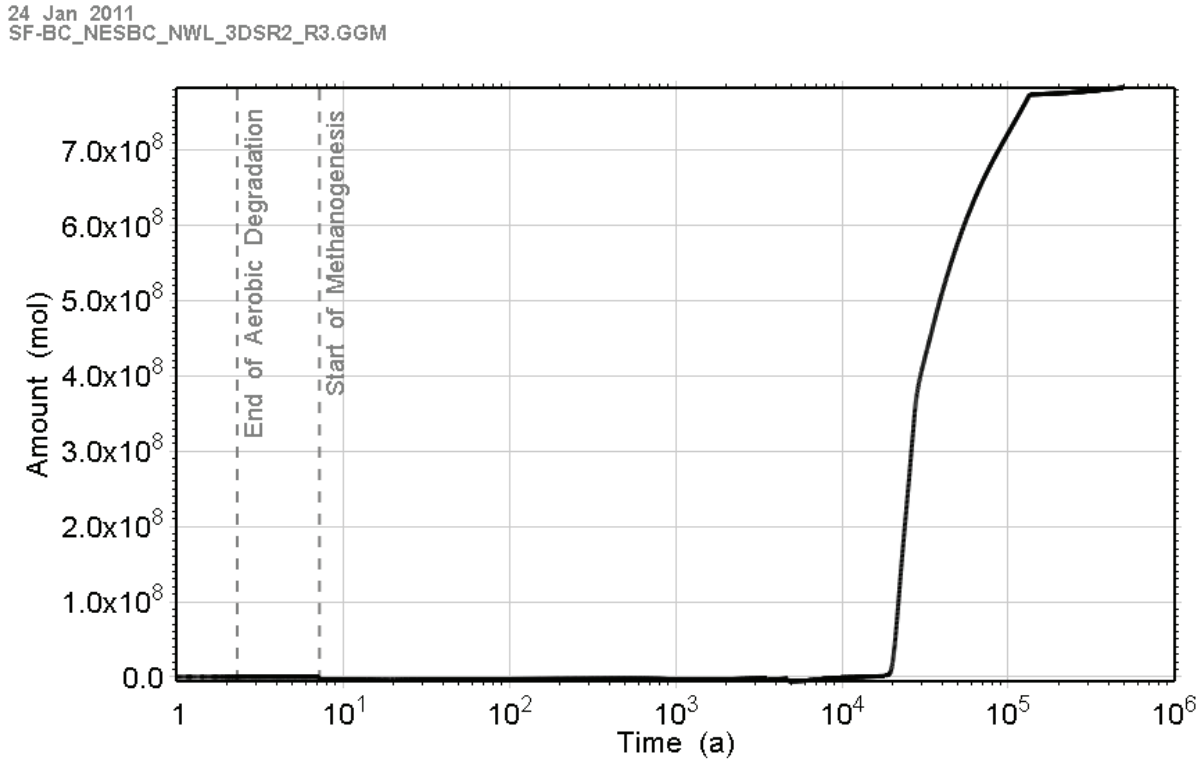

Figure 6.2: SF-BC: Total Amount of Gas that has Left the Repository

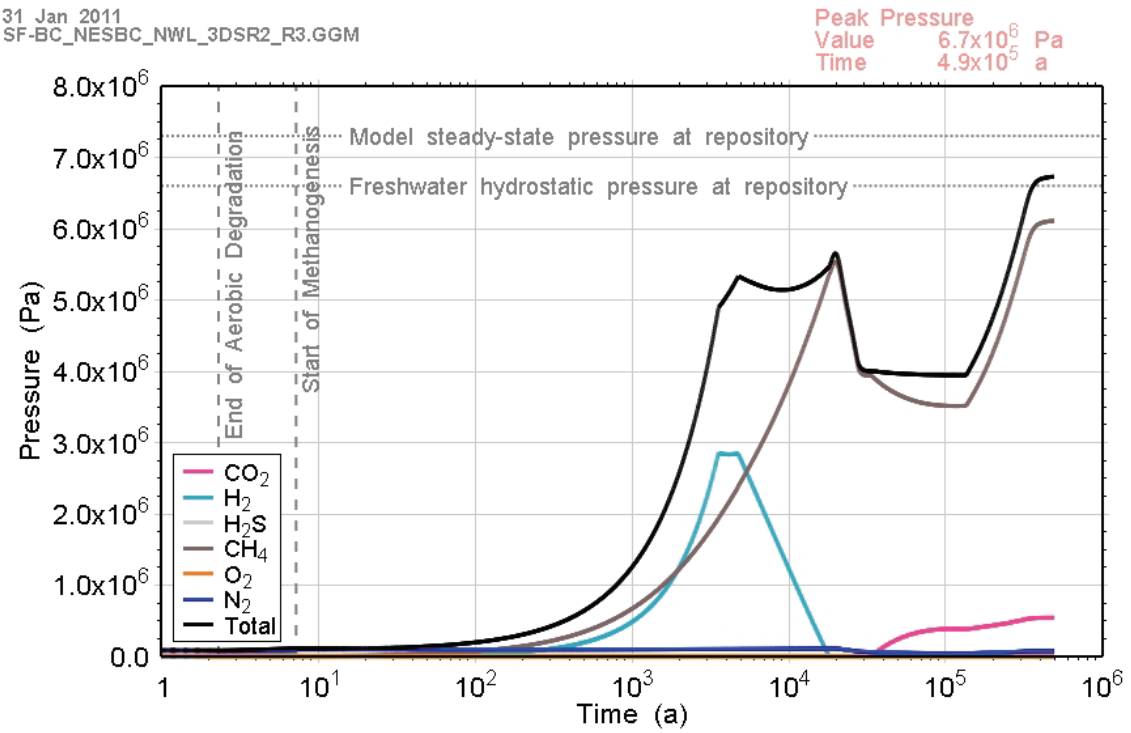

Figure 6.3: SF-BC: Total and Partial Gas Pressures within the Repository

6.1.2 Gas and Water Flows

Initially, SF-BC results are similar to NE-SBC, with similar repository pressurization up until approximately 3000 a. However, inflow from the shaft serves to resaturate the repository faster than in the NE-SBC case. After 2000 a, the repository pressure increases until it exceeds the pressure at the bottom of the shaft. At approximately 20,000 a, there is a breakthrough event where pressurized gas vents up the shaft to the top of the model domain (Guelph Formation). Subsequently, a desaturated pathway is established in the shaft to vent off additional gas as it is generated. Gas continues to be transmitted up the shaft until the water level in the repository rises above the top of the HDZ at approximately 150,000 a. This terminates the high-permeability gas connection between the shaft and the repository through the HDZ and gas transport up the shaft ceases. Water continues to flow down the shaft as the repository resaturates and repressurizes. The simulation terminated before complete resaturation and repressurization had occurred. Beyond that 500,000 a, shaft flows would be expected to reverse, as water flowing into the repository from the geosphere would exit the system via the shaft. Flow rates would be very low, limited by the low-permeability of the geosphere.

6.1.2.1 Shaft

The shaft is fully resaturated within 500 a (Figure 6.4), slightly faster than the NE-SBC case. Figure 6.5 through Figure 6.9 illustrate the sequence of events described above, with breakthrough of the gas (Figure 6.5), flow up the shaft (Figure 6.6 and Figure 6.7), repository saturation above the HDZ (Figure 6.8), and longer term liquid flow (Figure 6.9).

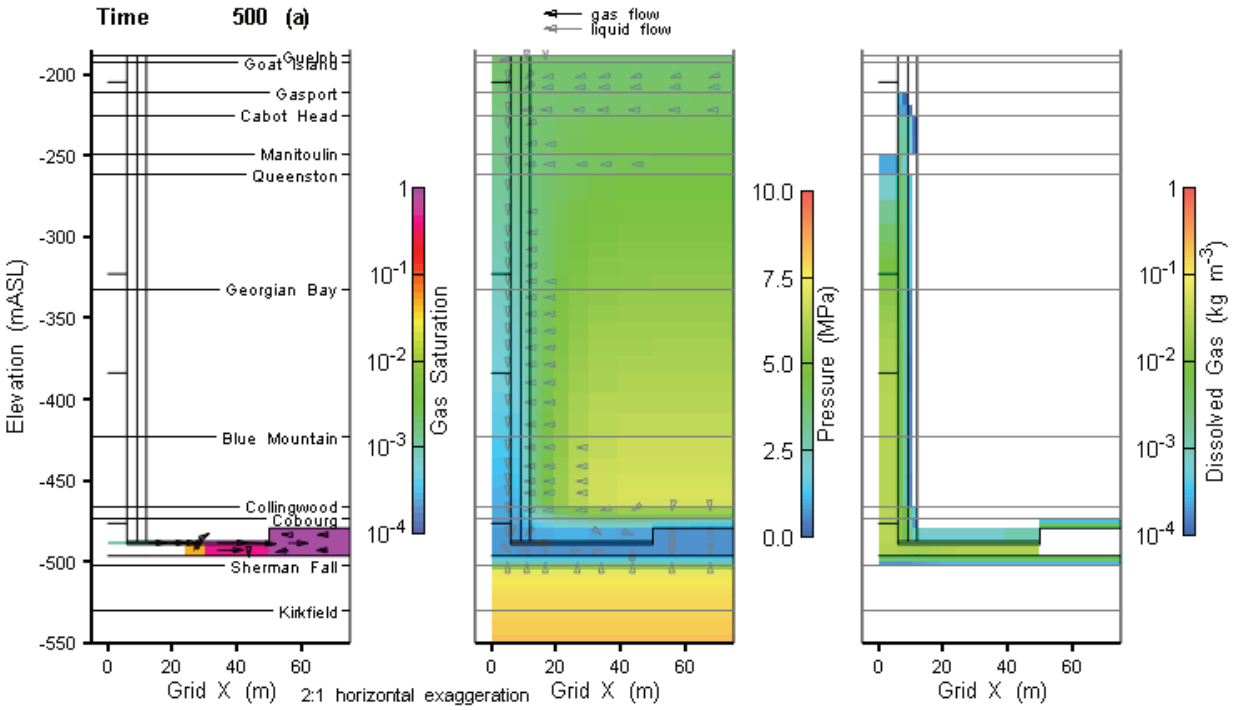

Figure 6.4: SF-BC: 3DSRS Model Shaft Saturations, Flows and Pressures (500 a)

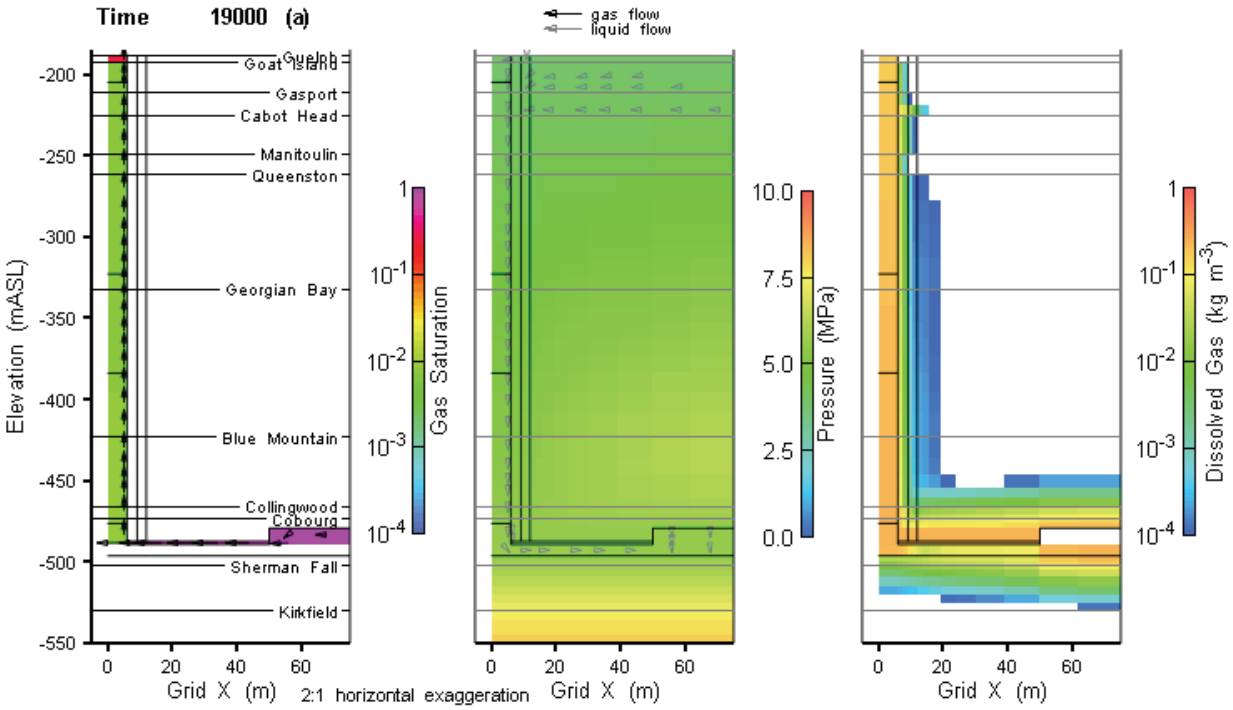

Figure 6.5: SF-BC: 3DSRS Model Shaft Saturations, Flows and Pressures (19,000 a)

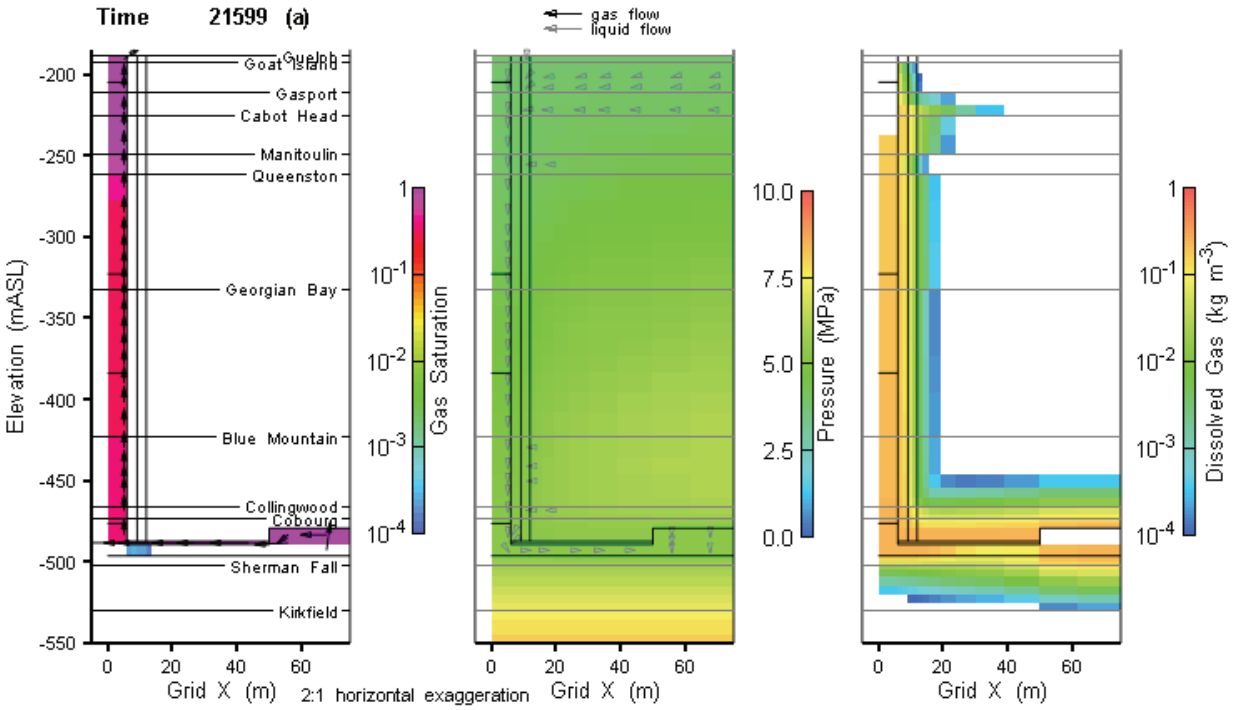

Figure 6.6: SF-BC: 3DSRS Model Shaft Saturations, Flows and Pressures (21,600 a)

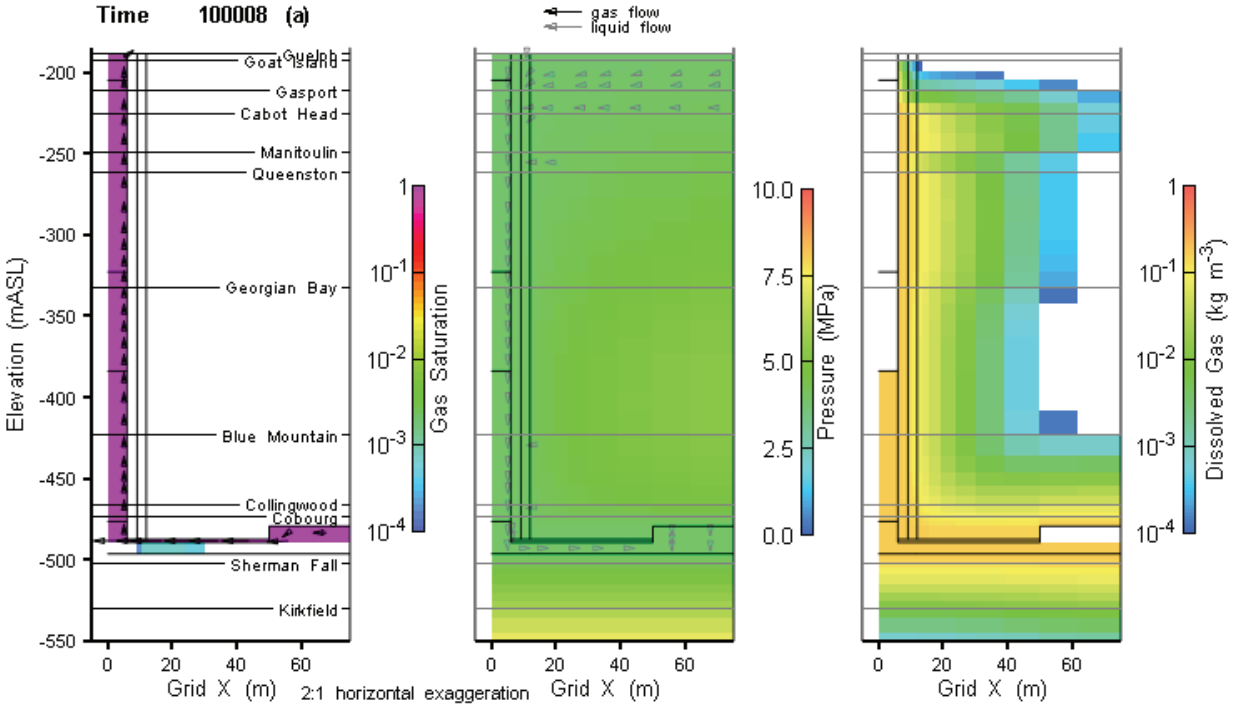

Figure 6.7: SF-BC: 3DSRS Model Shaft Saturations, Flows and Pressures (100,000 a)

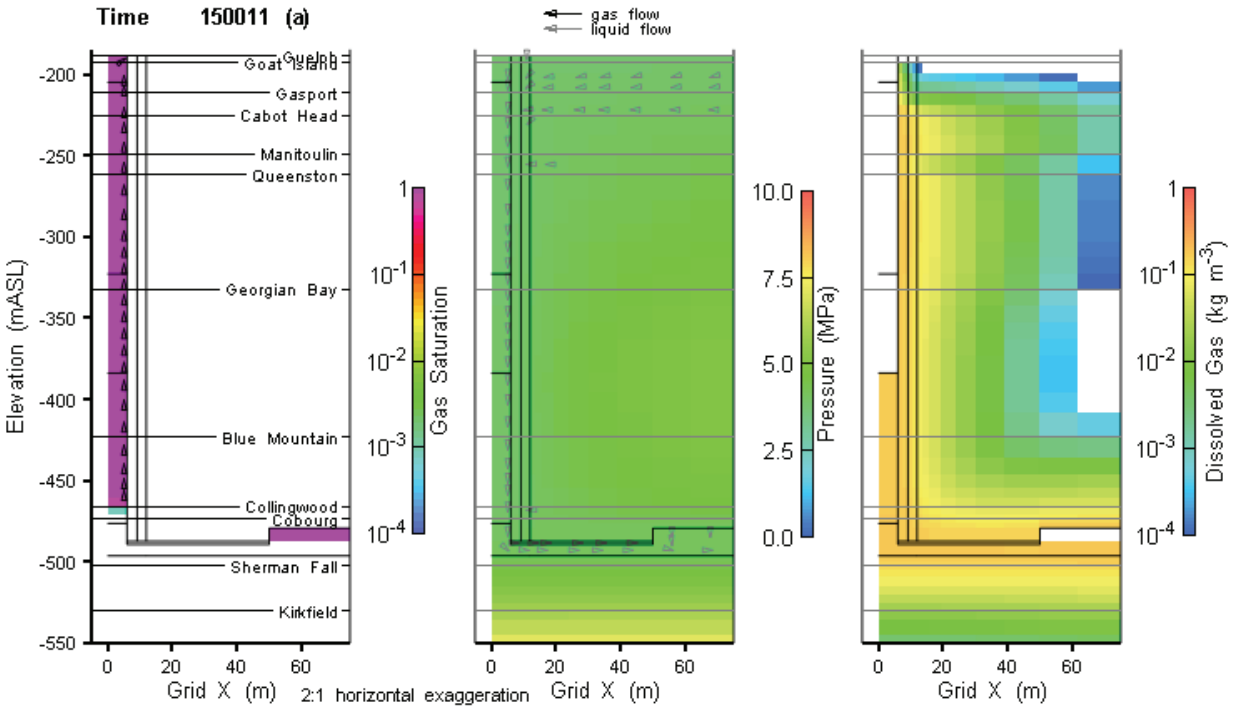

Figure 6.8: SF-BC: 3DSRS Model Shaft Saturations, Flows and Pressures (125,000 a)

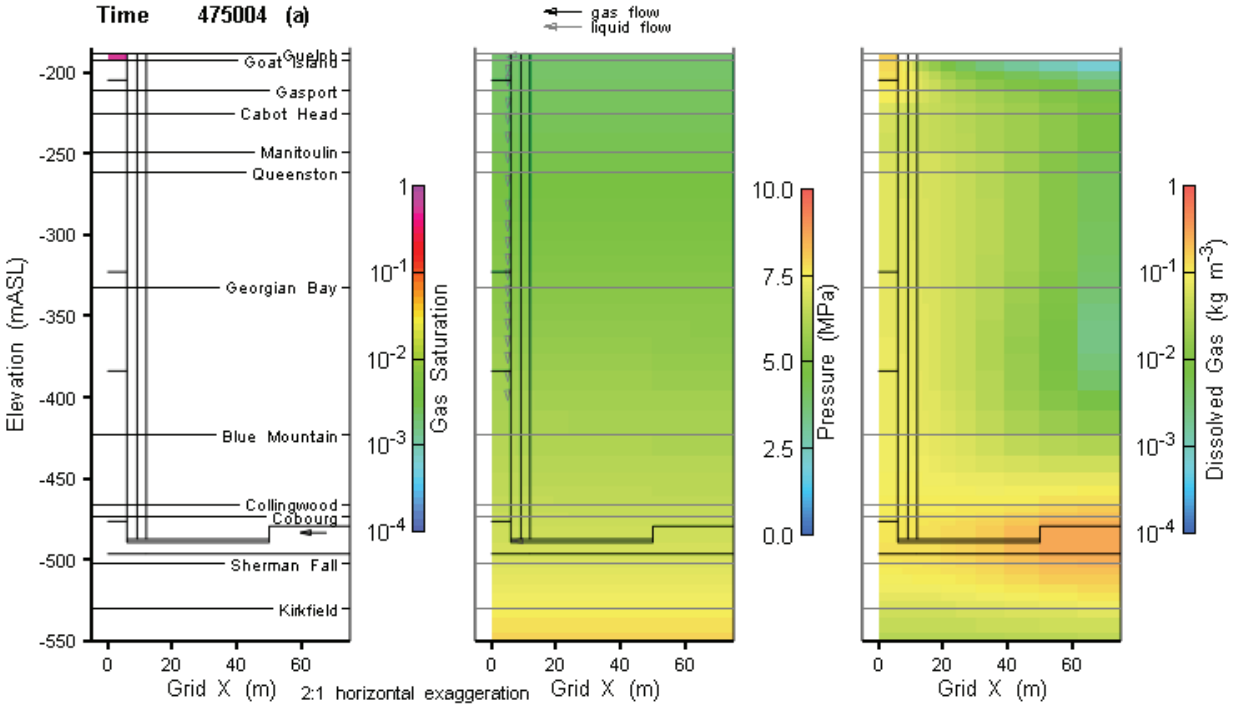

Figure 6.9: SF-BC: 3DSRS Model Shaft Saturations, Flows and Pressures (475,000 a)

A time profile of gas flow in the shaft is presented in Figure 6.10

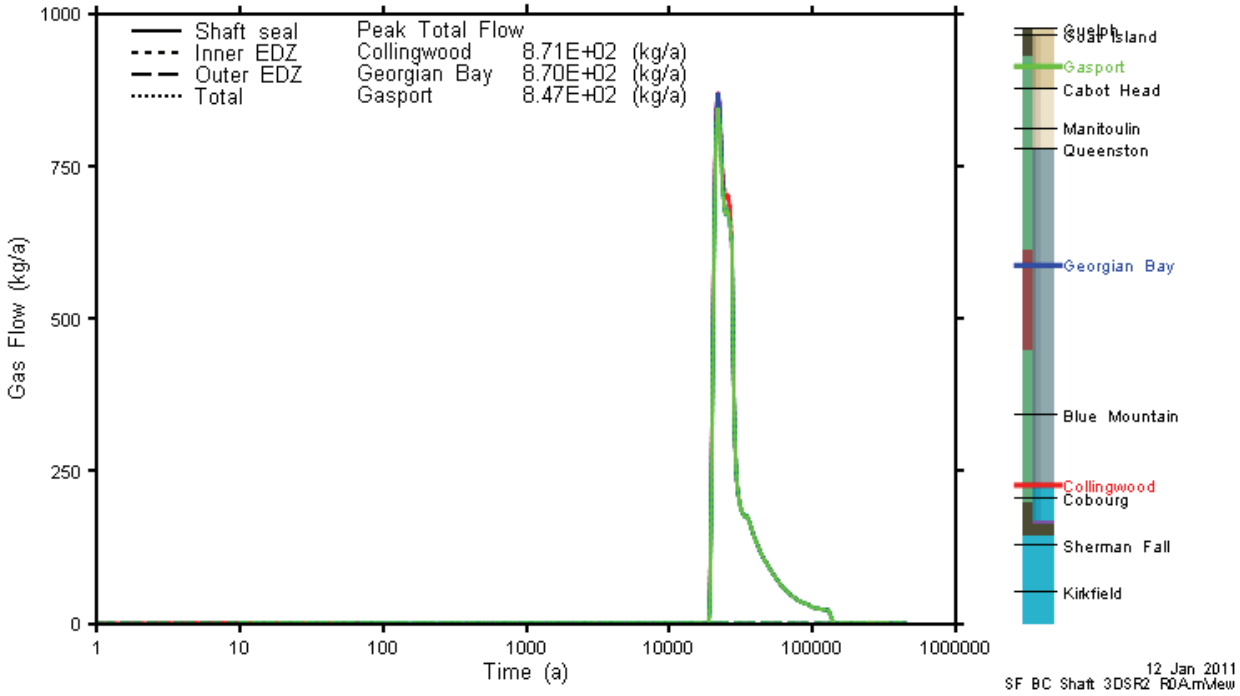

Figure 6.10: SF-BC: 3DSRS Model Shaft Gas Flow at Selected Monitoring Planes

There is no dissolved gas transport up the shaft, as liquid flow is down the shaft for the duration of the simulation. Dissolved gas may start to flow up the shaft at late times (beyond 500,000 a) and at very low rates.

In evaluating the SF-BC case, an important point to remember is the parameterization of the shaft gas transport properties. As specified, the zero capillary pressure in the shaft seal materials has two significant implications:

1. Once gas reaches the shaft through the HDZ, it forms an almost immediate pathway up through the shaft, and moves quickly upwards due to buoyancy; and
2. Unlike Normal Evolution cases with gas transport up the shaft, there is little likelihood that a significant fraction of the gas would discharge from the shaft into the more permeable Guelph or Salina A1 upper carbonate formations. The majority of the gas flux measured at the Gasport will discharge directly into the shaft backfill at the bottom of the Shallow Bedrock Groundwater Zone.

For these reasons, the 2DRS model was not run for the SF-BC case. Results of the 3DSRS model indicated that gas flow measured in the shaft would likely be continuous to the top of the Silurian system.

However, if the SF-BC case was parameterized with a similar capillary pressure relationship to intact bentonite/sand, but with a reduced air-entry pressure as per the Davies relationship (see Section 4.2.1), the pressure threshold for transport would be increased, and the rate of

transport possibly decreased. Furthermore, depending upon the exact relationship of the capillary pressure curves, the Guelph and Salina A1 upper carbonate may also act as complete or partial gas sinks, reducing the mass flux to the Shallow Bedrock Groundwater Zone.

6.1.2.2 Repository System

Figure 6.11 presents SF-BC repository pressures and liquid saturations compared to NE-SBC results. Cumulative gas and liquid flows are shown in Figure 6.12. Liquid inflows are primarily through the shaft, as is all gas outflow.

6.1.2.3 Geosphere

Geosphere impacts of the SF-BC model are significant, as shown in Figure 6.13. Pressures above the repository are influenced by the low shaft pressures.

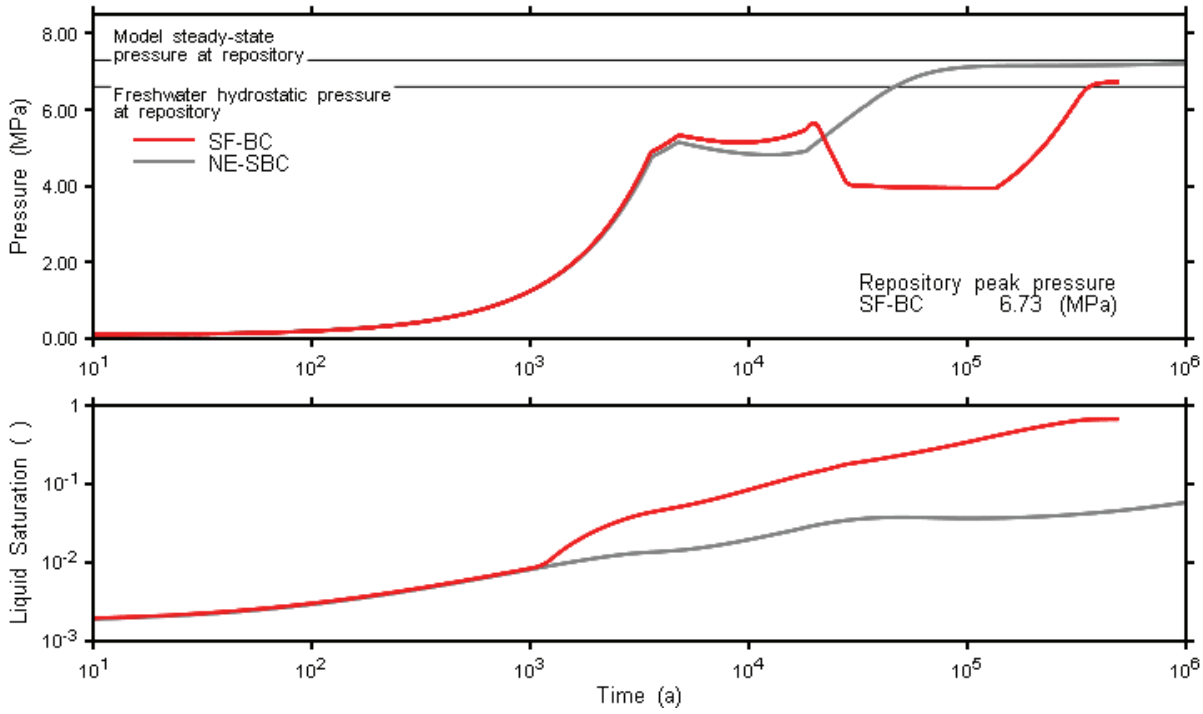

Figure 6.11: SF-BC: 3DSRS Model Repository Pressure and Saturation

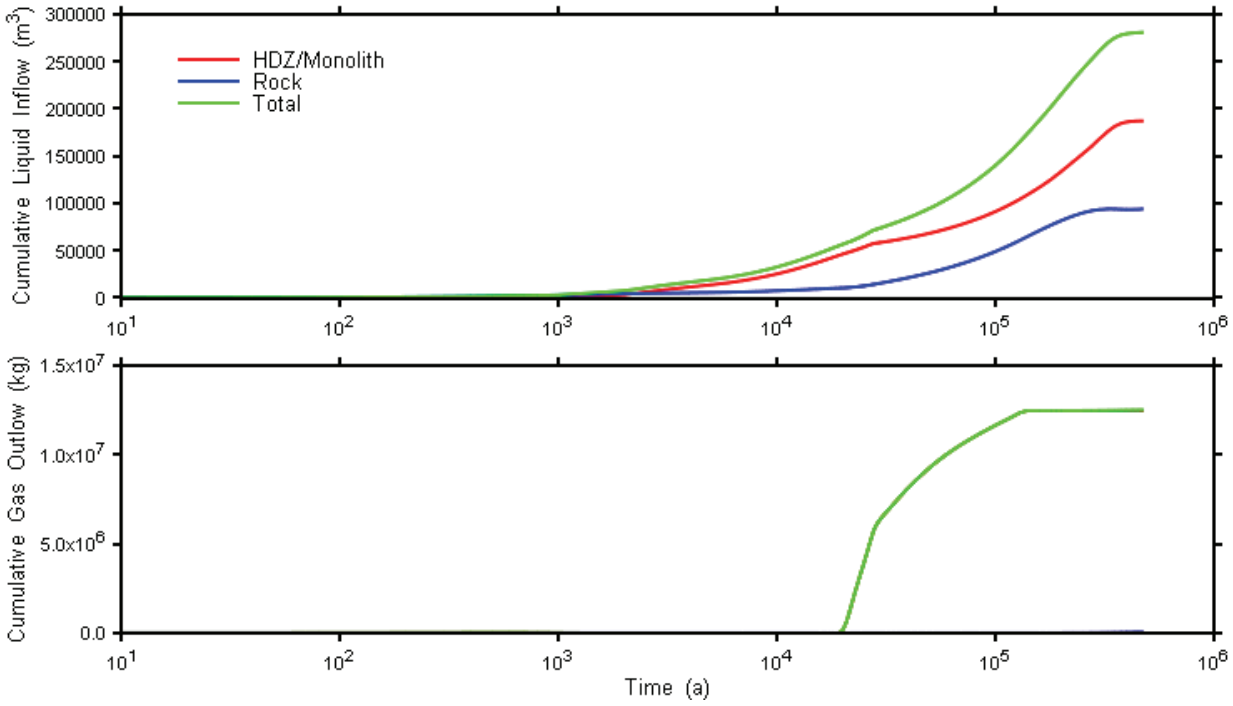

Figure 6.12: SF-BC: Repository Liquid Inflow and Gas Outflow

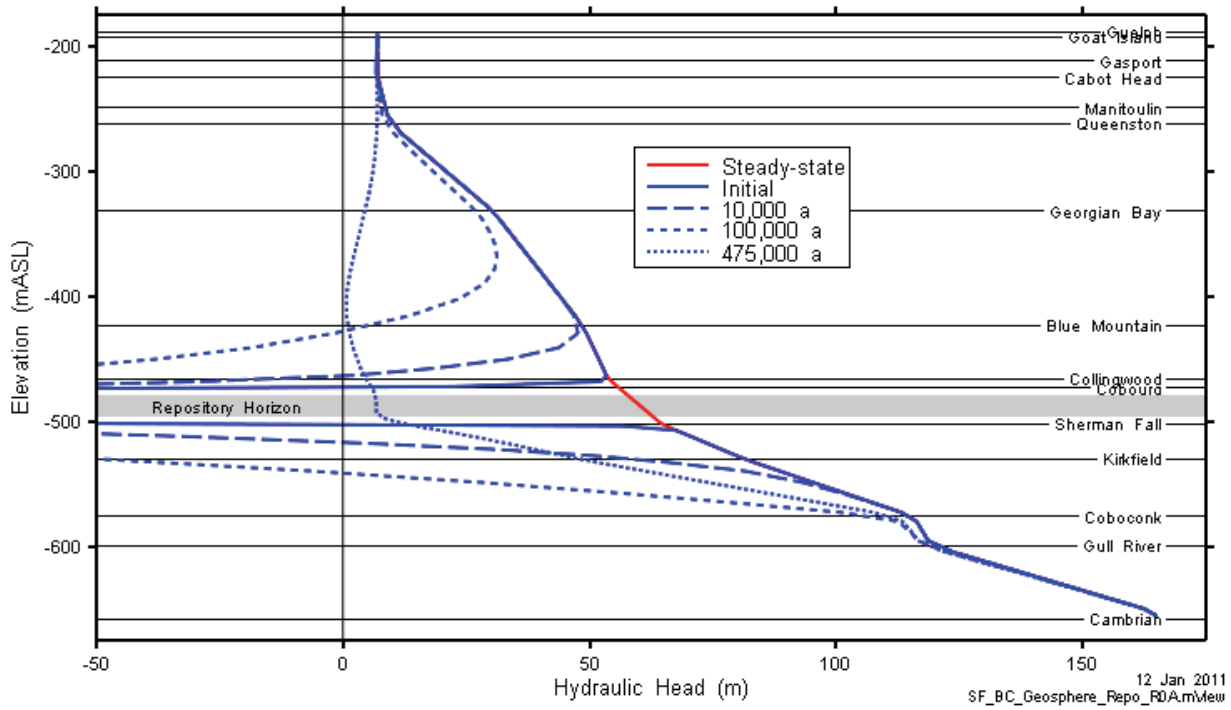

Figure 6.13: SF-BC: 3DSRS Geosphere Head Profile

6.2 SF-ED Shaft Seal Failure – Extra Degradation Case (10^{-7} m/s)

The Severe Shaft Seal Failure-Extra Degradation (SF-ED) case assumes more conservative values for shaft seal hydraulic conductivity (10^{-7} m/s) in order to understand the sensitivity of the model performance to shaft seal properties. Simulations were performed with the 3DSRS model.

6.2.1 Gas Generation

The high permeabilities in the shaft and EDZ allow much more water to flow into the repository than for the NE-SBC case. This influx of water causes the gas pressure within the repository to build up far more rapidly. A peak in water saturation of approximately 85% at 500 a is followed by a peak in gas pressure of 7.6 MPa shortly afterwards at 1000 a (see Figure 6.14 and Figure 6.15). This build-up in pressure causes a pulse of gas to leave the repository at approximately 1100 a (see Figure 6.16). As a result of the slightly earlier higher CO_2 partial pressures in this case approximately double the amount of siderite is produced compared to the Simplified Base Case and SF-BC cases (Figure 6.17).

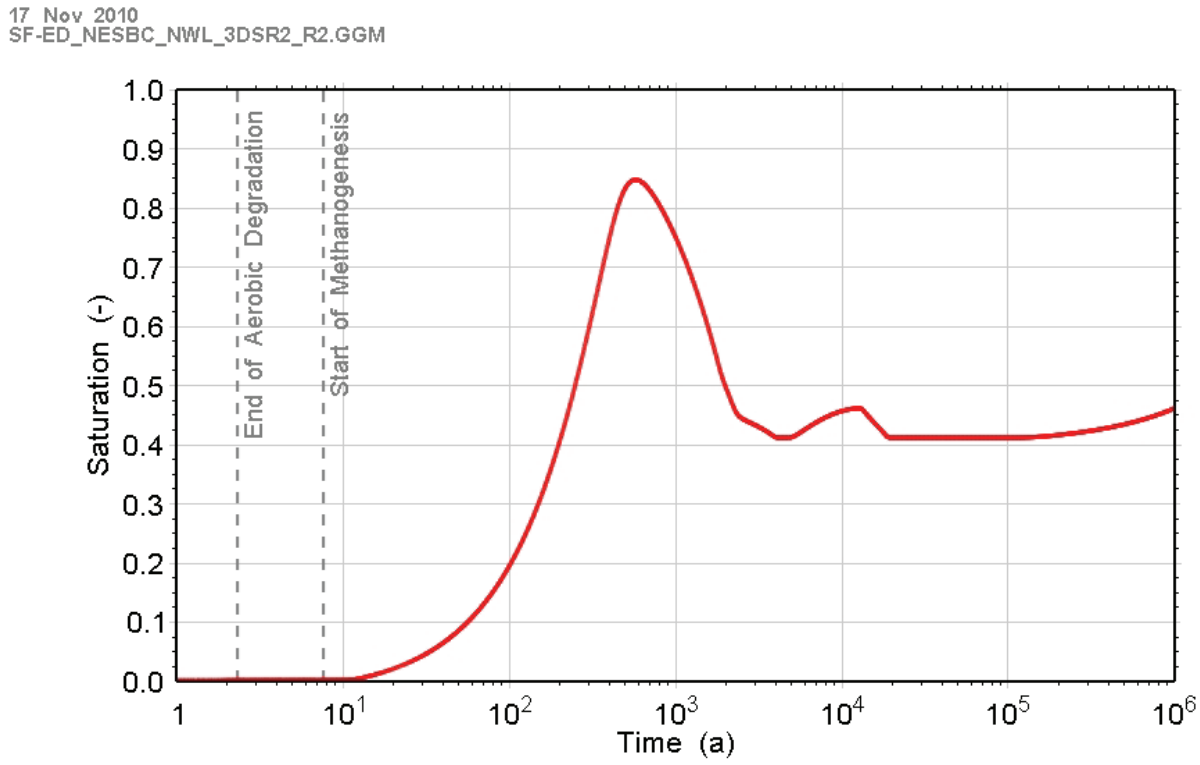

Figure 6.14: SF-ED: Water Saturation

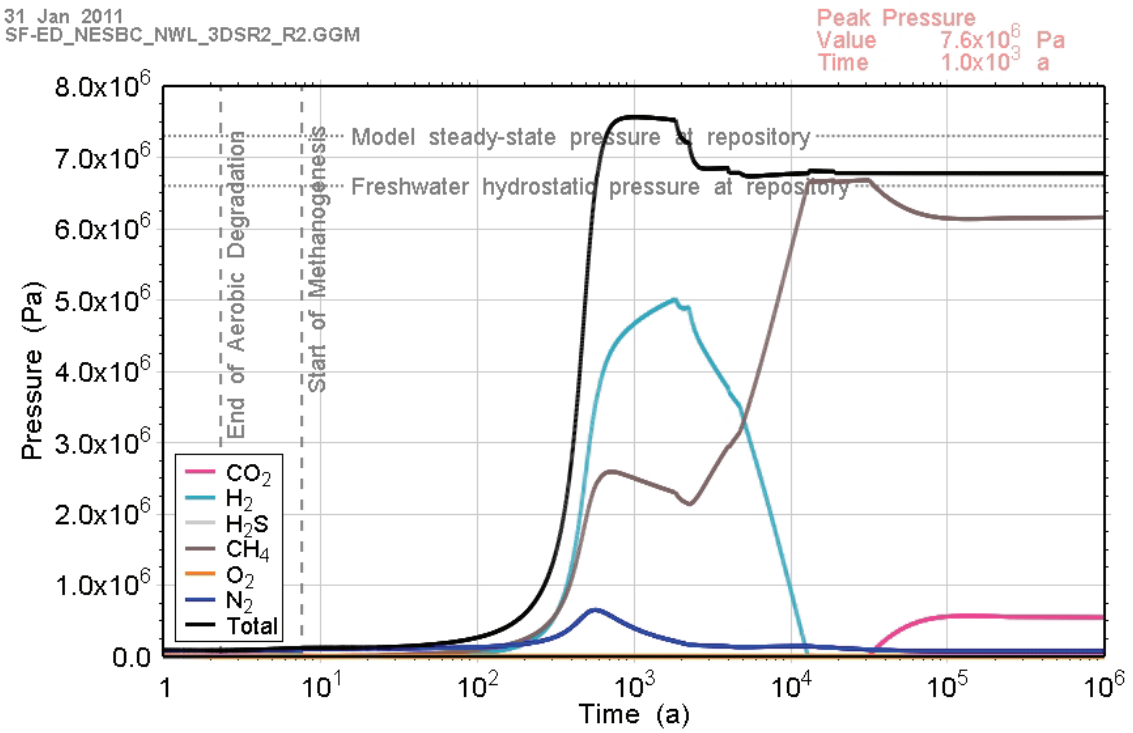

Figure 6.15: SF-ED: Total and Partial Gas Pressures within the Repository

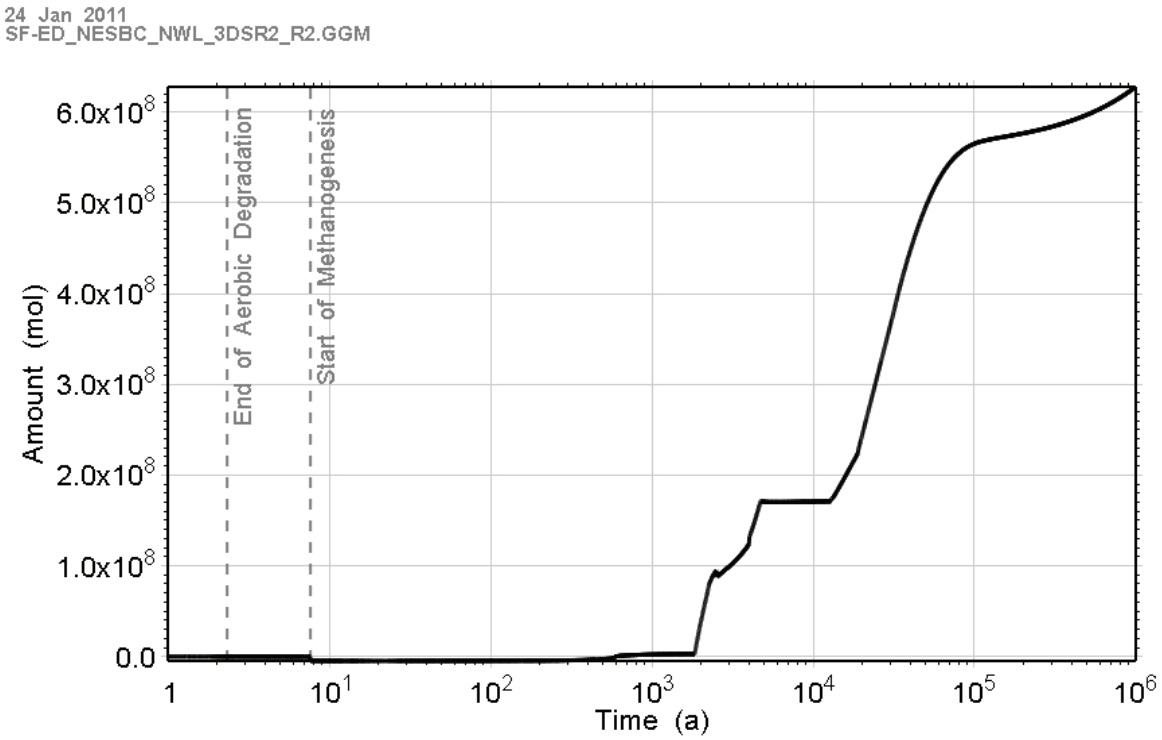

Figure 6.16: SF-ED: Total Amount of Gas that has Left the Repository

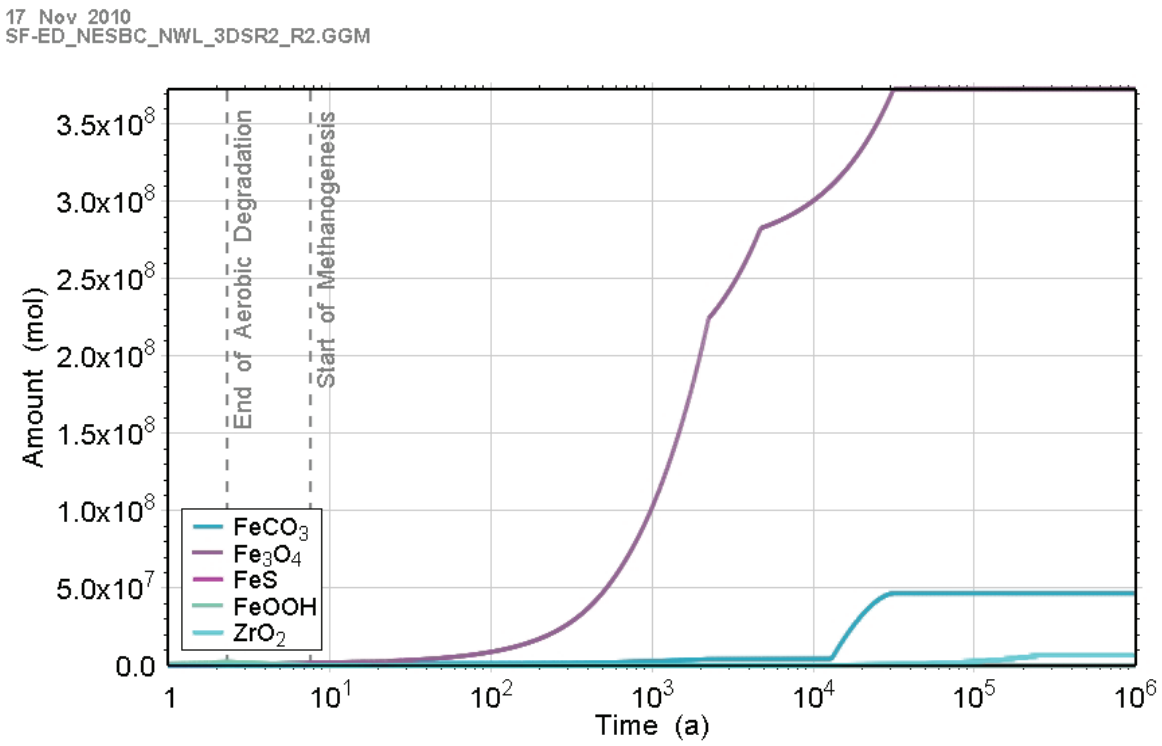

Figure 6.17: SF-ED: Amounts of Corrosion Products

6.2.2 Gas and Water Flows

SF-ED results are strongly dependent on the geometry assumptions made for the case. Specifically, the assumption of instant rockfall leads to a repository with significant void space at an elevation higher than the monolith HDZ. This "headspace" is available to trap generated gas after the water level in the repository rises above the top of the HDZ. In an alternative conceptual model, where rockfall has not occurred, generated gas would not build up in the headspace, but would instead leave the repository through the HDZ as it was generated. This would result in earlier, but lower, peak mass flow rates.

The general sequence of gas and water flows in this case is as follows: virtually instantaneous resaturation of the shaft, and initial saturation of the repository from shaft inflows, sourced from the permeable Guelph Formation. The water level in the repository rises above the top of the HDZ. Subsequent gas generation is trapped in the rockfall void. As sufficient gas is generated to cause gas pressures to exceed the shaft pressure, the gas forces water out of the repository through the HDZ and up the shaft, creating an initial pulse of contaminated water with high mass flows of dissolved gas. Eventually gas generation has proceeded to the point that the water level in the repository drops below the top of the HDZ. At this point, gas flows through the HDZ and up the shaft in a large initial pulse. Subsequent changes in gas generation rates cause additional pulses to occur at later times.

6.2.2.1 Shaft

The shaft is fully resaturated within 10 a (Figure 6.18). Groundwater flow is down the shaft and into the repository.

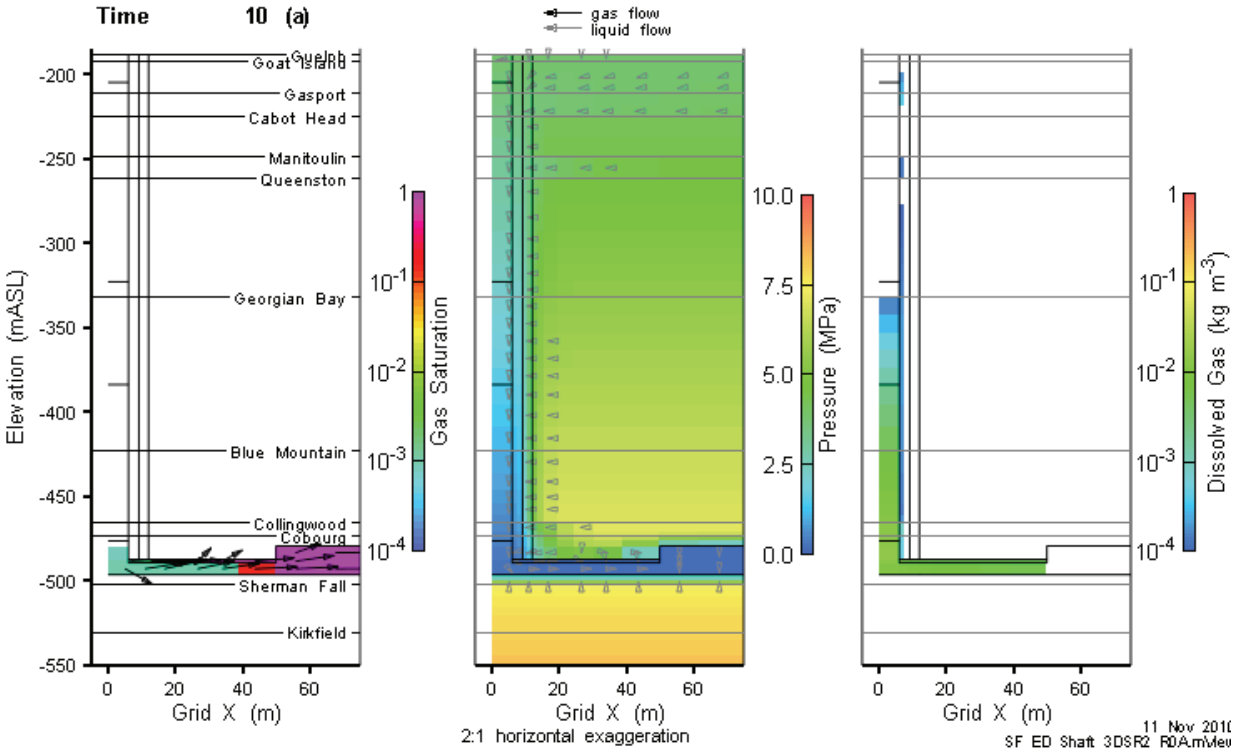

Figure 6.18: SF-ED: 3DSRS Model Shaft Saturations, Flows and Pressures (10 a)

Within 300 a, the groundwater level is above the top of the HDZ. At 500 a, the repository reaches a peak liquid saturation of approximately 85%, at a height well above the top of the HDZ (Figure 6.19). Subsequently, gas generation processes start to increase gas volumes and pressures, pushing water out of the head space, and subsequently up the shaft. Liquid flow directions are reversed at 600 a, with a maximum gas pressure of 7.6 MPa reached by 900 a (Figure 6.20).

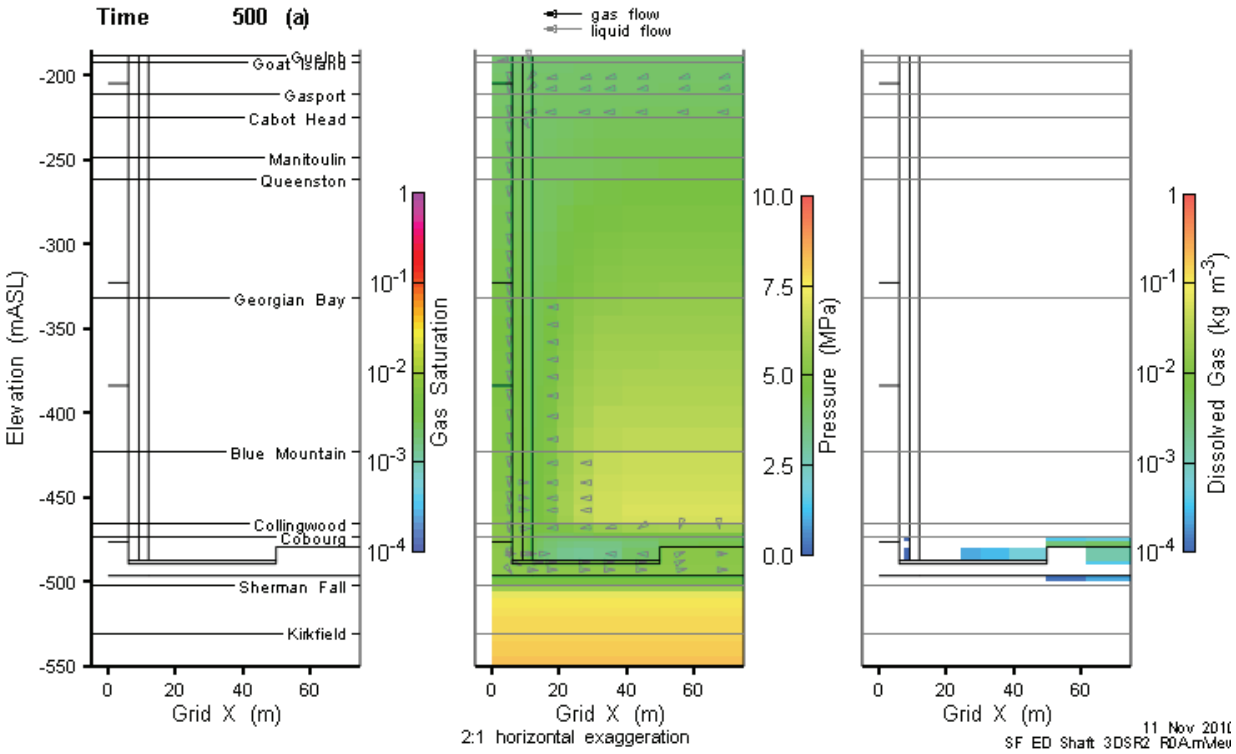

Figure 6.19: SF-ED: 3DSRS Model Shaft Saturations, Flows and Pressures (500 a)

For the next 950 a, contaminated water is pushed out from the repository and up the shaft. As shown in Figure 6.21 (at 1800 a), free gas exsolves from this water as it rises up the shaft and pressure is reduced.

Between 1800 a and 1850 a, repository water levels drop below the top of the HDZ and gas is transmitted through the HDZ and into the shaft, where it quickly develops a pathway through the shaft sealing material (Figure 6.22).

A time profile of gas flow is presented in Figure 6.23. Note that the results from all monitoring planes are visually identical. The overpressure in the repository is dissipated as gas escapes, with gas flow rates reducing significantly from the peak. A second, short duration, but high magnitude peak, occurs at approximately 4000 a. After that peak, gas continues to flow up the shaft at significant rates until approximately 4750 a, at which time flow drops to near zero. This level is maintained until approximately 13,000 a, when increased gas generation causes a second series of gas flows. This second series also includes a single, very short duration peak.

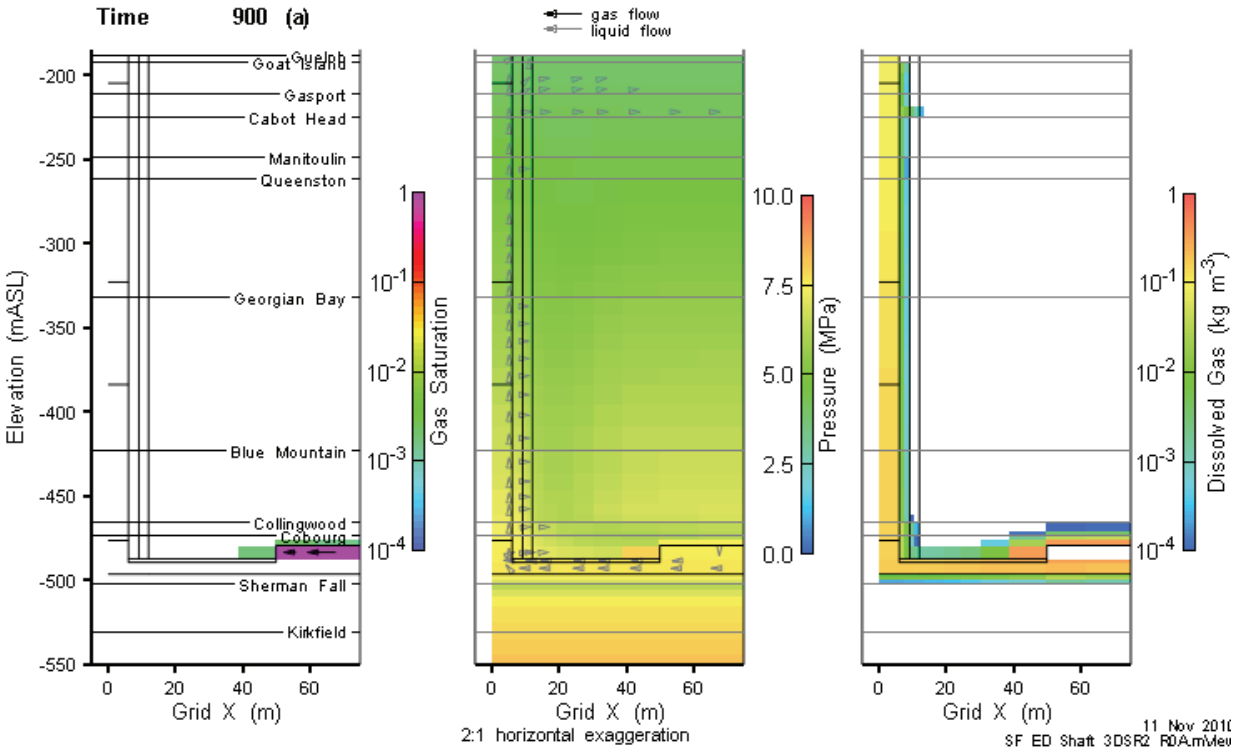

Figure 6.20: SF-ED: 3DSRS Model Shaft Saturations, Flows and Pressures (900 a)

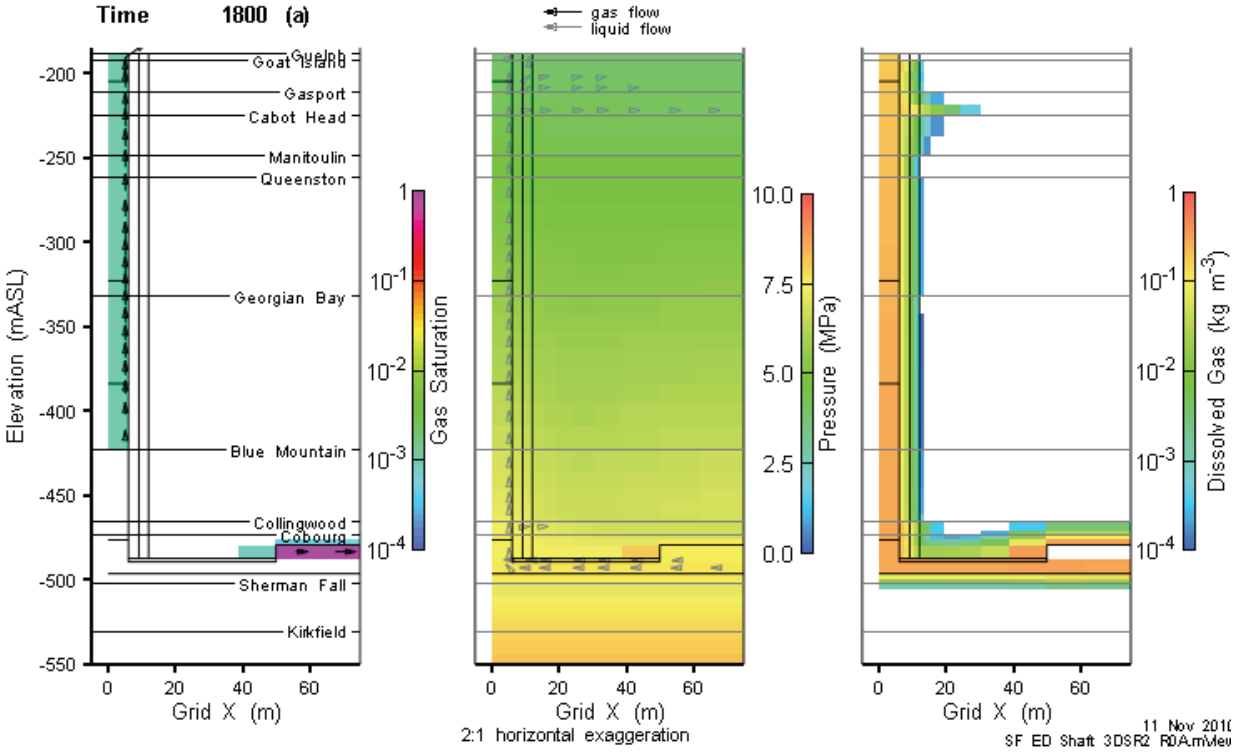

Figure 6.21: SF-ED: 3DSRS Model Shaft Saturations, Flows and Pressures (1800 a)

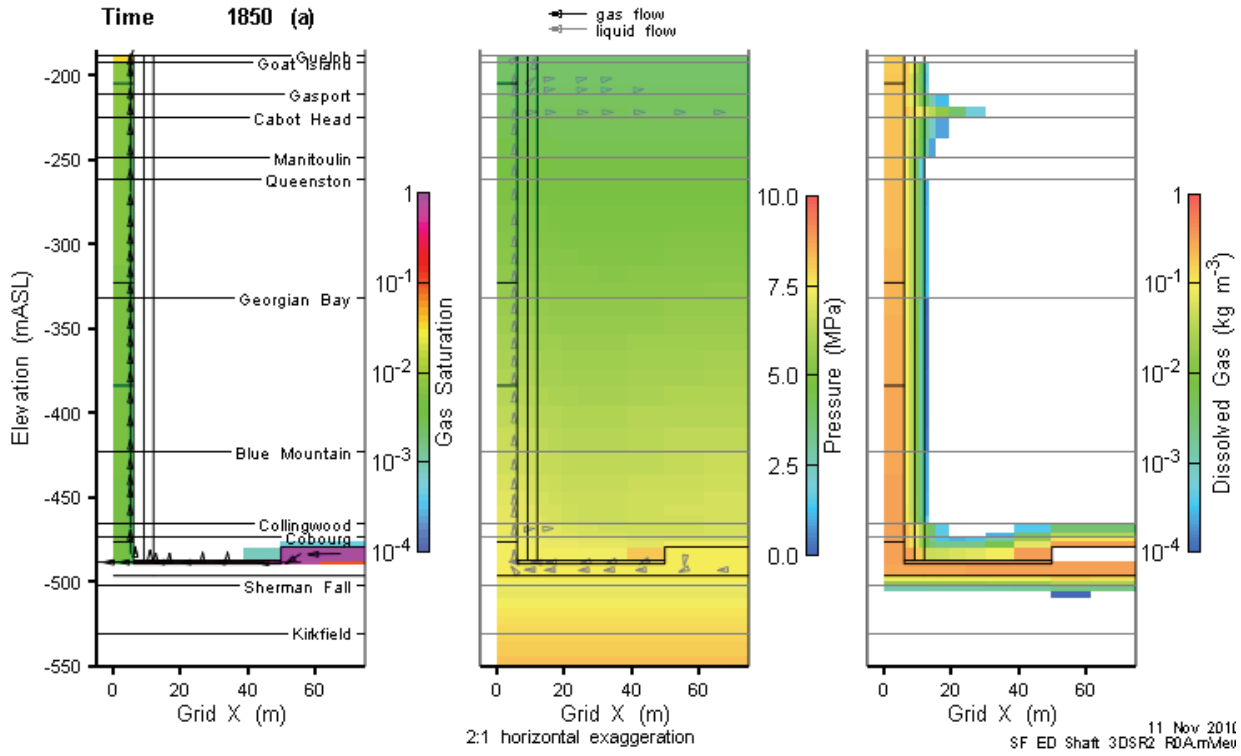

Figure 6.22: SF-ED: 3DSRS Model Shaft Saturations, Flows and Pressures (1850 a)

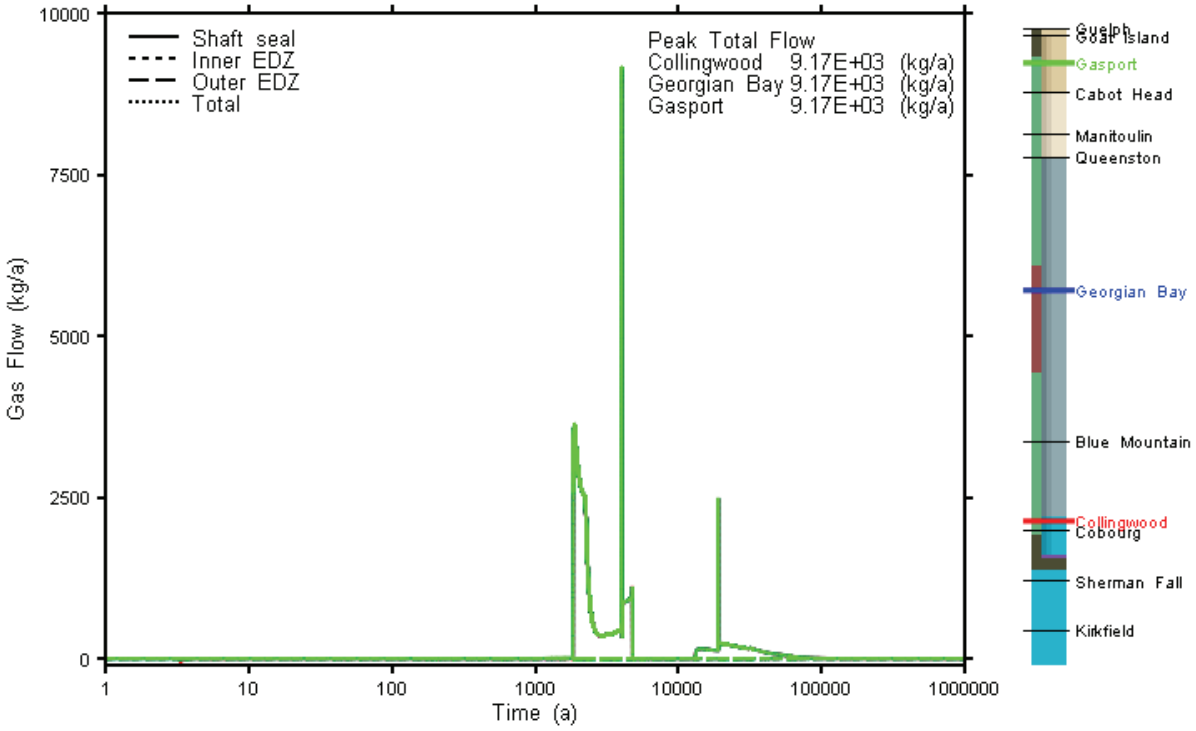

Note: Results from all planes overlap.

Figure 6.23: SF-ED: 3DSRS Model Shaft Gas Flow at Selected Monitoring Planes

As for the SF-BC case, there is no capillary pressure in the shaft material. For the same reasons as the SF-BC case, there was no requirement to simulate the SF-ED case with the 2DRS model. The gas flux measured at the Gasport will discharge directly into the shaft backfill at the bottom of the Shallow Bedrock Groundwater Zone, as the permeability of the shaft is higher than that of any of the Silurian formations.

A time profile of dissolved gas flow is presented in Figure 6.24. The peak dissolved gas flow occurs during the initial outflow of water from the repository as the headspace is pressurized.

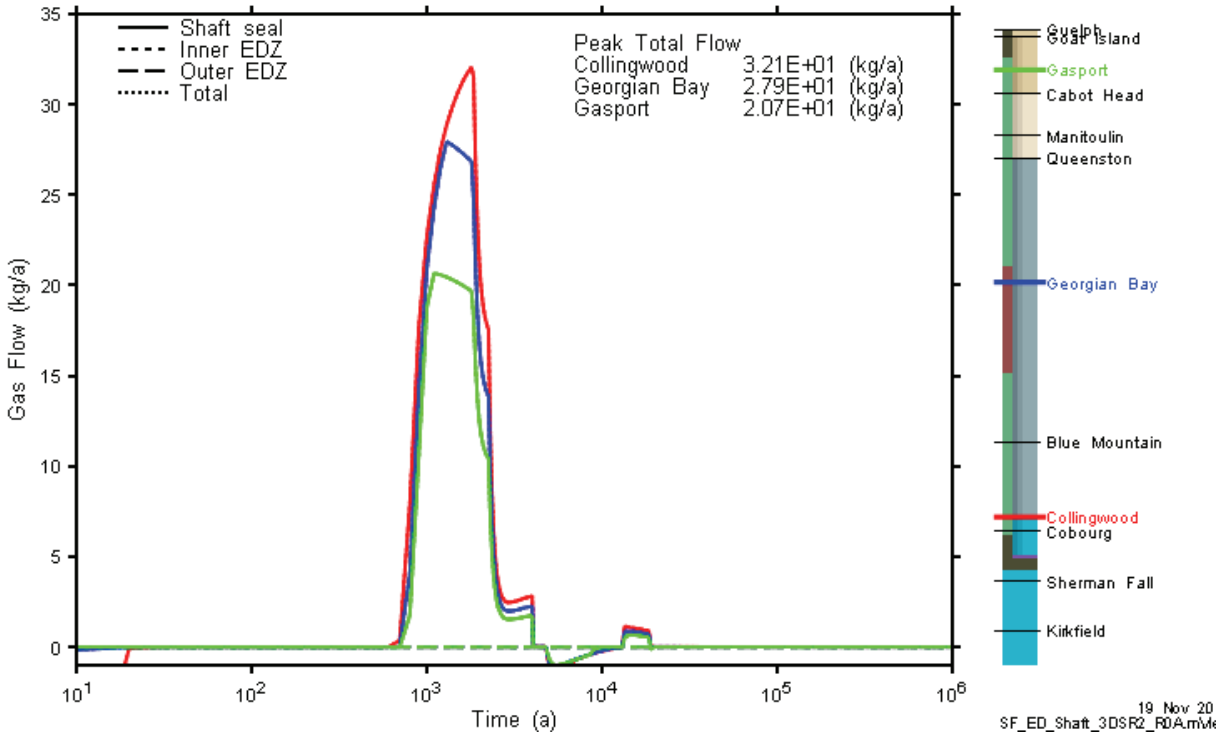

Figure 6.24: SF-ED: 3DSRS Model Shaft Dissolved Gas Flow at Selected Monitoring Points

6.2.2.2 Repository System

Figure 6.25 presents SF-ED repository pressures and liquid saturations in comparison to NE-SBC results. The long-term pressure achieves a near steady-state response between the initial geosphere steady-state, and freshwater hydrostatic pressure. This reflects the influence of the high-permeability shaft in modifying the geosphere pressure profile.

Cumulative gas and liquid flows are shown in Figure 6.26. Inflow and outflows are nearly entirely through the shaft. The rock makes a contribution to liquid inflows after repository pressures are below those of the surrounding geosphere, beyond 10,000 a.

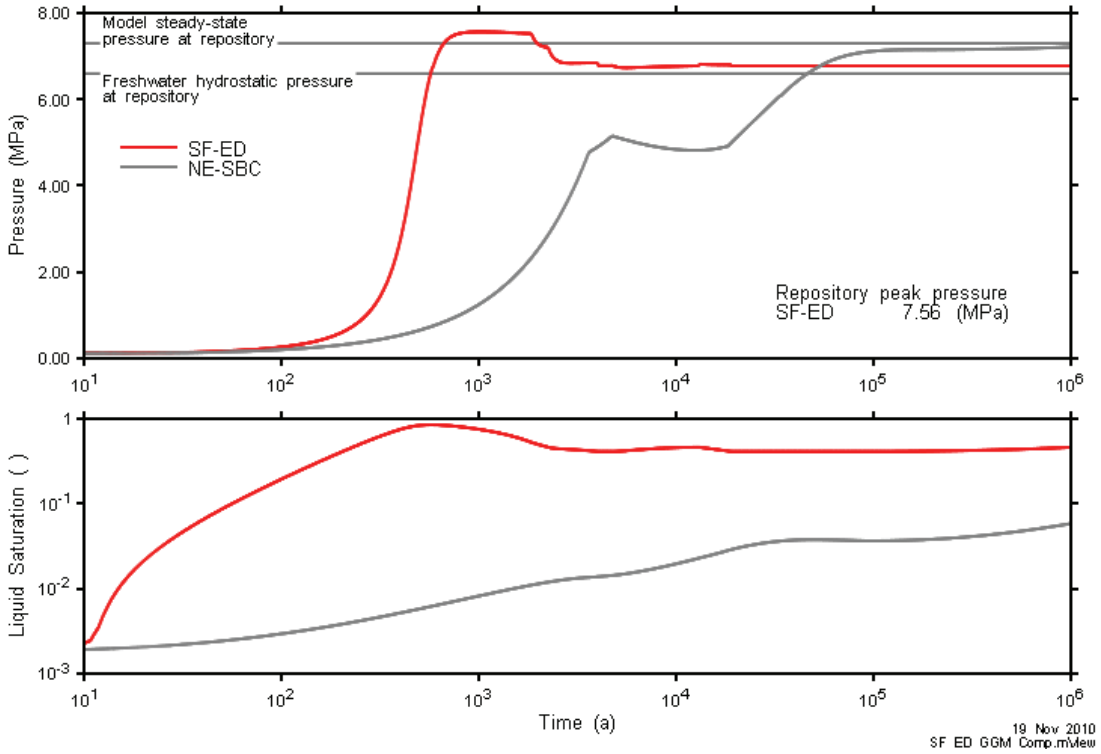

Figure 6.25: SF-ED: 3DSRS Model Repository Pressure and Saturation

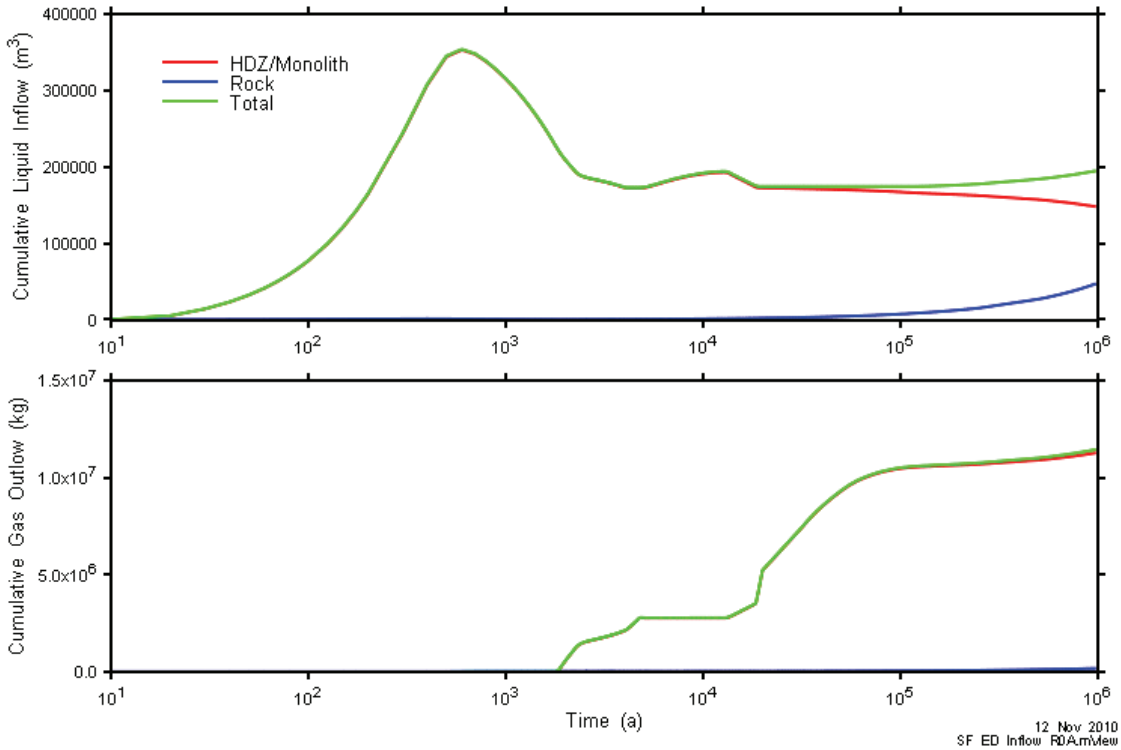

Figure 6.26: SF-ED: Repository Liquid Inflow and Gas Outflow

6.2.2.3 Geosphere

As shown in Figure 6.27, the long-term underpressure of the repository relative to the geosphere results in depressurization of the geosphere over an interval of approximately 100 m above and below the repository. Late time repository pressures are higher than for the SF-BC case, so the depressurization does not extend as far.

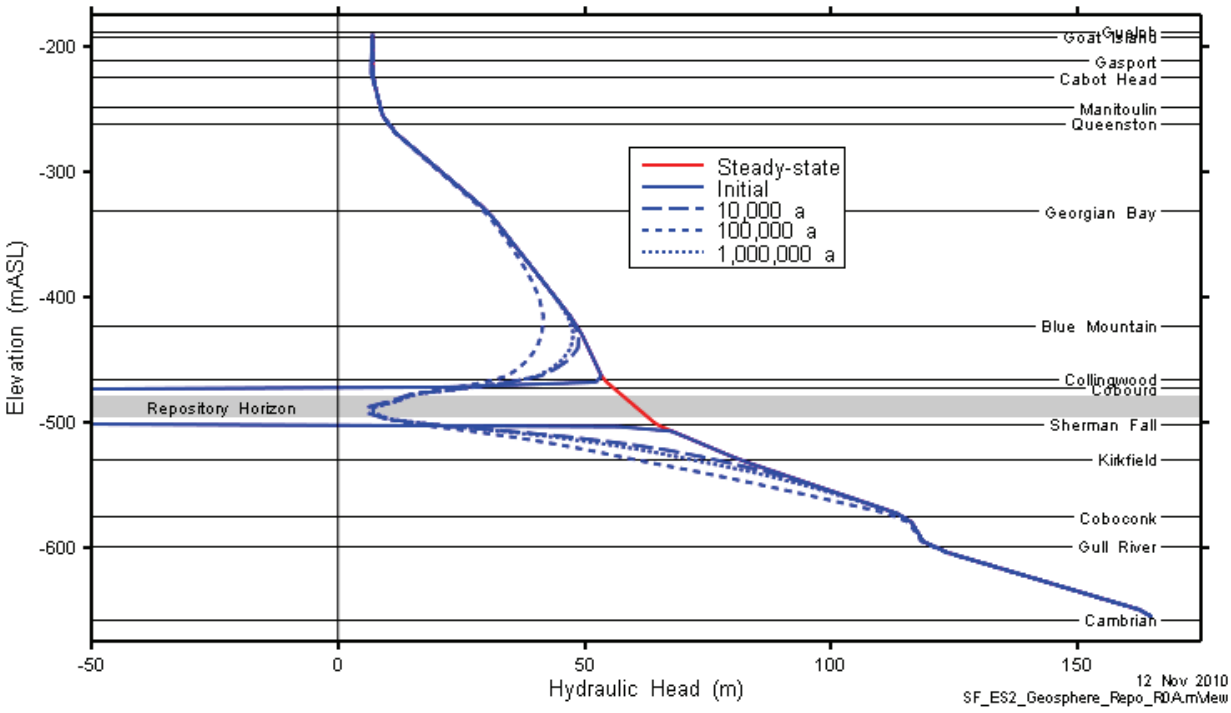

Figure 6.27: SF-ED: 3DSRS Geosphere Head Profile

7. RESULTS FOR WATER-LIMITED CALCULATION CASES

This section provides a brief discussion of results from water-limited (WL) simulations. Most WL simulations share a characteristic pressure and resaturation profile. Pressure build-up in the repository is significantly delayed relative to the corresponding non-water-limited (NWL) case, and the repository never reaches an overpressured condition relative to the geosphere. As a consequence, water flow is always into the repository from the surrounding geosphere and from the shaft. Initial repository liquid saturations are quickly consumed, after which saturation is maintained at a virtually "dry" level until water consuming reactions are complete. While the repository is virtually dry, water consuming corrosion and degradation processes are limited by the rate at which water is supplied to the repository from the geosphere, slowing gas generation. This can affect the balance of gases within the repository at intermediate times, but most WL cases complete with a similar gas composition to their NWL counterpart.

The vapour phase gas generation processes are dependent on the relative humidity, which can change rapidly once water is consumed and which can undergo small fluctuations. To help with the stability of T2GGM, methane biomass generation was switched off for some of the WL cases. It can be seen for the equivalent NWL cases that methane biomass generation played only a very minor role and so this does not greatly influence the results.

Only a subset of WL results is described in detail, with comparison of most cases presented in summary only.

7.1 NE-RC - Reference Case

The NE-RC WL case was simulated with 3DD, 3DSRS and 3DSR models.

7.1.1 Gas Generation

Results for the 3DSRS model are presented here. Unlike the NWL variant, the saturation drops to a virtually dry state at approximately 400 a due to consumption of water by gas generation reactions. The relative humidity then drops towards the lower threshold at which vapour phase reactions become inactive (60%) (see Figure 7.1 and Figure 7.2). Water consuming organic degradation and metallic corrosion processes then become limited by the rate at which water enters the repository from geosphere, so that corrosion of metallic waste streams and degradation of organic waste streams proceeds more slowly than the NWL variant case. Virtually all corrosion and degradation has halted by 200,000 a (see Figure 7.3 and Figure 7.4). The gas pressure builds very slowly, reaching 6.7 MPa at 1,000,000 a. The slow rate of organic degradation causes the repository to become CO_2 limited, so that the repository atmosphere contains both CH_4 and H_2 at 1,000,000 a (Figure 7.5). As with the NWL variant, gas bleeds from the rock into the repository over the 1 Ma time period.

The 3DSR results are almost the same, but for a brief recovery in relative humidity around 300,000 a. This allows corrosion and degradation to accelerate briefly. As more CO_2 is produced and the microbial methane generation reaction restarts, the H_2 in the repository is consumed leaving the final atmosphere methane dominated.

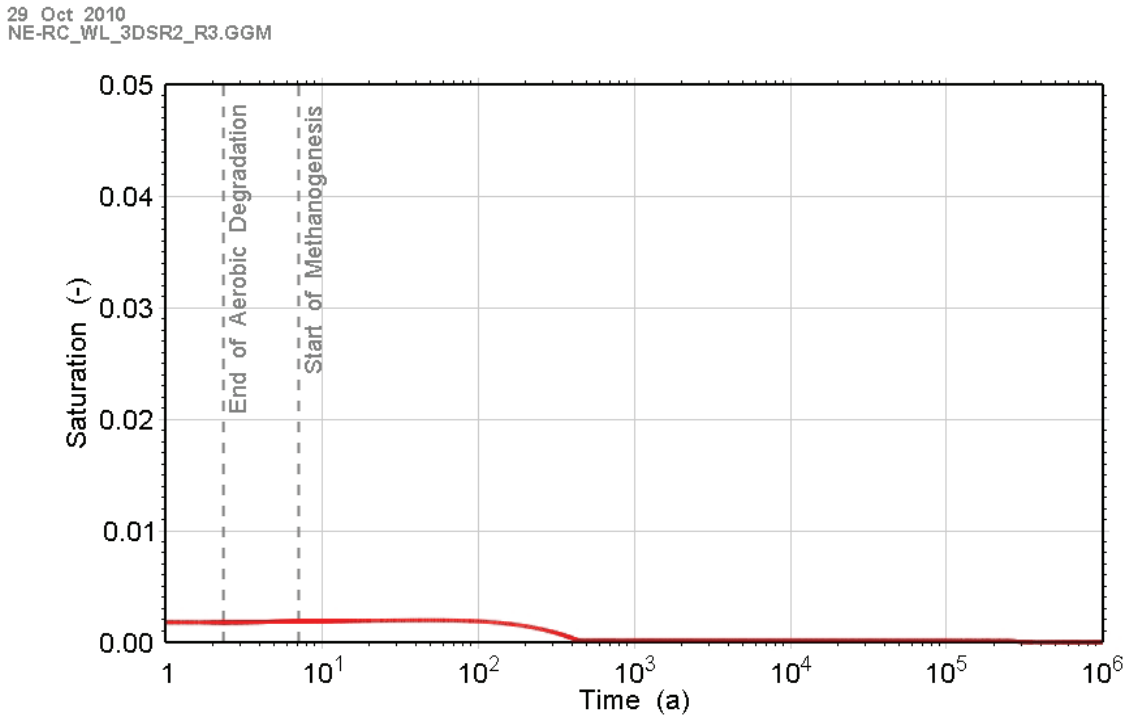

Figure 7.1: NE-RC WL: Water Saturation

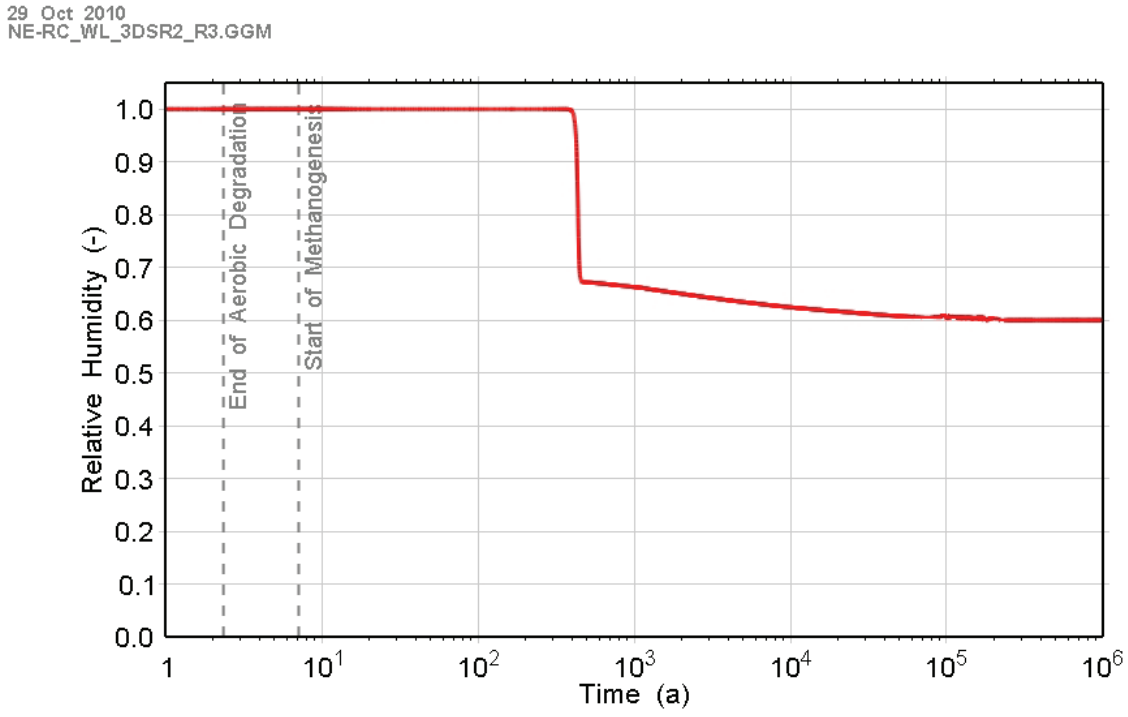

Figure 7.2: NE-RC WL: Relative Humidity

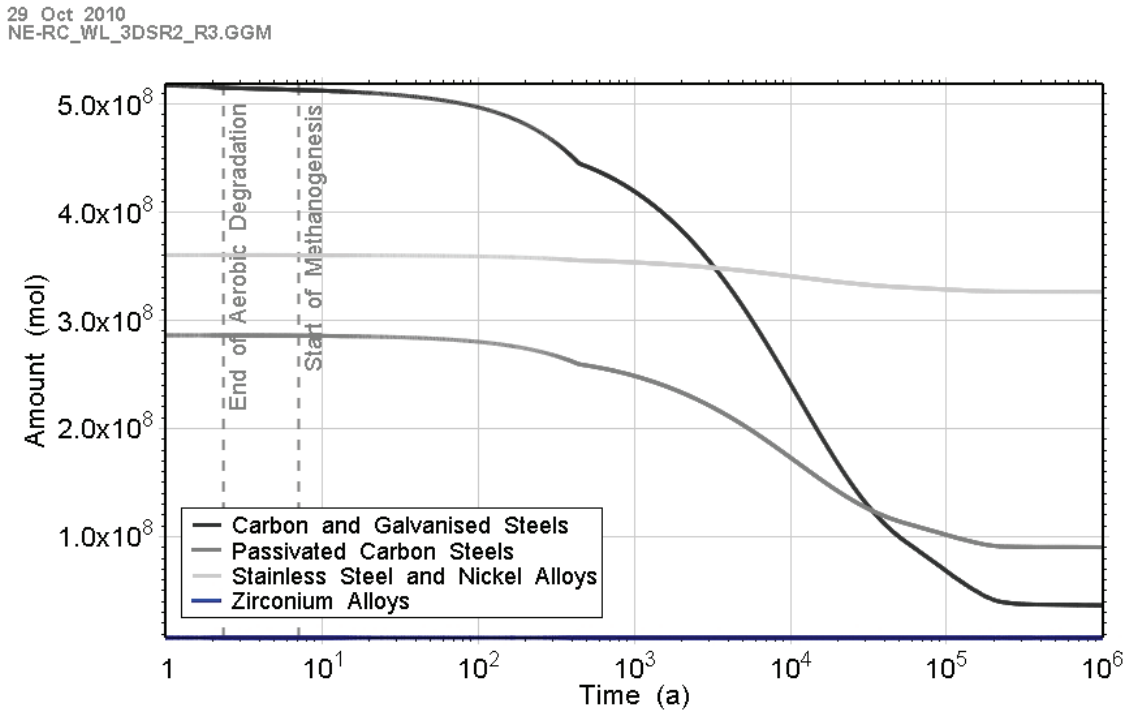

Figure 7.3: NE-RC WL: Amounts of Metallic Waste

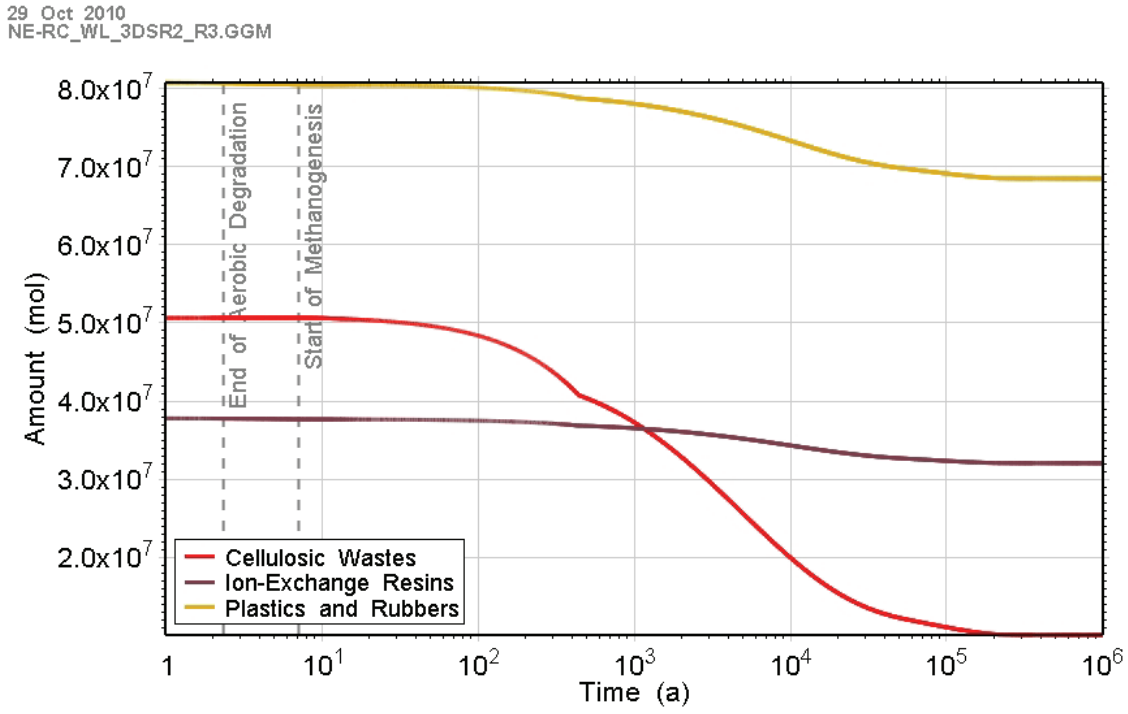

Figure 7.4: NE-RC WL: Amounts of Organic Waste

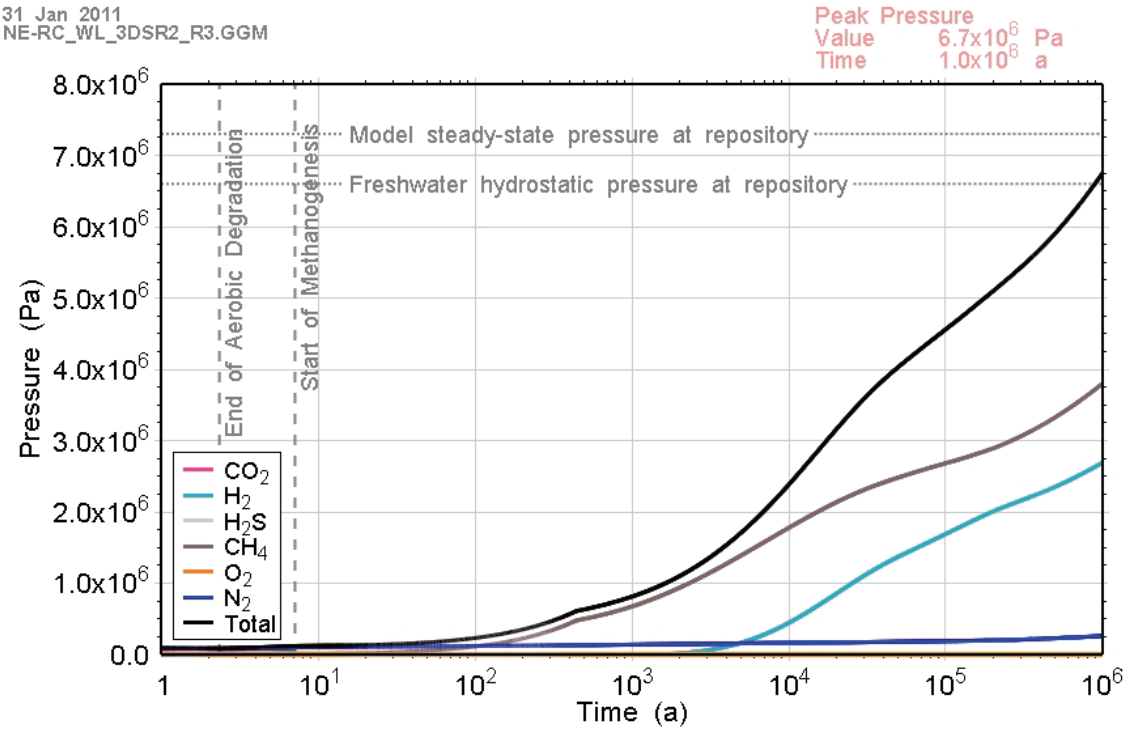

Figure 7.5: NE-RC WL: Total and Partial Gas Pressures within the Repository

7.1.2 Gas and Water Flows

Figure 7.6 presents NE-RC WL repository pressures and liquid saturations in comparison to NWL results. The WL 3DD and 3DSRS pressure responses are visually coincident, while saturation curves are very similar. The 3DSR WL pressure shows a slight excursion at 300,000 a, coincident with the brief period of higher RH noted in the previous section. In comparison to the NWL results, pressures are lower, and there is a long-period of near-zero saturation while gas generation reactions proceed at a reduced (RH limited) rate.

Cumulative gas and liquid flows are shown in Figure 7.7. The shaft makes a significant contribution to liquid inflows only for the 3DD model, although gas inflows are similar for both models.

Figure 7.8 shows a characteristic flow regime, with gas and water from the formation entering the shaft, and then flowing down the shaft to the HDZ and tunnel leading to the repository.

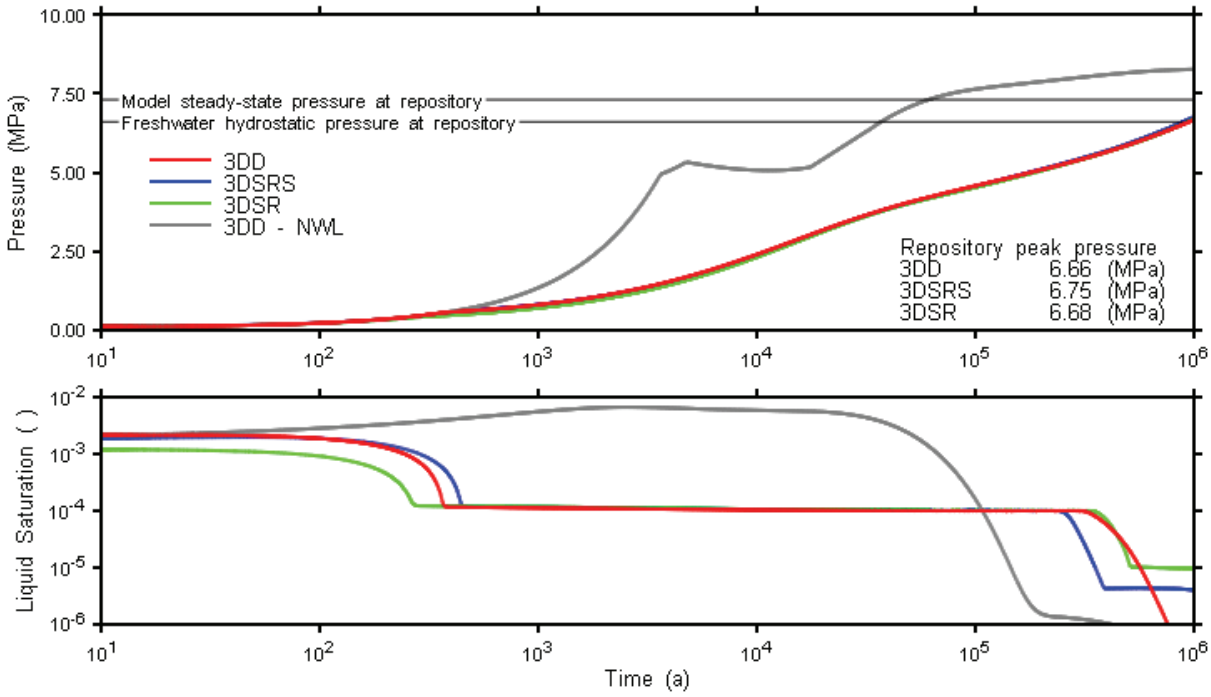

Figure 7.6: NE-RC WL: 3DD, 3DSRS and 3DSR Model Repository Pressure and Saturation

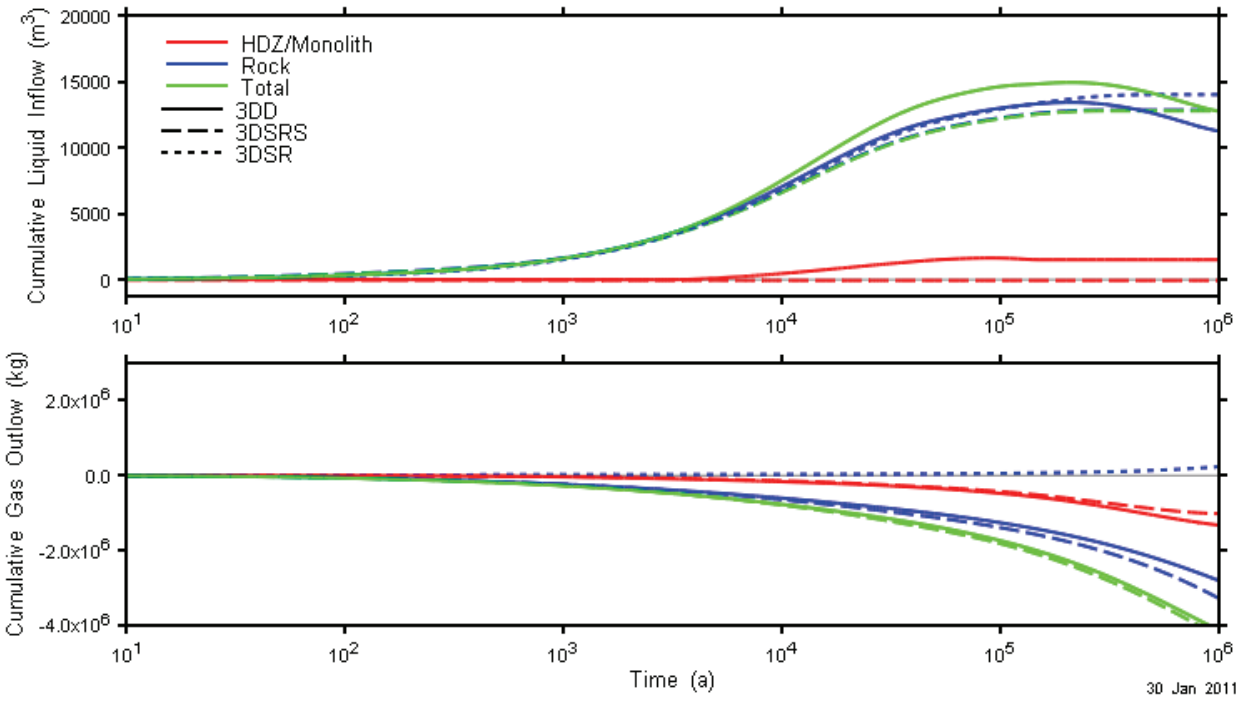

Figure 7.7: NE-RC WL: Repository Liquid Inflow and Gas Outflow

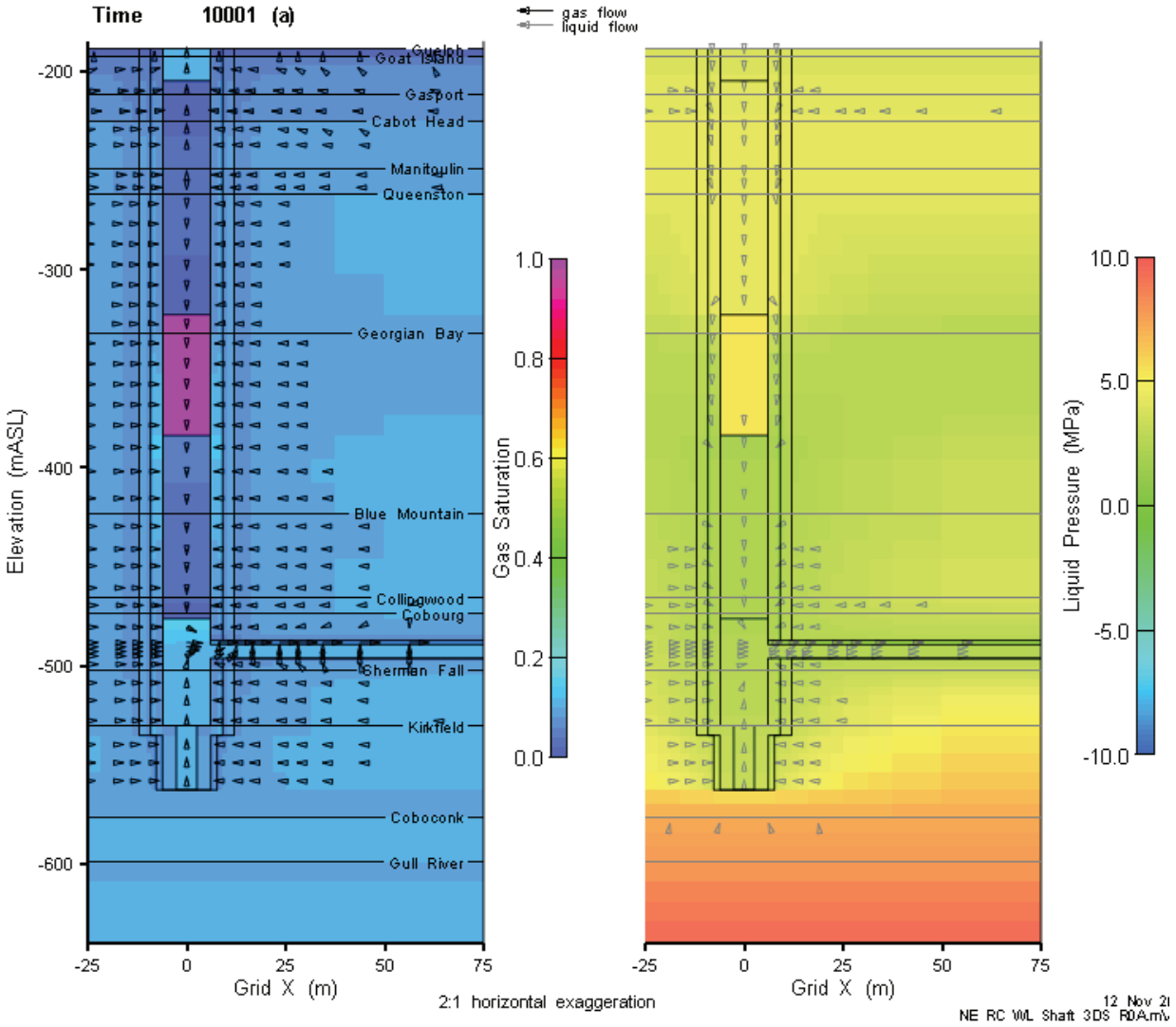

Figure 7.8: NE-RC WL: 3DD Model Pressures and Saturations at 10,000 a

7.2 NE-SBC - Simplified Base Cases

The NE-SBC WL case was simulated with 3DD, 3DSRS and 3DSRmodels. 3DD model results are available to 905,000 a.

7.2.1 Gas Generation

The 3DSRS model results are described in this section. As with the NE-RC case, the saturation and relative humidity drop at approximately 1000 a due to build-up of gas pressure and consumption of water by gas generating processes. However, unlike the NE-RC case, the rate of ingress of water increases sufficiently to overcome consumption by corrosion and degradation processes at approximately 20,000 a (see Figure 7.9 and Figure 7.10). Once the saturation starts to increase, corrosion, degradation and gas pressure evolve following a similar profile to the NWL variant, only delayed due to the intermediate dry period (see Figure 7.11).

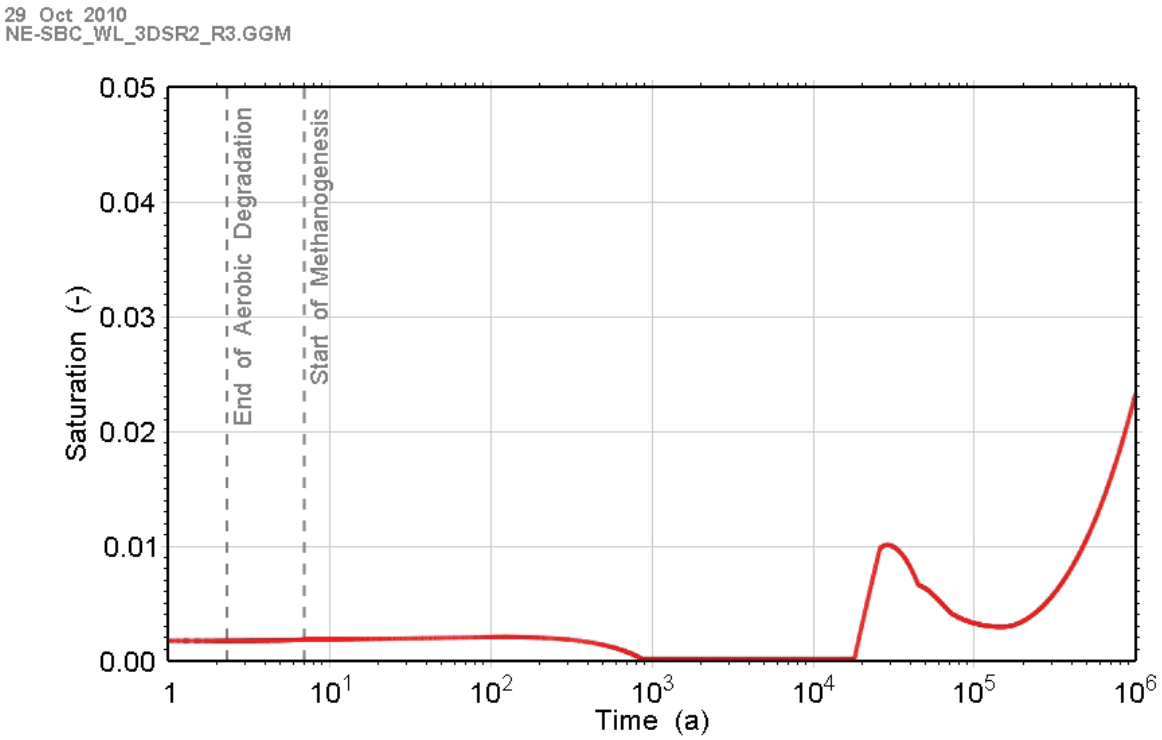

Figure 7.9: NE-SBC WL: Water Saturation

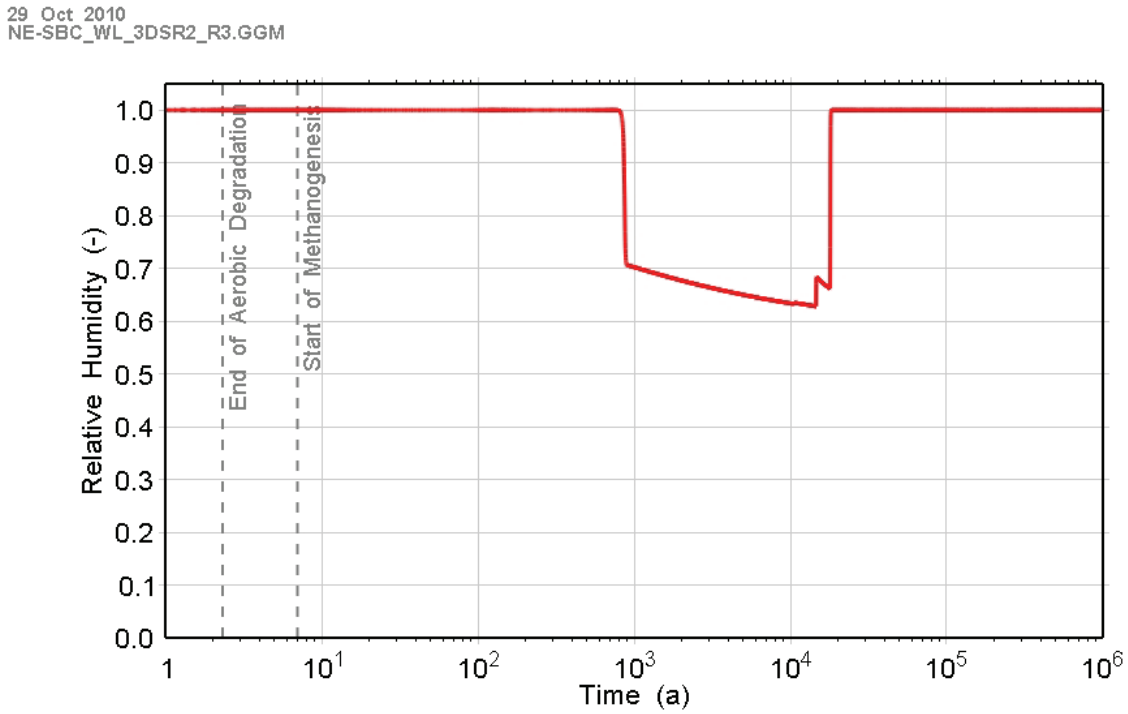

Figure 7.10: NE-SBC WL: Relative Humidity

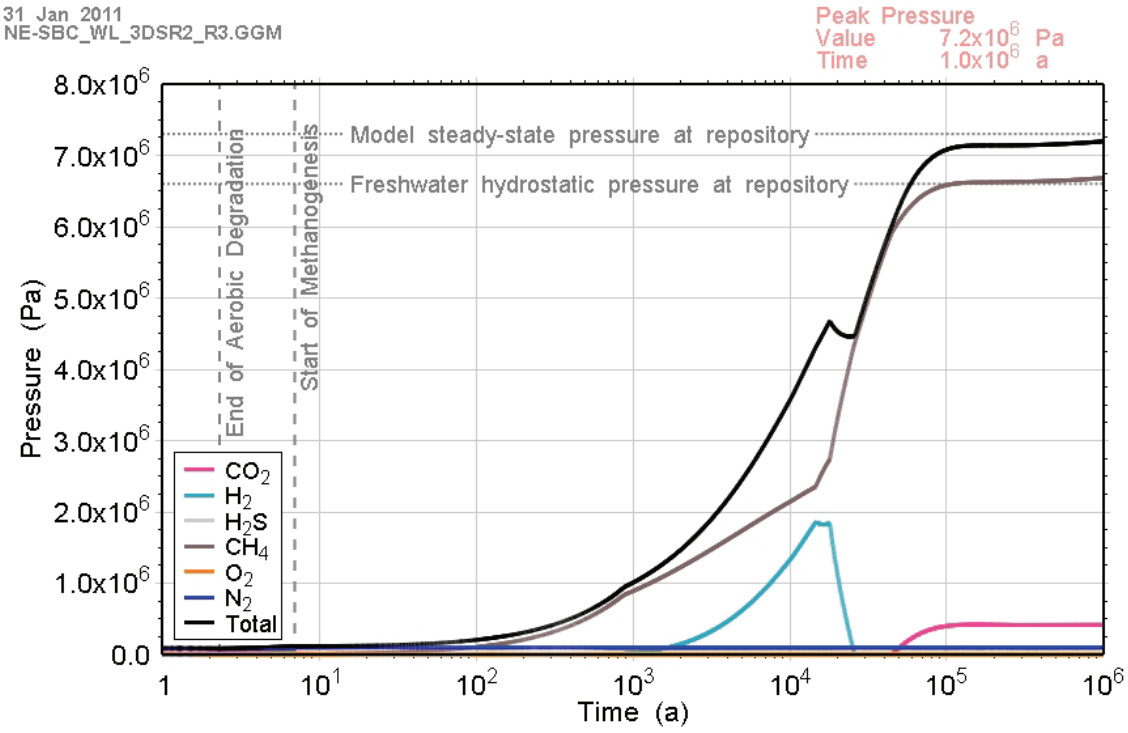

Figure 7.11: NE-SBC WL: Total and Partial Gas Pressures within the Repository

7.2.2 Gas and Water Flows

Figure 7.12 presents NE-SBC WL repository pressures and liquid saturations in comparison to NWL results. WL 3DD and 3DSRS pressure and saturation results are very similar, and delayed considerably from the NWL results. The timing and magnitude of the first peak pressure differ slightly for the 3DSR model, with the subsequent pressure recovery to a lower pressure than the 3DD and 3DSRS models. This is due to the lack of liquid inflow from the shaft, which causes 3DD and 3DSRS saturations to rise earlier. Liquid inflows for the NE-SBC WL model are higher than for the NE-RC WL model, and as a result water consuming reactions are limited for only approximately 17,500 a, after which saturations rise rapidly.

Cumulative gas and liquid flows are shown in Figure 7.13. As for the NE-RC WL case, most gas and liquid flows are through the intact rock. The shaft makes a small contribution to liquid inflows, with the 3DD model showing a slightly larger shaft inflow than the 3DSRS.

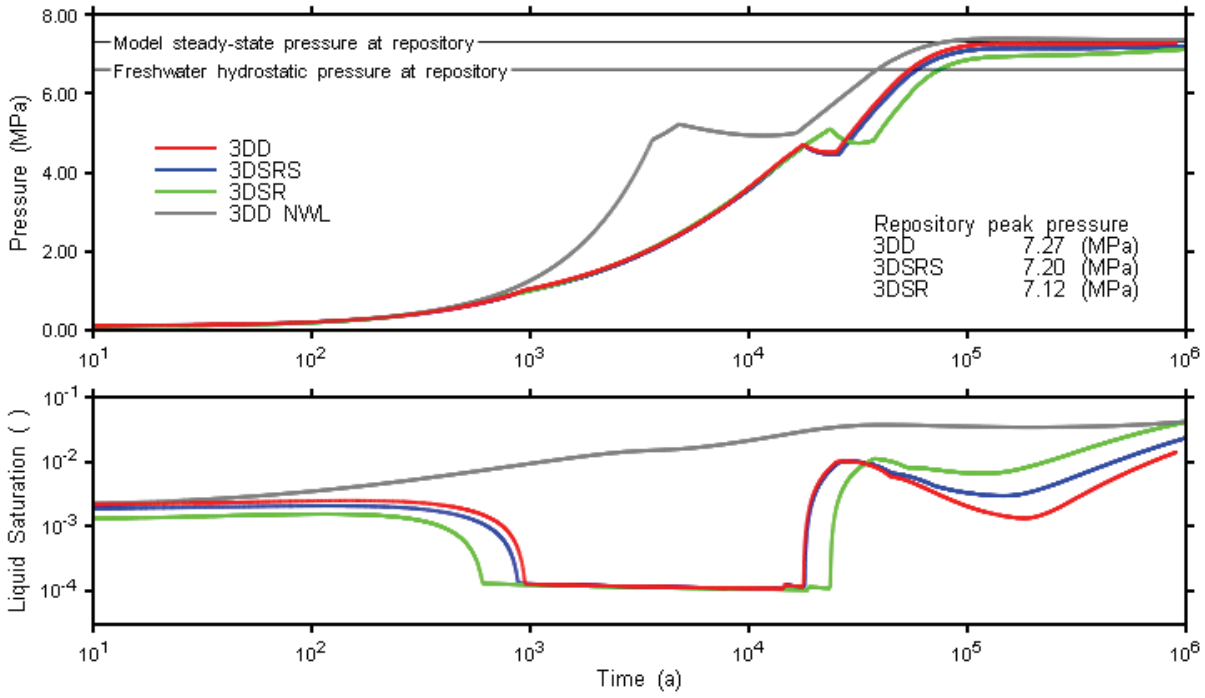

Figure 7.12: NE-SBC WL: 3DD and 3DSRS Model Repository Pressure and Saturation

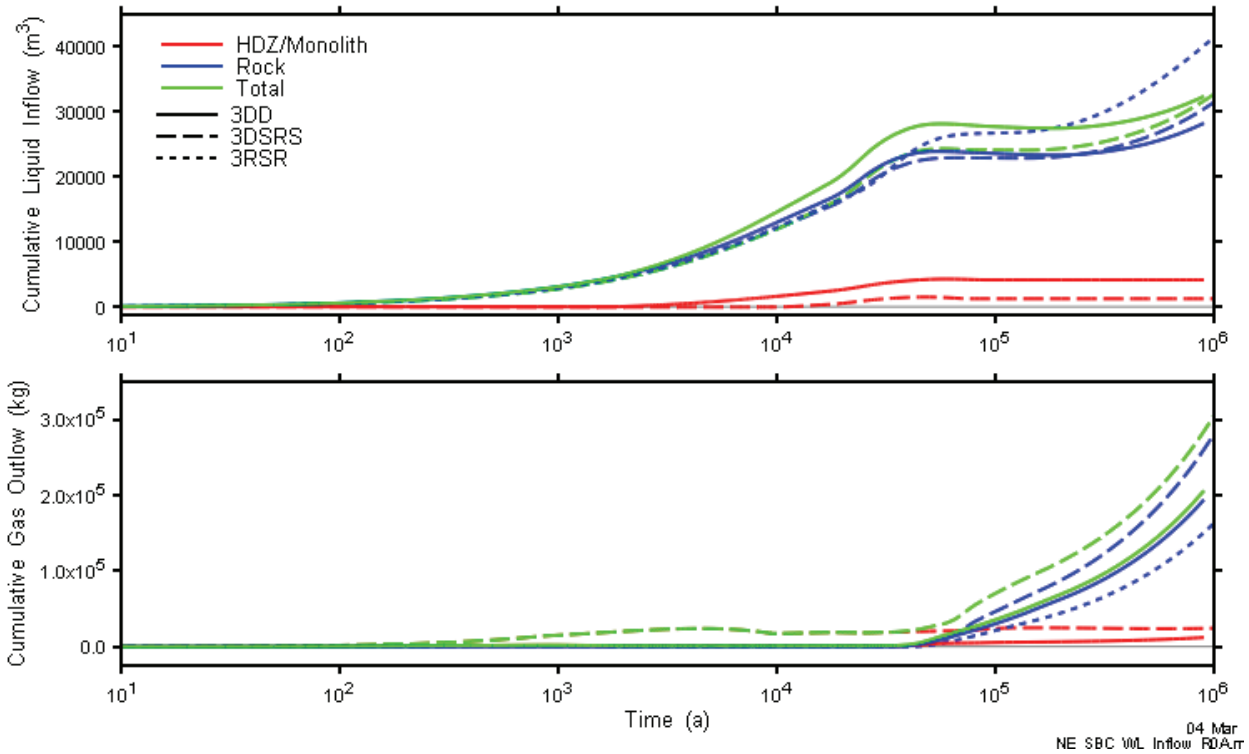

Figure 7.13: NE-SBC WL: Repository Liquid Inflow and Gas Outflow

7.3 Case NE-AN3 WL – Reduced Geosphere Anisotropy

7.3.1 Gas Generation

Compared to the NWL case, there is a small drop in saturation at around 2000 a, but the saturation quickly recovers. It does not drop sufficiently far for the repository to become water-limited and the relative humidity remains at 100%. The small drop in saturation has little impact on the corrosion and microbial degradation processes and the pressure profile is almost identical to that for the NWL case as shown below.

7.3.2 Gas and Water Flows

Figure 7.14 presents NE-SBC WL repository pressures and liquid saturations in comparison to NWL results. The WL pressures are only slightly different than those of the NWL case. Saturations diverge somewhat more over the period from 1000 a to 10,000 a where some reduction in saturation occurs in the WL case as water is consumed. The reductions are not sufficient to limit the water consuming reactions.

Cumulative gas and liquid flows are shown in Figure 7.15. Flows are very similar to those calculated for the NWL case (Figure 5.80), further indication that the WL or NWL assumptions have only minor impact on system response for the NE-AN3 case.

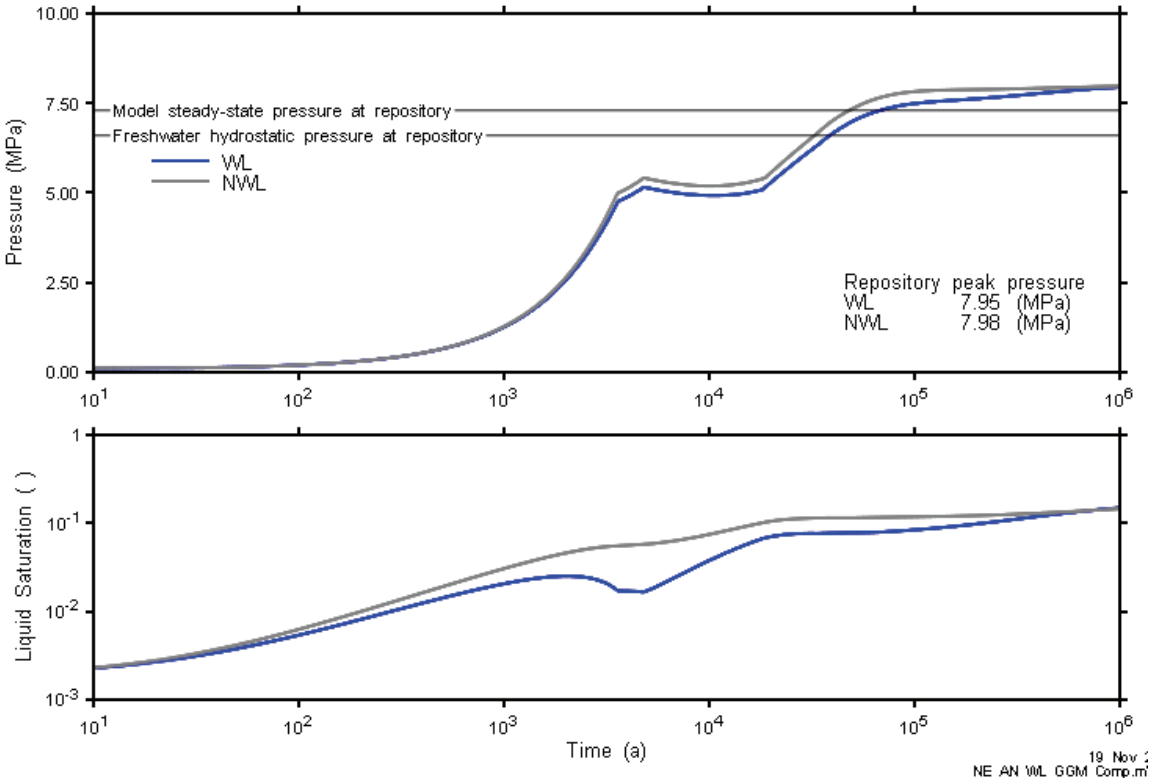

Figure 7.14: NE-AN3 WL: 3DSRS Model Repository Pressure and Saturation

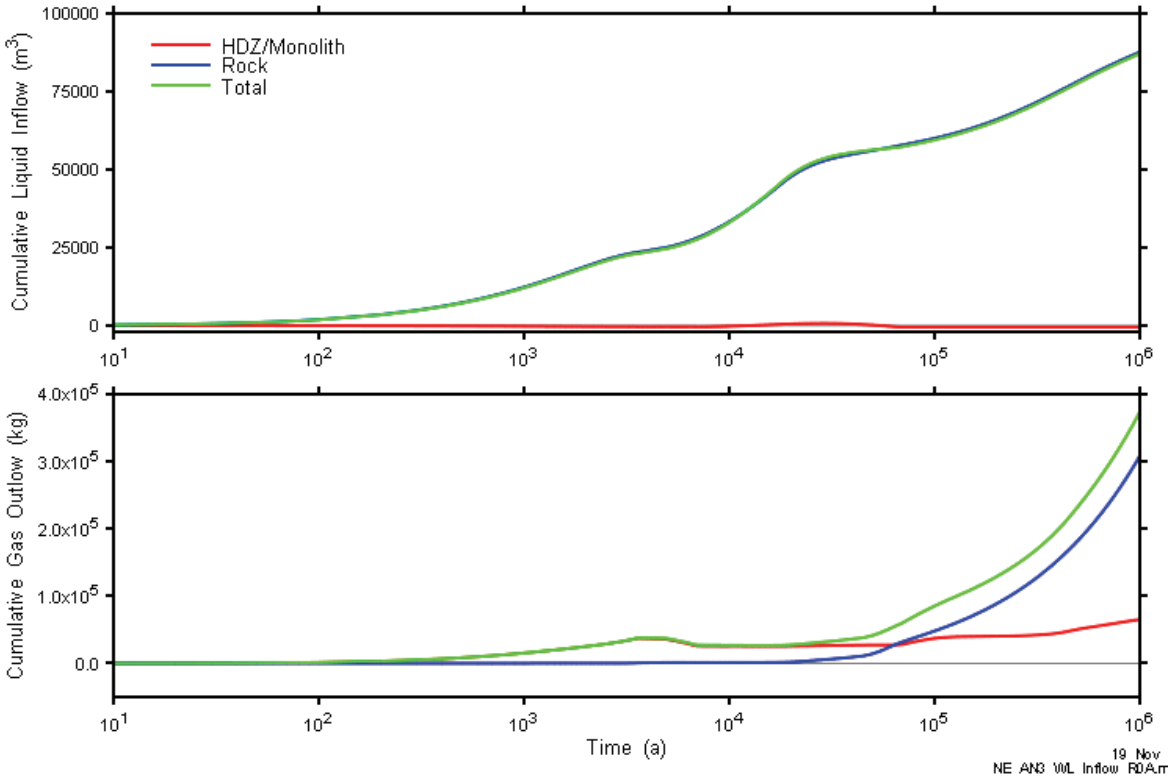

Figure 7.15: NE-AN3 WL: Repository Liquid Inflow and Gas Outflow

7.4 Other Normal Evolution Water-Limited Cases

The changes to remaining Normal Evolution cases as a result of WL assumptions are similar in character to those described above for the NE-RC and NE-SBC cases. In all cases except for late-time NE-GG2, the WL assumptions result in no periods where repository overpressures occur, and consequently no cases where there is significant flow of gas up and through the shaft seals.

The saturation and relative humidity drop, resulting in an intermediate "virtually dry" period where corrosion and microbial processes are limited by the rate at which water is supplied by the geosphere. This slows the build-up of gas pressure. The maximum gas pressures over the 1 Ma time period are generally slightly lower than for the NWL counterparts.

The repository pressure and liquid saturations for selected cases are presented in Figure 7.16. Only cases with distinct results are shown (i.e., NE-GT1, NE-GT2, and NE-GT3 are very similar to NE-GG1; they are not presented). In all cases, except NE-GG2, pressure build-up is reduced and retarded relative to the corresponding NWL case. The very late-time overpressure for NE-GG2 case results in a limited pulse of dissolved gas up the lower reaches of the shaft. As shown in Figure 7.17, the pulse does not extend to the top of the modelled shaft. With NE-GG2 case, methanogenesis at late times causes a reduction in pressure, leading to a relatively rapid increase in saturation. This increase provides sufficient water for further gas generation leading to the overpressure.

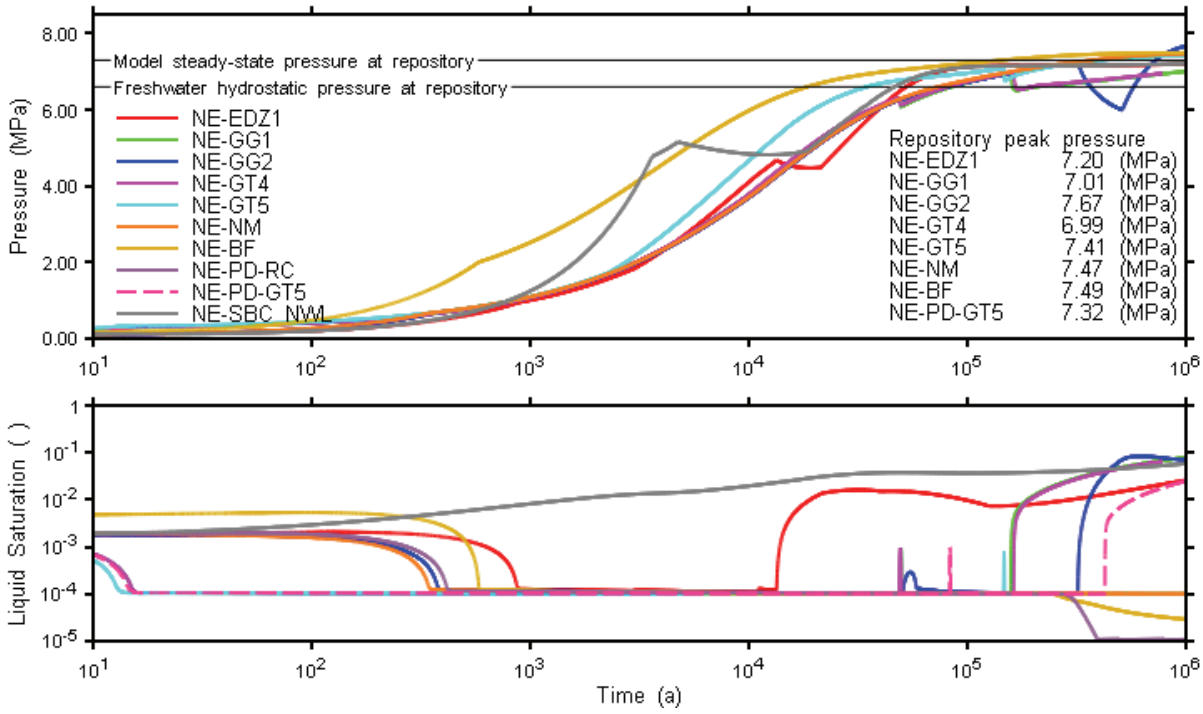

Figure 7.16: NE WL: 3DSRS Model Repository Pressure and Saturations for Selected Cases

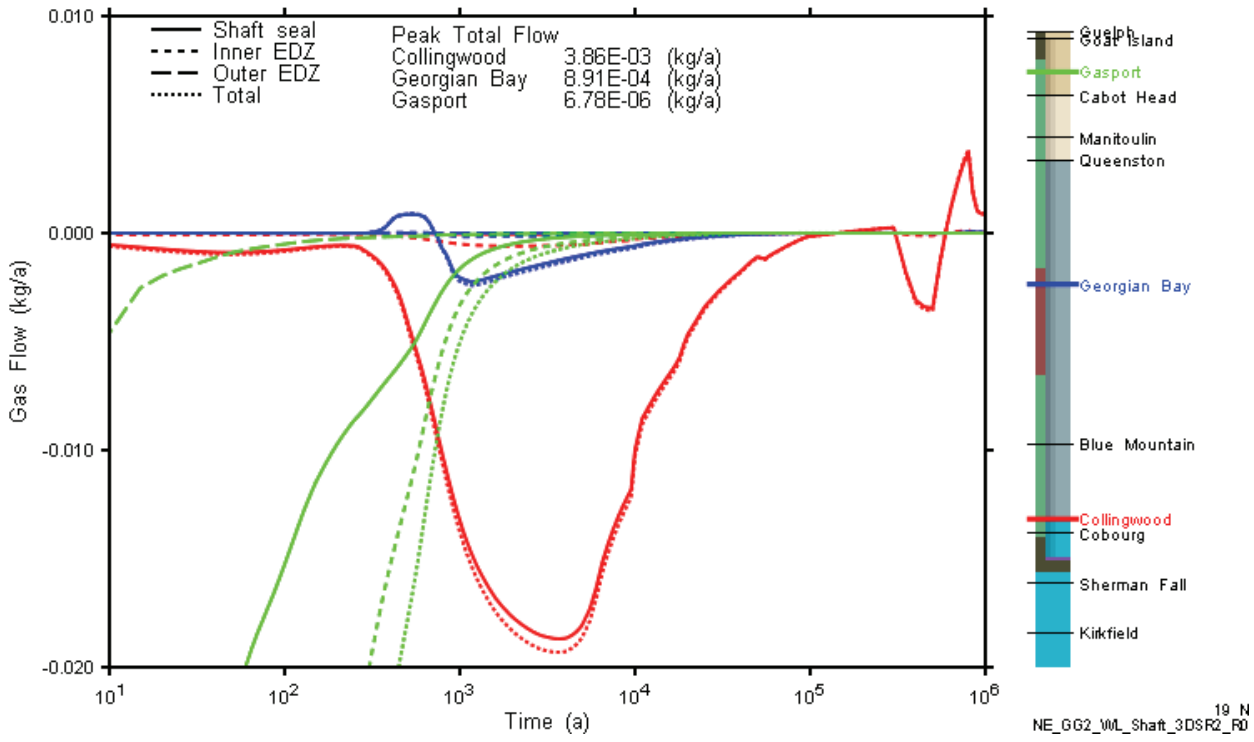

Figure 7.17: NE GG2 WL: 3DSRS Model Shaft Dissolved Gas Flow at Selected Planes

7.5 NE-PD-RC and NE-PD-GT5 WL - Final Preliminary Design Water-Limited Cases

As shown in Figure 7.18, the increased volume associated with the final preliminary design has very little impact on the NE-RC WL or NE-PD-GT5 results. Gas generation for the final preliminary design is almost identical for NE-RC and NE-PD-RC, and very similar for NE-GT5 and NE-PD-G5.

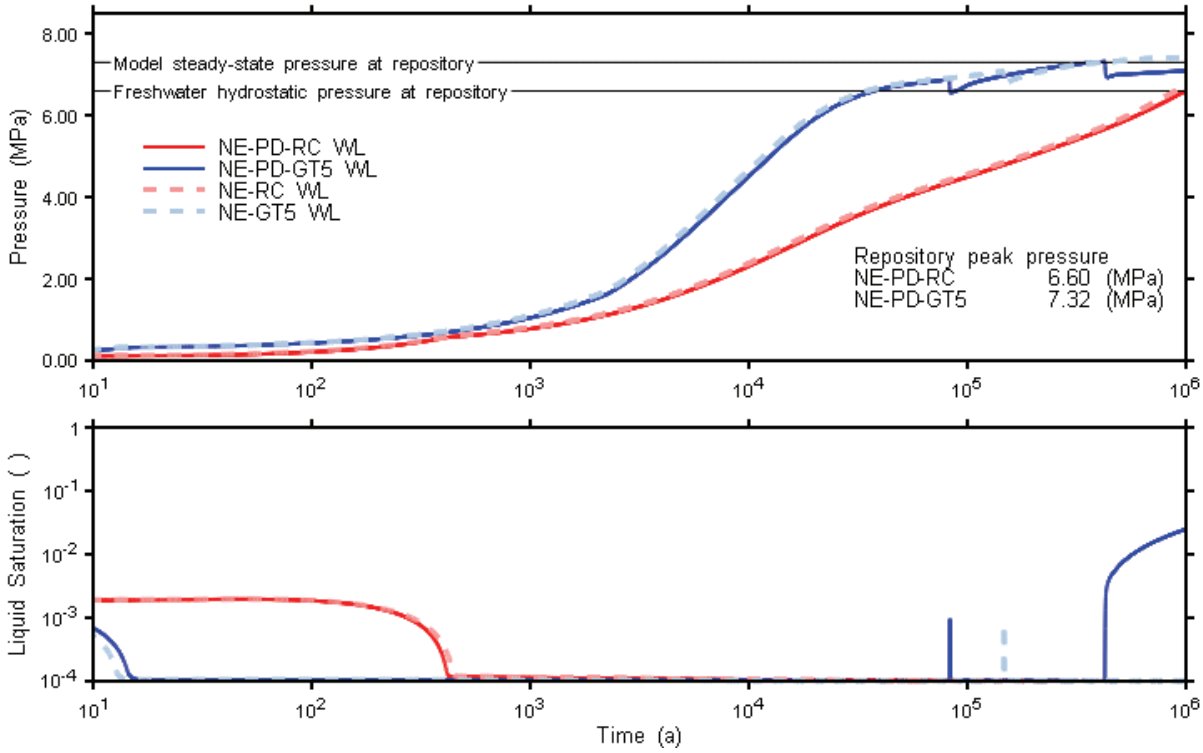

Figure 7.18: NE-PD WL: 3DSRS Model Repository Pressure and Saturations

7.6 Shaft Seal Failure Water-Limited Cases

As shown in Figure 7.19, the WL assumptions have a minor impact on the SF-BC results where there is a short early time period where repository liquid saturations are reduced relative to the NWL case. The SF-ED WL case results are virtually the same as for the NWL case since the water saturation remains positive throughout.

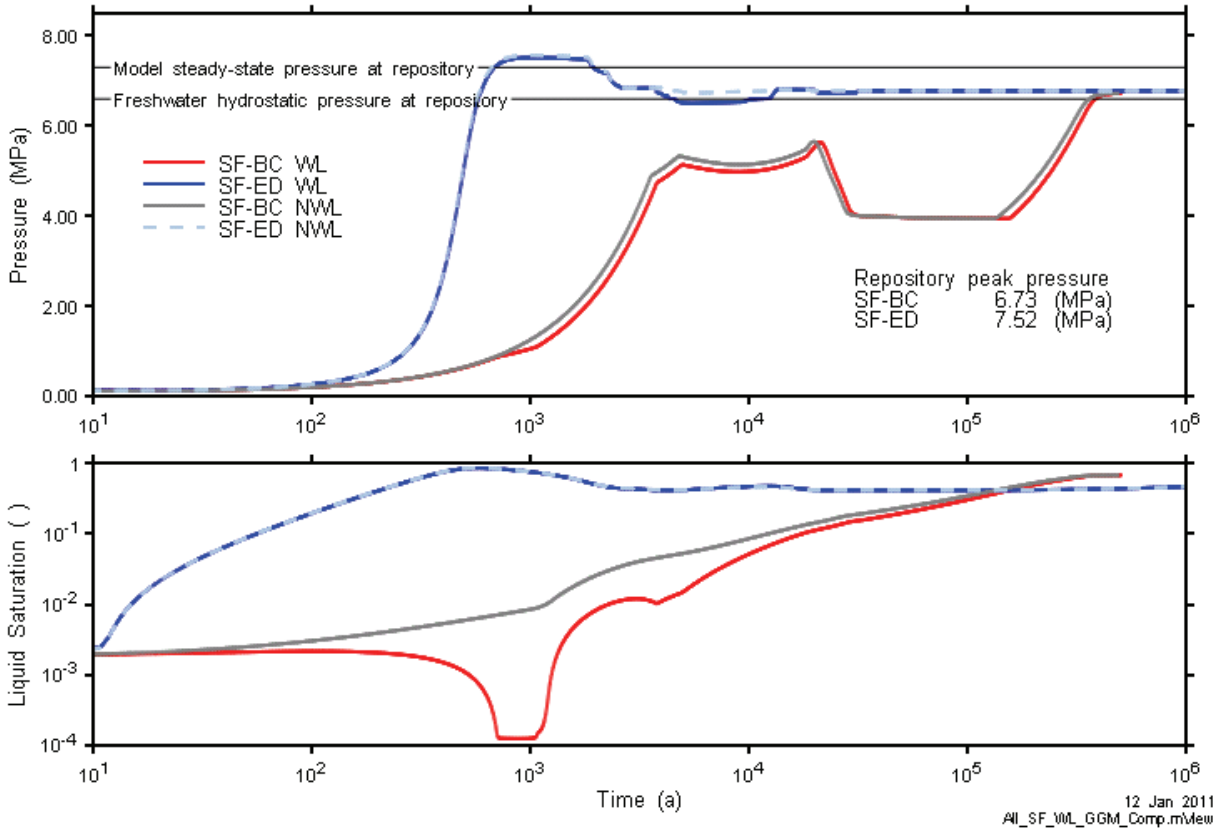

Figure 7.19: SF WL: 3DSRS Model Repository Pressure and Saturations

8. RESULTS ASSESSMENT AND COMPARISON

This section provides graphical and tabular comparative summaries of gas and water flows for all calculation cases. In general, only results from 3DSRS models are presented in this section so as to remove the minor effects of model differences from comparisons. For cases where only 3DSR results are available, their use is explicitly indicated. On graphs where Normal Evolution and Shaft Failure cases are plotted together, the Shaft Failure cases are plotted with dashed lines to indicate the different status of the cases. Cases representing the final preliminary design (NE-PD-RC and NE-PD-GT5) are plotted with dotted lines.

8.1 Repository Pressure and Saturation

Figure 8.1 shows repository pressure as a function of time for NWL cases simulated with the 3DSRS model. Only those cases with distinct responses are presented. Cases not presented are: NE-GT1, NE-GT2, NE-GT3, and NE- GT4 (similar to NE-GG1); NE-RC2 (similar to NE-RC); and NE-RC1 and NE-MG (similar to NE-SBC).

None of the case pressures exceed the estimated lithostatic pressure at the repository horizon (17 MPa).

Most normal evolution cases come to a long-term steady-state pressure at a value near the model steady-state pressure within 1,000,000 a. Other cases are still approaching this point by 1,000,000 a, and in the NE-NM case (no methane generating reactions) the pressure initially rises above this pressure and then decreases towards it.

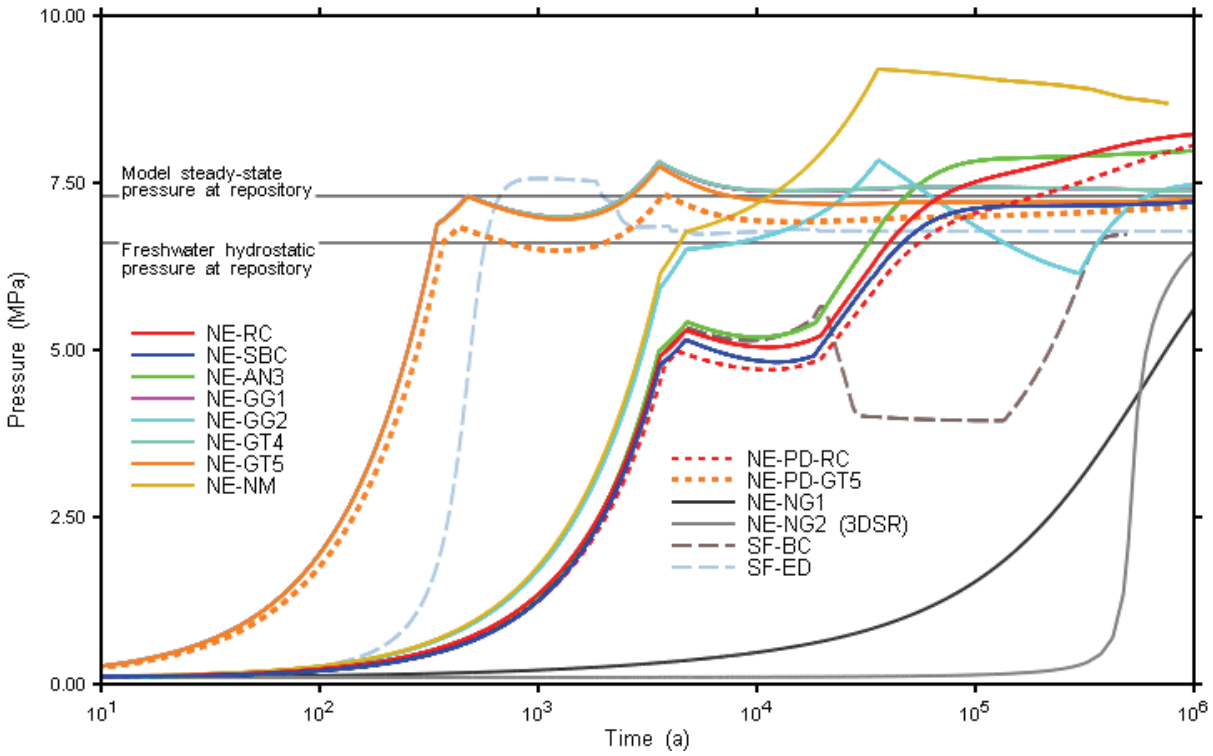

Figure 8.1: Average Repository Gas Pressure for all NWL Cases

The case with gas saturations in the host rock (NE-RC) present long-term overpressures as there is slow long-term formation gas influx into the repository. In this case the pressure would stabilize after 1,000,000 a as egress of gas through the shaft balances the inflow from the formation.

The Severe Shaft Seal Failure cases have similar repository gas pressure responses.

Pressure responses for WL cases are shown in Figure 8.2. Nearly all WL case pressure responses are substantially delayed relative to the corresponding NWL cases. Exceptions include the SF cases and the NE-AN3 case, where sufficient water for reactions is provided by the shaft and higher permeability geosphere respectively. Again, there is the tendency towards a long-term pressure consistent with or slightly above the model steady-state pressure.

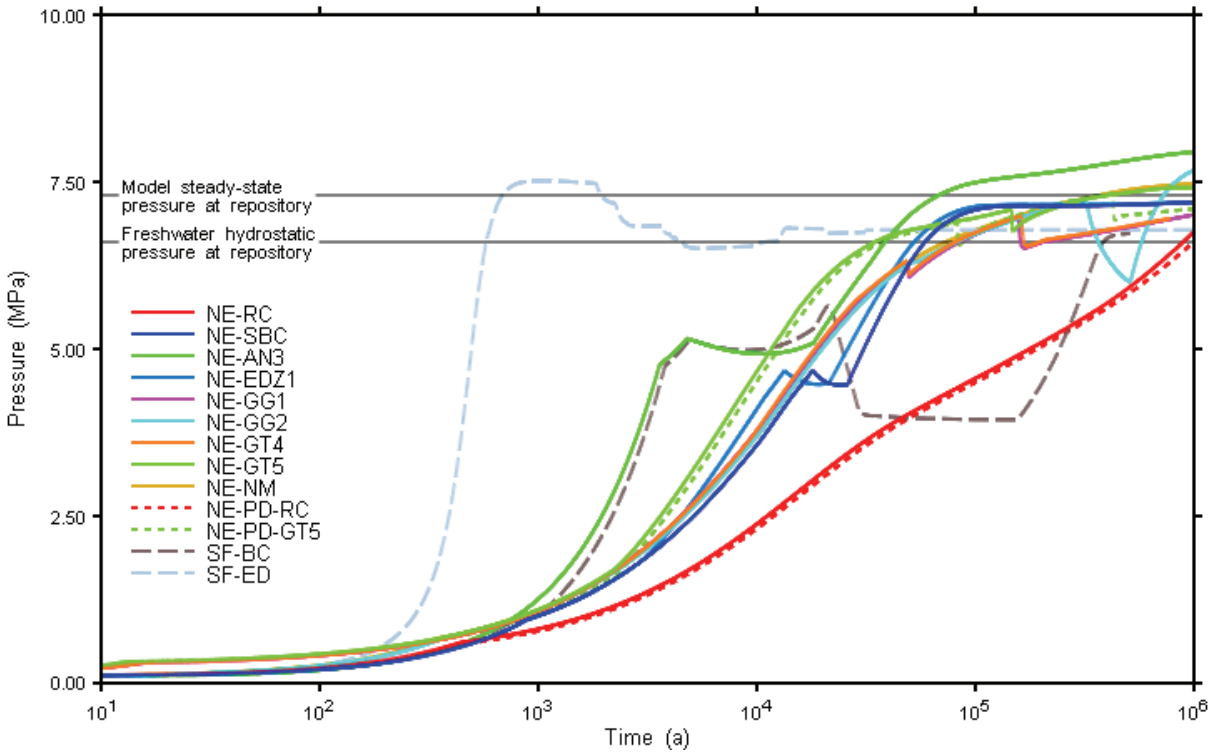

Figure 8.2: Average Repository Gas Pressure for all WL Cases

Repository liquid saturation for all distinct NWL and WL cases are presented below in Figure 8.3 and Figure 8.4, respectively. Unlike most other repository saturation figures previously presented in this report, these figures use a linear Y axis, which provides a visual representation that reflects the actual relative level of water in the repository. For most cases, resaturation is limited, with correspondingly low water levels within the repository for the duration of the simulation. Only shaft failure cases (SF-BC and SF-ED), and cases with no gas generation (NE-NG1 and NE-NG2) result in saturations in excess of 25%.

NE-AN3, NE-GG2, NE-EDZ1 (WL) and NE-GG1 (WL only) results present perceptible, albeit low, liquid saturations.

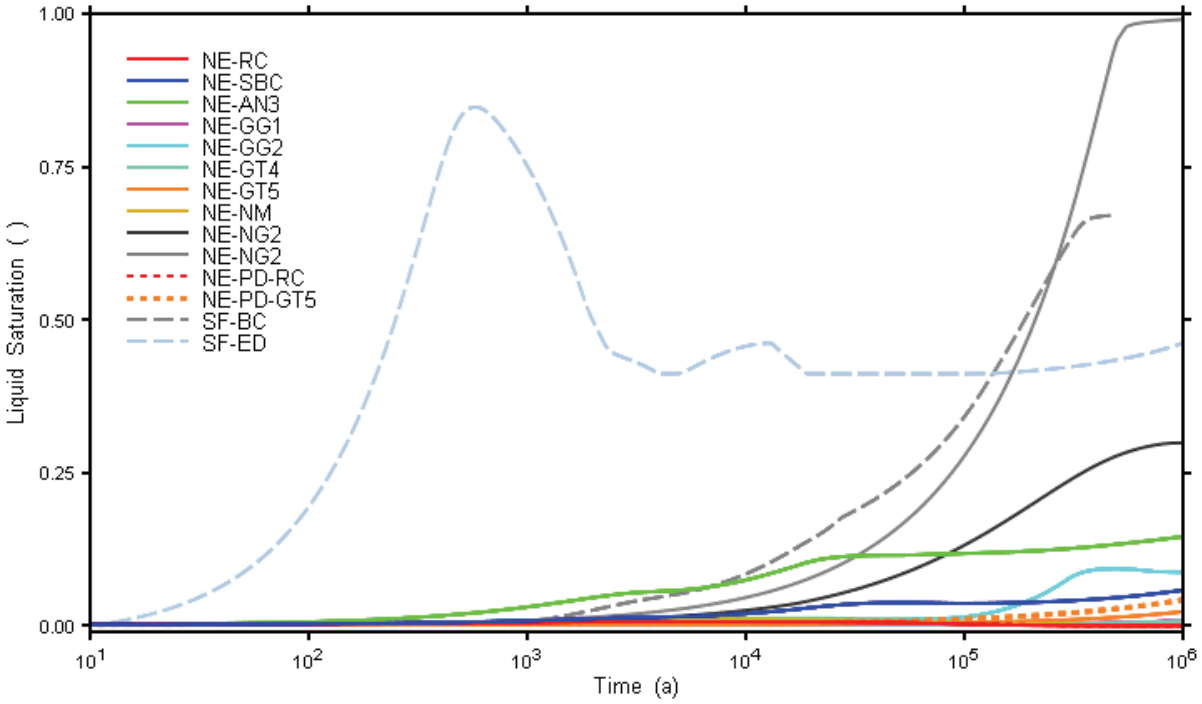

Figure 8.3: Average Repository Water Saturation for all NWL Cases

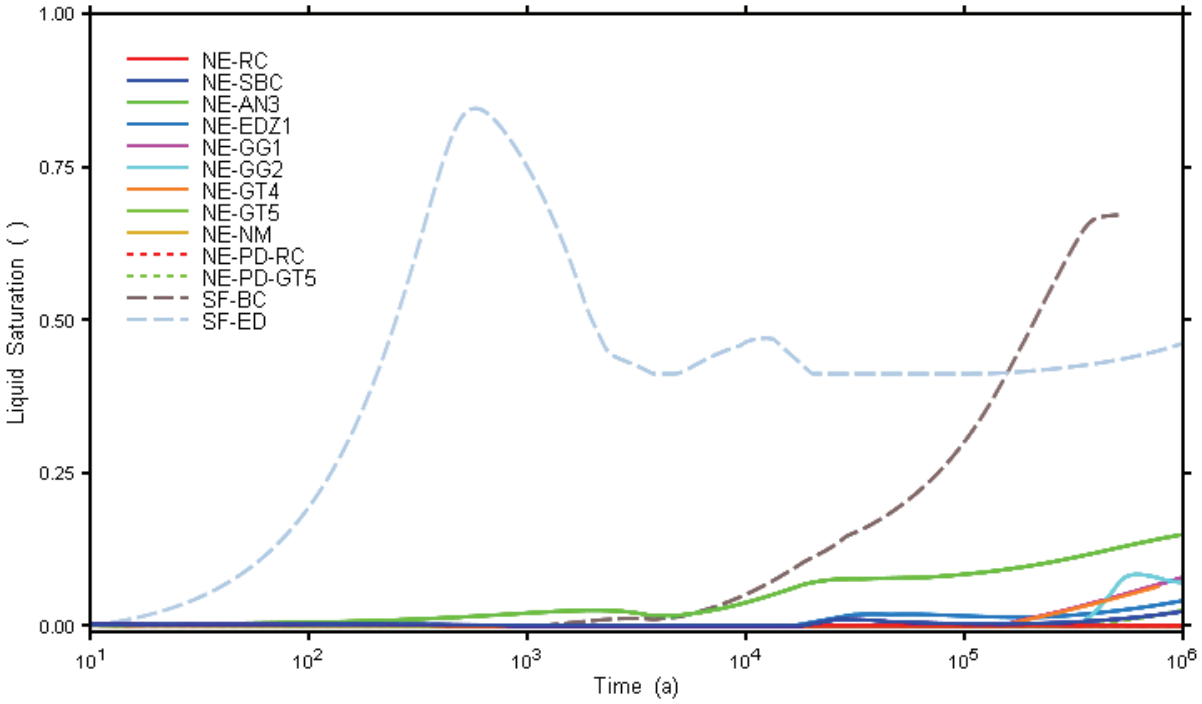

Figure 8.4: Average Repository Water Saturation for all WL Cases

Peak pressure data for all cases are summarized in Table 8.1. Due to the low-permeability rock and shaft, backfilling the repository (NE-BF) reduces the available void space to hold the generated gas, and results in a higher peak repository gas pressure. However, this is not the reference design basis. All other cases have peak pressures of 6-9 MPa.

8.2 Gas Flow

Figure 8.5 presents gas flow rates up the shaft for all 3DSRS Normal Evolution cases where such flow occurred (i.e., there was no gas flow up the shaft for the other cases).

NE-NM results are based on the transport of H_2, with a lower molecular weight than the CH_4 gas used for other runs.

NE-RC shaft gas flows are primarily formation gas. At early-times they are gas moving into the shaft from Upper Ordovician formations and thence upwards (see Figure 5.18). At later times the NE-RC flows represent the long-term efflux of formation gas that originally entered the repository from the geosphere. There may be a component of repository gas; however, at this time the radioactive components of the gas will be minimal due to radioactive decay.

Shaft gas flows for the NWL Severe Shaft Seal Failure cases are presented in Figure 8.6. Results are shown for gas flow through the Gasport formation level only, as flow rates for all locations in the shaft are visually coincident.

2DRS model results presented in previous sections for NE cases show that there is no flow of gas in the shaft above the Guelph Formation, as the permeable formation acts as a sink. 2DRS models were not executed for SF-BC and SF-ED cases, but it is unlikely that the Guelph and Salina A1 upper carbonate would act as gas sinks for these cases, given the assumption of zero capillary pressure in the degraded shaft seal material, and the high permeability of the shaft materials.

Table 8.1: Summary of 3DSRS Model Peak Repository Pressures

Mode	NWL		WL	
Calculation Case	Peak Repository Gas Pressure (MPa)	Time of Peak Gas Pressure (Ma)	Peak Repository Gas Pressure (MPa)	Time of Peak Gas Pressure (Ma)
NE-RC	8.22	1	6.75	1
NE-SBC	7.21	1	7.20	1
NE-AN3	7.98	1	7.95	1
NE-EDZ1	7.23	1	7.20	1
NE-GG1	7.81	0.004	7.01	1
NE-GG2	7.84	0.036	7.67	1
NE-GT(1,2,3)	All 3DSR, same as NE-GG1			
NE-GT4	7.82	0.004	6.99	0.83 (end of run)
NE-GT5	7.75	0.004	7.41	0.96
NE-MG	7.18	1	n/a	n/a
NE-NG1	5.61	1	same as NWL	same as NWL
NE-NG2 (3DSR)	6.47	1	same as NWL	same as NWL
NE-NM	9.20	0.036	7.47	1
NE-RC1 (3DSR)	7.22	1	6.14	1
NE-RC2 (3DSR)	8.05	1	6.14	1
NE-BF	16.21	0.005	7.49	1
NE-PD-RC	8.06	1	6.60	1
NE-PD-GT5	7.33	0.004	7.32	1
SF-BC	6.73	0.49 (end of run)	6.73	0.5 (end of run)
SF-ED	7.56	0.001	7.52	0.001

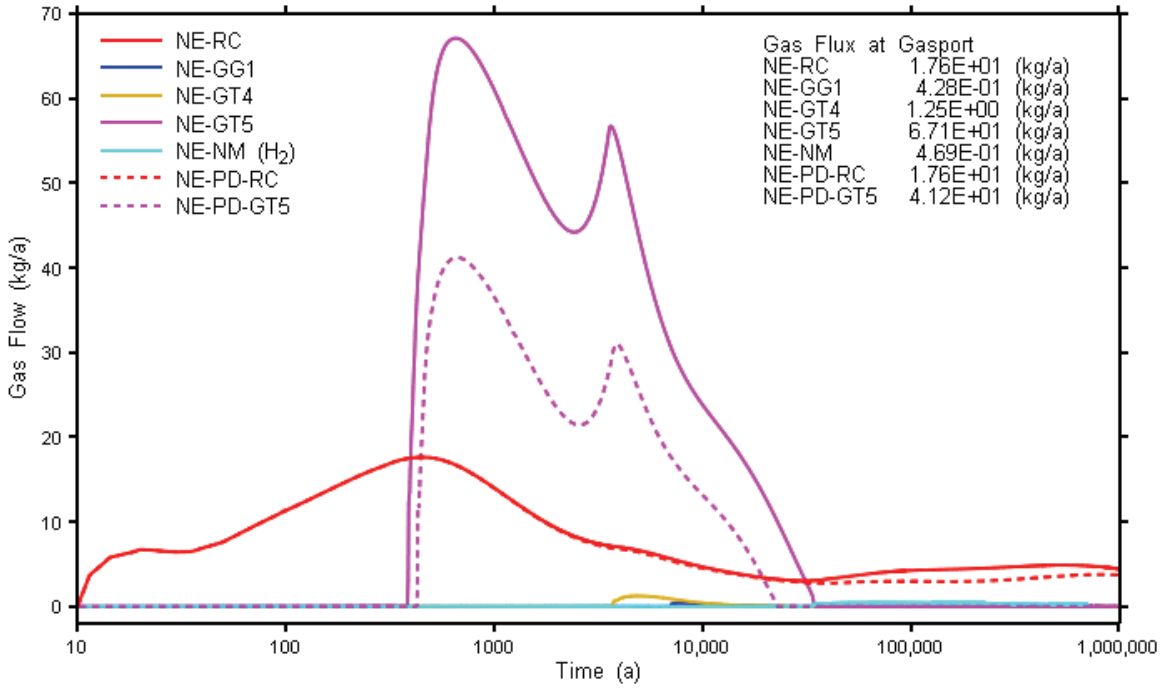

Figure 8.5: 3DSRS Gas Flow Rates up Shaft at Gasport Formation for NWL NE-RC, NE-GG1, NE-GT5, NE-NM, NE-PD-RC and NE-PD-GT5 Cases

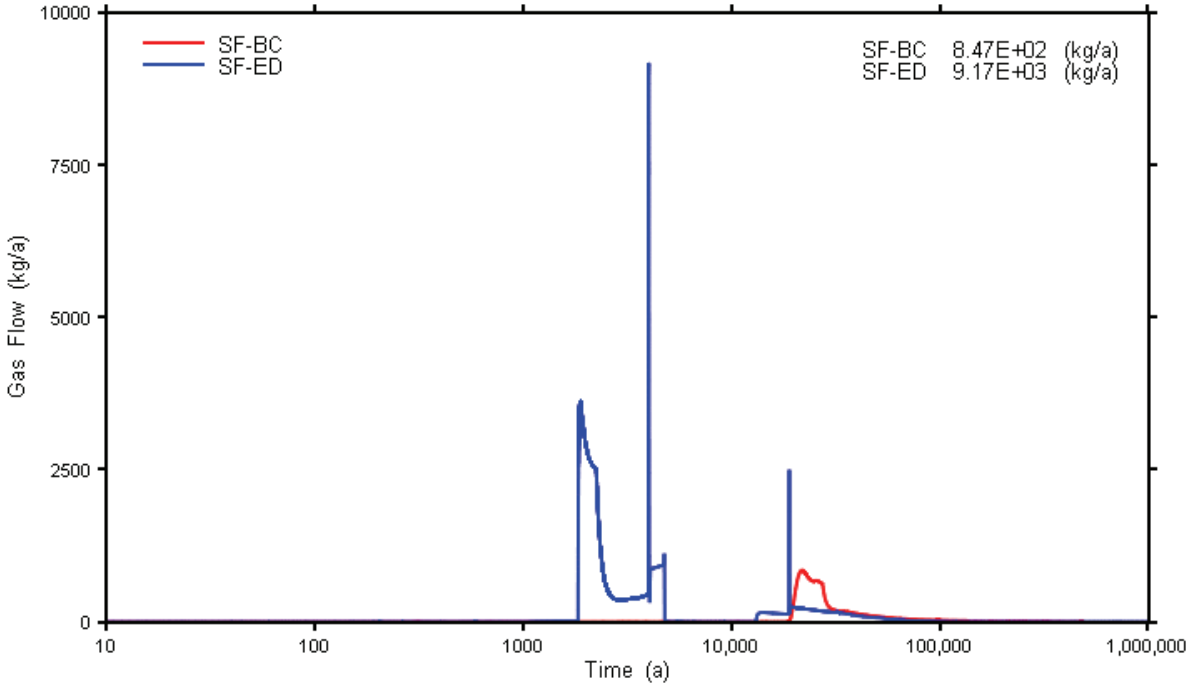

Figure 8.6: 3DSRS Gas Flow Rates up Shaft at Gasport Formation for SF-BC and SF-ED Cases

Dissolved gas flow rates for selected 3DSRS models are shown in Figure 8.7. In addition to NE-RC and NE-SBC cases, only those NE cases with a positive dissolved gas flow up the shaft in excess of 2.0×10^{-4} kg/a are shown. All cases shown are NWL cases as none of the WL normal evolution cases had positive liquid flow up the shaft at the Gasport horizon within the 1 Ma simulation period.

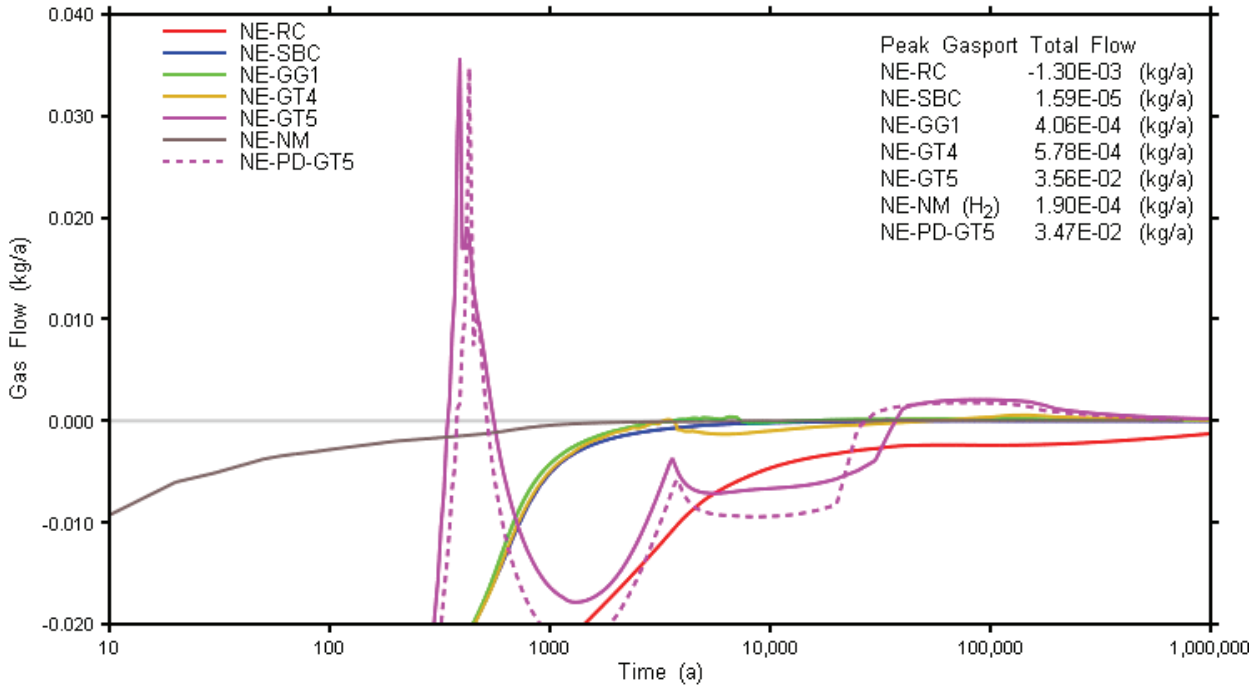

Figure 8.7: 3DSRS Dissolved Gas Flow Rates for Selected NWL Cases

Table 8.2 provides a summary of gas and dissolved gas flows from 3SDRS NWL model results. Only positive upwards fluxes are entered in the table. Zero or negative (downward) fluxes are represented as "--".

Table 8.2: Summary of 3DSRS NWL Peak Gas Flow Rates at Gasport

Calculation Case	Gas Flow		Dissolved Gas	
	Peak Rate	Time	Peak Rate	Time
	(kg/a)	(ka)	(kg/a)	(ka)
NE-RC	1.8E+01	0.46	--	--
NE-SBC	--	--	1.6E-05	85
NE-AN3	--	--	2.2E-05	
NE-EDZ1	--	--	1.5E-04	110
NE-GG1	4.3E-01	8	4.1E-04	7
NE-GG2	--	--	2.0E-05	40
NE-GT4	1.2E+00	5	5.8E-04	150
NE-GT5	6.7E+01	0.65	3.6E-02	0.39
NE-NG	--	--	--	--
NE-NM (H_2)	4.7E-01	76	1.9E-04	34
NE-BF	1.2E+02	42	2.3E-02	4
NE-PD-RC	1.8E+01	0.455		
NE-PD-GT5	4.1E+01	0.675	3.5E-02	0.41
SF-BC	8.5E+02 *	22 *	--	--
SF-ED	9.2E+03 **	4 **	2.1E+01	2

Notes:

* The peak gas flow for SF-BC (WL) is similar, 840 kg/a at 23 ka.

** The peak gas flow for SF-ED (WL) is similar, 9300 kg/a at 3.8 ka.

9. UNCERTAINTIES

Uncertainties in model results presented in this report arise from a variety of sources, including: the modelling approach, limitations of the model, parameterization (for both the gas generation and gas transport models), and the conceptual model of the geosphere. The calculation cases presented in this report are intended to illustrate and bound the uncertainty in key model results such as repository gas pressure and gas flux. Sources of uncertainty and possible approaches to reducing uncertainty are discussed in the following subsections.

9.1 Gas Generation Model

GGM is a simple model of the gas generation processes within the repository, which is sufficiently detailed to consider the key processes that govern the fluxes of water and gases between the repository and the geosphere, and to estimate the repository gas pressure. The following GGM simplifications are potential areas of uncertainty.

1. **Microbial activity**: The water in the repository is expected to be highly saline, and the water chemistry will vary locally – e.g. high pH near cement wastes, high dissolved metal levels - which will affect the types of bacteria which operate and, in particular, the viability of methanogens and the microbial reaction rates. There will also be other competing microbial processes rather than gas generation. The current model assumes that microbes will be active given that there are energy sources present, that microbial gas generation occurs and that all materials are fully degrade, which maximizes gas generation. Microbial activity has both positive and negative effects on the gas content in the repository. The highest calculated pressures occur only if there is no microbial activity, and only H_2 gas generated by chemical corrosion reactions on steel. In this case, the peak gas pressure is expected to rise about 2 MPa (Case NE-NM, Section 5.11) above steady-date pressures.

2. **Carbonation reaction with concrete and limestone**: CO_2 gas in the repository will interact both with the cement in the repository, and with the calcium carbonate in the surrounding host rock. The reaction with cement could consume some CO_2, but could be rate-limited by carbonation of cement surfaces. The CO_2 gas pressure will also develop into an equilibrium with dissolved carbonate in water and the surrounding host rock.

3. **Reaction Rate Variability**: The wastes are treated as a small number of relatively homogenous materials that all corrode or degrade at the same rate under given conditions (aerobic/anaerobic, saturated/unsaturated). In reality, the wastes even within a given waste type will be more heterogeneous in their parameters (e.g., dimensions such as surface area), their chemical environment, and their spatial location. As a result, their overall behaviour may be better described by a range of corrosion or degradation rates. This could result in higher rates at shorter times and slower rates at longer times, with similar average behaviour.

4. **The composition of gas entering the repository**: For the reference NE-RC case, gas initially present in the geosphere enters the repository. However, the model assumes that the composition of any gases entering the repository is the same as the composition of gases existing within the repository. This is not exact, since the early repository atmosphere has significant hydrogen or methane, while the geosphere gas is mostly methane. However, since the repository gas is mostly methane on long time scales, this is expected to be a small effect.

5. **Transport of gas via water**: Currently any gases dissolved within the water in the repository are assumed by GGM to remain within the repository rather than being transported out with the water when it leaves or diffusing out over long timescales. However, the results show that the water generally flows into the repository and, therefore, the effect of gas transport out of the repository via the water is likely to be insignificant.

9.2 Gas Transport Model

9.2.1 Modelling Approach

The gas transport modelling is numerically difficult because of the desire to include two-phase transport, transient conditions, detailed geometry, a wide range of spatial scales, a wide range of permeabilities and sharp permeability contrasts, and a long (1 Ma) simulation period.

The modelling approach developed for this work and presented in this report uses a complementary sequence of models that provide differing levels of detail. The 3DD model is a spatially complex model, which represents the repository layout with reasonable geometric fidelity, while the 3DSRS model simplifies the physical attributes of the 3DD model. The 3DSR and 2DRS models concentrate on single aspects of performance, the repository and geosphere for the former, and the shaft and geosphere for the latter.

Confidence in the modelling approach is obtained by comparison of the results. Shaft flows from 3DD, 3DSRS and 2DRS models compare well (see Figure 5.107 and Figure 5.108 for 3DD/2DRS comparison, Figure 5.139 and Figure 5.143 for 3DSRS/2DRS comparison) as do repository pressures and inflows from 3DD, 3DSRS and 3DSR models. Steady-state and transient geosphere head profiles also compare well to groundwater modelling results presented in GEOFIRMA (2011) (see Figure 5.170 through Figure 5.173). The GEOFIRMA (2011) results were produced with another numeric code, FRAC3DVS-OPG (groundwater model), which provides an extra degree of confidence in the approach. Appendix B also presents results of a simple gas transport calculation for steady-state flow of gas in the shaft. It compares well to T2GGM shaft fluxes for a period of the SF-ED case where shaft gas flows are relatively constant.

However, there are a number of issues inherent in selection of the TOUGH2/EOS3 code as the underlying numeric code for the all gas transport models. In particular, those issues which may have an impact on simulation results are as follows.

1. **Single bulk gas**. The current modelling assumes a single gas as the bulk gas transported through the geosphere. Most of the cases presented here used CH_4, although cases with air (NE-MG) and H_2 (NE-NM) were simulated. Gas generation results show the composition of the bulk gas to be a mixture of gases, the composition of which evolves with time. Also, site characterization data suggests initial gases in the geosphere are primarily CH_4, with some CO_2. The consequences of the differences between the single gas used in each case and the actual gas mixtures are not straightforward, due to the combination and different properties of these gases. However, as the repository pressure response is determined by the ideal gas law, calculated from repository void volume and molar rates of gas generation and consumption, and these rates are calculated using multiple gases, the differences are unlikely to be significant. TMVOC, another TOUGH2 family code that considers multiple gases may provide insight into the minor variations expected.

2. **Uncontaminated gases**. The repository and shaft system contain initial uncontaminated gases, and in the reference cases (NE-RC, NE-RC1 and NE-RC2), the rock also contains initial uncontaminated gases. However, the current modelling approach is unable to differentiate between initial uncontaminated gases and gases potentially contaminated by waste degradation. In the cases where dissolved gas is transported up the shaft, it is impossible to tell whether the gas at any point is contaminated, uncontaminated or a mixture of the two. Resolving this issue requires use of a multi-gas model such as TMVOC. Currently, the safety assessment model conservatively assumes that any gas released could be contaminated.

3. **Constant density fluid.** Many of the effects of using variable density fluid are incorporated though use of an equivalent environmental head approach. Appendix A of GEOFIRMA (2011) contains a detailed explanation of the concepts and applicability of environmental head to modelling the local flow system at the Bruce nuclear site. Furthermore, sensitivity case NE-SE in GEOFIRMA (2011) compares results from variable density simulations with those using constant density and environmental head and concludes that results are very similar. This supports the use here of the computationally simpler constant density approach. However, there is a TOUGH2 equation of state module, EOS7R, which does include salinity and could allow direct testing of a saline geosphere.

4. **Geosphere pressure at repository**. This issue is partially related with that of constant density fluid as the use of environmental head with TOUGH2/EOS3 fresh water fluid densities results in pressures at the repository horizon that are lower than would be the case in a steady-state saline system. A scoping simulation conducted using measured Guelph and Cambrian pressures as upper and lower boundary conditions yielded a steady-state pressure at the repository horizon of approximately 7.7 MPa rather than the 7.3 MPa of the current NE-SBC case. Alternative permeability profiles will also change the steady-state pressure distribution at the repository horizon. For example, the NE-AN3 case yields a steady-state repository pressure of 7.5 MPa.

   As a consequence, several of the cases that produced overpressures relative to the steady-state freshwater geosphere pressures would not be overpressured relative to a steady-state saline geosphere (or different permeability distribution) and, therefore, would not produce flows up the shaft of similar magnitudes. In specific, flows from NE-GG1 and NE-GT5 NWL would be most affected. The current approach can be considered conservative for most cases, as it will maximize upwards shaft gas flow. For the WL cases, a higher pressured geosphere would result in a higher gradient into the repository which could result in slightly higher liquid inflow rates; however, it is unlikely that the increase would be sufficient to significantly alter the results.

   Quantitative assessment of the impacts of this approach could be addressed by comparison to a TOUGH2/EOS7R GGM model.

9.2.2 Model Limitations and Geosphere Conservatisms

Although the gas modelling results presented in this report show virtually no transport of repository gases in the host rock, these results may still be conservative. This subsection describes various aspects of the current modelling approach that may under-represent the impact of various geosphere attributes.

1. The applicability of the van Genuchten models for capillary pressure and relative permeability has not been demonstrated for the low permeability rocks of the DGR system. For example, the relative permeability curves may under-estimate actual permeability reduction and, thence over-estimate system response. However, there are no clearly superior alternative models, and the van Genuchten model has widespread acceptance in international programs. If the effective permeability were to be further reduced, the repressurization of the Ordovician underpressures present in the NE-RC and related cases would be further delayed. Water inflow into the repository may also be reduced.

2. The T2GGM model, coupled with the assigned boundary conditions in the Cambrian and Lower Silurian sediments, will bleed gas off the lower and upper boundaries. This effect can be noted by examining saturation profiles presented in Figure 5.169. In geologic time (far beyond the time simulated), this could lead to a significant depletion of gas in the formation. However, field evidence indicates that the partial gas saturation of the Ordovician rock mass, if it exists, is likely very old and has not moved. This suggests that the estimated two-phase flow parameters used in T2GGM analyses may not fully capture 'stagnant' system performance, and may overestimate the gas transport rates in the rock. As there is virtually no transport of repository gases into the geosphere over the 1 Ma simulation period (see Figure 5.123), this is also of little significance.

3. TOUGH2/EOS3 does not include dispersion as a transport process for dissolved gases. Dispersion has the effect of "smearing" the concentration front in areas where advective transport dominates. In all cases, dissolved gas flow in the geosphere is diffusion dominated, and thus dispersion would not change the distribution of dissolved gas in the geosphere. Advection is limited to flow up the shaft in the current models, so inclusion of dispersion could possibly alter the arrival time (making it earlier) and reduce the magnitude of dissolved gas pulses in the shaft. This would affect the SF-ED case only, and would likely not be significant.

4. Up-scaling of core properties to formation scale diminishes the importance of local changes in permeability, such as those due to carbonate and shale interlayering seen in the Ordovician shales. This alternating of more and less permeable layers could affect the accumulation of gas in the system, causing zones of high gas saturation at the interfaces. This in turn may create capillary barriers that could affect system response. The NE-RC or NE-RC2 models would not be expected to reveal existence of these barrier(s), as the models are not discretized at the scale of lithologic change. This up-scaling problem is a universal issue for all gas and groundwater models where averaging is required both for numeric tractability and to represent the limited ability to completely characterize a geologic system. Even if these barriers were present, they would likely have very little impact on repository pressures. They would have no impact on transport within the shaft.

5. T2GGM assumes that the relative permeability curve can be used to scale calculated effective diffusion (D_e) coefficients. In the low permeability rocks of the DGR system, this approach may over-estimate D_e leading to a simulated overestimate of dissolved gas migration from the system in the intact rock. As there is no significant transport of dissolved or free-phase gas in the geosphere in any of the cases presented in this report, this effect is inconsequential.

Application of possibly more representative geosphere attributes as described above would not appreciably change the simulation results.

9.2.3 Parameter Uncertainty

The Reference Case and variant cases for the Normal Evolution Scenario considered in this report were intended to illustrate possible or feasible conceptual models. The following list enumerates the major sources of parameter uncertainty.

1. **Geosphere capillary pressure and relative permeability parameters:**

   Geosphere capillary pressure and relative permeability functions used in the modelling are parameterized by fitting the van Genuchten functions to laboratory test results. As described in Section 4.2.1, there are a range of responses for individual formations. A representative set of two-phase flow properties were developed that provided a reasonable representation of the various formation responses. Sensitivity cases NE-GT1 and NE-GT2 investigated bounding capillary pressure curves, while NE-GT3 used an alternative relative permeability curve. Simulation results for these cases showed virtually no sensitivity to these parameters; in all cases there is essentially no transport of a separate phase gas in the intact rock, when the rock is assumed fully liquid saturated.

   The capillary pressure curves are particularly important in defining conditions for the NE-RC and related cases with initial gas saturation. For the NE-RC and NE-RC2 cases, the capillary pressure assumptions slightly impact the repository pressure history during the 1 Ma simulation period. The NE-RC2 case used formation-specific two-phase flow parameters rather than the representative set; this did not appreciably change repository pressures in comparison to NE-RC, but did induce more transient behaviour in the geosphere. The NE-RC, NE-RC1 and NE-RC2 cases are sensitive to assumptions on residual gas saturation for the relative permeability curve. The 5% residual saturation selected for the representative curves in NE-RC and NE-RC1 is within the range of the site specific S_{gr} values used for NE-RC2 (1% to 15%).

2. **Shaft seal capillary pressure and relative permeability parameters:** Shaft material two-phase flow properties were based on literature values. There are few data describing two-phase flow parameters for the specified formulations of seal materials, particularly the asphalt. Sensitivity case NE-GT4 determined sensitivity to the presence of the asphalt seal as opposed to replacement by bentonite/sand. No significant differences in shaft flow rates were seen. Sensitivity case NE-GT5 tested model sensitivity to bentonite/sand permeability and a corresponding decrease in air entry pressure as per the Davies relationship. In combination, these changes significantly increased shaft gas flow rates in comparison to the NE-GG1 case.

3. **Shaft EDZ characterization and shaft seal effectiveness:** Effectiveness of the overall shaft seal is clearly important. Case NE-EDZ1 assessed the impact of increased EDZ permeabilities and found little change from the NE-SBC case. The current EDZ characterization is largely based on international experience and expert judgement. Also, the range of cases presented here (NE-RC, NE-GT5, SF-BC, SF-ED) are likely conservative representations of the expected variation. Site specific measurement of the shaft EDZ is considered as part of the DGR construction (NWMO 2011b).

4. **Tunnel HDZ Characterization:** In all normal evolution cases with gas transport up the shaft, repository gas moves to the shaft through the access tunnel HDZ above the concrete monolith. This was conservatively modelled as a high permeability system. Sensitivity to HDZ permeability or two-phase flow parameters was not assessed. However, gas transport

was generally found to be limited by the shaft seals, so a more permeable HDZ is unlikely to increase gas and liquid flow up the shaft. However, if the HDZ size and/or permeability could be reduced, such as by removing a significant length of HDZ during closure, that would likely reduce gas flow up the shaft.

5. **Geosphere permeability:** Permeabilities used in these models were based on formation averages of hydraulic testing results (INTERA 2011). These tests estimate horizontal hydraulic conductivity only. Vertical conductivity is calculated from an estimated anisotropy, for which no direct in-situ physical estimates are possible. A 10:1 K_h:K_v anisotropy is specified for most formations in INTERA (2011). Sensitivity case NE-AN3 evaluated a decrease in anisotropy to 1:1 for most formations, which effective increased vertical permeability in the vicinity of the repository by a factor of 10. The NWL results of the NE-AN3 case show a resulting slight increase in repository pressure. The WL results showed a more significant change as the increased liquid inflow allows gas generation to proceed at close to the NWL rate. These results provide further confirmation that the NWL results represent a more conservative approach.

9.3 Geosphere Conceptual Model Uncertainty

Our understanding of the geosphere properties, its history and its future evolution is described in the Descriptive Geosphere Site Model (INTERA 2011) and Geosynthesis report (NWMO 2011a). The repository system evolution is summarized in Chapter 4 of the System and Its Evolution report (QUINTESSA 2011b). Specific areas of uncertainty that may impact gas transport results are listed below, along with how they are addressed in this study.

1. **Mechanism of Ordovician underpressures:** Transport of any dissolved gas from the repository will be significantly reduced for as long as underpressures persist in the Ordovician units. During this period prevailing liquid gradients will be downward at all points above the repository horizon, including the shaft and EDZ system. Most cases in the current study make the conservative assumption that the underpressures have been dissipated. Even with this assumption, dissolved gas transport within the rock is minimal.

   In the cases which incorporate an underpressure (NE-RC, NE-RC1, and NE-RC2), the initial pressure is based on pressures measured in Westbay casings installed in site characterization boreholes. It is likely that these pressures are not yet at local equilibrium and the actual underpressure is greater. If such were the case, the duration of downward gradients above the repository would be of a greater magnitude and persist for even longer.

2. **Time dependence of Cambrian overpressure:** The high pressure in the Cambrian unit drives the transport of water and dissolved gas upwards from the surrounding rocks into the repository and subsequently upwards through the shaft system. Although this pressure is proven present from site characterization results, its future evolution is unknown. However, any changes in Cambrian pressure will take very long times to propagate through the geosphere. In the current study, the Cambrian pressure has been assumed constant.

3. **Gas saturations in the Ordovician:** The NE-RC and related cases demonstrate the effect of gas saturations and pressures on repository performance. Site characterization data suggest that gas saturations exist in the rock mass at the repository horizon and the existence of gas at these horizons is the likely explanation for the observed underpressures. However, quantification of gas saturations is uncertain, as the permeability and porosity of the rock mass are at the threshold at which existing measurement techniques can be

applied. The NE-RC1 and NE-RC2 case results show that the selected gas saturations have limited impact on system performance.

4. **Silurian flow system:** Measured pressures in the DGR boreholes indicate that overpressures exist in the lower Silurian (below the Guelph Formation) with limited or nonexistent vertical gradients above the Guelph. Horizontal gradients exist in the more permeable formations (Guelph and Salina A1 upper carbonate) and slow horizontal groundwater flow through these units will occur. These processes are not represented in the models used in this report, but may be expected to reduce, if not eliminate, any vertical transport of gas and dissolved gases above these formations. The 2DRS model incorporates these units (but without horizontal gradients), and results show that the Guelph acts as an effective sink for any gas transported up the shaft.

5. **Future glaciation events:** The impact of sequential future glaciation events on the repository system has not been evaluated in the T2GGM models. The primary effects are expected to be transient overpressurization of all stratigraphic units and the repository during glacial advances followed by dissipation during glacial retreats. The extent of overpressures is likely limited (see results of coupled hydro-mechanical modelling in Chapter 5, Geosynthesis, NWMO 2011a). Glaciation may have mechanical impacts such as causing roof failure within the repository; however, calculations presented here all assumed complete roof failure from an early period. The complete inclusion of glaciation effects will require the use of a code with coupled two-phase and hydro-mechanical processes.

6. **Porewater and rock mass interactions with gases**: There may be interactions of dissolved and free phase CO_2 with the carbonate rocks and porewaters that could affect CO_2 transport. However, any interaction will be limited to the immediate vicinity of the repository and is unlikely to impact repository pressure or saturation.

9.4 Repository Layout

The final preliminary design differs in minor aspects from the original preliminary design used in the bulk of the analyses presented in this report. Specifically, the final design void volume is approximately 8% larger than that of the original preliminary design. The effect of this variation was assessed with two cases, NE-PD-RC, and NE-PD-GT5. In both cases, peak repository pressure was slightly diminished, and in the case of NE-PD-GT5, gas flows up the shaft reduced for the final design.

10. SUMMARY AND CONCLUSIONS

The long-term performance of the proposed L&ILW repository at the Bruce nuclear site has been assessed with the use of numeric models of two-phase gas and groundwater flow. Reference Case and sensitivity analyses have been performed for the Normal Evolution Scenario and for a 'what if' Disruptive Scenario (Severe Shaft Seal Failure).

The modelling approaches used include simplified two- and three-dimensional models which incorporate aggregate properties of the repository and shaft in a computationally efficient model. The T2GGM model was employed, which couples the GGM repository gas generation model with the TOUGH2/EOS3 two-phase flow model.

The following narrative is a qualitative description of gas generation and water processes within the repository.

1. Oxygen within the repository is consumed and conditions become anaerobic.

2. Moisture initially present in the wastes, plus water that seeps slowly into the repository from the surrounding rock and the shaft, support the anaerobic corrosion of metals and the degradation of organic wastes, resulting in generation of hydrogen, CO_2 and CH_4 gases. The gas pressure in the repository rises gradually.

3. There is a pressure balance between the water seepage into the repository and the gas generation within the repository. For most cases, the very low permeability of the rock precludes significant water saturation of the repository for the 1 Ma simulation period. In some sensitivity cases the repository is virtually dry (or completely unsaturated) after 100,000 a.

4. Over the 1 Ma period, the peak repository gas pressure is in the range of 7 to 9 MPa, converging towards or somewhat higher than the steady-state pressure at the repository horizon of around 7 MPa, and much less than the lithostatic pressure of 17 MPa.

5. Methane is generally the dominant gas throughout the evolution of the repository, due to degradation of organic wastes and the consumption of hydrogen and carbon dioxide via the microbial methanogenic reaction given by Equation (2-3). The balance of the initial inventories of metallic and organic wastes results in the repository atmosphere containing small levels of either hydrogen or carbon dioxide. Generally, hydrogen is more apparent at early times.

6. Due to the low-permeability rock and shaft, backfilling the repository reduces the available void space to hold the generated gas, and results in a higher peak repository gas pressure. However, this is not the reference design basis.

The following describes the general flow of gas and water within the host-rock and shaft system in qualitative terms.

1. Rock formation porewater and gas (if present) flow into the shaft from the rock after closure. The shaft seals generally resaturate with water within a several hundred year period as initial gas dissolves and disperses into the incoming water.

2. Porewater and formation gas (if present) flow into the repository from the host rock. The shaft is a minor source of water and gas. As the repository pressure rises, due to both liquid

inflow and gas generation, the flow rate into the repository decreases. This equilibration is a slow process due to the large repository volume and the low rock permeability.

3. If the geosphere contains gas above a residual level of gas saturation, formation gas will continue to seep into the repository until an equilibrium between repository and geosphere pressures is reached. This may take millions of years.

4. As pressures in the repository develop, small amounts of gas are pushed out into the shaft and the rock mass. The high capillary pressures in the Ordovician rock mass and bentonite/sand seals ensure that leakage of gas out of the repository is very slow. Gas saturations in the rock remain very small beyond a few metres from the repository.

5. In the Reference and Simplified Base Cases, repository gas pressure never exceeds the air-entry pressure of the shaft seal materials. However, in several variant cases, the gas pressure at the base of the shaft is sufficient to initiate flow up the shaft.

6. If gas reaches the Guelph Formation, the differences in relative capillary pressures between the low-permeability shaft seal materials and the permeable Guelph Formation results in the gas flowing into the formation. The Guelph acts as an effective sink, preventing free gas from reaching the Shallow Bedrock Groundwater Zone. However, free gas at this level could then be a source of dissolved gas that could diffuse upwards.

7. Some dissolved gas from repository level reaches the top of the Intermediate Groundwater Zone, in very small amounts and at long times.

8. The repository remains largely unsaturated over the 1 million years evaluated in the normal evolution scenario. As gas generation is eliminated, slow gas dissolution and permeation may allow eventual resaturation on very long time scales.

While all the cases for the Normal Evolution Scenario exhibit the same series of gas and water flow processes, they differ in the timing of these processes, as well as the magnitude of the repository response (both water saturation and pressure). Similar processes occur in the Severe Shaft Seal Failure Scenario, where the main difference is that gas reaches the top of the Intermediate Bedrock Groundwater Zone.

The results of the detailed gas modelling presented here are used in the safety assessment-level modelling to inform:

- The water level in the repository with time;
- The relative proportions of CO_2 and CH_4 and hence partitioning of gaseous C-14 between CO_2 and CH_4;
- The partitioning of radioactive gases between gas and groundwater in the repository;
- The release rates of radioactive gas entrained in bulk gas to the shaft and geosphere; and
- The bulk gas travel time from the repository to the ground surface via the shafts and geosphere.

Uncertainties have been taken into account through use of variant cases, conservative representation and a gas generation model that incorporates the key processes. Confidence in the results can be increased by considering:

- Further data on geosphere initial gas pressures, gas saturations, and two-phase flow parameters (capillary pressure and relative permeability);

- Further data on shaft seal and EDZ characteristics;
- Additional information on the time dependence of the Cambrian overpressure and Ordovician underpressures, as well as the response of the repository and geosphere system to glaciation events; and
- Confirmation simulations of selected cases with enhanced models capable of multiple gases and saline geosphere liquids.

Results from cases presented in this report show that the site geosphere acts as a very effective barrier, with no significant flow of free-phase or dissolved gas within the host rocks. In case where transport occurs, all movement of gas is through the shaft seals, and in some cases, through the shaft EDZ. The shaft seals are an effective barrier, and, in conjunction with the higher permeability Guelph Formation, prevent the transport of any gas to the Shallow Bedrock Groundwater Zone. Only under the disruptive scenarios does gas reach the shallow groundwater, and then only if extreme assumptions are made about the properties of the degraded shaft materials that characterize the scenarios.

11. REFERENCES

Calder, N. 2011. Two-Phase Flow Parameters from DGR-2, DGR-3 and DGR-4 Petrophysics Data. Intera Engineering Ltd. Report TR-08-33 R0. Ottawa, Canada.

Davies, P.B. 1991. Evaluation of the Role of Threshold Pressure in Controlling Flow of Waste-generated Gas into Bedded Salt at the Waste Isolation Pilot Plant (WIPP). Sandia Report SAND 90-3246. Albuquerque, USA.

European Commission (EU). 1999. Gas Migration and Two-Phase Flow through Engineered and Geological Barriers for a Deep Repository for Radioactive Waste. A Joint EC/NEA Status Report EUR 19122 EN. Luxembourg.

Finsterle, S. 1999. iTOUGH2 Command Reference, Version 4. Earth Sciences Division, Lawrence Berkeley National Laboratory. University of California, Berkeley, USA.

GEOFIRMA. 2011. Postclosure Safety Assessment: Groundwater Modelling. Geofirma Engineering Ltd. report for the Nuclear Waste Management Organization DGR-TR-2011-30 R000. Toronto, Canada.

Incropera, F.P. and D.P. DeWitt. 1996. Fundamentals of Heat and Mass Transfer. John Wiley and Sons, New York, USA.

INTERA. 2011. Descriptive Geosphere Site Model. Intera Engineering Ltd. report for the Nuclear Waste Management Organization DGR-TR-2011-24 R000. Toronto, Canada.

Jorgensen, D.G., T. Gogel and D.C. Signor. 1982. Determination of flow in aquifers containing variable-density water, Groundwater Monitoring Review, Vol. 2 No. 2, pp. 40-45.

Lanyon, G.W., P. Marschall, M. Fukaya, J. Croise, S. Yamamoto and G. Mayer. 2001 Laboratory Data Compilation Report. Nagra Project Report NBP-00-20. Wettingen, Switzerland.

Luckner, L., M.Th. van Genuchten and D. Nielsen. 1989. A consistent set of parametric models for the two-phase flow of immiscible fluids in the subsurface, Water Resources Research, Vol. 25(10), 2187–2193.

Lusczynski, N J. 1961. Head and flow of groundwater of variable density, Journal of Geophysical Research, Vol. 66, pp. 4247-4256.

NWMO. 2011a. Geosynthesis. Nuclear Waste Management Organization Report NWMO DGR-TR-2011-11 R000. Toronto, Canada.

NWMO. 2011b. Geoscientific Verification Plan. Nuclear Waste Management Organization Report NWMO DGR-TR-2011-38. Toronto, Canada.

OPG. 2011a. Deep Geologic Repository for Low and Intermediate Level Waste: Environmental Impact Statement. Ontario Power Generation Report 00216-REP-07701-00001 R000. Toronto, Canada.

OPG. 2011b. Deep Geologic Repository for Low and Intermediate Level Waste: Preliminary Safety Report. Ontario Power Generation Report 00216-SR-01320-00001 R000. Toronto, Canada.

Pruess, K., C. Oldenburg and G. Moridis. 1999. TOUGH2 User's Guide, Version 2.0. Lawrence Berkeley National Laboratory LBNL-43134. Berkeley, USA.

QUINTESSA. 2010. Postclosure Safety Assessment Services for OPG's Proposed Deep Geologic Repository: Project Quality Plan. Quintessa Ltd. Document QRS-1335B-PQP v3.0. Henley-on-Thames, United Kingdom.

QUINTESSA. 2011a. Postclosure Safety Assessment: Analysis of the Normal Evolution Scenario. Quintessa Ltd. report for the Nuclear Waste Management Organization NWMO DGR-TR-2011-26 R000. Toronto, Canada.

QUINTESSA. 2011b. Postclosure Safety Assessment: System and Its Evolution. Quintessa Ltd. report for the Nuclear Waste Management Organization NWMO DGR-TR-2011-28 R000. Toronto, Canada.

QUINTESSA and GEOFIRMA. 2011a. Postclosure Safety Assessment: Data. Quintessa Ltd. and Geofirma Engineering Ltd. report for the Nuclear Waste Management Organization NWMO DGR-TR-2011-32 R000. Toronto, Canada.

QUINTESSA and GEOFIRMA. 2011b. T2GGM Version 2: Gas Generation and Transport Code. Quintessa Ltd. and Geofirma Engineering Ltd. report for the Nuclear Waste Management Organization NWMO DGR-TR-2011-33 R000. Toronto, Canada.

QUINTESSA and SENES. 2011. Postclosure Safety Assessment: Analysis of Human Intrusion and Other Disruptive Scenarios. Quintessa Ltd. and SENES Consultants Ltd. report for the Nuclear Waste Management Organization NWMO DGR-TR-2011-27 R000. Toronto, Canada.

QUINTESSA, INTERA and SENES. 2009. Postclosure Safety Assessment (V1). Quintessa Ltd., Intera Engineering Ltd. and SENES Consultants Ltd. report for the Nuclear Waste Management Organization NWMO DGR-TR-2009-01 R000. Toronto, Canada.

QUINTESSA, GEOFIRMA and SENES. 2011a. Postclosure Safety Assessment. Quintessa Ltd., Geofirma Engineering Ltd. and SENES Consultants Ltd. report for the Nuclear Waste Management Organization NWMO DGR-TR-2011-25 R000. Toronto, Canada.

QUINTESSA, SENES and GEOFIRMA. 2011b. Postclosure Safety Assessment: Features, Events and Processes. Quintessa Ltd., SENES Consultants Ltd. and Geofirma Engineering Ltd. report for the Nuclear Waste Management Organization NWMO DGR-TR-2011-29 R000. Toronto, Canada.

Walsh, R. 2011. Compilation and Consolidation of Field and Laboratory Data for Hydrogeological Properties, Intera Engineering Ltd. Report TR-08-10 R0. Ottawa, Canada.

12. ABBREVIATIONS AND ACRONYMS

2DRS	2-dimensional Radial Shaft Model
3DD	3-Dimensional Detailed Model
3DSR	3-Dimensional Simplified Repository Model
3DSRS	3-Dimensional Simplified Repository and Shaft Model
BH	Poorly Sealed Borehole Scenario
DGR	Deep Geologic Repository
EDZ	Excavation Damaged Zone
EIS	Environmental Impact Statement
EOS	Equation-of-State
FEP	Features, Events and Processes
GGM	Gas Generation Model
HDZ	Highly Damaged Zone
HI	Human Intrusion Scenario
L&ILW	Low and Intermediate Level Waste
NE	Normal Evolution Scenario
NE-AN3	Reduced Geosphere Anisotropy Case
NE-BF	Backfilled Repository Case
NE-EDZ1	Increased Permeability EDZ Case
NE-GG1	Increased Gas Generation Case
NE-GG2	Reduced Degradation Rate Case
NE-GT 1	Decreased Geosphere Air Entry Pressure Case
NE-GT 2	Increased Geosphere Air Entry Pressure Case
NE-GT 3	Modified Geosphere Relative Permeability Case
NE-GT4	Asphalt Replacement Case
NE-GT5	Reduced Shaft Seal Performance Case
NE-MG	Alternative Gas (Air) Case
NE-NG	No Gas Generation Cases

NE-NM	No Methanogenic Gas Reactions Case
NE-PD-GT5	Reduced Shaft Seal Performance - Final Preliminary Design Case
NE-PD-RC	Reference Case - Final Preliminary Design Case
NE-RC	Reference Case
NE-RC1	Geosphere Gas Phase at Residual Saturation Case
NE-RC2	Variable Geosphere Gas Saturation and Transport Properties Case
NE-SBC	Simplified Base Case
NWL	Non-Water-Limiting Case
OPG	Ontario Power Generation
PD	Final Preliminary Design
PSR	Preliminary Safety Report
SA	Safety Assessment
SF	Shaft Failure Scenario
SF-BC	Shaft Seal Failure Base Case
SF-ED	Severe Shaft Seal Failure – Extra Degradation Case
UTM	Universal Transverse Mercator
VF	Vertical Fault Scenario
WI	Work Instruction
WL	Water-Limiting Case
WWMF	Western Waste Management Facility

APPENDICES

THIS PAGE HAS BEEN LEFT BLANK INTENTIONALLY

APPENDIX A: FEP AUDIT OF GAS GENERATION AND TRANSPORT MODEL

This appendix provides an audit of the T2GGM mathematical model against the list of FEPs (Features, Events and Processes) outlined in the FEPs report (QUINTESSA et al. 2011).

THIS PAGE HAS BEEN LEFT BLANK INTENTIONALLY

FEP			Included in Mathematical Model for Gas Generation and Gas Migration (T2GGM) Models
2. REPOSITORY SYSTEM FACTORS			
2.1	Waste, Waste Form & Engineered Components		
	2.1.01	Waste inventory	
		2.1.01.01 Radionuclide content	**No**, Not applicable since T2GGM does not explicitly identify or track radioactive isotopes within the waste streams.
		2.1.01.02 Chemical content	**Yes**, although specific chemicals or derivatives of them may be modelled as belonging to a metallic or organic waste stream, rather than being explicitly modelled. See, for example, the discussion of ion-exchange resins in Section 4.2.1.1 of the Software Documentation (QUINTESSA and GEOFIRMA 2011a).
	2.1.02	Waste-form characteristics	
		2.1.02.01 Metallic wastes	**Yes**, see Section 4.3 of the Software Documentation (QUINTESSA and GEOFIRMA 2011a).
		2.1.02.02 Organic wastes	**Yes**, see Section 4.2 of the Software Documentation (QUINTESSA and GEOFIRMA 2011a).
		2.1.02.03 Non-metallic, inorganic wastes	**Yes**, but only in terms of effects on metallic/organic waste streams and gas generation. The volume of non-metallic, inorganic wastes (concrete, ash, asbestos) are taken into account when calculating the repository void volume used by the GGM. See the Data report (QUINTESSA and GEOFIRMA 2011b). The presence of cementitious material on the corrosion rates of metals is taken into account through consideration of a passivated carbon steel waste stream. Carbonation of concrete is not modelled explicitly by T2GGM, but this considered through scoping calculations in the System and Its Evolution report (QUINTESSA 2011).
	2.1.03	Waste-packaging characteristics	
		2.1.03.01 Containers	**Yes**, inventories of organic and metallic components that fall into the main waste streams considered by T2GGM are explicitly modelled. See Sections 4.2 and 4.3 of the Software Documentation (QUINTESSA and GEOFIRMA 2011a). Containers are also included in the calculations of the surface areas of those waste

FEP			Included in Mathematical Model for Gas Generation and Gas Migration (T2GGM) Models
			streams and the initial void volume. See Section 3.2 of the Data Report (QUINTESSA and GEOFIRMA 2011b).
	2.1.03.02	Overpacks	**Yes**, inventories of organic and metallic components that fall into the main waste streams considered by the GGM are explicitly modelled. See Sections 4.2 and 4.3 of the Software Documentation (QUINTESSA and GEOFIRMA 2011a). Overpacks are also included in the calculations of the surface areas of those waste streams and the initial void volume. See Section 3.2 of the Data report (QUINTESSA and GEOFIRMA 2011b).
2.1.04	Emplacement room and access and shaft service area tunnel characteristics		
	2.1.04.01	Roofs and walls	**Yes (partly)**, although individual room and tunnels are not explicitly modelled, their dimensions are used in developing the model's representation of the DGR, and their concrete lining and associated steel reinforcement are accounted for in the estimate of repository void volume and metal inventory.
	2.1.04.02	Floors	**Yes (partly)**, see FEP 2.1.04.01.
	2.1.04.03	Rock bolts	**Yes**, included in the inventory of the metals in the repository. See Section 4.3 of the Software Documentation (QUINTESSA and GEOFIRMA 2011a).
	2.1.04.04	Room and closure walls	**Yes (partly)**, although repository is modelled as contiguous void space, walls and associated steel reinforcement are accounted for in the calculation of repository void volume and metal inventory.
	2.1.04.05	Backfill	**Yes (partly)**, but only considered for the backfill (NE-BF) calculation case (all other cases assume no backfill). For the NE-BF case, backfill is accounted for by reducing the repository void volume.
2.1.05	Shaft characteristics		
	2.1.05.01	Lining	**Yes (partly)**, the presence in the repository of materials from the decommissioned ventilation shaft liner is accounted for in the

FEP			Included in Mathematical Model for Gas Generation and Gas Migration (T2GGM) Models
			available void volume and the mass of passivated carbon steel (see Tables 4.5 and 4.9 of the Data report, QUINTESSA and GEOFIRMA 2011b). Shaft lining is removed in Intermediate and Deep Bedrock Groundwater zones according to closure plan and so is not represented in flow calculations.
	2.1.05.02	Backfill	**Yes**, backfill in the shaft (bentonite/sand and engineered fill) are explicitly represented in the model.
	2.1.05.03	Plugs	**Yes**, concrete and asphalt seals are explicitly represented in the model.
	2.1.05.04	Rock bolts	**n/a**, screened out in conceptual model.
2.1.06	Mechanical processes and conditions (in wastes and emplacement rooms, tunnels and shafts)		Note. The effect of mechanical processes and conditions, such as failure of shaft seals, can be modelled through alteration of geometry and expected volumes. The effect of gas and water flow due to the altered conditions can also be taken into account. Thus mechanical effects are principally taken into account through consideration of different scenarios using T2GGM.
	2.1.06.01	Packaging collapse	
		A Steel failure	**No**, the collapse of steel as it corrodes is not explicitly modelled by T2GGM. However, this can be taken into account in selection of the corresponding corrosion rates and in the change of waste surface area.
		B Concrete failure	**No**, this is not explicitly modelled by T2GGM, but the consequences of concrete failure on T2GGM can be modelled through interaction with gas and water flows in the geosphere and through changes in repository void volume.
	2.1.06.02	Material volume changes	
		A Concrete shrinkage/expansion	**No**, low-shrinkage concrete specified for preliminary.
		B Bentonite swelling	**No**, not explicitly modelled. Good contact is assumed at bentonite/rock interface with no interface zone of different properties.

FEP			Included in Mathematical Model for Gas Generation and Gas Migration (T2GGM) Models
		C Corrosion products	**No**, effect of corrosion products on time-dependent corrosion rate not accounted for.
	2.1.06.03	Emplacement room/ tunnel collapse	**Yes**, roof fall is assumed to have occurred at time = 0.
	2.1.06.04	Container movement	**Yes**, container compaction due to rock fall included.
	2.1.06.05	Fracture formation	**No**, geomechanical modelling has shown that calculated gas pressures (8-10 MPa) (Figure 8.1 and Figure 8.2) will not cause fracturing (Chapter 6 of the Geosynthesis report, NWMO 2011).
	2.1.06.06	Stress-corrosion cracking	**n/a**, screened out in conceptual model.
	2.1.06.07	Gas explosion	**n/a**, screened out in conceptual model.
	2.1.06.08	Influence of climate change	**Yes**, 10 m rockfall in the repository is attributed to possible glaciation.
2.1.07	Hydraulic/hydrogeological processes and conditions (in wastes, emplacement rooms, tunnels and shafts)		
	2.1.07.01	Resaturation/desaturation	**Yes**, T2GGM models the evolution of saturated and vapour phases and uses this as an input to gas and liquid transport across the repository boundaries. See Chapter 4 of the Software Documentation (QUINTESSA and GEOFIRMA 2011a).
	2.1.07.02	Water flow	**Yes**, T2GGM calculates the rate of water generation due to corrosion and degradation processes within the repository. This is used to model the flow of water into and out of the repository.
	2.1.07.03	Gas-mediated water flow	**Yes**, T2GGM calculates the rate of gas generation due to corrosion and degradation processes within the repository. This is used to model gas-mediated water flow.
	2.1.07.04	Failure of drainage system	**n/a**, screened out in conceptual model.
	2.1.07.05	Fracturing of repository components due to hydraulic pressure	**n/a**, screened out in conceptual model.
	2.1.07.06	Coupled hydraulic processes including	**n/a**, screened out in conceptual model.

FEP			Included in Mathematical Model for Gas Generation and Gas Migration (T2GGM) Models
		temperature, chemical or electrical gradients	
	2.1.07.07	Influence of climate change	**No**, this is not explicitly modelled in T2GGM, although value for concrete bulkheads and monolith permeability is set at degraded value to account for potential impact of glacial cycling.
2.1.08	Chemical/geochemical processes and conditions (in wastes, emplacement rooms, tunnels and shafts)		
	2.1.08.01	pH conditions	**No**, T2GGM does not explicitly calculate the pH of the environment. However an enhanced corrosion rate is used in the presence of CO_2 which implicitly takes into account the acidification resulting from the dissolution of CO_2 in the aqueous phase. See Section 4.3.1.1 of the Software Documentation (QUINTESSA and GEOFIRMA 2011a).
	2.1.08.02	Redox conditions	**Yes**, T2GGM models redox processes through a series of terminal electron acceptor stages. See Chapter 4 of the Software Documentation (QUINTESSA and GEOFIRMA 2011a).
	2.1.08.03	Chloride and sulphate conditions	**Yes** (partly). Chloride is not explicitly modelled by T2GGM, although corrosion rates take into account the saline conditions in the DGR (see Appendix E of the Data report, QUINTESSA and GEOFIRMA 2011b). The impact of sulphates on microbial degradation is modelled (see Section 4.2.1 of the Software Documentation, QUINTESSA and GEOFIRMA 2011a).
	2.1.08.04	Corrosion	
		A General	**Yes**, explicitly modelled by T2GGM. See Section 4.3 of the Software Documentation (QUINTESSA and GEOFIRMA 2011a).
		B Localized	**n/a**, screened out in conceptual model.
		C Galvanic	**n/a**, screened out in conceptual model.
	2.1.08.05	Polymer degradation	**Yes**, see Section 4.2 of the Software Documentation (QUINTESSA and GEOFIRMA 2011a).

FEP			Included in Mathematical Model for Gas Generation and Gas Migration (T2GGM) Models
	2.1.08.06	Mineralization	
		A Leaching	**No**, the effect of leaching of concrete and other repository material is not considered. See FEP 2.1.08.01.
		B Chloride attack	**No**, the effect of chloride ions in the water on repository materials is not considered.
		C Sulphate attack	**No**, the effect of sulphate ions on concrete is not considered. However, the reduction of sulphate ions through the degradation of organic wastes and the subsequent rapid precipitation of iron sulphides is. See Section 4.2.1 and 4.4.1 of the Software Documentation. (QUINTESSA and GEOFIRMA 2011a).
		D Carbonation	**n/a**, screened out in conceptual model.
		E Illitization	**n/a**, screened out in conceptual model.
	2.1.08.07	Precipitation reactions	**Yes** (partly). Only the precipitation of metal sulphides is modelled.
	2.1.08.08	Chelating agent effects	**n/a**, screened out in conceptual model.
	2.1.08.09	Colloid formation	**n/a**, screened out in conceptual model.
	2.1.08.10	Osmotic effects	**n/a**, screened out in conceptual model.
	2.1.08.11	Chemical concentration gradients	**n/a**, screened out in conceptual model.
	2.1.08.12	Influence of climate change	**n/a**, screened out in conceptual model.
2.1.09	Biological/biochemical processes and conditions (in wastes, emplacement rooms, tunnels and shafts)		
	2.1.09.01	Microbial growth and poisoning	**Yes**, growth and death of biomass and recycling of biomass as organic waste are all modelled by T2GGM. See Section 4.2.1.3 of the Software Documentation (QUINTESSA and GEOFIRMA 2011a). Poisoning of microbial processes due to biocides or increased temperatures is not, but the cessation of microbial processes under conditions of low relative humidity in the vapour phase is.

FEP			Included in Mathematical Model for Gas Generation and Gas Migration (T2GGM) Models
	2.1.09.02	Microbially/biologically mediated processes	**Yes**, degradation of cellulosic wastes, nitrate and sulphate reduction and biomass growth are all explicitly modelled. See Section 4.2 of the Software Documentation (QUINTESSA and GEOFIRMA 2011a).
	2.1.09.03	Microbial/biological effects of evolution on redox (Eh) and acidity/alkalinity (pH)	**No**, neither the reduction potential nor the pH is explicitly calculated. However, redox reactions are modelled through a series of terminal electron acceptor stages and the effect of decreased pH due to dissolution of CO_2 is modelled through the enhanced corrosion of carbon and galvanized steels under high CO_2 partial pressures. See Section 4.2 of the Software Documentation (QUINTESSA and GEOFIRMA 2011a).
	2.1.09.04	Influence of climate change	**n/a**, screened out in conceptual model.
2.1.10	Thermal processes and conditions (in wastes, emplacement rooms, tunnels and shafts)		
	2.1.10.01	Radiogenic, chemical and biological heat production from the waste packages	**n/a**, screened out in conceptual model.
	2.1.10.02	Heat production from engineered features	**n/a**, screened out in conceptual model.
	2.1.10.03	Temperature evolution	**n/a**, screened out in conceptual model.
	2.1.10.04	Temperature dependence of processes	
		A Mechanical	**n/a**, screened out in conceptual model.
		B Hydraulic	**n/a**, screened out in conceptual model.
		C Chemical	**n/a**, screened out in conceptual model.
		D Biological	**n/a**, screened out in conceptual model.

FEP	Included in Mathematical Model for Gas Generation and Gas Migration (T2GGM) Models
2.1.10.05 Influence of climate change	**n/a**, screened out in conceptual model.
2.1.11 Gas sources (in wastes, emplacement rooms, tunnels and shafts)	
2.1.11.01 Radioactive decay	**n/a,** screened out in conceptual model.
2.1.11.02 Metal corrosion	**Yes**, see Section 4.3 of the Software Documentation (QUINTESSA and GEOFIRMA 2011a).
2.1.11,03 Organic waste degradation	**Yes**, see Section 4.2 of the Software Documentation (QUINTESSA and GEOFIRMA 2011a).
2.1.11.04 Cement degradation	**n/a**, screened out in conceptual model.
2.1.11.05 Asphalt degradation	**n/a**, screened out in conceptual model.
2.1.12 Radiation effects (in wastes, emplacement rooms, tunnels and shafts)	**n/a**, screened out in conceptual model.
2.1.13 Effects of extraneous materials	**n/a**, screened out in conceptual model.
2.1.14 Nuclear criticality	**n/a**, screened out in conceptual model.
2.2 Geological Environment	
2.2.01 Stratigraphy	**Yes**, consider Deep, Intermediate and Shallow Bedrock Groundwater Zones.
2.2.02 Host rock lithology	**Yes**, consider all bedrock units down to Precambrian.
2.2.03 Disturbed zone (in geosphere)	
2.2.03.01 Emplacement rooms and tunnels	**Yes**, explicitly consider excavation damaged zone around access tunnels. EDZ around repository is neglected, but would not provide significant additional permeability as compared to the repository itself.
2.2.03.02 Shafts	**Yes**, explicitly consider excavation damaged zone around shaft.
2.2.04 Large-scale discontinuities (in geosphere)	

FEP			Included in Mathematical Model for Gas Generation and Gas Migration (T2GGM) Models
	2.2.04.01	Faults and shear zones	**n/a**, screened out in conceptual model. Disruptive event case VF considers vertical fault.
	2.2.04.02	Fractures and joints	**No**, although field evidence shows that there are localized fracture zones and palaeokarst horizons, there are no continuous discrete fracture networks. So the presence of fractures is subsumed within the measured formation hydraulic conductivities (see FEPs report, QUINTESSA et al. 2011).
	2.2.04.03	Dykes	**n/a**, screened out in conceptual model.
2.2.05	Mechanical processes and conditions (in geosphere)		
	2.2.05.01	Geomechanical properties	**Yes**, consider rockfall in emplacement rooms and tunnels.
	2.2.05.02	Current stress regime	**Yes**, consider stress regime in determining EDZ parameters.
	2.2.05.03	Future stress regime	**Yes**, consider evolution of stress regime around the repository that causes rockfall.
2.2.06	Hydraulic/hydrogeological processes and conditions (in geosphere)		
	2.2.06.01	Hydraulic properties	**Yes**, geosphere properties assigned on a formation basis.
	2.2.06.02	Current hydraulic potentials and gradients	**Yes**, Reference Case includes underpressures. Horizontal hydraulic gradients assessed in sensitivity cases.
	2.2.06.03	Future hydraulic potentials and gradients	**Yes**, Reference Case is transient and includes equilibration of underpressures.
2.2.07	Chemical/geochemical processes and conditions (in geosphere)		
	2.2.07.01	Mineralogical properties	**No**, interactions of water and gas with rock minerals not evaluated by T2GGM models.

FEP			Included in Mathematical Model for Gas Generation and Gas Migration (T2GGM) Models
	2.2.07.02	Geochemical properties	**Yes** (partly), the impact of geosphere-derived sulphates on microbial degradation in the repository is modelled. Carbonate control of dissolved carbonate in repository water also assumed. Impact of salinity on corrosion rates is also considered (see FEP 2.1.08.03).
	2.2.07.03	Effects of engineered barriers	**n/a**, screened out in conceptual model.
	2.2.07.04	Effects of climate change	**n/a**, screened out in conceptual model.
2.2.08	Biological/biochemical processes and conditions (in geosphere)		**n/a**, screened out in conceptual model.
2.2.09	Thermal processes and conditions (in geosphere)		
	2.2.09.01	Thermal properties	**n/a**, screened out in conceptual model.
	2.2.09.02	Effects of waste and repository materials	**n/a**, screened out in conceptual model.
	2.2.09.03	Effects of climate change	**No**, the system at depth is expected to be isolated from the effects of climate change and so it is assumed to evolve under constant climate conditions. T2GGM does not represent the shallow geosphere which is expected to be affected by climate change.
2.2.10	Gas processes and effects (in geosphere)		
	2.2.10.01	Gas sources (excluding waste and repository materials)	**Yes**, formation gas is considered in the T2GGM gas calculations (Table 3.1).
	2.2.10.02	Gas migration	**Yes**, explicitly modelled.
	2.2.10.03	Gas dissolution	**Yes**, explicitly modelled.
	2.2.10.04	Gas-induced fractures	**n/a**, screened out in conceptual model.
2.2.11	Geological resources (in geosphere)		**No**, no economically viable resources in deep and intermediate geosphere (see Section 2.3.5 of the System and Its Evolution report, QUINTESSA 2011).

FEP	**Included in Mathematical Model for Gas Generation and Gas Migration (T2GGM) Models**
2.2.12 Undetected features (in geosphere)	**n/a**, screened out in conceptual model.
2.3 Surface Environment	**No**, not represented in the T2GGM models which focus on the repository and deep and intermediate geosphere.
2.4 Human Behaviour	**No**, not represented in the T2GGM models which focus on the repository and deep and intermediate geosphere.
3. CONTAMINANT FACTORS	T2GGM calculates the rate of generation of gas and water within the repository, and calculates the flux of gas and water from/to the geosphere, including the amounts of individual gas components. Assessment level codes can then use this information to track contaminants based on assumptions about initial levels within the wastes.

REFERENCES FOR APPENDIX A

NWMO. 2011. Geosynthesis. Nuclear Waste Management Organization Report NWMO DGR-TR-2011-11 R000. Toronto, Canada.

QUINTESSA. 2011. Postclosure Safety Assessment: System and Its Evolution. Quintessa Ltd. report for the Nuclear Waste Management Organization NWMO DGR-TR-2011-28 R000. Toronto, Canada.

QUINTESSA, SENES and GEOFIRMA. 2011. Postclosure Safety Assessment: Features, Events and Processes. Quintessa Ltd., SENES Consultants Ltd. and Geofirma Engineering Ltd. report for the Nuclear Waste Management Organization NWMO DGR-TR-2011-29 R000. Toronto, Canada.

QUINTESSA and GEOFIRMA. 2011a. T2GGM Version 2: Gas Generation and Transport Code. Quintessa Ltd. and Geofirma Engineering Ltd. report for the Nuclear Waste Management Organization NWMO DGR-TR-2011-33 R000. Toronto, Canada.

QUINTESSA and GEOFIRMA. 2011b. Postclosure Safety Assessment: Data. Quintessa Ltd. and Geofirma Engineering Ltd. report for the Nuclear Waste Management Organization NWMO DGR-TR-2011-32 R000. Toronto, Canada.

APPENDIX B: SIMPLE GAS PRESSURE AND FLOW CALCULATIONS

B.1 GAS PRESSURE

Appendix B of the System and Its Evolution report (QUINTESSA 2011) describes some simple calculations to estimate the maximum gas pressures within the repository as waste is converted to gaseous forms by corrosion and degradation. These calculations are based on the amounts of gases that could be produced from the initial waste inventory assuming certain processes. These amounts are used to estimate gas pressures assuming that all the gas is contained within the void space of the repository (no leakage). The following additional assumptions were made:

- no oxygen, no nitrate, no sulphate;
- no biomass;
- an unlimited supply of water; and
- a repository temperature of 22 ºC.

The processes considered for the three cases were:

1. Anaerobic Corrosion & Degradation[3];
2. Anaerobic Corrosion & Degradation with $FeCO_3$ Formation; and
3. Anaerobic Corrosion & Degradation with the Microbial Hydrogen Methanogenic Reaction ($4H_2+CO_2 \rightarrow CH_4 + 2H_2O$).

For comparison, a fourth case has been added here, with no microbial activity, only corrosion. The results are summarized in Table B.1. Table B.1 shows that the microbial hydrogen methanogenic reaction is expected to be the most important process for reducing gas pressure.

Table B.1: Estimated Maximum Repository Gas Pressures

Gas Generation	Initial Mass of Metals or Organics (kg)	Maximum Gas Pressure (MPa)			
		Case 1	Case 2	Case 3	Case 4
		Anaerobic Corrosion & Degradation	Case 1 with $FeCO_3$ Formation	Case 1 with Methanogenic Reaction	No microbial activity. Corrosion only
H_2 from metal corrosion	6.6E+07	9.1	8.1	0.0	9.1
CO_2 from organic degradation	2.2E+07	3.0	0.0	0.7	0.0
CH_4 from organic degradation		4.4	4.4	6.6	0.0
N_2 from initial air	-	0.1	0.1	0.1	0.1
Total	8.8E+07	16.6	12.6	7.4	9.2

[3] Microbes are active in degrading organics and producing gases like methane, but are not active in the gas methanogenic reaction $H_2 + CO_2 \rightarrow CH_4 + 2H_2O$.

B.2 CALCULATION OF GAS FLOW RATES IN THE SHAFT

The calculations in this section provide "back of the envelope" confirmation of the gas flow rates calculated for the SF-ED case. They use the pressures calculated at the top and bottom of the shaft, the permeability of the shaft, and the relative permeability calculated from the T2GGM average gas saturations. The flow area is taken from the single element of the three shaft elements (in cross-section) that has increased gas saturation. Flow takes a preferential path through this single column of elements. The 1-D Darcy flow equation for mass flow of gas can be written as:

$$Q_{gas} = \frac{m_{gas} P}{RT} \frac{k}{\mu} k_{rg} A \frac{dP}{dl} \quad \text{(B-1)}$$

where

$$k_{rg} = \frac{S_g - S_{min}}{S_{max} - S_{min}}$$

and

$$P = \frac{P_{upper} + P_{lower}}{2}$$

$$dP = P_{upper} - P_{lower}$$

$$dl = z_{upper} - z_{lower}$$

where

Q_{gas}	=	gas flow	(kg/s)
m_{gas}	=	molar weight of gas	(kg/mol)
P	=	average pressure	(Pa)
R	=	universal gas constant	(J/(K mol))
T	=	temperature	(K)
k	=	intrinsic permeability	(m^2)
k_{rg}	=	relative permeability to gas	(-)
μ	=	gas viscosity	(Pa s)
A	=	flow area	(m^2)
dP/dl	=	pressure gradient in shaft	(Pa/m)
S_g	=	gas saturation	(-)
S_{min}	=	gas saturation at k_{rg} = 0.0	(-)
S_{max}	=	gas saturation at k_{rg} = 1.0	(-)
P_{upper}	=	pressure at top of shaft	(Pa)
P_{lower}	=	pressure at bottom of shaft	(Pa)
z_{upper}	=	elevation at top of shaft	(m)
z_{lower}	=	elevation at bottom of shaft	(m)

Values used in the calculation (Table B.2) are defined by the SF-ED case at 3200 a when a near steady-state flow of gas is occurring in the shaft.

Table B.2: Shaft gas flow parameters

Parameter	Value	Unit	Source
m_{gas}	0.016	kg/mol	molecular weight of methane
R	8.314472	J/(K mol)	
T	295.15	K	SF-ED case
k	1.16E-14	m^2	SF-ED shaft permeability
μ	1.12E-05	Pa s	CRC (1992)
A	9	m^2	SF-ED grid property
S_g	1.97E-03	-	SF-ED average gas saturation of flowing nodes in shaft
S_{min}	0.001	-	SF-ED shaft relative permeability
S_{max}	0.999	-	SF-ED shaft relative permeability
P_{upper}	3,970,000	Pa	SF-ED case results at 3200 a
P_{lower}	6,370,000	Pa	SF-ED case results at 3200 a
z_{upper}	-202	mASL	Elevation of node at top of shaft
z_{lower}	-441	mASL	Elevation of node at bottom of shaft

The calculated gas mass flow rate up the shaft is 3.1×10^{-6} kg/s. This compares very well to the T2GGM calculated gas flow rate of 2.9×10^{-6} kg/s.

REFERENCES FOR APPENDIX B

QUINTESSA. 2011. Postclosure Safety Assessment: System and Its Evolution. Quintessa Ltd. report for the Nuclear Waste Management Organization NWMO DGR-TR-2011-28 R000. Toronto, Canada.

CRC. 1992. CRC Handbook of Chemistry and Physics, 73ed edition, p.6-164. CRC Press, Ann Arbor, USA.